A. Kaveh

Optimal Analysis of Structures by Concepts of Symmetry and Regularity

Springer

Optimal Analysis of Structures by Concepts of Symmetry and Regularity

A. Kaveh

Optimal Analysis of Structures by Concepts of Symmetry and Regularity

Springer

A. Kaveh
Centre of Excellence for Fundamental Studies
in Structural Engineering
Department of Civil Engineering
Iran University of Science and Technology
Tehran, Iran

ISBN 978-3-7091-1564-0 ISBN 978-3-7091-1565-7 (eBook)
DOI 10.1007/978-3-7091-1565-7
Springer Wien Heidelberg New York Dordrecht London

Library of Congress Control Number: 2013937845

Printed on acid-free paper

Springer is part of Springer Science+Business Media (www.springer.com)

Foreword

Recent advances in structural technology require greater accuracy, efficiency and speed in the analysis of structural systems, referred to as *Optimal Analysis of Structures Using Concepts of Symmetry and Regularity*. It is, therefore, not surprising that new methods have been developed for the analysis of structures with a large number of nodes and members.

The requirement of accuracy in analysis has been brought about by the need for demonstrating structural safety. Consequently, accurate methods of analysis had to be developed, since conventional methods, although perfectly satisfactory when used on simple structures, have been found inadequate because of the requirement of high computational effort for large-scale structures. Another reason why greater accuracy is required is the need to achieve efficient and optimal use of the material, i.e. optimal design.

In this book, different mathematical concepts are combined to make the optimal analysis of structures feasible. Canonical forms from matrix algebra, product graphs from graph theory and symmetry groups from group theory are some of the concepts involved in the variety of efficient methods and algorithms presented.

The methods and algorithms elucidated in this book enable the analysts to handle large-scale structural systems by lowering their computational cost fulfilling the requirement for faster analysis and design of future complex systems. The value of the presented methods becomes all the more evident in cases where the analysis needs to be repeated hundreds or even thousands of times, as is the case with the optimal design of structures using different meta-heuristic algorithms.

This book is of interest to all those engaged in computer-aided analysis and design, and also to software developers in this field. Though the methods are illustrated mainly through skeletal structures, however, some continuum models have also been added to show the generality of the methods. The concepts presented in this book are not only applicable to different types of structures, but can equally be used for the analysis of other systems, such as hydraulic and electrical networks.

The author has been involved in various developments and applications of graph theory in the last four decades. The present book contains part of this research, suitable for various aspects of matrix structural analysis.

The present book is intended to serve as a textbook for the optimal analysis of large-scale structures utilising concepts of symmetry and regularity. Special attention is focused on efficient methods for eigensolution of matrices involved in static, dynamic and stability analyses of symmetric and regular structures, or those general structures containing such components. Powerful tools are also developed for configuration processing, which is an important issue in the analysis and design of space structures and finite element models.

The book is written in an attractive dynamic style that immediately goes to the heart of each subtopic. The many worked out examples will help the reader to appreciate the theory. The book is likely to be of interest to pure and applied mathematicians who use and teach graph theory as well as to students and researchers in structural engineering and architecture.

Vienna University of Technology
Austria

Professor Emeritus
Dr. Dr. h.c. Franz Ziegler

Preface

Concepts from different fields of mathematics are combined to obtain powerful tools and algorithms for efficient analysis of structures. Many structures are either symmetric or regular, and some others can be made symmetric or regular by addition or elimination of a small number of nodes and/or members. For these structures, the matrices have canonical forms and the corresponding equations can easily be solved using some concepts from matrix algebra, linear algebra, graph theory, and group theory.

The methods and algorithms developed in this book make the analysis of large-scale structures possible by reducing their computational time and storage, fulfilling the requirements for a faster analysis of complex systems. The power of the presented methods becomes more evident when analysis needs to be repeated many times, as is the case with optimum design of structures utilizing different meta-heuristic algorithms.

The author has been involved in various developments and applications of graph theory in the last four decades. The present book contains part of this research, suitable for matrix analysis of symmetric and regular structures.

Methods of this book can efficiently be used in computer-aided analysis and design, and commercial software developments. Though these methods are mainly illustrated through skeletal structures, some continuum models have also been included to show the generality of the algorithms.

The present book is intended to serve as a textbook for the optimal analysis of large-scale structures utilising concepts of symmetry and regularity. Special attention is focused on efficient methods for eigensolution of matrices involved in static, dynamic and stability analyses of symmetric and regular structures, or those general structures containing such components. Powerful tools are also developed for configuration processing, which is an important issue in the analysis and design of space structures and finite element models.

In Chap. 1, an introduction is provided to the definitions and basic concepts of symmetry and regularity. Chapter 2 presents a background of the mathematics extensively used in this book, consisting of definitions from graph theory and algebraic graph theory. Standard definitions of graph products and their extensions

are provided in Chap. 3 and utilised in the important topic of configuration processing of structures. Basic definitions of canonical forms and their properties involved in symmetric and regular structures are discussed in Chap. 4. The canonical forms are applied to two important combinatorial optimisation problems consisting of nodal ordering to improve the patterns of the structural matrices, and graph partitioning for use in parallel computing in Chap. 5. Chapter 6 utilises graph products for similar purposes as in the previous chapter. Canonical forms have important applications in structural mechanics. These applications are discussed in Chap. 7. Graph products make the efficient analysis of regular structures feasible, providing closed-form solutions for this purpose as discussed in Chap. 8. Some structural models are not regular but can be made regular by adding and/or deleting of some members. Chapter 9 contains efficient methods for eigensolution and analysis of such structures using direct methods. Iterative methods for similar purposes are presented in Chap. 10. Group theory is known as the language of symmetry. Basic concepts and applications of group theory are discussed in Chap. 11. Finally, the interrelation of canonical forms, graph products and group theory and their applications to the analysis of symmetric-regular structures are presented in Chap. 12.

I would like to take this opportunity to acknowledge a deep sense of gratitude to a number of colleagues and friends who in different ways have helped in the preparation of this book. Mr. J.C. de C. Henderson, formerly of Imperial College of Science and Technology, first introduced me to the subject with most stimulating discussions on various aspects of topology and combinatorial mathematics. Professor F. Ziegler encouraged and supported me to write this book. My special thanks are due to Mrs. Silvia Schilgerius, the senior editor of the applied sciences of Springer, for her constructive comments, editing and unfailing kindness in the course of the preparation of this book. My sincere appreciation is extended to our Springer colleagues Mr. C. Bachem and Ms. G. Umamaheswari.

I would like to thank my former Ph.D. and M.Sc. students, Dr. H. Rahami, Dr. H. Fazli, Dr. M. Nikbakht, Dr. K. Koohestani, Dr. M.A. Sayarinejad, Dr. B. Salimbahrami, Dr. L. Shahryari, Dr. M. Nouri, Dr. H.A. Rahimi Bonderabady, Mr. H. Mehanpour, Mr. F. Nemati and Mr. S. Najafian and Mr. S. Beheshti, for permitting me to use our joint papers and for their help in various stages of writing this book. I would like to thank the publishers who permitted some of our papers to be utilised in the preparation of this book, consisting of Springer Verlag, John Wiley and Sons, and Elsevier.

My warmest gratitude is due to my wife, Mrs. Leopoldine Kaveh, for her continued support in the course of preparing this book and my son, Mr. Babak Kaveh, for proof reading.

Every effort has been made to render the book error free. However, the author would appreciate any remaining errors being brought to his attention through the following email address: alikaveh@iust.ac.ir.

Tehran, Iran A. Kaveh
January 2013

Contents

Chapter 1
Introduction to Symmetry and Regularity

1.1 Symmetric Structures

1.1.1 Definition of Symmetry

Symmetry is not only one of the most fundamental concepts in science and engineering, but it is also an ideal bridging idea crossing various branches of sciences and different fields of engineering. In the past, symmetry has been considered important for its aesthetic appeal; however, this century has witnessed a great enhancement in its recognition as a basis of scientific and engineering principle. At the same time, the meaning and utility of symmetry have greatly expanded. It is not surprising that many valuable books are published in this field and regular annual conferences are devoted to symmetry in various fields of science and engineering. In the following, different definitions are provided for symmetry.

Symmetry is the classical Greek word **Σ**Y**M-M**ETP**IA**, *the same measure*, due proportion. Proportion means equal division, and 'due' implies that there is some higher moral criterion. In Greek culture due proportion in everything was the ideal. The word and usage have been taken over as a technical term into most European languages.

Some other definitions and comments on symmetry are as follows:

To say that an object or a situation is symmetrical in space–time coordinate x, y, z, t means that part of the object (etc.) has the same measure as another part. Measure implies identity to within the limits of the measuring device employed.

'Symmetry' is one more fundamental scientific concept, which alongside with the 'harmony' concept has a relation practically to all frames of the nature, science and art.

The outstanding mathematician Hermann Weil highly evaluated the role of symmetry in modern science:

> Symmetry, as though is wide or narrow we did not perceive this word, there is the idea, with the help of which a man attempted to explain and to create the order, beauty and perfection.

A. Kaveh, *Optimal Analysis of Structures by Concepts of Symmetry and Regularity*,
DOI 10.1007/978-3-7091-1565-7_1,

In a simple language, when we look in the mirror, we can see in it our reflection; this is the example of the 'mirror' symmetry. The mirror reflection is the example of the so-called 'orthogonal' transformation varying orientation.

In the most general case, 'symmetry' in mathematics is perceived as such transformation of space (plane), at which each point of M passes in other point of M' regarding to some plane (or straight line) a, when the line segment of MM' is perpendicular to the plane (or to the straight line) a and is divided by it in halves. The plane (or the straight line) a is called as the *plane (or axis) of symmetry*. The *plane of symmetry, symmetry axis and centre of symmetry* are fundamental concepts of symmetry. The *plane of symmetry* is called such plane, which divides the figure into two mirror-equal parts arranged from each other as some subject and its mirror reflection. It is easy to establish that the cube has nine planes of symmetry. The *symmetry axis L* is called such straight line, around of which the symmetrical figure can be turned around some times in such manner that each time the figure is 'combined' with itself in space. A number of such turns around of the symmetry axis are called the *order* of the axis. For example, the equilateral triangle has the symmetry axis L_3, that is, there are three ways of turn of the triangle around the axis, at which there is its 'self-alignment'. It is clear that the square has the symmetry axis L_4 and the pentagon has L_5. The cone has also the symmetry axis, and as the number of turns of the cone around of the symmetry axis resulting in 'self-alignment' is infinitely, thus the cone has the symmetry axis of the type L_∞. Finally, the *symmetry centre C* is called such singular point inside the figure that any straight line drawn through the point C and on the equal distances from the centre C meets identical points of the figure. 'Ideal' example of such figure is a sphere, which the centre is its centre of symmetry.

The concept of 'symmetry' with reference to the physical laws is used widely in modern physics. If the laws, establishing relations between values or determining a change of these values in the course of time, do not vary at definite operations (transformations), to which the system can be subjected, we say that these laws have symmetry (or are invariant) concerning to the given transformations. For example, the law of gravitation acts in any points of space, that is, it is invariant regarding to carry of a system as the whole in space.

In the opinion of academician Vernadski, the outstanding Russian scientist, 'the symmetry encompasses properties of all fields of physics and chemistry'.

Still and Pythagoreans paid attention to the phenomenon of symmetry in the live nature in connection with development of their harmony doctrine. It is established that in nature two kinds of symmetry, the 'mirror' and 'radial' symmetry, are most widespread. The butterfly, the leaf and the beetle have the 'mirror' symmetry, and often such kind of symmetry is called as the 'leaf symmetry' or the 'bilateral symmetry'. The mushroom, the chamomile and the pine tree have the 'radial' symmetry and often such kind of symmetry is called as the 'chamomile–mushroom' symmetry.

Still in the nineteenth century, the researches in this area resulted in the conclusion that the symmetry of the natural forms largely depends on the influence of the Earth gravitation forces, which have the symmetry of the cone in each point.

In outcome, the following law was found, to which the forms of natural bodies are subjected:

> Everything that grows or moves in vertical direction, that is up or down regarding to the Earth surface is subjected by the "radial" ("chamomile- mushroom") symmetry. Everything that grows and moves horizontally or sloping regarding to the Earth surface is subjected by the "bilateral" symmetry, the "leaf symmetry".

In modern science, the interest in symmetry and its diverse applications to nature, science, art and engineering increased extremely, and the establishment in 1989 of the *International Society for Interdisciplinary Study of Symmetry (ISIS-Symmetry)* became the beginning of considerable intellectual motion.

Symmetry has been categorised to help us study it. As we look for patterns, we will also learn the language of symmetry. Here were a few definitions to start with that were mainly quoted from an excellent book of *Symmetry 2: Unifying Human Understanding*, edited by István Hargittai, 1994. Do not worry too much about them now; they are here for reference and will make more sense later. A *transformation* is an operation which maps, or moves, a figure to a new position. We will be looking at several transformations. An *isometry* is a transformation which preserves lengths. That is, a figure is moved, turned and/or flipped, but it still has the same size and shape. All transformations we will be working with are isometries.

An image has rotational symmetry if there is a centre point where an object is turned a certain number of degrees and still looks the same. An image has translational symmetry if it can be divided by straight lines into a sequence of identical figures. Translational symmetry results from moving a figure a certain distance in a certain direction also called translating (moving) by a vector (length and direction).

1.1.2 History of the Developments of Symmetry in Structural Engineering

In this section, the history of the developments of symmetry in structural engineering is presented that is mainly adopted from the excellent review paper of Kangwai et al. [1].

A symmetric structure is a structure that is left unaltered, geometrically and mechanically, after a symmetry operation is performed. These operations can be reflection, rotation, improper rotation (a reflection in a plane followed by a rotation about an axis perpendicular to that plane), translation or dilations. Only infinite structures can be left unaltered by a translation or dilation, so the last two symmetry operation will be dealt separately. Some repetitive structures are left unaltered by a translation or dilation, apart from regions near the boundaries, and can be analysed by symmetry techniques.

The development of methods to exploit the symmetry properties of a structure does not have a clearly defined origin nor a continuous historical path. In common with other areas of structural analysis, there has been an increase in work done in

this area with the advent of the electronic computer and especially since the development of finite element structural package.

The main advances in the analysis of symmetric structures have come through two differing approaches. The first approach usually exploits only rotational symmetry of the structure with a method based on the discrete Fourier transformation, which can be extended to translation and dilation symmetry. The second more recent development is a method which can exploit any symmetry, based on the application of representation theory to structural analysis.

The Fourier approach was first developed by Fortescue [2], for the analysis of polyphase electrical circuits. He used a tensor analysis approach to find a new symmetry-adapted coordinate system, which reduces the governing system of equations into a number of independent subsystems of equations. Another electrical engineer [3] presented Fortescue's method of symmetric components in matrix form and set up a transformation matrix (the Fourier matrix) which reduces the governing matrix to a block-diagonalised form. A detailed description of symmetric components in matrix form is given in [4].

The first application of discrete Fourier transformation methods to structural analysis was made by Renton [5], who was concerned with the stability analysis of symmetric frameworks. Further development has been carried out by several authors. Hussey [6] has applied the discrete Fourier transformation method in order to decouple the stiffness equations and investigate the buckling under cyclically symmetric loading. Thomas [7] and Williams [8–10] have provided exact methods for solving eigenvalue problems of rotationally periodic structures purely from the stiffness equations of the repeating symmetry substructure. Thomas [7] has analysed the dynamics of rotationally periodic structures to show that any forced vibrations can be decomposed into independent rotating components. References [5, 11] have shown how the Fourier approach can be extended to repetitive structures.

Although the Fourier approach has been shown to be useful for rotational symmetry and some other simple symmetry types, it is not easily extended to structures with more complicated symmetry properties. To do this, the alternative approach, based on group theory, was required.

Group theory provides a systematic way to describe the full symmetry of any structure, and the extension to group representation theory allows for the maximum utilisation of a structure's symmetry properties. The theoretical basis of the abstract group representation theory has been extensively developed [12–14]. It is widely used in physics and chemistry [15–17] to simplify calculation concerning the vibration of molecules or crystals. Reference [18] provides a detailed review of the history and application of the group representation theory approach and also shows that the Fourier method is simply a special case of group representation theory, a point which is expanded in [1].

The first application of group representation theory to structural analysis was by Zolkovic [19, 20], who formulated the so-called G-vector analysis based on group representation theory and applied it to problems in static, vibration and stability. The development and application of this method to finite element analysis is

described in [21] and [22]. However, because G-vector analysis is based on the characters of irreducible representations, rather than the representations themselves, it is not able to directly split subspaces corresponding to more-than-one-dimensional irreducible representations. For two-dimensional representations, this is usually easily rectified.

Bossavit [23–25] has considered using group representation theory to find reduced linear systems of equations for boundary value problems. Bossavit has also shown that the Fourier method is a special case of group representation theory. References [26–28] show how the group theoretical techniques aid the understanding of bifurcation problems with symmetry. References [29–33] apply group representation theory to bifurcation problems in non-linear mechanics and consider symmetry-breaking solutions. References [34–50] show applications of group representation theory to eigenvalue problems associated with static and vibrations of mechanical systems, in order to find reduced solutions.

The writer and colleagues have performed extensive amount of research on symmetry using linear algebra, graph theory and group theory [51–54]. In early stage, the symmetry of graphs was of interest to calculate the eigenvalues of the adjacency and Laplacian matrices of such graphs. For this purpose, a decomposition followed by healing approach was used for canonical forms and the corresponding graphs. Later this method was extended to eigensolution of symmetric truss and frame structures [55–59]. The developed methods were applied to efficient calculation of buckling load and finding the eigenfrequencies and eigenmodes of these structures. More complex symmetries and regular structures were studied [60–77]. The latter can be viewed as a generalised symmetry. Methods were developed for eigensolution of the regular graph models. These methods were utilised for nodal ordering and graph partitioning. The ideas were then extended to skeletal structures for efficient stability analysis for vibration of such structures. The tools used for the above-mentioned methods were based on linear algebra and graph theory. Group theory was also used extensively in our research. Pure group theory and combination group theory and linear algebra (in the form of canonical forms) are applied to many problems in structural analysis [78–83]. Mixed group and graph theory is found very attractive in simplifying the pure group theoretical methods [84]. The forthcoming chapters of this book contain some of the most useful theories and results of the above-mentioned researches.

1.2 Regular Structures

1.2.1 Repetitive and Cyclic Structures

A structure is said to be repetitive if it consists of a number of identical units which are connected together in a regular form. Repetitive structures may be categorised as consisting of a finite or infinite number of repetitive units. Repetitive trusses are

periodically stiffened shells; are widely used in construction, aeronautic engineering and shipbuilding; and have repetitive geometric form.

The symmetry properties of the repetitive structures are systematically treated in the symmetry group theory. The symmetric structure, accordingly, is defined as one invariant to a symmetry operation. The basic spatial symmetry operations are reflections, rotations, translations and dilatations.

In these methods the analysis of the entire structure is reduced to the analysis of the repeating module under transformed loading and boundary conditions. Consequently, both the design parameters and the analysis variables constitute a relatively small set which facilitates the analysis process. Such method is especially rewarding when the analysis should be performed many times such as in optimisation and non-linear analysis.

The main difficulty in developing repetitive structures lies in devising a way of interconnecting the basic components comprising the structure.

1.2.2 Definition of Regularity

A structural model is called *regular* if it can be considered as the graph product of two or three subgraphs. The most well-known graph products are Cartesian, strong Cartesian, direct and lexicographic products. However, in order to be able to define the model of practical space structures and different finite element models, other graph products are defined which will be discussed in this book.

Graph products have been known to mathematician for a long time. However, the application to structural mechanics has been made by Kaveh and Rahami [60–64], and in the last decade extensively developed and applied to many problems in combinatorial optimisation and eigensolution in structural mechanics.

Many structural models can be generated as the graph products of two or three subgraphs known as their *generators*. The main types of graph products consist of Cartesian, strong Cartesian, direct and lexicographic products. This simplifies many complicated calculations, particularly in relation with eigensolution of regular structures. In this book, a general method is presented for the factorisation of these graph products, such that the eigenvalues of the entire graph is obtained as the union of the eigenvalues of the weighted subgraphs defined here. The adjacency and Laplacian for each graph product is separately studied. For graphs with missing elements (cut-outs) or additional elements, the eigenvalues are calculated with the additional use of the Rayleigh quotient approach. The main idea steams from the rules recently developed by the authors for block diagonalisation of matrices. These products have many applications in computational mechanics, such as ordering, graph partitioning, dynamic analysis and stability analysis of structures. Finally group theory as the language of symmetry is utilised in eigensolution and analysis of structures. Then some concepts of graph theory and group theory together with ideas from linear algebra are combined to provide powerful means for the analysis of structures. Though the main structure discussed here will be skeletal structures,

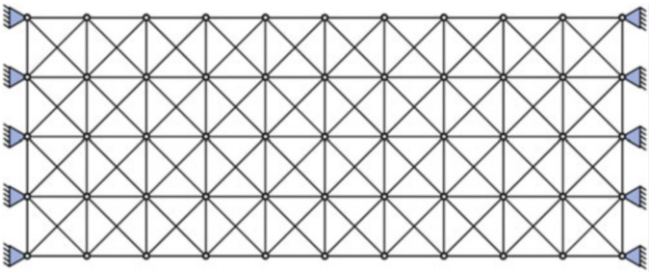

Fig. 1.1 A 2D truss model with two axis of symmetry

Fig. 1.2 A 3D bridge with a plane of symmetry

however, the ideas can easily be extended to finite element analysis of continuum structures.

There is a close relationship between symmetry and regularity which will also be exploited in subsequent chapters.

1.3 Examples of Symmetric and Regular Structural Models

In this section, some examples of symmetry and regularity are provided utilising their configurations.

Example 1.1. A 2D model with two axes of symmetry is shown in Fig. 1.1.

Example 1.2. A 3D bridge model with a plane of symmetry is shown in Fig. 1.2.

Example 1.3. A 2D and 3D circular (circulant) models with many axes of symmetry are shown in Fig. 1.3a, b, respectively.

Example 1.4. A 3D dome with 660 nodes, shown in Fig. 1.4a, is considered. This model is called a regular model, with generators being shown in Fig. 1.4b.

Example 1.5. A 3D model with 750 nodes, shown in Fig. 1.5a, is considered. The corresponding generators are illustrated in Fig. 1.5b.

Example 1.6. A regular 3D double-layer cylinder with 768 nodes, shown in Fig. 1.6a, is considered. The corresponding generators are illustrated in Fig. 1.6b.

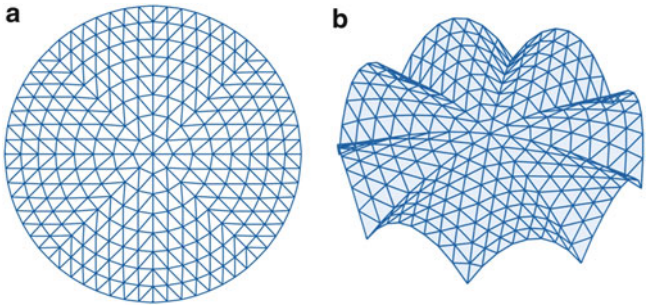

Fig. 1.3 (**a**) A 2D model with many axes of symmetry. (**b**) A 3D model with many axes of symmetry (circular or circulant models)

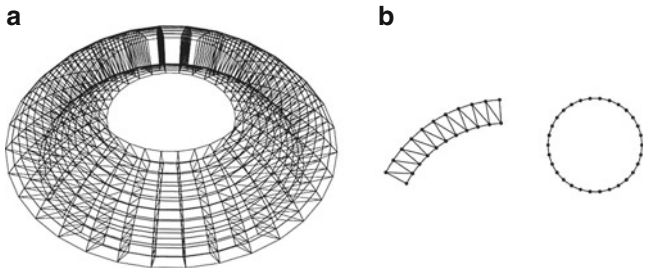

Fig. 1.4 A 3D regular dome and its generators. (**a**) A dome-shaped model. (**b**) Generators of the dome

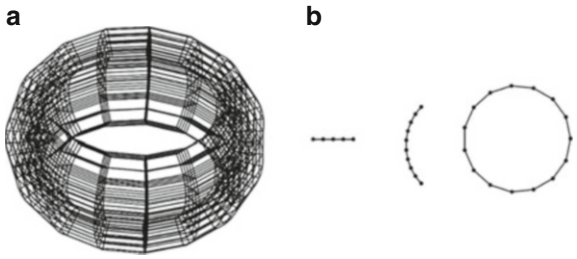

Fig. 1.5 A regular 3D torus-shaped model and the corresponding generators. (**a**) A torus-shaped model. (**b**) Generators of the torus

Example 1.7. A hypercube with 750 nodes is considered, as shown in Fig. 1.7a. The corresponding generators are illustrated in Fig. 1.7b.

Example 1.8. A double-layer grid with 352 nodes is considered, as shown in Fig. 1.8a. The corresponding generators are illustrated in Fig. 1.8b.

Example 1.9. Some additional regular structures are shown in Fig. 1.9.

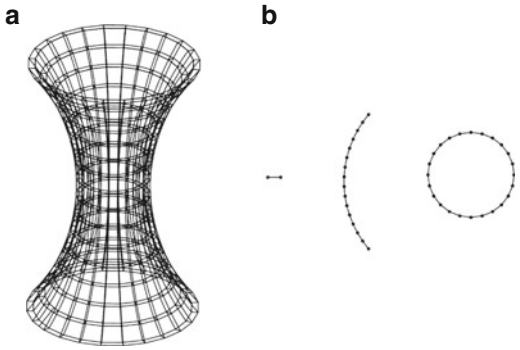

Fig. 1.6 A regular 3D double-layer cylinder and its generators. (**a**) A double-layer cylinder. (**b**) Generators of the model

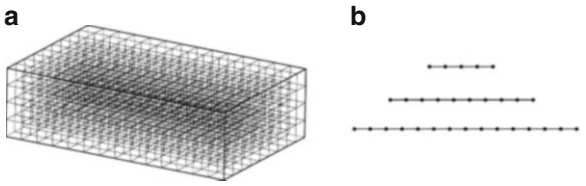

Fig. 1.7 A regular 3D hypercube and its generators. (**a**) A double-layer cylinder. (**b**) Generators of the model

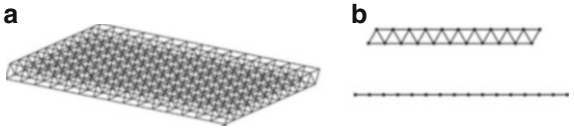

Fig. 1.8 A regular model in the form of a double-layer grid and its generators. (**a**) A double-layer grid. (**b**) Generators of the grid

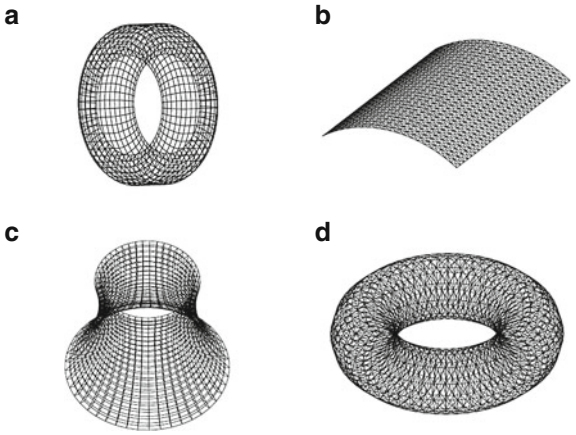

Fig. 1.9 Different regular structures. (**a**) The model of a cylindrical model. (**b**) Model of a barrel vault. (**c**) Model of a double-layer tower. (**d**) Model of a torus-shaped structure

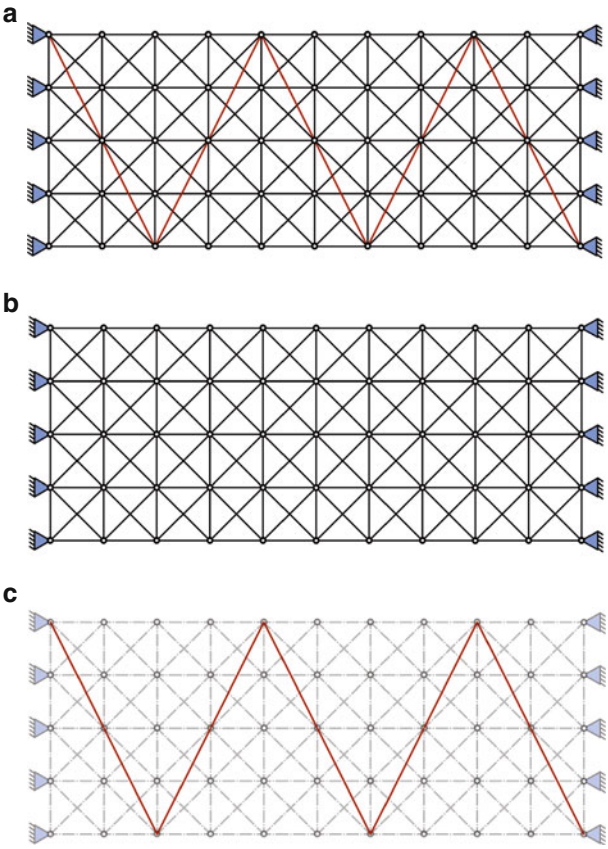

Fig. 1.10 A non-regular model decomposed into two parts. (**a**) A non-regular truss. (**b**) The regular part of the structure. (**c**) The excessive members being highlighted

Example 1.10. A non-regular graph is considered as shown in Fig. 1.10a. This structure can be considered as a regular model as shown in Fig. 1.10b and an additional model as illustrated in Fig. 1.10c.

1.4 Optimal Analysis of Structures

An analysis is called *optimal* if the matrices involved in the analysis are sparse, well structured and well conditioned. Methods for the formation of such matrices are developed in a book by the author, entitled *Optimal Structural Analysis*, Kaveh [84]. Sparsity can be provided by selection of localised self-compatible and self-equilibrating systems for the stiffness and flexibility matrices of structures,

respectively. The matrices can be made well structured by ordering the considered variables of the structures (nodes and cycles of the structural models). Conditioning can be improved by selecting suitable kinematic and static bases for stiffness and flexibility methods, respectively. In the above methods, the entire models have been used for the solution of the structure.

In this book, methods are developed for configuration processing, eigensolution and analysis of structures utilising some concepts of symmetry and regularity. The use of these concepts permits the analysis of these structures to be performed considering only small parts of the structures, and in some cases, matrices of much smaller dimensions are utilised to perform the eigensolution of matrices of very large dimensions. However, this does not mean that only symmetric and regular structures can be dealt with by the methods of the present book. Those structures which can be obtained by addition or removal of members and/or nodes can also be efficiently analysed.

Graph products often correspond to special block matrices, the so-called canonical forms. On the other hand canonical forms are often encountered in structural mechanics because of the repeated nature of some structural models. This is why the titles of chapters of the present book are selected in terms of *canonical forms* and *graph products*.

References

1. Kangwai RD, Guest SD, Pellegrino S (1999) An introduction to the analysis of symmetric structures. Comput Struct 71:671–688
2. Fortescue CL (1918) Method of symmetrical co-ordinates applied o the solution of polyphase networks. Trans AIEE 38:1027–1140
3. Kron G (1963) Diakoptics; the piecewise solution of large-scale systems. MacDonald, London
4. Pipes LA (1996) Circulant matrices and the theory of symmetrical components. Matrix Tensor Quart 17:35–50
5. Renton JD (1964) On the stability analysis of symmetrical frameworks. Quart J Mech Appl Math 17:175–197
6. Hussey MJL (1967) General theory of cyclically symmetric frames. J Struct Div ASCE 93 (ST2):163–176
7. Thomas DL (1979) Dynamics of rotationally periodic structures. Int J Numer Methods Eng 14:81–102
8. Williams FW (1978) A warning on the use of symmetry in classical eigenvalue analyses. Int J Numer Methods Eng 12:379–383
9. Williams FW (1986) An algorithm for exact eigenvalue calculations for rotationally periodic structures. Int J Numer Methods Eng 23:609–622
10. Williams FW (1986) Exact eigenvalue calculations for rotationally periodic sub-structures. Int J Numer Methods Eng 23:695–706
11. Samartin A (1988) Analysis of spatially periodic structures-application to shell and spatial structures. In: Proceedings of the international symposium on innovative applications of shells and spatial forms. Oxford/IBH Publishing, Bangalore/New Delhi, pp 205–221
12. Weyl H (1946) The classical groups, their invariants and representations. Princeton University Press, Princeton
13. Leech JW, Newman DJ (1969) How to use groups. Methuen, London

14. Serre J-P (1977) Linear representations of finite groups. Springer, Berlin
15. Hammermesh M (1962) Group theory and its applications to physical problems. Addison-Wesely, Reading
16. Schonland DS (1965) Molecular symmetry, an introduction to group theory and its uses in chemistry. Van Nostrand, New York
17. Chung F, Sterberg S (1993) Mathematics and the buckyball. Am Scientist 81:56–71
18. Mackay GW (1980) Harmonic analysis as the exploitation of symmetry-a historical survey. Bull Am Math Soc 3:543–696
19. Zoloković GM (1973) Group theory and G-vector spaces in structural analysis: vibration, stability and statics of structures. ICS, Beograd
20. Zoloković GM (1989) Group theory and G-vector spaces in structural analysis: vibration, stability and statics of structures. Ellis Horwood, Chichester
21. Zoloković GM (1992) Group supermatrices in finite element analysis. Ellis Horwood, Chichester
22. Zoloković GM (1994) Group supermatrix procedure in computing of engineering structures. Struct Eng Rev 6:39–50
23. Bossavit A (1986) Symmetry, groups and boundary value problems, a progressive introduction to noncommutative harmonic analysis of partial differential equations in domains with geometrical symmetry. Comput Methods Appl Mech Eng 56:167–215
24. Bossavit A (1988) On the exploitation of geometrical symmetry in structural computations of space power stations. Space Power 7:199–210
25. Bossavit A (1992) On the computation of strains and stresses to symmetrical articulated structures. In: George K, Allower EL, Miranda R (eds) Proceedings of AMS seminar Aug 1992, Fort Collins Basel. Birkhauser
26. Sattinger DH (1979) Group theoretic methods in bifurcation theory. Springer, Berlin/Heidelberg/New York
27. Sattinger DH (1980) Bifurcation and symmetry breaking in applied mathematics. Bull Am Math Soc 3:779–819
28. Golubitsky M, Stewart I, Schaeffer DG (1988) Singularities and groups in bifurcation theory. In: Applied mathematical sciences, vol 69, Part II. Springer, Berlin
29. Healey TJ (1988) A group theoretic approach to computational bifurcation problems. Comput Methods Appl Mech Eng 67:257–295
30. Healey TJ (1989) Symmetry and equivalence in nonlinear elasto-statics. Part I Arch Rotational Mech Anal 105:205–228
31. Wohlever TJ (1993) A group theoretic approach to the nonlinear bifurcation analysis of shells of revolution. Ph.D. thesis, Cornel University, Ithaca
32. Ikeda K, Murota K (1991) Bifurcation analysis of symmetric structures using block-diagonalisation. Comput Methods Appl Mech Eng 86:215–243
33. Ikeda K, Murota K (1991) Bifurcation hierarchy of symmetric structures. Int J Solids Struct 27:1551–1573
34. Chang P, Healey TJ (1988) Computation of symmetry modes and exact reduction in nonlinear structural analysis. Comput Struct 28:135–142
35. Dinkevich S (1984) The spectral method of calculation of symmetric structures of finite size. Trans Can Soc Mech Eng 8:167–215
36. Dinkevich S (1986) The fast method of block elimination for the solution of large regular mechanical structures. Trans Can Soc Mech Eng 10:91–98
37. Dinkevich S (1991) Finite symmetric systems and their analysis. Int J Solids Struct 27:1215–1253
38. Healey TJ, Treacy JA (1991) Exact block diagonalization of large eigenvalue problems for structures with symmetry. Int J Numer Methods Eng 31:265–285
39. Ikeda K, Ario I, Tori K (1992) Block-diagonalization analysis of symmetric plates. Int J Solids Struct 29:2779–2793

40. Zhong W, Qui C (1983) Analysis of symmetric or partially symmetric structures. Comput Methods Appl Mech Eng 38:1–8
41. Zingoni A, Pavlović MN, Zoloković GM (1995) A symmetry adapted flexibility approach for multi-story space frames. Part 1: general outline and symmetry-adapted redundants. Struct Eng Rev 7:107–119
42. Zingoni A, Pavlović MN, Zoloković GM (1995) A symmetry adapted flexibility approach for multi-story space frames. Part 2: symmetry-adapted loads. Struct Eng Rev 7:121–130
43. Glockner PG (1973) Symmetry in structural mechanics. J Struct Div ASCE 99:71–89
44. Zingoni A (1996) An efficient computational scheme for the vibration analysis of high-tension cable nets. J Sound Vib 189:55–79
45. Zingoni A (1996) Truss and beam finite elements revisited: a derivation based on displacement-field decomposition. Int J Space Struct 11:371–380
46. Zingoni A (2002) Group-theoretical applications in solid and structural mechanics: a review, chapter 12. In: Topping BHV, Bittnar Z (eds) Computational structures technology. Saxe-Coburg, Edinburgh
47. Zingoni A (2005) On the symmetries and vibration modes of layered space grids. Eng Struct 27:629–638
48. Zingoni A (2009) Group-theoretic exploitations of symmetry in computational solids and structural mechanics. Int J Numer Methods Eng 79:253–289
49. Zingoni A (2008) On group-theoretic computation of natural frequencies for spring-mass dynamic systems with rectilinear motion. Commun Numer Methods Eng 24:973–987
50. Zingoni A (2012) Symmetry recognition in group-theoretic computational schemes for complete systems. Comput Struct 94–95:34–44
51. Kaveh A, Sayarinejad MA (2003) Eigensolutions for matrices of special structures. Commun Numer Methods Eng 19:125–136
52. Kaveh A, Sayarinejad MA (2004) Graph symmetry in dynamic systems. Comput Struct 82 (23–26):2229–2240
53. Kaveh A, Sayarinejad MA (2005) Eigenvalues of factorable matrices with Form IV symmetry. Commun Numer Methods Eng 21(6):269–278
54. Kaveh A, Sayarinejad MA (2006) Eigensolution of specially structured matrices with hyper-symmetry. Int J Numer Methods Eng 67(7):1012–1043
55. Kaveh A, Salimbahrami B (2004) Eigensolutions of symmetric frames using graph factorization. Commun Numer Methods Eng 20:889–910
56. Kaveh A, Salimbahrami B (2007) Buckling load of symmetric frames using canonical forms. Comput Struct 85(11):1420–1430
57. Kaveh A, Salimbahrami B (2008) Analysis of symmetric structures using canonical forms. Commun Numer Methods Eng 24(3):195–218
58. Kaveh A, Shahryari L (2007) Buckling load of planar frames with semi-rigid joints using weighted symmetric graphs. Comput Struct 85:1704–1728
59. Kaveh A, Shahryari L (2010) Eigenfrequencies of symmetric planar trusses via weighted graph symmetry and new canonical forms. Eng Comput 27(3):409–439
60. Kaveh A, Rahami H (2006) Block diagonalization of adjacency and Laplacian matrices for graph products; applications in structural mechanics. Int J Numer Methods Eng 68(1):33–63
61. Kaveh A, Rahami H (2006) Special decompositions for eigenproblems in structural mechanics. Commun Numer Methods Eng 22(9):943–953
62. Kaveh A, Rahami H (2007) Compound matrix block diagonalization for efficient solution of eigenproblems in structural matrices. Acta Mech 188(3–4):155–166
63. Kaveh A, Rahami H (2007) Tri-diagonal and penta-diagonal block matrices for efficient eigensolutions of problems in structural mechanics. Acta Mech 192(1–4):77–87
64. Kaveh A, Rahami H (2008) Factorization for efficient solution of eigenproblems of adjacency and Laplacian matrices for graph products. Int J Numer Methods Eng 75(1):58–82
65. Kaveh A, Fazli H (2008) Analysis of frames by substructuring technique based on using algebraic and graph methods. Commun Numer Methods Eng 24(10):867–874

66. Kaveh A, Koohestani K (2008) Graph products for configuration processing of space structures. Comput Struct 86:1219–1236
67. Kaveh A, Nouri M (2009) Weighted graph products for configuration processing of planar and space structures. Int J Space Struct 24(1):13–26
68. Kaveh A, Rahami H (2010) An efficient analysis of repetitive structures generated by graph products. Int J Numer Methods Eng 84(1):108–126
69. Kaveh A, Nemati F (2010) Eigensolution of rotationally repetitive space structures using a canonical form. Int J Numer Methods Eng 26(12):1781–1796
70. Kaveh A, Rahami H (2010) Eigenvalues of the adjacency and Laplacian matrices for modified regular structural models. Int J Numer Methods Eng 26(12):1836–1855
71. Kaveh A, Rahami H (2011) Block circulant matrices and their applications to free vibration analysis of cyclically repetitive structures. Acta Mech 217(1–2):51–62
72. Kaveh A, Fazli H (2011) Approximate eigensolution of locally modified regular structures using a substructuring technique. Comput Struct 89:529–537
73. Kaveh A, Fazli H (2011) Approximate eigensolution of Laplacian matrices for locally modified graph products using implicitly restarted Lanczos method. J Comput Appl Math 236:1591–1603
74. Kaveh A, Beheshti S (2012) Weighted triangular and circular graph products for configuration processing. Period Polytech-Civil Eng 56(1):1–9
75. Kaveh A, Fazli H (2012) Canonical forms for symmetric and regular structures. J Math Model Algorithms 11(2):119–157
76. Rahami H, Kaveh A, Mehanpour H (2012) Optimal analysis of non-regular graphs using the results of regular models via an iterative method. Int J Optim Civil Eng 2(2):153–171
77. Kaveh A, Rahami H, Mehanpour H (2012) Static and modal analyses of structures with different repeated patterns. Adv Eng Softw 51:1–9
78. Kaveh A, Nikbakht M (2006) Buckling load of symmetric plane frames using canonical forms and group theory. Acta Mech 185(1–2):89–128
79. Kaveh A, Nikbakht M (2007) Block diagonalization of Laplacian matrices of symmetric graphs via group theory. Int J Numer Methods Eng 69(5):908–947
80. Kaveh A, Nikbakht M (2008) Stability analysis of hyper symmetric skeletal structures using group theory. Acta Mech 200(3–4):177–197
81. Kaveh A, Jahanmohammadi A (2008) Group-theoretic method for forced vibration analysis of symmetric structures. Acta Mech 199(1–4):1–16
82. Kaveh A, Nikbakht M (2010) Improved group-theoretical method for eigenvalue problems of special symmetric structures, using graph theory. Adv Eng Softw 41:22–31
83. Kaveh A, Nikbakht M, Rahami H (2010) Improved group theoretic method using graphs products, for the analysis of symmetric-regular structures. Acta Mech 210(3–4):265–289
84. Kaveh A (1997) Optimal structural analysis, 2nd edn. Wiley, Chichester

Chapter 2
Introduction to Graph Theory and Algebraic Graph Theory

2.1 Introduction

Graph theory is a branch of mathematics started by Euler [1] as early as 1736. It took a hundred years before the second important contribution of Kirchhoff [2] had been made for the analysis of electrical networks. Cayley [3] and Sylvester [4] discovered several properties of special types of graphs known as *trees*. Poincaré [5] defined in principle what is known nowadays as the *incidence matrix* of a graph. It took another century before the first book was published by König [6]. After the Second World War, further books appeared on graph theory (Ore [7], Behzad and Chartrand [8], Tutte [9], Berge [10], Harary [11], Gould [12], Wilson [13], Wilson and Watkins [14] and West [15], among many others).

Algebraic graph theory can be viewed as an extension to graph theory in which algebraic methods are applied to problems about graphs (Biggs [16]). *Spectral graph theory*, as the main branch of algebraic graph theory, is the study of properties of graphs in relationship to the characteristic polynomial, eigenvalues and eigenvectors of matrices associated with graphs, such as its *adjacency matrix* or *Laplacian matrix*. Spectral graph theory emerged in the 1950s and 1960s. The 1980 monograph *Spectra of Graphs* [17] by Cvetković, Doob and Sachs has summarised nearly all research to date in the area. In 1988 it was updated by the survey *Recent Results in the Theory of Graph Spectra* [18].

Graph theory has found many applications in engineering and science, such as chemical, electrical, civil and mechanical engineering, architecture, management and control, communication, operational research, sparse matrix technology, combinatorial optimisation and computer science. Therefore, many books have been published on applied graph theory such as those by Bondy and Murty [19], Chen [20], Thulasiraman and Swamy [21], Beineke and Wilson [22], Mayeda [23], Christofides [24], Gondran and Minoux [25], Deo [26], Cooke et al. [27] and Kaveh [28, 29]. In recent years, due to the extension of the concepts and applications of the graph theory, many journals such as *Journal of Graph Theory, Journal of Combinatorial Theory A & B, Discrete and Applied Mathematics, SIAM*

A. Kaveh, *Optimal Analysis of Structures by Concepts of Symmetry and Regularity*,
DOI 10.1007/978-3-7091-1565-7_2, © Springer-Verlag Wien 2013

Journal of Discrete Mathematics, European Journal of Combinatorics and *Graphs and Combinatorics* are being published to cover the advances made in this field.

In this chapter basic definitions and concepts of graph theory and algebraic graph theory are briefly presented; however, for proofs and details the reader may refer to textbooks on this subject, Refs. [11, 15, 28, 29].

2.2 Basic Concepts and Definitions of Graph Theory

There are many physical systems whose performance depends not only on the characteristics of their components but also on their relative location. As an example, in a structure, if the properties of a member are altered, the overall behaviour of the structure will be changed. This indicates that the performance of a structure depends on the characteristics of its members. On the other hand, if the location of a member is changed, the properties of the structure will again be different. Therefore, the connectivity (topology) of the structure influences the performance of the entire structure. Hence, it is important to represent a system so that its topology can clearly be understood. The graph model of a system provides a powerful means for this purpose.

In this section, basic concepts and definitions of graph theory are presented. Since some of the readers may be unfamiliar with the theory of graphs, simple examples are included to make it easier to understand the main concepts.

Some of the uses of the theory of graphs in the context of civil engineering are as follows. A graph can be a model of a structure, a hydraulic network, a traffic network, a transportation system, a construction system or a resource allocation system. These are only some of such models, and the applications of graph theory are much extensive. In this book, the theory of graphs is used as the model of a skeletal structure, and it is employed also as a means for transforming the connectivity properties of finite element meshes to those of graphs. This section will also enable the readers to develop their own ideas and methods in the light of the principles of graph theory. For further definitions and proofs, the reader may refer to Harary [11] and West [15].

2.2.1 Definition of a Graph

A *graph* S consists of a non-empty set N(S) of elements called *nodes* (vertices or points) and a set M(S) of elements called *members* (edges or arcs) together with a relation of *incidence* which associates with each member a pair of nodes (not necessarily distinct), called its *ends*.

Two or more members joining the same pair of nodes are known as *multiple members,* and a member joining a node to itself is called a *loop*. A graph with no loops and multiple members is called a *simple graph*. If N(S) and M(S) are

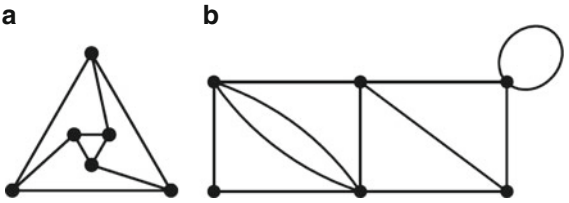

Fig. 2.1 Simple and non-simple graphs. (**a**) A simple graph. (**b**) A graph with a loop and multiple members

countable sets, then the corresponding graph S is *finite*. In this book only finite graphs are needed, which are referred to as graphs.

The above definitions correspond to abstract graphs; however, a graph may be visualised as a set of points connected by line segments in Euclidean space; the nodes of a graph are identified with points, and its members are identified as line segments without their end points. Such a configuration is known as a *topological graph*. These definitions are illustrated in Fig. 2.1.

2.2.2 Adjacency and Incidence

Two nodes of a graph are called *adjacent* if these nodes are the end nodes of a member. A member is called *incident with a node* if this node is an end node of the member. Two members are called *incident* if they have a common end node. The *degree* (valency) of a node n_i of a graph, denoted by deg (n_i), is the number of members incident with that node. Since each member has two end nodes, the sum of node degrees of a graph is twice the number of its members.

2.2.3 Graph Operations

A *subgraph* S_i of S is a graph for which $N(S_i) \subseteq N(S)$ and $M(S_i) \subseteq M(S)$, and each member of S_i has the same ends as in S.

The *union* of subgraphs $S_1, S_2, \ldots, S_k$ of S, denoted by $S^k = \bigcup_{i=1}^{k} S_i = S_1 \cup S_2 \cup \ldots \cup S_k$, is a subgraph of S with $N(S^k) = \bigcup_{i=1}^{k} N(S_i)$ and $M(S^k) = \bigcup_{i=1}^{k} M(S_i)$. The *intersection* of two subgraphs S_i and S_j is similarly defined using intersections of node sets and member sets of the two subgraphs. The *ring sum* of two subgraphs $S_i \oplus S_j$ is a subgraph which contains the nodes and members of S_i and S_j except those elements common to S_i and S_j. These definitions are illustrated in Fig. 2.2.

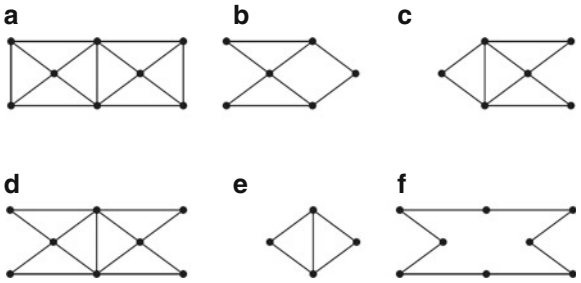

Fig. 2.2 A graph, two of its subgraphs, their union, intersection and ring sum. (**a**) S. (**b**) S_i. (**c**) S_j. (**d**) $S_i \cup S_j$. (**e**) $S_i \cap S_j$. (**f**) $S_i \oplus S_j$

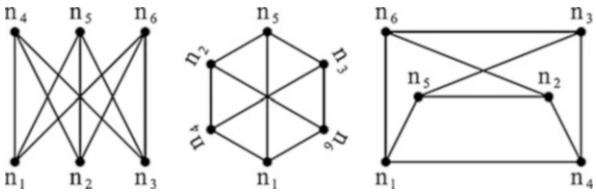

Fig. 2.3 Three isomorphic graphs

There are other important graph operations consisting of different graph products which will be described in detail in Chap. 3 of this book. These products and their applications in structural mechanics are the main concern of the present book.

Two graphs are called *isomorphic* if they have the same number of nodes and the adjacency is preserved. As an example three isomorphic graphs are shown in Fig. 2.3.

2.2.4 Walks, Trails and Paths

A *walk* P_k of S is a finite sequence $P_k = \{n_0, m_1, n_1, \ldots, m_p, n_p\}$ whose terms are alternately nodes n_i and members m_i of S for $1 \leq i \leq p$, and n_{i-1} and n_i are the two ends of m_i. A *trail* in S is a walk in which no member of S appears more than once. A *path* is a trail in which no node appears more than once. The *length* of a path P_i, denoted by $L(P_i)$, is taken as the number of its members. P_i is called the *shortest path* between the two nodes n_0 and n_p, if for any other path P_j between these nodes $L(P_i) \leq L(P_j)$. The *distance* between two nodes of a graph is defined as the number of the members of a shortest path between these nodes.

Two nodes n_i and n_j are said to be *connected* in S if there exists a path between these nodes. A graph S is called *connected* if all pairs of its nodes are connected. A *component* of a graph S is a maximal connected subgraph, that is, it is not a subgraph of any other connected subgraph of S.

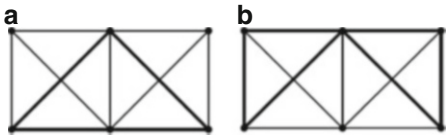

Fig. 2.4 A cycle and a hinged cycle of S. (**a**) A cycle of S. (**b**) A hinged cycle of S

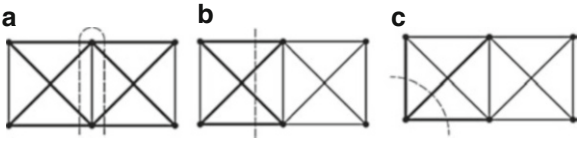

Fig. 2.5 A disconnecting set, a cutset and a co-cycle of S. (**a**) A disconnecting set. (**b**) A cutset. (**c**) A co-cycle

2.2.5 Cycles and Cutsets

A *cycle* is a path (n_0, m_1, n_1, … , m_p, n_p) for which $n_0 = n_p$ and $p \geq 1$; that is, a cycle is a closed path. Similarly a *closed trail (hinged cycle)* and a *closed walk* can be defined. A cycle of a graph and a hinged cycle are shown in Fig. 2.4a, b, respectively.

A *disconnecting set* of a connected graph S is a set of members whose removal disconnects S. As an example the removal of bold members in Fig. 2.5a will result in three disconnected subgraphs. A *cutset* is defined as a disconnecting set, no proper subset of which a disconnecting set. Obviously the removal of the members of a cutset will separate the remainder of the graph into two disjoint components S_1 and S_2, which are linked by each member of the cutset, Fig. 2.5b. Notice that no proper subsets of a cutset have this property. A *link* is a member which has its ends in S_1 and S_2. If one of S_1 or S_2 consists of a single node, the cutset is called a *co-cycle* (Fig. 2.5c).

2.2.6 Trees, Spanning Trees and Shortest Route Trees

A *tree* T of S is a connected subgraph of S which contains no cycle. A set of trees of S forms a *forest*. Obviously a forest with k trees contains N(S) − k members. If a tree contains all the nodes of S, it is called a *spanning tree* of S. Henceforth, for simplicity it will be referred to as a *tree*. The complement of T in S is called a *cotree*, denoted by T*. The members of T are known as *branches* and those of T* are called *chords*.

A *shortest route tree* (SRT) rooted at a specified node n_0 of S is a tree for which the distance between every node n_j of T and n_0 is minimum. An SRT of a graph can be generated by the following simple algorithm:

Label the selected root n_0 as ‘0’ and the adjacent nodes as ‘1’. Record the members incident to ‘0’ as tree members. Repeat the process of labelling with

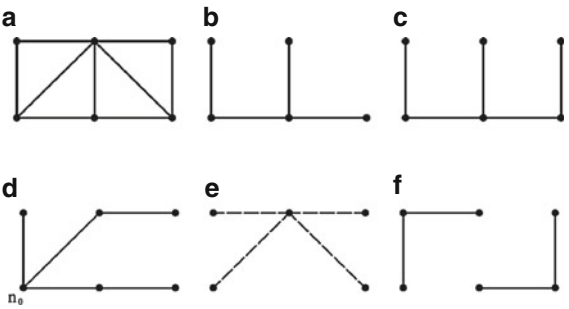

Fig. 2.6 Different subgraphs in relation with tree of S. (**a**) A graph S. (**b**) A tree T of S. (**c**) A spanning tree T′ of S. (**d**) An SRT rooted from n_0. (**e**) The cotree of T′. (**f**) A forest with two trees

'2' the unnumbered ends of all the members incident with nodes labelled as '1', again recording the tree members. This process terminates when each node of S is labelled and all the tree members are recorded. This algorithm has many applications in engineering, and it is also called a *breadth-first-search* algorithm.

The above definitions are illustrated in Fig. 2.6.

It is easy to prove that for a tree T

$$M(T) = N(T) - 1 \tag{2.1}$$

where M(T) and N(T) are the numbers of members and nodes of T, respectively.

For a connected graph S, the number of chords is given by

$$M(T^*) = M(S) - M(T). \tag{2.2}$$

Since N(T) = N(S), hence,

$$M(T^*) = M(S) - N(S) + 1, \tag{2.3}$$

where M(S) and N(S) are the numbers of members and nodes of S, respectively. Notice that for a set and its cardinality, the same notation is used and the difference should be obvious from the context.

2.2.7 Directed Graphs

A directed graph or digraph D is a set of nodes N(D), a set of members M(D), together with a relationship which associates a pair of ordered nodes with each member. The first node of an ordered pair is called the start node, and the second is known as the end node of a directed member. We say a member is directed from its start node to its end node. Naturally the underlying graph a directed graph D is a graph S with the members of D being treated as unordered pairs. A directed graph D and its underlying graphs S are shown in Fig. 2.7.

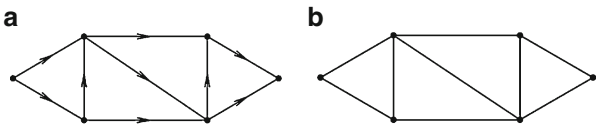

Fig. 2.7 A directed graph and its underlying graph. (**a**) A directed graph D. (**b**) The underlying graph of D

Fig. 2.8 Three different types of graphs. (**a**) A null graph N_6. (**b**) A path graph P_4. (**c**) A cycle graph C_5

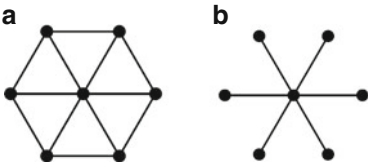

Fig. 2.9 Two different types of graphs. (**a**) A wheel graph W_7. (**b**) A star graph

Fig. 2.10 Different types of graphs. (**a**) A complete graph K_6. (**b**) A bipartite graph with $r = 3$ and $s = 4$. (**c**) A complete bipartite graph $K_{3,4}$

2.2.8 Different Types of Graphs

In order to simplify the study of properties of graphs, different types of graphs have been defined. Some important and relevant to our study are as follows:

A *null graph* is a graph which contains no members, Fig. 2.8a. Thus, N_k is a graph containing k isolated nodes.

A *path graph* is a graph consisting of a single path, Fig. 2.8b. Hence, P_k is a path with k nodes and $(k-1)$ members.

A *cycle graph* is a graph consisting of a single cycle, Fig. 2.8c. Therefore, C_k is a polygon with k members.

A *wheel graph* W_k is defined as the union of a star graph with $k-1$ members and a cycle graph C_{k-1}, connected as shown in Fig. 2.9, for $k = 6$. Alternatively a wheel graph W_k can be obtained from the cycle graph C_{k-1} by adding a node O and members (spokes) joining O to each nodes of C_{k-1}.

A *complete graph* is a graph in which every two distinct nodes are connected by exactly one member, Fig. 2.10a. A complete graph with N nodes is denoted by K_N. It can easily be proved that a complete graph with N nodes has $N(N-1)/2$ members.

A graph is called *bipartite* if the corresponding node set can be split into two sets N_1 and N_2 in such a way that each member of S joins a node of N_1 to a node of N_2. This graph is denoted by $B(S) = (N_1, M, N_2)$, Fig. 2.10b. A *complete bipartite* graph is a bipartite graph in which each node N_1 is joined to each node of N_2 by exactly one member. If the numbers of nodes in N_1 and N_2 are denoted by r and s, respectively, then a complete bipartite graph is denoted by $K_{r,s}$, Fig. 2.10c.

A graph S is called *regular* if all of its nodes have the same degree. If this degree is k, then S is k-*regular graph*. As an example, a triangle graph is 2-regular and a cubic graph is 3-regular.

2.3 Vector Spaces Associated with a Graph

A vector space can be associated with a graph by defining a vector, the field and the binary operations as follows:

Any subset of the M(S) members of a graph S can be represented by a vector **x** whose M(S) components are elements of the field of integer modulo 2, where component $x_i = 1$ when the *i*th member is an element of the subset, and $x_i = 0$ otherwise. The sum of two subset vectors **x** and **y**, a vector **z** with entries defined by $z_i = x_i + y_i$, represents the symmetric difference of the original subsets. The scalar product of **x** and **y** defined by $\Sigma x_i y_i$ is 0 or 1 according as the original subsets have an even or an odd number of members in common. Although this vector space can be constructed over an arbitrary field, for simplicity the field of integer modulo 2 is considered, in which $1 + 1 = 0$.

Two important subspaces of the above vector space of a graph S are the cycle subspace and cutset subspace, known as *cycle space* and *cutset space* of S.

2.3.1 Cycle Space

Let a cycle set of members of a graph be defined as a set of members which form a cycle or form several cycles having no common member, but perhaps common nodes. The null set is also defined as a cycle set. A vector representing a cycle set is called a *cycle set vector*. It can be shown that the sum of two cycle set vectors of a graph is also a cycle set vector. Thus, the cycle set vectors of a graph form a vector space over the field of integer modulo 2. The dimension of a cycle space is given by

$$\text{nullity } (S) = \nu(S) = b_1(S) = M(S) - N(S) + b_0(S), \tag{2.4}$$

where $b_1(S)$ and $b_0(S)$ are the first and zero Betti numbers of S, respectively. As an example, the nullity of the graph S in Fig. 2.11a is $\nu(S) = 10 - 8 + 1 = 3$.

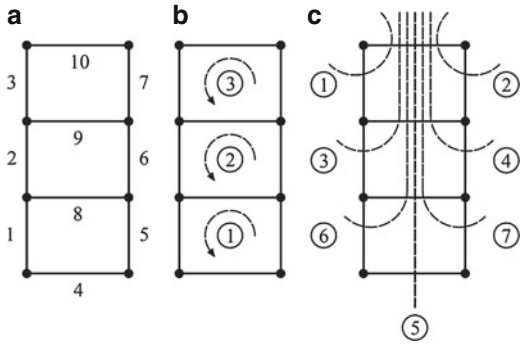

Fig. 2.11 A graph S with a cycle basis and a cutset basis. (**a**) A graph model S. (**b**) A cycle basis. (**c**) A cutest basis

2.3.2 Cutset Space

Consider a cutset vector similar to that of a cycle vector. Let the null set be also defined as a cutset. It can be shown that the sum of two cutset vectors of a graph is also a cutset vector. Therefore, the cutset vectors of a graph form a vector space, the dimension of which is given by

$$\text{rank } (S) = \rho(S) = N(S) - b_0(S). \tag{2.5}$$

As an example, the rank of S in Fig. 2.11a is $\rho(S) = 8 - 1 = 7$.

2.3.3 Cycle Bases Matrices

The cycle–member incidence matrix $\bar{\mathbf{C}}$ of a graph S has a row for each cycle or hinged cycle and a column for each member. An entry c_{ij} of $\bar{\mathbf{C}}$ is 1 if cycle C_i contains member m_j, and it is 0 otherwise. In contrast to the node adjacency and node–member incidence matrix, the cycle–member incidence matrix does not determine a graph up to isomorphism; that is, two totally different graphs may have the same cycle–member incidence matrix.

For a graph S there exist $2^{b_1(S)} - 1$ cycles or hinged cycles. Thus, $\bar{\mathbf{C}}$ is a $(2^{b_1(S)} - 1) \times M$ matrix. However, one does not need all the cycles of S, and the elements of a cycle basis are sufficient. For a cycle basis, a cycle–member incidence matrix becomes a $b_1(S) \times M$ matrix, denoted by $\mathbf{C}$, known as the *cycle basis incidence matrix* of S. As an example, matrix $\mathbf{C}$ for the graph shown in Fig. 2.11, for the following cycle basis,

$$C_1 = (m_1,\ m_4,\ m_5,\ m_8),\ C_2 = (m_2,\ m_8,\ m_6,\ m_9),\ C_3 = (m_3,\ m_9,\ m_7,\ m_{10})$$

is given by

$$\mathbf{C} = \begin{matrix} C_1 \\ C_2 \\ C_3 \end{matrix} \begin{bmatrix} 1 & 0 & 0 & 1 & 1 & 0 & 0 & 1 & 0 & 0 \\ 0 & 1 & 0 & 0 & 0 & 1 & 0 & 1 & 1 & 0 \\ 0 & 0 & 1 & 0 & 0 & 0 & 1 & 0 & 1 & 1 \end{bmatrix} \tag{2.6}$$

The *cycle adjacency matrix* **D** is a $b_1(S) \times b_1(S)$ matrix, each entry d_{ij} of which is 1 if C_i and C_j have at least one member in common, and it is 0 otherwise. This matrix is related to the cycle–member incidence matrix by the following relationship:

$$\mathbf{C}\mathbf{C}^t = \mathbf{D} + \mathbf{W}, \tag{2.7}$$

where **W** is diagonal matrix with w_{ii} being the length of the *i*th cycle and its trace being equal to the total length of the cycles of the basis.

2.3.4 Cutset Bases Matrices

The *cutset–member incidence matrix* $\bar{\mathbf{C}}^*$ for a graph S has a row for each cutset of S and a column for each member. An entry $\bar{c}^*_{ij}$ of $\bar{\mathbf{C}}^*$ is 1 if cutset C^*_i contains member m_j, and it is 0 otherwise. This matrix, like $\bar{\mathbf{C}}$, does not determine a graph completely.

Independent rows of $\bar{\mathbf{C}}^*$ for a cutset basis, denoted by **C***, form a matrix known as a *cutset basis incidence matrix*, which is a $\eta(S) \times M$ matrix, $\eta(S)$ being the rank of graph S. As an example, **C*** for the cutset of Fig. 2.11 with members labelled as in Fig. 2.11a is given below.

$$\mathbf{C}^* = \begin{bmatrix} 0 & 0 & 1 & 0 & 0 & 0 & 0 & 0 & 0 & 1 \\ 0 & 0 & 0 & 0 & 0 & 0 & 1 & 0 & 0 & 1 \\ 0 & 1 & 0 & 0 & 0 & 0 & 0 & 0 & 1 & 1 \\ 0 & 0 & 0 & 0 & 0 & 1 & 0 & 0 & 1 & 1 \\ 0 & 0 & 0 & 1 & 0 & 0 & 0 & 1 & 1 & 1 \\ 1 & 0 & 0 & 0 & 0 & 0 & 0 & 1 & 1 & 1 \\ 0 & 0 & 0 & 0 & 1 & 0 & 0 & 1 & 1 & 1 \end{bmatrix}. \tag{2.8}$$

The *cutset adjacency matrix* **D*** is a $\eta(S) \times \eta(S)$ matrix defined analogously to cycle adjacency matrix **D**.

2.4 Graphs Associated with Matrices

Through these matrices, many concepts from matrix algebra can be related to those of graph theory. Three types of matrices and the corresponding graphs are shown in Fig. 2.12. The sign * is used to indicate a non-zero number. M_1 is a

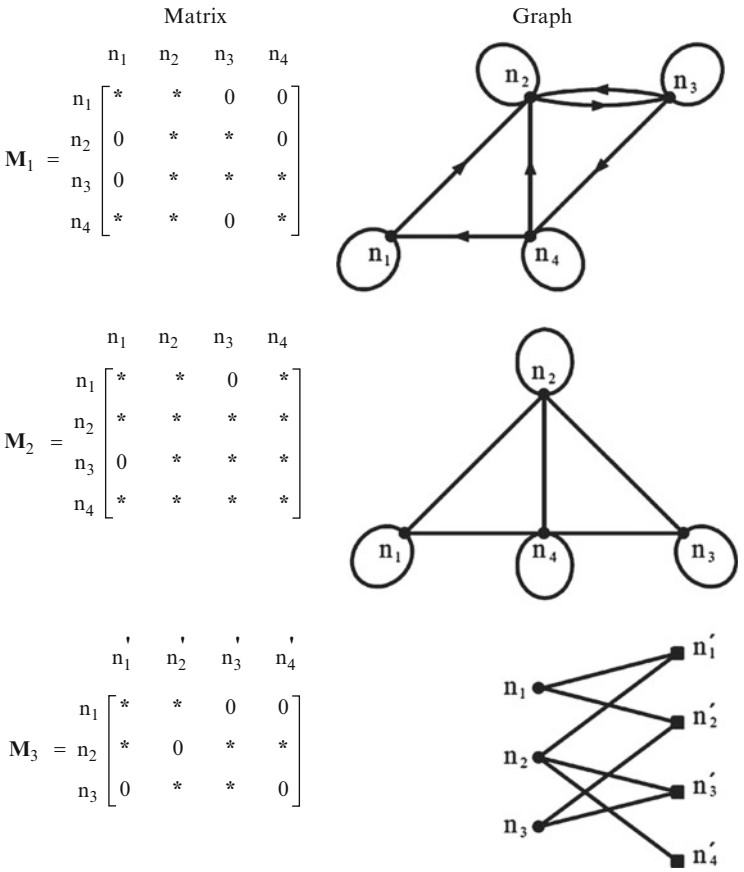

Fig. 2.12 Matrices and the associated graphs

nonsymmetric square matrix, and the corresponding graph is a directed graph with N nodes, where N is the dimension of the matrix. M_2 is a symmetric square matrix, and the corresponding graph is a nondirected graph with N nodes, where N is the dimension of the matrix. M_3 is an arbitrary rectangular matrix of dimension $M \times N$, and the corresponding graph is a bipartite graph $K_{M,N}$. In fact M_1, M_2 and M_3 are the node adjacency matrices of these graphs.

2.5 Planar Graphs: Euler's Polyhedron Formula

Graph theory and properties of planar graphs were first discovered by Euler in 1736. After 190 years Kuratowski found a criterion for a graph to be planar. Whitney developed some important properties of embedding graphs in the plane. MacLane

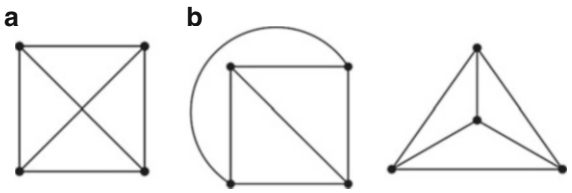

Fig. 2.13 K_4 and two of its drawings. (**a**) A complete graph K_4. (**b**) Planar drawings of K_4

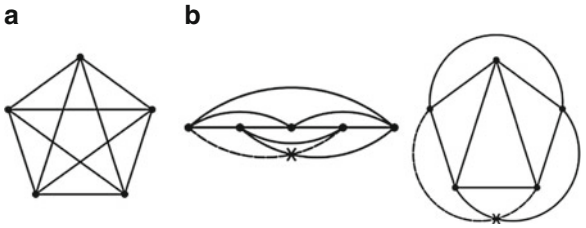

Fig. 2.14 K_5 and two of its drawings. (**a**) A complete graph K_5. (**b**) Two drawings of K_5 with one crossing

expressed the planarity of a graph in terms of its cycle basis. In this section, some of these criteria are studied, and Euler's polyhedron formula is proved.

2.5.1 Planar Graphs

A graph S is called *planar* if it can be drawn (embedded) in the plane in such a way that no two members cross each other. As an example, a complete graph K_4 shown in Fig. 2.13 is planar since it can be drawn in the plane as shown.

On the other hand K_5, Fig. 2.14, is not planar, since every drawing of K_5 contains at least one crossing.

Similarly $K_{3,3}$ is not planar.

A planar graph S drawn in the plane divides the plane into regions, all of which are bounded and only one is unbounded. If S is drawn on a sphere, all the regions will be bounded; however, the number of regions will not change. The cycle bounding a region is called a *regional cycle*. Obviously the sum of the lengths of regional cycles is twice the number of members of the graph.

Theorem. (Euler [1]): *Let S be a connected planar graph. Then,*

$$R(S) - M(S) + N(S) = 2. \tag{2.9}$$

Proof. For a proof, S is re-formed in two stages. In the first stage a spanning tree T of S is considered in the plane for which $R(T) - M(T) + N(T) = 2$. This is true

since R(T) = 1 and M(T) = N(T) − 1. In the second stage chords are added one at a time. Addition of a chord increases the number of members and regions each by unity, leaving the left-hand side of Eq. 2.9 unchanged during the entire process, and the result follows.

2.6 Definitions from Algebraic Graph Theory

Spectral graph theory, as a branch of algebraic graph theory, is the study of properties of a graph in relationship to the characteristic polynomial, eigenvalues and eigenvectors of matrices associated to the graph, such as its adjacency matrix or Laplacian matrix. An undirected graph has a symmetric adjacency matrix and therefore has real eigenvalues (the multiset of which is called the graph's *spectrum*) and a complete set of orthonormal eigenvectors. While the adjacency matrix depends on the vertex labelling, its spectrum is a graph invariant.

2.6.1 Incidence, Adjacency and Laplacian Matrices of a Graph

A directed graph S consists of node set N(S) and member set M(S), where a member, or directed member, is an ordered pair of distinct nodes. An undirected graph can be equally viewed as a directed graph where (n_i,n_j) is a member whenever (n_j,n_i) is a member.

The incidence matrix $\mathbf{B} = \left[b_{ij}\right]_{n\times m}$ of a graph S, whose nodes are labelled as 1,2, . . . , n, and members as 1, 2, 3, . . . , m, is defined as

$$b_{ij} = \begin{cases} 1 & \text{if node } n_i \text{ is incident with member } m_j \\ 0 & \text{otherwise} \end{cases} \tag{2.10}$$

The adjacency matrix $\mathbf{A} = \left[a_{ij}\right]_{n\times n}$ of a graph S, whose nodes are labelled as 1,2, . . . , n, is defined as

$$a_{ij} = \begin{cases} 1 & \text{if node } n_i \text{ is adjacent to } n_j \\ 0 & \text{otherwise} \end{cases} \tag{2.11}$$

The degree matrix $\mathbf{D} = \left[d_{ij}\right]_{n\times n}$ is a diagonal matrix containing node degrees. d_{ij} is equal to the degree of the *i*th node.

The Laplacian matrix $\mathbf{L} = \left[l_{ij}\right]_{n\times n}$ is defined as

Fig. 2.15 A graph S

$$\mathbf{B} = \begin{array}{c} \\ n_1 \\ n_2 \\ n_3 \\ n_4 \\ n_5 \end{array} \begin{array}{c} \begin{array}{ccccccc} m_1 & m_2 & m_3 & m_4 & m_5 & m_6 & m_7 \end{array} \\ \begin{bmatrix} 1 & 0 & 1 & 0 & 0 & 0 & 0 \\ 1 & 0 & 1 & 1 & 1 & 0 & 0 \\ 0 & 1 & 0 & 0 & 0 & 1 & 0 \\ 0 & 0 & 1 & 1 & 0 & 0 & 1 \\ 0 & 0 & 0 & 0 & 1 & 1 & 1 \end{bmatrix} \end{array} \quad \mathbf{A} = \begin{array}{c} \\ n_1 \\ n_2 \\ n_3 \\ n_4 \\ n_5 \end{array} \begin{array}{c} \begin{array}{ccccc} n_1 & n_2 & n_3 & n_4 & n_5 \end{array} \\ \begin{bmatrix} 0 & 1 & 0 & 1 & 0 \\ 1 & 0 & 1 & 1 & 1 \\ 0 & 1 & 0 & 0 & 1 \\ 1 & 1 & 0 & 0 & 1 \\ 0 & 1 & 1 & 1 & 0 \end{bmatrix} \end{array}$$

$$\mathbf{D} = \begin{array}{c} \\ n_1 \\ n_2 \\ n_3 \\ n_4 \\ n_5 \end{array} \begin{array}{c} \begin{array}{ccccc} n_1 & n_2 & n_3 & n_4 & n_5 \end{array} \\ \begin{bmatrix} 2 & 0 & 0 & 0 & 0 \\ 0 & 4 & 0 & 0 & 0 \\ 0 & 0 & 2 & 0 & 0 \\ 0 & 0 & 0 & 3 & 0 \\ 0 & 0 & 0 & 0 & 3 \end{bmatrix} \end{array} \quad \mathbf{L} = \begin{array}{c} \\ n_1 \\ n_2 \\ n_3 \\ n_4 \\ n_5 \end{array} \begin{array}{c} \begin{array}{ccccc} n_1 & n_2 & n_3 & n_4 & n_5 \end{array} \\ \begin{bmatrix} 2 & -1 & 0 & -1 & 0 \\ -1 & 4 & -1 & -1 & -1 \\ 0 & -1 & 2 & 0 & -1 \\ -1 & -1 & 0 & 3 & -1 \\ 0 & -1 & -1 & -1 & 3 \end{bmatrix} \end{array}$$

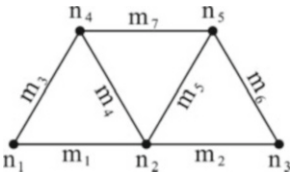

$$\mathbf{L} = \mathbf{D} - \mathbf{A}. \tag{2.12}$$

Therefore, the entries of **L** are as follows:

$$l_{ij} = \begin{cases} -1 \text{ node } n_i \text{ is adjacent to } n_j \\ \deg(n_i) \qquad \text{if} \quad i = j \\ 0 \qquad \text{otherwise.} \end{cases} \tag{2.13}$$

As an example, the incidence, adjacency, degree and Laplacian matrices of the graph S shown in Fig. 2.15 are as follows:

2.6.2 Incidence and Adjacency Matrices of a Directed Graph

The incidence matrix $\mathbf{B} = \left[b_{ij}\right]_{n\times m}$ of a directed graph S, whose nodes are labelled as 1,2, . . . , n, and members as 1, 2, 3, . . . , m, is defined as

$$b_{ij} = \begin{cases} +1 & \text{if node } n_i \text{ is connected to } n_j \text{ and } n_i \text{ is the start node of member } m_j \\ -1 & \text{if node } n_i \text{ is connected to } n_j \text{ and } n_i \text{ is the end node of member } m_j \\ 0 & \text{otherwise} \end{cases} \tag{2.14}$$

Fig. 2.16 A graph S

$$\mathbf{B} = \begin{array}{c} \\ n_1 \\ n_2 \\ n_3 \\ n_4 \\ n_5 \end{array} \begin{array}{c} \begin{array}{ccccccc} m_1 & m_2 & m_3 & m_4 & m_5 & m_6 & m_7 \end{array} \\ \begin{bmatrix} 1 & 0 & 1 & 0 & 0 & 0 & 0 \\ -1 & 0 & 1 & -1 & 1 & 0 & 0 \\ 0 & -1 & 0 & 0 & 0 & -1 & 0 \\ 0 & 0 & -1 & 1 & 0 & 0 & 1 \\ 0 & 0 & 0 & 0 & -1 & 1 & -1 \end{bmatrix} \end{array} \qquad \mathbf{A} = \begin{array}{c} \\ n_1 \\ n_2 \\ n_3 \\ n_4 \\ n_5 \end{array} \begin{array}{c} \begin{array}{ccccc} n_1 & n_2 & n_3 & n_4 & n_5 \end{array} \\ \begin{bmatrix} 0 & 1 & 0 & 1 & 0 \\ -1 & 0 & 1 & -1 & 1 \\ 0 & -1 & 0 & 0 & -1 \\ -1 & 1 & 0 & 0 & 1 \\ 0 & -1 & 1 & -1 & 0 \end{bmatrix} \end{array}$$

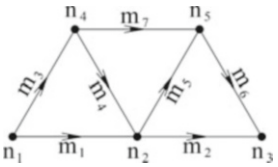

The adjacency matrix $\mathbf{A} = \left[a_{ij}\right]_{n\times n}$ of a directed graph D, whose nodes are labelled as 1,2, . . ., n, is defined as

$$a_{ij} = \begin{cases} +1 & \text{if node } n_i \text{ is connected to } n_j \text{ and directed from } n_i \text{ to } n_j \\ -1 & \text{if node } n_i \text{ is connected to } n_j \text{ and directed from } n_j \text{ to } n_i \\ 0 & \text{otherwise} \end{cases} \tag{2.15}$$

As an example, the incidence and adjacency matrices of the directed graph of Fig. 2.16 are shown in the following:

2.6.3 Adjacency and Laplacian Matrices of a Weighted Graph

Consider a graph with weights assigned to its nodes and edges. The nodal weight vector is

$$\mathbf{NW} = [nw_i];\ i = 1, 2, \ldots, N, \tag{2.16}$$

and edge weight vector is defined as follows:

$$\mathbf{EW} = \left[ew_{ij}\right];\ (i, j) = 1, , \ldots, N, \tag{2.17}$$

The adjacency matrix $\mathbf{A} = \left[a_{ij}\right]_{n\times n}$ of a weighted graph S, containing n nodes, is defined as follows:

$$a_{ij} = \begin{cases} ew_{ij} & \text{if } n_i \text{ is adjacent to } n_j \\ 0 & \text{otherwise} \end{cases} \tag{2.18}$$

For a non-weighted graph ew_{ij} should be replaced by unity.

The entries of the weighted Laplacian matrix **L** of a weighted graph is defined as

$$\mathbf{L} = \mathbf{D} - \mathbf{A}, \tag{2.19}$$

The entries of **L** are as follows:

$$l_{ij} = \begin{cases} -ew_{ij} = -ew_{ji} & \text{if nodes } n_i \text{ and } n_j \text{ are adjacent} \\ ew_i = \sum_{j=1}^{D_i} ew_{ij} & \text{for } i = j \\ 0 & \text{otherwise} \end{cases} \tag{2.20}$$

For non-weighted graph this reduces to Eq. 2.13.

2.6.4 Eigenvalues and Eigenvectors of an Adjacency Matrix

Consider the eigenproblem as

$$\mathbf{A}\boldsymbol{\phi}_i = \mu_i \boldsymbol{\phi}_i \tag{2.21}$$

where μ_i is the eigenvalue and $\boldsymbol{\phi}_i$ is the corresponding eigenvector. Since **A** is a symmetric real matrix, all its eigenvalues are real and can be expressed as

$$\mu_1 \leq \mu_2 \leq \ \cdots \leq \mu_{n-1} \leq \mu_n \tag{2.22}$$

The largest eigenvalue μ_n is the single root of the characteristic equation of **A**. The corresponding eigenvector $\boldsymbol{\phi}_n$ is the only eigenvector with positive entries. This vector has attractive properties employed in geography and structural mechanics. The characteristic polynomial of a matrix **A** is a polynomial

$$\phi(\mathbf{A}, \lambda) = \det\ (\lambda \mathbf{I} - \mathbf{A}). \tag{2.23}$$

Consider $\phi(\mathbf{A},\lambda)$ as the characteristic polynomial of **A**. The spectrum of a matrix is the list of its eigenvalues together with their multiplicities. The spectrum of a graph S is the spectrum of its adjacency matrix **A**. For two isomorphic graphs S and S′, $\phi(S, \lambda) = \phi(S', \lambda)$. However, two graphs may have the same spectrum and yet be non-isomorphic. Information such as valencies of nodes or planarity cannot be determined by the spectrum.

The following properties can easily be proved:

1. The number of walks with length k from n_i to n_j in a graph S is equal to (i,j)th entry of $\mathbf{A}^k$. This can be proved by induction on k.
2. The trace of a square matrix **A** is the sum of its diagonal entries, denoted by trace **A**. The number of closed walks with length k in a graph is equal to trace $\mathbf{A}^k$. Thus, for a graph with M members and T triangles, trace $\mathbf{A} = 0$, trace $\mathbf{A}^2 = 2M$,

and trace $\mathbf{A}^3 = 6T$. Since the trace of a square matrix is also equal to the sum of its eigenvalues, therefore, the eigenvalues of $\mathbf{A}^k$ are the kth power of the eigenvalues of $\mathbf{A}$. Hence, trace $\mathbf{A}^k$ is determined by the spectrum of $\mathbf{A}$, that is, the spectrum of a graph S determines the number of nodes, members and triangles in S.

3. The complement $\bar{S}$ of a graph S has the same node set as S, where nodes n_i and n_j are adjacent in $\bar{S}$ if and only if they are not adjacent in S. Let $\bar{S}$ be the complement of S. Then the adjacency matrix of the complement S is given by

$$\mathbf{A}(\bar{S}) = \mathbf{J} - \mathbf{I} - \mathbf{A}(S), \tag{2.24}$$

where $\mathbf{J}$ is all-one matrix and $\mathbf{I}$ is a unit matrix.

2.6.5 Eigenvalues and Eigenvectors of a Laplacian Matrix

Consider the following eigenproblem:

$$\mathbf{L}\mathbf{v}_i = \lambda_i \mathbf{v}_i, \tag{2.25}$$

where λ_i is the eigenvalue and $\mathbf{v}_i$ is the corresponding eigenvector. As for $\mathbf{A}$, all the eigenvalues of $\mathbf{L}$ are real. It can be shown that matrix $\mathbf{L}$ is a positive semi-definite matrix with

$$0 = \lambda_1 \leq \lambda_2 \leq \ldots \leq \lambda_n. \tag{2.26}$$

And

$$\mathbf{v}_1^t = \{1,\ 1, \ldots, 1\}. \tag{2.27}$$

The second eigenvalue λ_2 and the corresponding eigenvector $\mathbf{v}_2$ have attractive properties. Fiedler [30] has investigated various properties of λ_2. This eigenvalue is also known as the *algebraic connectivity* of a graph.

2.6.6 Additional Properties of a Laplacian Matrix

Consider a graph S with an arbitrary orientation. The Laplacian of S is a matrix $\mathbf{L}(S) = \mathbf{B}\mathbf{B}^t$, where $\mathbf{B}$ is the member–node incidence matrix. Naturally the Laplacian does not depend on the orientation considered for the graph. The following results can be proved:

The rank of the Laplacian matrix $\mathbf{L}(S)$ of S is equal to the rank of $\mathbf{L}(S) = N–b_0(S)$.

1. If S is a graph on N nodes and $2 \leq i \leq N$, then $\lambda_i(\bar{S}) = N - \lambda_{N-i+2}(S)$, where $\bar{S}$ is the complement of S.

Proof. It can be observed that

$$\mathbf{L}(S) + \mathbf{L}(\bar{S}) = N\mathbf{I} - \mathbf{J}. \tag{2.28}$$

The vector $\mathbf{I} = \{1\ 1\ 1\ \ldots\ 1\}^t$ is an eigenvector of $\mathbf{L}(S)$ and $\mathbf{L}(\bar{S})$ with the corresponding eigenvector 0. Let x be another eigenvector of $\mathbf{L}(S)$ with eigenvalue λ. One can assume that x is orthogonal to $\mathbf{I}$. Then $\mathbf{Jx} = 0$, and

$$N\mathbf{x} = (N\mathbf{I} - \mathbf{J})\mathbf{x} = \mathbf{L}(\bar{S})\mathbf{x} + \mathbf{L}(\bar{S})\mathbf{x} = \lambda\mathbf{x} + \mathbf{L}(\bar{S})\mathbf{x}. \tag{2.29}$$

Therefore, $\mathbf{L}(\bar{S}) = (N - \lambda)\mathbf{x}$, and the proof follows.

2. Let S be a graph on N nodes with Laplacian $\mathbf{L}$. Then for any vector $\mathbf{x}$, we have

$$\mathbf{x}^t\mathbf{L}\mathbf{x} = \sum_{(i,j)\in M(S)} (x_i - x_j)^2 \tag{2.30}$$

Proof. This follows from the observation that

$$\mathbf{x}^t\mathbf{L}\mathbf{x} = \mathbf{x}^t\mathbf{B}\mathbf{B}^t\mathbf{x} = (\mathbf{B}^t\mathbf{x})^t(\mathbf{B}^t\mathbf{x}), \tag{2.31}$$

and that if $(i,j) \in M(S)$, then the entry of $\mathbf{B}^t\mathbf{x}$ corresponding to (i,j) is $\pm (x_i - x_j)$.

2.7 Matrix Representation of a Graph in Computer

A graph can be represented in various forms. Some of these representations are of theoretical importance; others are useful from the programming point of view when applied to realistic problems. In this section, six different representations of a graph are described.

Two important matrices, namely, incidence matrix $\mathbf{B}$ and the adjacency matrices A defined in Sect. 2.6.3, can be used for representing a graph to a computer. However, the storage requirements for these matrices are high and proportional to $N \times N$ and $M \times (N - 1)$, respectively. In fact large numbers of unnecessary zeros are stored in these matrices. In practice one can use different approaches to reduce the storage required, some of which are described in the following.

Member List: This type of representation is a common approach in structural mechanics. A member list consists of two rows (or columns) and M columns

(or rows). Each column (or row) contains the labels of the two end nodes of each member, in which members are arranged sequentially. For example, the member list of S in Fig. 2.15 is

$$\mathbf{ML} = \begin{array}{c} \\ n_i \\ n_j \end{array} \begin{array}{c} \begin{array}{ccccccc} m_1 & m_2 & m_3 & m_4 & m_5 & m_6 & m_7 \end{array} \\ \begin{bmatrix} 1 & 2 & 1 & 2 & 2 & 3 & 4 \\ 2 & 3 & 4 & 4 & 5 & 5 & 5 \end{bmatrix} \end{array}. \tag{2.32}$$

It should be noted that a member list can also represent orientations on members. The storage required for this representation is 2 × M. Some engineers prefer to add a third row containing the member's labels, for easy addressing. In this case, the storage is increased to 3 × M.

A different way of preparing a member list is to use a vector containing the end nodes of members sequentially; for example, for the previous example, this vector becomes

$$(1,2;\ 2,3;\ 1,4;\ 2,4;\ 2,5;\ 3,5;\ 4,5). \tag{2.33}$$

This is a compact description of a graph; however, it is impractical because of the extra search required for its use in various algorithms.

Adjacency List: This list consists of N rows and D columns, where D is the maximum degree of the nodes of S. The *i*th row contains the labels of the nodes adjacent to node i of S. For the graph S shown in Fig. 2.15, the adjacency list is

$$\mathbf{AL} = \begin{array}{c} \\ n_1 \\ n_2 \\ n_3 \\ n_4 \\ n_5 \end{array} \begin{array}{c} \begin{array}{cccc} & & & \end{array} \\ \begin{bmatrix} 2 & 4 & & \\ 1 & 3 & 4 & 5 \\ 2 & 5 & & \\ 1 & 2 & 5 & \\ 2 & 3 & 4 & \end{bmatrix}_{N\times D} \end{array} \tag{2.34}$$

The storage needed for an adjacency list is N × D.

Compact Adjacency List: In this list the rows of **AL** are continually arranged in a row vector **R**, and an additional vector of pointers **P** is considered. For example, the compact adjacency list of Fig. 2.15 can be written as

$$\begin{aligned} \mathbf{R} &= (\mathbf{2},4,\mathbf{1},3,4,5,\mathbf{2},5,\mathbf{1},2,5,\mathbf{2},3,4), \\ \mathbf{P} &= (1,3,7,9,12,15). \end{aligned} \tag{2.35}$$

P is a vector (p_1, p_2, p_3, ...) which helps to list the nodes adjacent to each node. For node n_i one should start reading **R** at entry p_i and finish at $p_{i+1} - 1$.

An additional restriction can be put on **R**, by ordering the nodes adjacent to each node n_i in ascending order of their degrees. This ordering can be of some

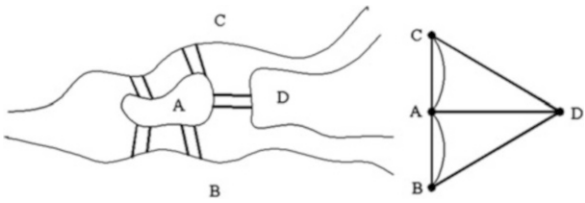

Fig. 2.17 Königsberg Bridge Problem

advantage, an example of which is nodal ordering for bandwidth optimisation. The storage required for this list is 2M + N + 1.

2.8 Historical Problem of Graph Theory

As mentioned before, in a topological graph the nodes are shown by points and the edges are usually identified by arcs or lines. However, an abstract graph can model a much more general set of object and relations. The following problem shows this general aspect even in the earliest application.

Euler began his paper on graphs by discussing a puzzle, the so-called Königsberg Bridge Problem. The city of Königsberg (now Kaliningrad) in East Prussia is located at the banks and on two islands of the river Pregel. The various parts of the city were connected by seven bridges. The problem arose: Is it possible to plan a tour in such a manner that starting from home, one can return there after having crossed each river bridge just once?

A schematic map of the Königsberg is reproduced in Fig. 2.17. The four parts of the city are denoted by letters A, B, C and D. Since we are interested only in the bridge crossings, we may think of A, B, C and D as the vertices of the graph with connecting edges corresponding to the bridges.

Euler showed that this graph cannot be traversed completely in a single circular path; in other words, no matter at which vertex one begins, one cannot cover the graph and come back to the starting point without retracing one's steps. Such a path would have to enter each vertex as many times as it departs from it; hence, it requires an even number of edges at each vertex, and this condition is not fulfilled in the graph representing the map of Königsberg.

In this historical problem, the incidence of different parts of a city is considered with edges representing the bridges, that is, even the first graph model has been such a general one and has not been confined to points and edges as imagined by some users.

For definition on topology, the reader may refer to any textbook on topology, for example, Cooks [31].

References

1. Euler L (1736) Solutio problematic ad Geometrian situs pertinentis, Comm Acad Petropolitanae 8:128–140. Translated in: Speiser klassische Stücke der Mathematik, Zürich (1927)127–138
2. Kirchhoff G (1847) Über die Auflösung der Gleichungen auf welche man bei der Untersuchung der Linearen Verteilung Galvanischer Ströme geführt wird. Ann Physik Chemie, 72:497–508. English translation, IRE Trans Circuit Theory, CT5(1958)4-7
3. Cayley A (1889–1897) On the theory of the analytical forms called trees. Math. Papers, Cambridge, vol III, pp. 242–246
4. Sylvester JJ (1909) On the geometrical forms called trees. Math. Papers, Cambridge University Press, vol III, pp. 640–641
5. Poincaré H (1901) Second complement à l′analysis situs. Proc Lond Math Soc 32:277–308
6. König D (1936) Theory der endlichen und unendlichen Graphen. Chelsea, 1950, 1st edn. Akad. Verlag, Leipzig
7. Ore O (1962) Theory of graphs, vol 38. American Mathematical Society Colloquium Publication, Providence
8. Behzad M, Chartrand G (1971) Introduction to the theory of graphs. Allyn and Bacon, Boston
9. Tutte WT (1966) Connectivity in graphs. University of Toronto Press, Toronto
10. Berge C (1973) Graphs and hypergraphs. North-Holland, Amsterdam
11. Harary F (1969) Graph theory. Addison-Wesley, Reading, Mass
12. Gould RJ (1988) Graph theory. Benjamin/Cummings. Menlo Park, CA
13. Wilson RJ (1996) Introduction to graph theory. Longman, University of California, USA
14. Wilson RJ, Beineke LW (1979) Applications of graph theory. Academic, London
15. West DB (1996) Introduction to graph theory. Prentice Hall, USA
16. Biggs N (1993) Algebraic graph theory, 2nd edn. Cambridge University Press, Cambridge
17. Cvetković DM, Doob M, Sachs H (1980) Spectra of graphs, theory and application. Academic, New York
18. Cvetković DM, Doob M, Gutman IA, Torgasev A (1988) Recent results in the theory of graph spectra. Ann Discrete Math 36. North-Holland, Amsterdam
19. Bondy A, Murty SR (1979) Graph theory and related topics. Academic, New York
20. Chen WK (1971) Applied graph theory. North-Holland, Amsterdam
21. Thulasiraman K, Swamy MNS (1992) Graphs, theory and algorithms. Wiley, New York
22. Beineke LW, Wilson RJ (1996) Graph connections. Oxford Science, Oxford
23. Mayeda W (1972) Graph theory. Wiley, New York
24. Christofides N (1975) Graph theory; an algorithmic approach. Academic, London
25. Gondran M, Minoux M (1984) Graphs and algorithms. (trans: Vajda S). Wiley, New York
26. Deo N (1998) Graph theory with applications to engineering and computer science. Prentice-Hall, Englewood-Cliffs (PHI, Delhi, 1995)
27. Cook WJ, Cunningham WH, Pulleyblank WR, Schrijver A (1998) Combinatorial optimization, Wiley-Interscience series in discrete mathematics and optimization. Wiley, New York
28. Kaveh A (1995) Structural mechanics: graph and matrix methods, 3rd edn. Research Studies Press and Wiley, Exeter
29. Kaveh A (1997) Optimal structural analysis, 2nd edn. Wiley, Chichester
30. Fiedler M (1973) Algebraic connectivity of graphs. Czech Math J 23:298–305
31. Cooke GE, Finney RL (1967) Homology of cell complexes. Princeton University Press, Princeton

Chapter 3
Graph Products and Configuration Processing

3.1 Introduction

Graph products are defined and developed in the past 50 years (see, e.g. Berge [1], Sabidussi [2], Harary and Wilcox [3]). An excellent book covering the mathematics of graph products is that of Imrich and Klavzar [4]. In this chapter, the necessary definitions from graph products are presented and examples are included to illustrate the definitions pictorially. The number of graph products in literature is far more than four; however, products which have extensively been studied in mathematics are as follows:

Cartesian graph product
Strong Cartesian graph product
Direct graph product
Lexicographic graph product

For configuration processing in structural engineering, additional new products were needed. Four such products were named and Type I, Type II, Type III and Type IV products are defined by Kaveh and Koohestani [5]. The latter types of products were obtained for subgraphs with directed members and containing loops. The corresponding product graphs have configurations most suitable for representing space structures and finite element models.

Though there is no restriction in the number of subgraphs for the graph products, however, in structural mechanics the product of two subgraphs is sufficient for studying of the practical models. Again though the subgraphs can be general ones, however paths and cycles are sufficient to form most of the models encountered in structural engineering.

Finally weighted graph are introduced by assigning weights to the nodes and members of the subgraphs, leading to triangular and circular products [6, 7, 8].

A. Kaveh, *Optimal Analysis of Structures by Concepts of Symmetry and Regularity*,
DOI 10.1007/978-3-7091-1565-7_3,

3.2 Definitions of Different Graph Products

Many structures have regular patterns and can be viewed as the Cartesian product, strong Cartesian product or direct product of a number of simple graphs. These subgraphs, used in the formation of a model, are called the *generators* of that model.

In order to show different graph products with no direction (undirected graphs), the symbol (X) will be used. The indices C, SC, D and LEX will be employed to show Cartesian, strong Cartesian, direct and lexicographic, respectively. As an example, C_5 $(X)_{SC}$ P_7 shows the strong Cartesian product of the cycle C_5 by the path P_7.

3.2.1 Boolean Operation on Graphs

In order to explain the products of graphs, let us consider a graph S as a subset of all unordered pairs of its nodes. The node set and member set of S are denoted by N(S) and M(S), respectively. The nodes of S are labelled as s_1, s_2,. . .,s_m,. . ., s_n, and the resulting graph is a *labelled graph*. Two distinct adjacent nodes, s_m and s_n, form a member, denoted by $s_m s_n \in M(S)$.

A Boolean operation on an ordered pair of disjoint labelled graphs K and H results in a labelled graph S, which has $N(K) \times N(H)$ as its nodes. The set M(S) of members of S is expressed, in terms of the members in M(K) and M(H), differently for each Boolean operations. In the first part of this chapter, four different operations are provided, corresponding to Cartesian product, strong Cartesian product, direct product and Lexicographic product of two graphs. In the second part, another four products, namely, Type I, Type II, Type III and Type IV graph products, are presented. Triangular and circular products will then be discussed in the third part.

3.2.2 Cartesian Product of Two Graphs

The simplest Boolean operation on a graph is the Cartesian product K $(X)_C$ H introduced by Sabidussi [2]. The Cartesian product is a Boolean operation S = K $(X)_C$ H, in which, for any two nodes $s_m = (u_i,v_k)$ and $s_n = (u_j,v_l)$ in $N(K) \times N(H)$, the member $s_m s_n$ is in M(S) whenever

$$u_i = u_j \text{ and } v_k v_l \in M(H), \tag{3.1a}$$

Or

$$v_k = v_l \text{ and } u_i u_j \in M(K). \tag{3.1b}$$

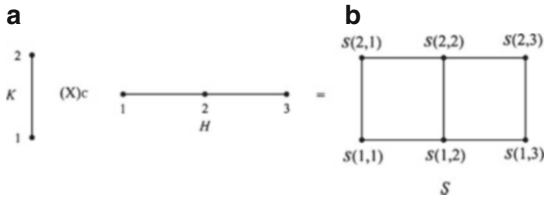

Fig. 3.1 The Cartesian product S of two simple graphs K and H. (**a**) $K = P_2$ and $H = P_3$. (**b**) $S = P_2 (X)_C P_3$

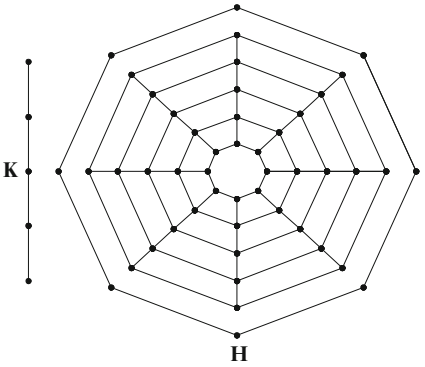

Fig. 3.2 Representation of $C_8 (X)_C P_5$

As an example, the Cartesian product of $K = P_2$ and $H = P_3$ is shown in Fig. 3.1.

In this product, the two nodes (u_1,v_2) and (u_2,v_2) are joined by a member, since the condition (3.1b) is satisfied.

The Cartesian product of two graphs K and H, denoted by K $(X)_C$ H, can be constructed by taking one copy of H for each node of K and joining copies of H corresponding to adjacent nodes of K by matching of size N(H).

The graphs K and H will be referred to as the *generators* of S. The Cartesian product operation is symmetric, that is, K $(X)_C$ H $\cong$ H $(X)_C$ K. For other useful graph operations, the reader may refer to the work by Gross and Yellen [9].

Examples. In this example, the Cartesian product $C_8 (X)_C P_5$ of the path graph with five nodes K denoted by P_5 and a cycle graph H shown by C_8 is illustrated in Fig. 3.2.

A product graph can be represented in different forms. As an example two representations of the Cartesian product $C_3 (X)_C P_4$ are illustrated in Fig. 3.3.

The Cartesian product $P_{m1} (X)_C P_{m2} (X)_C P_{m3}$ of three paths forms a three-dimensional mesh. As an example, the Cartesian product of $P_6 (X)_C P_4 (X)_C P_5$, resulting in a $5 \times 3 \times 4$ grid, is shown in Fig. 3.4.

A graph can be the product of more than two specific graphs, such as paths and cycles. As an example, the product of three graphs, $P_2 (X)_C K_3 (X)_C P_4$, is shown in Fig. 3.5. The product of a general graph S and the P_4, denoted by S $(X)_C$ P_4, is illustrated in Fig. 3.6.

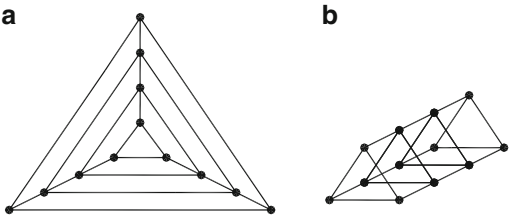

Fig. 3.3 Two different representations of C_3 $(X)_C$ P_4. (**a**) A 2D representation. (**b**) A 3D representation

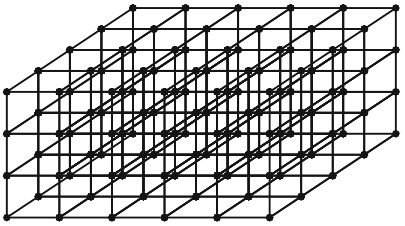

Fig. 3.4 Representation of a 5 × 3 × 4 mesh

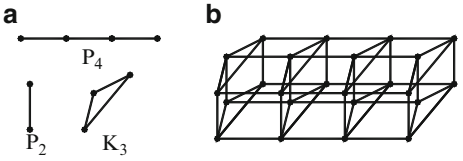

Fig. 3.5 The Cartesian product of three graphs P_2 $(X)_C$ K_3 $(X)_C$ P_4. (**a**) Generators. (**b**) Product

It can be proved that the Cartesian product of two graphs is connected if and only if both generators are connected [4].

3.2.3 Strong Cartesian Product of Two Graphs

This is another Boolean operation, known as the *strong Cartesian product*. The strong Cartesian product is a Boolean operation $S = K(X)_{SC} H$ in which, for any two distinct nodes $s_m = (u_i,v_k)$ and $s_n = (u_j,v_l)$ in N(K) × N(H), the member $s_m s_n$ is in M(S) if

$$u_i = u_j \text{ and } v_k v_l \in M(H), \tag{3.2a}$$

or

$$v_k = v_l \text{ and } u_i u_j \in M(K), \tag{3.2b}$$

or

$$u_i u_j \in M(K) \text{ and } v_k v_l \in M(H). \tag{3.2c}$$

As an example, the strong Cartesian product of $K = P_2$ and $H = P_3$ is shown in Fig. 3.7.

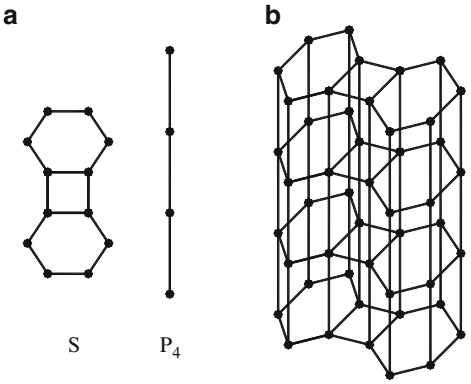

Fig. 3.6 The Cartesian product S $(X)_C$ P_4 of S by P_4. (**a**) Generators sand P_4. (**b**) Product S $(X)_C$ P_4

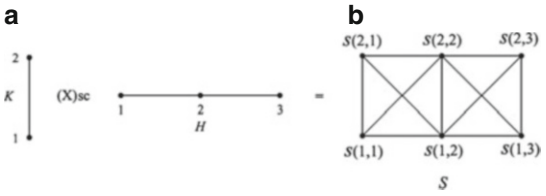

Fig. 3.7 The strong Cartesian product of two simple graphs. (**a**) Generators $K = P_2$ and $H = P_3$. (**b**) S $= P_2$ $(X)_{SC}$ P_3

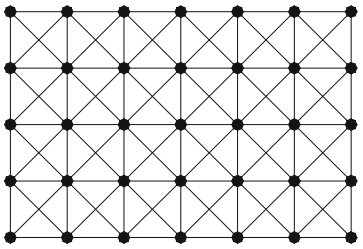

Fig. 3.8 Strong product representation of P_7 $(X)_{SC}$ P_5

In this example, the nodes (u_1,v_1) and (u_2,v_2) are joined, since the condition (3.2c) is satisfied.

Examples. In this example, the strong Cartesian product P_7 $(X)_{SC}$ P_5 of the path P_7 and the path graph P_5 is illustrated in Fig. 3.8. As a second example, the strong Cartesian product C_7 $(X)_{SC}$ P_4 is shown in Fig. 3.9.

3.2.4 Direct Product of Two Graphs

This is another Boolean operation, known as the *direct product*, introduced by Weichsel [10], who called it the *Kronecker product*. However, in this book,

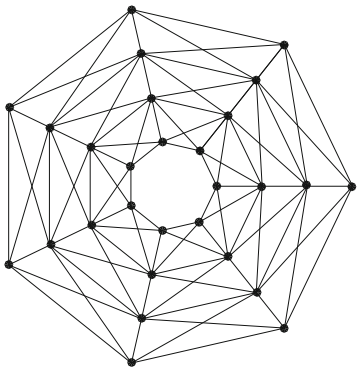

Fig. 3.9 Strong product representation of C_7 $(X)_{SC}$ P_4

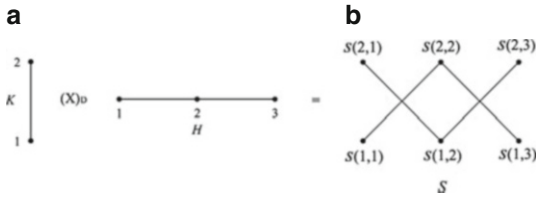

Fig. 3.10 The direct product of two simple graphs. (**a**) K = generators P_2 and H = P_3. (**b**) S = P_2 $(X)_D$ P_3

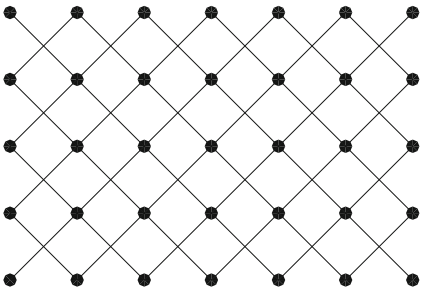

Fig. 3.11 Direct product representation of P_7 $(X)_D$ P_5

Kronecker product will be defined and used in matrix algebraic sense. The direct product is a Boolean operation S = K $(X)_D$ H, in which, for any two nodes $s_m = (u_i,v_k)$ and $s_n = (u_j,v_l)$ in N(K) × N(H), the member $s_m s_n$ is in M(S) if

$$u_i u_j \in \mathrm{M(K)} \text{ and } v_k v_l \in \mathrm{M(H)}. \tag{3.3}$$

As an example, the direct product of K = P_2 and H = P_3 is shown in Fig. 3.10.

Here, the two nodes (u_1,v_1) and (u_2,v_2) are joined, since the condition (3.3) is satisfied.

Examples. The direct product P_7 $(X)_D$ P_5 of the path graph P_7 and path graph P_5 is illustrated in Fig. 3.11. As a second example, the direct product C_7 $(X)_D$ P_4 is shown in Fig. 3.12.

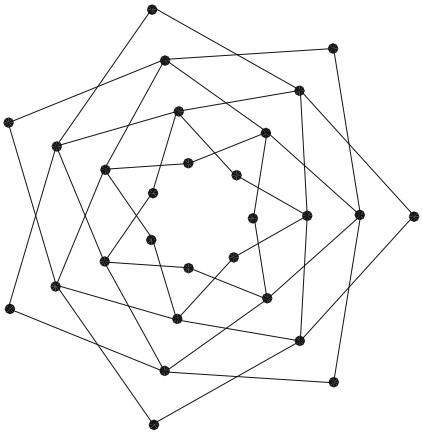

Fig. 3.12 Direct product representation of C_7 $(X)_D$ P_4

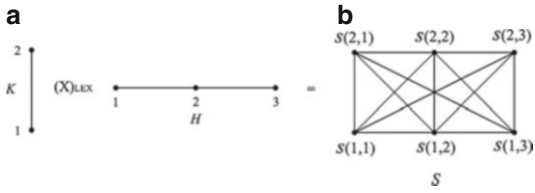

Fig. 3.13 The lexicographic product K $(X)_{LEX}$ H of two path graphs P_2 and P_3. (**a**) Generators K = P_2 and H = P_3. (**b**) S = P_2 $(X)_{LEX}$ P_3

3.2.5 Lexicographic Product of Two Graphs

This is another Boolean operation known as the *lexicographic product* introduced by Harary and Wilcox [3], and occasionally it is referred to as the *composition product*. The lexicographic product is a Boolean operation S = K $(X)_{LEX}$ H in which for any two nodes $s_m = (u_i,v_k)$ and $s_n = (u_j,v_l)$ in N(K) × N(H), the edge $s_m s_n$ is in M(S) if

$$u_i u_j \in \mathrm{M(K)}, \tag{3.4a}$$

or

$$u_i = u_j \text{ and } v_k v_l \in \mathrm{M(H)}. \tag{3.4b}$$

More concretely, the lexicographic product can be formed by replacing each node of K with a copy of H and drawing all possible edges between adjacent copies.

As an example, the lexicographic product of K = P_3 and H = P_2 is shown in Fig. 3.13.

Here, the two nodes (u_1,v_1) and (u_2,v_3) are joined, since the condition (3.4a) is satisfied.

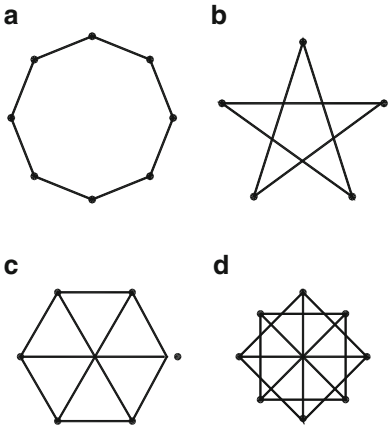

Fig. 3.14 Four generators G_1, G_2, G_3 and G_4. (**a**) G_1. (**b**) G_2. (**c**) G_3. (**d**) G_4

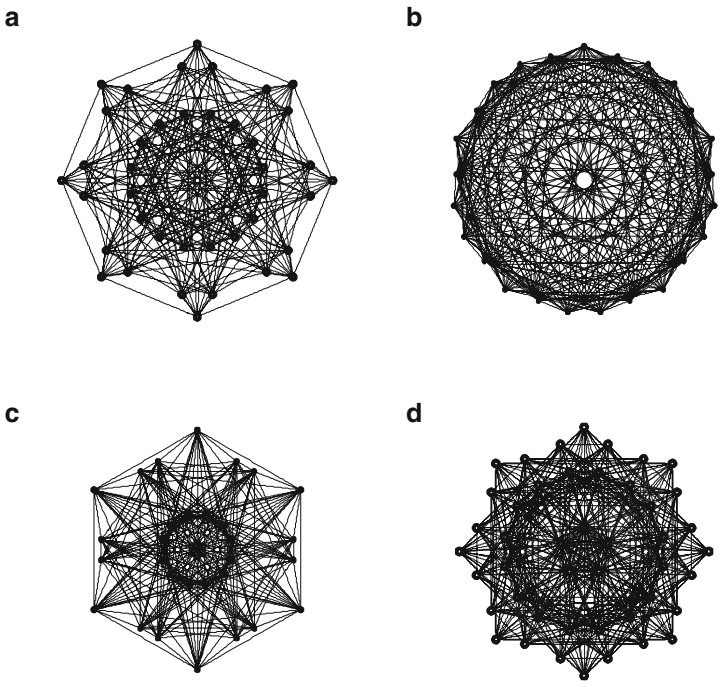

Fig. 3.15 The lexicographic graph products. (**a**) The lexicographic product $G_1\,(X)_{LEX}\,G_2$. (**b**) The lexicographic product $G_2\,(X)_{LEX}\,G_1$. (**c**) The lexicographic product $G_3\,(X)_{LEX}\,G_2$. (**d**) The lexicographic product $G_1\,(X)_{LEX}\,G_4$

Cartesian, strong Cartesian and direct products are extensively studied and applied in structural mechanics, as will be described in Chap. 6. Therefore, only additional examples from the lexicographic product are presented. The lexicographic products of the two graphs shown in Fig. 3.14 are illustrated in Fig. 3.15.

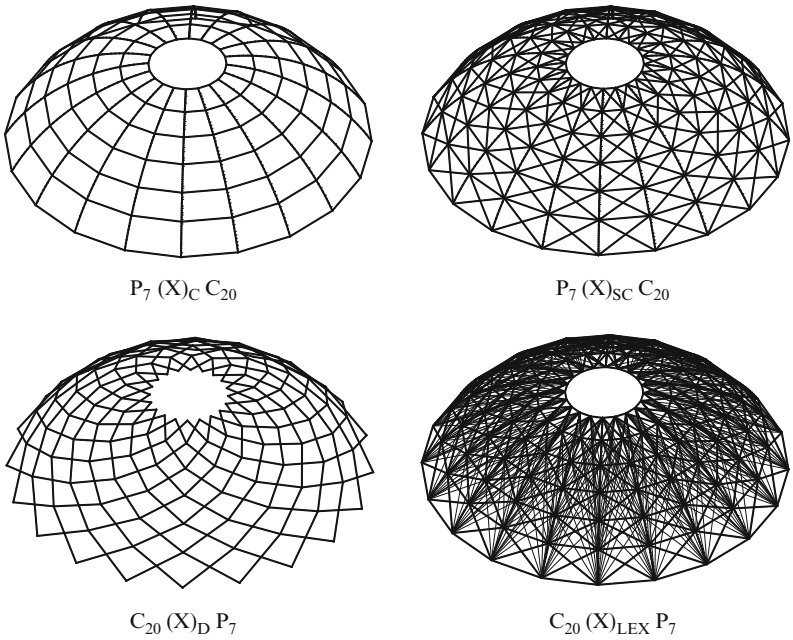

Fig. 3.16 Four domes generated by four undirected graph products

Example. In this example four domes are generated using the four undirected graph products defined in this section, Fig. 3.16.

3.3 Directed Graph Products

Graph products introduced in Sect. 3.2 are extensively used in combinatorial optimisation and structural mechanics; however, the directed graph products are recently developed [5], which are discussed in this section.

In this section four types of directed graph products are presented. Operators for the union and ring sum of these products are also defined and utilised.

Since in these products the graphs are directed and often contain loops, therefore for better explanation of the generators, the following notations are adopted:

In general a path and a cycle with no direction and no loop are denoted by P_n and C_n, respectively. If a path contains some loops, it will have super indices a, e, o, b or m, designating loops in all the nodes, in the nodes with even numbers, in the nodes with odd numbers, in end nodes and in non-end nodes, respectively. The sign ':' has the same implication as in MATLAB, that is, the total number of the list or a loop. In an expression, when the sign ':' is used twice, then the number in between shows the increment of interval. Some paths together with the corresponding signs are illustrated in Fig. 3.17.

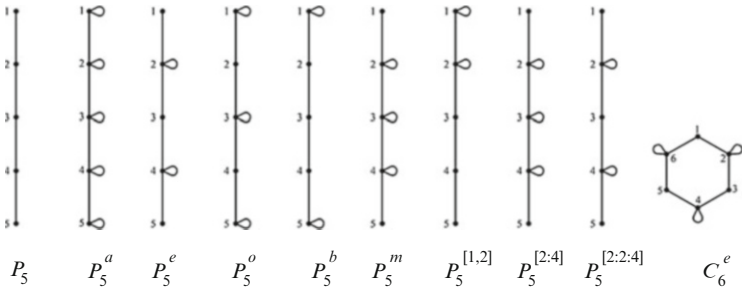

Fig. 3.17 Examples of paths with different loop systems

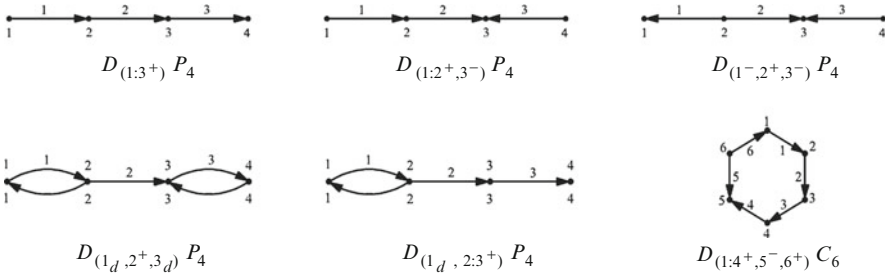

Fig. 3.18 Notations used for directed graphs

In order to show the directed graphs and for specifying the direction and the number of members, the index D for P and C is used. The indices consist of one or some numbers with + and − signs as their superscripts. Therefore, the numbers show the number of directed member with the same direction. For members with both directions, the subscript d is employed. The direction for + and − direction is quite optional, and members with no direction have no sign. Some examples for the above notation are shown in Fig. 3.18.

3.3.1 Type I Directed Graph Products

One shortcoming of the products defined in Sect. 3.2 is their incapability in generating triangular submodels. This reduces the applicability of undirected graph products in configuration processing of the practical structures and emphasises the need for employing directed graph products. The use of directed strong Cartesian product can be considered as an efficient tool for creating diagonal members for the panels. Thus, the formation of space structures with different connectivity becomes feasible.

The product for two directed graphs K and H is denoted by $(X)_1$, and it is defined as follows:

- The product has $N_K \times N_H$ nodes, where N_K, N_H are the numbers of nodes of K and H, respectively.

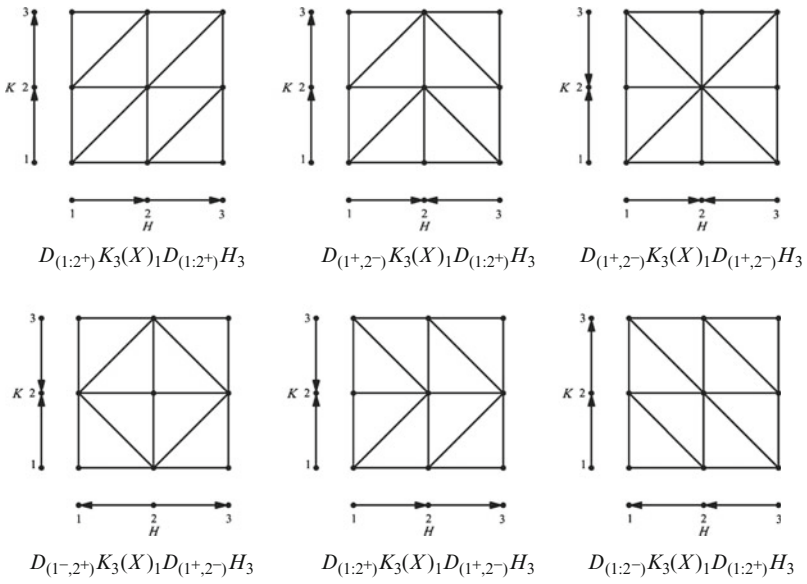

$D_{(1:2^+)}K_3(X)_1D_{(1:2^+)}H_3$ $D_{(1^+,2^-)}K_3(X)_1D_{(1:2^+)}H_3$ $D_{(1^+,2^-)}K_3(X)_1D_{(1^+,2^-)}H_3$

$D_{(1^-,2^+)}K_3(X)_1D_{(1^+,2^-)}H_3$ $D_{(1:2^+)}K_3(X)_1D_{(1^+,2^-)}H_3$ $D_{(1:2^-)}K_3(X)_1D_{(1:2^+)}H_3$

Fig. 3.19 Examples of Type I directed graph products

- Two nodes $s_m = (u_i,v_k)$ and $s_n = (u_j,v_l)$ are connected by a member s_ms_n if one of the following conditions holds:

$$\left(u_i = u_j \text{ and } \left(v_l.\text{adj}.v_k \text{ or } v_k.\text{adj}.v_l\right)\right) \tag{3.5a}$$

or
$$\left(\left(u_i.adj.u_j \text{ and } v_k.\text{adj}.v_l\right) \text{ or } \left(u_j.\text{adj}.u_i \text{ and } v_l.\text{adj}.v_k\right)\right) \tag{3.5b}$$

or
$$\left(v_k = v_l \text{ and } \left(u_j.\text{adj}.u_i \text{ or } u_i.\text{adj}.u_j\right)\right) \tag{3.5c}$$

where *adj* is an abbreviation for 'adjacent'.

Some examples of this product are shown in Fig. 3.19, where the method for controlling the diagonal members is clearly illustrated.

3.3.2 Type II Directed Graph Products

In this type of product, loops are used to control the inclusion or exclusion of members in different parts of the model. The product of K and H is denoted by $(X)_2$, and it is defined as follows:

- The product has $N_K \times N_H$ nodes, where N_K, N_H are the numbers of nodes of K and H, respectively.
- Two nodes $s_m = (u_i,v_k)$ and $s_n = (u_j,v_l)$ are connected by a member s_ms_n if one of the following conditions holds:

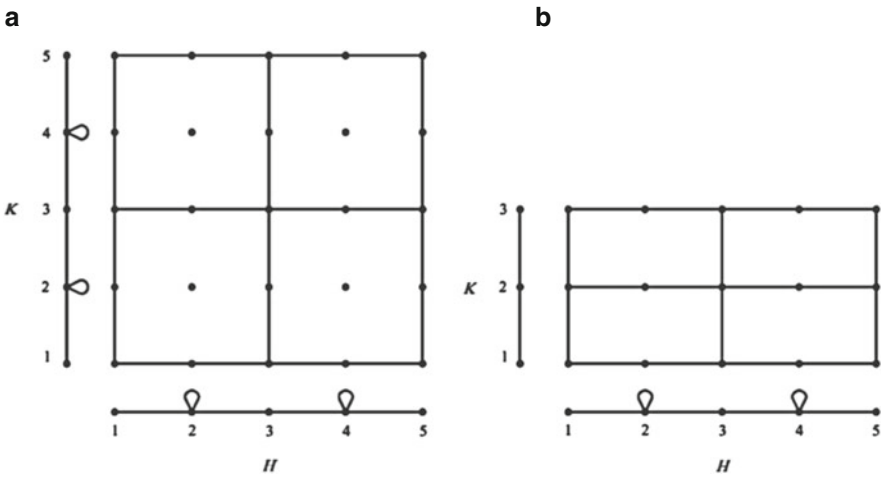

Fig. 3.20 Two examples of Type II directed graph products. (**a**) $K_5^e(X)_2H_5^e$. (**b**) $K_5^e(X)_2H_3$

$$\left(u_i = u_j \text{ and } u_i.\sim \text{adj}.u_i(\text{no\_loop}) \text{ and } v_k.\text{adj}.v_l\right) \tag{3.6a}$$

or
$$\left(v_k = v_l \text{ and } v_k.\sim \text{adj}.v_k(\text{no\_loop}) \text{ and } u_i.\text{adj}.u_j\right). \tag{3.6b}$$

where *adj* refers to 'adjacent' and *~adj* means 'not adjacent'.

Two examples of this type of products are shown in Fig. 3.20.

3.3.3 Type III Directed Graph Products

In Type II product, it is possible to delete the members of one complete row. Since this is required for the formation of complicated graphs, therefore, in Type III product, loops and directed members are simultaneously used to control the inclusion or exclusion of members. Using this product one can form graphs in the form of honeycombs. This product for two graphs G and H is denoted by $(X)_3$, and it is defined as follows:

- The product has $N_K \times N_H$ nodes.
- Two nodes $s_m = (u_i,v_k)$ and $s_n = (u_j,v_l)$ are connected by a member s_ms_n if one of the following conditions holds:

$$\left(u_i = u_j \text{ and } u_i.\text{adj}.u_i(\text{loop}) \text{ and } v_k.\text{adj}.v_l \text{ and } v_l.\text{adj}.v_k\right) \tag{3.7a}$$

or
$$\left(u_i = u_j \text{ and } u_i.\sim \text{adj}.u_i(\text{no\_loop}) \text{ and } v_k.\text{adj}.v_l \text{ and } v_l.\sim \text{adj}.v_k\right) \tag{3.7b}$$

or
$$\left(v_k = v_l \text{ and } u_i.\text{adj}.u_j\right). \tag{3.7c}$$

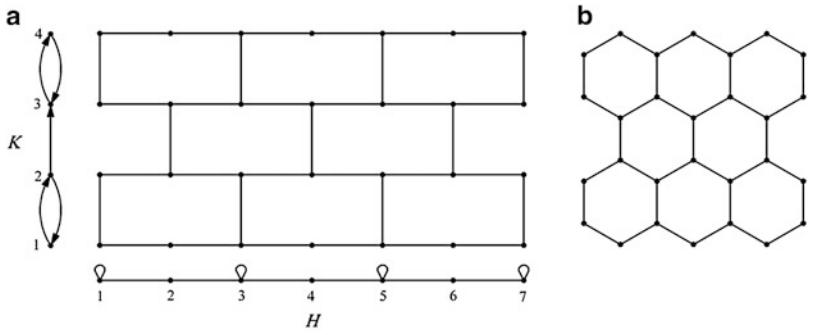

Fig. 3.21 (**a**) Type III directed graph product. (**b**) Product with geometric transformation

It should be mentioned that the topological properties of the presented products contain the properties of their generators. However, the configurations can be changed with different geometric transformations. Examples of this type of products together with their geometric transformations are shown in Fig. 3.21. Further explanations will be provided in subsequent section.

3.3.4 Type IV Directed Graph Products

In this section a summation of different types of graph products is presented. This approach is particularly suitable for the formation of the double-layer grids.

The product and sum of two graphs K and H is a graph S with algebraic representation denoted by $S = K(X)H(+)_4EK(X)EH$, where K and H are the main subgraphs and EK and EH are two subgraphs which can easily be obtained from the main subgraphs. In fact these subgraphs are graphs with each node being associated with a member of the main subgraph, and two nodes are connected if the corresponding members are incident in the main subgraphs.

- Therefore, the graph S has the nodes as $N_K \times N_H + M_K \times M_H$, where M_K and M_H are the numbers of members of K and H, respectively.
- The graph S has two subgraphs $K(X)H$ and $EK(X)\,EH$, and the product can be an arbitrary product introduced in the previous sections.
- The nodes of these two subgraphs which are denoted by (u, v) for $K(X)H$ and (eu, ev) for $EK(X)EH$ are connected to each other if the following condition holds:

$$(u, v), (eu, ev) - - - - > (u \ inc \ eu \text{ and } v \text{ inc } ev). \tag{3.8}$$

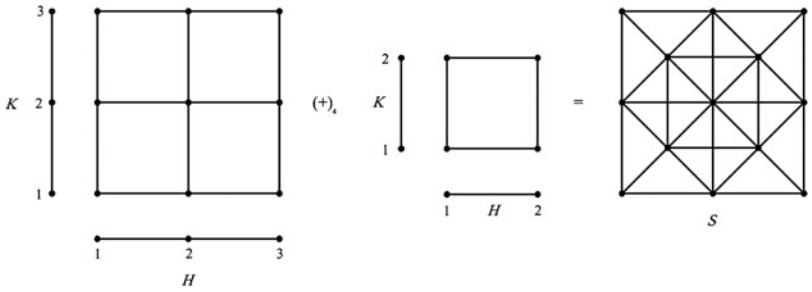

Fig. 3.22 An example of Type IV directed graph product and sum

Here, *inc* represents *incidence*. The above relationship indicates that for the node u corresponding to the member eu, and the node v corresponding to member ev, the (u, v) is connected to (eu, ev). The above operation has extremely good capability for generating double-layer grids. Examples of simultaneous product and summation are shown in Fig. 3.22. In these examples the products used are Cartesian products.

3.4 Weighted Triangular and Circular Graph Products for Configuration Processing

In this section new weighted triangular and circular graph products are presented for configuration processing of the new forms of structural models. Here, the weighted triangular and circular products are employed for the configuration processing of space structures that are of triangular shapes or a combination of triangular and rectangular shapes and also of the solid circular shapes as domes and some space structural models. The covered graph products are represented for selecting or eliminating some parts or panels from the product graph by using the second weights for the nodes of the generators. Cut-out products are other types of graph products which are defined to eliminate all of the connected elements to a specified node, to configure the model or grid with some vacant panels inside of the model [7, 8].

3.4.1 Extension of Classic Graph Products

For generating the configurations encountered in practice, some elements should be removed with an additional rule. In order to avoid such a complication, weighted

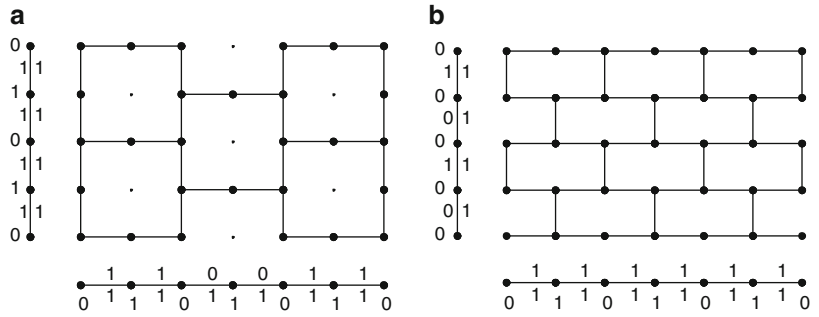

Fig. 3.23 Two weighted Cartesian graph products

graphs can be employed. Here, zero weights are assigned to the nodes and members which are supposed to be removed.

After the formation of the nodes according to the nodes of the generators, a member is added between two typical nodes (U_k,V_l) and (U_i,V_j), with the weights W_{ik}, $W_{ki,}$ W_{jl} and W_{lj} for elements and W_i and W_j for the nodes, if the following conditions are fulfilled:

$$\begin{aligned}\text{If } \{ &[U_i = U_k \text{ and } W_i = 0 \text{ and } (W_{jl} \neq 0 \text{ and } W_{lj} \neq 0)] \\ &\text{or } [U_i = U_k \text{ and } W_i \neq 0 \text{ and } (W_{jl}{}^* W_{lj} = 0 \text{ and } (W_{jl} \neq 0 \text{ or } W_{lj} \neq 0))] \\ &\text{or } [V_j = V_l \text{ and } W_j = 0 \text{ and } (W_{ik} \neq 0 \text{ and } W_{ki} \neq 0)] \\ &\text{or } [V_j = V_l \text{ and } W_j \neq 0 \text{ and } (W_{ik}{}^* W_{ki} = 0 \text{ and } (W_{ik} \neq 0 \text{ or } W_{ki} \neq 0))]\}\end{aligned} \tag{3.9}$$

Figure 3.23 illustrates the constructed configurations by the above rules. Though the formulae for both configurations in this figure are identical, however, due to the use of different weighted generators, dissimilar configurations are obtained.

3.4.2 Formulation of Weighted Strong Cartesian Product

Simple graph products can only generate panels with two crossing members, and in order to generate configurations with panels having single bracing elements, weighted strong Cartesian products cannot be used. In order to produce configurations with triangular panels, weighted generators should be employed. Here, zero weights are assigned to the nodes and members which should be removed. After the formation of the nodes according to the nodes of the generator, a member is added between two typical nodes (U_k,V_l) and (U_i,V_j), with the weights W_{ik}, $W_{ki,}$ W_{jl} and W_{lj} for elements, if the following conditions are fulfilled:

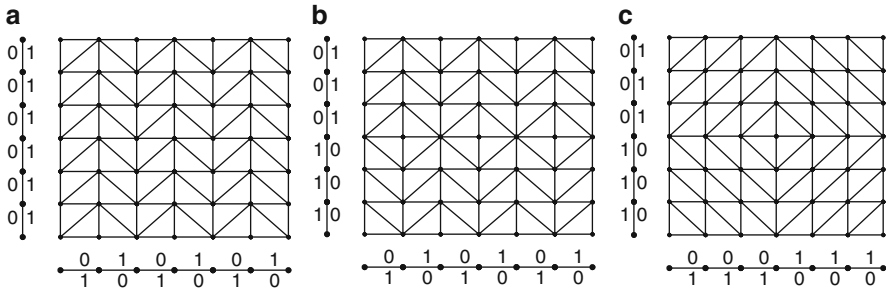

Fig. 3.24 Three weighted strong Cartesian graph products

$$\begin{aligned} \text{If } \{ & [U_i = U_k \text{ and } (W_{jl} \neq 0 \text{ or } W_{lj} \neq 0)] \\ & \text{or } [V_j = V_l \text{ and } (W_{ik} \neq 0 \text{ or } W_{ki} \neq 0)] \\ & \text{or } [W_{ki} \neq 0 \text{ or } W_{lj} \neq 0] \} \end{aligned} \tag{3.10}$$

Three examples of grids generated by these relationships are shown in Fig. 3.24. For each configuration the corresponding weighted generator are also depicted.

3.4.3 Formulation of Weighted Direct New Product

Here, zero weights are assigned to the nodes and also to the members which should be removed. After the formation of the nodes according to the nodes of the generator, a member is added between two typical nodes (U_k,V_l) and (U_i,V_j), with the weights W_{ik}, W_{ki}, W_{jl}, and W_{lj} for elements, if the following conditions are fulfilled:

$$\text{If } \{W_{ki} \neq 0 \text{ and } W_{lj} \neq 0\} \tag{3.11}$$

Two examples of weighted direct products of PW7*PW7 are illustrated in Fig. 3.25. The considered weights for the paths are different, thus resulting in different configurations.

3.4.4 Weighted Cartesian Direct Graph Products

By combining the weighted Cartesian and direct graph products, weighted Cartesian direct graph product is defined. In the weighted Cartesian product, both elements and nodes have weights, and the conditions are implemented by using these weights. But in the weighted direct product, only the nodes of the generators are weighted, so the

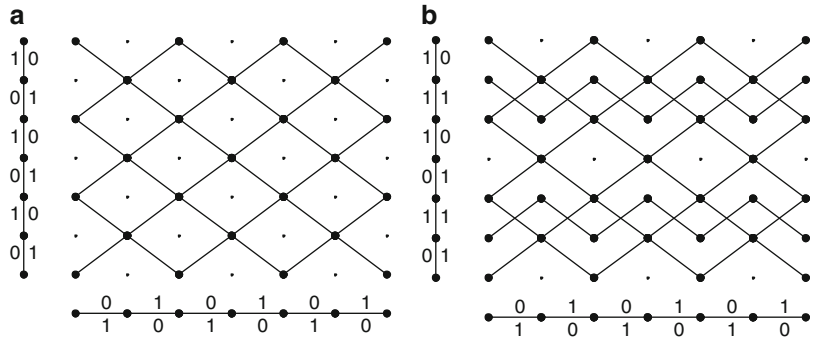

Fig. 3.25 Two weighted direct graph products

conditions are defined based on the weights of the elements. In the weighted Cartesian direct product, both the elements and nodes are weighted. For configuring vertical and horizontal elements, both weights are implemented and the conditions of weighted Cartesian product must be fulfilled. But for configuring diagonal elements, only nodal weights and weighted direct product must be satisfied. By simultaneous use of the product's conditions, a new graph product can be defined for configuring some special models with the horizontal, vertical and diagonal elements. After the formation of the nodes according to the nodes of the generators, a member is added between two typical nodes (U_k,V_l) and (U_i,V_j), with the weights W_{ik}, W_{ki}, W_{jl} and W_{lj} for elements and W_i and W_j for the nodes, if one of the following conditions is fulfilled:

$$
\begin{aligned}
\text{If } \{ & [[U_i = U_k \text{ and } W_i = 0 \text{ and } (W_{jl} \neq 0 \text{ and } W_{lj} \neq 0)] \\
& \text{or } [U_i = U_k \text{ and } W_i \neq 0 \text{ and } (W_{jl}{}^* W_{lj} = 0 \text{ and } (W_{jl} \neq 0 \text{ or } W_{lj} \neq 0))] \\
& \text{or } [V_j = V_l \text{ and } W_j = 0 \text{ and } (W_{ik} \neq 0 \text{ and } W_{ki} \neq 0)] \\
& \text{or } [V_j = V_l \text{ and } W_j \neq 0 \text{ and } (W_{ik}{}^* W_{ki} = 0 \text{ and } (W_{ik} \neq 0 \text{ or } W_{ki} \neq 0))]] \\
& \textbf{or } [W_{ki} \neq 0 \text{ or } W_{lj} \neq 0] \}
\end{aligned}
\tag{3.12}
$$

Some examples of this product are demonstrated in Fig. 3.26.

3.5 Definition of Weighted Triangular Graph Products

Since the classic graph products use only the adjacency conditions in the generators, therefore these products can only form simple shapes and models. For configuring other classes of models, it is necessary to assign other conditions and definitions to the previously mentioned generators and also to the conditions of the products. Assigning weights to the nodes and elements can be considered as new additions to the conditions and definitions. For creating the new graph products

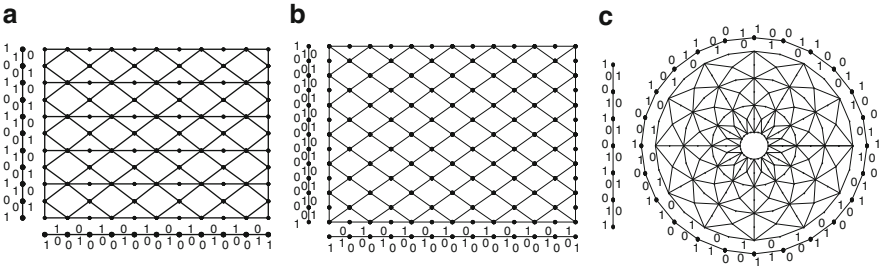

Fig. 3.26 Three weighted Cartesian direct graph products

and new configurations, Kaveh and Nouri [6] generated new models in the forms of the classic products with assigning weights to the nodes and elements of the generators.

Assigning weights to the nodes and defining new conditions according to these weights can have a wide range of applications and can make it possible to generate many other different configurations which are impossible to be generated by using classic products. In other words, the new definitions obtained by assigning nodal weights, new variables become available to consider as the adjacency conditions of the nodes in a product graph.

Using the existing graph products, only models in the form of rectangular or circular shapes can be generated with no centre node. For generating other types of configurations, we define a new graph product for generating the triangular and a wide range of polygonal shapes. By using this product, it becomes possible to generate triangular, trapezoid, parallelogram and many other combinations of triangular and rectangular shapes.

3.5.1 Weights Assigned to Nodes of the Generators and Product Graphs

The weights for the nodes of a product graph are considered the same as the sum of the weights of the nodes of the corresponding subgraphs, Fig. 3.27. Obviously assigning the weights to the nodes of a product graph according to the weights of the generators can have different types such as sum, difference or product.

After assigning weights to the nodes of a product graph, some conditions should be imposed to assess the adjacency of the nodes. First W_{MAX} is defined as the maximum weight of the subgraphs. For example, for two subgraphs with the weights [1 2 3 4 5] and [2 3 2 3 4], W_{MAX} is equal to 5. Considering the significance of W_{MAX} and using $W_{i,j}(i,j)$ and $W_{i,j}(k,l)$, the new conditions are implemented.

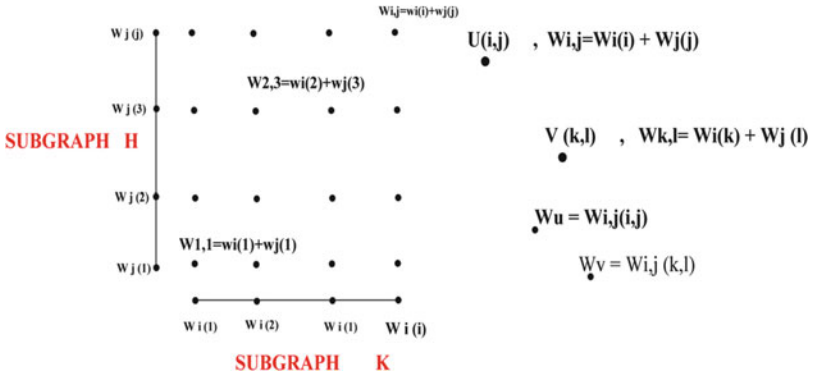

Fig. 3.27 Assigning weights to the nodes of a product graph

3.5.2 *Weighted Triangular Strong Cartesian Graph Product*

After the formation of weights of the nodes in a product graph, a member should be added between two typical nodes (U_k,V_l) and (U_i,V_j) if the following conditions are satisfied:

$$\text{Weights of the nodes}: W_{k,l} = W_i(k) + W_j(l),\ W_{i,j} = W_i(i) + W_j(j) \tag{3.13a}$$

$$\text{Weights of the elements}: W_{ik}, W_{ki,} W_{jl}, W_{lj} \tag{3.13b}$$

$$\begin{aligned}\text{If } \{&[[U_iU_k \in E(K) \text{ and } V_jV_l \in E(H)] \text{ and } [W_{i,j,}W_{k,l} = W_{\max}]]\\ &\text{or } [[[V_j = V_l \text{ and } (W_{ik} \neq 0 \text{ or } W_{ki} \neq 0)] \text{ or } [(W_{ki*}W_{lj} \neq 0 \text{ or } W_{ik*}W_{jl} \neq 0)\\ &\text{or } (W_{ik*}W_{lj} \neq 0 \text{ or } W_{ki*}W_{jl} \neq 0)]] \text{ and } [W_{i,j,}W_{k,l} \leq W_{\max}]]\}\end{aligned} \tag{3.14}$$

Four examples of grids generated by these relationships are shown in Fig. 3.28. For each configuration the corresponding weighted generators are also depicted.

3.5.3 *Weighted Triangular Semistrong Cartesian Graph Product*

In this product, both diagonal and horizontal elements can be connected. After the formation of weights of the nodes in the product graph, a member should be added between two typical nodes (U_k,V_l) and (U_i,V_j) if the following conditions are satisfied:

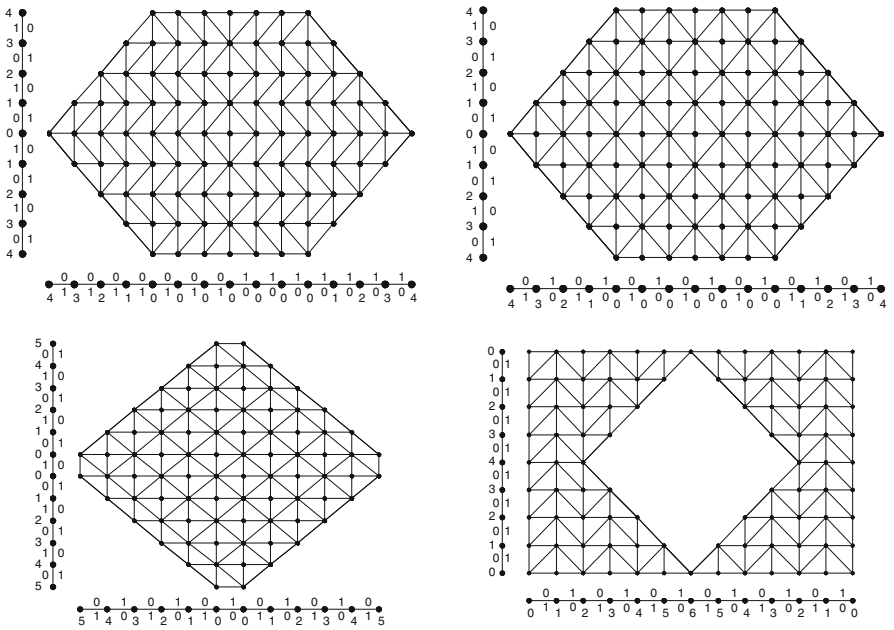

Fig. 3.28 Four weighted triangular strong Cartesian graph products

Using the same definitions as Eqs. 3.13a and 3.13b,

$$\begin{aligned}\text{If } \{ [[U_i U_k \in E(K) \text{ and } V_j V_l \in E(H)] \text{ and } [W_{i,j}, W_{k,l} = W_{\max}]] \\ \text{or } [[[V_j = V_l \text{ and } (W_{ik} \neq 0 \text{ or } W_{ki} \neq 0)] \text{ or } [(W_{ki} * W_{lj} \neq 0 \text{ or } W_{ik} * W_{jl} \neq 0) \\ \text{or } (W_{ik} * W_{lj} \neq 0 \text{ or } W_{ki} * W_{jl} \neq 0)]] \text{ and } [W_{i,j}, W_{k,l} \leq W_{\max}]] \}\end{aligned} \tag{3.15}$$

Two examples of grids generated by these relationships are shown in Fig. 3.29. For each configuration the corresponding weighted generators are also depicted.

3.6 Definition of a Weighted Circular Graph Product

In the field of space structures, domes are of special importance. From the structural point of view, domes are always similar to solid circular-shaped models. For configuring solid circles using graph products, one should either use the transformation of product graph of two paths or the graph product of a path, and a cycle should be employed. Another graph for covering the central part can be added. In this section, a new graph product is defined to configure solid circular-shaped models.

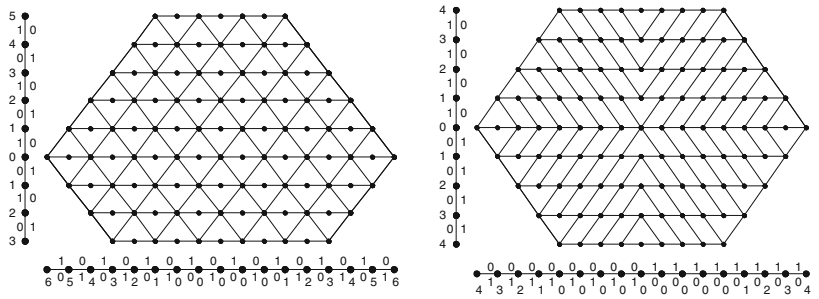

Fig. 3.29 Two weighted triangular semistrong Cartesian products

3.6.1 Weighted Circular Cartesian Graph Products

In this product weights are assigned to the nodes of the subgraphs, and the conditions and definitions of this product are based on these weights. In this product, the conditions are merely provided for the adjacency of the vertical and horizontal elements. Two nodes, (U_i,V_j) and (U_k,V_l), in the product graph, with the weights W_i, W_j, W_k and W_l, and with the weights W_{ik}, $W_{ki,}$ W_{jl} and W_{lj} for elements, are adjacent if the following conditions are fulfilled:

$$
\begin{aligned}
&\text{If } \{[[[U_i = U_k \text{ and } W_i = 0 \text{ and } (W_{jl} \neq 0 \text{ and } W_{lj} \neq 0)]\\
&\quad \text{or } [U_i = U_k \text{ and } W_i \neq 0 \text{ and } (W_{jl} * W_{lj} = 0 \text{ and } (W_{jl} \neq 0 \text{ or } W_{lj} \neq 0))]\\
&\quad \text{or } [V_j = V_l \text{ and } W_j = 0 \text{ and } (W_{ik} \neq 0 \text{ and } W_{ki} \neq 0)]\\
&\quad \text{or } [V_j = V_l \text{ and } W_j \neq 0 \text{ and } (W_{ik} * W_{ki} = 0 \text{ and } (W_{ik} \neq 0 \text{ or } W_{ki} \neq 0))]]\\
&\quad \text{and } [W_{j,} W_l \leq 1]] \textbf{ or } [[[V_j V_l \in \mathrm{E(K)}] \text{ and } [W_j > 1 \text{ and } i = 1]]\\
&\quad \text{and } [[W_k = 0 \text{ and } W_{jl} * W_{lj} \neq 0]\\
&\quad \text{or } [W_k \neq 0 \text{ and } W_{jl} * W_{lj} = 0 \text{ and } (W_{jl} \neq 0 \text{ or } W_{lj} \neq 0)]]]\}
\end{aligned}
\tag{3.16}
$$

Some examples of this product are demonstrated in Fig. 3.30.

3.6.2 Weighted Circular Strong Cartesian Graph Product

In this product, the nodes of generators are assigned some weights, and conditions are defined based on the weights. Using this product the nodes (U_i,V_j) and (U_k,V_l) in the product graph which the weights W_i, W_j, W_k and W_l are assigned to the nodes and also the weights W_{ik}, $W_{ki,}$ W_{jl}, W_{lj} assigned to the elements will be connected if the following conditions are fulfilled:

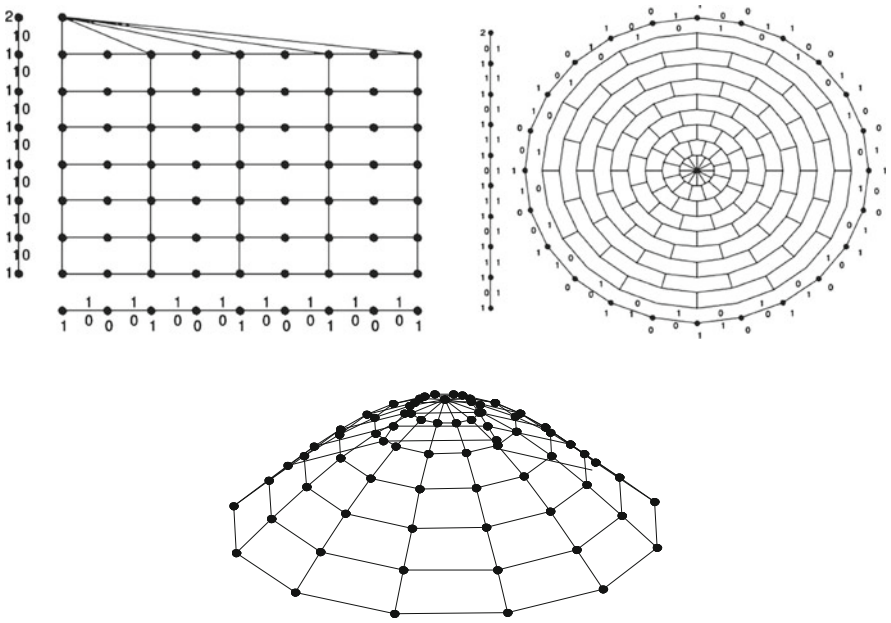

Fig. 3.30 Three weighted circular Cartesian products

$$\begin{aligned}\text{If } \{&[[[U_i = U_k \text{ and } (W_{jl} \neq 0 \text{ or } W_{lj} \neq 0)] \text{or} [V_j = V_l \text{ and } (W_{ik} \neq 0 \text{ or } W_{ki} \neq 0)]\\ &\text{or} [W_{ki} \neq 0 \text{ or } W_{lj} \neq 0]] \text{and} [W_j, W_l \leq 1]]\\ &\textbf{or} [[V_j V_l \in E(K)] \text{and} [W_j > 1 \text{ and } i = 1]]\}\end{aligned} \tag{3.17}$$

Some examples of this product are illustrated in Fig. 3.31.

3.6.3 Weighted Circular Direct Graph Product

In this product only the diagonal elements will be connected. The nodes of generators are weighted and conditions are defined based on the weights. Using this product, the nodes (U_i,V_j) and (U_k,V_l) in the product graph which the weights W_i, W_j, W_k and W_l assigned to them will be connected if the following conditions are fulfilled:

$$\begin{aligned}\text{If } \{&[[W_{ki} \neq 0 \text{ or } W_{lj} \neq 0] \text{ and} [W_j, W_l \leq 1]]\\ &\textbf{or} [[V_j V_l \in \text{E(K)}] \text{and} [W_j > 1 \text{ and } i = 1]]\}\end{aligned} \tag{3.18}$$

Some examples of this product are demonstrated in Fig. 3.32.

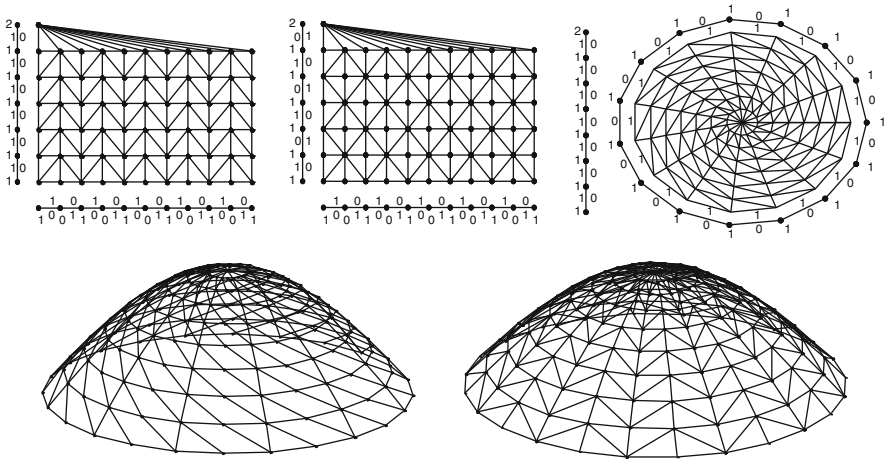

Fig. 3.31 Five weighted circular strong Cartesian products

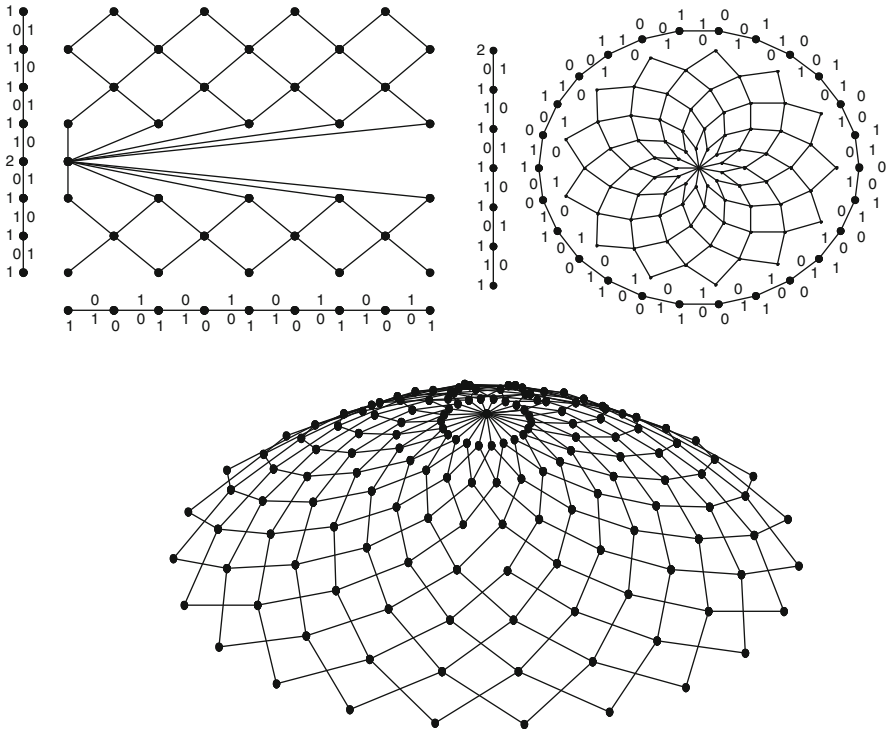

Fig. 3.32 Three weighted circular direct products

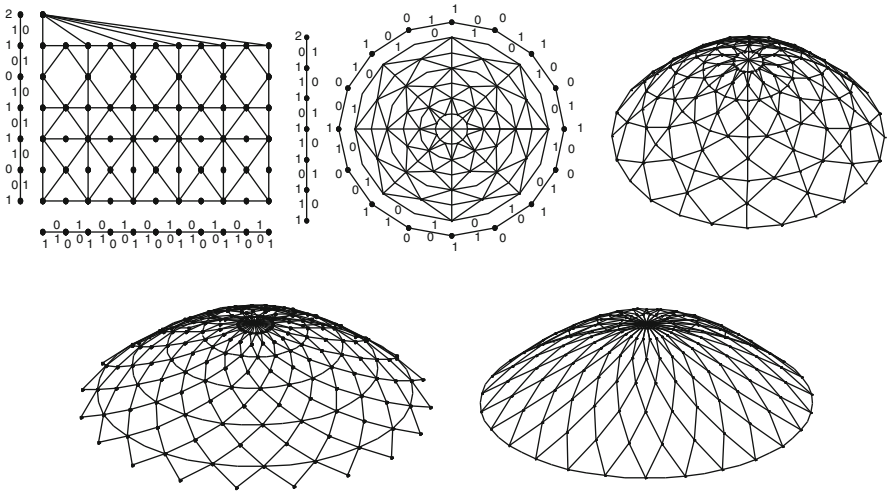

Fig. 3.33 Five weighted circular Cartesian direct products

3.6.4 Weighted Circular Cartesian Direct Graph Product

In this product, only the diagonal elements will be connected. The nodes of generators are weighted and conditions are defined based on the weights. Using this product, the nodes (U_i,V_j) and (U_k,V_l) in the product graph which the weights W_i, W_j, W_k and W_l are assigned to them will be connected if the following conditions are fulfilled:

$$
\begin{aligned}
\text{If } \{ & [[[U_i = U_k \text{ and } W_i = 0 \text{ and} (W_{jl} \neq 0 \text{ and } W_{lj} \neq 0)]. \\
& \text{or} [U_i = U_k \text{ and } W_i \neq 0 \text{ and} (W_{jl}{}^* W_{lj} = 0 \text{ and } (W_{jl} \neq 0 \text{ or } W_{lj} \neq 0))] \\
& \text{or} [V_j = V_l \text{ and } W_j = 0 \text{ and} (W_{ik} \neq 0 \text{ and } W_{ki} \neq 0)] \\
& \text{or} [V_j = V_l \text{ and } W_j \neq 0 \text{ and} (W_{ik} * W_{ki} = 0 \text{ and } (W_{ik} \neq 0 \text{ or } W_{ki} \neq 0))]] \\
& \text{and} [W_j, W_l \leq 1]] \textbf{ or} [[W_{ki} \neq 0 \text{ or } W_{lj} \neq 0] \text{and} [W_j, W_l \leq 1]] \\
& \textbf{or} [[V_j V_l \in E(K)] \text{and} [W_j > 1 \,\&\, i = 1]] \}
\end{aligned}
\tag{3.19}
$$

Some examples of this product are demonstrated in Fig. 3.33.

3.7 Weighted Cut-Out in Graph Products

Utilising all the previous products, the product graphs have continuous and regular shapes, and all of the nodes in the inner panels are connected. However, some models are in forms where there exist some inner panels as hollow and some nodes have no connections with the other nodes. On the other hand, the connected elements to some

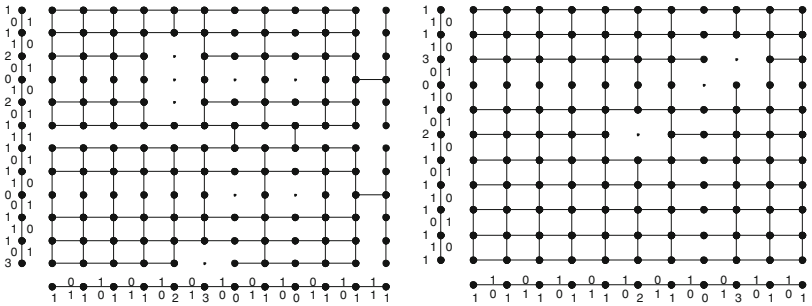

Fig. 3.34 Two weighted cut-out Cartesian products

nodes must be eliminated. In this section a new graph product for eliminating an optional node or nodes with the connected elements (stars) is defined. Using this product, all the nodes in the product graph which have equal or larger weight than a specified value will have no connections with the other nodes and elements.

3.7.1 Weighted Cut-Outs in Cartesian Graph Product Models

This graph product provides the conditions for connecting vertical and horizontal elements according to the weights of the generators. Using this product, the nodes (U_i,V_j) and (U_k,V_l) in the product graph with weights W_i, W_j, W_k and W_l assigned to them are connected if the following conditions are fulfilled:

$$
\begin{aligned}
\text{If } \{ & [[U_i = U_k \text{ and } W_i = 0 \text{ and } (W_{jl} \neq 0 \text{ and } W_{lj} \neq 0)] \\
& \text{or } [U_i = U_k \text{ and } W_i \neq 0 \text{ and } (W_{jl}{}^* W_{lj} = 0 \text{ and } (W_{jl} \neq 0 \text{ or } W_{lj} \neq 0))] \\
& \text{or } [V_j = V_l \text{ and } W_j = 0 \text{ and } (W_{ik} \neq 0 \text{ and } W_{ki} \neq 0)] \\
& \text{or } [V_j = V_l \text{ and } W_j \neq 0 \text{ and } (W_{ik}{}^* W_{ki} = 0 \text{ and } (W_{ik} \neq 0 \text{ or } W_{ki} \neq 0))]] \\
& \textbf{and } [[W_i,\ W_j,\ W_k,\ W_l \leq 1] \text{or} [W_i \neq W_j \text{ and } W_k \neq W_l]]\}
\end{aligned}
\tag{3.20}
$$

Examples of this product are demonstrated in Fig. 3.34.

3.7.2 Weighted Cut-Out Cartesian Direct Graph Product

This product provides the conditions for connecting vertical, horizontal and diagonal elements according to the weights of the generators. Using this product, the nodes (U_i,V_j) and (U_k,V_l) in the product graph which the weights W_i, W_j, W_k and W_l assigned to them and also the weights W_{ik}, W_{ki}, W_{jl} and W_{lj} assigned to the elements will be connected if the following conditions are fulfilled:

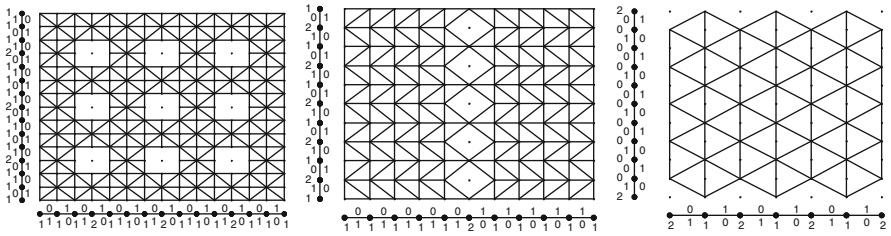

Fig. 3.35 Weighted cut-out Cartesian direct products

$$
\begin{aligned}
&\text{If } \{[[U_i = U_k \text{ and } W_i = 0 \text{ and} (W_{jl} \neq 0 \text{ and } \ W_{lj} \neq 0)] \\
&\quad \text{or} [U_i = U_k \text{ and } W_i \neq 0 \text{ and} (W_{jl}{}^* \, W_{lj} = 0 \text{ and} (W_{jl} \neq 0 \text{ or } W_{lj} \neq 0))] \\
&\quad \text{or} [V_j = V_l \text{ and } W_j = 0 \text{ and} (W_{ik} \neq 0 \text{ and } W_{ki} \neq 0)] \\
&\quad \text{or} [V_j = V_l \text{ and } W_j \neq 0 \text{ and} (W_{ik}{}^* \, W_{ki} = 0 \text{ and} (W_{ik} \neq 0 \text{ or } W_{ki} \neq 0))] \\
&\quad \text{or} [W_{ki} \neq 0 \text{ or } W_{lj} \neq 0]] \\
&\quad \textbf{and} [[W_i, \ W_j, \ W_k, \ W_l \ \leq 1] \text{or} [W_i \neq W_j \,\&\, W_k \neq W_l]]\}
\end{aligned}
\tag{3.21}
$$

Some examples of this product are demonstrated in Fig. 3.35.

3.7.3 Weighted Cut-Out Strong Cartesian Graph Product

In this product conditions consist of direct graph product conditions and a new condition for deleting the special nodes with special weights. Thus, in this product, only the diagonal elements will be connected.

Using this product, the nodes (U_i,V_j) and (U_k,V_l) in the product graph which the weights W_i, W_j, W_k and W_l are assigned to them will be connected if the following conditions are fulfilled:

$$
\begin{aligned}
&\text{If } \{[[U_i = U_k \text{ and } (W_{jl} \neq 0 \text{ or } W_{lj} \neq 0)] \\
&\quad \text{or} [V_j = V_l \text{ and } (W_{ik} \neq 0 \text{ or } \ W_{ki} \neq 0)] \text{or} [W_{ki} \neq 0 \text{ or } W_{lj} \neq 0]] \\
&\quad \textbf{and} [[W_i, \ W_j, \ W_k, \ W_l \leq 1] \text{or} [W_i \neq W_j \text{ and } W_k \neq W_l]]\}
\end{aligned}
\tag{3.22}
$$

Some examples of this product are demonstrated in Fig. 3.36.

3.7.4 Weighted Cut-Out Semistrong Cartesian Graph Product

In this product conditions consist of direct graph product conditions and a new condition for deleting the special nodes with special weights. Thus, in this product, only the diagonal elements will be connected.

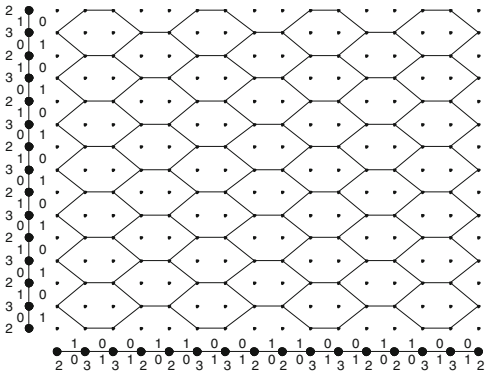

Fig. 3.36 Weighted cut-out strong Cartesian product

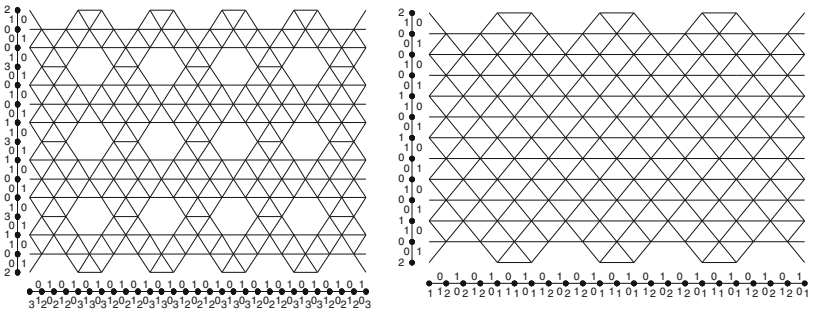

Fig. 3.37 Weighted cut-out semistrong Cartesian products

Using this product, the nodes (U_i,V_j) and (U_k,V_l) in the product graph which the weights W_i, W_j, W_k and W_l are assigned to them will be connected if the following conditions are fulfilled:

$$\begin{aligned}\text{If } \{ [[V_j = V_l \text{ and } (W_{ik} \neq 0 \text{ or } W_{ki} \neq 0)] \text{or} [W_{ki} \neq 0 \text{ or } W_{lj} \neq 0]] \\ \textbf{and} [[W_i,\ W_j,\ W_k,\ W_l \leq 1] \text{or} [W_i \neq W_j \text{ and } \mathrm{W_k} \neq \mathrm{W_l}]] \}\end{aligned} \tag{3.23}$$

Some examples of this product are demonstrated in Fig. 3.37.

3.8 Covered Graph Products

By using the new graph products, a vast amount of different shapes and models can be generated; however, in some product graphs, it is necessary to choose or eliminate some parts of the shape of the product graph to generate the desired models. On the other hand, for generating the other shapes, it is often necessary to select some parts of the previous models. In this section by adding a condition to

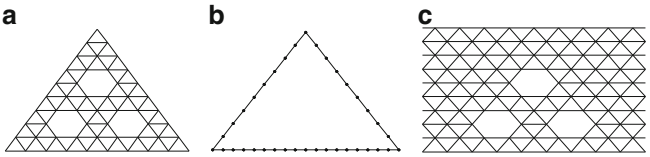

Fig. 3.38 Three cut-out direct products

the previous conditions, it becomes possible to select the desired part of the product graph. This condition is implemented by assigning some other weights to the nodes of the subgraphs. This means that the primary elemental and nodal weights generate the full parts of the shapes and the secondary nodal weights select or eliminate the desired part of the original shape or model. Even it is possible to increase the number of selecting process by assigning additional weights to the nodes of the subgraphs. For understanding the importance of this product, three shapes are illustrated where the shape 3.38a can not directly be generated by the prior graph products, but by cutting the shape 3.38b from the shape 3.38c, shape 3.38a can be produced. The constitution of the covered product is similar to this cutting process.

3.8.1 Covered Cut-Out Cartesian Graph Product

After the formation of weights of the nodes in the product graph according to the following relations:

$$\begin{aligned}&\text{Weights of the nodes for product graph}: W_{2i,2j}\\&= W_{2i}(i) + W_{2j}(j), W_{2k,2l} = W_{2i}(k) + W_{2j}(l)\end{aligned} \tag{3.24a}$$

$$\text{Weights of the nodes for subgraph}: W_{1i}, W_{1j},\ W_{1k}, W_{1l} \text{ and } W_{2i}, W_{2j},\ W_{2k}, W_{2l} \tag{3.24b}$$

$$\text{Weights of the elements}: W_{ik},\ W_{ki,}W_{jl},\ W_{lj} \tag{3.24c}$$

A member should be added between two typical nodes (U_k,V_l) and (U_i,V_j) if the following conditions are satisfied:

$$\begin{aligned}\text{If } \{&[[U_i = U_k \text{ and } V_jV_l \in \mathrm{E(K)}] \text{or} [U_iU_k \in \mathrm{E(H)} \text{ and } V_j = V_l]]\\&\textbf{and}\,[W_{1i},\ W_{1j},\ W_{1k},\ W_{1l} \le 1] \text{or} [W_{1i} \ne W_{1j} \text{ and } W_{1k} \ne W_{1l}]\\&\textbf{and}\,[W_{2i,2j,}W_{2k,2l} \le W_{2\max}]\}\end{aligned} \tag{3.25}$$

Some examples of this product are demonstrated in Fig. 3.39.

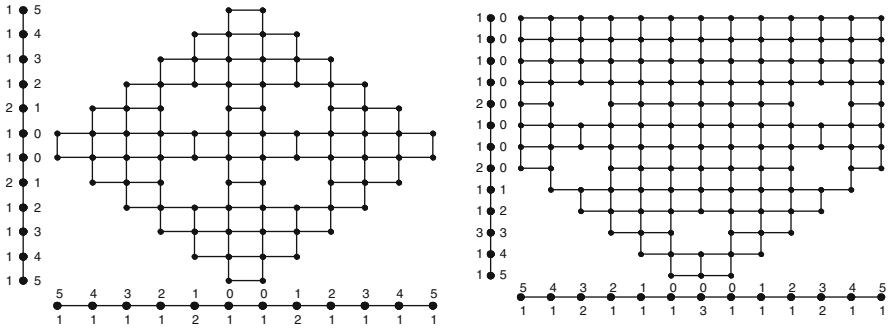

Fig. 3.39 Covered cut-out Cartesian graph products

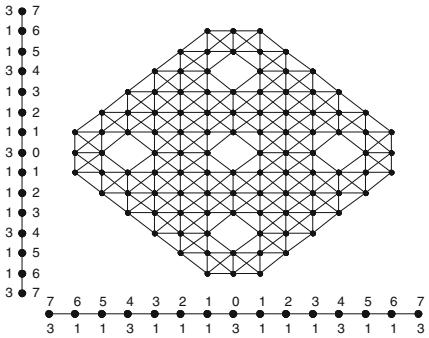

Fig. 3.40 Covered cut-out strong Cartesian graph product

3.8.2 Covered Cut-Out Strong Cartesian Graph Product

Using this product, the nodes (U_i,V_j) and (U_k,V_l) in the product graph which the weights W_i, W_j, W_k and W_l are assigned to them will be connected if the following conditions are fulfilled:

$$\begin{aligned}
&\text{If } \Big\{\Big[\big[U_i = U_k \text{ and } V_jV_l \in \mathrm{E(K)}\big] \text{or} \big[U_iU_k \in \mathrm{E(H)} \text{ and } V_j = V_l\big]\\
&\quad \text{or} \big[U_iU_k \in \mathrm{E(K)} \text{ and } V_jV_l \in \mathrm{E(H)}\big]\Big]\\
&\quad \textbf{and} \Big[\big[W_{1i},\ W_{1j},\ W_{1k},\ W_{1l} \le 1\big] \text{or} \big[W_{1i} \ne W_{1j} \text{ and } W_{1k} \ne W_{1l}\big]\Big]\\
&\quad \textbf{and} \big[W_{2i,2j,}W_{2k,2l} \le W_{2\max}\big]\Big\}
\end{aligned} \tag{3.26}$$

Some examples of this product are demonstrated in Fig. 3.40.

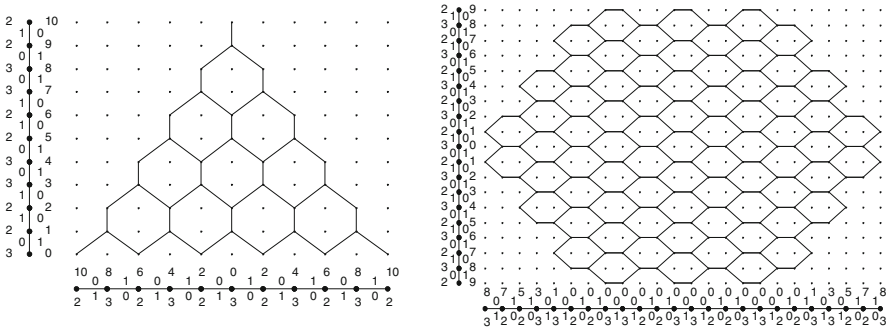

Fig. 3.41 Weighted covered cut-out strong Cartesian graph products

3.8.3 Weighted Covered Cut-Out Strong Cartesian Graph Product

Using this product the nodes (U_i,V_j) and (U_k,V_l) in the product graph which the weights W_i, W_j, W_k and W_l are assigned to them will be connected if the following conditions are fulfilled:

$$\begin{aligned}&\text{If } \{[[U_i = U_k \text{ and} (W_{jl} \neq 0 \text{ or } W_{lj} \neq 0)] \text{or} [V_j = V_l \text{ and } (W_{ik} \neq 0 \text{ or } W_{ki} \neq 0)]\\ &\quad \text{or} [W_{ki} \neq 0 \text{ or } W_{lj} \neq 0]\\ &\quad \textbf{and} [[W_{1i},\ W_{1j},\ W_{1k},\ W_{1l} \leq 1] \text{or} [W_{1i} \neq W_{1j} \text{ and } W_{1k} \neq W_{1l}]]\\ &\quad \textbf{and} [W_{2i,2j,} W_{2k,2l} \leq W_{2\max}]\}\end{aligned} \tag{3.27}$$

Some examples of this product are demonstrated in Fig. 3.41.

3.8.4 Weighted Covered Cut-Out Semistrong Cartesian Graph Product

Using this product, the nodes (U_i,V_j) and (U_k,V_l) in the product graph where the weights W_i, W_j, W_k and W_l are assigned to them will be connected if the following conditions are fulfilled:

$$\begin{aligned}&\text{If } \{[[V_j = V_l \text{ and } (W_{ik} \neq 0 \text{ or } W_{ki} \neq 0)] \text{or} [W_{ki} \neq 0 \text{ or } W_{lj} \neq 0]]\\ &\quad \textbf{and} [[W_{1i},\ W_{1j},\ W_{1k},\ W_{1l} \leq 1] \text{or} [W_{1i} \neq W_{1j} \text{ and } \mathrm{W}_{1k} \neq \mathrm{W}_{1l}]]\\ &\quad \textbf{and} [W_{2i,2j,} W_{2k,2l} \leq W_{2\max}]\}\end{aligned} \tag{3.28}$$

Some examples of this product are shown in Fig. 3.42.

Using the weighted triangular graph product, it becomes possible to generate triangular and a wide range of polygonal-shaped configurations. It is also

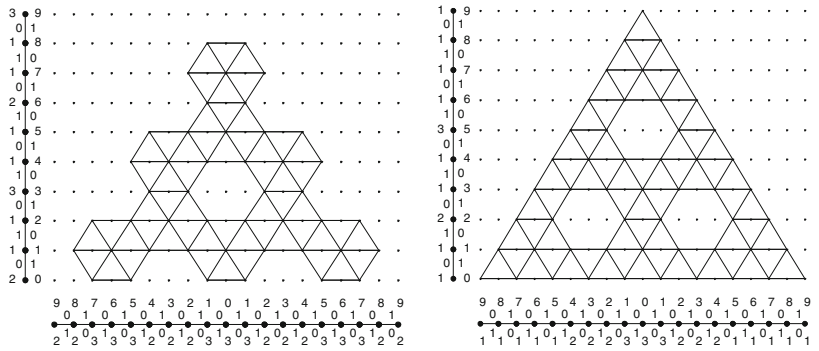

Fig. 3.42 Weighted covered cut-out semistrong Cartesian products

possible to configure triangle, trapezoid, parallelogram and many combinations of triangular- and rectangular-shaped models. Employing triangular graph products, the formation of different configurations based on a simple algebra and graph theory becomes feasible. Circular graph products make it possible to generate the solid circles which are the models of some space structures like domes.

The use of graph products reduces the storage requirement for data processing of structures, and it makes it much easier and less costly in the computer. This is obvious since in place of the data for the entire model, only the information for two much smaller subgraphs (generators) is needed to be stored.

References

1. Berge C (1973) Graphs and hypergraphs. North-Holland, Amsterdam
2. Sabidussi G (1960) Graph multiplication. Math Zeit 72:446–457
3. Harary F, Wilcox GW (1967) Boolean operations on graphs. Math Scand 20:41–51
4. Imrich W, Klavžar S (2000) Product graphs; structure and recognition. Wiley, New York
5. Kaveh A, Koohestani K (2008) Graph products for configuration processing of space structures. Comput Struct 86:1219–1236
6. Kaveh A, Nouri M (2009) Weighted graph products for configuration processing of planar and space structures. Int J Space Struct 24(1):13–26
7. Kaveh A, Beheshti S (2012) Weighted triangular and circular graph products for configuration processing. Period Polytech-Civil Eng 56(1):1–9
8. Kaveh A, Beheshti S (2013) New graph products for configuration processing. Int J Civil Eng 11(2):67–76
9. Gross J, Yellen J (1998) Graph theory and its applications. CRC Press, New York
10. Weichsel PM (1962) The Kronecker product of graphs. Proc Amer Math Soc 13:47–52

Chapter 4
Canonical Forms, Basic Definitions and Properties

4.1 Introduction

In this chapter, linear algebra is employed for the study of symmetry, followed by graph-theoretical interpretations. The application of the methods presented in this chapter is not limited to geometric symmetry. Thus, the symmetry studied here can more appropriately be considered as *topological symmetry*. The methods considered in this chapter can be considered as special techniques for transforming the matrices into block triangular forms. These forms allow good saving of computation effort for many important problems such as computing determinants, eigenvalue problems and solution of linear system of equations. For each of these tasks with dimension N, the computing cost grows approximately with N^3. Therefore, reducing, for example, the dimension to N/2, the effort decreases eight times which is a great advantage.

Here different canonical forms are presented. Methods are developed for decomposing and healing of the graph models associated with these forms for efficient calculation of the eigenvalues of matrices associated with these forms [1–5]. The formation of divisors and co-divisors, using a graph-theoretical approach, is developed by Rempel and Schwolow [6] and well described in reference [7]. Here, only symmetric forms are presented, since simple graph-theoretical concepts are sufficient for their formation. Two important forms known as tri-diagonal and penta-diagonal forms are also presented, and methods are provided for their decomposition. It is shown that different canonical forms can be derived from the block tri-diagonal form [8, 9].

4.2 Decomposition of Matrices to Special Forms

In this section, a $2N \times 2N$ symmetric matrix $\mathbf{M}$ is considered with all entries being real. For four canonical forms, the eigenvalues of $\mathbf{M}$ are obtained using the properties of its submatrices.

A. Kaveh, *Optimal Analysis of Structures by Concepts of Symmetry and Regularity*,
DOI 10.1007/978-3-7091-1565-7_4,

4.2.1 Canonical Form I

In this case, matrix $\mathbf{M}$ has the following pattern:

$$\mathbf{M} = \left[\begin{array}{c|c} \mathbf{A}_{N\times N} & \mathbf{0}_{N\times N} \\ \hline \mathbf{0}_{N\times N} & \mathbf{A}_{N\times N} \end{array}\right]_{2N\times 2N} \tag{4.1}$$

Considering the set of eigenvalues of the submatrix $\mathbf{A}$ as $\{\lambda\mathbf{A}\}$, the set of eigenvalues of $\mathbf{M}$ can be obtained as follows:

$$\{\lambda\mathbf{M}\} = \{\lambda\mathbf{A}\}\overline{\cup}\{\lambda\mathbf{A}\}. \tag{4.2}$$

where the sign $\overline{\cup}$ is used for the collection of the eigenvalues of the submatrices and not necessarily their union.

Since $\det \mathbf{M} = \det \mathbf{A} \times \det \mathbf{A}$, the proof becomes evident. Here 'det' stands for the determinant.

Form I can be generalised to a decomposed form with diagonal submatrices $\mathbf{A}_1$, $\mathbf{A}_2$, $\mathbf{A}_3$, …, $\mathbf{A}_p$ of different dimensions, and the eigenvalues can be calculated as follows:

$$\{\lambda\mathbf{M}\} = \{\lambda\mathbf{A}_1\}\overline{\cup}\{\lambda\mathbf{A}_2\}\overline{\cup}\{\lambda\mathbf{A}_3\}\overline{\cup}\ \ldots\ \overline{\cup}\{\lambda\mathbf{A}_p\}. \tag{4.3}$$

The proof follows from the fact that $\det \mathbf{M} = \det \mathbf{A}_1 \times \det \mathbf{A}_2 \times \det \mathbf{A}_3 \times \ldots \times \det \mathbf{A}_p$.

Example 4.1. Consider the matrix $\mathbf{M}$ as follows:

$$\mathrm{M} = \left[\begin{array}{cc|cc} 1 & 2 & 0 & 0 \\ 3 & 4 & 0 & 0 \\ \hline 0 & 0 & 1 & 2 \\ 0 & 0 & 3 & 4 \end{array}\right],$$

with $\mathbf{A} = \begin{bmatrix} 1 & 2 \\ 3 & 4 \end{bmatrix}$.

Since $\{\lambda\mathbf{A}\} = \{-0.3723,\ 5.3723\}$, therefore $\{\lambda\mathbf{M}\} = \{-0.3723,\ 5.3723,\ -0.3723,\ 5.3723\}$.

4.2.2 Canonical Form II

For this case, matrix $\mathbf{M}$ can be decomposed into the following form:

$$\mathbf{M} = \left[\begin{array}{c|c} \mathbf{A}_{N\times N} & \mathbf{B}_{N\times N} \\ \hline \mathbf{B}_{N\times N} & \mathbf{A}_{N\times N} \end{array}\right]_{2N\times 2N} \tag{4.4}$$

The eigenvalues of $\mathbf{M}$ can be calculated as follows:

$$\{\lambda\mathbf{M}\} = \{\lambda\mathbf{C}\}\overline{\cup}\{\lambda\mathbf{D}\}. \tag{4.5}$$

$\mathbf{C}$ and $\mathbf{D}$ are called *condensed submatrices* of $\mathbf{M}$.

Proof. In block form, addition of the second column of the matrix $\mathbf{M}$ to the first column and reducing the first row from the second row results in

$$\begin{bmatrix} \mathbf{A}+\mathbf{B} & \mathbf{B} \\ \mathbf{A}+\mathbf{B} & \mathbf{A} \end{bmatrix} \Rightarrow \left[\begin{array}{c|c} \mathbf{A}+\mathbf{B} & \mathbf{B} \\ \hline \mathbf{0} & \mathbf{A}-\mathbf{B} \end{array}\right] = \left[\begin{array}{c|c} \mathbf{C} & \mathbf{B} \\ \hline \mathbf{0} & \mathbf{D} \end{array}\right] \tag{4.6}$$

where

$$\mathbf{C} = \mathbf{A}+\mathbf{B} \text{ and } \mathbf{D} = \mathbf{A}-\mathbf{B}, \tag{4.7}$$

and

$$\det\,\mathbf{M} = \det\mathbf{C} \times \det\mathbf{D}, \tag{4.8}$$

and the proof is complete.

Example 4.2. Consider the matrix $\mathbf{M}$ as follows:

$$\mathbf{M} = \left[\begin{array}{cc|cc} 10 & 15 & 8 & 2 \\ 16 & 20 & 4 & -3 \\ \hline 8 & 2 & 10 & 15 \\ 4 & -3 & 16 & 20 \end{array}\right]$$

This matrix has the pattern of Form II and is decomposed according to Eq. 4.4, leading to

$$\mathbf{A} = \begin{bmatrix} 10 & 15 \\ 16 & 20 \end{bmatrix} \text{and } \mathbf{B} = \begin{bmatrix} 8 & 2 \\ 4 & -3 \end{bmatrix}.$$

Matrices $\mathbf{C}$ and $\mathbf{D}$ are formed using Eq. 4.5 as

$$\mathbf{C} = \mathbf{A}+\mathbf{B} = \begin{bmatrix} 18 & 17 \\ 20 & 17 \end{bmatrix}, \text{ and } \mathbf{D} = \mathbf{A}-\mathbf{B} = \begin{bmatrix} 2 & 13 \\ 12 & 23 \end{bmatrix}.$$

For these matrices, the eigenvalues are

$$\{\lambda\mathbf{C}\} = \{35.9459, -0.9459\} \text{ and } \{\lambda\mathbf{D}\} = \{-3.8172,\ 28.8172\};$$

hence,

$$\{\lambda\mathbf{M}\} = \{\lambda\mathbf{C}\}\overline{\cup}\{\lambda\mathbf{D}\} = \{-0.9459, -3.8172,\ 28.8172,\ 35.9459\}.$$

4.2.3 Canonical Form III

This form has a Form II submatrix augmented by some rows and columns as shown in the following:

$$\mathbf{M} = \begin{bmatrix} \mathbf{A} & \mathbf{B} & L_{11} \ldots L_{1k} \\ & & L_{21} \ldots L_{2k} \\ & & \vdots \quad \vdots \\ & & L_{N1} \ldots L_{Nk} \\ \mathbf{B} & \mathbf{A} & L_{11} \ldots L_{1k} \\ & & L_{21} \ldots L_{2k} \\ & & \vdots \quad \vdots \\ & & L_{N1} \ldots L_{Nk} \\ C(2N+1,1) \ldots C(2N+1,2N) & & C(2N+1,2N+1) \ldots C(2N+1,2N+k) \\ \vdots \quad \vdots & & \vdots \quad \vdots \\ Z(2N+k,1) \ldots Z(2N+k,2N) & & Z(2N+k,2N+1) \ldots Z(2N+k,2N+k) \end{bmatrix} \tag{4.9}$$

where $\mathbf{M}$ is a $(2N + k) \times (2N + k)$ matrix, with a $2N \times 2N$ submatrix with the pattern of Form II, and k augmented columns and rows. The entries of the augmented columns at the top right-hand side are $L_{1i}, L_{2i}, \ldots, L_{Ni}$ $(i = 1, \ldots, k)$ and then repeated again, and all the entries of $\mathbf{M}$ are real numbers.

Now $\mathbf{D}$ is obtained as $\mathbf{D} = \mathbf{A} - \mathbf{B}$, and $\mathbf{E}$ is constructed as the following:

$$\mathbf{E} = \begin{bmatrix} \mathbf{A}+\mathbf{B} & L_{11} \ldots L_{1k} \\ & L_{21} \ldots L_{2k} \\ & \vdots \quad \vdots \\ & L_{N1} \ldots L_{Nk} \\ C(2N+1,1)+C(2N+1,N+1) \ldots & C(2N+1,2N+1) \ldots C(2N+1,2N+k) \\ \vdots \quad \vdots & \vdots \quad \vdots \\ Z(2N+k,1)+Z(2N+k,N+1) \ldots & Z(2N+k,2N+1) \ldots Z(2N+k,2N+k) \end{bmatrix} \tag{4.10}$$

$\mathbf{D}$ is an $N \times N$ matrix and $\mathbf{E}$ is an $(N + k) \times (N + k)$ matrix. The set of eigenvalues for $\mathbf{M}$ is obtained as follows:

$$\{\lambda\mathbf{M}\} = \{\lambda\mathbf{D}\}\overline{\cup}\{\lambda\mathbf{E}\}. \tag{4.11}$$

Proof. Similar to Form II, $\mathbf{M}$ can be factored by rows and columns permutation. In this case, first the augmented rows and columns are transformed into the central part of the matrix. The last column (in block form) is added to the first column, followed by reducing the first row from the last row.

$$\begin{aligned}\mathbf{M} = \begin{bmatrix} \mathbf{A} & \mathbf{B} & \mathbf{P} \\ \mathbf{B} & \mathbf{A} & \mathbf{P} \\ \mathbf{Q} & \mathbf{H} & \mathbf{R} \end{bmatrix} \Rightarrow \begin{bmatrix} \mathbf{A} & \mathbf{P} & \mathbf{B} \\ \mathbf{B} & \mathbf{P} & \mathbf{A} \\ \mathbf{Q} & \mathbf{R} & \mathbf{H} \end{bmatrix} \Rightarrow \\ \begin{bmatrix} \mathbf{A} & \mathbf{P} & \mathbf{B} \\ \mathbf{Q} & \mathbf{R} & \mathbf{H} \\ \mathbf{B} & \mathbf{P} & \mathbf{A} \end{bmatrix} \Rightarrow \begin{bmatrix} \mathbf{A}+\mathbf{B} & \mathbf{P} & \mathbf{B} \\ \mathbf{Q}+\mathbf{H} & \mathbf{R} & \mathbf{H} \\ \mathbf{B}+\mathbf{A} & \mathbf{P} & \mathbf{A} \end{bmatrix} \Rightarrow \begin{bmatrix} \mathbf{A}+\mathbf{B} & \mathbf{P} & \mathbf{B} \\ \mathbf{Q}+\mathbf{H} & \mathbf{R} & \mathbf{H} \\ \mathbf{0} & \mathbf{0} & \mathbf{A}-\mathbf{B} \end{bmatrix}\end{aligned} \tag{4.12}$$

that is, the matrix is now in a factored form.

$$\mathbf{M} = \left[\begin{array}{c|c} \mathbf{E} & \mathbf{K} \\ \hline \mathbf{0} & \mathbf{D} \end{array}\right], \tag{4.13}$$

where $\mathbf{D}$ and $\mathbf{E}$ are constructed as follows:

$$\mathbf{D} = \mathbf{A} - \mathbf{B},$$

$$\mathbf{E} = \begin{bmatrix} & & \mathrm{L}_{11} & \cdots & \mathrm{L}_{1k} \\ & \mathbf{A}+\mathbf{B} & \mathrm{L}_{21} & \cdots & \mathrm{L}_{2k} \\ & & \vdots & \cdots & \vdots \\ & & \mathrm{L}_{N1} & \cdots & \mathrm{L}_{Nk} \\ \mathrm{C}(2N+1,1)+\mathrm{C}(2N+1,N+1) & \cdots & \mathrm{C}(2N+1,2N+1) & \cdots & \mathrm{C}(2N+1,2N+k) \\ \vdots & \cdots & \vdots & \cdots & \vdots \\ \mathrm{Z}(2N+k,1)+\mathrm{Z}(2N+k,N+1) & \cdots & \mathrm{Z}(2N+k,2N+1) & \cdots & \mathrm{Z}(2N+k,2N+k) \end{bmatrix}$$

and

$$\det \mathbf{M} = \det \mathbf{D} \times \det \mathbf{E}. \tag{4.14}$$

Example 4.3. Consider a matrix $\mathbf{M}$ as follows:

$$\mathbf{M} = \left[\begin{array}{cccc|c} -1 & 0.5 & -0.7 & -0.7 & -10.3 \\ 3 & 4 & 0.8 & 0.9 & -10.3 \\ \hline -0.7 & -0.7 & -1 & 0.5 & -10.3 \\ 0.8 & 0.9 & 3 & 4 & -10.3 \\ \hline -11.3 & -12.3 & -13.3 & 1.3 & -5.7 \end{array}\right].$$

Condensed submatrices are calculated using Eq. 4.15 as follows:

$$\mathbf{D} = \begin{bmatrix} -1 & 0.5 \\ 3 & 4 \end{bmatrix} - \begin{bmatrix} -0.7 & -0.7 \\ 0.8 & 0.9 \end{bmatrix} = \begin{bmatrix} -0.3 & 1.2 \\ 2.2 & 3.1 \end{bmatrix},$$

and

$$\mathbf{E} = \begin{bmatrix} -1-0.7 & 0.5-0.7 & -10.3 \\ 3+0.8 & 4+0.9 & -10.3 \\ -13.3-11.3 & -12.3+1.3 & -5.7 \end{bmatrix} = \begin{bmatrix} -1.7 & -0.2 & -10.3 \\ 3.8 & 4.9 & -10.3 \\ -24.6 & -11 & -5.7 \end{bmatrix}.$$

Eigenvalues for **D** and **E** are calculated as follows:

$$\{\lambda\mathbf{D}\} = \{-0.9516,\ 3.7516\},$$

$$\{\lambda\mathbf{E}\} = \{1.6224,\ 17.6885, -21.8109\}.$$

Therefore, the eigenvalues of **M** are obtained:

$$\{\lambda\mathbf{M}\} = \{\lambda\mathbf{D}\}\overline{\cup}\{\lambda\mathbf{E}\} = \{-0.9516,\ 3.7516,\ 1.6224,\ 17.6885, -21.8109\}.$$

4.2.4 Transformation of Form III into Form II

In this section, it is shown that the canonical Form III can be obtained from the canonical Form II, Ref. [10]. In order to show this property, the following results are first considered:

Let a 2N × 2N matrix **L** be augmented by an arbitrary row and a column with all zero entries, as follows:

$$\mathbf{C} = \left[\begin{array}{c|c} \mathbf{L} & \mathbf{0} \\ \hline \mathbf{X} & \mathbf{0} \end{array}\right]_{(2N+1)(2N+1)}. \tag{4.15}$$

The matrix **C** has in its (2N + 1)th column all zero entries, and the eigenvalues of **C** and **L** are identical, with the exception of an additional zero eigenvalue for **C**. This can be proved as follows:

The first 2N rows of **C** are multiplied by $k_1, k_2, \ldots, k_{2N}$, respectively, and the sum is equated to zero. Since any multiple of the last column will be zero, therefore the following equations are obtained:

$$\mathbf{LK} + \mathbf{X} = \mathbf{0}. \tag{4.16}$$

If **L** is invertible (i.e. if det (**L**) ≠ 0), then $\mathbf{K} = -\mathbf{L}^{-1}\mathbf{X}$ and $k_1, k_2, \ldots, k_{2N}$ can be found and the last row of **C** becomes zero. However, if det (**L**) = 0, then there are many sets of k_i which put the last row of **C** into zero. Therefore, one can

conclude that there is always at least one transformation that makes the last row of **C** as zero.

If the *k*th row of a matrix is multiplied in m and the *k*th column is divided by m, the eigenvalues of this matrix stay unchanged. The reason is that the magnitude of the diagonal entry stays constant, and if it is expanded with respect to a row and column, the determinant of the submatrices stays unaltered.

Algorithm. Add a zero column together with an arbitrary row with zero entry in the second column as shown in the following:

$$\begin{bmatrix} \mathbf{A} & \mathbf{B} & \mathbf{P} \\ \mathbf{B} & \mathbf{A} & \mathbf{P} \\ \mathbf{Q} & \mathbf{H} & \mathbf{R} \end{bmatrix} \Rightarrow \begin{bmatrix} \mathbf{A} & \mathbf{0} & \mathbf{B} & \mathbf{P} \\ \frac{(\mathbf{H}-\mathbf{Q})}{2} & \mathbf{0} & \frac{(\mathbf{H}-\mathbf{Q})}{2} & \mathbf{0} \\ \mathbf{B} & \mathbf{0} & \mathbf{A} & \mathbf{P} \\ \mathbf{Q} & \mathbf{0} & \mathbf{H} & \mathbf{R} \end{bmatrix}. \tag{4.17}$$

Add half of the 4th column to column 2, and add half of 4th row to row 2. Now interchange column 2 with column 4. These operations are shown in the following:

$$\begin{bmatrix} \mathbf{A} & \mathbf{P}/2 & \mathbf{B} & \mathbf{P} \\ \mathbf{H}/2 & \mathbf{R}/4 & \mathbf{Q}/2 & \mathbf{R}/2 \\ \mathbf{B} & \mathbf{P}/2 & \mathbf{A} & \mathbf{P} \\ \mathbf{Q} & \mathbf{R}/2 & \mathbf{H} & \mathbf{R} \end{bmatrix} \Rightarrow \begin{bmatrix} \mathbf{A} & \mathbf{P} & \mathbf{B} & \mathbf{P}/2 \\ \mathbf{H}/2 & \mathbf{R}/2 & \mathbf{Q}/2 & \mathbf{R}/4 \\ \mathbf{B} & \mathbf{P} & \mathbf{A} & \mathbf{P}/2 \\ \mathbf{Q} & \mathbf{R} & \mathbf{H} & \mathbf{R}/2 \end{bmatrix}. \tag{4.18}$$

Column 4 is multiplied by 2 and row 4 is multiplied by 1/2, resulting in

$$\left[\begin{array}{cc|cc} \mathbf{A} & \mathbf{P} & \mathbf{B} & \mathbf{P} \\ \frac{\mathbf{H}}{2} & \frac{\mathbf{R}}{2} & \frac{\mathbf{Q}}{2} & \frac{\mathbf{R}}{2} \\ \hline \mathbf{B} & \mathbf{P} & \mathbf{A} & \mathbf{P} \\ \frac{\mathbf{Q}}{2} & \frac{\mathbf{R}}{2} & \frac{\mathbf{H}}{2} & \frac{\mathbf{R}}{2} \end{array}\right] \Rightarrow \left[\begin{array}{c|c} \mathbf{M} & \mathbf{N} \\ \hline \mathbf{N} & \mathbf{M} \end{array}\right] \tag{4.19}$$

where

$$\begin{bmatrix} \mathbf{A} & \frac{\mathbf{P}}{2} & \mathbf{B} & \mathbf{P} \\ \frac{\mathbf{H}}{2} & \frac{\mathbf{R}}{4} & \frac{\mathbf{Q}}{2} & \frac{\mathbf{R}}{2} \\ \mathbf{B} & \frac{\mathbf{P}}{2} & \mathbf{A} & \mathbf{P} \\ \mathbf{Q} & \frac{\mathbf{R}}{2} & \mathbf{H} & \mathbf{R} \end{bmatrix} \Rightarrow \begin{bmatrix} \mathbf{A} & \mathbf{P} & \mathbf{B} & \frac{\mathbf{P}}{2} \\ \frac{\mathbf{H}}{2} & \frac{\mathbf{R}}{2} & \frac{\mathbf{Q}}{2} & \frac{\mathbf{R}}{4} \\ \mathbf{B} & \mathbf{P} & \mathbf{A} & \frac{\mathbf{P}}{2} \\ \mathbf{Q} & \mathbf{R} & \mathbf{H} & \frac{\mathbf{R}}{2} \end{bmatrix}$$

$$\mathbf{M}+\mathbf{N} = \begin{bmatrix} \mathbf{A}+\mathbf{B} & 2\mathbf{P} \\ \frac{(\mathbf{Q}+\mathbf{H})}{2} & \mathbf{R} \end{bmatrix}, \quad \mathbf{M}-\mathbf{N} = \begin{bmatrix} \mathbf{A}-\mathbf{B} & \mathbf{0} \\ \frac{(\mathbf{H}-\mathbf{Q})}{2} & \mathbf{0} \end{bmatrix}. \tag{4.20}$$

Column 2 is multiplied by 1/2, and the second row is multiplied by 2, resulting in **E**.

$$\mathbf{E} = \begin{bmatrix} \mathbf{A}+\mathbf{B} & \mathbf{P} \\ \mathbf{Q}+\mathbf{H} & \mathbf{R} \end{bmatrix}. \tag{4.21}$$

The right-hand matrix $\mathbf{M} - \mathbf{N}$ in Eq. 4.20 has the same eigenvalues as those of $\mathbf{A} - \mathbf{B}$ with exception of having 2N extra zeros. **E** and **D** are the same matrices obtained for Form III in the previous section.

4.2.5 Form IV Symmetry

Definition. Consider the following 6 × 6 matrix in a tri-diagonal form:

$$\mathbf{M} = \begin{bmatrix} s-h & h-s & & & & \\ h-s & s & -h & h-s & & \\ & -h & s & & & \\ & & h-s & s & -h & \\ & & & -h & s & h-s \\ & & & & h-s & s-h \end{bmatrix}_{6\times 6} \tag{4.22}$$

The entries of **M** have the following properties:

1. Each row-sum of this matrix is equal to zero and the row-sum of non-diagonal entries has the same value as its diagonal entry with reverse sign.
2. Matrix **M** has a central core in the following form:

$$\mathbf{C} = \left[\begin{array}{cc|cc} s & -h & & \\ -h & s & & \mathbf{Q} \\ \hline & & s & -h \\ \mathbf{Q}^t & & -h & s \end{array}\right]_{4\times 4} \quad \text{where} \quad \mathbf{Q} = \begin{bmatrix} 0 & 0 \\ h-s & 0 \end{bmatrix}. \tag{4.23}$$

The core **C** consists of two parts in Form II, with **Q** showing the type of the link between these two parts.

Matrix **M** is obtained by the addition of two rows and two columns to the beginning and end of **C**.

The characteristic polynomial of **M** can be expressed as follows:

$$\mathrm{PM}(\lambda) = [\lambda(2h - 2s + \lambda)]\left[\lambda^2 - 2s\lambda + sh - h^2\right]\left[\lambda^2 - 2s\lambda + 3sh - 3h^2\right]. \tag{4.24}$$

- The first term of this equation can be considered as the characteristic equation of the following matrix;

$$\mathbf{e}_1 = \begin{bmatrix} s-h & h-s \\ h-s & s-h \end{bmatrix} \Rightarrow \lambda\mathbf{e}_1 = \{0, -2h + 2s\}; \tag{4.25}$$

  $\mathbf{e}_1$ is a matrix of Form II.
- The second term of Eq. 4.24 can be taken as the characteristic equation of the following matrix:

$$\mathbf{e}_2 = \begin{bmatrix} s+h & -s \\ s & s-h \end{bmatrix} \Rightarrow \lambda\mathbf{e}_2 = \left\{s + \sqrt{s^2 + h^2 - sh}, s - \sqrt{s^2 + h^2 - sh}\right\}. \tag{4.26}$$

- The third part of Eq. 4.24 is treated as the characteristic equation of

$$\mathbf{e}_3 = \begin{bmatrix} 2s & 3h \\ h-s & 0 \end{bmatrix} \Rightarrow \lambda\mathbf{e}_3 = \left\{s + \sqrt{s^2 - 3sh + 3h^2}, s - \sqrt{s^2 - 3sh + 3h^2}\right\}. \tag{4.27}$$

Rearranging the entries of an arbitrary matrix **M**, one may find one or more submatrices such that the eigenvalues of these submatrices are among the eigenvalues of **M**. Then **M** is called a *reflective matrix*, and the submatrices with the above properties are called the *principal submatrices* of **M**.

Now we want to know when **M** is a reflective matrix and which submatrices of **M** are principal. Suppose

$$\mathbf{SM} = \begin{bmatrix} s & -h \\ -h & s \end{bmatrix} \tag{4.28}$$

be a principal submatrix of **M**. For **SM** we have

$$\mathbf{PSM}(\lambda) = \lambda^2 - 2s\lambda + s^2 - h^2.$$

In order to relate the eigenvalues of **SM** to those of $\mathbf{e}_3$, the polynomials of **SM** and $\mathbf{e}_3$ are equated as

$$\lambda^2 - 2s\lambda + s^2 - h^2 = \lambda^2 - 2s\lambda + 3sh - 3h^2, \tag{4.29}$$

resulting in

$$s_1 = 2h \quad \text{and} \quad s_2 = h.$$

Thus, for $s = 2h$ and $s = h$, the matrix **M** becomes reflective, and **SM** in Eq. 4.28 becomes its principal submatrix.

For $s = 2h$,

$$\mathbf{Pe}_2(\lambda) = \lambda^2 - 4h\lambda - h^2,$$

and

$$\mathbf{Pe}_3\ (\lambda) = \lambda^2 - 4h\lambda + 3h^2.$$

It is easy to show that for $s = 2h$,

$$\{\lambda\mathbf{e}_2\} \neq \{\lambda\mathbf{e}_3\},$$

and similarly

$$\{\lambda\mathbf{e}_3\} \neq \{\lambda\mathbf{e}_1\}.$$

Therefore

$$\{\lambda\mathbf{e}_1\} \cap \{\lambda\mathbf{e}_2\} \cap \{\lambda\mathbf{e}_3\} = \emptyset. \tag{4.30}$$

Hence, for $s = 2h$, the matrix **M** becomes a well-structured reflective matrix.

4.2.6 *Method for the Formation of e_1 and e_2 Matrices*

The matrix **M** of Eq. 4.22 can be considered as two Form III matrices connected to each other by a submatrix **Q** as follows:

$$\mathbf{M} = \begin{bmatrix} \text{Form III} & \mathbf{Q} \\ \mathbf{Q}^t & \text{Form III} \end{bmatrix}. \tag{4.31}$$

The upper-left part being a Form III matrix having the following condensed matrix:

$$\mathbf{M}' = \begin{bmatrix} s-h & h-s & 0 \\ h-s & s & -h \\ 0 & -h & s \end{bmatrix}. \tag{4.32}$$

This matrix has a Form II core as follows:

$$\mathbf{e}_1 = \begin{bmatrix} s-h & h-s \\ h-s & s-h \end{bmatrix}.$$

Hence, using Eq. 4.7, its factorisation leads to

$$\mathbf{e}_C = [s-h+h-s] = [0],$$

$$\mathbf{e}_D = [s-h-h+s] = [2s-2h].$$

The lower-right part of $\mathbf{M}$ in Eq. 4.22 has Form III symmetry as

$$\mathbf{M}' = \begin{bmatrix} s & -h & 0 \\ -h & s & h-s \\ 0 & h-s & s-h \end{bmatrix}, \tag{4.33}$$

with a condensed matrix:

$$\mathbf{e}_2 = \begin{bmatrix} s-(-h) & h-s+(-h) \\ h-s & s-h \end{bmatrix} = \begin{bmatrix} s+h & -s \\ h-s & s-h \end{bmatrix}.$$

The submatrices $\mathbf{e}_1$ and $\mathbf{e}_2$ are called *operative submatrices* of $\mathbf{M}$.

Example 4.4. Consider a 6×6 matrix $\mathbf{M}$ as follows:

$$\mathbf{M} = \begin{bmatrix} 3 & -3 & 0 & 0 & 0 & 0 \\ -3 & 5 & -2 & 0 & 0 & 0 \\ 0 & 2 & 5 & -3 & 0 & 0 \\ 0 & 0 & -3 & 5 & -2 & 0 \\ 0 & 0 & 0 & -2 & 5 & -3 \\ 0 & 0 & 0 & 0 & -3 & 3 \end{bmatrix}.$$

For this matrix, $s = 5$ and $h = 2$, and since $s \neq h$ and $s \neq 2h$, therefore $\mathbf{M}$ cannot be a reflective matrix.

The eigenvalues of $\mathbf{M}$ are as follows:

$$\lambda\mathbf{M} = \{0.6411, 0, 2.3542, 6, 7.6458, 9.3589\}.$$

The operative submatrices are constructed as follows:

$$\mathbf{e}_1 = \begin{bmatrix} 3 & -3+(0) \\ -3 & 5+9-2) \end{bmatrix} = \begin{bmatrix} 3 & -3 \\ -3 & 3 \end{bmatrix} \Rightarrow \lambda\mathbf{e}_1 = \{0, 6\},$$

$$\mathbf{e}_2 = \begin{bmatrix} 5-(-2) & -3+(-2) \\ -3-(0) & 3+(0) \end{bmatrix} = \begin{bmatrix} 7 & -5 \\ -3 & 3 \end{bmatrix} \Rightarrow \lambda\mathbf{e}_2 = \{9.3589, 0.6411\},$$

$$\mathbf{e}_3 = \begin{bmatrix} 2\times 5 & 3\times 2 \\ 2-5 & 0 \end{bmatrix} = \begin{bmatrix} 10 & 6 \\ -3 & 0 \end{bmatrix} \Rightarrow \lambda\mathbf{e}_3 = \{7.6458, 2.3542\}.$$

Therefore,

$$\lambda\mathbf{M} = \{\lambda\mathbf{e}_1\} \cup \{\lambda\mathbf{e}_2\} \cup \{\lambda\mathbf{e}_3\}.$$

Now if we select s = 2h with h = 1, then a reflective matrix will be formed as follows:

$$\mathbf{M} = \left[\begin{array}{cccccc} 1 & -1 & 0 & 0 & 0 & 0 \\ -1 & 2 & -1 & 0 & 0 & 0 \\ 0 & -1 & 2 & -1 & 0 & 0 \\ 0 & 0 & -1 & 2 & -1 & 0 \\ 0 & 0 & 0 & -1 & 2 & -1 \\ 0 & 0 & 0 & 0 & -1 & 1 \end{array}\right],$$

with

$$\{\lambda\mathbf{M}\} = \{0.2679, 0, 1, 2,\ 3,\ 3.7321\}.$$

The submatrix $\mathbf{e}_3$ is a principal submatrix of $\mathbf{M}$, since the eigenvalues of $\mathbf{e}_2$ are reflected in those of $\mathbf{M}$. As the eigenvalues of $\mathbf{e}_3$ have no common overlap with those of $\mathbf{e}_1$ and $\mathbf{e}_2$, hence, $\mathbf{M}$ is a well-structured reflective matrix.

The submatrices and their eigenvalues are calculated as follows:

$$\mathbf{e}_1 = \begin{bmatrix} 1 & -1 \\ -1 & 1 \end{bmatrix} \Rightarrow \lambda\mathbf{e}_1 = \{0, 2\}, \mathbf{e}_2 = \begin{bmatrix} 3 & -2 \\ -1 & 1 \end{bmatrix} \Rightarrow \lambda\mathbf{e}_2 = \{3.7321, 0.2679\},$$

$$\mathbf{e}_3 = \begin{bmatrix} 2 & -1 \\ -1 & 2 \end{bmatrix} \Rightarrow \lambda\mathbf{e}_3 = \{3, 1\}.$$

4.3 Generalization of Form IV to Higher-Order Matrices

In order to maintain the properties of the previous matrices, the row-sum of non-diagonal entries should be the same as the diagonal entry of the considered row with reverse sign.

Consider an N × N block symmetric matrix $\mathbf{M}_g$ for which the cores $\mathbf{E}_1$, $\mathbf{E}_2$ and $\mathbf{E}_3$ contain submatrices **S** and **H** in place of the entries s and h. Therefore, $\mathbf{M}_g$ can be written as follows:

$$\mathbf{M}_g = \begin{bmatrix} \mathbf{S}-\mathbf{H} & \mathbf{H}-\mathbf{S} & \mathbf{0} & \mathbf{0} & \mathbf{0} & \mathbf{0} \\ \mathbf{H}-\mathbf{S} & \mathbf{S} & -\mathbf{H} & \mathbf{0} & \mathbf{0} & \mathbf{0} \\ \mathbf{0} & -\mathbf{H} & \mathbf{S} & \mathbf{H}-\mathbf{S} & \mathbf{0} & \mathbf{0} \\ \mathbf{0} & \mathbf{0} & \mathbf{H}-\mathbf{S} & \mathbf{S} & -\mathbf{H} & \mathbf{0} \\ \mathbf{0} & \mathbf{0} & \mathbf{0} & -\mathbf{H} & \mathbf{S} & \mathbf{H}-\mathbf{S} \\ \mathbf{0} & \mathbf{0} & \mathbf{0} & \mathbf{0} & \mathbf{H}-\mathbf{S} & \mathbf{S}-\mathbf{H} \end{bmatrix}_{6N\times 6N}. \tag{4.34}$$

Since $[\mathbf{H}-\mathbf{S}]^t = [\mathbf{H}-\mathbf{S}]$, therefore $\mathbf{S}_{6\times 6}$ and $\mathbf{H}_{6\times 6}$ are both symmetric. For this matrix $\mathbf{E}_1$, $\mathbf{E}_2$ and $\mathbf{E}_3$ are calculated as follows:

$$\mathbf{E}_1 = \begin{bmatrix} \mathbf{S}-\mathbf{H} & \mathbf{H}-\mathbf{S} \\ \mathbf{H}-\mathbf{S} & \mathbf{S}-\mathbf{H} \end{bmatrix}_{2N\times 2N}, \quad \mathbf{E}_2 = \begin{bmatrix} \mathbf{S}+\mathbf{H} & -\mathbf{S} \\ \mathbf{H}-\mathbf{S} & \mathbf{S}-\mathbf{H} \end{bmatrix}_{2N\times 2N},$$
$$\text{and } \mathbf{E}_3 = \begin{bmatrix} 2\mathbf{S} & 3\mathbf{H} \\ \mathbf{H}-\mathbf{S} & \mathbf{0} \end{bmatrix}_{2N\times 2N}. \tag{4.35}$$

Example 4.5. The following 12 × 12 matrix has the required properties.

$$\mathbf{M}_g = \begin{bmatrix} 6 & -2 & -6 & 2 & 0 & 0 & 0 & 0 & 0 & 0 & 0 & 0 \\ -2 & 6 & 2 & -6 & 0 & 0 & 0 & 0 & 0 & 0 & 0 & 0 \\ -6 & 2 & 8 & 0 & -2 & -2 & 0 & 0 & 0 & 0 & 0 & 0 \\ 2 & -6 & 0 & 8 & -2 & -2 & 0 & 0 & 0 & 0 & 0 & 0 \\ 0 & 0 & -2 & -2 & 8 & 0 & -2 & -2 & 0 & 0 & 0 & 0 \\ 0 & 0 & -2 & -2 & 0 & 8 & -2 & -2 & 0 & 0 & 0 & 0 \\ 0 & 0 & 0 & 0 & -2 & -2 & 8 & 0 & -2 & -2 & 0 & 0 \\ 0 & 0 & 0 & 0 & -2 & -2 & 0 & 8 & -2 & -2 & 0 & 0 \\ 0 & 0 & 0 & 0 & 0 & 0 & -2 & -2 & 8 & 0 & -6 & 2 \\ 0 & 0 & 0 & 0 & 0 & 0 & -2 & -2 & 0 & 8 & 3 & -6 \\ 0 & 0 & 0 & 0 & 0 & 0 & 0 & 0 & -6 & 2 & 6 & -2 \\ 0 & 0 & 0 & 0 & 0 & 0 & 0 & 0 & 2 & -6 & -2 & 6 \end{bmatrix}_{12\times 12}.$$

Considering the partitioning with 2 × 2 submatrices, **S** and **H** are as follows:

$$\mathbf{S}=\begin{bmatrix}8 & 0\\ 0 & 8\end{bmatrix} \text{ and } \mathbf{H}=\begin{bmatrix}2 & 2\\ 2 & 2\end{bmatrix} \Rightarrow \mathbf{S}-\mathbf{H}=\begin{bmatrix}6 & -2\\ -2 & 6\end{bmatrix} \text{ and } \mathbf{H}-\mathbf{S}=\begin{bmatrix}-6 & 2\\ 2 & -6\end{bmatrix}.$$

Now the cores $\mathbf{E}_1$, $\mathbf{E}_2$ and $\mathbf{E}_3$ are formed as follows:

$$\mathbf{E}_1=\left[\begin{array}{cc|cc} 6 & -2 & -6 & 2\\ -2 & 6 & 2 & -6\\ \hline -6 & 2 & 6 & -2\\ 2 & -6 & -2 & 6\end{array}\right].$$

$\mathbf{E}_1$ itself has a Form II symmetry, and using Eq. 4.15 it is decomposed as follows:

$$\mathbf{E}_{1\mathrm{C}}=\begin{bmatrix}6+(-6) & -2+2\\ -2+2 & 6+(-6)\end{bmatrix}=\begin{bmatrix}0 & 0\\ 0 & 0\end{bmatrix} \Rightarrow \lambda\mathbf{E}_{1\mathrm{C}}=\{0,0\},$$

$$\mathbf{E}_{1\mathrm{D}}=\begin{bmatrix}6-(-6) & -2-(2)\\ -2-2 & 6-(-6)\end{bmatrix}=\begin{bmatrix}12 & -4\\ -4 & 12\end{bmatrix} \Rightarrow \chi\mathbf{E}_{1\mathrm{D}}=\{8,16\}.$$

Therefore,

$$\lambda\mathbf{E}_1=\{0,0,8,16\}.$$

The matrices $\mathbf{E}_2$ and $\mathbf{E}_3$ are constructed by substituting $\mathbf{S}$ and $\mathbf{H}$ in Eq. 4.38. The calculation for the eigenvalues of the submatrices in a similar manner leads to

$$\lambda\mathbf{E}_2=\{0,16,14.9282,1.0718\} \text{ and } \lambda\mathbf{E}_3=\{16,0,12,4\}.$$

Thus,

$$\lambda\mathbf{M}_{\mathrm{g}}=\{0,0,8,16,0,16,14.9282,1.0718,0,16,12,4\}.$$

Remark. Consider the central core of $\mathbf{M}_{\mathrm{g}}$ as a principal submatrix $\mathbf{M}_{\mathrm{gP}}$, that is,

$$\mathbf{M}_{\mathrm{gP}}=\left[\begin{array}{cc|cc} 8 & 0 & -6 & 2\\ 0 & 8 & 2 & -6\\ \hline -6 & 2 & 8 & 0\\ 2 & -6 & 0 & 8\end{array}\right],$$

then the eigenvalues will be

$$\lambda\mathbf{E}_3=\{0,4,12,16\}.$$

Therefore, $\mathbf{M}_{\mathrm{g}}$ is a well-structured reflective matrix.

4.4 Special Pattern Form IV Matrices

Here, the conditions are derived for having well-structured reflective matrices. Consider the following matrix:

$$\mathbf{M}_s = \begin{bmatrix} s-h & -h & & & & \\ -h & s & -h & & & \\ & -h & \boxed{\begin{matrix} s & -h \\ -h & s \end{matrix}} & -h & & \\ & & & -h & s & -h \\ & & & & -h & s-h \end{bmatrix}_{6\times 6} \tag{4.36}$$

The difference between this matrix and that of Eq. 4.22 is that in $\mathbf{M}_s$ the row-sum for rows is $s - 2h$ and not zero. The characteristic polynomial of $\mathbf{M}_s$ is as follows:

$$\begin{aligned} P\mathbf{M}_s(\lambda) = (\lambda - s)(2h - s + \lambda) \times (h - s + \lambda)(-h - s + \lambda) \\ \times \left(-3h^2 + s^2 - 2s\lambda + \lambda^2\right). \end{aligned} \tag{4.37}$$

The first term can be taken as the polynomial for the following $\mathbf{e}_1$ matrix:

$$\mathbf{e}_1 = \begin{bmatrix} s-h & -h \\ -h & s-h \end{bmatrix} \Rightarrow \lambda\mathbf{e}_1 = \{s, s-2h\}. \tag{4.38}$$

The second part of the polynomial corresponds to

$$\mathbf{e}_3 = \begin{bmatrix} s & -h \\ -h & s \end{bmatrix} \Rightarrow \lambda\mathbf{e}_3 = \{s-h, s+h\}. \tag{4.39}$$

This matrix is a principal submatrix of $\mathbf{M}_s$, since its eigenvalues are reflected in those of $\mathbf{M}_s$. It has Form II symmetry and the eigenvalues can be obtained using this property.

The third part belongs to

$$\mathbf{e}_2 = \begin{bmatrix} s+h & -2h \\ 2h & \mathbf{s}-h \end{bmatrix} \Rightarrow \lambda e_2 = \left\{s + \sqrt{3}h, s - \sqrt{3}h\right\}. \tag{4.40}$$

Therefore,

$$\lambda(\mathbf{M}_s)\} = \lambda\mathbf{e}_1 \cup \lambda\mathbf{e}_2 \cup \lambda\mathbf{e}_3 = \left\{s, s-2h, s-h, s+h, s+\sqrt{3}h, s-\sqrt{3}h\right\}. \quad (4.41)$$

This special case can also be generalised to matrices of higher dimensions, by considering submatrices **S** and **H** in place of the entries s and h.

For this form, one can easily identify the principal submatrix positioned at the central part of the matrix. The submatrices **S** and **H** can immediately be formed and used in the formation of $\mathbf{E}_2$ and $\mathbf{E}_3$ matrices.

Example 4.6. Consider a 12×12 matrix as follows, which has the properties of special Form IV matrices.

$$\mathbf{M}_s = \begin{bmatrix}
2 & -1 & -1 & 0 & 0 & 0 & 0 & 0 & 0 & 0 & 0 & 0 \\
-1 & 2 & 0 & -1 & 0 & 0 & 0 & 0 & 0 & 0 & 0 & 0 \\
-1 & 0 & 3 & -1 & -1 & 0 & 0 & 0 & 0 & 0 & 0 & 0 \\
0 & -1 & -1 & 3 & 0 & -1 & 0 & 0 & 0 & 0 & 0 & 0 \\
0 & 0 & -1 & 0 & 3 & -1 & -1 & 0 & 0 & 0 & 0 & 0 \\
0 & 0 & 0 & -1 & -1 & 3 & 0 & -1 & 0 & 0 & 0 & 0 \\
0 & 0 & 0 & 0 & -1 & 0 & 3 & -1 & -1 & 0 & 0 & 0 \\
0 & 0 & 0 & 0 & 0 & -1 & -1 & 3 & 0 & -1 & 0 & 0 \\
0 & 0 & 0 & 0 & 0 & 0 & -1 & 0 & 3 & -1 & -1 & 0 \\
0 & 0 & 0 & 0 & 0 & 0 & 0 & -1 & -1 & 3 & 0 & -1 \\
0 & 0 & 0 & 0 & 0 & 0 & 0 & 0 & -1 & 0 & 2 & -1 \\
0 & 0 & 0 & 0 & 0 & 0 & 0 & 0 & 0 & -1 & -1 & 2
\end{bmatrix}_{12\times 12}$$

The principal submatrix can easily be identified as

$$\mathbf{E}_3 = \left[\begin{array}{cc|cc}
3 & -1 & -1 & 0 \\
-1 & 3 & 0 & -1 \\
\hline
-1 & 0 & 3 & -1 \\
0 & -1 & -1 & 3
\end{array}\right] \Rightarrow \lambda\mathbf{E}_3 = \{1,3,3,5\},$$

and we have

$$\mathbf{S} = \begin{bmatrix} 3 & -1 \\ -1 & 3 \end{bmatrix}, \mathbf{H} = \begin{bmatrix} 1 & 0 \\ 0 & 1 \end{bmatrix}, \ \mathbf{S}-\mathbf{H} = \begin{bmatrix} 2 & -1 \\ -1 & 2 \end{bmatrix} \text{ and } \ \mathbf{S}-2\mathbf{H} = \begin{bmatrix} 1 & -1 \\ -1 & 1 \end{bmatrix}.$$

$\mathbf{E}_1$ and $\mathbf{E}_2$ and the corresponding eigenvalues can then easily be calculated as follows:

$$\mathbf{E}_1 = \begin{bmatrix} \mathbf{S}-\mathbf{H} & -\mathbf{H} \\ -\mathbf{H} & \mathbf{S}-\mathbf{H} \end{bmatrix} \Rightarrow \lambda\mathbf{E}_1 = \{0,2,2,4\}.$$

Similarly

$$\mathbf{E}_2 = \begin{bmatrix} \mathbf{S}+\mathbf{H} & -\mathbf{2H} \\ -\mathbf{H} & \mathbf{S}-\mathbf{H} \end{bmatrix} \Rightarrow \lambda\mathbf{E}_2 = \{5.7321, 0.2679, 3.7321, 2.2679\}.$$

Leading to

$$\begin{aligned} \lambda\mathbf{M}_s &= \lambda\mathbf{E}_1 \cup \lambda\mathbf{E}_2 \cup \lambda\mathbf{E}_3 \\ &= \{0, 2, 2, 4, 5.731, 0.2679, 3.7321, 2.2679, 1, 3, 3, 5\}. \end{aligned}$$

4.5 Eig[M] Operator

For a matrix $\mathbf{M}$, Eig[$\mathbf{M}$] is defined as an operator which acts on $\mathbf{M}$ and results its eigenvalues. For example, for an N × N matrix $\mathbf{M}$ we have

$$\text{Eig}[\mathbf{M}_{\text{N}\times\text{N}}] = \vec{\mathbf{V}}_{\text{n}} = \{\lambda_1, \lambda_2, \ldots, \lambda_{\text{n}}\}. \tag{4.42}$$

For the factors $\mathbf{E}_1$, $\mathbf{E}_2$ and $\mathbf{E}_3$, we had

$$\begin{aligned} &\text{Eig}[\mathbf{E}_1] = \{\mathbf{S}, \mathbf{S}-2\mathbf{H}\}^{\text{t}},\ \text{Eig}[\mathbf{E}_2] = \{\mathbf{S}+3\mathbf{H}, \mathbf{S}-3\mathbf{H}\}^{\text{t}},\ \text{and} \\ &\text{Eig}[\mathbf{E}_3] = \{\mathbf{S}-\mathbf{H}, \mathbf{S}+\mathbf{H}\}^{\text{t}}. \end{aligned}$$

The most interesting property of Form IV is that if $\mathbf{S}$ and $\mathbf{H}$ submatrices are replaced by s and h, then the operator 'Eig' will be as follows:

$$\begin{aligned} \text{Eig}[\mathbf{E}_1] &= \text{Eig}[\mathbf{S}, \mathbf{S}-2\mathbf{H}]^{\text{t}} = \{\text{Eig}[\mathbf{S}], \text{Eig}[\mathbf{S}-2\mathbf{H}]\}^{\text{t}}, \\ \text{Eig}[\mathbf{E}_2] &= \text{Eig}\left\{\mathbf{S}+\sqrt{3}\mathbf{H}, \mathbf{S}-\sqrt{3}\mathbf{H}\right\}^{\text{t}} = \left\{\text{Eig}\left[\mathbf{S}+\sqrt{3}\mathbf{H}\right], \text{Eig}\left[\mathbf{S}-\sqrt{3}\mathbf{H}\right]\right\}^{\text{t}}, \\ \text{Eig}[\mathbf{E}_3] &= \text{Eig}\{\mathbf{S}-\mathbf{H}, \mathbf{S}+\mathbf{H}\}^{\text{t}} = \{\text{Eig}[\mathbf{S}-\mathbf{H}], \text{Eig}[\mathbf{S}+\mathbf{H}]\}^{\text{t}}. \end{aligned} \tag{4.44}$$

This simplifies the computation, since once $\mathbf{S}$ and $\mathbf{H}$ are formed, all the eigenvalues of $\mathbf{M}$ can be obtained as follows:

$$\begin{aligned} \text{Eig}[\mathbf{M}] = \Big\{&\text{Eig}[\mathbf{S}], \text{Eig}[\mathbf{S}-2\mathbf{H}], \text{Eig}[\mathbf{S}-\mathbf{H}], \text{Eig}[\mathbf{S}+\mathbf{H}], \text{Eig}\left[\mathbf{S}+\sqrt{3}\mathbf{H}\right], \\ &\text{Eig}\left[\mathbf{S}-\sqrt{3}\mathbf{H}\right]\Big\}^{\text{t}}, \end{aligned} \tag{4.45}$$

and there is no need for explicit formation of $\mathbf{E}_1$, $\mathbf{E}_2$ and $\mathbf{E}_3$. The application is presented in the following section.

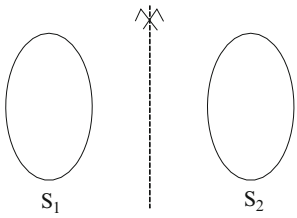

Fig. 4.1 Symmetry of Form I

4.6 Laplacian Matrices for Different Forms

The Laplacian matrix $\mathbf{L}(S)$ is an important matrix associated with a graph S. The list of eigenvalues together with their multiplicities of $\mathbf{L}(S)$ is known as the *spectrum* of S. There are interesting relationships between the properties of a graph and the Laplacian spectrum. Since a graph is the underlying model of a vibrating structure or a system, therefore eigenvalues of graphs are of great importance in their study.

The Laplacian $\mathbf{L}(S) = [l_{ij}]_{N \times N}$ of a weighted graph S is an $N \times N$ matrix defined as follows:

$$\mathbf{L}(S) = \mathbf{D}(S) - \mathbf{A}(S), \tag{4.46}$$

where N is the number of vertices of the graph and

$$l_{ij} = \begin{cases} -(\text{sum of the member weights connecting } n_i \text{ to } n_j) & \text{for } n_i \text{ connected to } n_j, \\ \text{sum of the weights of members connected to } n_i & \text{for } n_i = n_j, \\ 0 & \text{otherwise.} \end{cases} \tag{4.47}$$

When the weights of members are considered as one, then $\mathbf{D}(S)$ and $\mathbf{A}(S)$ become the degree matrix and adjacency matrix of S, respectively.

4.6.1 Symmetry and Laplacian of Graphs

In this section, **M** is taken as the Laplacian of S, and for different forms of **M**, the corresponding graphs are introduced. This correspondence provides an efficient means for calculating the eigenvalues of the Laplacian of graphs.

Consider a symmetric graph S with an axis of symmetry. The following cases may arise:

Symmetry of Form I: The axis of symmetry does not pass through members and nodes. In this case, S is a disjoint graph and its components S_1 and S_2 are isomorphic subgraphs, Fig. 4.1. In order to have the Laplacian matrix in Form I,

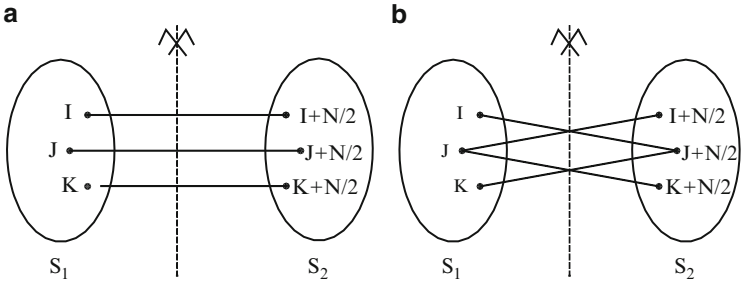

Fig. 4.2 Symmetry of Form II. (**a**) A direct connection. (**b**) A cross-connection

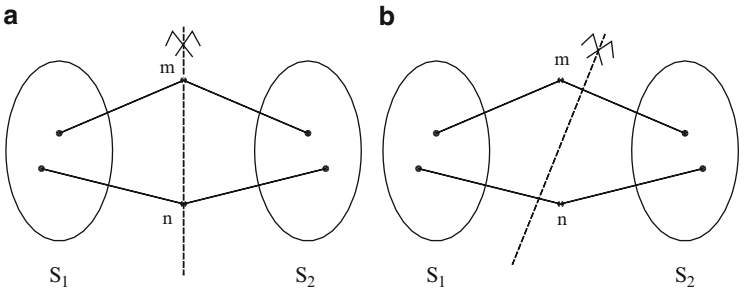

Fig. 4.3 Symmetry of Form II with axis passing through nodes. (**a**) The axis of symmetry. (**b**) Altering the axis of symmetry

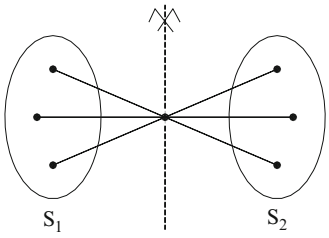

Fig. 4.4 A symmetry of Form III

the nodes of S_1 are numbered first as 1, 2, . . ., N/2, followed by the labelling of the nodes of S_2 as N/2 + 1, N/2 + 2,. . .,N, such that for a typical node I in S_1, the corresponding symmetric counterpart in S_2 is labelled as I + N/2.

Symmetry of Form II: The axis of symmetry passes through members, and the graph S has an even number of nodes. The members cut by the axis of symmetry are called *link members*, and their end nodes are taken as *linked nodes*, Fig. 4.2. Link members connect the two isomorphic subgraphs S_1 and S_2 to each other. For this case, two different types of connections can be considered, as illustrated in

Fig. 4.2a, b. The first one is a *direct connection* and the second is called a *cross-connection*.

In a direct connection, a typical node I in S_1 is connected to the node labelled as I + N/2 in S_2 by a link member. In cross-connection, a typical pair of nodes I and J in S_1 is connected to J + N/2 and I + N/2, respectively. A combination of the direct and cross-connection is also possible.

For some graphs, the axis of symmetry may pass through an even number of nodes, as illustrated in Fig. 4.3a. Then, one may still consider the graph as Form II by altering the axis of symmetry, as shown in Fig. 4.3b, while maintaining the topological symmetry of the model.

Symmetry of Form III: In this case, the axis of symmetry passes through nodes, while the conditions of direct or cross-connections are not fulfilled, Fig. 4.4. The nodes on the axis of symmetry are called *central nodes*.

A combination of Form II and Form III connections may also exist in a model.

4.6.2 Factorisation of Symmetric Graphs

Once the three types of symmetry are identified, the isomorphic subgraphs S_1 and S_2 are modified such that the union of eigenvalues of the Laplacian matrices of the two modified subgraphs becomes the same as the eigenvalues of the entire graph S. The process of the modifications applied to the subgraphs is called *healing* of the subgraphs, and the entire process may be considered as the *factorisation* of a graph. The subgraphs obtained for a graph S after healings are called the *divisor* and *co-divisor* of S. The following operations should be performed for different forms.

Factorisation for Symmetry of Form I: No healing is required, and S_1 and S_2 are the factors of S.

Factorisation for Symmetry of Form II: For direct connection, link members are removed and S_1 resulting in the subgraph C, known as the *divisor* of S, is obtained. Loops are added to the linked nodes of the subgraph S_2 to form the *co-divisor* D of S.

For cross-connection, after removal of the link members, new members are added between I and J in S_1 in order to obtain the divisor C. For S_2, k loops are added to each linked node, where k is the number of links connected to that particular linked node. The members between a typical pair of nodes labelled as J + N/2 and I + N/2 are then removed, in order to obtain the co-divisor D.

Factorisation for Symmetry of Form III: The nodes on the axis of symmetry are changed to neutral nodes in S_1 to obtain the divisor D. A *neutral node* is a node which is drawn in the graph; however, it does not take part in the formation of the Laplacian matrix. In order to obtain the co-divisor E, the nodes on the axis of symmetry are added to S_2, and each central node is connected to the corresponding linked nodes in S_2 by directed members.

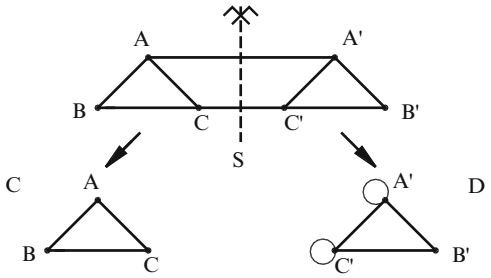

Fig. 4.5 A symmetric graph S and its factorisation

The above rules provide simple means for factorising graphs with symmetry. Therefore, simple calculation of eigenvalues of the Laplacian matrices of such graphs becomes feasible.

Example 4.7. Consider the symmetric graph S shown in Fig. 4.5.

The nodes A, B and C in the first subgraph have the corresponding nodes A′, B′ and C′ in the second subgraph. If A, B, C, A′, B′ and C′ are numbered as 1–6, then the Laplacian of S in Fig. 4.5 can be written as follows:

$$\mathbf{L} = \left[\begin{array}{ccc|ccc} 3 & -1 & -1 & -1 & 0 & 0 \\ -1 & 2 & -1 & 0 & 0 & 0 \\ -1 & -1 & 3 & 0 & 0 & -1 \\ \hline -1 & 0 & 0 & 3 & -1 & -1 \\ 0 & 0 & 0 & -1 & 2 & -1 \\ 0 & 0 & -1 & -1 & -1 & 3 \end{array}\right] = \left[\begin{array}{c|c} \mathbf{G} & \mathbf{LI} \\ \hline \mathbf{LI} & \mathbf{G} \end{array}\right]_{N\times N}.$$

The -1 entries in **LI** correspond to the link members AA′ and CC′.

The condensed matrices **C** and **D** in this form are obtained as follows:

$$\mathbf{C} = \mathbf{G} + \mathbf{LI} \quad \text{and} \quad \mathbf{D} = \mathbf{G} - \mathbf{LI}. \tag{4.48}$$

Matrix **C** is the same as **G** with -1 added to its linked nodes A and C, and **D** is the same as **G** with $-(-1)$ added to its linked nodes A′ and C′. Therefore, **C** and **D** can be viewed as the Laplacian matrices of two subgraphs C and D as shown in Fig. 4.5, healed with loops being added to D at A′ and C′. Thus, a factorisation of S is obtained where healings are made to include the effect of link members AA′ and CC′.

The matrices **C** and **D** are calculated as follows:

$$\mathbf{C} = \begin{bmatrix} 3 & -1 & -1 \\ -1 & 2 & -1 \\ -1 & -1 & 3 \end{bmatrix} + \begin{bmatrix} -1 & 0 & 0 \\ 0 & 0 & 0 \\ 0 & 0 & -1 \end{bmatrix} = \begin{bmatrix} 2 & -1 & -1 \\ -1 & 2 & -1 \\ -1 & -1 & 2 \end{bmatrix},$$

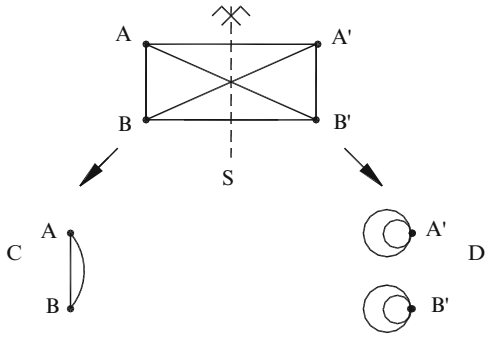

Fig. 4.6 A graph S and its factors C and D

and

$$[\mathbf{D}] = \begin{bmatrix} 3 & -1 & -1 \\ -1 & 2 & -1 \\ -1 & -1 & 3 \end{bmatrix} - \begin{bmatrix} -1 & 0 & 0 \\ 0 & 0 & 0 \\ 0 & 0 & -1 \end{bmatrix} = \begin{bmatrix} 4 & -1 & -1 \\ -1 & 2 & -1 \\ -1 & -1 & 4 \end{bmatrix}.$$

Therefore, in place of finding the eigenvalues of the Laplacian of S, those of C and D can be calculated, and

$$\begin{aligned} \lambda\mathbf{L}(\mathrm{S}) &= \{\lambda\mathbf{C}(\mathrm{S})\}\overline{\cup}\{\lambda\mathbf{D}(\mathrm{S})\} \\ \lambda\mathbf{C}(\mathrm{S}) &= \{0,3,3\}, \{\lambda\mathbf{D}(\mathrm{S})\} = \{1,4,5\}, \end{aligned} \tag{4.49}$$

and

$$\{\lambda\mathbf{L}(\mathrm{S})\} = \{0,1,3,3,4,5\}.$$

Example 4.8. Consider a graph S with symmetry of Form II and cross-connections, as shown in Fig. 4.6. For this graph the Laplacian matrix is as follows:

$$\mathbf{L} = \left[\begin{array}{cc|cc} 3 & -1 & -1 & -1 \\ -1 & 3 & -1 & -1 \\ \hline -1 & -1 & 3 & -1 \\ -1 & -1 & -1 & 3 \end{array}\right].$$

In this example, the link members 1–3 and 2–4 have direct connections and 1–4 and 2–3 have cross-connections. Therefore, one loop in node 1 and one in node 2 are produced with respect to direct symmetry, and additional loops are due to the cross symmetry. The deletion of member 1–2 and the addition of an extra member between 3 and 4 are also the healing required because of the cross-connection. The factorisation is shown in Fig. 4.6 and the corresponding **C** and **D** matrices are as follows:

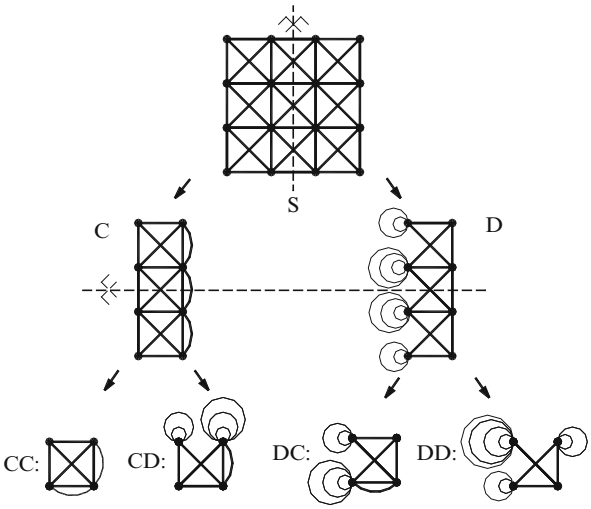

Fig. 4.7 A graph S with symmetry and its decomposition

Table 4.1 Subgraphs of S and their eigenvalues

Subgraphs	Eigenvalues
CC	0, 7, 4, 5
DC	1.4364, 9.8053, 6.3596
CD	1.4364, 9.8053, 4.3987, 6.3596
DD	2.1518, 5.6727, 7, 9.1755

$$\mathbf{C} = \begin{bmatrix} 2 & -2 \\ -2 & 2 \end{bmatrix} \text{ and } \mathbf{D} = \begin{bmatrix} 4 & 0 \\ 0 & 4 \end{bmatrix}.$$

Example 4.9. A graph S is considered as shown in Fig. 4.7. The Laplacian of S is a 16 × 16 matrix, which is put in Form II with suitable ordering. The subgraphs corresponding to the condensed submatrices **C** and **D** are obtained as shown in Fig. 4.7. Here the members in C with both ends as linked nodes are changed into multiple members, and the linked nodes in D have received the appropriate number of loops. Further decompositions result in the subgraphs illustrated in Fig. 4.7. The eigenvalues are then calculated for the subgraphs as provided in Table 4.1.

The eigenvalues for the Laplacian **L** of S are obtained as follows:

$$\{\lambda\mathbf{L}(\mathrm{S})\} = \{0,\ 7,\ 4,\ 5,\ 1.4364,\ 9.8053,\ 6.3596,\ 1.4364,\ 9.8053,\ 4.3987,\ 6.3596,\ 2.1518,\ 5.6727,\ 7,\ 9.1755\}.$$

Using the symmetry, the Laplacian matrix of S with dimension 16 × 16 having 256 entries is reduced to four matrices of dimension 4 × 4 having counted together 64 entries.

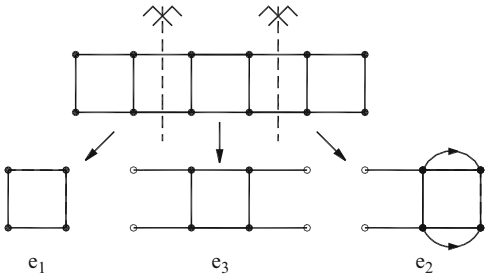

Fig. 4.8 A graph and its factors

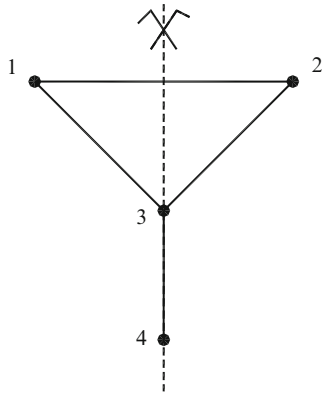

Fig. 4.9 A graph S

Factorisation for Symmetry of Form IV: Consider the matrix **M** as given in the example of Sect. 4.4. This matrix can be considered as the Laplacian matrix of the graph G in Fig. 4.8.

4.6.3 Form III as an Augmented Form II

Consider the Laplacian for Form II and augment it by a row and a column as follows:

$$\mathbf{L} = \left[\begin{array}{cc|c} \multicolumn{2}{c|}{\multirow{2}{*}{\begin{tabular}{cc} \textbf{G} & \textbf{LI} \\ \textbf{LI} & \textbf{G} \end{tabular}}} & \begin{matrix} a \\ b \\ c \\ . \\ . \\ . \end{matrix} \\ \hline \multicolumn{2}{c|}{a\ b\ c\ .\ .\ .\ z} & \end{array}\right] \tag{4.50}$$

Here, we have no column with equal entries, and the only augmented row is the transpose of the augmented column. Similar to the general case, many augmented rows and columns may be included.

Consider the graph shown in Fig. 4.9:

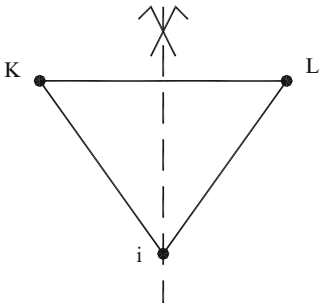

Fig. 4.10 A graph with a symmetric core

The Laplacian is formed as follows:

$$[\mathbf{L}] = \left[\begin{array}{cc|c|c} 2 & -1 & -1 & 0 \\ \hline -1 & 2 & -1 & 0 \\ \hline -1 & -1 & 3 & -1 \\ \hline 0 & 0 & -1 & 1 \end{array}\right],$$

where $\mathbf{G} = [2]$ and $\mathbf{I} = [-1]$.

The condensed matrices **D** and **E** and their eigenvalues are obtained as follows:

$$\mathbf{D} = [2] - [-1] = [3] \text{ and } \lambda\mathbf{D} = \{3\},$$

and

$$[\mathbf{E}] = \begin{bmatrix} 2+(-1) & -1 & 0 \\ -1+(-1) & 3 & -1 \\ 0+0 & -1 & 1 \end{bmatrix} = \begin{bmatrix} 1 & -1 & 0 \\ -2 & 3 & -1 \\ 0 & -1 & 1 \end{bmatrix} \text{ and } \{\lambda\mathbf{E}\} = \{0, 1, 4\}.$$

Hence, $\{\lambda\mathbf{L}(\mathrm{S})\} = \{0, 1, 4, 3\}$.

In Form III, the matrix **L** contains a submatrix **H** corresponding to the symmetric core of the graph. A *symmetric core* of a graph is a subgraph for which the corresponding Laplacian matrix is of Form II. As an example, for the graph shown in Fig. 4.10, the edge KL is the symmetric core.

Node I is linked to nodes K and L in a symmetric manner. K and L are called *in-core* nodes and I is known as the *out-of-core* node.

In order to construct Form III, the in-core nodes and the out-of-core nodes should be ordered. In-core nodes are numbered in a suitable manner for Form II, followed by an arbitrary ordering of the out-of-core nodes.

For constructing the graph model of the condensed matrix **E**, it should be noticed that the addition of the last augmenting row and column results in a nonsymmetric matrix. Therefore, we should define a directed subgraph. In a directed graph, the members are directed, and the degree of a node is the number of arrows leaving that node. A member with two opposing arrows can be treated as a member with no direction.

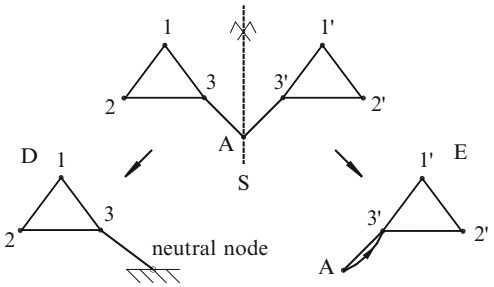

Fig. 4.11 A symmetric graph with seven nodes and its factors D and E

Example 4.10. Consider the symmetric graph of Fig. 4.11 with an odd number of nodes. This graph has seven nodes and contains a symmetric core of Form II. The additional node A is connected to symmetric nodes 3 and 3′. It can be seen that the symmetry is preserved.

The Laplacian of the graph shown in Fig. 4.11 has Form III. The nodal numbering of the core is the same as for Form II, followed by node A numbered as 7. The corresponding Laplacian has the following pattern:

$$\mathbf{L} = \begin{bmatrix} 2 & -1 & -1 & 0 & 0 & 0 & 0 \\ -1 & 2 & -1 & 0 & 0 & 0 & 0 \\ -1 & -1 & 3 & 0 & 0 & 0 & -1 \\ 0 & 0 & 0 & 2 & -1 & -1 & 0 \\ 0 & 0 & 0 & -1 & 2 & -1 & 0 \\ 0 & 0 & 0 & -1 & -1 & 3 & -1 \\ 0 & 0 & -1 & 0 & 0 & -1 & 2 \end{bmatrix}.$$

The corresponding condensed matrices are as follows:

$$\mathbf{D} = \begin{bmatrix} 2 & -1 & -1 \\ -1 & 2 & -1 \\ -1 & -1 & 3 \end{bmatrix} \Rightarrow \{\lambda \mathbf{D}\} = \{3.7321, 3, 0.2679\},$$

$$\mathbf{E} = \begin{bmatrix} 2 & -1 & -1 & 0 \\ -1 & 2 & -1 & 0 \\ -1 & -1 & 3 & -1 \\ 0 & 0 & -2 & 2 \end{bmatrix} \Rightarrow \{\lambda \mathbf{E}\} = \{0, 3, 4.4142, 1.5858\}.$$

The matrix $\mathbf{L}$ without partitioning leads to $\{\lambda \mathbf{L}\} = \{\lambda \mathbf{D}\} \bar{\cup} \{\lambda \mathbf{E}\} = \{3, 3.7321, 3, 0.2679, 4.4142, 1.5858, 0\}$. Here, $\mathbf{L}$ has 49 entries, while the sum of entries for two condensed matrices $\mathbf{D}$ and $\mathbf{E}$ is $3 \times 3 + 4 \times 4 = 25$. For cores with higher numbers of nodes, partitioning leads to higher saving in numerical calculations.

In this example, the diagonal entry of $\mathbf{D}$ in the third row is 3, while the sum of non-diagonal entries in that row is -2. Here, unlike the condensed matrix of

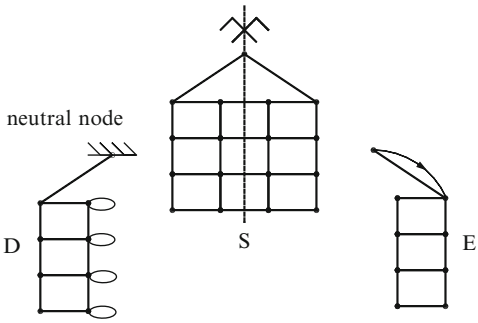

Fig. 4.12 A graph S and its factors D and E

Form II, where the sum of absolute values of non-diagonal entries is bigger than the diagonal entry by an even number, the sum is bigger by an odd number. The reason is that one non-diagonal non-zero entry is in the augmented column which does not take part in the subtraction for calculating **D**. Therefore, a *neutral node* is defined as a node which we draw in the graph; however, it does not take part in the formation of the Laplacian matrix.

Example 4.11. For the graph shown in Fig. 4.12, the subgraphs of E and D are illustrated in this figure.

For the subgraph D, the Laplacian and its eigenvalues are as follows:

$$\mathbf{D} = \begin{bmatrix} 3 & -1 & -1 & 0 & 0 & 0 & 0 & 0 \\ -1 & 4 & 0 & -1 & 0 & 0 & 0 & 0 \\ -1 & 0 & 3 & -1 & -1 & 0 & 0 & 0 \\ 0 & -1 & -1 & 5 & 0 & -1 & 0 & 0 \\ 0 & 0 & -1 & 0 & 3 & -1 & -1 & 0 \\ 0 & 0 & 0 & -1 & -1 & 5 & 0 & -1 \\ 0 & 0 & 0 & 0 & -1 & 0 & 2 & -1 \\ 0 & 0 & 0 & 0 & 0 & -1 & -1 & 4 \end{bmatrix},$$

$$\{\lambda\mathbf{D}\} = \{4, 4.1815, 3.4613, 2.8305, 1.5179, 5.4664, 0.6958, 6.8423\}.$$

For the subgraph E, the Laplacian and the corresponding eigenvalues are as follows:

$$\mathbf{E} = \begin{bmatrix} 3 & -1 & -1 & 0 & 0 & 0 & 0 & 0 & -1 \\ -1 & 2 & 0 & -1 & 0 & 0 & 0 & 0 & 0 \\ -1 & 0 & 3 & -1 & -1 & 0 & 0 & 0 & 0 \\ 0 & -1 & -1 & 3 & 0 & -1 & 0 & 0 & 0 \\ 0 & 0 & -1 & 0 & 3 & -1 & -1 & 0 & 0 \\ 0 & 0 & 0 & -1 & -1 & 3 & 0 & -1 & 0 \\ 0 & 0 & 0 & 0 & -1 & 0 & 2 & -1 & 0 \\ 0 & 0 & 0 & 0 & 0 & -1 & -1 & 2 & 0 \\ -2 & 0 & 0 & 0 & 0 & 0 & 0 & 0 & 2 \end{bmatrix},$$

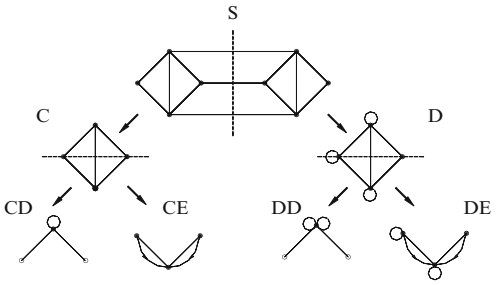

Fig. 4.13 A symmetric graphs S and the corresponding decomposition and healing

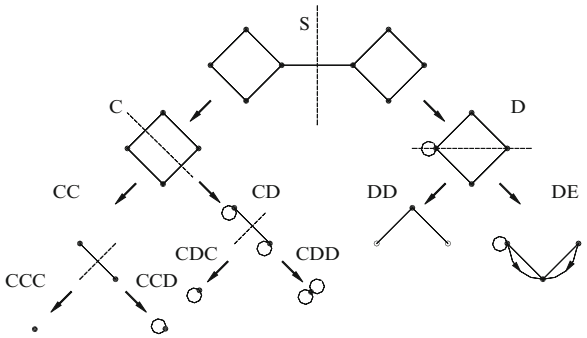

Fig. 4.14 A symmetric graph S, its decomposition and healing

$$\{\lambda \mathbf{E}\} = \{0, 5.5254, 1.4470, 4.4778, 2.3028, 3.1780, 3.5584, 2, 0.5105\}.$$

The set of eigenvalues of **L** is the union of the eigenvalues of **E** and **D**.

The main graph has $17 \times 17 = 289$ entries in **L**, while the sum of entries of **E** and **D** is $9 \times 9 + 8 \times 8 = 145$, which is nearly half of that of **L**.

4.6.4 Mixed Models

A graph may have different symmetries in the process of sequential decomposition. In the following, examples are considered containing both Form II and Form III symmetries.

Example 4.12. For this example, operations for decomposing and healing are shown in Fig. 4.13, where S is first decomposed to C and D, both being Form III. Then C is decomposed to CD and CE. Similarly, D is decomposed to DD and DE.

Example 4.13. For this model, operations for decomposing and healing are shown in Fig. 4.14, where S is first decomposed to C and D having Form II and Form III, respectively. Then C is decomposed to CC and CD, both being Form II. Similarly, D is decomposed to DD and DE, which have Form II and Form III, respectively. CC is decomposed to CCC and CCD, and CD is decomposed to CDC and CDD.

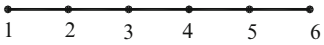

Fig. 4.15 The graph representation of [**M**] in Eq. 4.35

Remark. A graph may contain different symmetries, and an optimal sequence of using these symmetries for decomposition can have a decisive effect on the size and quality of the factors of the graph.

4.7 Graph Representation of Form IV Symmetry

4.7.1 Graph Representation

Matrix [**M**] can be viewed as the Laplacian matrix of the graph, as shown in Fig. 4.15.

For [**M**] in Eq. 4.22, the submatrices $[\mathbf{e_1}]$, $[\mathbf{e_2}]$ and $[\mathbf{e_3}]$ correspond to the subgraphs shown in Fig. 4.16.

This graph has two symmetries of Form III, connected to each other by a Form II symmetry. Using the previously developed factorisation method of [1, 2], one obtains the factors as illustrated in Fig. 4.17. The decomposition is performed by a Form II factorisation, followed by a Form III factorisation.

A comparison of Figs. 4.16 and 4.17 shows that the factors are quite different. In the latter factorisation, a core is resulted with a matrix having the dimension as $\frac{N}{2} \times \frac{N}{2}$, while the present method results in factors with smaller dimensions.

The graph e_3 is a *principal factor* of S, since its eigenvalues are exactly reflected in those of S, and this is an attractive result for graphs.

Consider six identical subgraphs g, connected by subgraphs c, as shown in Fig. 4.18.

Let $\left[\mathbf{L}_g\right]$ be the Laplacian matrix of an internal graph g and $[\mathbf{L}_c]$ be the Laplacian matrix of the connecting graph c. For a typical internal unit, we have

$$[\mathbf{L}_c] - 2[\mathbf{H}] = \left[\mathbf{L}_g\right], \tag{4.51}$$

and for an external unit,

$$[\mathbf{L}'_c] - [\mathbf{H}] = \left[\mathbf{L}_g\right], \tag{4.52}$$

where $[\mathbf{L}_c^{'}]$ is the Laplacian matrix of the external graphs g. The necessary and sufficient condition of the Laplacian of S to have Form IV symmetry is that $[\mathbf{H}]^t = [\mathbf{H}]$. This equality holds when $[\mathbf{L}_c]$ and $\left[\mathbf{L}_c^{'}\right]$ are also symmetric. This form simplifies the eigensolution of grid type of models.

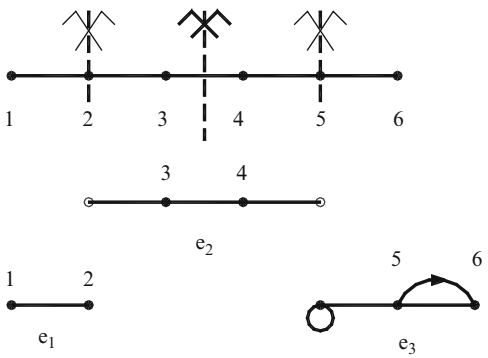

Fig. 4.16 A graph and its factors

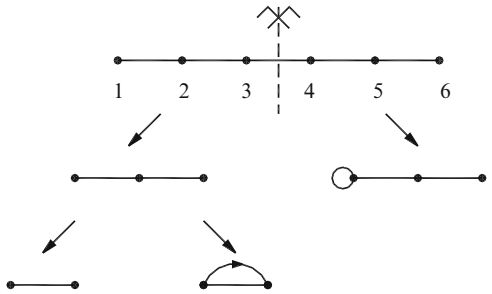

Fig. 4.17 Factorisation of the graph S

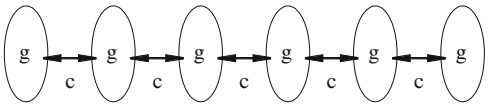

Fig. 4.18 A general sketch of a graph with identical subgraphs

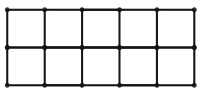

Fig. 4.19 A simple grid G

4.7.2 Examples

Example 4.14. Consider the grid G shown in Fig. 4.19.

The Laplacian matrix $\mathbf{L}(G)$ can easily be constructed. For calculating the eigenvalues of $\mathbf{L}(G)$, the submatrices $[\mathbf{L}_c]$ and $[\mathbf{H}]$ can be identified as follows:

$$[\mathbf{L}_c] = \begin{bmatrix} 3 & -1 & 0 \\ -1 & 4 & -1 \\ 0 & -1 & 3 \end{bmatrix} \Rightarrow \text{Eig}[\mathbf{L}_c] = \{2, 3, 5\},$$

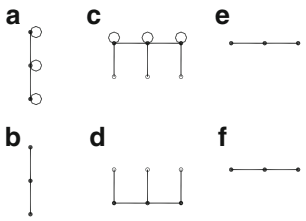

Fig. 4.20 The factors of G obtained by operator Eig. **(a)** $\mathbf{L}_c$, **(b)** $\mathbf{L}_c - 2\mathbf{H}$, **(c)** $\mathbf{L}_c + \mathbf{H}$, **(d)** $\mathbf{L}_c - \mathbf{H}$, **(e)** $\mathbf{L}_c + \sqrt{3}\mathbf{H}$, **(f)** $\mathbf{L}_c - \sqrt{3}\mathbf{H}$

$$[\mathbf{H}] = \begin{bmatrix} 1 & 0 & 0 \\ 0 & 1 & 0 \\ 0 & 0 & 1 \end{bmatrix}.$$

Now the submatrices of Eq. 4.44 are formed and the corresponding Eigs are calculated:

$$\text{Eig}[\mathbf{L}_c - 2\mathbf{H}] = \{0, 1, 3\}, \quad \text{Eig}[\mathbf{L}_c + \mathbf{H}] = \{3{,}4{,}6\}, \quad \text{Eig}[\mathbf{L}_c - \mathbf{H}] = \{1, 2, 4\},$$
$$\text{Eig}[\mathbf{L}_c + \sqrt{3}\mathbf{H}] = \{3.7321, 4.7321, 6.7321\}, \text{ and}$$
$$\text{Eig}[\mathbf{L}_c - \sqrt{3}\mathbf{H}] = \{0.2679, 1.2679, 3.2679\}.$$

Eig$[\mathbf{M}_s]$ is then found as the union of the above eigenvalues. Six factors of the grid are shown in Fig. 4.20a–f. These factors have Form III symmetry and can further be factorised.

Example 4.15. Consider the graph shown in Fig. 4.21. For the numbering provided in this figure, a 48 × 48 Laplacian matrix $\mathbf{L}$(G) can easily be constructed. For calculating the eigenvalues of $\mathbf{L}$(G), the submatrices $[\mathbf{L}_c]$ and $[\mathbf{H}]$ can be expressed as follows:

$$\mathbf{L}_c = \begin{bmatrix} 4 & -1 & 0 & 0 & 0 & 0 & 0 & -1 \\ -1 & 4 & -1 & 0 & 0 & 0 & 0 & 0 \\ 0 & -1 & 4 & -1 & 0 & 0 & 0 & 0 \\ 0 & 0 & -1 & 4 & -1 & 0 & 0 & 0 \\ 0 & 0 & 0 & -1 & 4 & -1 & 0 & 0 \\ 0 & 0 & 0 & 0 & -1 & 4 & -1 & 0 \\ 0 & 0 & 0 & 0 & 0 & -1 & 4 & -1 \\ -1 & 0 & 0 & 0 & 0 & 0 & -1 & 4 \end{bmatrix} \text{ and } \mathbf{H} = \begin{bmatrix} 1 & 0 & 0 & 0 & 0 & 0 & 0 & 0 \\ 0 & 1 & 0 & 0 & 0 & 0 & 0 & 0 \\ 0 & 0 & 1 & 0 & 0 & 0 & 0 & 0 \\ 0 & 0 & 0 & 1 & 0 & 0 & 0 & 0 \\ 0 & 0 & 0 & 0 & 1 & 0 & 0 & 0 \\ 0 & 0 & 0 & 0 & 0 & 1 & 0 & 0 \\ 0 & 0 & 0 & 0 & 0 & 0 & 1 & 0 \\ 0 & 0 & 0 & 0 & 0 & 0 & 0 & 1 \end{bmatrix}.$$

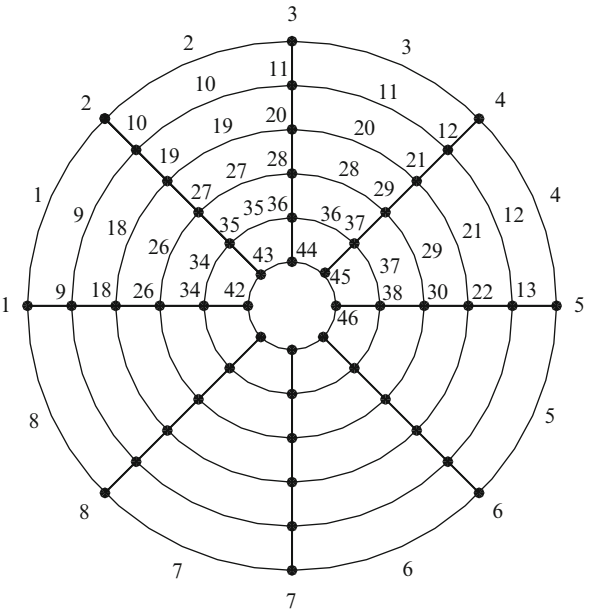

Fig. 4.21 A graph with circular node and member numbering

The eigenvalues for the factors are obtained as follows:

$$\text{Eig}[\mathbf{L}_c] = \{4.0000, 4.000, 2.5858, 2.5858, 5.4142, 5.4142, 2.0000, 6.0000\},$$
$$\text{Eig}[\mathbf{L}_c - 2\mathbf{H}] = \{2.0000, .0000, 0.5858, 0.5858, 3.4142, 3.4142, 0.0000, 4.0000\},$$
$$\text{Eig}[\mathbf{L}_c - \mathbf{H}] = \{3.0000, 3.0000, 1.5858, 1.5858, 4.4142, 4.4142, 1.0000, 5.0000\},$$
$$\text{Eig}[\mathbf{L}_c + \mathbf{H}] = \{5.0000, 5.0000, 3.5858, 3.5858, 6.4142, 6.4142, 3.0000, 7.0000\},$$
$$\text{Eig}\left[\mathbf{L}_c + \sqrt{3}\mathbf{H}\right] = \{5.7321, 5.7321, 4.3178, 4.3178, 7.1463, 7.1463, 3.7321, 3.7321\}, \text{ and}$$
$$\text{Eig}\left[\mathbf{L}_c - \sqrt{3}\mathbf{H}\right] = \{0.8537, 0.8537, 2.2679, 2.2679, 3.6822, 3.6822, 0.2679, 4.2679\}.$$

The eigenvalues of the entire graph is now obtained as the union of the eigenvalues of its factors as $\text{Eig}[\mathbf{L}(G)] =$

$$\{4.0000, 4.000, 2.5858, 2.5858, 5.4142, 5.4142, 2.0000, 6.0000, 2.0000, .0000,$$
$$0.5858, 0.5858, 3.4142, 3.4142, 0.0000, 4.0000, \ 3.0000, 3.0000, 1.5858, 1.5858,$$
$$4.4142, 4.4142, 1.0000, 5.0000, 5.0000, 5.0000, 3.5858, 3.5858, 6.4142, 6.4142,$$
$$3.0000, 7.0000, \ 5.7321, 5.7321, 4.3178, 4.3178, 7.1463, 7.1463, 3.7321, 3.7321,$$
$$0.8537, 0.8537, 2.2679, 2.2679, 3.6822, 3.6822, 0.2679, 4.2679\}.$$

4.8 Generalised Form III Matrix

Now the question arises whether rows and columns with other properties can be added to the core of a Form II pattern. When the sum of the absolute values for the entries of an augmenting row is the same as that of its column, then **D** and **E** can be formed as before. It should be noted that such a restriction is not necessary to be imposed on the last row and column.

Consider the following form:

$$\mathbf{M}=\left[\begin{array}{cc|c} [\mathbf{A}] & [\mathbf{B}] & * \\ \hline [\mathbf{B}] & [\mathbf{A}] & \mathrm{H} \\ * & \mathrm{H} & \mathrm{P} \end{array}\right] \rightarrow \text{ith row}, \tag{4.53}$$

where P is a real number.

For the ith row,

$$\begin{aligned} &\mathrm{H}+\mathrm{b}_{(\mathrm{i},1)}+\ldots+\mathrm{b}_{(\mathrm{i},\,\mathrm{n})}+\mathrm{a}_{(\mathrm{i},\mathrm{n}+1)}+\ldots+\mathrm{a}_{(\mathrm{i},2\mathrm{n})}=\left|\mathrm{a}_{(\mathrm{i},\mathrm{i})}\right|, \\ \text{or} \\ &\mathrm{H}+\sum_{\mathrm{j}=1}^{\mathrm{n}}\mathrm{b}_{(\mathrm{i},\mathrm{j})}+\sum_{\mathrm{j}=\mathrm{n}\ \&\ \mathrm{j}\neq\mathrm{i}}^{2\mathrm{n}}\mathrm{a}_{(\mathrm{i},\mathrm{j})}=\left|\mathrm{a}_{(\mathrm{i},\mathrm{i})}\right|. \end{aligned} \tag{4.54}$$

Example 4.16. Consider a core in Form II:

$$\mathbf{N}=\left[\begin{array}{c|c} -6 & 2 \\ \hline 2 & -6 \end{array}\right]_{2\times 2}.$$

Add an augmenting row and column to form **M** with the following properties:

1. Matrix **M** is symmetric.
2. **M** has condensed submatrices **D** and **E**.
3. Two numerical values are considered for H in **M**, namely $\mathrm{H}_1=4$ and $\mathrm{H}_2=-8$.

$$\mathbf{M}=\left[\begin{array}{cc|c} -6 & 2 & \mathrm{H} \\ \hline 2 & -6 & \mathrm{H} \\ \mathrm{H} & \mathrm{H} & \mathrm{P} \end{array}\right] \tag{4.55}$$

For $\mathrm{H}=4$, P is taken arbitrarily as 8, that is,

$$\mathbf{M}_1=\left[\begin{array}{cc|c} -6 & 2 & 4 \\ \hline 2 & -6 & 4 \\ 4 & 4 & 8 \end{array}\right] \Rightarrow \{\lambda\mathbf{M}_1\}=\{-8,-6.2462,10.2462\}$$

The condensed submatrices are as follows:

$$\mathbf{D}_1 = [-6-2] = [-8] \Rightarrow \{\lambda \mathbf{D}_1\} = \{-8\}.$$

$$\mathbf{E}_1 = \begin{bmatrix} -4 & 4 \\ 8 & 8 \end{bmatrix} \Rightarrow \{\lambda \mathbf{E}_1\} = \{-6.2462, 10.2462\}.$$

These submatrices will contain the eigen-properties of part of the **M**.
For H = 8, the numerical value of P is taken as −16, and

$$\mathbf{M}_2 = \left[\begin{array}{c|c|c} -6 & 2 & -8 \\ \hline 2 & -6 & -8 \\ \hline -8 & -8 & -16 \end{array}\right] \Rightarrow \{\lambda \mathbf{M}_2\} = \{-8, 2.8062, -22.8062\}.$$

The corresponding condensed submatrices are as follows:

$$\mathbf{D}_2 = [-8] \Rightarrow \{\lambda \mathbf{D}_2\} = \{-8\},$$

$$\mathbf{E}_2 = \begin{bmatrix} -4 & -8 \\ -16 & -16 \end{bmatrix} \Rightarrow \{\lambda \mathbf{E}_2\} = \{2.8062, -22.8062\}.$$

As mentioned before, in both $\mathbf{M}_1$ and $\mathbf{M}_2$ matrices some properties of the core are left unaltered. These eigenvalues correspond to those of **D**. In this example, H = −8, the eigenvalue corresponding to $\mathbf{D}_1$ has this property.

All the properties of Sect. 4.5 are applicable to this special pattern. As an example, the eigenvalues of $\mathbf{M}_2$ are:

$$\lambda_1 = -8 \Rightarrow \mathbf{v}_1 = \left\{\begin{array}{c} -1 \\ \hline 1 \\ \hline 0 \end{array}\right\}; \lambda_2 = 2.8062 \Rightarrow \mathbf{v}_2 = \left\{\begin{array}{c} 1 \\ \hline 1 \\ \hline -0.85 \end{array}\right\};$$

$$\lambda_3 = -22.8062 \Rightarrow \mathbf{v}_3 = \left\{\begin{array}{c} 0.4253 \\ \hline 0.4253 \\ \hline 1 \end{array}\right\}.$$

It should be mentioned that the above argument is also applicable when *k* rows and columns are added to the symmetric core of Form II.

4.9 Block Diagonalization of Compound Matrices

In linear algebra it is known that a square matrix can be diagonalised using the normalised eigenvectors, provided all the eigenvectors are orthogonal. It is also proved that if the matrix is Hermitian, then it can be diagonalised and diagonal

entries constitute the eigenvalues of this matrix. A matrix is Hermitian if its conjugate is the same as its transpose. Therefore, if a matrix is real, then symmetry is the only requirement for the matrix to be Hermitian. The eigenvalues of Hermitian matrices are real, and the eigenvectors corresponding to any arbitrary pairs of distinct eigenvalues are orthogonal.

If $\mathbf{M}$ is a Hermitian matrix, then using $\mathbf{U}^t\mathbf{M}\mathbf{U}$ it can be diagonalised. All what is required, is the formation of an orthogonal matrix $\mathbf{U}$. This can in fact be achieved by the singular value decomposition (SVD) approach for symmetric matrices.

Definition. The *Kronecker product* of two matrices $\mathbf{A}$ and $\mathbf{B}$ is the matrix we get by replacing the ij, the entry of $\mathbf{A}$ by $a_{ij}\mathbf{B}$, for all i and j.

As an example,

$$\begin{bmatrix} 1 & 1 \\ 1 & 0 \end{bmatrix} \otimes \begin{bmatrix} a & b \\ c & d \end{bmatrix} = \begin{bmatrix} a & b & a & b \\ c & d & c & d \\ a & b & 0 & 0 \\ c & d & 0 & 0 \end{bmatrix}, \tag{4.56}$$

where entry 1 in the first matrix has been replaced by a complete copy of the second matrix.

Now the main question is how one can block diagonalise a compound matrix. For a matrix $\mathbf{M}$ defined as a single Kronecker product, in the form $\mathbf{M} = \mathbf{A}_1 \otimes \mathbf{B}_1$, it is obvious that if $\mathbf{A}_1$ is Hermitian, then the diagonalisation leads to a block diagonal matrix of the form $\mathbf{D}_{\mathbf{A}_1} \otimes \mathbf{B}_1$.

Now suppose a compound matrix $\mathbf{M}$ can be written as the sum of two Kronecker products:

$$\mathbf{M} = \mathbf{A}_1 \otimes \mathbf{B}_1 + \mathbf{A}_2 \otimes \mathbf{B}_2. \tag{4.57}$$

We want to find a matrix $\mathbf{P}$, which diagonalises $\mathbf{A}_1$ and $\mathbf{A}_2$ simultaneously. In such a case, one should show that $\mathbf{U} = \mathbf{P} \otimes \mathbf{I}$ block diagonalises $\mathbf{M}$, that is, we have to show that $\mathbf{U}^t\mathbf{M}\mathbf{U}$ is a block diagonal matrix.

From algebra we have $(\mathbf{A} \otimes \mathbf{B})^t = \mathbf{A}^t \otimes \mathbf{B}^t$ and $(\mathbf{A} \otimes \mathbf{B})(\mathbf{C} \otimes \mathbf{D}) = \mathbf{AC} \otimes \mathbf{BD}$. Then

$$\begin{aligned} (\mathbf{U}^t\mathbf{M}\mathbf{U}) &= (\mathbf{P}^t \otimes \mathbf{I}^t)(\mathbf{A}_1 \otimes \mathbf{B}_1 + \mathbf{A}_2 \otimes \mathbf{B}_2)(\mathbf{P} \otimes \mathbf{I}) \\ &= [(\mathbf{P}^t\mathbf{A}_1 \otimes (\mathbf{I}\mathbf{B}_1) + (\mathbf{P}^t\mathbf{A}_2) \otimes (\mathbf{I}\mathbf{B}_2)](\mathbf{P} \otimes \mathbf{I})) \\ &= (\mathbf{P}^t\mathbf{A}_1\mathbf{P}) \otimes (\mathbf{B}_1\mathbf{I}) + (\mathbf{P}^t\mathbf{A}_2\mathbf{P}) \otimes (\mathbf{B}_2\mathbf{I}) \\ &= (\mathbf{P}^t\mathbf{A}_1\mathbf{P}) \otimes (\mathbf{B}_1) + (\mathbf{P}^t\mathbf{A}_2\mathbf{P}) \otimes (\mathbf{B}_2). \end{aligned} \tag{4.58}$$

Since it is assumed that $\mathbf{P}$ diagonalises $\mathbf{A}_1$ and $\mathbf{A}_2$, thus

$$\mathbf{P}^t\mathbf{A}_1\mathbf{P} = \mathbf{D}_{\mathbf{A}_1} \text{ and } \mathbf{P}^t\mathbf{A}_2\mathbf{P} = \mathbf{D}_{\mathbf{A}_2}, \tag{4.59}$$

and therefore,

$$\mathbf{U}^{t}\mathbf{M}\mathbf{U} = \mathbf{D}_{\mathbf{A}_1} \otimes \mathbf{B}_1 + \mathbf{D}_{\mathbf{A}_2} \otimes \mathbf{B}_2. \tag{4.60}$$

In this way, $\mathbf{U}$ becomes block diagonalised and in order to calculate the eigenvalues of $\mathbf{M}$, one can evaluate the eigenvalues of the blocks on the diagonal. The matrices $\mathbf{M}$ and $\mathbf{U}^{t}\mathbf{M}\mathbf{U}$ are similar matrices, since $\mathbf{P}$ is orthogonal, thus $\mathbf{U}$ is also orthogonal and its inverse is equal to its transpose.

Now an important question is whether the assumptions made at the beginning of this section are feasible; that is, can one always find a matrix $\mathbf{P}$, which diagonalises $\mathbf{A}_1$ and $\mathbf{A}_2$ simultaneously?

For a matrix to be diagonalisable, it is necessary to be Hermitian. However, for two matrices to be diagonalisable, not only these two matrices should be Hermitian, but these matrices should also commute [10]; that is,

$$\mathbf{A}_1\mathbf{A}_2 = \mathbf{A}_2\mathbf{A}_1. \tag{4.61}$$

Therefore, if $\mathbf{A}_1$ and $\mathbf{A}_2$ commute with respect to multiplication, then

$$\lambda_{\mathbf{M}} = \bigcup_{i=1}^{n} [\mathrm{eig}(\lambda_i(\mathbf{A}_1)\mathbf{B}_1 + \lambda_i(\mathbf{A}_2)\mathbf{B}_2)]. \tag{4.62}$$

The $\lambda_i(\mathbf{A}_j)$ for $j = 1,2$ is a diagonal matrix containing all the eigenvalues of $\mathbf{A}_j$, and n is the dimension of the matrix $\mathbf{A}_i$. It should be noticed that the order of the eigenvalues in $\mathbf{A}_1$ and $\mathbf{A}_2$ is important. The order is the same as obtained after simultaneous diagonalisation of the two matrices, which appear on the diagonal of the matrices.

As an example, for the special case with $\mathbf{A}_1 = \mathbf{I}$, it is obvious that $\mathbf{I}\mathbf{A}_2 = \mathbf{A}_2\mathbf{I}$, and we have

$$\begin{aligned} &\mathbf{M} = \mathbf{I} \otimes \mathbf{B}_1 + \mathbf{A}_2 \otimes \mathbf{B}_2 \\ &\lambda_{\mathbf{M}} = \bigcup_{i=1}^{n} [\mathrm{eig}(\mathbf{B}_1 + \lambda_i(\mathbf{A}_2)\mathbf{B}_2)] \quad \text{and } \lambda_i(\mathbf{A}_1) = 1. \end{aligned} \tag{4.63}$$

These special cases are already shown in early sections of this chapter.

One can use another $\mathbf{A}_1$ matrix except $\mathbf{I}$, provided it commutes with respect to $\mathbf{A}_2$. The Hermitian property is obvious, due to the symmetry, and it is real; though for complex matrices this property still holds. For the formation of $\mathbf{P}$, it is sufficient to use SVD decomposition for a linear combination of $\mathbf{A}_1$ and $\mathbf{A}_2$, that is, if we use the SVD decomposition on $\mathbf{N} = a_1\mathbf{A}_1 + a_2\mathbf{A}_2$, then $\mathbf{P}$ can be obtained; here, a_1 and a_2 are two arbitrary nonequal numbers.

As an example, consider the following matrix which has the Form II form:

$$\mathbf{M} = \begin{bmatrix} \mathbf{A} & \mathbf{B} \\ \mathbf{B} & \mathbf{A} \end{bmatrix} = \mathbf{I} \otimes \mathbf{A} + \mathbf{T} \otimes \mathbf{B}, \quad \text{where} \quad \mathbf{T} = \begin{bmatrix} 0 & 1 \\ 1 & 0 \end{bmatrix}. \tag{4.64}$$

Since $\mathbf{I}$ and $\mathbf{T}$ commute, one can, for example, decompose $\mathbf{N} = 2\mathbf{I} + \mathbf{T}$. Here, $\mathbf{I}$ and $\mathbf{T}$ have much smaller dimensions compared to that of $\mathbf{M}$, and in this particular case, these are 2×2 matrices. Decomposition of $\mathbf{N}$ leads to

$$\mathbf{P} = \frac{\sqrt{2}}{2}\begin{bmatrix} 1 & 1 \\ 1 & -1 \end{bmatrix} \Rightarrow \mathbf{U} = \mathbf{P} \otimes \mathbf{I} = \frac{\sqrt{2}}{2}\begin{bmatrix} \mathbf{I} & \mathbf{I} \\ \mathbf{I} & -\mathbf{I} \end{bmatrix} \Rightarrow \mathbf{U}^{\mathrm{t}}\mathbf{M}\mathbf{U} = \begin{bmatrix} \mathbf{A}+\mathbf{B} & \mathbf{0} \\ \mathbf{0} & \mathbf{A}-\mathbf{B} \end{bmatrix}. \quad (4.65)$$

Therefore, it is only necessary to calculate the eigenvalues of $\mathbf{A} + \mathbf{B}$ and $\mathbf{A} - \mathbf{B}$, and if the diagonal entries are not needed, then using Eq. 4.63

$$\begin{aligned} \lambda_{\mathbf{M}} = \bigcup_{i=1}^{n} [\mathrm{eig}(\mathbf{A} + \lambda_i(\mathbf{T})\mathbf{B})] \quad \text{and } \lambda_{\mathbf{T}} = \{1, -1\}. \\ \lambda_{\mathbf{M}} = \cup[\mathrm{eig}(\mathbf{A} + \mathbf{B}), \mathrm{eig}(\mathbf{A} - \mathbf{B})]. \end{aligned} \quad (4.66)$$

As another example, consider a matrix $\mathbf{M}$ in the following form:

$$\mathbf{M} = \begin{bmatrix} \mathbf{A} & \mathbf{B} & \mathbf{0} \\ \mathbf{B} & \mathbf{A} & \mathbf{B} \\ \mathbf{0} & \mathbf{B} & \mathbf{A} \end{bmatrix} = \mathbf{I} \otimes \mathbf{A} + \mathbf{T} \otimes \mathbf{B}, \quad \text{where} \quad \mathbf{T} = \begin{bmatrix} 0 & 1 & 0 \\ 1 & 0 & 1 \\ 0 & 1 & 0 \end{bmatrix}. \quad (4.67)$$

As before, $\mathbf{P}$ can be obtained from a linear combination of $\mathbf{I}$ and $\mathbf{T}$ as follows:

$$\begin{aligned} \mathbf{P} = \frac{1}{2}\begin{bmatrix} 1 & \sqrt{2} & 1 \\ -\sqrt{2} & 0 & \sqrt{2} \\ 1 & -\sqrt{2} & 1 \end{bmatrix} \Rightarrow \mathbf{U} = \mathbf{P} \otimes \mathbf{I} \Rightarrow \mathbf{U}^{\mathrm{t}}\mathbf{M}\mathbf{U} \\ = \begin{bmatrix} \mathbf{A} - \sqrt{2}\mathbf{B} & \mathbf{0} & \mathbf{0} \\ \mathbf{0} & \mathbf{A} & \mathbf{0} \\ \mathbf{0} & \mathbf{0} & \mathbf{A} + \sqrt{2}\mathbf{B} \end{bmatrix}. \end{aligned} \quad (4.68)$$

Using Eq. 4.66 leads to

$$\begin{aligned} \lambda_{\mathbf{M}} = \cup[\mathrm{eig}(\mathbf{A} + \lambda_i(\mathbf{T})\mathbf{B})] \quad \text{and } \lambda_{\mathbf{T}} = \left\{\pm\sqrt{2}, 0\right\} \Rightarrow \\ \lambda_{\mathbf{M}} = \cup\left\{\mathrm{eig}\left(\mathbf{A} \pm \sqrt{2}\mathbf{B}, \mathbf{A}\right)\right\} \end{aligned}. \quad (4.69)$$

The interesting point about the matrices of the above form is that the determinant of the matrix is calculated after they are put in block forms, decomposition is performed, and the components are then obtained. As the first example, consider

$$\det(\mathbf{M}) = \mathbf{A}^2 - \mathbf{B}^2 = (\mathbf{A} + \mathbf{B})(\mathbf{A} - \mathbf{B}), \quad (4.70)$$

and as the second example consider

$$\det(\mathbf{M}) = \mathbf{A}^3 - 2\mathbf{A}\mathbf{B}^2 = \mathbf{A}\left(\mathbf{A}^2 - 2\mathbf{B}^2\right) = \mathbf{A}\left(\mathbf{A} + \sqrt{2}\mathbf{B}\right)\left(\mathbf{A} - \sqrt{2}\mathbf{B}\right). \quad (4.71)$$

It should be noted that here blocks are treated as numbers, that is, these have the commuting property. In general, one can show that

$$\mathbf{M}_{mn} = \begin{bmatrix} \mathbf{A}_m & \mathbf{B}_m & & & \\ \mathbf{B}_m & \mathbf{A}_m & . & & \\ & . & . & . & \\ & & . & \mathbf{A}_m & \mathbf{B}_m \\ & & & \mathbf{B}_m & \mathbf{A}_m \end{bmatrix}_n = \mathbf{F}_n(\mathbf{A}_m, \mathbf{B}_m, \mathbf{A}_m) \tag{4.72}$$

$$\Rightarrow \det(\mathbf{M}) = \sum_{n=0}^{\left[\frac{n}{2}\right]} (-1)^n \binom{n-i}{n} \mathbf{A}^{(n-2i)} \mathbf{B}^{2i} = \sum_{i=1}^{n} (\mathbf{A} + \alpha_i \mathbf{B}). \tag{4.73}$$

Comparing with Eq. 4.63, we have $\alpha_i = \lambda_T$. Since $\mathbf{T} = \mathbf{F}(0, 1, 0)$, therefore as mentioned before, we have $\alpha_i = \lambda_{\mathbf{T}} = 2\cos\frac{k\pi}{n+1}$, where k = 1:n.

Applications of these relationships will be demonstrated in Examples 7.20 and 7.21 of Chap. 7. As it will be shown, one may need to multiply rows or columns with certain numbers to transform the matrix into the above form.

The present approach is always applicable. As an example, consider the following matrix:

$$\mathbf{M}_{mn} = \begin{bmatrix} \mathbf{0} & \mathbf{A} & \mathbf{B} & & & & & \\ \mathbf{A} & \mathbf{B} & \mathbf{A} & \mathbf{B} & & & & \\ \mathbf{B} & \mathbf{A} & \mathbf{B} & . & . & & & \\ & \mathbf{B} & . & . & . & \mathbf{B} & & \\ & & . & . & . & \mathbf{A} & \mathbf{B} & \\ & & & \mathbf{B} & \mathbf{A} & \mathbf{B} & \mathbf{A} & \\ & & & & \mathbf{B} & \mathbf{A} & \mathbf{0} & \end{bmatrix}, \tag{4.74}$$

which is a block penta-diagonal matrix and can be presented more simply by **F** matrices as

$$\begin{aligned} \mathbf{M} &= \mathbf{F}(\mathbf{0}, \mathbf{A}, \mathbf{B}, \mathbf{B}) = \mathbf{F}(0, 1, 0) \otimes \mathbf{A} + \mathbf{F}(0, 0, 1, 1) \otimes \mathbf{B} \\ &= \mathbf{T} \otimes \mathbf{A} + \mathbf{S} \otimes \mathbf{B}. \end{aligned} \tag{4.75}$$

Here **M** shown by an **F** matrix in a similar manner to that of Eq. 4.72, The only difference is that in this case an additional argument is introduced, which is the magnitude of the entries in the additional diagonals introduced compared to a tri-diagonal matrix.

It can be shown that **S** and **T** are not unit matrices, and therefore, Eq. 4.63 is not applicable. However, since **TS** = **ST**, thus Eq. 4.62 should be employed.

$$\lambda_T = 2\cos\frac{k\pi}{n+1}, \quad \lambda_S = 1 + 2\cos\frac{2k\pi}{n+1}, \quad k = 1:n \tag{4.76}$$

$$\lambda_{\mathbf{M}} = \cup\left[\text{eig}\left\{2\left(\mathbf{A}\cos\frac{\text{k}\pi}{\text{n}+1} + \mathbf{B}\cos\frac{2\text{k}\pi}{\text{n}+1}\right) + \mathbf{B}\right\}\right],\ \text{k} = 1:\text{n} \tag{4.77}$$

As an example, for $\text{m} = 8$ and $\text{n} = 5$, instead of calculating the eigenvalues of a 40×40 matrix, the eigenvalues of five 8×8 matrices will be needed, since **T** and **S** commute and **M** is block diagonalisable.

4.10 Matrices as the Sum of Three Kronecker Products

Now we assume **M** to be the sum of three Kronecker products as

$$\mathbf{M} = \sum_{\text{i}=1}^{3} \mathbf{A}_\text{i} \otimes \mathbf{B}_\text{j}. \tag{4.78}$$

If the block diagonalisation of **M** is required, as for the case with two terms, $\mathbf{A}_\text{i}$ (i = 1:3) should commute for any two matrices $\mathbf{A}_\text{i}$, that is,

$$\mathbf{A}_\text{i}\mathbf{A}_\text{j} = \mathbf{A}_\text{j}\mathbf{A}_\text{i} \quad \text{i,j} = 1:3,\ \ \text{i} \neq \text{j}. \tag{4.79}$$

With these conditions holding, the matrix **M** can be transformed into tri-diagonal matrix and then to a diagonal matrix.

Consider a penta-diagonal matrix as

$$\mathbf{M} = \begin{bmatrix} \mathbf{A} & \mathbf{B} & \mathbf{I} & & & \\ \mathbf{B} & \mathbf{A}+\mathbf{I} & . & . & & \\ \mathbf{I} & . & . & . & . & \\ & . & . & . & . & \mathbf{I} \\ & & . & . & \mathbf{A}+\mathbf{I} & \mathbf{B} \\ & & & \mathbf{I} & \mathbf{B} & \mathbf{A} \end{bmatrix} = \mathbf{I}\otimes\mathbf{A} + \mathbf{T}\otimes\mathbf{B} + \mathbf{S}\otimes\mathbf{I} = \sum_{\text{i}=1}^{3} \mathbf{A}_\text{i} \otimes \mathbf{B}_\text{i} \tag{4.80}$$

where

$$\mathbf{T} = \mathbf{F}(0,1,0) \ \text{ and } \ \mathbf{S} = \mathbf{F}(0,0,1,1).$$

Here, $\mathbf{A}_\text{i}\mathbf{A}_\text{j} = \mathbf{A}_\text{j}\mathbf{A}_\text{i}$ $\text{i,j} = 1:3,\ \text{i} \neq \text{j}$ holds and **M** can be diagonalised. A matrix with numerical entries can be decomposed by SVD to obtain **P**. Then $\mathbf{U} = \mathbf{P} \otimes \mathbf{I}$ is selected (e.g. $\mathbf{N} = \mathbf{A}_1 + 2\mathbf{A}_2 + 3\mathbf{A}_3$) as

$$\mathbf{P} = \frac{\sqrt{3}}{6}\begin{bmatrix} 1 & -1 & \sqrt{3} & 2 & -\sqrt{3} \\ \sqrt{3} & \sqrt{3} & \sqrt{3} & 0 & \sqrt{3} \\ 2 & -2 & 0 & -2 & 0 \\ \sqrt{3} & \sqrt{3} & -\sqrt{3} & 0 & -\sqrt{3} \\ 1 & -1 & -\sqrt{3} & 2 & \sqrt{3} \end{bmatrix} \Rightarrow \mathbf{U} = \mathbf{P}\otimes\mathbf{I} \Rightarrow \mathbf{U}^\text{t}\mathbf{M}\mathbf{U} \tag{4.81}$$

resulting in a block matrix $\mathbf{U}^{t}\mathbf{M}\mathbf{U}$. Therefore, instead of calculating $\mathbf{U}$, we calculate the block matrices by

$$\lambda_{\mathbf{M}} = \bigcup_{j=1}^{n} \left[\operatorname{eig} \sum_{i=1}^{3} \lambda_j(\mathbf{A}_i)\mathbf{B}_i \right]. \tag{4.82}$$

In order to demonstrate the applications, in Examples 7.22 and 7.23 of Chap. 7, a plate will be studied under uniaxial forces, and their buckling loads will be calculated. Example 7.24 will study the natural frequency of a system with continuous distributed mass.

4.11 The Commutating Condition

In this section, the condition for two matrices of the form $\mathbf{F}$ to commute is investigated.

Theorem 1. *For two penta-diagonal (tri-diagonal as a special case) matrices of the form* $\mathbf{A}_i = \mathbf{F}(a_i, b_i, c_i, d_i)$, $\mathbf{A}_i\mathbf{A}_j = \mathbf{A}_j\mathbf{A}_i$ if $t_1 = \frac{a_i - c_i}{d_i}$ and $t_2 = \frac{a_i - c_i + d_i}{b_i}$ *for both matrices* $\boldsymbol{A}_i$ *and* $\boldsymbol{A}_j$ *are identical.*

Proof. Consider

$$\mathbf{A}_i = \mathbf{F}(a_i, b_i, c_i, d_i) = c_i\mathbf{I} + b_i\mathbf{F}(0,1,0) + (a_i - c_i)\mathbf{F}(1,0,0) + d_i\mathbf{F}(0,0,0,1) \tag{4.83}$$

a_i to d_i are all numbers. From definition of t_1 and t_2, we have

$$(a_i - c_i) = t_1 d_i, \quad t_2 = (1 + t_1)\frac{d_i}{b_i}. \tag{4.84}$$

Substituting $\mathbf{A}_i$ we obtain

$$\mathbf{A}_i = c_i\mathbf{I} + \left(\frac{1+t_1}{t_2}\right) d_i\mathbf{F}(0,1,0) + t_1 d_i\mathbf{F}(1,0,0) + d_i\mathbf{F}(0,0,0,1) = c_i\mathbf{I} + d_i\mathbf{R}. \tag{4.85}$$

In the last three terms, d_i is factorised and $\mathbf{R}$ is obtained. If t_1 and t_2 are the same for both matrices, then they have identical $\mathbf{R}$, and it is only necessary to show that

$$(c_i\mathbf{I} + d_i\mathbf{R})\big(c_j\mathbf{I} + d_j\mathbf{R}\big) = \big(c_j\mathbf{I} + d_j\mathbf{R}\big)(c_i\mathbf{I} + d_i\mathbf{R}). \tag{4.86}$$

This is obvious since $\mathbf{I}$ and $\mathbf{R}$ commute and $\mathbf{R}^2$ can be cancelled from two sides. The proof is then complete.

It should be noted that if one of the above expressions for t_1 and t_2 becomes $\frac{0}{0}$, then the condition for commuting will hold and no control is required. We also consider the result of dividing two nonequal numbers as non-zero. Therefore, for

two tri-diagonal matrices, the above condition holds for t_1's (since the divisor is always zero and the magnitude of dividend is not important), and t_2's should be equal. As an example, in Example 7.22 we will have

$$\begin{aligned} \mathbf{T} &= \mathbf{F}(0,1,0,0); t_1 = \frac{0}{0}, \\ \mathbf{S} &= \mathbf{F}(0,0,1,1);\ t_2 = \frac{0}{0}. \end{aligned} \tag{4.87}$$

Since t_1 of the matrix **T** is equal to $\frac{0}{0}$, thus there is no need to calculate t_1 of **S**, and also $t_2 = \frac{0}{0}$ for S. Therefore, these two matrices (**S** and **T**) commute. One can also control **T**, **I**, **S**, **I** for commuting. However, in Example 7.23, it will be seen that after block diagonalisation, **M** is transformed into **N**, and **N** does not satisfy the above condition, since

$$\begin{aligned} \mathbf{T} &= \mathbf{F}(0,1,0,0); t_1 = \frac{0}{0} \qquad t_2 = \frac{0}{1}, \\ \mathbf{S} &= \mathbf{F}(0,0,-1,1); \qquad\quad t_2 = \frac{2}{0}. \end{aligned} \tag{4.88}$$

t_1 requires no control; however, t_2 for **S** and **T** are not identical. Therefore, no further simplification can be made for **N**. While in Example 7.22, **N** had **S** and **T** similar to **M**, and we can reduce it into simple non-matrix equation.

4.12 A Block Tri-diagonal Matrix with Corner Blocks and Its Block Diagonalisation

In this section, a canonical form is introduced and an efficient method is developed for its block diagonalisation.

Consider a matrix **M** as

$$\mathbf{M} = \begin{bmatrix} \mathbf{A} & \mathbf{B} & & & & & \mathbf{B}^t \\ \mathbf{B}^t & \mathbf{A} & \mathbf{B} & & & & \\ & \mathbf{B}^t & \mathbf{A} & \mathbf{B} & & & \\ & & . & . & . & & \\ & & & . & . & . & \\ & & & & \mathbf{B}^t & \mathbf{A} & \mathbf{B} \\ \mathbf{B} & & & & & \mathbf{B}^t & \mathbf{A} \end{bmatrix}_{nm\times nm}. \tag{4.89}$$

This matrix is a block symmetric matrix which has $n \times n$ blocks. The blocks of this matrix are $\mathbf{A}_{m\times m}, \mathbf{B}_{m\times m}$ and $\mathbf{B}^t_{m\times m}$; thus, this matrix generally has $nm \times nm$ entries. Block **A** is located on the main diagonal and blocks **B** and $\mathbf{B}^t$ are situated on

the upper and lower adjacent diagonals and also in the lower-left corner and the upper-right corner, respectively.

The problem is to find the eigenvalues and eigenvectors of $\mathbf{M}$. This matrix is symmetric and a set of nm real eigenvalues μ_i and real eigenvectors $\boldsymbol{\varphi}_i$ can be calculated in such a manner that $\mathbf{M}\boldsymbol{\varphi}_i = \mu_i\boldsymbol{\varphi}_i$ $(i = 1, \ldots, nm)$. Now, using the decomposed form of $\mathbf{M}$, an efficient method is presented for its eigensolution.

Matrix $\mathbf{M}$ can be decomposed as the sum of three Kronecker products:

$$\mathbf{M}_{nm\times nm} = \mathbf{I}_{n\times n} \otimes \mathbf{A}_{m\times m} + \mathbf{H}_{n\times n} \otimes \mathbf{B}_{m\times m} + \mathbf{H}^{t}_{n\times n} \otimes \mathbf{B}^{t}_{m\times m} \tag{4.90}$$

where, $\mathbf{I}$ is an n × n identity matrix and $\mathbf{H}$ is an n × n unsymmetric matrix as

$$\mathbf{H} = \begin{bmatrix} 0 & 1 & & & & 0 \\ & 0 & 1 & & & \\ & & . & . & & \\ & & & . & . & \\ & 0 & & & . & . \\ & & & & 0 & 1 \\ 1 & & & & & 0 \end{bmatrix}_{\mathbf{n}\times\mathbf{n}} . \tag{4.91}$$

Since $\mathbf{H}$ is unsymmetric, the block diagonalisation of $\mathbf{M}$ needs additional considerations. Firstly, $\mathbf{H}$ is a permutation matrix and thus it is orthogonal. Therefore,

$$\mathbf{H}^{t}\mathbf{H} = \mathbf{I}. \tag{4.92}$$

Secondly, $\mathbf{H}$ and $\mathbf{H}^{t}$ have commutative property. On the other hand

$$\mathbf{H}^{t}\mathbf{H} = \mathbf{H}\mathbf{H}^{t}. \tag{4.93}$$

This means that these two matrices can simultaneously be diagonalised. Now, using a matrix such as $\mathbf{U} = \mathbf{X} \otimes \mathbf{I}$, $\mathbf{M}$ is diagonalised.

$$\begin{aligned} \mathbf{U}^{-1}\mathbf{M}\mathbf{U} &= \mathbf{U}^{-1}(\mathbf{I} \otimes \mathbf{A} + \mathbf{H} \otimes \mathbf{B} + \mathbf{H}^{t} \otimes \mathbf{B}^{t})\mathbf{U} \\ &= (\mathbf{X} \otimes \mathbf{I})^{-1}(\mathbf{I} \otimes \mathbf{A} + \mathbf{H} \otimes \mathbf{B} + \mathbf{H}^{t} \otimes \mathbf{B}^{t})(\mathbf{X} \otimes \mathbf{I}) \\ &= \left(\mathbf{X}^{-1} \otimes \mathbf{I}^{-1}\right)(\mathbf{I} \otimes \mathbf{A} + \mathbf{H} \otimes \mathbf{B} + \mathbf{H}^{t} \otimes \mathbf{B}^{t})(\mathbf{X} \otimes \mathbf{I}) \\ &= \left(\mathbf{X}^{-1} \otimes \mathbf{A} + \mathbf{X}^{-1}\mathbf{H} \otimes \mathbf{B} + \mathbf{X}^{-1}\mathbf{H}^{t} \otimes \mathbf{B}^{t}\right)(\mathbf{X} \otimes \mathrm{I}) \\ &= \left(\mathbf{I} \otimes \mathbf{A} + \mathbf{X}^{-1}\mathbf{H}\mathbf{X} \otimes \mathbf{B} + \mathbf{X}^{-1}\mathbf{H}^{t}\mathbf{X} \otimes \mathbf{B}^{t}\right). \end{aligned} \tag{4.94}$$

Since a similarity transformation is used, thus the eigenvalues do not change. In Eq. 4.94, $\mathbf{I}$ is a diagonal matrix and it is sufficient to show that $\mathbf{X}$ diagonalises $\mathbf{H}$ and $\mathbf{H}^{t}$. On the other hand, it is assumed that

$$\mathbf{X}^{-1}\mathbf{H}\mathbf{X} = \mathbf{D}_1 \tag{4.95}$$

$$\mathbf{X}^{-1}\mathbf{H}^{\mathbf{t}}\mathbf{X} = \mathbf{D}_2 \tag{4.96}$$

in which $\mathbf{D}_1$ and $\mathbf{D}_2$ are diagonal matrices. Thus, the block diagonal form of $\mathbf{M}$ can be written as

$$\mathbf{U}^{-1}\mathbf{M}\mathbf{U} = \left(\mathbf{I} \otimes \mathbf{A} + \mathbf{D}_1 \otimes \mathbf{B} + \mathbf{D}_2 \otimes \mathbf{B}^{\mathbf{t}}\right). \tag{4.97}$$

Generally, Eqs. 4.95 and 4.96 are eigenvalue decomposition of matrices $\mathbf{H}$ and $\mathbf{H}^{\mathbf{t}}$ in which $\mathbf{X}$ and $\mathbf{D}$ are eigenvector and eigenvalue matrices, respectively. Since $\mathbf{H}$ is orthogonal, a relationship between $\mathbf{D}_1$ and $\mathbf{D}_2$ can be established. If we find the inverse of Eq. 4.95, then with respect to the orthogonal property of $\mathbf{H}$, we will have

$$\mathbf{X}^{-1}\mathbf{H}^{-1}\mathbf{X} = \mathbf{D}_1^{-1} \tag{4.98}$$

$$\mathbf{X}^{-1}\mathbf{H}^{\mathrm{t}}\mathbf{X} = \mathbf{D}_2. \tag{4.99}$$

Thus,

$$\mathbf{D}_2 = \mathbf{D}_1^{-1}. \tag{4.100}$$

Now the eigenvalues and eigenvectors of matrix $\mathbf{H}$ (entries of $\mathbf{D}$ and $\mathbf{X}$) are analytically calculated. As previously mentioned, $\mathbf{H}$ is an $n \times n$ permutation matrix and its characteristic polynomial (using variable λ) can be written as

$$\lambda^{\mathrm{n}} - 1 = 0. \tag{4.101}$$

In general, Eq. 4.101 has n real and complex roots. It is clear that if n is even or odd, then $(-1, 1)$ and (1) are only real roots of Eq. 4.101, respectively. Other complex roots of this equation can easily be calculated. Since the absolute value of each root is unit, therefore the roots of Eq. 4.101 are identical to those of Eq. 4.102.

$$\cos \mathrm{n}\theta + \mathrm{i} \sin \mathrm{n}\theta = 1. \tag{4.102}$$

These complex and real roots are presented in Table 4.2.

According to Table 4.2, depending on n being even or odd, two real and $\mathrm{n} - 2$ complex roots or a real and $\mathrm{n} - 1$ complex roots should be calculated, respectively. In addition, the normalised eigenvectors $\mathbf{x}^i$ associated with the eigenvalues λ_{i} $(\mathrm{i} = 1, \ldots, \mathrm{n})$ can analytically be evaluated by solving the following equation:

$$(\mathbf{H} - \lambda_{\mathrm{i}}\mathbf{I})\mathbf{x}^{\mathrm{i}} = 0. \tag{4.103}$$

Table 4.2 Roots of the characteristic polynomial associated with matrix H

	Real roots	Complex roots
n is even	$-1,\ 1$	$\cos\theta \pm \mathbf{i}\ \sin\theta, \quad \theta = \frac{2k\pi}{n}, \quad k = 1, 2, \ldots, \frac{(n-2)}{2}$
n is odd	1	$\cos\theta \pm \mathbf{i}\ \sin\theta, \quad \theta = \frac{2k\pi}{n}, \quad k = 1, 2, \ldots, \frac{(n-1)}{2}$

This is a linear equation and by selecting $\mathbf{x}_1$, all other entries of $\mathbf{x}^i$ (unknown eigenvector) are found as follows:

$$\lambda_i,\ x^i = \left[x_1, x_j, x_n\right]^t,\ i = 1, \ldots, n \tag{4.104}$$

$$\mathbf{x}_1 = \frac{1}{\sqrt{n}},\ \left(\mathbf{x}_j = \lambda_i \mathbf{x}_{j-1}\ \ j = 2, \ldots, n-1\right),\ \mathbf{x}_n = \frac{\mathbf{x}_1}{\lambda_i}. \tag{4.105}$$

It is important to note that if $\mathbf{x}_1 = \frac{1}{\sqrt{n}}$ is assumed, each eigenvector will be calculated in a normalised form with no additional effort. Also the matrix $\mathbf{X}$ with its columns being the eigenvectors of $\mathbf{H}$, can easily be generated as

$$X = \left[x^1, x^2, \ldots, x^n\right]. \tag{4.106}$$

Now, Eq. 4.97 can be expressed in a much simpler form. Since λ_is are located on the diagonal entries of $\mathbf{D}(d_{ii} = \lambda_i)$, and the absolute value of each λ_i is unit, thus, the inverse of the complex diagonal matrix equals to its conjugate, and Eq. 4.100 can simply be written as

$$\mathbf{D}_2 = \bar{\mathbf{D}}_1. \tag{4.107}$$

Finally, according to Eq. 4.108, the eigenvalues of matrix $\mathbf{M}$ can be found using the union of the eigenvalues of n blocks as

$$\mathbf{eig}(\mathbf{M}) = \bigcup_{j=1}^{n} \mathbf{eig}\left(\mathbf{BL}_j\right) = \bigcup_{j=1}^{n} \mathbf{eig}\left(\mathbf{A} + \lambda_j(\mathbf{H})\mathbf{B} + \bar{\lambda}_j(\mathbf{H})\mathbf{B}^t\right) \tag{4.108}$$

where $\left(\mathbf{BL}_j\right)$ is the jth diagonal block of $\mathbf{U}^{-1}\mathbf{MU}$ associated with λ_j, that is, the calculation of the eigenvalues of an $nm \times nm$ matrix is transformed into those of n times $m \times m$ matrices. Clearly, this process leads to a significant decrease in computational time and memory.

Also, for each eigenvalue μ_i which is obtained from Eq. 4.108 (for the jth block), an eigenvector y_i is calculated as

$$\mathbf{BL}_j \mathbf{y}_i = \mu_i \mathbf{y}_i. \tag{4.109}$$

This eigenvector can easily be transformed into an eigenvector of **M** using the following relationships:

$$\boldsymbol{\varphi}_i = \mathbf{U}\left(\mathbf{e}_j \otimes \mathbf{y}_i\right) = (\mathbf{X} \otimes \mathbf{I})\left(\mathbf{e}_j \otimes \mathbf{y}_i\right) = \mathbf{X}\mathbf{e}_j \otimes \mathbf{I}\mathbf{y}_i \tag{4.110}$$

$$\boldsymbol{\varphi}_i = \mathbf{x}^j \otimes \mathbf{y}_i. \tag{4.111}$$

Therefore, if μ_i is a simple root of characteristic polynomial corresponding to **M**, Eq. 4.111 leads to an eigenvector with real entries. However, if μ_i is a multiple root of characteristic polynomial, Eq. 4.111 leads to eigenvectors with complex entries. As we know, λ_j and $\overline{\lambda}_j$ are the roots of Eq. 4.101, leading to two conjugate blocks $\left(\mathbf{BL}_j\right)$ which have identical eigenvalues, and their conjugate eigenvectors are found by Eq. 4.111. For such eigenvalues, the eigenvectors with real entries can be generated. This is done by simply adding two complex conjugate eigenvectors. Obviously, the imaginary parts of these two vectors will be eliminated. The remaining vector is also orthogonal to other eigenvectors and should be normalised. However, other orthogonal real eigenvectors for multiple eigenvalues should be calculated by an orthogonalisation algorithm, such as *Gram–Schmidt* method [11], if needed.

References

1. Kaveh A, Sayarinejad MA (2003) Eigensolutions for matrices of special structures. Commun Numer Methods Eng 19:125–136
2. Kaveh A, Sayarinejad MA (2004) Eigensolutions for factorable matrices of special patterns. Commun Numer Methods Eng 20(2):133–146
3. Kaveh A, Sayarinejad MA (2005) Eigenvalues of factorable matrices with Form IV symmetry. Commun Numer Methods Eng 21(6):269–278
4. Kaveh A, Sayarinejad MA (2006) Augmented canonical forms and factorization of graphs. Int J Numer Methods Eng 65(10):1545–1560
5. Kaveh A, Sayarinejad MA (2006) Eigensolution of specially structured matrices with hypersymmetry. Int J Numer Methods Eng 67(7):1012–1043
6. Rempel J, Schwolow KH (1977) Ein Verfahren zur Faktorisierung des charakteristiscen Polynoms eines Graphen. Wissenschaftliche Zeitschrift der TH Ilmenau 23:25–39
7. Cvetkovié DM, Doob M, Sachs H (1980) Spectra of graphs. Academic, New York
8. Kaveh A, Rahami H (2007) Compound matrix block diagonalization for efficient solution of eigenproblems in structural matrices. Acta Mech 188(3–4):155–166
9. Kaveh A, Rahami H (2006) Unification of three canonical forms with application to stability analysis. Asian J Civil Eng 7(2):125–138
10. Kaveh A, Rahami H (2006) Block digonalization of adjacency and Laplacian matrices for graph products; applications in structural mechanics. Int J Numer Methods Eng 68:33–63
11. Jacques I, Judd C (1987) Numerical analysis. Chapman and Hall, London

Chapter 5
Canonical Forms for Combinatorial Optimisation, Nodal Ordering and Graph Partitioning

5.1 Introduction

Ordering is an important issue in the analysis of large-scale structures. In the standard approach depending on the solution scheme, the bandwidth, profile or front width of the structural matrices should be optimised. For parallel computing, the model of the structure (domain) should be partitioned (decomposed) into a number of substructures (subdomain) having certain properties. The latter can also be considered as an ordering problem.

There are many applications of algebraic graph theory in nodal and element ordering and graph partitioning. However, despite of the efficiency of graph spectra for combinatorial optimisation, the calculation of eigenvalues and eigenvectors of large graphs and their corresponding structural models without considering patterns and the sparsity of their matrices requires additional memory and computational time.

There are numerous applications of graph theory and algebraic graph theory in optimal structural analysis, Kaveh [1, 2]. In this chapter, a canonical form as well as its relation with four structural models often encountered in practice and their corresponding graphs are presented, Kaveh and Koohestani [3]. Furthermore, the block diagonalisation of this form, which is performed using three Kronecker products and unsymmetric matrices, is studied. This block diagonalisation leads to an efficient method for the eigensolution of adjacency and Laplacian matrices of special graphs. The eigenvalues and eigenvectors are used for efficient nodal ordering and partitioning of large structural models.

5.2 Preliminary Definitions

Consider the solution of sparse linear system of equations

$$\mathbf{A}\mathbf{x} = \mathbf{b}, \tag{5.1}$$

where the $n \times n$ matrix $\mathbf{A}$ is a sum of elemental matrices.

A. Kaveh, *Optimal Analysis of Structures by Concepts of Symmetry and Regularity*,
DOI 10.1007/978-3-7091-1565-7_5, © Springer-Verlag Wien 2013

The *bandwidth* of the matrix **A** is defined as

$$B = \max\{b_i\}, \tag{5.2}$$

where

$$b_i = \max\{i - j + 1\} \text{ with } a_{ij} \neq 0 \tag{5.3}$$

The *profile* of the matrix **A** is the total number of coefficients in the lower triangle when any zero ahead of the first entry in its row is excluded. That is,

$$P = \sum_{i=1}^{n} \max\{b_i\}. \tag{5.4}$$

Note that since **A** is assumed to have a symmetric pattern of non-zeros, it follows that

$$P = \sum_{i=1}^{n} f_i. \tag{5.5}$$

5.3 Algebraic Graph Theory for Ordering and Partitioning

Algebraic graph theory can be considered as a branch of mathematics that connects the algebra and theory of graph. In this theory, eigenvalues and eigenvectors of certain matrices are employed to deduce the principal properties of a graph. In fact eigenvalues are closely related to most of the invariants of a graph, linking one extremal property to another. These eigenvalues play a central role in our fundamental understanding of graphs. There are interesting books on algebraic graph theory such as Biggs [4], Cvetković et al. [5] and Seidel [6].

The Laplacian matrix of a graph is already introduced in Chap. 2, and here the eigen-properties of this matrix will be employed for bisection of graphs and its nodal ordering.

One of the major contributions in algebraic graph theory is due to Fiedler [7, 8], where the properties of the second eigenvalue and eigenvector of the Laplacian of a graph have been introduced. The latter, known as the *Fiedler vector*, is used in nodal ordering and bipartition of skeletal structures as well as finite element models, Mohar [9], Pothen et al. [10] and Topping and Sziveri [11].

Mohar [9] has applied (λ_2,$\mathbf{v}_2$) to different problems such as graph partitioning and ordering. Paulino et al. [12] used $\mathbf{v}_2$ for element ordering and nodal numbering. Pothen et al. [10], Simon [13], Seale and Topping [14], Kaveh [15], Kaveh and Davaran [16] and Kaveh and Rahimi Bondarabady [17, 18] have used the properties of $\mathbf{v}_2$, for

partitioning graphs. However, for calculating λ_2, when the entire model is considered, a fair amount of computational time and storage space is required. In this chapter, for regular structural models, this goal is achieved by far more efficient method.

General methods are available in the literature for calculating the eigenvalues of matrices; however, for matrices corresponding to special models, it is beneficial to make use of their extra properties.

5.4 Eigenvalue Problems and Similarity Transformation

A complex scalar λ_i is called an *eigenvalue* of the square matrix $\mathbf{A}_{n\times n}$ if a nonzero vector v_i of $\mathbf{C}^n$ exists such that $\mathbf{A}\mathbf{v}_i = \lambda_i \mathbf{v}_i$. The vector $\mathbf{v}_i$ is called an *eigenvector* of $\mathbf{A}$ associated with λ_i. The set of eigenvalues of $\mathbf{A}$ is called the *spectrum* of $\mathbf{A}$.

A scalar λ_i is an eigenvalue of $\mathbf{A}$ if and only if $\det(\mathbf{A} - \lambda_i \mathbf{I}) = 0$. That is true if and only if λ_i is a root of the characteristic polynomial.

Two matrices $\mathbf{A}$ and $\mathbf{B}$ are said to be *similar* if there is a nonsingular matrix $\mathbf{U}$ such that

$$\mathbf{B} = \mathbf{U}^{-1}\mathbf{A}\mathbf{U}. \tag{5.6}$$

The mapping $\mathbf{A} \rightarrow \mathbf{B}$ is called a *similarity transformation*. It can easily be shown that similarity transformations preserve the eigenvalues of matrices.

$$\mathbf{A}\mathbf{v}_i = \lambda_i \mathbf{v}_i \ (i = 1, \ldots, n) \tag{5.7}$$

$$\mathbf{U}^{-1}\mathbf{A}\mathbf{U}\mathbf{U}^{-1}\mathbf{v}_i = \lambda_i \mathbf{U}^{-1}\mathbf{v}_i. \tag{5.8}$$

By substituting $\mathbf{B} = \mathbf{U}^{-1}\mathbf{A}\mathbf{U}$ and $\mathbf{y}_i = \mathbf{U}^{-1}\mathbf{v}_i$, we will have

$$\mathbf{B}\mathbf{y}_i = \lambda_i \mathbf{y}_i. \tag{5.9}$$

Equation 5.9 which is a standard representation of eigenproblems means that λ_i ($i = 1,\ldots,n$) are also the eigenvalues of the matrix $\mathbf{B}$. This transformation is used in the next sections for block diagonalisation of adjacency and Laplacian matrices with special pattern.

5.5 A Special Canonical Form and Its Block Diagonalisation

Matrix $\mathbf{M}$ with a pattern shown in Eq. 5.10 is a block symmetric matrix which has $n \times n$ blocks. The blocks of this matrix are $\mathbf{A}_{m\times m}$, $\mathbf{B}_{m\times m}$ and $\mathbf{B}^t_{m\times m}$; thus, this matrix generally has $nm \times nm$ entries. Block $\mathbf{A}$ is located on the main diagonal

and blocks $\mathbf{B}$ and $\mathbf{B}^t$ are located on the upper and lower adjacent diagonals and also in the lower-left corner and the upper-right corner, respectively.

$$\mathbf{M} = \begin{bmatrix} \mathbf{A} & \mathbf{B} & & & & & \mathbf{B}^t \\ \mathbf{B}^t & \mathbf{A} & \mathbf{B} & & & & \\ & \mathbf{B}^t & \mathbf{A} & \mathbf{B} & & & \\ & & . & . & . & & \\ & & & . & . & . & \\ & & & & \mathbf{B}^t & \mathbf{A} & \mathbf{B} \\ \mathbf{B} & & & & & \mathbf{B}^t & \mathbf{A} \end{bmatrix}_{nm \times nm} \tag{5.10}$$

The problem is to find the eigenvalues and eigenvectors of $\mathbf{M}$. This matrix is symmetric and a set of nm real eigenvalues μ_i and real eigenvectors $\boldsymbol{\varphi}_i$ can be calculated in such a manner that $\mathbf{M}\boldsymbol{\varphi}_i = \mu_i \boldsymbol{\varphi}_i \quad (i = 1, \ldots, nm)$. Using the decomposed form of $\mathbf{M}$, an efficient method is already presented in Sect. 4.12 of the previous chapter for its eigensolution. In the following only the main necessary relationships are restated.

The eigenvalues of matrix $\mathbf{M}$ can be found using the union of the eigenvalues of n blocks as

$$\mathbf{eig}(\mathbf{M}) = \bigcup_{j=1}^{n} \mathbf{eig}\left(\mathbf{BL}_j\right) = \bigcup_{j=1}^{n} \mathbf{eig}\left(\mathbf{A} + \lambda_j(\mathbf{H})\mathbf{B} + \bar{\lambda}_j(\mathbf{H})\mathbf{B}^t\right) \tag{5.11}$$

where $\left(\mathbf{BL}_j\right)$ is the jth diagonal block of $\mathbf{U}^{-1}\mathbf{MU}$ associated with λ_j, that is, the calculation of the eigenvalues of a $nm \times nm$ matrix is transformed into those of n times $m \times m$ matrices. Clearly, this process leads to a significant decrease in computational time and memory. Also, for each eigenvalue μ_i which is obtained from Eq. 5.11 (for the *j*th block), an eigenvector $\mathbf{y}_i$ is calculated as

$$\mathbf{BL}_j \mathbf{y}_i = \mu_i \mathbf{y}_i \tag{5.12}$$

This eigenvector can easily be transformed into an eigenvector of $\mathbf{M}$ using the following equations:

$$\boldsymbol{\varphi}_i = \mathbf{U}\left(\mathbf{e}_j \otimes \mathbf{y}_i\right) = (\mathbf{X} \otimes \mathbf{I})\left(\mathbf{e}_j \otimes \mathbf{y}_i\right) = \mathbf{X}\mathbf{e}_j \otimes \mathbf{I}\mathbf{y}_i \tag{5.13}$$

$$\boldsymbol{\varphi}_i = \mathbf{x}^j \otimes \mathbf{y}_i \tag{5.14}$$

Therefore, if μ_i is a simple root of characteristic polynomial corresponding to $\mathbf{M}$, Eq. 5.14 leads to an eigenvector with real entries. However, if μ_i is a multiple root of characteristic polynomial, Eq. 5.14 leads to eigenvectors with complex entries. As we know, λ_j and $\bar{\lambda}_j$ are the roots of the characteristic equation of $\mathbf{H}$ (defined in Eq. 4.91), leading to two conjugate blocks $\left(\mathbf{BL}_j\right)$ which have identical eigenvalues, and their conjugate eigenvectors are found by Eq. 5.14. For such eigenvalues, the eigenvectors with real entries can be generated. This can be done by simply adding

two complex conjugate eigenvectors. Obviously, the imaginary parts of these two vectors will be eliminated. The remaining vector is also orthogonal to other eigenvectors and should be normalised. However, other orthogonal real eigenvectors for multiple eigenvalues should be calculated by an orthogonalisation algorithm, such as *Gram–Schmidt* method, if needed [19].

5.6 Adjacency and Laplacian Matrices for Models of Different Topologies

In this section, the graph models of four configurations (having different topology) often encountered in structural mechanics and space structures are studied. Matrices associated with these graphs have the same pattern as those presented in the previous section. These configurations can also be generated using graph products which are different standard products. In this chapter, the spectral properties of these graphs are studied in relation with the present canonical form, without reference to their representations as graph products.

5.6.1 Configuration of Type 1

The first type of configurations is shown in Fig. 5.1. The pattern of adjacency and Laplacian matrices for such a model and the corresponding graph is completely dependent on its nodal numbering. However, using the numbering scheme shown in Fig. 5.1, a desired pattern (introduced form in Sect. 5.5) can be achieved. On the other hand, nodes on each edge (nodes which are shown in the hidden bounding box) should be numbered sequentially. If such a numbering scheme is used, the adjacency and Laplacian matrices will have $nm \times nm$ entries with $m \times m$ blocks. Then the size of matrices $\mathbf{A}$ and $\mathbf{B}$ will be $m \times m$. Obviously, the graph shown in Fig. 5.1, for clarity in topology and nodal numbering, is depicted by small number of nodes and members ($n = 6$ and $m = 3$). However, the related matrices which are utilised for large models in the subsequent section are illustrated in their general forms.

$$\mathbf{A}_{\mathbf{adj}} = \begin{bmatrix} 0 & 1 & & & & & & & 0 \\ 1 & 0 & 1 & & & & & & \\ & 1 & 0 & 1 & & & & & \\ & & \cdot & \cdot & \cdot & & & & \\ & & & \cdot & \cdot & \cdot & & & \\ & & & & \cdot & \cdot & \cdot & & \\ & & & & & \cdot & \cdot & \cdot & \\ & & & & & & 1 & 0 & 1 \\ 0 & & & & & & & 1 & 0 \end{bmatrix}_{m\times m} \quad \mathbf{B}_{\mathbf{adj}} = \begin{bmatrix} 1 & 1 & & & & & & & 0 \\ & 1 & 1 & & & & & & \\ & & 1 & 1 & & & & & \\ & & & \cdot & \cdot & & & & \\ & & & & \cdot & \cdot & & & \\ & & & & & \cdot & \cdot & & \\ & & & & & & \cdot & \cdot & \\ & & & & & & & 1 & 1 \\ 0 & & & & & & & & 1 \end{bmatrix}_{m\times m}$$

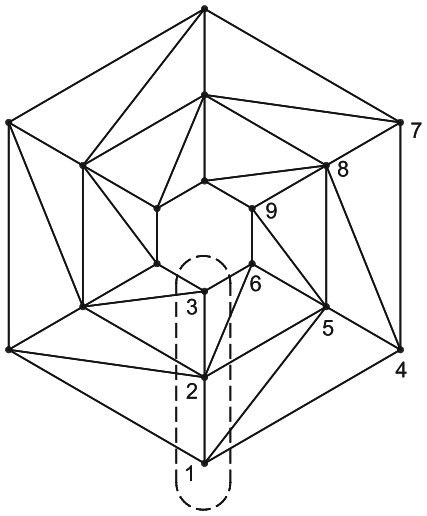

Fig. 5.1 Configuration of Type 1

$$\mathbf{A_{Lap}} = \begin{bmatrix} 4 & -1 & & & & & & 0 \\ -1 & 6 & -1 & & & & & \\ & -1 & 6 & -1 & & & & \\ & & \cdot & \cdot & \cdot & & & \\ & & & \cdot & \cdot & \cdot & & \\ & & & & \cdot & \cdot & \cdot & \\ & & & & & -1 & 6 & -1 \\ 0 & & & & & & -1 & 4 \end{bmatrix}_{m\times m} \qquad \mathbf{B_{Lap}} = -\mathbf{B_{adj}}$$

5.6.2 *Configurations of Type 2, Type 3 and Type 4*

Here, block matrices **A** and **B** as well as suitable nodal numbering scheme are presented for other three types, Figs. 5.2, 5.3, and 5.4. In these types of configurations, if the number of nodes of a member is k, then the total number of nodes which are shown in the hidden bounding box will be $2k - 1$. In fact, this is the size of internal blocks. On the other hand, a member with k nodes and a cycle with n nodes lead to a graph with nm nodes in which $m = 2k - 1$.

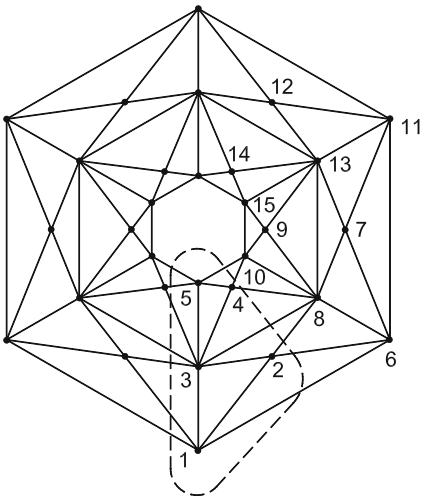

Fig. 5.2 Configuration of Type 2

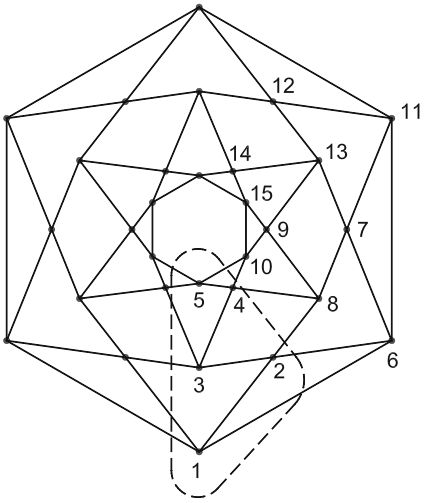

Fig. 5.3 Configuration of Type 3

$$\mathbf{A}_{\mathbf{adj}} = \begin{bmatrix} 0 & 1 & 1 & & & & & & 0 \\ 1 & 0 & 1 & 0 & & & & & \\ 1 & 1 & 0 & 1 & 1 & & & & \\ & 0 & 1 & . & . & . & & & \\ & & 1 & . & . & . & . & & \\ & & & . & . & . & . & 0 & \\ & & & & . & 1 & 0 & 1 & 1 \\ & & & & & 0 & 1 & 0 & 1 \\ 0 & & & & & & 1 & 1 & 0 \end{bmatrix}_{m \times m} \quad \mathbf{B}_{\mathbf{adj}} = \begin{bmatrix} 1 & & & & & & & & 0 \\ 1 & 0 & 1 & & & & & & \\ & & 1 & & & & & & \\ & & 1 & 0 & 1 & & & & \\ & & & & . & & & & \\ & & & & . & . & 1 & & \\ & & & & & & 1 & & \\ & & & & & & 1 & 0 & 1 \\ 0 & & & & & & & & 1 \end{bmatrix}_{m \times m}$$

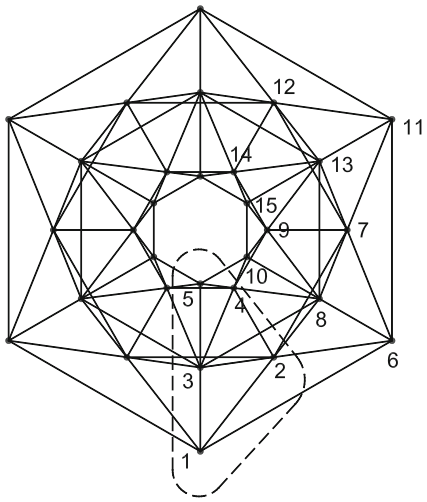

Fig. 5.4 Configuration of Type 4

$$\mathbf{A_{Lap}} = \begin{bmatrix} 5 & -1 & -1 & & & & & & 0 \\ -1 & 4 & -1 & 0 & & & & & \\ -1 & -1 & 8 & -1 & -1 & & & & \\ & 0 & -1 & 4 & -1 & . & & & \\ & & -1 & . & . & . & . & & \\ & & & . & . & . & . & 0 & \\ & & & & . & -1 & 8 & -1 & -1 \\ & & & & & 0 & -1 & 4 & -1 \\ 0 & & & & & & -1 & -1 & 5 \end{bmatrix}_{m\times m} \qquad \mathbf{B_{Lap}} = -\mathbf{B_{adj}}$$

It should be noted that Types 2 and 3 configurations are only similar to the configurations which can be made by strong Cartesian and direct graph products of cycles and paths, already defined in Chap. 3. In fact, the present types have different number of nodes and members and have nodes in all the crossing points of the members which make their topologies completely different from those of the above-mentioned graph products.

$$\mathbf{A_{adj}} = \begin{bmatrix} 0 & 1 & & & & & & & 0 \\ 1 & 0 & 1 & & & & & & \\ & 1 & 0 & 1 & & & & & \\ & & & . & . & & & & \\ & & & . & . & . & & & \\ & & & & . & . & . & & \\ & & & & & 1 & 0 & 1 & \\ & & & & & & 1 & 0 & 1 \\ 0 & & & & & & & 1 & 0 \end{bmatrix}_{m\times m} \qquad \mathbf{B_{adj}} = \begin{bmatrix} 1 & & & & & & & & 0 \\ 1 & 0 & 1 & & & & & & \\ & & 0 & & & & & & \\ & & 1 & 0 & 1 & & & & \\ & & & & . & & & & \\ & & & & . & . & 1 & & \\ & & & & & & 0 & & \\ & & & & & & 1 & 0 & 1 \\ 0 & & & & & & & & 1 \end{bmatrix}_{m\times m}$$

$$\mathbf{A_{Lap}} = \begin{bmatrix} 4 & -1 & & & & & & & 0 \\ -1 & 4 & -1 & & & & & & \\ & -1 & 4 & -1 & & & & & \\ & & . & . & . & & & & \\ & & & . & . & . & & & \\ & & & & . & . & . & & \\ & & & & & -1 & 4 & -1 & \\ & & & & & & -1 & 4 & -1 \\ 0 & & & & & & & -1 & 4 \end{bmatrix}_{m\times m} \quad \mathbf{B_{Lap}} = -\mathbf{B_{adj}}$$

$$\mathbf{A_{adj}} = \begin{bmatrix} 0 & 1 & 1 & & & & & & 0 \\ 1 & 0 & 1 & 1 & & & & & \\ 1 & 1 & 0 & 1 & 1 & & & & \\ & 1 & 1 & . & . & . & & & \\ & & 1 & . & . & . & . & & \\ & & & . & . & . & . & 1 & \\ & & & & . & 1 & 0 & 1 & 1 \\ & & & & & 1 & 1 & 0 & 1 \\ 0 & & & & & & 1 & 1 & 0 \end{bmatrix}_{m\times m} \quad \mathbf{B_{adj}} = \begin{bmatrix} 1 & & & & & & & & 0 \\ 1 & 1 & 1 & & & & & & \\ & & 1 & & & & & & \\ & & 1 & 1 & 1 & & & & \\ & & & & . & & & & \\ & & & & . & . & 1 & & \\ & & & & & & 1 & & \\ & & & & & & 1 & 1 & 1 \\ 0 & & & & & & & & 1 \end{bmatrix}_{m\times m}$$

$$\mathbf{A_{Lap}} = \begin{bmatrix} 5 & -1 & -1 & & & & & & 0 \\ -1 & 7 & -1 & -1 & & & & & \\ -1 & -1 & 8 & -1 & -1 & & & & \\ & -1 & . & . & . & . & & & \\ & & . & . & . & . & . & & \\ & & & . & . & . & . & -1 & \\ & & & & -1 & -1 & 8 & -1 & -1 \\ & & & & & -1 & -1 & 7 & -1 \\ 0 & & & & & & -1 & -1 & 5 \end{bmatrix}_{m\times m} \quad \mathbf{B_{Lap}} = -\mathbf{B_{adj}}$$

5.7 Examples from Structural Models

In this section, using the developed canonical form, the eigensolutions of various structural models are studied through some examples. In these examples, the largest eigenvalue of the adjacency matrices and the second eigenvalue and eigenvector of the Laplacian matrices are calculated for efficient nodal ordering and graph partitioning.

In the present method, eigenvalues and eigenvectors of a $nm \times nm$ matrix are found only by n times eigensolutions of different $m \times m$ matrices. This is achieved by block diagonalisation of the related matrices. This process guarantees the high accuracy and considerable decrease in computational times. The present method

Fig. 5.5 A circular dome

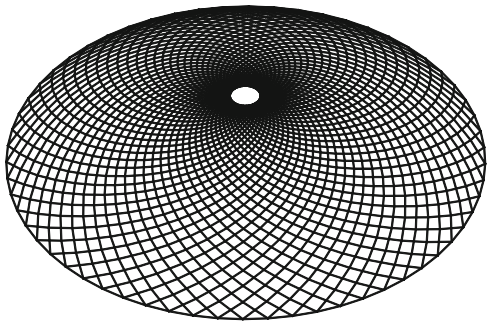

has a complexity of $n\ O(\mathrm{m}^r)$ compared to classical methods which have a complexity of $O(nm^r)$. Thus, a considerable decrease in computational times is achieved. For larger models this difference becomes more noticeable, and the usage of any program or programming language (uniformly) does not change the efficiency. However, in this chapter for all eigensolutions (n times $m \times m$ matrices), MATLAB functions are used. For a correct comparison this uniformity has been maintained.

Example 5.1. A circular dome is considered as shown in Fig. 5.5. This model has 2940 nodes and 5880 members in which $\mathrm{n} = 60$ and $\mathrm{k} = 25$. Adjacency and Laplacian matrices of this model are generated using matrices which are presented for configuration of Type 3. The largest eigenvalue of the adjacency and second eigenvalue and eigenvector of Laplacian are calculated and utilised for ordering. Also the computational time of presented method and eigensolutions using MATLAB program are compared.

The largest eigenvalue of adjacency matrices has some special properties which can be used to decrease the complexity of the calculation. According to *Perron–Frobenius* theorem, the largest eigenvalue of an adjacency matrix is a simple root of corresponding characteristic polynomial, Kaveh [3]. This means that $\mu_{\max}(\mathbf{Adj})$ cannot be found from blocks associated with complex λ_i. Then real λ_i and obviously $\lambda = 1$ should be used for this calculation. Using Eq. 5.11 the block with $\mu_{\max}(\mathbf{Adj})$ which can be found from it has the following form:

$$\mathbf{A} + \mathbf{B} + \mathbf{B}^{\mathbf{t}} = \begin{bmatrix} 2 & 2 & & & & \\ 2 & 0 & 2. & & & \\ & . & . & . & & \\ & & 2 & 0 & 2 & \\ & & & 2 & 2 & \end{bmatrix}.$$

The sum of all rows of this matrix is equal to 4, and therefore, 4 is an eigenvalue associated with the eigenvector $[\,1 \quad 1 \quad . \quad . \quad 1\,]^{\mathbf{t}}$. This is also the largest eigenvalue because 4 is the upper eigenvalue bound of this matrix. This can easily be revealed from the *Gerschgorin* first theorem, Jacques and Judd [19].

Table 5.1 The bandwidth and profile of the Laplacian matrix before and after ordering

Bandwidth of the Laplacian matrix		Profile of the Laplacian matrix	
Initial bandwidth	Bandwidth after ordering	Initial profile	Profile after ordering by $\boldsymbol{\varphi}_2$
2892	98	1502220	150906

Finally, $\mu_{max}(\mathbf{Adj}) = 4$ and the corresponding normalised eigenvector is $\boldsymbol{\varphi} = \left(\frac{1}{2940}\right) \times [1 \quad 1 \quad . \quad . \quad 1]^{\mathbf{t}}$.

Unfortunately, the second eigenvalue of Laplacian matrices is not always a simple root. However, such a clarification can be used for a simpler solution. On the other hand, using the *Gerschgorin* theorem, $\mu_2(\mathbf{Lap})$ should be found from blocks which correspond to λ_j with a large positive real parts. Since such λ_i leads to a considerable decrease in the diagonal entries of blocks, therefore, the centre of the well-known *Gerschgorin* circles will be closer to the origin. If $\mu_2(\mathbf{Lap})$ is a simple root, it can be found from the block associated with $\lambda = 1$.

For this example, the second eigenvalue of the Laplacian matrix is a double root and equals $\mu_2(\mathbf{Lap}) = 0.0058068$ which are found from the blocks associated with complex conjugate $\lambda = 0.9945 \pm 0.1045i$. For a realistic comparison between the computational times, all λ_j are used and after the calculation of eigenvalues, the second of them is selected. Also, the computational time of the present method for all the eigenvalues' calculations is 0.975 s compared to the 411.27 s extracted from MATLAB program.

Finally, using the second eigenvector of the Laplacian (Fiedler vector), a nodal ordering is performed. The remarkable reduction in bandwidth compared to the initial value can be observed from Table 5.1.

Example 5.2. In Fig. 5.6 the skeleton graph of a finite element model of a cooling tower is shown. This graph and the corresponding matrices are generated using Type 1 configuration. This graph has 1650 nodes and 4850 members with $n = 50$ and $m = 33$. The largest eigenvalue of the adjacency matrix as well as the second eigenvalue and eigenvector of the Laplacian matrix are calculated, and using the second eigenvector a nodal ordering is performed and the model is bisected. Also, the bandwidth and profile of the Laplacian matrix of the model before and after ordering are compared in Table 5.2.

As previously mentioned, the largest eigenvalue of adjacency matrix is a simple root of the characteristic polynomial, and this value must be calculated from the block which corresponds to $\lambda = 1$. This block is a tri-diagonal matrix with its entries equal to 2. The decomposed form of such a matrix can be written as

$$\mathbf{A} + \mathbf{B} + \mathbf{B}^{\mathrm{t}} = 2\mathbf{I}_{m\times m} + 2\mathbf{F}_{m\times m}(0,1,0) = \begin{bmatrix} 2 & 2 & & & \\ 2 & 2 & 2 & & \\ & . & . & . & \\ & & 2 & 2 & 2 \\ & & & 2 & 2 \end{bmatrix}_{m\times m}$$

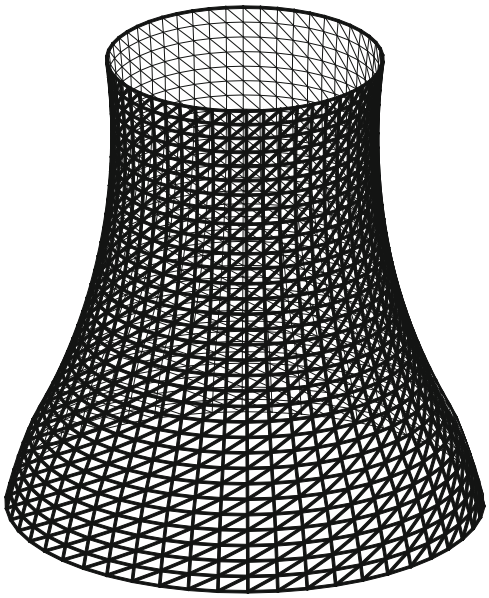

Fig. 5.6 Skeleton graph for the finite element model of a cooling tower

Table 5.2 The bandwidth and profile of the Laplacian matrix before and after ordering

Bandwidth of the Laplacian matrix		Profile of the Laplacian matrix	
Initial bandwidth	Bandwidth after ordering	Initial profile	Profile after ordering by $\boldsymbol{\varphi}_2$
1616	54	107201	81703

where $\mathbf{F}(0,1,0)$ is only a compact representation of a matrix. A comprehensive explanation of this representation and its corresponding eigenvalues can be found in Sect. 4.9. However, the largest eigenvalue can analytically be calculated as

$$\mu_{\max}(\mathbf{Adj}) = 2 + 4\ \max\left(\cos\frac{i\pi}{m+1}\right)\ i = 1,\ldots,m.$$

Since $i = 1$ maximises the term which is in the brackets, therefore,

$$\mu_{\max}(\mathbf{Adj}) = 5.982936.$$

The second eigenvalue of the Laplacian matrix is calculated as $\mu_2(\mathbf{Lap}) = 0.0181123$, and the corresponding eigenvector is also obtained using the present method. The model is also bisected using the Fiedler vector, and its partitioned form is illustrated in Fig. 5.7.

For this example, the computational time for the present method when all the eigenvalues are calculated is 0.093 s compared to the 58.29 s extracted from MATLAB program.

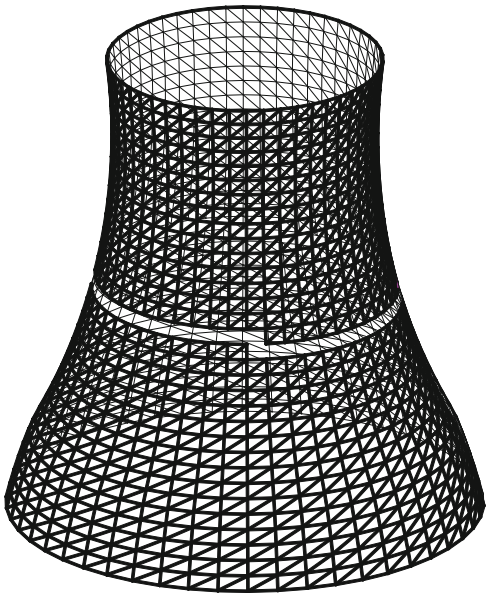

Fig. 5.7 The bisected form of cooling tower through the Fiedler vector

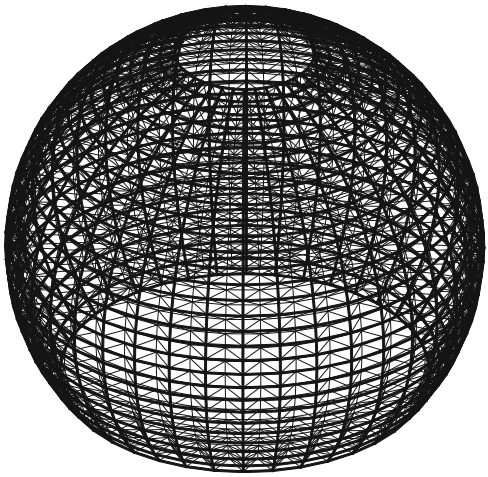

Fig. 5.8 Spherical double-layer dome

Example 5.3. In Fig. 5.8 a double-layer spherical dome is shown. The total number of nodes and elements of this graph are 2360 and 9280, respectively, with n = 40 and k = 30. This graph and the corresponding matrices are generated by the details of Type 4 configuration. The largest eigenvalue of adjacency and the second eigenvalue and eigenvector of Laplacian matrices are also calculated. The bandwidth and profile of the Laplacian matrix of the model before and after ordering are also shown in Table 5.3.

Table 5.3 The bandwidth and profile of the Laplacian matrix before and after ordering

Bandwidth of the Laplacian matrix		Profile of the Laplacian matrix	
Initial bandwidth	Bandwidth after ordering	Initial profile	Profile after ordering by $\boldsymbol{\varphi}_2$
2302	101	269283	184130

The largest eigenvalue of the adjacency matrix can easily be calculated by finding the largest eigenvalue of the following matrix (block associated with $\lambda = 1$):

$$\mathbf{A}+\mathbf{B}+\mathbf{B}^{\mathrm{t}} = 2\mathbf{I}_{m\times m} + 2\mathbf{F}_{m\times m}(0,1,0) + \mathbf{F}_{m\times m}(0,0,1,0) = \begin{bmatrix} 2 & 2 & 1 & & \\ 2 & 2 & 2 & . & \\ 1 & . & . & . & 1 \\ & . & 2 & 2 & 2 \\ & & 1 & 2 & 2 \end{bmatrix}_{m\times m} .$$

Therefore, $\mu_{\max}(\mathbf{Adj}) = 7.9837910$. This value and the corresponding eigenvector can be used for the selection of a good starting node for graph-theoretical-based ordering methods, Kaveh [1, 2]. Also the largest eigenvalue of Laplacian matrix which is a simple root is calculated as $\mu_2(\mathbf{Lap}) = 0.0169988$, and using the corresponding eigenvector, a nodal ordering is performed. The results shown in Table 5.3 indicate a considerable reduction in the bandwidth and profile of the Laplacian matrix of this model. For this example, the computational time of presented method for all eigenvalues' calculations is *0.234* s compared to the *196.59* s extracted from MATLAB program. Thus, using the present method, all the eigenvalues can be calculated in a fraction of a second.

The efficiency of algebraic graph theory in combinatorial optimisation, especially in nodal ordering and partitioning of graphs, is well known. However, large structural models and their corresponding graphs require considerable computational time for evaluating their eigenvalues and eigenvectors. In this chapter, using a special canonical form, a highly efficient method was presented for eigensolution of some special structural and finite element models which are often encountered in structural mechanics.

References

1. Kaveh A (2004) Structural mechanics: graph and matrix methods, 3rd edn. Research Studies Press, Exeter
2. Kaveh A (2006) Optimal structural analysis, 2nd edn. Wiley, Chichester
3. Kaveh A, Koohestani K (2008) Graph products for configuration processing of space structures. Comput Struct 86:1219–1236
4. Biggs NL (1993) Algebraic graph theory, 2nd edn. Cambridge University Press, Cambridge
5. Cvetković DM, Doob M, Sachs H (1980) Spectra of graphs, theory and applications. Academic, New York
6. Seidel JJ (1989) Graphs and their spectra, combinatorics and graph theory. PWN-Polish Scientific, Warsaw

7. Fiedler M (1973) Algebraic connectivity of graphs. Czech Math J 23:298–305
8. Fiedler M (1975) An algebraic approach to connectivity of graphs. In: Fiedler M (ed) Recent advances in graph theory. Academia, Praha, pp 193–196
9. Mohar B et al (1991) The Laplacian spectrum of graphs. In: Alavi Y (ed) Graph theory, combinatorics and applications, vol 2. Wiley, New York, pp 871–898
10. Pothen A, Simon H, Liou KP (1990) Partitioning sparse matrices with eigenvectors of graphs. SIAM J Matrix Anal Appl 11:430–452
11. Topping BHV, Sziveri J (1995) Parallel subdomain generation method. In: proceedings of Civil-Comp, Edinburgh
12. Paulino GH, Menezes IFM, Gattass M, Mukherje S (1994) Node and element resequencing using Laplacian of a finite element graph, Part-I-general concepts and algorithms. Int J Numer Methods Eng 37:1511–1530
13. Simon HD (1991) Partitioning of unstructured problems for parallel processing. Comput Syst Eng 2:135–148
14. Seale C, Topping BHV (1995) Parallel implementation of recursive spectral bisection. In: proceedings of Civil Comp 95, Edinburgh, pp. 459–473
15. Kaveh A (1991) Algebraic and topological graph theory for ordering. Z Angew Math Mech 71: T739–T742
16. Kaveh A, Davaran A (2006) Spectral bisection of adaptive finite element meshes for parallel processing. Comput Struct 70:315–323
17. Kaveh A, Rahimi Bondarabady HA (2002) A multi-level finite element nodal ordering using algebraic graph theory. Finite Elem Anal Des 38:245–261
18. Kaveh A, Rahimi Bondarabady HA (2004) Bisection using Fiedler and Ritz vectors. Acta Mech 167(3–4):131–144
19. Jacques I, Judd C (1987) Numerical analysis. Chapman and Hall, London

Chapter 6
Graph Products for Ordering and Domain Decomposition

6.1 Introduction

A number of algorithms based on domain decomposition methods have been proposed for the solution of the partial differential equations arising in solid and fluid mechanics problems, among others. These methods are generally spurred by the advent of parallel processors and are motivated by the fact that domain decomposition provides a natural route to parallelism. Given a number of available processors q, an arbitrary finite element model (FEM) is decomposed into q subdomains where formation of element matrices, assembly of global matrices, partial factorisation of the stiffness matrix and state determination or evaluation of generalised stresses can be carried out independently of similar computations for the other subdomains and hence can be performed in parallel.

While the subdomains are processed in a parallel architecture, the time to complete a task will be the time to compute the longest subtask. An algorithm for domain decomposition will be efficient if it yields subdomains that require an equal amount of execution time. In other words, the algorithm has to achieve a load balance among the processors. In general, this will be particularly ensured if each subdomain contains an equal number of elements or equal total number of degrees of freedom.

In the previous chapter ordering and graph partitioning were performed using special canonical forms. In this chapter, the properties of graph products are utilised for efficient ordering and decomposition. Here, an efficient analytical method is presented for calculating the eigenvalues of space structures and finite element meshes (FEMs) with regular topologies. In this method, the graph model of a FEM is considered as the Cartesian product of its generators. The eigenvalues of the Laplacian matrix for this graph model is then easily calculated using the eigenvalues of their generators [1, 2]. An exceptionally fast method is also proposed for computing the second eigenvalue and eigenvector $\mathbf{v}_2$ of the Laplacian of the graph model. The entries of $\mathbf{v}_2$ are then ordered and accordingly the graph is partitioned, and the corresponding finite element mesh is bisected. This vector is

A. Kaveh, *Optimal Analysis of Structures by Concepts of Symmetry and Regularity*,
DOI 10.1007/978-3-7091-1565-7_6,

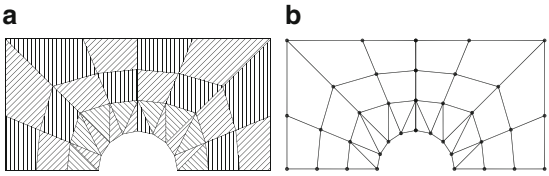

Fig. 6.1 A FE mesh and its skeleton graph. (**a**) A simple finite element mesh. (**b**) The skeleton graph of the FE mesh

also employed for the nodal numbering to reduce the profile of the stiffness matrices. The idea study is extended to other graph products and an efficient approximate method is presented. Examples are included to illustrate the efficiency of the method.

It should be noted that in this chapter, the two words 'generator' and 'regular' are used in their literal senses and their meaning should not be taken identical to those employed in topology and graph theory. Here, the geometry of the models need not be regular, and the only requirement is the regularity of the topology, that is, a regular model affected by an arbitrary geometrical transformation can also be bisected with the method of this chapter.

6.2 Graph Models of Finite Element Meshes

There are at least ten different graph models in the literature for transforming the connectivity properties of FE meshes into the topological properties of their graphs, Kaveh [3, 4]. In this chapter the simplest one, known as the skeleton graph, is used for this transformation.

The *skeleton graph* of a FE mesh is a graph whose nodes are the same as those of the FE mesh, and the boundaries of the elements form the edges of the skeleton graph. A small FE mesh containing linear rectangular and triangular elements is depicted in Fig. 6.1a, and the skeleton graph of this FE mesh is shown in Fig. 6.1b.

Many mechanical models can be viewed as the Cartesian product of a number of simple graphs. Such models are called *regular* in this chapter. The subgraphs used in the formation of a model are called the *generators* of that model, as discussed in Chap. 3.

6.3 Eigenvalues of Graph Matrices for Cartesian Product

6.3.1 Properties of Kronecker Product

The Kronecker product, previously defined in Sect. 4.9, has the property that if **B**, **C**, **D** and **E** are four matrices, such that **BD** and **CE** exist, then

$$(\mathbf{B} \otimes \mathbf{C})(\mathbf{D} \otimes \mathbf{E}) = \mathbf{BD} \otimes \mathbf{CE}. \tag{6.1}$$

Thus, if **u** and **v** are vectors of the correct dimensions, then

$$(\mathbf{B} \otimes \mathbf{C})(\mathbf{u} \otimes \mathbf{v}) = \mathbf{Bu} \otimes \mathbf{Cv}. \tag{6.2}$$

If u and v are eigenvectors of **B** and **C**, with eigenvalues λ and μ, respectively, then,

$$\mathbf{Bu} \otimes \mathbf{Cv} = \lambda\mu\mathbf{u} \otimes \mathbf{v}, \tag{6.3}$$

Whence, $\mathbf{u} \otimes \mathbf{v}$ is an eigenvector of $\mathbf{B} \otimes \mathbf{C}$ with eigenvalue λμ.

For a Cartesian product K × H, the adjacency matrix **A** can be written as follows:

$$\mathbf{A}(\mathrm{K} \times \mathrm{H}) = \mathbf{A}(\mathrm{K}) \otimes \mathbf{I}_{\mathrm{N(H)}} + \mathbf{I}_{\mathrm{N(K)}} \otimes \mathbf{A}(\mathrm{H}). \tag{6.4}$$

In this relation, $\mathbf{A}(\mathrm{K}) \otimes \mathbf{I}_{\mathrm{N(H)}}$ is the adjacency matrix of N(H) node-disjoint copies of K, and $\mathbf{I}_{\mathrm{N(K)}} \otimes \mathbf{A}(\mathrm{H})$ is the adjacency matrix of N(K) node-disjoint copies of H, Refs. [1, 2].

In the case of Cartesian product, similar relationship holds for the Laplacian matrices, that is,

$$\mathbf{L}(\mathrm{K} \times \mathrm{H}) = \mathbf{L}(\mathrm{K}) \otimes \mathbf{I}_{\mathbf{N(H)}} + \mathbf{I}_{\mathbf{N(K)}} \otimes \mathbf{L}(\mathrm{H}). \tag{6.5}$$

6.3.2 Theorem

Let $\lambda_1,\lambda_2,\ldots,\lambda_m$ and $\mu_1,\mu_2,\ldots,\mu_n$ be the eigenvalues for the Laplacian matrices of K and H, respectively. Then m×n eigenvalues of the Laplacian of G = K × H are $\{\lambda_i + \mu_j\}$ i = 1:m and j = 1:n.

Proof. Using the above relationship, we have

$$\mathbf{L}(\mathrm{K} \times \mathrm{H})(\mathbf{u}_i \otimes \mathbf{v}_j) = \big(\mathbf{L}(\mathrm{K}) \otimes \mathbf{I}_{\mathrm{N(H)}}\big)(\mathbf{u}_i \otimes \mathbf{v}_j) + \big(\mathbf{I}_{\mathrm{N(K)}} \otimes \mathbf{L}(\mathrm{H})\big)(\mathbf{u}_i \otimes \mathbf{v}_j). \tag{6.6}$$

The associativity property of the Kronecker product results in

$$\begin{aligned}&\big(\mathbf{L}(\mathrm{K}) \otimes \mathbf{I}_{\mathrm{N(H)}}\big)\big(\mathbf{u}_i \otimes \mathbf{v}_j\big) + \big(\mathbf{I}_{\mathrm{N(K)}} \otimes \mathbf{L}(\mathrm{H})\big)\big(\mathbf{u}_i \otimes \mathbf{v}_j\big)\\ &= (\mathbf{L}(\mathrm{K}))(\mathbf{u}_i) \otimes \big(\mathbf{I}_{\mathrm{N(H)}}\big)\big(\mathbf{v}_j\big) + \big(\mathbf{I}_{\mathrm{N(H)}}\big)\big(\mathbf{u}_j\big) \otimes (\mathbf{L}(\mathrm{K}))(\mathbf{u}_i) = \lambda_i\mathbf{u}_i \otimes \mathbf{v}_j + \mathbf{u}_i \otimes \mu_j\mathbf{v}_j\end{aligned} \tag{6.7}$$

leading to

$$\mathbf{L}(\mathrm{K}\times\mathrm{H})(\mathbf{u}_\mathrm{i}\otimes\mathbf{v}_\mathrm{j}) = (\lambda_\mathrm{i}+\mu_\mathrm{j})\mathbf{u}_\mathrm{i}\otimes\mathbf{v}_\mathrm{j}, \tag{6.8}$$

and the proof is complete.

Once the eigenvalues are found, the corresponding eigenvectors can be calculated. However, this can be done much simpler considering that the eigenvectors of G are the Kronecker product of the eigenvectors of K and H, that is, $\mathbf{w}_\mathrm{k} = \mathbf{u}_\mathrm{i}\otimes\mathbf{v}_\mathrm{j}$, where $\mathbf{w}_\mathrm{k}$, $\mathbf{u}_\mathrm{i}$ and $\mathbf{v}_\mathrm{j}$ are the eigenvectors of G, K and H, respectively.

6.3.3 Eigenvalues of Graph Matrices for Cycle and Path Graphs

Consider the adjacency matrix $\mathbf{A}$ of a cycle graph $\mathrm{C_n}$. When $\mathbf{A}$ is expanded with respect to the first row, the characteristic polynomial of $\mathrm{C_n}$ is obtained as $|\mathbf{A}-\lambda\mathbf{I}| = 0$. The eigenvalues corresponding to the above relations can simply be expressed as

$$\lambda_\mathrm{r} = 2\cos\left(\frac{2\pi\mathrm{r}}{\mathrm{n}}\right) : \mathrm{r} = 1:\mathrm{n}. \tag{6.9}$$

Now λ_r is obtained for the Laplacian matrix $\mathbf{L}$ of a graph. For a cycle graph we have $\mathbf{D} = 2\mathbf{I}_\mathrm{n}$. In fact for a regular graph $\mathbf{D} = \mathrm{k}\mathbf{I}_\mathrm{n}$ and for a cycle $\mathrm{k} = 2$. Therefore,

$$\det(\mathbf{L}-\lambda\mathbf{I}) = 0 \Rightarrow \det[(\mathbf{D}-\mathbf{A})-\lambda\mathbf{I}] = 0 \Rightarrow \det[-\mathbf{A}-(\lambda-2)\mathbf{I}] = 0. \tag{6.10}$$

The eigenvalues of $-\mathbf{A}$ are the same as those of $\mathbf{A}$ with a reverse sign. Therefore, once the eigenvalues of $\mathbf{A}$ are obtained, the signs are reversed and two units are added.

For the Laplacian matrix $\mathbf{L}$, the equation $|\mathbf{L}-\lambda\mathbf{I}| = 0$ should be solved as

$$\begin{aligned}\lambda_\mathrm{r} &= 2-2\cos\left(\frac{2\pi\mathrm{r}}{\mathrm{n}}\right) = \left(\frac{2\sin\pi\mathrm{r}}{\mathrm{n}}\right)^2 : \mathrm{r} = 0:\mathrm{n}-1 \text{ and}\\ \mathrm{r} &= 0 \Rightarrow \lambda_1 = 0.\end{aligned} \tag{6.11}$$

Obviously the maximum value of λ_r for matrix $\mathbf{A}$ is equal to 2, and the minimum value of λ_r for Laplacian, by ignoring 0, is equal to $\left(\frac{2\sin\pi}{\mathrm{n}}\right)^2$. As an example, for $\mathrm{n} = 10$, $\lambda_2 = 0.3820$. The above equation reveals that $\lambda_\mathrm{r} \in \{0,4\}$.

Repeating the above arguments, for the adjacency matrix of a path graph $\mathrm{P_n}$, we have

$$\lambda_\mathrm{r} = 2\cos\left[\frac{\pi\mathrm{r}}{(\mathrm{n}+1)}\right] : \mathrm{r} = 1:\mathrm{n}, \tag{6.12}$$

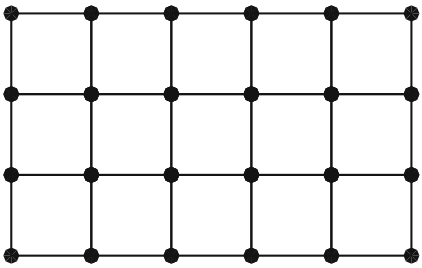

Fig. 6.2 Cartesian product $P_6\ (X)_C\ P_4$ of two path graphs

and for the Laplacian matrix of P_n,

$$\lambda_r = 2 - 2\cos\left(\frac{\pi r}{n}\right) = \left(\frac{2\sin\pi r}{2n}\right)^2 : r = 0 : n-1 \text{ and } r = 0 \Rightarrow \lambda_1 = 0. \quad (6.13)$$

Again here we have $\lambda_r \in \{0,4\}$.

Obviously, the maximum value of λ_r for the adjacency matrix is $2\cos\left[\frac{\pi}{(n+1)}\right]$, and λ_2 for the Laplacian matrix is $\left(\frac{2\sin\pi}{2n}\right)^2$.

6.3.4 Example

Consider the Cartesian product of two paths P_6 and P_4 as shown in Fig. 6.2. In order to calculate the eigenvalues of the Laplacian matrix **L** of the graph obtained by the Cartesian product of P_6 and P_4, first, the eigenvalues for these paths should be obtained. Then the first eigenvalue of P_6 is added to all the eigenvalues of P_4. Next the second eigenvalue of P_6 is added to those of P_4. This process is continued until all eigenvalues of $S = P_6\ (X)_C\ P_4$ are obtained.

As a numerical example, consider the two path graphs as P_6 and P_4. The eigenvalues for the Laplacian matrix **L** of S are calculated as follows:

$$\lambda(P_6) : \{0;\ 0.2679;\ 1;\ 2;\ 3;\ 3.7321\},$$
$$\lambda(P_4) : \{0;\ 0.5858;\ 2;\ 3.4142\},$$
$$\lambda(S) = \lambda(P_6) + \lambda(P_4) = \{0;\ 0.5858;\ 2;\ 3.4142;\ 0.2679;\ \ldots;\ 7.1463\}.$$

For the Laplacian matrix **L** of each path graph, the eigenvalues lie in the range [0,4]. Thus, the final results are contained in the range [0,8]. For this case, the first eigenvalue is zero, and therefore, for calculating the second eigenvalues, λ_2, one should choose the smallest eigenvalue from P_6 and P_4, so that when added to zero, λ_2 for S is obtained. Obviously as the number of nodes of a graph increases, the corresponding λ_2 will decrease. Hence, for evaluating λ_2 of S, it is sufficient to select the generator with the higher number of nodes (i.e. $\lambda_2(P_6)$ in this example):

$$\lambda_2(S) = \lambda_2(P_6) \text{ since } n(P_6) > n(P_4). \quad (6.14)$$

For this case, the eigenvalues of the path P_3 and the cycle C_7 are calculated:

$$\lambda(P_3) : \{0;\ 1;\ 3\},$$
$$\lambda(C_7) : \{0;\ 0.7530;\ 0.7530;\ 2.4450;\ 2.4450;\ 3.8019;\ 3.8019\},$$
$$\lambda_2(S) = \lambda_2(C_7) = 0.7530,$$

and all the eigenvalues of **L** for S can be obtained, similar to the previous example. Further simplification can be achieved if the cycle has an even number of nodes more than two. For such a case, two eigenvalues are 0 and 4. For evaluating the remaining eigenvalues, one can divide the number of nodes by 2 and consider an equivalent path graph with this number of nodes, and each eigenvalue obtained should be repeated once.

6.4 Spectral Method for Bisection

6.4.1 Computing λ_2 for Laplacian of Regular Models

In the method of the previous section, if only the magnitude of λ_2 is required, then the method can further be simplified. As an example, in the above problem half of the nodes of the cycle should be compared to the number of nodes of the path generator, and the one with the largest number of nodes should be selected. For this graph, the second eigenvalue λ_2 has the same value as that of the main graph S.

The above idea can easily be generalised to three-dimensional models. Consider a three-dimensional grid as $S = P_8\ (X)_C\ P_5\ (X)_C\ P_4$. This graph has 160 nodes, and P_8, P_5 and P_4 have 8, 5 and 4 nodes, respectively. Thus, $\lambda_2(S) = \lambda_2(P_8) = 0.1522$, since P_8 has more nodes than the other generators.

Consider a simple model as shown in Fig. 6.3a. After some geometric transformations, the models shown in Fig. 6.3b–c are obtained (see Nooshin [5] for such transformations). These models are equivalent to a circle with 25 and 72 sectors. Since $72/2 = 36 > 26$, therefore $\lambda_2 = \left(\frac{2\sin\pi}{72}\right)^2 = 0.0076$.

6.4.2 Algorithm

This method is simple and consists of the following steps:

Step 1. Calculate the second eigenvalue λ_2 of the Laplacian matrix **L** of the model.
Step 2. Construct the second eigenvector $\mathbf{v}_2$ corresponding to λ_2.
Step 3. Order the entries of $\mathbf{v}_2$ in an ascending order.
Step 4. Construct the status vector **Sv** for bisection of the model according to their occurrence in $\mathbf{v}_2$, and correspondingly number the nodes of the FEM.

The above algorithm can easily be used for graph partitioning, and correspondingly the domain decomposition can easily be performed.

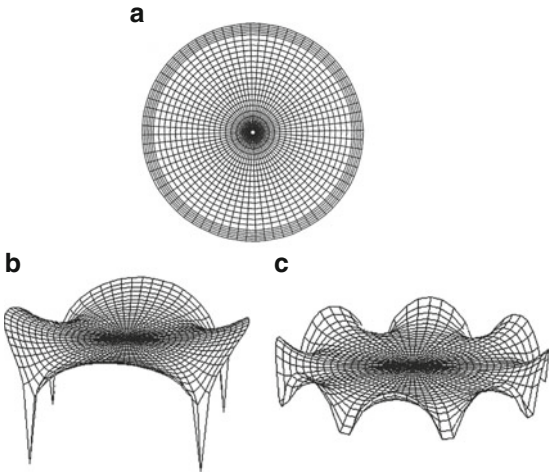

Fig. 6.3 Models as the Cartesian product of a circle and a path. (**a**) A simple finite element mesh

6.5 Numerical Results

In this section the results for three FE meshes are presented. The models are chosen from those encountered in practice having different topologies. Here, for the standard method, MATLAB is employed for calculating λ_2 and $\mathbf{v}_2$. However, for the present method, no computational time is provided for the examples since unlike the standard known methods, for each example it takes a fraction of a second to calculate the eigenvalues and eigenvectors.

Example 6.1. A simply connected rectangular FE mesh with rectangular elements is considered as shown in Fig. 6.4. This model consists of 3,168 nodes and 3,045 elements. The skeleton graph is considered as $P_{88}\ (X)_C\ P_{36}$ and is partitioned with $\lambda_2 = 0.00127$ corresponding to P_{88}, and the corresponding FEM is bisected. The process is repeated for further decomposition of the FEM into four, eight, sixteen and thirty-two subdomains as illustrated in the same figure.

The computational time was 119.7 s for evaluating λ_2, and 614.7 s for calculating λ_2 and $\mathbf{v}_2$, while the present method takes a few seconds to evaluate λ_2 and $\mathbf{v}_2$ analytically.

Example 6.2. A circular FE mesh is considered as shown in Fig. 6.5. This model consists of 1,872 nodes and 1,800 rectangular elements. The skeleton graph is considered as $C_{72}\ (X)_C\ P_{26}$ and is partitioned with $\lambda_2 = 0.007611$ corresponding to C_{72}, and the corresponding FEM is bisected. The process is repeated for further decomposition of the FEM into four, eight and sixteen subdomains as illustrated in the same figure.

The computational time was 19.8 s for evaluating λ_2, and 103.5 s for calculating λ_2 and $\mathbf{v}_2$, while the present method takes a few seconds to evaluate λ_2 and $\mathbf{v}_2$ analytically.

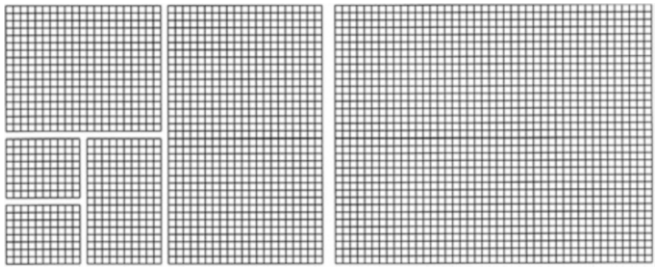

Fig. 6.4 A rectangular FE mesh and its sequential bisections

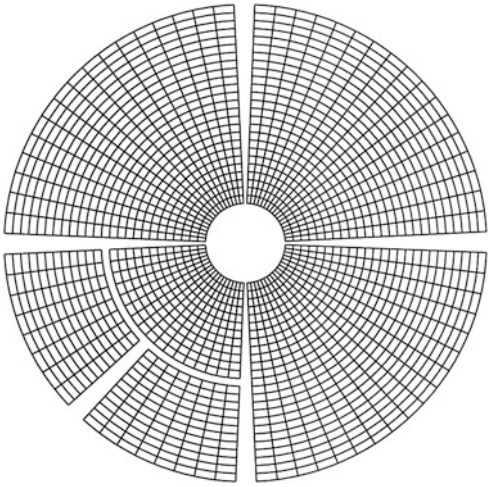

Fig. 6.5 A circular FE mesh and its sequential bisections

Example 6.3. A finite element mesh of a nuzzle is considered as shown in Fig. 6.6a. This model consists of 4,000 nodes and 3,960 rectangular shell elements. The skeleton graph is considered as $P_{100}\ (X)_C\ C_{40}$ and is partitioned with $\lambda_2 = 0.000987$ corresponding to P_{100}, and the corresponding FEM is bisected, Fig. 6.6b. The process is repeated for further decomposition of the FEM into four subdomains as illustrated in Fig. 6.6c.

The computational time was 269.5 s for evaluating λ_2, and 1072.3 s for calculating λ_2 and $\mathbf{v}_2$, while the present method takes a few seconds to evaluate λ_2 and $\mathbf{v}_2$ analytically.

In the above examples, the generators were chosen as paths and or cycles. In the following examples one of the generators is selected as an arbitrary graph. Again λ_2 for the entire model can easily be obtained by comparison of the λ_2 for the generators. In this case, however, the second eigenvalue of the generators should be calculated using classical methods.

Example 6.4. Consider a model with an arbitrary subgraph S_1 as its generator, Fig. 6.7. The Cartesian products of $S_1\ (X)_C\ P_4$ and $S_1\ (X)_C\ C_4$ are considered. The corresponding eigenvalues are as follows:

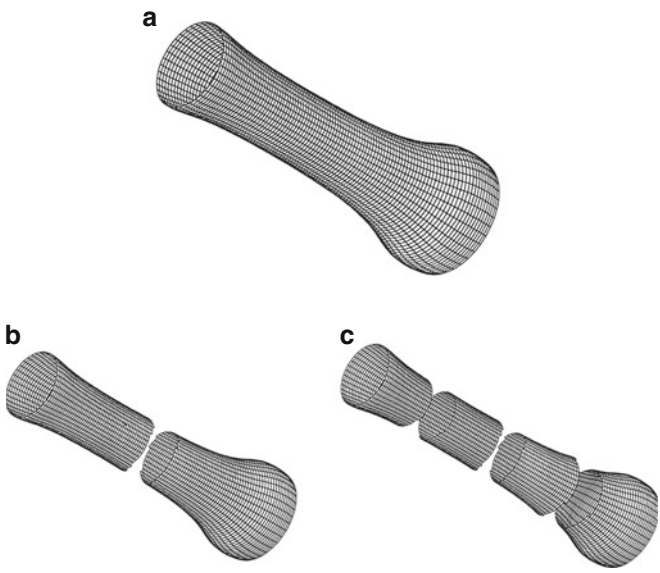

Fig. 6.6 A cylindrical shaped FE mesh and its decompositions. (**a**) A simple finite element mesh for a nuzzle. (**b**) Bisected model. (**c**) Further bisection

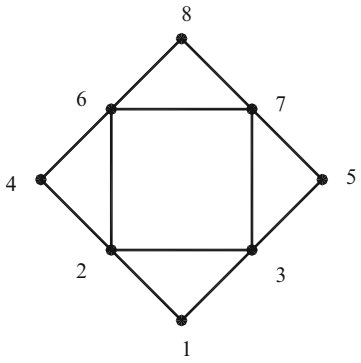

Fig. 6.7 The arbitrary generator S_1 of the considered model

$$\lambda_2(S_1) = 1.2679 \text{ and } \lambda_2(P_4) = 0.5858, \text{ and therefore } \lambda_2\left(S_1\,(X)_C\,P_4\right) = 0.5858;$$
$$\lambda_2(S_1) = 1.2679 \text{ and } \lambda_2(C_4) = 2.0000, \text{ and therefore } \lambda_2\left(S_1\,(X)_C\,C_4\right) = 1.2679. \quad (6.15)$$

Since in this problem a small number of nodes are involved, therefore the computational time using MATLAB is also small. However, if $S_1\,(X)_C\,P_{100}$ and $S_1\,(X)_C\,C_{100}$ are considered, the computational time becomes significant with MATLAB, namely, 1.6540 and 7.1500 for computing λ_2 and $\mathbf{v}_2$ for $S_1\,(X)_C\,P_{100}$ and 1.6380 and 6.2890 for those of $S_1\,(X)_C\,C_{100}$. While the present method requires only the use of simple analytical relationships as discussed in Sect. 6.3.

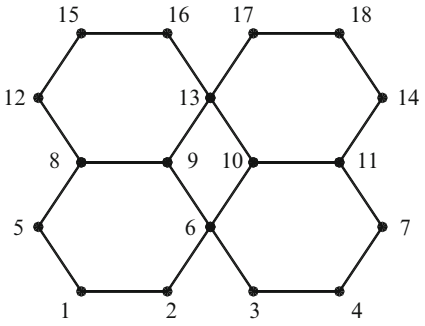

Fig. 6.8 The arbitrary generator S_2 of the considered model

Example 6.5. Consider a model with an arbitrary subgraph S_2 as its generator, Fig. 6.8. The Cartesian products of $S_2\ (X)_C\ P_{10}$ and $S_2\ (X)_C\ C_{10}$ are considered. The corresponding eigenvalues are as follows:

$$\lambda_2(S_2) = 0.2765 \text{ and } \lambda_2(P_{10}) = 0.0979, \text{ and therefore } \lambda_2\left(S_2\ (X)_C\ P_{10}\right) = 0.0979;$$
$$\lambda_2(S_2) = 0.2765 \text{ and } \lambda_2(C_{10}) = 0.3820, \text{ and therefore } \lambda_2\left(S_2\ (X)_C\ C_{10}\right) = 0.2765. \quad (6.16)$$

Since in this problem a small number of nodes are involved, therefore the computational time using MATLAB is also small. However, if $S_2\ (X)_C\ P_{100}$ and $S_2\ (X)_C\ C_{100}$ are considered, the computational time becomes substantial with MATLAB, namely, 31.6170 and 151.0570 for computing λ_2 and $\mathbf{v}_2$ for $S_2\ (X)_C\ P_{100}$ and 31.1570 and 125.4680 for those of $S_2\ (X)_C\ C_{100}$. While the present method requires only the use of simple analytical relationships as discussed in Sect. 6.4.

From these examples it can easily be observed that the present analytical method is highly efficient and makes the calculation of eigenvalues for Laplacian matrices of regular FE meshes very simple and fast, compared to the use of classic numerical methods. The only restriction corresponds to irregular models, for which additional effort is needed to regularisation. However, for irregular models, the results of the present approach can always be used as a primary approximation for further optimisation.

6.6 Spectral Method for Nodal Ordering

This method is simple and consists of the following steps:

Step 1. Calculate the second eigenvalue λ_2 of the Laplacian matrix $\mathbf{L}$ of the model.
Step 2. Construct the second eigenvector $\mathbf{v}_2$ corresponding to λ_2.
Step 3. Order the entries of $\mathbf{v}_2$ in an ascending order.
Step 4. Renumber the nodes of the model according to their occurrence in $\mathbf{v}_2$.

The above algorithm leads to well-structured stiffness matrices with low bandwidth and low profile. In the following examples are included to illustrate the performance of the present method.

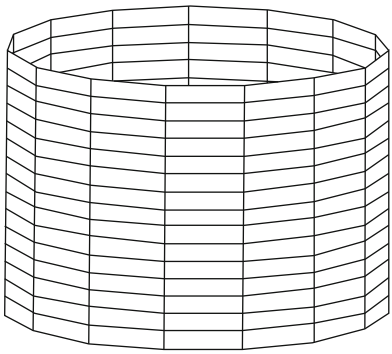

Fig. 6.9 A cylindrical grid S

Table 6.1 Results of Example 6.6

	Profile	Bandwidth
Initial	16,258	239
New	3,642	16

Example 6.6. A cylindrical grid S with two generators P_{16} and C_{15} is shown in Fig. 6.9. This model has 240 nodes and 465 members. Since $16 > 15/2$, thus for P_{16} we have $\lambda_2 = \left(\frac{2\sin\pi}{2\times 16}\right)^2 = 0.038429$ corresponding to the second eigenvalue of the entire model. The results corresponding to the bandwidth and profile of S before and after nodal ordering, using the second eigenvector of its Laplacian, are illustrated in Table 6.1.

Example 6.7. A circular grid S with beam elements is shown in Fig. 6.10. This grid S has two generators P_{13} and C_{96}. This model has 1,248 nodes and 1,152 members. Since $96/2 > 13$, thus for C_{96} we have $\lambda_2 = \left(\frac{2\sin\pi}{96}\right)^2 = 0.01711$ corresponding to the second eigenvalue of the entire model. The results corresponding to the bandwidth and profile of S before and after nodal ordering, using the second eigenvector of its Laplacian, are illustrated in Table 6.2.

For these examples, no comparison is made with other methods, since in the present approach calculating λ_2 takes only a fraction of a second. However, for the present method additional effort is needed to identify the generators.

6.7 Spectral Method for Different Product Graphs: An Approximate Method

In this section, an approximate method is introduced. In this approach, using the Laplacian matrix and exerting some modifications on its entries, one can directly write this matrix in algebraic terms, and the corresponding eigensolution becomes a straightforward process. These modifications lead to a better approximation, and it is simpler than the existing methods, since in the new approach the construction of a

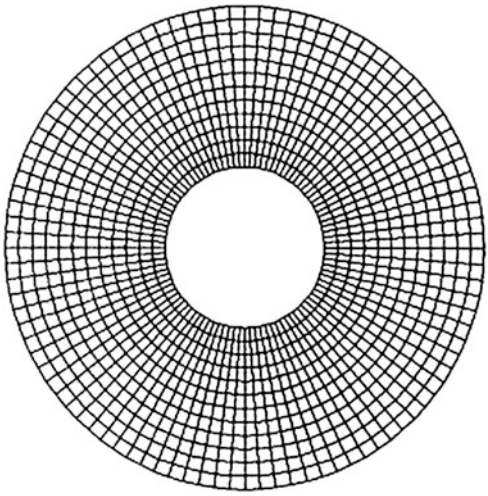

Fig. 6.10 A circular grid S

Table 6.2 Results of Example 6.7

	Profile	Bandwidth
Initial	49,972	239
New	34,848	46

new model by adding members and rewriting the Laplacian matrix for the modified model can be avoided.

In graph product of two subgraphs K and H with degree n and degree m, respectively, one can express the Laplacian matrix as

$$\mathbf{L} = \mathbf{F}_{\mathrm{n}}(\mathbf{A}_{\mathrm{m}}, \mathbf{B}_{\mathrm{m}}, \mathbf{C}_{\mathrm{m}}) = \begin{bmatrix} \mathbf{A}_{\mathrm{m}} & \mathbf{B}_{\mathrm{m}} & & & & & \\ \mathbf{B}_{\mathrm{m}} & \mathbf{C}_{\mathrm{m}} & \mathbf{B}_{\mathrm{m}} & & & & \\ & \mathbf{B}_{\mathbf{m}} & \mathbf{C}_{\mathbf{m}} & \mathbf{B}_{\mathrm{m}} & & & \\ & & \cdot & \cdot & \cdot & & \\ & & & \mathbf{B}_{\mathrm{m}} & \mathbf{C}_{\mathrm{m}} & \mathbf{B}_{\mathrm{m}} & \\ & & & & \mathbf{B}_{\mathbf{m}} & \mathbf{A}_{\mathrm{m}} & \end{bmatrix}. \tag{6.17}$$

It can be seen that the Laplacian matrix has a three-diagonal form with degree $nm \times nm$. For calculating the eigenvalues of such a matrix in terms of the eigenvalues of its subgraphs, one has to write the Laplacian matrix in algebraic terms. Most of the approximate methods exert some modifications into the Laplacian matrices. Such condition can be attained by writing a relation between the blocks of the considered matrix. For example, in the methods develop by Pothen et al. [6] or Kaveh and Rahami [2], the modifications lead to a relation between blocks of Laplacian matrix as $\mathbf{A}_{\mathrm{m}} = \mathbf{B}_{\mathrm{m}} + \mathbf{C}_{\mathrm{m}}$ that makes an easy eigensolution feasible. Now in the present method, without using the graphical model, we rewrite the Laplacian matrix in algebraic terms which can be expressed as the sum of some Kronecker products as

$$\mathbf{L} = \mathbf{I}_n \otimes (\mathbf{A}_m + \mathbf{B}_m) - \mathbf{T}_n \otimes \mathbf{B}_m + \mathbf{K}_n \otimes (\mathbf{C}_m - \mathbf{A}_m + \mathbf{B}_m) \tag{6.18}$$

in which $\mathbf{T}_n = \mathbf{F}_n(1, -1, 2)$ and $\mathbf{K}_n = \mathbf{F}_n(0, 0, 1)$. However, the blocks $\mathbf{A}_m, \mathbf{B}_m$ and $\mathbf{C}_m$ have a similar three-diagonal pattern similar to the main Laplacian matrix $\mathbf{L}$. Thus, we can write these as

$$\begin{cases} \mathbf{A}_m = \mathbf{F}_m(a_1, b_1, c_1) \\ \mathbf{B}_m = \mathbf{F}_m(a_2, b_2, c_2) \\ \mathbf{C}_m = \mathbf{F}_m(a_3, b_3, c_3) \end{cases} \tag{6.19}$$

$$\begin{cases} \mathbf{A}_m = \mathbf{I}_m \otimes (a_1 + b_1) - \mathbf{T}_m \otimes b_1 + \mathbf{K}_m \otimes (c_1 - a_1 + b_1) \\ \mathbf{B}_m = \mathbf{I}_m \otimes (a_2 + b_2) - \mathbf{T}_m \otimes b_2 + \mathbf{K}_m \otimes (c_2 - a_2 + b_2) \\ \mathbf{C}_m = \mathbf{I}_m \otimes (a_3 + b_3) - \mathbf{T}_m \otimes b_3 + \mathbf{K}_m \otimes (c_3 - a_3 + b_3) \end{cases}$$

Now employing the above relationships, the Laplacian matrix can be rewritten as

$$\begin{aligned} \mathbf{L} = {} & \mathbf{I}_n \otimes (\{\mathbf{I}_m \otimes (a_1 + b_1) - \mathbf{T}_m \otimes b_1 + \mathbf{K}_m \otimes (c_1 - a_1 + b_1)\} + \{\mathbf{I}_m \otimes (a_2 + b_2) \\ & - \mathbf{T}_m \otimes b_2 + \mathbf{K}_m \otimes (c_2 - a_2 + b_2))\} - \mathbf{T}_n \otimes \{\mathbf{I}_m \otimes (a_2 + b_2) \\ & - \mathbf{T}_m \otimes b_2 + \mathbf{K}_m \otimes (c_2 + a_3 + b_2)\} + \mathbf{K}_m \otimes (\{\mathbf{I}_m \otimes (a_3 + b_3) - \\ & - \mathbf{T}_m \otimes b_3 + \mathbf{K}_m \otimes (c_3 - a_3 + b_3)\} - \{\mathbf{I}_m \otimes (a_1 + b_1) - \mathbf{T}_m \otimes (a_1 + b_1) - \mathbf{T}_m \otimes b_1 + \\ & + \mathbf{K}_m \otimes (c_1 - a_1 + b_1)\} + \{\mathbf{I}_m \otimes (a_2 + b_2) - \mathbf{T}_m \otimes b_2 + \mathbf{K}_m \otimes (c_2 - a_2 + b_2)\}. \end{aligned} \tag{6.20}$$

For calculating the eigenvalues of the sum of the Kronecker products, the following theorem is available.

6.7.1 Main Theorem

Theorem. (Kaveh and Rahami [2]): *The necessary conditions for the following to hold*

$$\mathrm{eig}\left(\sum_{i=1}^{n} \mathbf{A}_i \otimes \mathbf{B}_i\right) = \sum_{i=1}^{n} \mathrm{eig}(\mathbf{A}_i \otimes \mathbf{B}_i) \tag{6.21}$$

is as follows:

$$\mathbf{A}_i \mathbf{A}_j = \mathbf{A}_j \mathbf{A}_i, \quad \mathbf{B}_i \mathbf{B}_j = \mathbf{B}_j \mathbf{B}_i, \quad i, j = 1, ..., n \tag{6.22}$$

In writing the Laplacian matrix, three types of matrices as $\mathbf{I}, \mathbf{T}, \mathbf{K}$ are encountered. In the first term $\mathbf{I}_n, \mathbf{T}_n, \mathbf{K}_n$ and in the second term $\mathbf{I}_m, \mathbf{T}_m, \mathbf{K}_m$ are present, respectively.

The commutative property holds for each pair of the matrices $\mathbf{K}_i$ and $\mathbf{T}_i$. By some modifications in the entries of $\mathbf{K}_i$, one can change it to such a form that for the above theorem all the necessary conditions are satisfied. If $\mathbf{K}'_i$ is the modified form of $\mathbf{K}_i$, then clearly $\mathbf{K}'_i$ will commute with $\mathbf{T}_i$.

Using the above theorem, the eigensolution equation for Laplacian matrix can be written as

$$\begin{aligned}\mathrm{eig}(\mathbf{L}) = {} & (a_1+b_1) - b_1\lambda_m + \mu_m(c_1 - a_1 + b_1) + (a_2+b_2) - b_2\lambda_m \\ & + \mu_m(c_2 - a_2 + b_2) - \lambda_n\{(a_2+b_2) - b_2\lambda_m + \mu_m(c_2 - a_2 + b_2)\} \\ & + \mu_n\{(a_3+b_3) - b_3\lambda_m + \mu_m(c_3 - a_3 + b_3) - (a_1+b_1) \\ & + b_1\lambda_m - \mu_m(c_1 - a_1 + b_1) + (a_2+b_2) - b_2\lambda_m + \mu_m(c_2 - a_2 + b_2)\} \quad (6.23)\end{aligned}$$

in which λ_m, λ_n are the eigenvalues of the Laplacian matrices corresponding to two subgraphs of product and μ_n and μ_m are the eigenvalues of the modified matrices K'_n and K'_m, respectively. Since $(i-2)$ eigenvalues for K_i are equal to '1' and only two eigenvalues are '0', thus the best modification in entries of K_i can be considered as changing them to the unit matrices I_i. For this purpose, it is sufficient to change the first and last entries of K_i from '0' to '1'. However, one may also change the K_i matrix in a different manner such that it becomes commutative to T_i. As an example, K_i can be considered as I_i in the modified form by replacing each μ_i with '1' in Eq. 6.20.

6.7.2 Eigensolution in Cartesian Product of Two Graphs

In order to find a formula for calculating the eigenvalues of the Laplacian matrix in Cartesian product of graphs, one can write

$$\begin{aligned}&\mathbf{L} = \mathbf{F}_n(\mathbf{A}_m, \mathbf{B}_m, \mathbf{C}_m) \\ &\begin{cases}\mathbf{A}_m = \mathbf{F}_m(a_1, b_1, c_1) \\ \mathbf{B}_m = \mathbf{F}_m(a_2, b_2, c_2) \\ \mathbf{C}_m = \mathbf{F}_m(a_2, b_3, c_3),\end{cases}\end{aligned} \quad (6.24)$$

$$\begin{cases}a_1 = 2 \\ b_1 = -1 \\ c_1 = 3,\end{cases} \quad \begin{cases}a_2 = -1 \\ b_2 = 0 \\ c_2 = -1,\end{cases} \quad \begin{cases}a_3 = 3 \\ b_3 = -1 \\ c_3 = 4.\end{cases} \quad (6.25)$$

After replacing these quantities in eig($\mathbf{L}$), one obtains

$$\text{eig}(\mathbf{L}) = \lambda_m + \lambda_n. \tag{6.26}$$

From Kaveh [4], we know that this equation is an exact relationship. The approximation parameters, μ_i, are deleted in Eq. 6.23, leading to an exact relationship for the Cartesian products.

6.7.3 Eigensolution in Direct Product of Two Graphs

In order to find a relationship for calculating the eigenvalues of the Laplacian matrix in direct product of graphs, one can write

$$\begin{gathered}\mathbf{L} = \mathbf{F}_n(\mathbf{A}_m, \mathbf{B}_m, \mathbf{C}_m) \\ \begin{cases} \mathbf{A}_m = \mathbf{F}_m(a_1, b_1, c_1) \\ \mathbf{B}_m = \mathbf{F}_m(a_2, b_2, c_2) \\ \mathbf{C}_m = \mathbf{F}_m(a_2, b_3, c_3), \end{cases}\end{gathered} \tag{6.27}$$

$$\begin{cases} a_1 = 1 \\ b_1 = 0 \\ c_1 = 2, \end{cases} \quad \begin{cases} a_2 = 0 \\ b_2 = -1 \\ c_2 = 0, \end{cases} \quad \begin{cases} a_3 = 2 \\ b_3 = 0 \\ c_3 = 4. \end{cases} \tag{6.28}$$

After replacing these quantities in eig($\mathbf{L}$), we obtain

$$\text{eig}(\mathbf{L}) = 2\lambda_m + 2\lambda_n - \lambda_m\lambda_n + \mu_m\lambda_n + \mu_n\lambda_m, \tag{6.29}$$

and from the above discussions, the best relationship is attained by replacing μ_n, μ_m with '1' as

$$\text{eig}(\mathbf{L}) = 2\lambda_m + 2\lambda_n - \lambda_m\lambda_n. \tag{6.30}$$

This equation is the same as the one used by Pothen et al. [6].

6.7.4 Eigensolution in Strong Cartesian Product of Two Graphs

In order to find a relationship for calculating the eigenvalues of the Laplacian matrix in the strong Cartesian product of graphs, one can also write

$$\mathbf{L} = \mathbf{F}_n(\mathbf{A}_m, \mathbf{B}_m, \mathbf{C}_m) \text{ where} \begin{cases} \mathbf{A}_m = \mathbf{F}_m(a_1, b_1, c_1) \\ \mathbf{B}_m = \mathbf{F}_m(a_2, b_2, c_2), \\ \mathbf{C}_m = \mathbf{F}_m(a_3, b_3, c_3) \end{cases} \tag{6.31}$$

$$\begin{cases} a_1 = 3 \\ b_1 = -1 \\ c_1 = 5, \end{cases} \quad \begin{cases} a_2 = -1 \\ b_2 = -1 \\ c_2 = -1, \end{cases} \quad \begin{cases} a_3 = 5 \\ b_3 = -1 \\ c_3 = 8. \end{cases} \tag{6.32}$$

And by substituting these quantities in eig($\mathbf{L}$), we have

$$\text{eig}(\mathbf{L}) = 2\lambda_m + 2\lambda_n - \lambda_n\lambda_m + \mu_m\lambda_n + \mu_n\lambda_m. \tag{6.33}$$

Assuming $\mu_n = \mu_m = 1$,

$$\text{eig}(\mathbf{L}) = 3\lambda_m + 3\lambda_n - \lambda_n\lambda_m. \tag{6.34}$$

This approximate relationship for calculating the eigenvalues of the Laplacian matrix of strong Cartesian product is also the same as those obtained by Pothen et al. [6].

In the following two examples are provided to further clarify the difference of the three methods.

6.7.5 *Examples*

Example 6.8. The strong Cartesian product $P_3\ (X)_{SC}\ P_6$ is considered as shown in Fig. 6.11a.

In this example, the Laplacian matrix before modification is as follows:

$$\mathbf{L} = \mathbf{F}_n(\mathbf{A}_m, \mathbf{B}_m, \mathbf{C}_m)$$

$$\mathbf{F}_n(\mathbf{A}_m, \mathbf{B}_m, \mathbf{C}_m) = \begin{bmatrix} \mathbf{A}_m & \mathbf{B}_m & & & & \\ \mathbf{B}_m & \mathbf{C}_m & \mathbf{B}_m & & & \\ & \mathbf{B}_m & \mathbf{C}_m & \mathbf{B}_m & & \\ & & . & . & . & \\ & & & \mathbf{B}_m & \mathbf{C}_m & \mathbf{B}_m \\ & & & & \mathbf{B}_m & \mathbf{A}_m \end{bmatrix} \tag{6.35}$$

where $\begin{cases} \mathbf{A}_m = \mathbf{F}_m(3, -1, 5) \\ \mathbf{B}_m = \mathbf{F}_m(-1, -1, -1) \\ \mathbf{C}_m = \mathbf{F}_m(5, -1, 8) \end{cases}$

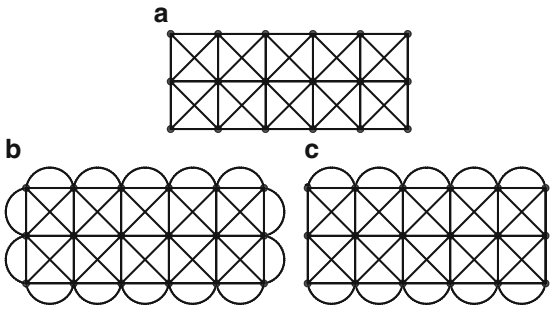

Fig. 6.11 A strong Cartesian product and its modified models. (**a**) Strong Cartesian product of P_3 $(X)_{SC}$ P_6 in graphical model. (**b**) The modified model of P_3 $(X)_{SC}$ P_6 by Pothen et al. method. (**c**) The modified model of P_3 $(X)_{SC}$ P_6 by Kaveh–Rahami method

Table 6.3 Comparison of some of the eigenvalues

Eigenvalue	Real (exact)	Pothen et al. method	Kaveh–Rahami method
λ_2	0.6226	0.8038	0.8038
λ_3	2.2828	3.000	2.5663
λ_{10}	5.7053	9.000	6.7184

1. Pothen et al. [6] Modification: In this approach, members are added to four sides of the model. Algebraically this is equivalent to

$$\mathbf{L} = \mathbf{F}_n(\mathbf{A}_m, \mathbf{B}_m, \mathbf{C}_m) \quad \text{where} \quad \begin{cases} \mathbf{A}_m = \mathbf{F}_m(5, -2, 7) \\ \mathbf{B}_m = \mathbf{F}_m(-2, -1, -1) \\ \mathbf{C}_m = \mathbf{F}_m(7, -1, 8) \end{cases} \tag{6.36}$$

   It can be seen that after this modification, we have $\mathbf{A}_m = \mathbf{B}_m + \mathbf{C}_m$ and this enables us to decompose the Laplacian matrix.
2. Kaveh–Rahami Modification [1]: In this approach, members are added to only two opposite sides of the model. Algebraically this is equivalent to

$$\mathbf{L} = \mathbf{F}_n(\mathbf{A}_m, \mathbf{B}_m, \mathbf{C}_m) \quad \text{where} \quad \begin{cases} \mathbf{A}_m = \mathbf{F}_m(4, -2, 7) \\ \mathrm{B}_m = \mathbf{F}_m(-1, -1, -1) \\ \mathrm{C}_m = \mathbf{F}_m(5, -1, 8) \end{cases} \tag{6.37}$$

   It can also be seen that after modification of Kaveh-Rahami, the relationship $\mathbf{A}_m = \mathbf{B}_m + \mathbf{C}_m$ holds.

In Table 6.3 the exact and approximate values for strong Cartesian product of P_3 $(X)_{SC}$ P_6 are compared.

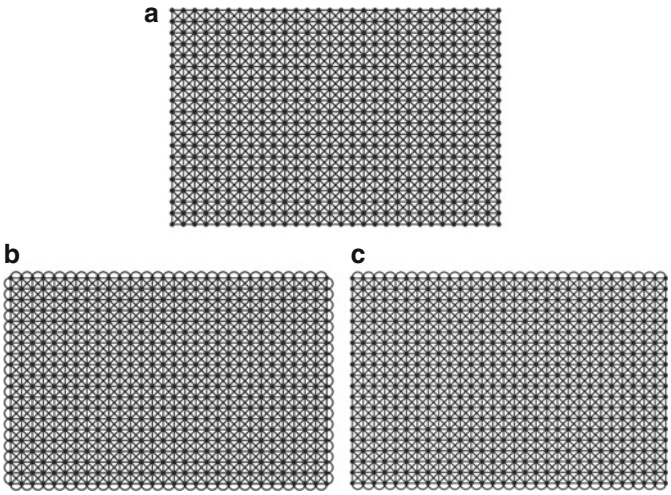

Fig. 6.12 A strong Cartesian product and its modified model. (**a**) Strong Cartesian product of P_{20} $(X)_{SC}$ P_{30} in graphical model. (**b**) The modified model of P_3 $(X)_{SC}$ P_6 by Pothen et al. method. (**c**) The modified model of P_3 $(X)_{SC}$ P_6 by Kaveh–Rahami method

The table shows that in general, Kaveh–Rahami method performs better as an approximate approach. For this example, which is not a large-scale problem, the difference between the approximate and exact solutions is considerable; however, as the number of nodes increases, this difference reduces, as will be shown in the subsequent example.

Example 6.9. P_{20} $(X)_{SC}$ P_{30} for strong Cartesian product is considered as shown in Fig. 6.12.

In this example, the Laplacian matrix before modification is as follows:

$$\mathbf{L} = \mathbf{F}_n(\mathbf{A}_m, \mathbf{B}_m, \mathbf{C}_m)$$

$$\mathbf{F}_n(\mathbf{A}_m, \mathbf{B}_m, \mathbf{C}_m) = \begin{bmatrix} \mathbf{A}_m & \mathbf{B}_m & & & & & \\ \mathbf{B}_m & \mathbf{C}_m & \mathbf{B}_m & & & & \\ & \mathbf{B}_m & \mathbf{C}_m & \mathbf{B}_m & & & \\ & & \cdot & \cdot & \cdot & & \\ & & & \mathbf{B}_m & \mathbf{C}_m & \mathbf{B}_m & \\ & & & & \mathbf{B}_m & \mathbf{A}_m & \end{bmatrix} \quad \text{where} \quad \begin{cases} \mathbf{A}_m = \mathbf{F}_m(3,-1,5) \\ \mathbf{B}_m = \mathbf{F}_m(-1,-1,-1) \\ \mathbf{C}_m = \mathbf{F}_m(5,-1,8) \end{cases} \tag{6.38}$$

Table 6.4 Comparison of some of the eigenvalues

Eigenvalue	Real (exact)	Pothen et al. method [6]	Kaveh–Rahami method [2]
λ_2	0.0318	0.029	0.0329
λ_3	0.0722	0.0739	0.0722
λ_{10}	0.3413	0.3651	0.03619

1. Pothen et al. modification:

$$\mathbf{L} = \mathbf{F}_{\mathrm{n}}(\mathbf{A}_{\mathrm{m}}, \mathbf{B}_{\mathrm{m}}, \mathbf{C}_{\mathrm{m}}) \quad \text{where} \quad \begin{cases} \mathbf{A}_{\mathrm{m}} = \mathbf{F}_{\mathrm{m}}(5, -2, 7) \\ \mathbf{B}_{\mathrm{m}} = \mathbf{F}_{\mathrm{m}}(-2, -1, -1) \\ \mathbf{C}_{\mathrm{m}} = \mathbf{F}_{\mathrm{m}}(7, -1, 8) \end{cases} \tag{6.39}$$

It can be observed that after modification, we have

$$\mathbf{A}_{\mathrm{m}} = \mathbf{B}_{\mathrm{m}} + \mathbf{C}_{\mathrm{m}}, \tag{6.40}$$

and this can help to decompose the Laplacian matrix for eigensolution.

2. Kaveh–Rahami modification:

$$\mathbf{L} = \mathbf{F}_{\mathrm{n}}(\mathbf{A}_{\mathrm{m}}, \mathbf{B}_{\mathrm{m}}, \mathbf{C}_{\mathrm{m}}) \quad \text{where} \quad \begin{cases} \mathbf{A}_{\mathrm{m}} = \mathbf{F}_{\mathrm{m}}(4, -2, 7) \\ \mathbf{B}_{\mathrm{m}} = \mathbf{F}_{\mathrm{m}}(-1, -1, -1) \\ \mathbf{C}_{\mathrm{m}} = \mathbf{F}_{\mathrm{m}}(5, -1, 8) \end{cases} \tag{6.41}$$

Also one can see that after the modification by Kaveh–Rahami method, we have $\mathbf{A}_{\mathrm{m}} = \mathbf{B}_{\mathrm{m}} + \mathbf{C}_{\mathrm{m}}$.

Comparison of the exact and approximate eigenvalues for strong Cartesian product of P_{20} $(X)_{SC}$ P_{30} is made in Table 6.4.

It can be observed that the new algebraic method can be used easily in eigensolution of the Laplacian matrix of any other graph product with two generators and can also be applied to the graph product of three generators and more.

In Fig. 6.13 the comparison of the computational time consumed for eigensolution in the two existing methods and the present approximate approach is illustrated. It can be observed that the present method requires much less computational time for the eigensolution of Laplacian matrices.

6.8 Numerical Examples

Example 6.10. The finite element model of a cooling tower is considered as shown in Fig. 6.14a. This model consists of 875 nodes and 816 rectangular shell elements.

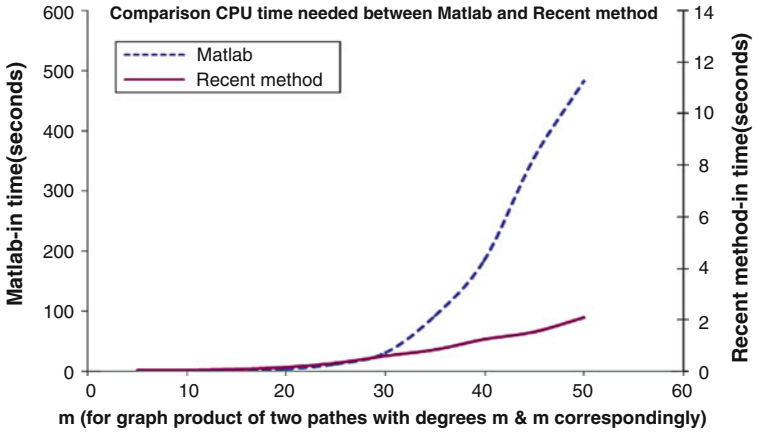

Fig. 6.13 The comparison for computational time for the existing and present methods

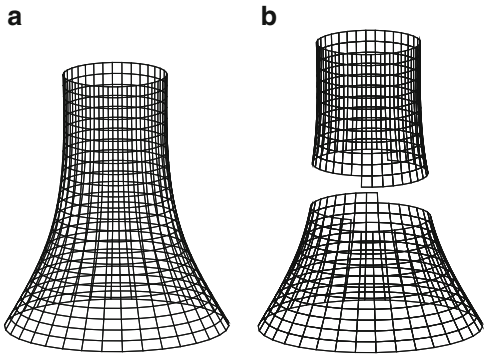

Fig. 6.14 The FE model of a cooling tower and its partitioning

The skeleton graph, as defined in Kaveh [4], is considered as P_{25} $(X)_C$ C_{35} and is partitioned with $\lambda_2 = 0.0158$. The corresponding bisected FEM is shown in Fig. 6.14b.

Example 6.11. In this example, the finite element model of a shell structure is considered, as shown in Fig. 6.15a. This model has 1,225 nodes and 1,156 rectangular shell elements. The model is trisected as illustrated in Fig. 6.15b corresponding to $\lambda_3 = 0.0081$. The skeleton graph is considered as P_{35} $(X)_C$ P_{35}.

Example 6.12. In this example, the strong Cartesian product of P_{40} and C_{55}, includes 2,200 nodes and 8,424 triangular elements, is partitioned into 3 subdomains as illustrated in Fig. 6.16 corresponding to $\lambda_3 = 0.0384$. In Fig. 6.16, it can be seen that one of these subdomains includes two distinct parts as in left and right. MATLAB is also employed to calculate λ_3 and v_3, where the necessary CPU

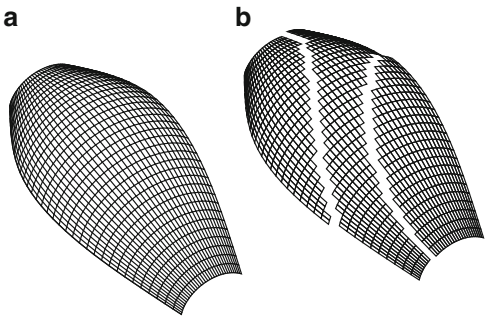

Fig. 6.15 The FE model of a shell and its partitioning

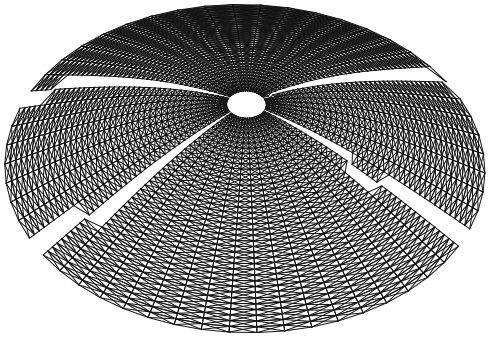

Fig. 6.16 The FE model of a dome and its partitioning

time for eigensolution was 87.834 s. However, the present method takes a few seconds to perform the subdomaining of this model by considering the eigenvalues of its generators.

In this chapter, using an algebraic approximate method on Laplacian matrices of graph products, a general equation for eigensolution is introduced which is not only applicable to all the existing graph products with two generators but also can be used for graph product of three or more subgraphs. Employing this method one can partition the graph model of a structure into two or more submodels. Each of these submodels can reflect the properties of initial model for parallel computation. The simplicity of the present method for eigensolution is that for constructing the derivation of the final relationship, one does not need the graph model of the product, and the Laplacian matrix is sufficient to obtain the necessary relationship.

References

1. Kaveh A, Rahami H (2004) A new spectral method for nodal ordering of regular space structures. Finite Elem Anal Des 40:1931–1945
2. Kaveh A, Rahami H (2004) An efficient method for decomposition of regular structures using graph products. Int J Numer Methods Eng 61:1797–1808

3. Kaveh A (2004) Structural mechanics: graph and matrix methods, 3rd edn. Research Studies Press, Somerset
4. Kaveh A (2006) Optimal structural analysis, 2nd edn. Wiley, Chichester
5. Nooshin H (1984) Formex configuration processing in structural engineering. Elsevier Applied Science, London
6. Pothen A, Simon H, Liou KP (1990) Partitioning sparse matrices with eigenvectors of graphs. SIAM J Matrix Anal Appl 11:430–452

Chapter 7
Canonical Forms Applied to Structural Mechanics

7.1 Introduction

The main objective of this chapter is to illustrate different applications of the canonical forms in structural mechanics with particular emphasis on calculating the buckling load and eigenfrequencies of the symmetric structures.

In the first part, the problem of finding eigenvalues and eigenvectors of symmetric mass–spring vibrating systems is transferred into calculating those of their modified subsystems. This decreases the size of the eigenvalue problems and correspondingly increases the accuracy of their solutions and reduces the computational time [1].

In the second part, a methodology is presented for efficient calculation of buckling loads for symmetric frame structures. This is achieved by decomposing a symmetric model into two submodels followed by their healing to obtain the factors of the model. The buckling load of the entire structure is then obtained by calculating the buckling loads of its factors [2].

In the third part, the graph models of planar frame structures with different symmetries are decomposed, and appropriate processes are designed for their healing in order to form the corresponding factors. The eigenvalues and eigenvectors of the entire structure are then obtained by evaluating those of its factors. The methods developed in this part simplify the calculation of the natural frequencies and natural modes of the planar frames with different types of symmetry [3].

In the fourth part, methods are presented for calculating the eigenfrequencies of structures. The first approach is graph theoretical and uses graph symmetry. The graph models are decomposed into submodels, and healing processes are employed such that the union of the eigenvalues of the healed submodels contains the eigenvalues of the entire model. The second method has an algebraic nature and uses special canonical forms [4].

In the fifth part, general forms are introduced for efficient eigensolution of special tri-diagonal and five-diagonal matrices. Applications of these forms are illustrated using problems from mechanics of structures [5].

A. Kaveh, *Optimal Analysis of Structures by Concepts of Symmetry and Regularity*,
DOI 10.1007/978-3-7091-1565-7_7,

In the sixth part, the decomposability conditions of matrices are studied. Matrices that can be written as the sum of three Kronecker products are studied; examples are included to show the efficiency of this decomposition approach [6].

In the seventh part, canonical forms are used to decompose the symmetric line elements (truss and beam elements) into sub-elements of less the number of degrees of freedom (DOFs). Then the matrices associated with each sub-element are formed, and finally the matrices associated with each subsystem are combined to form the matrices of the prime element [7].

In the final part, an efficient eigensolution is presented for calculating the buckling load and free vibration of rotationally cyclic structures [8]. This solution uses a canonical form linear algebra that often occurs in matrices associated with graph models. A substructuring method is proposed to avoid the generation of entire matrices. Utilising the aforementioned method, the geometric stiffness matrix is generated in an efficient time-saving manner. Then solution for the eigenproblem is presented for geometric nonlinearity via the canonical form based on block diagonalisation method.

7.2 Vibrating Cores for a Mass–Spring Vibrating System

Consider a symmetric system shown in Fig. 7.1a. This system is symmetric, and its properties can be studied using its substructures.

These properties consist of the mass m_1 and the stiffness k_1. The masses, stiffnesses and their connectivity are considered to be symmetric with respect to the axis shown in Fig. 7.1a.

This system can be considered as two identical subsystems connected to each other with a spring, knows as a *link spring*, as shown in Fig. 7.1b.

This system has two degrees of freedom v_1 and v_2. The natural frequencies and natural modes for the following eigenproblem

$$\{[\mathbf{K}] - \boldsymbol{\omega}^2[\mathbf{m}]\}\{\boldsymbol{\phi}\} = \{0\} \tag{7.1}$$

can be found as

$$\left| \, [\mathbf{K}] - \omega^2[\mathbf{m}] \, \right| = 0. \tag{7.2}$$

where $[\mathbf{K}]$ is the stiffness matrix and $[\mathbf{m}]$ is the mass matrix of the system. The eigenvalues and eigenvectors are denoted by ω_i and $\boldsymbol{\phi}_i$, respectively.

Since $[\mathbf{K}]$ and $[\mathbf{m}]$ are both symmetric, therefore the matrix $[[\mathbf{K}] - \omega^2[\mathbf{m}]]$ has Form II as the following:

$$\begin{bmatrix} k_1 + k_2 - \omega^2 m_1 & -k_2 \\ -k_2 & k_1 + k_2 - \omega^2 m_1 \end{bmatrix}. \tag{7.3}$$

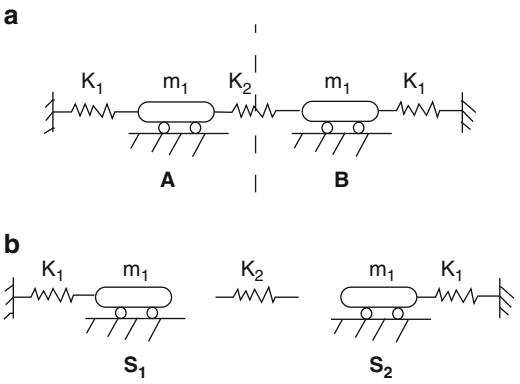

Fig. 7.1 A symmetric dynamic system and two subsystems with link spring

Using $\omega^2 m_1 = \lambda$, one can write

$$\begin{vmatrix} (k_1 + k_2) - \lambda & -k_2 \\ -k_2 & (k_1 + k_2) - \lambda \end{vmatrix} = 0. \tag{7.4}$$

Since the stiffness matrix has Form II, thus one can find its eigenvalues by calculating those of its condensed submatrices

$$\begin{aligned} \mathbf{C} &= [k_1 + k_2 - k_2] = [k_1] \\ \mathbf{D} &= [k_1 + k_2 + k_2] = [k_1 + 2k_2]. \end{aligned} \tag{7.5}$$

The matrices **C** and **D** partially contain the eigenvalues of S. Since these submatrices have a nature similar to that of the overall stiffness matrix, thus the condensed matrices **C** and **D** define the stiffness matrices of the subsystems as shown in Fig. 7.1.

The structure corresponding to the condensed submatrices are referred to as *vibrating cores*. These vibrating cores contain part of the properties of the vibrating system. Therefore, the eigenvalues and eigenvectors of the overall structure can be found using those of C and D subsystems, Fig. 7.2.

For the system S having N degrees of freedom, **m** and **K** are $N \times N$ matrices, and if the structure is symmetric, the corresponding submatrices will be $\frac{N}{2} \times \frac{N}{2}$.

For investigating the vibrating modes of S and vibrating cores, consider the following definitions:

Definition 1. Let matrix **M** be in Form II as follows:

$$\mathbf{M} = \left[\begin{array}{c|c} \mathbf{A} & \mathbf{B} \\ \hline \mathbf{B} & \mathbf{A} \end{array}\right]. \tag{7.6}$$

Let the corresponding eigenvalues of **M** be $\lambda_1, \lambda_2, \lambda_3, \ldots, \lambda_n$ with eigenvectors being as $\boldsymbol{\phi}_1, \boldsymbol{\phi}_2, \boldsymbol{\phi}_3, \ldots, \boldsymbol{\phi}_n$. The eigenvectors can be classified into two groups:

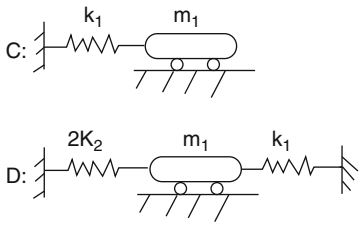

Fig. 7.2 Subsystems corresponding to condensed submatrices **C** and **D**

First group: those with eigenvectors having $\frac{N}{2}$ repeated entries
Second group: those with eigenvectors having $\frac{N}{2}$ repeated entries with reverse signs

Definition 2. If matrix **M** has a symmetry in Form II, then the condensed matrices are

$$\mathbf{C} = \mathbf{A} + \mathbf{B} \text{ and } \mathbf{D} = \mathbf{A} - \mathbf{B}. \tag{7.7}$$

The eigenvectors of **C** are of the first group type and those of **D** are of the second group type.

Therefore, if the eigenvectors for the eigenvalues of **C** (with $\frac{N}{2}$ entries) are calculated, then those of **M** can easily be obtained by addition of $\frac{N}{2}$ entries, and those of **D** with reversed signs should be added.

7.2.1 The Graph Model of a Mass–Spring System

The mathematical model of a dynamic system consists of masses and springs. These masses are connected by means of springs. As the mathematical model, a weighted graph is defined as follows:

1. The supports in the mathematical model are associated neutral nodes in the graph.
2. For each mass, a node of graph is associated, and its weight is taken as the magnitude of the mass.
3. An edge is considered for each spring, and its weight is taken as the stiffness of the spring.

As an example, the graph model G1 of a dynamic system shown in Fig. 7.3a is depicted in Fig. 7.3b.

For a dynamic system, we have

$$\mathbf{K}\boldsymbol{\phi} = \omega^2\mathbf{m}\boldsymbol{\phi} \Rightarrow \left[\mathbf{K} - \omega^2\mathbf{m}\right]\boldsymbol{\phi} = \mathbf{0}. \tag{7.8}$$

This is an eigenvalue problem for which ω is the eigenvalue and $\boldsymbol{\phi}$ is its eigenvector.

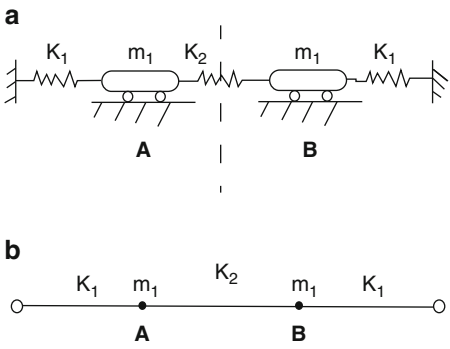

Fig. 7.3 A dynamic system and its graph model. (**a**) A symmetric dynamic system. (**b**) Graph model G1 of the system

If we assume $\mathbf{m}$ as a diagonal matrix, then its inverse can easily be found, and we will have

$$\mathbf{m}^{-1}\mathbf{K}\boldsymbol{\phi} = \mathbf{m}^{-1}\boldsymbol{\omega}^2\mathbf{m}\boldsymbol{\phi} \Rightarrow \mathbf{m}^{-1}\mathbf{K}\boldsymbol{\phi} = \boldsymbol{\omega}^2\boldsymbol{\phi} \Rightarrow [\mathbf{m}^{-1}\mathbf{K} - \boldsymbol{\omega}^2\mathbf{I}]\boldsymbol{\phi} = \mathbf{0}. \tag{7.9}$$

If $[\mathbf{m}^{-1}\mathbf{K}] = [\mathbf{L}_T]$ and $\lambda = \omega^2$, then we have

$$[\mathbf{L}_T - \lambda\mathbf{I}]\boldsymbol{\phi} = \mathbf{0}. \tag{7.10}$$

This is an eigenvalue problem corresponding to eigenvalues and eigenvectors of $\mathbf{L}_T$. This relationship can be associated with the corresponding graph. If $\mathbf{L}_T$ is the generalised Laplacian of the graph, then the above problem becomes an eigenproblem of a graph.

7.2.2 Vibrating Systems with Form II Symmetry

As an example, the generalised Laplacian matrix for the graph G1 in Fig. 7.3 has the following form:

$$\mathbf{L}_T = \left[\begin{array}{c|c} k_1 + k_2 - m_1 & -k_2 \\ \hline -k_2 & k_1 + k_2 - m_1 \end{array}\right] \tag{7.11}$$

For a symmetric graph, an appropriate numbering of the nodes results in a generalised Laplacian matrix with Form II.

Example 7.1. Consider a dynamic system as shown in Fig. 7.4 with graph model being G2.

This graph is symmetric and its Laplacian and generalised matrices are as follows:

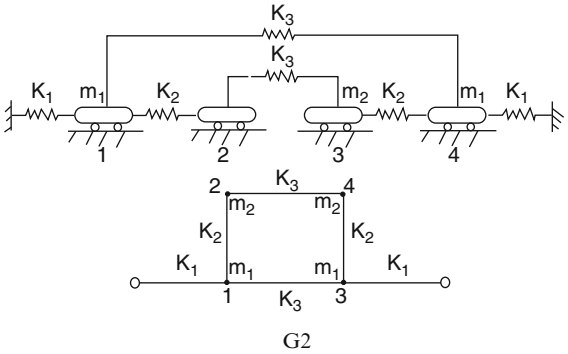

Fig. 7.4 A dynamic system and its graph model

$$\mathbf{L} = \left[\begin{array}{cc|cc} k_1+k_2+k_3 & -k_2 & -k_3 & 0 \\ -k_2 & k_2+k_3 & 0 & -k_3 \\ \hline -k_3 & 0 & k_1+k_2+k_3 & -k_2 \\ 0 & -k_3 & -k_2 & k_2+k_3 \end{array}\right] \tag{7.12}$$

$$\mathbf{L}_T = \left[\begin{array}{cc|cc} k_1+k_2+k_3-m_1 & -k_2 & -k_3 & 0 \\ -k_2 & k_2+k_3-m_2 & 0 & -k_3 \\ \hline -k_3 & 0 & k_1+k_2+k_3-m_1 & -k_2 \\ 0 & -k_3 & -k_2 & k_2+k_3-m_2 \end{array}\right]. \tag{7.13}$$

For the symmetry in Form II, the generalised Laplacian matrix can be written as

$$\mathbf{L}_T = \left[\begin{array}{c|c} \mathbf{S} & \mathbf{LI} \\ \hline \mathbf{LI} & \mathbf{S} \end{array}\right]. \tag{7.14}$$

The submatrix **S** is called the *shape matrix* and represents the properties of both subgraphs, which are identical, and **LI** is called the *link matrix* and shows the way two subgraphs are connected to each other. The submatrix **LI** represents the effect of the springs between two subgraphs in the stiffness matrix.

As mentioned before, we have an eigenproblem for the matrix $\mathbf{L}_T$. According to the properties of Form II, if $[\mathbf{S}+\mathbf{LI}] = \mathbf{C}$ and $[\mathbf{S}-\mathbf{LI}] = \mathbf{D}$, then $\mathbf{L}'_T$ can be expressed as

$$\mathbf{L}'_T = \begin{bmatrix} \mathbf{C} & \mathbf{0} \\ \mathbf{0} & \mathbf{D} \end{bmatrix}. \tag{7.15}$$

If $\mathbf{L}'_T$ is the generalised Laplacian matrix of a graph, then this graph will consist of two subgraphs with N/2 nodes for each subgraph which are not connected to each other, and $\mathbf{L}_T$ has eigenvalues as

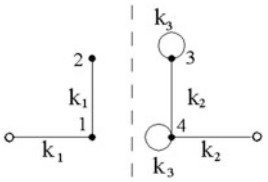

Fig. 7.5 The dynamic cores C and D of G2

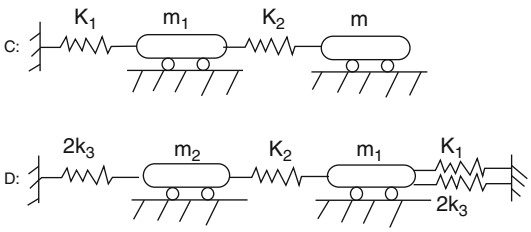

Fig. 7.6 The mathematical models for C and D

$$\mathrm{EIG}(\mathbf{L}_{\mathrm{T}}) = \mathrm{EIG}(\mathbf{C}) \cup \mathrm{EIG}(\mathbf{D}). \tag{7.16}$$

Thus, the subgraphs C and D are the dynamic cores of the model. Each core defines part of the natural frequencies ω_{i} of the entire system.

$$\{\boldsymbol{\omega}_{\mathbf{L}_{\mathrm{T}}}\} = \{\boldsymbol{\omega}_{\mathrm{D}}\} \cup \{\boldsymbol{\omega}_{\mathrm{E}}\}. \tag{7.17}$$

As an example, for graph G2, the cores C and D are shown in Fig. 7.5.

Laplacian matrices of C and D are as follows:

$$\mathbf{L}_C = \begin{bmatrix} \mathrm{k}_1 + \mathrm{k}_2 & -\mathrm{k}_2 \\ -\mathrm{k}_2 & \mathrm{k}_2 \end{bmatrix} \tag{7.18}$$

and

$$\mathbf{L}_{\mathrm{D}} = \begin{bmatrix} \mathrm{k}_1 + \mathrm{k}_2 + 2\mathrm{k}_3 & -\mathrm{k}_2 \\ -\mathrm{k}_2 & \mathrm{k}_2 + 2\mathrm{k}_3 \end{bmatrix} \tag{7.19}$$

As mentioned previously, the Laplacian matrix of the corresponding graphs is the same as the stiffness matrices of the mathematical model for each subgraph C and D as shown in Fig. 7.6.

7.2.3 Vibrating Systems with Form III Symmetry

For a symmetric system with odd number of masses, the corresponding graph will have Form III symmetry. For such a system, the vibrating cores can be identified using symmetry.

As the third example, consider the model shown in Fig. 7.7a.

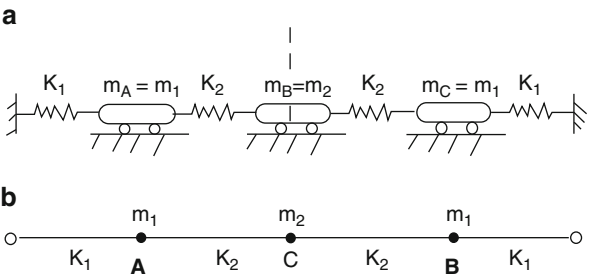

Fig. 7.7 A dynamic system and its graph model

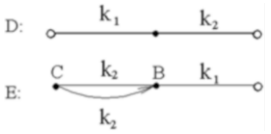

Fig. 7.8 The subgraphs for D and E

Fig. 7.9 A directed spring

The corresponding graph is shown in Fig. 7.7b.

The Laplacian and generalised Laplacian matrices are as follows:

$$\mathbf{L} = \begin{bmatrix} k_1 + k_2 & 0 & -k_2 \\ 0 & k_1 + k_2 & -k_2 \\ -k_2 & -k_2 & 2k_2 \end{bmatrix}, \tag{7.20}$$

$$\mathbf{L}_T = \left[\begin{array}{cc|c} k_1 + k_2 - m_1 & 0 & -k_2 \\ 0 & k_1 + k_2 - m_1 & -k_2 \\ \hline -k_2 & -k_2 & 2k_2 - m_2 \end{array}\right]. \tag{7.21}$$

As it can be seen, both $\mathbf{L}$ and $\mathbf{L}_T$ have Form III.

The Laplacian matrices corresponding to the vibrating cores are given below:

$$\mathbf{L}_D = [k_1 + k_2 - 0] = [k_1 + k_2], \tag{7.22}$$

and

$$\mathbf{L}_E = \begin{bmatrix} k_1 + k_2 & -k_2 \\ -2k_2 & 2k_3 \end{bmatrix}. \tag{7.23}$$

The graphs of these matrices are shown in Fig. 7.8.

If there is a directed edge between two nodes i and j directed from i to j, it represents a directed spring in the dynamic system, Fig. 7.9. The main characteristic

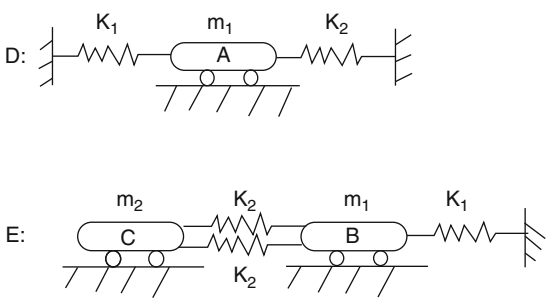

Fig. 7.10 Models corresponding to D and E

of such a spring is that the connection of this spring to masses is such that it does not take part in the stiffness of $k_{j,i}$, but it effects the $k_{i,j}$, that is,

The mathematical models corresponding to the cores D and E are shown in Fig. 7.10.

According to the properties of the cores,

$$\{\lambda \mathbf{L}_{\mathrm{T}}\} = \{\lambda_D\} \cup \{\lambda_E\}, \tag{7.24}$$

and

$$\{\omega \mathbf{L}_{\mathrm{T}}\} = \{\omega_D\} \cup \{\omega_E\}. \tag{7.25}$$

and from the vibrating cores E and D, the natural modes of the entire system can be found.

If each a vibrating system contains symmetry, then the cores can be decomposed accordingly. Further decomposition of the refined cores for symmetry is also possible.

7.2.4 Generalized Form III and Vibrating System

As described in Chap. 4, for a graph with symmetric core having Form III, if the complement of the core is connected by the nodes of degree 1, then the nodes can be ordered to produce a Laplacian matrix of Form III. This property can also be used for graphs corresponding to the vibrating systems.

Consider the system in Fig. 7.11a together with its graph being illustrated in Fig. 7.11b.

The subgraph containing the nodes A, B and C has a symmetric core of Form III. The nodes E and D are connected to this core through C. Therefore, the Laplacian matrix of this graph will be in the generalised Form III. $\mathbf{L}$ and $\mathbf{L}_{\mathrm{T}}$ are formed as follows:

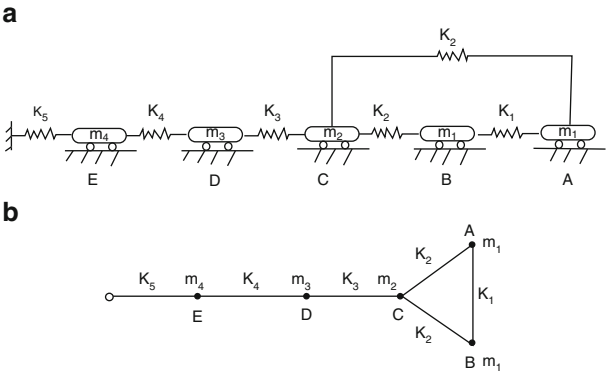

Fig. 7.11 A dynamic system and its graph model

$$\mathbf{L} = \begin{bmatrix} k_1 + k_2 & -k_1 & -k_2 & 0 & 0 \\ -k_1 & k_1 + k_2 & -k_2 & 0 & 0 \\ -k_2 & -k_2 & 2k_2 + k_3 & -k_3 & 0 \\ 0 & 0 & -k_3 & k_3 + k_4 & -k_4 \\ 0 & 0 & 0 & -k_4 & k_4 + k_5 \end{bmatrix}, \tag{7.26}$$

$$\mathbf{L}_T = \begin{bmatrix} k_1 + k_2 - m_1 & -k_1 & -k_2 & 0 & 0 \\ -k_1 & k_1 + k_2 - m_1 & -k_2 & 0 & 0 \\ -k_2 & -k_2 & 2k_2 + k_3 - m_2 & -k_3 & 0 \\ 0 & 0 & -k_3 & k_3 + k_4 - m_3 & -k_4 \\ 0 & 0 & 0 & -k_4 & k_4 + k_5 - m_4 \end{bmatrix}. \tag{7.27}$$

The connected submatrices **D** and **E** are formed for $\mathbf{L}_T$ as

$$\mathbf{D} = [k_1 + k_2 - m_1 - (-k_1)] = [2k_1 + k_2 - m_1], \tag{7.28}$$

$$\mathbf{E} = \begin{bmatrix} k_1 + k_2 - m_1 - k_1 & -k_2 - k_2 & 0 & 0 \\ -k_2 - k_2 & 2k_2 + k_3 - m_2 & -k_3 & 0 \\ 0 & -k_3 & k_3 + k_4 - m_3 & -k_4 \\ 0 & 0 & -k_4 & k_4 + k_5 - m_4 \end{bmatrix}, \tag{7.29}$$

or

$$\mathbf{E} = \begin{bmatrix} k_2 - m_1 & -k_2 & 0 & 0 \\ -2k_2 & 2k_2 + k_3 - m_2 & -k_3 & 0 \\ 0 & -k_3 & k_3 + k_4 - m_3 & -k_4 \\ 0 & 0 & -k_4 & k_4 + k_5 - m_4 \end{bmatrix}. \tag{7.30}$$

The subgraphs associated with the cores D and E are shown in Fig. 7.12.

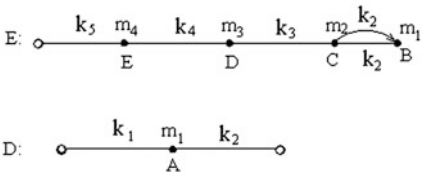

Fig. 7.12 Subgraphs D and E

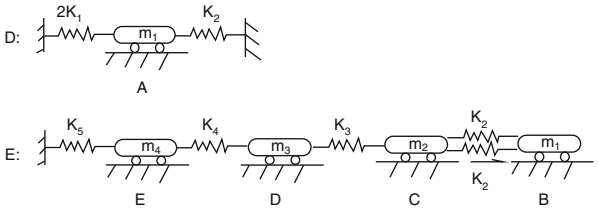

Fig. 7.13 Submodels D and E

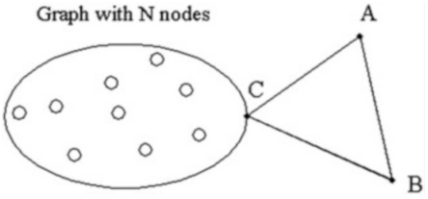

Fig. 7.14 A graph decomposable into D and E

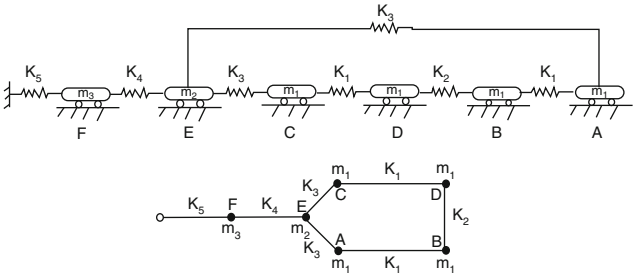

Fig. 7.15 A dynamic system and its graph model

The form of the vibrating cores corresponding to D and E is shown in Fig. 7.13.

It can be observed that due to the symmetry, the generalised Laplacian is decomposed into two submatrices of 1×1 and 4×4, and the cores are formed.

If N other nodes are connected to C in a similar manner, again the graph can be decomposed into two cores D and E, as shown in Fig. 7.14. It should be noted that the core D does not change.

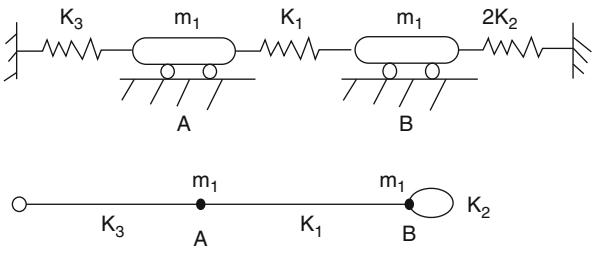

Fig. 7.16 The submodel D and the corresponding subgraph

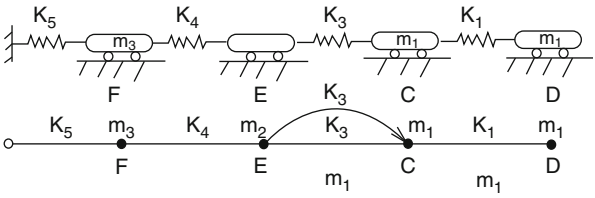

Fig. 7.17 The submodel E and the corresponding subgraph

Thus, the natural frequency of the core D and the corresponding mode of the system will be unaltered. Therefore, one can conclude that part of the natural frequency of the symmetric system with Form III will exactly be reflected in the whole system.

Consider the system shown in Fig. 7.15.

The $\mathbf{L}_{T,}$ $\mathbf{L}_D$ and $\mathbf{L}_E$ matrices are as follows:

$$\mathbf{L}_T = \begin{array}{c} \begin{matrix} A & B & C & D & E & F \end{matrix} \\ \begin{bmatrix} k_1+k_3-m_1 & -k_1 & 0 & 0 & -k_3 & 0 \\ -k_1 & k_1+k_2-m_1 & 0 & -k_2 & 0 & 0 \\ 0 & 0 & k_1+k_3-m_1 & -k_1 & -k_3 & 0 \\ 0 & -k_2 & -k_1 & k_1+k_2-m_1 & 0 & 0 \\ -k_3 & 0 & -k_3 & 0 & 2k_3+k_4-m_2 & -k_4 \\ 0 & 0 & 0 & 0 & -k_4 & k_4+k_5-m_3 \end{bmatrix} \end{array} \tag{7.31}$$

$$\mathbf{L}_D = \begin{bmatrix} k_1+k_3-m_1 & -k_1 \\ -k_1 & k_1+2k_2-m_1 \end{bmatrix}. \tag{7.32}$$

And the corresponding graph and model are illustrated in Fig. 7.16.

Also we have

$$\mathbf{L}_E = \begin{bmatrix} k_1+k_3-m_1 & -k_1 & -k_3 & 0 \\ -k_1 & k_1-m_1 & 0 & 0 \\ -2k_3 & 0 & 2k_3+k_4-m_2 & -k_4 \\ 0 & 0 & -k_4 & k_4+k_5-m_3 \end{bmatrix}. \tag{7.33}$$

And the corresponding model and graph are shown in Fig. 7.17.

7.2.5 Discussion

Symmetry of a mathematical model corresponds to the symmetric distribution of the physical properties comprising of masses and stiffnesses of the springs and the connectivity of the masses by means of springs.

For the graph model of a dynamic system, symmetry of Form II results in two vibrating cores C and D. These cores are physically identified with the difference of C being more flexible than D, and the main frequency and the corresponding mode are contained in this part of the model.

For the graph model of a vibrating system having Form III symmetry, the two vibrating cores D and E are produced. The number of masses and springs in D is less than E, and directed springs are included in the core E.

Although the systems studied in here are mass–spring systems, however, the application of the present method can be extended to other structural systems. The application can also be extended to stability analysis of frame structures.

7.3 Buckling Load of Symmetric Frames

In this part a method is presented for efficient calculation of buckling loads for symmetric frame structures. This is achieved by decomposing a symmetric model into two submodels followed by their healing to obtain the factors of the model. The buckling load of the entire structure is then obtained by calculating the buckling loads of its factors.

7.3.1 Buckling Load for Symmetric Frames with Odd Number of Spans per Storey

In this section, symmetric frames with an odd number of spans per storey are studied. The axis of symmetry for these structures passes through the central beams. For these frames, the matrices have canonical Form II patterns.

Non-sway Frames: Frames with no sway have no lateral displacement, and only rotational DOF specifies the deformation of the structure. In this study, for rigid-jointed frames in each joint, one rotational degree of freedom is considered.

For non-sway frames with odd number of spans per storey, if the loading is also symmetric, then the stiffness matrix with an appropriate numbering of the DOF will have canonical Form II pattern. In this case, the structure has two factors, one of which is stiffer than the other. Naturally the weaker factor will have smaller buckling load. Therefore, in order to find the buckling load for such a frame, with N DOF, it is sufficient to calculate the buckling load of a weaker factor with N/2 DOF. This process reduces the computational time and the necessary storage.

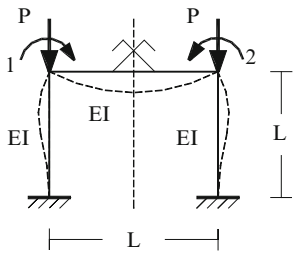

Fig. 7.18 A simple symmetric bending frame

Decomposition and Healing Process: The operations performed after decomposition is called the *healing* of substructures. The submodels obtained after the decomposition and healing are known as the *factors* of the structural model.

Healing for different types of symmetry requires different operations. These operations are designed such that the resulting factors correspond to the aforementioned condensed submatrices of the canonical forms.

For the non-sway frame with odd number of spans per storey, healing consists of the following steps:

Step 1. Delete the beams which are crossed by the axis of symmetry. These are *link beams* and are identified by Lb. Now the structure is decomposed into two substructures S_1 and S_2 in the left- and right-hand sides, respectively.

Step 2. For S_1, add one rotational spring, with a stiffness equal to $\frac{6EI_{lb}}{L_{Lb}^3} = k_{Ci}$, to the joint at the ith storey. This provides the necessary stiffness requirement for obtaining the factor C.

Step 3. Add a rotational spring to S_2, with a stiffness of magnitude $\frac{2EI_{lb}}{L_{Lb}^3} = k_{Di}$, at the joint of the ith storey. This provides the necessary stiffness requirement for obtaining the factor D.

S_1 and S_2 are now healed and the factors C and D are obtained.

The reason for selecting such stiffnesses for the springs is discussed by the following simple example.

Example 7.2. Consider a simple symmetric portal frame with symmetric buckling mode as shown in Fig. 7.18.

The stiffness matrix of the element with the numbering of the DOF as illustrated in Fig. 7.19 is formed using the standard stiffness method.

$$\mathbf{k} = \frac{EI}{L^3}\left[\begin{array}{cc|cc} 12 & -6 & -12 & 6 \\ -6 & 4 & 6 & -2 \\ \hline -12 & 6 & 12 & -6 \\ 6 & -2 & -6 & 4 \end{array}\right] - \frac{P}{L}\left[\begin{array}{cc|cc} \frac{6}{5} & \frac{-1}{10} & \frac{-6}{5} & \frac{1}{10} \\ \frac{-1}{10} & \frac{2}{15} & \frac{1}{10} & \frac{1}{30} \\ \hline \frac{-6}{5} & \frac{-1}{10} & \frac{6}{5} & \frac{-1}{10} \\ \frac{-1}{10} & \frac{1}{30} & \frac{-1}{10} & \frac{2}{15} \end{array}\right]. \tag{7.34}$$

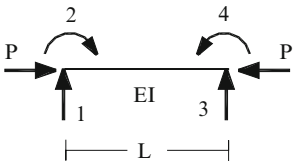

Fig. 7.19 Numbering of the DOF for a beam column

For the entire structure, the stiffness matrix is constructed as

$$\mathbf{K} = \frac{\mathrm{EI}}{\mathrm{L}^3}\left[\begin{array}{c|c} 8-4\lambda & 2 \\ \hline 2 & 8-4\lambda \end{array}\right], \text{ where } \lambda = \frac{\mathrm{PL}^2}{30\mathrm{EI}}. \tag{7.35}$$

The numbering of the DOF should be such that the difference between symmetric DOF becomes N/2.

The condensed submatrices of **K** are

$$\begin{aligned} \mathbf{A}-\mathbf{B} &= \left[\frac{6\mathrm{EI}}{\mathrm{L}^3} - \frac{4\mathrm{EI}}{\mathrm{L}^3}\times\frac{\mathrm{PL}^2}{30\mathrm{EI}}\right] = \frac{\mathrm{EI}}{\mathrm{L}^3}[6-4\lambda] \text{ and} \\ \mathbf{A}+\mathbf{B} &= \left[\frac{10\mathrm{EI}}{\mathrm{L}^3} - \frac{4\mathrm{EI}}{\mathrm{L}^3}\times\frac{\mathrm{PL}^2}{30\mathrm{EI}}\right] = \frac{\mathrm{EI}}{\mathrm{L}^3}[10-4\lambda], \end{aligned} \tag{7.36}$$

corresponding to the factors D and C, respectively.

Design of the Factor D: A factor for which the stiffness matrix is $\left[\frac{6\mathrm{EI}}{\mathrm{L}^3} - \frac{4\mathrm{EI}}{\mathrm{L}^3}\times\frac{\mathrm{PL}^2}{30\mathrm{EI}}\right]$ may be considered as a column under axial load P, with a spring of stiffness $\mathrm{k_C} = \frac{6\mathrm{EI}}{\mathrm{L}^3}$.

Design of the Factor C: Similarly, a factor for which the stiffness matrix is $\left[\frac{10\mathrm{EI}}{\mathrm{L}^3} - \frac{4\mathrm{EI}}{\mathrm{L}^3}\times\frac{\mathrm{PL}^2}{30\mathrm{EI}}\right]$ can be taken as a column under axial load P with a spring of stiffness $\mathrm{k_D} = \frac{10\mathrm{EI}}{\mathrm{L}^3}$.

In order to determine the buckling load of the frame, the determinant of the stiffness matrix is equated to zero:

$$\begin{aligned} \det\mathbf{K} = \det[\mathbf{A}-\mathbf{B}] \times \det[\mathbf{A}+\mathbf{B}] &= 0 \\ |6-4\lambda| = 0 \text{ and } |10-4\lambda| &= 0 \end{aligned} \tag{7.37}$$

leading to

$$\lambda_1 = 1.5 \text{ and } \lambda_2 = 2.5.$$

Therefore,

$$\lambda_{\min} = 1.5 = \frac{\mathrm{P_{cr}L}^2}{30\mathrm{EI}} \text{ leading to } \mathrm{P_{cr}} = \frac{45\mathrm{EI}}{\mathrm{L}^2}.$$

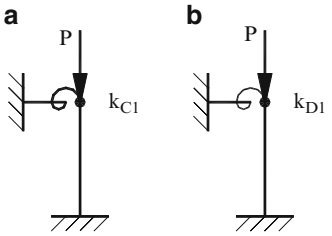

Fig. 7.20 Factors of the structure S. (**a**) Factor C (**b**) Factor D

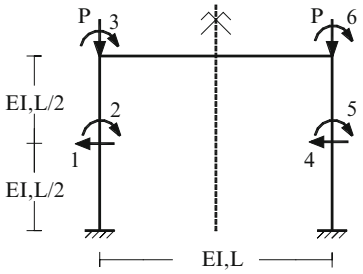

Fig. 7.21 A portal frame with six DOFs

Alternative Solution: First the factors are formed as shown in Fig. 7.20. The buckling load of the structure is obtained by finding the buckling load of the factor D.

$$\begin{aligned}\mathbf{K}_C &= \left[\frac{2EI}{L^3}(2) + \frac{6EI}{L^3} - \frac{2P}{15L}\right] = \left[\frac{10EI}{L^3} - \frac{2P}{15L}\right] \\ \mathbf{K}_D &= \left[\frac{2EI}{L^3}(2) + \frac{2EI}{L^3} - \frac{2P}{15L}\right] = \left[\frac{6EI}{L^3} - \frac{2P}{15L}\right]\end{aligned} \tag{7.38}$$

Equating the determinant of $\mathbf{K}_D$ to zero, the same buckling load is obtained. This approximation is very crude and can be improved by considering each column as two or more elements. As an example, the columns with two elements are considered as shown in Fig. 7.21.

Now the structure consists of four rotational degrees of freedom and two translation degrees of freedom. The corresponding stiffness matrix is obtained as

$$\mathbf{K} = \frac{8EI}{L^3} \times \left[\begin{array}{ccc|ccc} 24-72\lambda & 0 & -6+3\lambda & 0 & 0 & 0 \\ 0 & 8-8\lambda & 2+\lambda & 0 & 0 & 0 \\ -6+3\lambda & 2+\lambda & \frac{1}{2}+4-4\lambda & 0 & 0 & \frac{1}{4} \\ \hline 0 & 0 & 0 & 24-72\lambda & 0 & -6+3\lambda \\ 0 & 0 & 0 & 0 & 8-8\lambda & 2+\lambda \\ 0 & 0 & \frac{1}{4} & -6+3\lambda & 2+\lambda & \frac{1}{2}+4-4\lambda \end{array}\right] \tag{7.39}$$

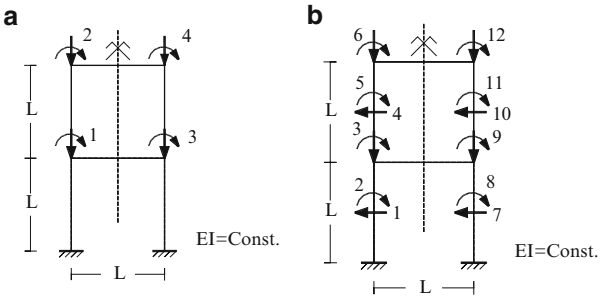

Fig. 7.22 A one-bay two-storey symmetric frame. (**a**) Each column as one element. (**b**) Each column as two elements

where $\lambda = \dfrac{PL^2}{120EI}$.

Forming the determinants of **A** + **B** and **A** − **B** and equating to zero results in $\lambda_{min} = 0.185$ corresponding to $P_{cr} = \dfrac{22.21EI}{L^2}$ which is quite close to the exact buckling load. In this case, the lowest critical load is known to correspond to antisymmetric mode, and as it will be shown in Sect. 3.2, the buckling load for that case will be $P_{cr} = \dfrac{7.44EI}{L^2}$.

Example 7.3. Consider a one-bay two-storey frame as shown in Fig. 7.22. This example is studied with two different discretisations. In the first model, each column is considered as one element as in Fig. 7.22a, and in the second model, each column is subdivided into two elements, as illustrated in Fig. 7.22b.

The overall stiffness matrix is formed as

$$\mathbf{K} = \frac{EI}{L^3}\left[\begin{array}{cc|cc} 12 & 2 & 2 & 0 \\ 2 & 8 & 0 & 2 \\ \hline 2 & 0 & 12 & 2 \\ 0 & 2 & 2 & 8 \end{array}\right] - \frac{P}{L}\left[\begin{array}{cc|cc} 0.4000 & -0.0333 & 0 & 0 \\ -0.0333 & 0.1333 & 0 & 0 \\ \hline 0 & 0 & 0.4000 & -0.0333 \\ 0 & 0 & -0.0333 & 0.1333 \end{array}\right].$$

The smallest eigenvalue, using det $\mathbf{K} = 0$, leads to the buckling load of the frame as

$$P_{cr} = \frac{19.7545EI}{L^2}.$$

However, this is not a good approximation, since only one element is used for each column. The result can easily be improved by idealising each column by two elements, as shown in Fig. 7.22b. For this model, the stiffness matrix is formed as

$$\mathbf{K} = \frac{EI}{l^3}\left[\begin{array}{cccccc|cccccc}
192 & 0 & -48 & 0 & 0 & 0 & 0 & 0 & 0 & 0 & 0 & 0 \\
0 & 64 & 16 & 0 & 0 & 0 & 0 & 0 & 0 & 0 & 0 & 0 \\
-48 & 16 & 36 & 0 & 0 & 0 & 0 & 0 & 2 & 0 & 0 & 0 \\
0 & 0 & 0 & 192 & 0 & -48 & 0 & 0 & 0 & 0 & 0 & 0 \\
0 & 0 & 0 & 0 & 64 & 16 & 0 & 0 & 0 & 0 & 0 & 0 \\
0 & 0 & 0 & -48 & 16 & 36 & 0 & 0 & 0 & 0 & 0 & 2 \\
\hline
0 & 0 & 0 & 0 & 0 & 0 & 192 & 0 & -48 & 0 & 0 & 0 \\
0 & 0 & 0 & 0 & 0 & 0 & 0 & 64 & 16 & 0 & 0 & 0 \\
0 & 0 & 2 & 0 & 0 & 0 & -48 & 12 & 36 & 0 & 0 & 0 \\
0 & 0 & 0 & 0 & 0 & 0 & 0 & 0 & 0 & 192 & 0 & -48 \\
0 & 0 & 0 & 0 & 0 & 0 & 0 & 0 & 0 & 0 & 64 & 16 \\
0 & 0 & 0 & 0 & 0 & 2 & 0 & 0 & 0 & -48 & 16 & 36
\end{array}\right]$$

$$-\frac{P}{l}\left[\begin{array}{cccccc|cccccc}
\frac{48}{5} & 0 & \frac{-2}{5} & 0 & 0 & 0 & 0 & 0 & 0 & 0 & 0 & 0 \\
0 & \frac{16}{15} & \frac{-2}{15} & 0 & 0 & 0 & 0 & 0 & 0 & 0 & 0 & 0 \\
\frac{-2}{5} & \frac{-2}{15} & \frac{8}{15} & 0 & 0 & 0 & 0 & 0 & 0 & 0 & 0 & 0 \\
0 & 0 & 0 & \frac{24}{5} & 0 & \frac{-1}{5} & 0 & 0 & 0 & 0 & 0 & 0 \\
0 & 0 & 0 & 0 & \frac{8}{15} & \frac{-1}{15} & 0 & 0 & 0 & 0 & 0 & 0 \\
0 & 0 & 0 & \frac{-1}{5} & \frac{-1}{15} & \frac{4}{15} & 0 & 0 & 0 & 0 & 0 & 0 \\
\hline
0 & 0 & 0 & 0 & 0 & 0 & \frac{48}{5} & 0 & \frac{-2}{5} & 0 & 0 & 0 \\
0 & 0 & 0 & 0 & 0 & 0 & 0 & \frac{16}{15} & \frac{-2}{15} & 0 & 0 & 0 \\
0 & 0 & 0 & 0 & 0 & 0 & \frac{-2}{5} & \frac{-2}{15} & \frac{8}{15} & 0 & 0 & 0 \\
0 & 0 & 0 & 0 & 0 & 0 & 0 & 0 & 0 & \frac{24}{5} & 0 & \frac{-1}{5} \\
0 & 0 & 0 & 0 & 0 & 0 & 0 & 0 & 0 & 0 & \frac{8}{15} & \frac{-1}{15} \\
0 & 0 & 0 & 0 & 0 & 0 & 0 & 0 & 0 & \frac{-1}{5} & \frac{-1}{15} & \frac{4}{15}
\end{array}\right].$$

The matrix $\mathbf{K}$ has Form II symmetry, and the smallest eigenvalue can be obtained leading to λ_1, corresponding to $P_{cr} = \dfrac{11.1049EI}{L^2}$. The exact value for the critical load is $P_{cr(exactl)} = \dfrac{12.6EI}{L^2}$.

Alternative Solution: The solution with one element per column indicates that for calculating the buckling load of the entire structure, one can calculate only the buckling load of the factor D of the frame, as shown in Fig. 7.23.

For this factor, $\det \mathbf{K}_D = 0$ leads to

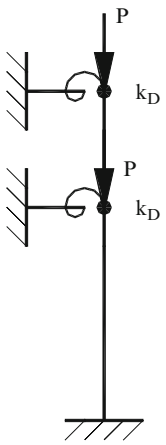

Fig. 7.23 The factor D of the structure

$$\det\begin{bmatrix} 10-15\lambda & 2+\lambda \\ 2+\lambda & 6-9\lambda \end{bmatrix} = 0 \tag{7.40}$$

or

$$\lambda_{\min} = 0.4273 \quad \text{and } P_{cr} = 12.82\frac{EI}{L^2},$$

and this is the same result as previously obtained.

Sway Frames: In this section, the buckling load of symmetric frames with sway is studied. For simplicity, the axial deformations of the beams are neglected. Therefore, for each storey, one lateral DOF is assumed, that is, the displacements of the two ends of each beam have the same magnitude.

In order to have the canonical Form III pattern, first, the rotational DOF should be numbered suitable for the formation of the Form II pattern with submatrices A and B, followed by free numbering of the translational DOFs of the stories forming the augmenting rows and columns. Then the stiffness matrix will have canonical Form III pattern.

In this case, for the formation of the factors of the frame, a new element should be defined, Fig. 7.24. Consider the following column with new values for its stiffness as

$$\mathbf{k} = \frac{2EI}{L^3}\begin{bmatrix} 6 & -6 & 3 & 3 \\ -6 & 6 & -3 & -3 \\ 0 & 0 & 0 & 0 \\ 0 & 0 & 0 & 0 \end{bmatrix}. \tag{7.41}$$

With an axial load P, the above matrix becomes

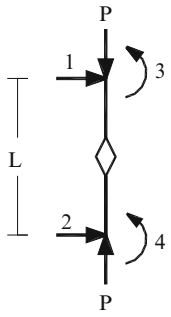

Fig. 7.24 A new column element

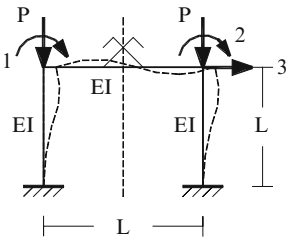

Fig. 7.25 A symmetric portal frame with antisymmetric sway buckling mode

$$\mathbf{k} = \frac{2EI}{L^3}\begin{bmatrix} 6 & -6 & 3 & 3 \\ -6 & 6 & -3 & -3 \\ 0 & 0 & 0 & 0 \\ 0 & 0 & 0 & 0 \end{bmatrix} - \frac{P}{L}\begin{bmatrix} \frac{6}{5} & \frac{-6}{5} & \frac{1}{10} & \frac{1}{10} \\ \frac{-6}{5} & \frac{6}{5} & \frac{-1}{10} & \frac{-1}{10} \\ 0 & 0 & 0 & 0 \\ 0 & 0 & 0 & 0 \end{bmatrix}. \tag{7.42}$$

7.3.1.1 Decomposition and Healing Process

For a sway frame with odd number of spans per storey, the process of the formation of the factors D and E consists of the following steps:

Step 1. All the beams crossed by the axis of symmetry are deleted.

Step 2. For the substructure in the left-hand side, a rotational spring with the stiffness $\frac{2EI_{lb}}{L^3_{Lb}}$ is added to obtain the substructure D. This provides the necessary stiffness requirement for obtaining the factor D.

Step 3. For the substructure in the right-hand side, the DOF for the beam is removed and a rotational DOF with stiffness equal to $\frac{6EI_{lb}}{L^3_{Lb}}$ is added.

Step 4. The translation DOF only affects the substructure E, and all the columns of E are doubled by the addition of the new column elements, introduced in the previous section, with corresponding stiffnesses.

Addition of the spring in the previous step, together with the new column, completes the formation of the factor E.

Example 7.4. The symmetric frame shown in Fig. 7.25 had a stiffness matrix with canonical Form II pattern when no lateral displacement was present. However, due to the presence of the lateral displacement, the corresponding stiffness matrix has canonical Form III pattern.

The stiffness matrix is now formed as

$$\mathbf{K} = \frac{EI}{L^3}\begin{bmatrix} 8 & 2 & -6 \\ 2 & 8 & -6 \\ -6 & -6 & 24 \end{bmatrix} - \frac{P}{L}\begin{bmatrix} 2/15 & 0 & -1/10 \\ 0 & 2/15 & -1/10 \\ -1/10 & -1/10 & 12/5 \end{bmatrix}. \tag{7.43}$$

This matrix is written as

$$\mathbf{K} = \frac{EI}{L^3}\begin{bmatrix} 8-4\lambda & 2 & -6+3\lambda \\ 2 & 8-4\lambda & -6+3\lambda \\ -6+3\lambda & -6+3\lambda & 24-72\lambda \end{bmatrix} \tag{7.44}$$

where $\lambda = \frac{PL^2}{30EI}$.

Consider a stiffness matrix in Form III as

$$\mathbf{K} = \begin{bmatrix} \mathbf{A} & \mathbf{B} & \mathbf{P} \\ \mathbf{B} & \mathbf{A} & \mathbf{P} \\ \mathbf{P} & \mathbf{P} & \mathbf{R} \end{bmatrix}. \tag{7.45}$$

The condensed submatrices of **K** are

$$[\mathbf{D}] = [\mathbf{A} - \mathbf{B}] = \frac{EI}{L^3}[8 - 4\lambda - 2] = \frac{EI}{L^3}[6 - 4\lambda], \tag{7.46}$$

and

$$[\mathbf{E}] = \begin{bmatrix} \mathbf{A}+\mathbf{B} & \mathbf{P} \\ 2\mathbf{P} & \mathbf{R} \end{bmatrix} = \frac{EI}{L^3}\begin{bmatrix} 10-4\lambda & -6+3\lambda \\ -12+6\lambda & 24-72\lambda \end{bmatrix}. \tag{7.47}$$

Design of D is the same as that of the non-sway frame, discussed in the previous section.

Design of E: The condensed matrix **E** for the present example can be written as

$$\mathbf{E} = \begin{bmatrix} \mathbf{E}_{22} & \mathbf{E}_{23} \\ \mathbf{E}_{32} & \mathbf{E}_{33} \end{bmatrix} = \begin{bmatrix} \frac{4EI}{L^3} + \frac{2EI}{L^3} - \frac{2P}{15L} & -\frac{3EI}{L^3} - \frac{3EI}{L^3} - \frac{P}{10L} \\ 2\left(\frac{-3EI}{L^3} - \frac{3EI}{L^3} - \frac{P}{10L}\right) & \frac{12EI}{L^3} + \frac{12EI}{L^3} - \frac{12P}{5L} \end{bmatrix}. \tag{7.48}$$

Deleting the second row and column, a one-by-one matrix $\mathbf{E}_{22}$ is obtained which corresponds to the factor C in non-sway frame and can be introduced to the factor E by adding a spring of stiffness equal to $\frac{6EI}{L^3}$. In order to incorporate the remaining submatrices of **E**, a new column element is introduced as shown in Fig. 7.24.

Consider the stiffness matrix of this column as

$$\mathbf{k}^* = \left[\begin{array}{c|c} \mathbf{k}_{\mathrm{I}} & \mathbf{k}_{\mathrm{II}} \\ \hline \mathbf{k}_{\mathrm{III}} & \mathbf{k}_{\mathrm{IV}} \end{array}\right], \tag{7.49}$$

where $\mathbf{k}_{\mathrm{I}}$ expresses relationship for translation DOF, $\mathbf{k}_{\mathrm{IV}}$ corresponds to rotation DOF and $\mathbf{k}_{\mathrm{II}}$ and $\mathbf{k}_{\mathrm{III}}$ express relationship for translation and rotation DOF.

Since the spring with stiffness $\frac{6\mathrm{EI}}{\mathrm{L}^3}$ is already included in the column, hence the new column element should have no additional effect on $\mathbf{E}_{22}$, and therefore, $\mathbf{k}_{\mathrm{IV}}$ should have all zero entries. For the formation of $\mathbf{E}_{23}$, the entry $\mathbf{K}_{23}$ in the overall stiffness matrix $\mathbf{K}$ should be introduced. Thus, the new column should have zero entries in $\mathbf{k}_{\mathrm{III}}$ position. According to Form III decomposition, for a symmetric matrix, $\mathbf{E}_{32}$ is equal to $2\mathbf{E}_{23}$, that is, the entry $\mathbf{E}_{32}$ is the same as $\mathbf{k}_{32}$ in the main column of the substructure C, plus itself, that is, the new column in $\mathbf{k}_{\mathrm{II}}$ position should have entries similar to those of a column element in the same position. In the present example, the entry $\mathbf{E}_{32}$ is obtained by the sum of $\mathbf{K}_{32}$ with itself:

$$\mathbf{k}_{\mathrm{II}} = \frac{\mathrm{EI}}{\mathrm{L}^3}\begin{bmatrix} 6 & 6 \\ -6 & -6 \end{bmatrix} - \frac{\mathrm{P}}{\mathrm{L}}\begin{bmatrix} \frac{1}{10} & \frac{1}{10} \\ -\frac{1}{10} & -\frac{1}{10} \end{bmatrix}. \tag{7.50}$$

In order to transfer the effect of translation from substructure D to that of E, the same stiffnesses as those of a general column (Eq. 7.34) are used, that is,

$$\mathbf{k}_{\mathrm{I}} = \frac{\mathrm{EI}}{\mathrm{L}^3}\begin{bmatrix} 12 & 12 \\ -12 & -12 \end{bmatrix} - \frac{\mathrm{P}}{\mathrm{L}}\begin{bmatrix} \frac{6}{5} & \frac{6}{5} \\ -\frac{6}{5} & -\frac{6}{5} \end{bmatrix}. \tag{7.51}$$

Thus, the stiffness matrix of the new column is obtained as

$$\mathbf{k}^* = \frac{\mathrm{EI}}{\mathrm{L}^3}\begin{bmatrix} 12 & -12 & 6 & 6 \\ -12 & 12 & -6 & -6 \\ 0 & 0 & 0 & 0 \\ 0 & 0 & 0 & 0 \end{bmatrix} - \frac{\mathrm{P}}{\mathrm{L}}\begin{bmatrix} \frac{6}{5} & \frac{-6}{5} & \frac{1}{10} & \frac{1}{10} \\ \frac{-6}{5} & \frac{6}{5} & \frac{-1}{10} & \frac{-1}{10} \\ 0 & 0 & 0 & 0 \\ 0 & 0 & 0 & 0 \end{bmatrix}, \tag{7.52}$$

and the reasoning is complete. This is an imaginary stiffness matrix, and such a column may not exist in the nature. However, the latter property has no effect on our calculations.

Now the determinant for the stiffness matrix of the entire structure is equated to zero as

$$\det \mathbf{K} = \det \mathbf{D} \times \det \mathbf{E} = \det[6 - 4\lambda] \times \det\begin{bmatrix} 10 - 4\lambda & -6 + 3\lambda \\ -12 + 6\lambda & 24 - 72\lambda \end{bmatrix} = 0, \tag{7.53}$$

leading to

$$\det \mathbf{D} = 0 \Rightarrow \lambda_1 = 1.5$$
$$\det \mathbf{E} = 0 \Rightarrow \lambda_2 = 2.5 \text{ and } \lambda_3 = 0.248.$$

Therefore,

$$\lambda_{\min} = 0.248 \text{ and } P_{cr} = 7.44\frac{EI}{L^2}.$$

The buckling load can be obtained by the direct eigensolution of a 3 × 3 matrix as $P_{cr} = 7.5\frac{EI}{L^2}$. More exact value of the buckling load is obtained by the solution of the corresponding differential equation leading to $P_{cr} = 7.34\frac{EI}{L^2}$.

For this example, the buckling load obtained by the present method is closer to the exact value compared to the case when the stability analysis of the entire structure is performed.

It can also be observed that for calculating the buckling load, only the formation of the factor E is needed. This reduces an eigensolution problem of size (m + n) × (m + n) to (m + n/2) × (m + n/2), where m and n are the translation and rotation degrees of freedom, respectively.

7.3.2 Buckling Load for Symmetric Frames with an Even Number of Spans per Storey

In this section, frames with an even number of spans per storey are studied. The axis of symmetry for these structures passes through columns, and we have no link beams. For these frames, the stiffness matrices have canonical Form III pattern.

Non-sway Frames: For this type of frame, first, the symmetric DOF is numbered suitable for canonical Form II part, followed by numbering the DOF corresponding to central joints. With this numbering, the stiffness matrix will have canonical Form III pattern.

7.3.2.1 Decomposition and Healing

Step 1. Cut the structure in a small distance ε to the left-hand side of the axis of symmetry.

Step 2. The cut ends are altered to clamped supports. The factor D is now obtained.

Step 3. For each central joint in the substructure of the right-hand side, add a simple support and connect this joint with a directed beam to the other end of the existing beam, as illustrated in the following example. Then the factor E is obtained.

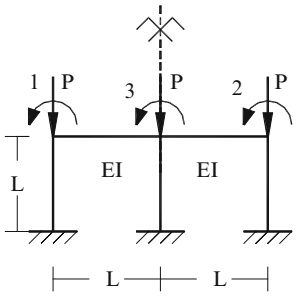

Fig. 7.26 A two-span symmetric non-sway frame

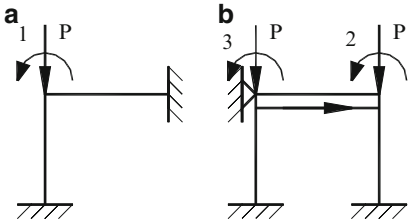

Fig. 7.27 Factors of the considered frame. (**a**) Factor D. (**b**) Factor E

Example 7.5. Consider the frame shown in Fig. 7.26. This frame has three DOFs, consisting of two symmetric DOFs and one central DOF.

The stiffness matrix, with canonical Form III pattern, is obtained as (Fig. 7.27)

$$\mathbf{K} = \frac{EI}{L^3}\begin{bmatrix} 4+4 & 0 & 2 \\ 0 & 4+4 & 2 \\ 2 & 2 & 4+4+4 \end{bmatrix} - \frac{P}{L}\begin{bmatrix} \frac{2}{15} & 0 & 0 \\ 0 & \frac{2}{15} & 0 \\ 0 & 0 & \frac{2}{15} \end{bmatrix}. \tag{7.54}$$

Assuming

$$\lambda = \frac{2Pl^2}{15EI},$$

we have

$$\mathbf{D} = \frac{EI}{L^3}[8-\lambda] \quad \text{and} \quad \mathbf{E} = \frac{EI}{L^3}\begin{bmatrix} 8-\lambda & 2 \\ 4 & 12-\lambda \end{bmatrix}, \tag{7.55}$$

leading to

$$\lambda_1 = 8, \quad \lambda_2 = 7.17, \quad \text{and } \lambda_3 = 12.82,$$

and $P_{cr} = 53.78\frac{EI}{L^2}$.

Alternative Solution: In this approach, the factors are formed using the decomposition and healing algorithm of the previous section. For each factor, the stiffness matrices are

$$\mathbf{D} = \frac{\mathrm{EI}}{\mathrm{L}^3}[8-\lambda] \quad \text{and } \mathbf{E} = \frac{\mathrm{EI}}{\mathrm{L}^3}\begin{bmatrix} 8-\lambda & 2 \\ 4 & 12-\lambda \end{bmatrix}, \tag{7.56}$$

leading to the same buckling load as

$$\lambda_1 = 8, \quad \lambda_2 = 7.17, \text{ and } \lambda_3 = 12.82,$$

and $\mathrm{P_{cr}} = 53.78\frac{\mathrm{EI}}{\mathrm{L}^2}$.

It was mentioned before that, with a suitable numbering of the DOF, for symmetric frames with an even number of spans, the overall stiffness matrix of the frame has a canonical Form III pattern as

$$\mathbf{K} = \begin{bmatrix} \mathbf{A} & \mathbf{B} & \mathbf{P} \\ \mathbf{B} & \mathbf{A} & \mathbf{L} \\ \mathbf{P} & \mathbf{L} & \mathbf{R} \end{bmatrix}, \tag{7.57}$$

where $\mathbf{P}$ expresses the relationship of the DOF for the left part with those of the central part, and $\mathbf{L}$ is the relationship of the DOF of the right-hand side and those of the central part. Since the frame is symmetric, therefore $\mathbf{P} = \mathbf{L}$, and the decomposition of

$$\mathbf{K} = \begin{bmatrix} \mathbf{A} & \mathbf{B} & \mathbf{P} \\ \mathbf{B} & \mathbf{A} & \mathbf{P} \\ \mathbf{P} & \mathbf{P} & \mathbf{R} \end{bmatrix} \tag{7.58}$$

results in

$$\mathbf{D} = [\mathbf{A} - \mathbf{B}] \text{ and } \mathbf{E} = \begin{bmatrix} \mathbf{A}+\mathbf{B} & \mathbf{P} \\ 2\mathbf{P} & \mathbf{R} \end{bmatrix}. \tag{7.59}$$

For a typical beam, the stiffness matrix is as follows:

$$\mathbf{k} = \begin{bmatrix} \mathbf{k}_{11} & \mathbf{k}_{12} \\ \mathbf{k}_{21} & \mathbf{k}_{22} \end{bmatrix} = \frac{\mathrm{EI}}{\mathrm{L}^3}\left[\begin{array}{cc|cc} 12 & -12 & 6 & 6 \\ -12 & 12 & -6 & -6 \\ \hline 6 & 6 & 4 & 2 \\ -6 & -6 & 2 & 4 \end{array}\right], \tag{7.60}$$

provided in the displacement vector, and rotations are multiplied by L.

For frames with no sway, only the rotation DOF of the beams is of interest, and therefore, only the submatrix $\mathbf{k}_{22}$ is important.

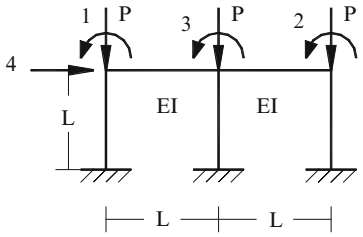

Fig. 7.28 A two-span sway frame

For a beam (i,j) the matrix **L** is as follows:

$$\mathbf{L} = \frac{EI}{L^3}\left[\begin{array}{c|c} 4 & 2 \\ \hline 2 & 4 \end{array}\right]\begin{matrix} i \\ j \end{matrix}. \tag{7.61}$$

After decomposition of S, the left-hand substructure corresponds to the condensed submatrix **D**. The effects of the central columns are all included in **E**, and therefore, the dimension of **E** is bigger than **D** by the number of DOF for central nodes, and for each column, one rotation DOF is considered on the top end of the column.

Design of D: The cut for decomposition is slightly towards the left of the axis of symmetry. In this way a correct number for the DOF of D which is half the symmetric DOF is obtained. Fixing the cut ends in D, the rotation DOF stays unaltered and hence provides the correct DOF.

Design of E: For the substructure in the right-hand side, the DOF of the central nodes is transferred to the right-hand substructure. The stiffness of the two ends of the beams is not the same; therefore, a directed beam is defined, leading to a nonsymmetric stiffness matrix.

As an example, for the frame shown in Fig. 7.28, we have

$$\mathbf{D} = \frac{EI}{L^3}[8] \quad \text{and} \quad \mathbf{E} = \begin{bmatrix} \mathbf{E}_{22} & \mathbf{E}_{23} \\ \mathbf{E}_{32} & \mathbf{E}_{33} \end{bmatrix} = \frac{EI}{L^3}\begin{bmatrix} 8 & 2 \\ 4 & 12 \end{bmatrix}. \tag{7.62}$$

For the substructure E, we should add a member such that in position $\mathbf{E}_{33}$, the stiffness is increased by k_{ii} in Eq. 7.62, and in $\mathbf{E}_{22}$, it should remain unchanged, that is, k_{jj} should be zero. This member should increase $\mathbf{E}_{32}$ by k_{ij}, but $\mathbf{E}_{23}$ should be left unaltered; that is, k_{ji} should have null value. Hence, the stiffness matrix of this beam will be in the following form:

$$\frac{EI}{L^3}\begin{bmatrix} 4 & 2 \\ 0 & 0 \end{bmatrix}. \tag{7.63}$$

With a direction on this member from i to j, corresponding to a nonsymmetric stiffness matrix, the above conditions are fulfilled. Here, i is the central node and j is the other end of the right-hand side beam.

Considering the entries of 2P in **E**, one finds out that these entries can be obtained by moments at the central DOF under the action of unit displacements

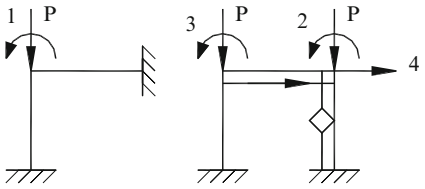

Fig. 7.29 The factors of the considered frame

in the DOF of the right-hand side. Thus, for the formation of the submatrix **E**, this moment is doubled, while the reverse action is not doubled. The importance of directed beams in the formation of the factor E becomes apparent.

Sway Frames

The stiffness matrices of these frames, with appropriate numbering of the DOF, have canonical Form III patterns. Here, the axis of symmetry passes through one or more joints. Similar to the non-sway case, first, symmetric DOF is numbered with n/2 difference suitable for canonical Form II pattern. Then the translational DOF is numbered. In this numbering, the central joint DOF for storey i is more than j if the symmetric DOF of storey i is bigger than those of j. With this numbering scheme, the stiffness matrix of the frame will have canonical Form III pattern.

7.3.2.2 Decomposition and Healing

Step 1. Cut the main structure with an axis passing from a small distance ε to the left of the axis of symmetry.
Step 2. Consider clamped supports for all the ends cut by this axis. The formation of the factor D is now completed.
Step 3. In the right-hand side substructure, for each cut beam, add a directed beam from central joint to symmetric joint to obtain E.

For this case, all the necessary elements are previously discussed and the necessity of above steps should be obvious.

Example 7.6. Consider the frame shown in Fig. 7.28.
This structure is factored to D and E as illustrated in Fig. 7.29.
The stiffness matrices of **D** and **E** are obtained as

$$\mathbf{D} = \frac{EI}{L^3}[8-\lambda] \Rightarrow \lambda_1 = 8$$
$$\mathbf{E} = \frac{EI}{L^3}\begin{bmatrix} 8-\lambda & 2 & -6-0.75\lambda \\ 4 & 12-\lambda & -6-0.75\lambda \\ -12-1.5\lambda & -6-0.75\lambda & 36-32\lambda \end{bmatrix} \tag{7.64}$$

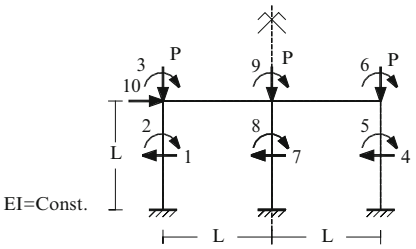

Fig. 7.30 A two-span one-storey symmetric frame

where $\lambda = \dfrac{2PL^2}{15EI}$.

The solution is obtained as

$$\lambda_2 = 0.729, \quad \lambda_3 = 6.88, \quad \text{and } \lambda_4 = 15.13,$$

and $P_{cr} = 5.47\dfrac{EI}{L^2}$.

The stiffness matrix of the factor E is

$$\mathbf{K} = \frac{EI}{L^3}\begin{bmatrix} 8 & 0 & 2 & -6 \\ 0 & 8 & 2 & -6 \\ 2 & 2 & 12 & -6 \\ -6 & -6 & -6 & 36 \end{bmatrix} - \frac{P}{L}\begin{bmatrix} \frac{2}{15} & 0 & 0 & \frac{-1}{10} \\ 0 & \frac{2}{15} & 0 & \frac{-1}{10} \\ 0 & 0 & \frac{2}{15} & \frac{-1}{10} \\ \frac{-1}{10} & \frac{-1}{10} & \frac{-1}{10} & \frac{18}{5} \end{bmatrix}. \tag{7.65}$$

Equating the determinant of this matrix to zero results in the same buckling load for the frame.

For a better approximation, columns are subdivided into two elements and the analysis is performed. As a second example, consider the frame shown in Fig. 7.30.

The stiffness matrix of this frame has canonical Form III with the following submatrices:

$$\mathbf{A} = \begin{bmatrix} 192 - 72\lambda & 0 & -48 + 3\lambda \\ 0 & 64 - 8\lambda & 16 + \lambda \\ -48 + 3\lambda & 16 + \lambda & 36 - 4\lambda \end{bmatrix} \quad \text{and} \quad \mathbf{B} = \begin{bmatrix} 0 & 0 & 0 \\ 0 & 0 & 0 \\ 0 & 0 & 0 \end{bmatrix}$$

$$\mathbf{P} = \begin{bmatrix} 0 & 0 & 0 & 96 - 36\lambda \\ 0 & 0 & 0 & -48 + 3\lambda \\ 0 & 0 & 2 & -48 + 3\lambda \end{bmatrix}$$

$$\text{and } \mathbf{H} = \begin{bmatrix} 192 - 72\lambda & 0 & -48 + 3\lambda & 96 - 36\lambda \\ 0 & 64 - 8\lambda & 16 + \lambda & -48 + 3\lambda \\ -48 + 3\lambda & 16 + \lambda & 40 - 4\lambda & -48 + 3\lambda \\ 96 - 36\lambda & -48 + 3\lambda & -48 + 3\lambda & 288 - 108\lambda \end{bmatrix}$$

$$\mathbf{M}+\mathbf{N}=\begin{bmatrix} 192-72\lambda & 0 & -48+3\lambda & 0 & 0 & 0 & 192-72\lambda \\ 0 & 64-8\lambda & 16+\lambda & 0 & 0 & 0 & -96+6\lambda \\ -48+3\lambda & 16+\lambda & 36-4\lambda & 0 & 0 & 4 & -96+6\lambda \\ 0 & 0 & 0 & 192-72\lambda & 0 & -48+3\lambda & 96-36\lambda \\ 0 & 0 & 0 & 0 & 64-8\lambda & 16+\lambda & -48+3\lambda \\ 0 & 0 & 2 & -48+3\lambda & 16+\lambda & 40-4\lambda & -48+3\lambda \\ 96-36\lambda & -48+3\lambda & -48+3\lambda & 96-48\lambda & -48+3\lambda & -48+3\lambda & 288-108\lambda \end{bmatrix}.$$

The eigenvalues corresponding to this matrix are obtained as

$$\lambda_{\mathbf{M+N}} = \{0.3423, 1.5268, 1.8055, 5.7650, 13.0571, 14.7588\}.$$

$$\mathbf{M}-\mathbf{N}=\begin{bmatrix} 192-72\lambda & 0 & -48+3\lambda & 0 & 0 & 0 & 0 \\ 0 & 64-8\lambda & 16+\lambda & 0 & 0 & 0 & 0 \\ -48+3\lambda & 16+\lambda & 32-4\lambda & 0 & 0 & 0 & 0 \\ 0 & 0 & 0 & 0 & 0 & 0 & 0 \\ 0 & 0 & 0 & 0 & 0 & 0 & 0 \\ 0 & 0 & 0 & 0 & 0 & 0 & 0 \\ 0 & 0 & 0 & 0 & 0 & 0 & 0 \end{bmatrix}.$$

and ignoring the last four rows and columns, the eigenvalues for the above matrix are obtained as

$$\lambda_{\mathbf{M-N}} = \{1.5695, 5.2540, 13.7989\}.$$

The smallest eigenvalue is therefore $\lambda_1 = 0.3423$, leading to $P_{cr} = 5.1344EI/L^2$.

7.3.3 Discussion

Exploiting the symmetry of structures can be made by using discrete mathematics. This prepares the ground for more efficient use of the computer and to an understanding which enables us to interpret the final results more readily. Factoring the symmetric structures has the following advantages:

1. The DOF of the problem is reduced.
2. The computational effort is decreased.
3. The solution of larger problems becomes feasible.

Though the examples are selected from small structures, however, the method shows its potential more when applied to large-scale structures.

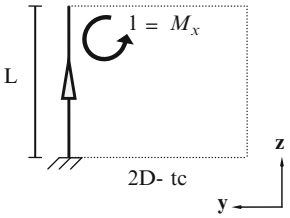

Fig. 7.31 The new column tc, fixed in F_y direction

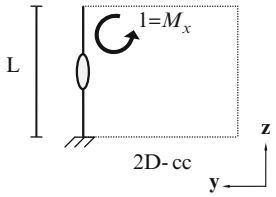

Fig. 7.32 The new column cc

7.4 Eigenfrequencies of Symmetric Planar Frame

In this part the graph models of planar frame structures with different symmetries are decomposed and appropriate processes are designed for their healing in order to form the corresponding factors. The eigenvalues and eigenvectors of the entire structure are then obtained by evaluating those of its factors. The methods developed in this part simplify the calculation of the natural frequencies and natural modes of the planar frames with different types of symmetry.

7.4.1 Eigenfrequencies of Planar Symmetric Frames with Odd Number of Spans

7.4.1.1 Definitions

The Element tc for 2D Case: The elements defined in the following are used in decomposition for doubling some columns in place of deleting the beams. The new column is denoted by tc, as shown in Fig. 7.31, and it is characterised by Eq. 7.66.

$$\text{The properties of the deleted beam} \quad L_b, \quad m_b, \quad EI_b$$

$$\mathbf{K}_{tc} = \frac{EI_b}{L_b} \times [6], \quad \mathbf{M}_{tc} = \frac{m_b L_b^3}{420} \times [1]. \tag{7.66}$$

The Element cc for 2D Case: This new column is denoted by cc, as shown in Fig. 7.32, and it is characterised by Eq. 7.67.

The properties of the deleted beam $\quad L_b, \quad m_b, \quad EI_b$

$$\mathbf{K}_{cc} = \frac{EI_b}{L_b} \times [2] \text{ and } \mathbf{M}_{cc} = \frac{m_b L_b^3}{420} \times [7]. \tag{7.67}$$

Algorithm (a): The algorithm for the decomposition of planar frames with odd number of spans, with or without sway, is designed as follows:

Step 1. Delete all the beams crossing the axis of symmetry.
Step 2. The columns corresponding to the left part, which are connected to the eliminated beams, are doubled by tc columns. This half for the case of non-sway forms the factor C and in the case of sway together with the translation DOFs forms the factor E.
Step 3. The columns of the right half, which were connected to the eliminated beams, are doubled by cc columns. This half for the cases of sway and non-sway forms the factor D and in the case of sway together with the translation DOFs is deleted.

*Definition of the Function f(**A**)*: Consider **A** as a matrix. If m is the number of translational DOFs, then f(**A**) multiplies the last m rows of **A** by 2.

Note: In the case of non-sway frame, the problem is solved by constructing the submatrices $\mathbf{M}_C, \mathbf{K}_C$ and $\mathbf{M}_D, \mathbf{K}_D$ corresponding to the Form II symmetry, and in the sway case, the problem is solved by forming $\mathbf{M}_D, \mathbf{K}_D$ and $f(\mathbf{M}_E), f(\mathbf{K}_E)$ corresponding to the Form III symmetry.

In this algorithm, the stiffness and mass matrices of the factor E are not the same as those obtained from the original structure. However, the responses consisting of the determinant and eigenvalues are identical, that is,

$$\mathbf{K},\ \mathbf{M} = \begin{bmatrix} \mathbf{A} & \mathbf{B} & \mathbf{S} & \mathbf{R} \\ \mathbf{B} & \mathbf{A} & \mathbf{S} & \mathbf{R} \\ \mathbf{S} & \mathbf{S} & \mathbf{Y} & \mathbf{X} \\ \mathbf{R} & \mathbf{R} & \mathbf{X} & \mathbf{Y} \end{bmatrix} \Rightarrow \mathbf{D} = \mathbf{A} - \mathbf{B} \text{ and } \mathbf{E} = \begin{bmatrix} \mathbf{A}+\mathbf{B} & \mathbf{S} & \mathbf{R} \\ 2\mathbf{S} & \mathbf{Y} & \mathbf{X} \\ 2\mathbf{R} & \mathbf{X} & \mathbf{Y} \end{bmatrix}. \tag{7.68}$$

The stiffness and mass matrices of the factor E in the algorithm (a) are obtained as

$$\mathbf{K}_E, \mathbf{M}_E = \begin{bmatrix} \mathbf{A}+\mathbf{B} & \mathbf{S} & \mathbf{R} \\ \mathbf{S} & \frac{\mathbf{Y}}{2} & \frac{\mathbf{X}}{2} \\ \mathbf{R} & \frac{\mathbf{X}}{2} & \frac{\mathbf{Y}}{2} \end{bmatrix}. \tag{7.69}$$

The properties of the new columns are obtained by considering the interrelation of the DOFs of the members. For the frames with odd number of spans, where the axis of symmetry passes through beams, the effect of the deleted beams should be included in the decomposed subgraphs. Adding the new columns serves as a means for

transferring the properties of the main structure into the decomposed substructures. These operations are healings which change the subgraphs into the factors.

Considering the Form II symmetry, we have

$$\begin{aligned} &\mathbf{K} = \begin{bmatrix} \mathbf{A} & \mathbf{B} \\ \mathbf{B} & \mathbf{A} \end{bmatrix}, \\ &\mathbf{C} = [\mathbf{A} + \mathbf{B}] \text{ and } \mathbf{D} = [\mathbf{A} - \mathbf{B}], \\ &\{\lambda \mathbf{K}\} = \{\lambda \mathbf{C}\} \overline{\cup} \{\lambda \mathbf{D}\}. \end{aligned} \tag{7.70}$$

If we can construct substructures with the stiffness and mass matrices corresponding to the above forms, then we can form the factors.

If the numbering is performed corresponding to the Form II symmetry, then the submatrix **B** will represent the relation between the DOFs of the right side and the left side of the frame, and the submatrix **A** represents the relation between the DOFs of each half of the structure.

In general, for a beam column with one rotational DOF per node, we have

$$\mathbf{K} = \frac{\mathrm{EI}}{\mathrm{L}} \times \begin{bmatrix} 4 & 2 \\ 2 & 4 \end{bmatrix}, \quad \mathbf{M} = \frac{\mathrm{mL}^3}{420} \times \begin{bmatrix} 4 & -3 \\ -3 & 4 \end{bmatrix}. \tag{7.71}$$

Considering the relationship between the DOFs of the connecting beams, it becomes obvious that the entries (1,1) and (1,2) in the mass and stiffness matrices of the substructures C and D should be added and subtracted, respectively.

$$\begin{aligned} \mathrm{C}: \quad & \mathbf{K} = \frac{\mathrm{EI}}{\mathrm{L}} \times [4+2] = \frac{\mathrm{EI}}{\mathrm{L}} \times [6], \quad \mathbf{M} = \frac{\mathrm{mL}^3}{420} \times [4+(-3)] = \frac{\mathrm{mL}^3}{420} \times [1], \\ \mathrm{D}: \quad & \mathbf{K} = \frac{\mathrm{EI}}{\mathrm{L}} \times [4-2] = \frac{\mathrm{EI}}{\mathrm{L}} \times [2], \quad \mathbf{M} = \frac{\mathrm{mL}^3}{420} \times [4-(-3)] = \frac{\mathrm{mL}^3}{420} \times [7]. \end{aligned} \tag{7.72}$$

It is obvious that the length and the elastic properties in these relationships correspond to the connecting beams which are supposed to be deleted.

$$\begin{aligned} \mathbf{K}_{\mathrm{tc}} &= \frac{\mathrm{EI_b}}{\mathrm{L_b}} \times [6], \quad \mathbf{M}_{\mathrm{tc}} = \frac{\mathrm{m_b L_b^3}}{420} \times [1], \\ \mathbf{K}_{\mathrm{cc}} &= \frac{\mathrm{EI_b}}{\mathrm{L_b}} \times [2], \quad \mathbf{M}_{\mathrm{cc}} = \frac{\mathrm{m_b L_b^3}}{420} \times [7]. \end{aligned} \tag{7.73}$$

In this way, the properties of the new columns are obtained.

Example 7.7. The symmetric frame shown in Fig. 7.33 is considered. This frame is assumed to be constrained against sway and has only two rotation DOFs, as shown in the figure.

The distribution of the mass in the link beam which crosses the axis of symmetry should also be symmetric.

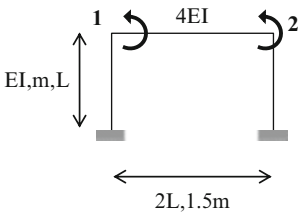

Fig. 7.33 A symmetric frame with two DOFs

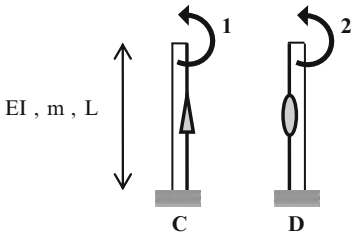

Fig. 7.34 Factors of the frame of Fig. 7.3

According to the algorithm (a), the decomposition of the frame is obtained in a step-by-step manner, whereas in the previously developed methods, the factors were obtained by adding springs and masses.

The properties of the added columns (Fig. 7.34) are as follows:

$$\begin{aligned} \mathbf{K}_{tc} &= \frac{EI_b}{L_b} \times [6] = \left[\frac{12EI}{L}\right] \quad \text{and} \quad \mathbf{M}_{tc} = \frac{m_b L_b^3}{420} \times [1] = \left[\frac{6mL^3}{210}\right], \\ \mathbf{K}_{cc} &= \frac{EI_b}{L_b} \times [2] = \left[\frac{4EI}{L}\right] \quad \text{and} \quad \mathbf{M}_{cc} = \frac{m_b L_b^3}{420} \times [7] = \left[\frac{42mL^3}{210}\right]. \end{aligned} \tag{7.74}$$

Now the stiffness and mass matrices of the factors C and D are formed as

$$\begin{aligned} &\mathbf{K}_C = \left[\frac{4EI}{L} + \frac{12EI}{L}\right] = \left[\frac{16EI}{L}\right] \text{ and } \mathbf{M}_C = \left[\frac{mL}{420} \times 4L^2 + \frac{6mL^3}{210}\right] = \left[\frac{8mL^3}{210}\right] \\ &\omega^2 = X \qquad \Rightarrow \omega_1^2 = \frac{420EI}{mL^4}, \\ &\mathbf{K}_D = \left[\frac{4EI}{L} + \frac{4EI}{L}\right] = \left[\frac{8EI}{L}\right] \text{ and } \mathbf{M}_D = \left[\frac{mL}{420} \times 4L^2 + \frac{42mL^3}{210}\right] = \left[\frac{44mL^3}{210}\right] \\ &\omega^2 = X \qquad \Rightarrow \omega_2^2 = \frac{420EI}{11mL^4}, \end{aligned} \tag{7.75}$$

and the natural frequencies are easily obtained.

Example 7.8. The frame shown in Fig. 7.35 has 10 DOFs and has the Form II symmetry.

The factors are constructed as shown in Fig. 7.36.

The stiffness and mass matrices of the added columns are as follows (Fig. 7.37):

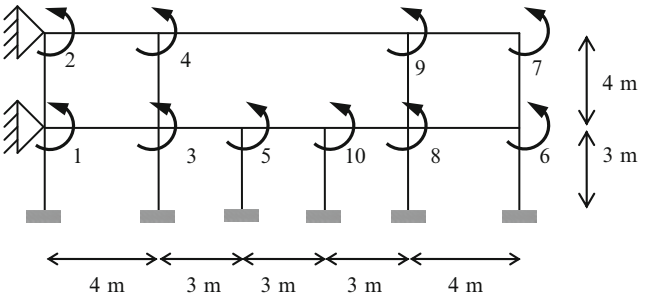

Fig. 7.35 A symmetric frame with 10 DOFs

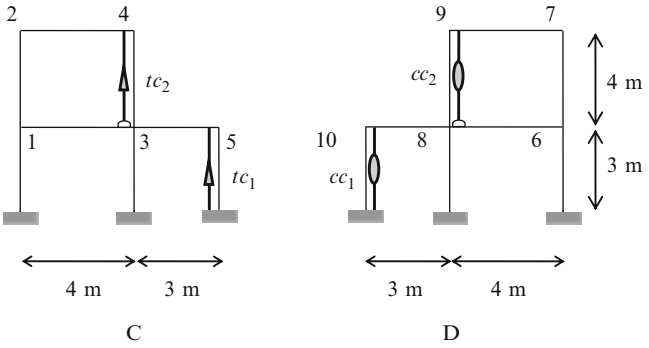

Fig. 7.36 Factors of the frame of Fig. 7.18

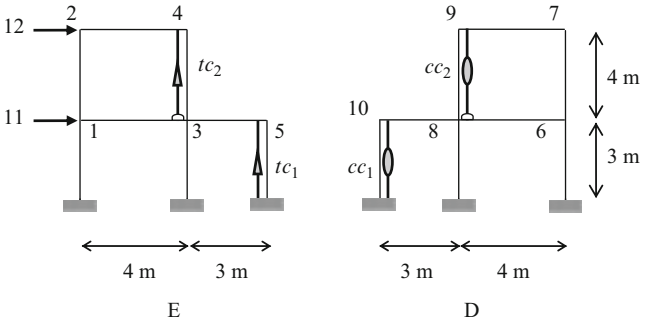

Fig. 7.37 Factors D and E of the sway frame of Fig. 7.36

$$\text{tc}_1 : \Rightarrow \mathbf{K}_{\text{tc}_1} = \frac{\text{EI}_\text{b}}{\text{L}_\text{b}} \times [6] = [2\text{EI}] \quad \& \quad \mathbf{M}_{\text{tc}_1} = \frac{\text{m}_\text{b}\text{L}_\text{b}^3}{420} \times [1] = \left[\frac{9\text{m}}{140}\right],$$

$$\text{cc}_1 : \Rightarrow \mathbf{K}_{\text{cc}_1} = \frac{\text{EI}_\text{b}}{\text{L}_\text{b}} \times [2] = \left[\frac{2\text{EI}}{3}\right] \quad \& \quad \mathbf{M}_{\text{cc}_1} = \frac{\text{m}_\text{b}\text{L}_\text{b}^3}{420} \times [7] = \left[\frac{9\text{m}}{20}\right].$$

$$\text{tc}_2 : \Rightarrow \mathbf{K}_{\text{tc}_2} = \frac{\text{EI}_\text{b}}{\text{L}_\text{b}} \times [6] = \left[\frac{2\text{EI}}{3}\right] \quad \& \quad \mathbf{M}_{\text{tc}_2} = \frac{\text{m}_\text{b}\text{L}_\text{b}^3}{420} \times [1] = \left[\frac{243\text{m}}{70}\right],$$

$$\text{cc}_2 : \Rightarrow \mathbf{K}_{\text{cc}_2} = \frac{\text{EI}_\text{b}}{\text{L}_\text{b}} \times [2] = \left[\frac{2\text{EI}}{9}\right] \quad \& \quad \mathbf{M}_{\text{cc}_2} = \frac{\text{m}_\text{b}\text{L}_\text{b}^3}{420} \times [7] = \left[\frac{243\text{m}}{10}\right]. \tag{7.76}$$

The stiffness and mass matrices of the factors C and D are constructed as

$$\mathbf{K}_\text{C} = \text{EI} \times \begin{bmatrix} \frac{4}{3}+\frac{4}{4}+\frac{4}{4} & \frac{2}{4} & \frac{2}{4} & 0 & 0 \\ \frac{2}{4} & \frac{4}{4}+\frac{4}{4} & 0 & \frac{2}{4} & 0 \\ \frac{2}{4} & 0 & \frac{4}{3}+\frac{4}{4}+\frac{4}{3}+\frac{4}{4} & \frac{2}{4} & \frac{2}{3} \\ 0 & \frac{2}{4} & \frac{2}{4} & \frac{4}{4}+\frac{4}{4}+\frac{2}{3} & 0 \\ 0 & 0 & \frac{2}{3} & 0 & \frac{4}{3}+\frac{4}{3}+2 \end{bmatrix}$$

$$= 2\text{EI} \begin{bmatrix} \frac{5}{3} & \frac{1}{4} & \frac{1}{4} & 0 & 0 \\ \frac{1}{4} & 1 & 0 & \frac{1}{4} & 0 \\ \frac{1}{4} & 0 & \frac{7}{3} & \frac{1}{4} & \frac{1}{3} \\ 0 & \frac{1}{4} & \frac{1}{4} & \frac{4}{3} & 0 \\ 0 & 0 & \frac{1}{3} & 0 & \frac{7}{3} \end{bmatrix},$$

$$\mathbf{M}_\text{C} = \frac{\text{m}}{420} \begin{bmatrix} 620 & -192 & -192 & 0 & 0 \\ -192 & 512 & 0 & -192 & 0 \\ -192 & 0 & 728 & -192 & -81 \\ 0 & -192 & -192 & 1241 & 0 \\ 0 & 0 & -81 & 0 & 243 \end{bmatrix}. \tag{7.77}$$

$$\mathbf{K}_{\mathrm{D}} = \mathrm{EI} \times \begin{bmatrix} \frac{4}{3}+\frac{4}{4}+\frac{4}{4} & \frac{2}{4} & \frac{2}{4} & 0 & 0 \\ \frac{2}{4} & \frac{4}{4}+\frac{4}{4} & 0 & \frac{2}{4} & 0 \\ \frac{2}{4} & 0 & \frac{4}{3}+\frac{4}{4}+\frac{4}{3}+\frac{4}{4} & \frac{2}{4} & \frac{2}{3} \\ 0 & \frac{2}{4} & \frac{2}{4} & \frac{4}{4}+\frac{4}{4}+\frac{2}{9} & 0 \\ 0 & 0 & \frac{2}{3} & 0 & \frac{4}{3}+\frac{4}{3}+\frac{2}{3} \end{bmatrix}$$

$$= 2\mathrm{EI} \begin{bmatrix} \frac{5}{3} & \frac{1}{4} & \frac{1}{4} & 0 & 0 \\ \frac{1}{4} & 1 & 0 & \frac{1}{4} & 0 \\ \frac{1}{4} & 0 & \frac{7}{3} & \frac{1}{4} & \frac{1}{3} \\ 0 & \frac{1}{4} & \frac{1}{4} & \frac{10}{9} & 0 \\ 0 & 0 & \frac{1}{3} & 0 & \frac{5}{3} \end{bmatrix}, \tag{7.78}$$

$$\mathbf{M}_{\mathrm{D}} = \frac{\mathrm{m}}{420} \begin{bmatrix} 620 & -192 & -192 & 0 & 0 \\ -192 & 512 & 0 & -192 & 0 \\ -192 & 0 & 728 & -192 & -81 \\ 0 & -192 & -192 & 5615 & 0 \\ 0 & 0 & -81 & 0 & 405 \end{bmatrix}.$$

In this way, the natural frequencies and the natural modes of this frame with 10 DOFs are obtained using the equation of the motion of two factors each having five DOFs as

$$\begin{aligned} &\det\left[\mathbf{K}_{\mathrm{C}} - \omega^2 \mathbf{M}_{\mathrm{C}}\right]_{5\times 5} = 0 \;\Rightarrow \\ &\omega_1^2 = \frac{0.6\mathrm{EI}}{\mathrm{m}},\ \omega_2^2 = \frac{1.42\mathrm{EI}}{\mathrm{m}},\ \omega_3^2 = \frac{2.15\mathrm{EI}}{\mathrm{m}},\ \omega_4^2 = \frac{5.24\mathrm{EI}}{\mathrm{m}} \text{ and } \omega_5^2 = \frac{9.56\mathrm{EI}}{\mathrm{m}}, \\ &\det\left[\mathbf{K}_{\mathrm{D}} - \omega^2 \mathbf{M}_{\mathrm{D}}\right]_{5\times 5} = 0 \;\Rightarrow \\ &\omega_6^2 = \frac{0.15\mathrm{EI}}{\mathrm{m}},\ \omega_7^2 = \frac{1.1\mathrm{EI}}{\mathrm{m}},\ \omega_8^2 = \frac{2\mathrm{EI}}{\mathrm{m}},\ \omega_9^2 = \frac{3.52\mathrm{EI}}{\mathrm{m}} \text{ and } \omega_{10}^2 = \frac{5.57\mathrm{EI}}{\mathrm{m}}. \end{aligned} \tag{7.79}$$

Example 7.9. Consider the sway frame shown in Fig. 7.38, having 12 DOFs.
The factors are shown in Fig. 7.22.
The natural frequencies are similar to those of Example 7.8, and therefore,

$$\omega_1^2 = \frac{0.15\mathrm{EI}}{\mathrm{m}}, \omega_2^2 = \frac{1.1\mathrm{EI}}{\mathrm{m}}, \omega_3^2 = \frac{2\mathrm{EI}}{\mathrm{m}}, \omega_4^2 = \frac{3.52\mathrm{EI}}{\mathrm{m}}, \omega_5^2 = \frac{5.57\mathrm{EI}}{\mathrm{m}}. \tag{7.80}$$

There is no need to solve the equation $\det\left[\mathbf{K}_{\mathrm{D}} - \omega^2 \mathbf{M}_{\mathrm{D}}\right]_{5\times 5} = 0$ for finding the eigenvalues. The formation of the factor D can be avoided.

$$\begin{aligned} &\mathrm{cc}_1 : \Rightarrow \mathbf{K}_{\mathrm{cc}_1} = \frac{\mathrm{EI_b}}{\ell_{\mathrm{b}}} \times [2] = \left[\frac{2\mathrm{EI}}{3}\right] \quad \text{and} \quad \mathbf{M}_{\mathrm{cc}_1} = \frac{\mathrm{m_b}\ell_{\mathrm{b}}^3}{420} \times [7] = \left[\frac{9\mathrm{m}}{20}\right], \\ &\mathrm{cc}_2 : \Rightarrow \mathbf{K}_{\mathrm{cc}_2} = \frac{\mathrm{EI_b}}{\ell_{\mathrm{b}}} \times [2] = \left[\frac{2\mathrm{EI}}{9}\right] \quad \text{and} \quad \mathbf{M}_{\mathrm{cc}_2} = \frac{\mathrm{m_b}\ell_{\mathrm{b}}^3}{420} \times [7] = \left[\frac{243\mathrm{m}}{10}\right]. \end{aligned} \tag{7.81}$$

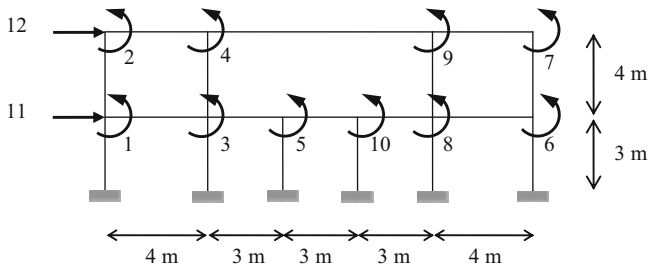

Fig. 7.38 A sway frame with 12 DOFs

The stiffness and the mass matrices of the factor E are as follows:

$$\mathbf{K}_{\mathrm{E}}=\mathrm{EI}\times\begin{bmatrix}
\frac{4}{3}+\frac{4}{4}+\frac{4}{4} & \frac{2}{4} & \frac{2}{4} & 0 & 0 & \frac{6}{3^2}-\frac{6}{4^2} & \frac{6}{4^2}\\
\frac{2}{4} & \frac{4}{4}+\frac{4}{4} & 0 & \frac{2}{4} & 0 & \frac{-6}{4^2} & \frac{6}{4^2}\\
\frac{2}{4} & 0 & \frac{4}{3}+\frac{4}{4}+\frac{4}{3}+\frac{4}{4} & \frac{2}{4} & \frac{2}{3} & \frac{6}{3^2}-\frac{6}{4^2} & \frac{6}{4^2}\\
0 & \frac{2}{4} & \frac{2}{4} & \frac{4}{4}+\frac{4}{4}+\frac{2}{3} & 0 & \frac{-6}{4^2} & \frac{6}{4^2}\\
0 & 0 & \frac{2}{3} & 0 & \frac{4}{3}+\frac{4}{3}+2 & \frac{6}{3^2} & 0\\
\frac{6}{3^2}-\frac{6}{4^2} & \frac{-6}{4^2} & \frac{6}{3^2}-\frac{6}{4^2} & \frac{-6}{4^2} & \frac{6}{3^2} & 3\times\frac{12}{3^3}+2\times\frac{12}{4^3} & -2\times\frac{12}{4^3}\\
\frac{6}{4^2} & \frac{6}{4^2} & \frac{6}{4^2} & \frac{6}{4^2} & 0 & -2\times\frac{12}{4^3} & 2\times\frac{12}{4^3}
\end{bmatrix},$$

$$\mathbf{M}_{\mathrm{E}}=\frac{\mathrm{m}}{420}\begin{bmatrix}
620 & -192 & -192 & 0 & 0 & -22\times3^2+22\times4^2 & 13\times4^2\\
-192 & 512 & 0 & -192 & 0 & -13\times4^2 & -22\times4^2\\
-192 & 0 & 728 & -192 & -81 & -22\times3^2+22\times4^2 & 13\times4^2\\
0 & -192 & -192 & 1241 & 0 & -13\times4^2 & -22\times4^2\\
0 & 0 & -81 & 0 & 243 & -22\times3^2 & 0\\
-22\times3^2+22\times4^2 & -13\times4^2 & -22\times3^2+22\times4^2 & -13\times4^2 & -22\times3^2 & 3\times156\times3+2\times156\times4 & 2\times54\times4\\
13\times4^2 & -22\times4^2 & 13\times4^2 & -22\times4^2 & 0 & 2\times54\times4 & 2\times156\times4
\end{bmatrix}. \tag{7.82}$$

In this way, the natural frequencies and the natural modes of this frame with 12 DOFs are obtained using the equation of the motion of two factors having five and seven DOFs.

The first five frequencies are as follows:

$$\omega_1^2=\frac{0.15\mathrm{EI}}{\mathrm{m}},\omega_2^2=\frac{1.1\mathrm{EI}}{\mathrm{m}},\omega_3^2=\frac{2\mathrm{EI}}{\mathrm{m}},\omega_4^2=\frac{3.52\mathrm{EI}}{\mathrm{m}},\omega_5^2=\frac{5.57\mathrm{EI}}{\mathrm{m}}. \tag{7.83}$$

The remaining seven frequencies are calculated from the factor E as

$$\begin{aligned}
&\det\left[\mathbf{K}_{\mathrm{E}}-\omega^2\mathbf{M}_{\mathrm{E}}\right]_{7\times7}=0\Rightarrow\\
&\omega_6^2=\frac{0.022\mathrm{EI}}{\mathrm{m}},\ \omega_7^2=\frac{0.25\mathrm{EI}}{\mathrm{m}},\ \omega_8^2=\frac{0.61\mathrm{EI}}{\mathrm{m}},\ \omega_9^2=\frac{1.81\mathrm{EI}}{\mathrm{m}},\\
&\omega_{10}^2=\frac{2.97\mathrm{EI}}{\mathrm{m}},\ \omega_{11}^2=\frac{5.67\mathrm{EI}}{\mathrm{m}}\ \text{ and }\omega_{12}^2=\frac{10.27\mathrm{EI}}{\mathrm{m}}.
\end{aligned} \tag{7.84}$$

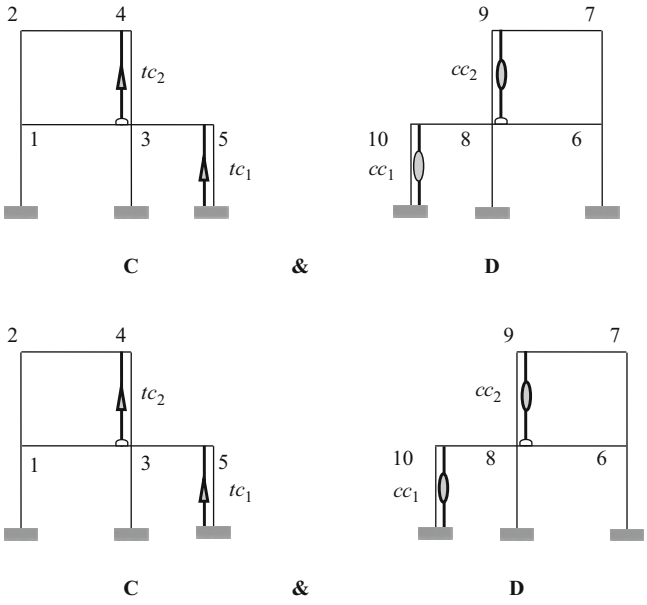

Fig. 7.39 Factors of the frame in non-sway and sway cases

The factors of the main frame in the case of sway and non-sway are identical, Figs. 7.22 and 7.39.

Only the factor E has the additional translation DOF. Thus, for calculating the responses of a frame in sway and non-sway cases, instead of solving a problem with $n \times n$ and $(n+m) \times (n+m)$ matrices, we need to solve three problems corresponding to $\frac{n}{2} \times \frac{n}{2}$, $\frac{n}{2} \times \frac{n}{2}$ and $\left(\frac{n}{2}+m\right) \times \left(\frac{n}{2}+m\right)$ matrices, Fig. 7.40.

7.4.2 *Decomposition of Symmetric Planar Frames with Even Number of Spans*

Algorithm for Decomposition: According to the present algorithm, each symmetric structure with an even number of spans can be decomposed into two factors, without introducing a new element. By obtaining dynamic properties of each factor and considering the union of the results, one can obtain the dynamic properties of the entire structure.

Definitions: A central element is defined as a column which coincides with the axis of symmetry. Central nodes are taken as the nodes that coincide with the axis of symmetry.

Algorithm (b): This algorithm is simple and consists of the following steps:

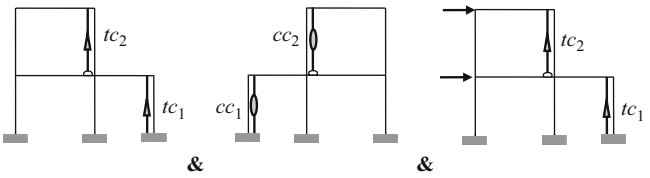

Fig. 7.40 Three factors to be considered for the solution

Step 1. Divide the frame into two halves from the axis of symmetry, such that the moment of inertia for the central column and the mass of their unit length, m, are reduced to half.

Step 2. Fix the central nodes in the left half. This half is the factor D and the right half forms the factor E.

Therefore, one can solve the main eigenproblem by constructing submatrices $\mathbf{K}_{\mathrm{D}}, \mathbf{M}_{\mathrm{D}}$ and $\mathbf{K}_{\mathrm{E}}, \mathbf{M}_{\mathrm{E}}$. In fact, the factors D and E obtained by this algorithm have the properties of the entire structure.

Proof: The stiffness and mass matrices of the factors D and E in the algorithm (b) are symmetric and can be formed as

$$\mathbf{D} = [\mathbf{G}]_{\frac{\mathrm{n}}{2}\times\frac{\mathrm{n}}{2}} \text{ and } \mathbf{E} = \begin{bmatrix} \mathbf{Q} & \mathbf{R} \\ \mathbf{R}^{\mathrm{t}} & \mathbf{Y} \end{bmatrix}_{\left(\frac{\mathrm{n}}{2}+\mathrm{m}\right)\times\left(\frac{\mathrm{n}}{2}+\mathrm{m}\right)} \tag{7.85}$$

where m is the total number of rotation and translation DOFs of central nodes and translation DOFs vertical to the plane of symmetry and n is the total number of symmetric translation and rotation DOFs.

If the numbering of the DOFs of main frame is performed in a special form corresponding to the Form III symmetry, then the matrices will be decomposable and can be formed as

$$\mathbf{K}, \mathbf{M} = \begin{bmatrix} \mathbf{A} & \mathbf{B} & \mathbf{S} \\ \mathbf{B}^{\mathrm{t}} & \mathbf{A} & \mathbf{S} \\ \mathbf{S}^{\mathrm{t}} & \mathbf{S}^{\mathrm{t}} & \mathbf{X} \end{bmatrix} \Rightarrow \mathbf{D}_{\mathrm{real}} = [\mathbf{A} - \mathbf{B}] \text{ and } \mathbf{E}_{\mathrm{real}} = \begin{bmatrix} \mathbf{A}+\mathbf{B} & \mathbf{S} \\ \mathbf{2S}^{\mathrm{t}} & \mathbf{X} \end{bmatrix}. \tag{7.86}$$

After considering the interrelationship between the DOFs in the main frame and in the factors and defining the function f, we will have

$$\begin{aligned} &\mathbf{G} = \mathbf{A} - \mathbf{B},\ \mathbf{Q} = \mathbf{A} + \mathbf{B},\ \mathbf{R} = \mathbf{S} \text{ and } \mathbf{Y} = \frac{\mathbf{X}}{2} \\ &\Rightarrow \mathbf{D} = [\mathbf{A} - \mathbf{B}] = \mathbf{D}_{\mathrm{real}} \text{ and } \mathbf{E} = \begin{bmatrix} \mathbf{A}+\mathbf{B} & \mathbf{S} \\ \mathbf{S}^{\mathrm{t}} & \frac{\mathbf{X}}{2} \end{bmatrix} \Rightarrow \mathbf{E}_{\mathrm{real}} = \mathrm{f}(\mathbf{E}). \end{aligned} \tag{7.87}$$

In this algorithm, the stiffness and mass matrices of the factor E are not the same as those of $\mathbf{M}_{\mathrm{E}}$ and $\mathbf{K}_{\mathrm{E}}$ of the stiffness and mass matrices of the main structure. However, as has been mentioned in the previous section, the responses consisting of

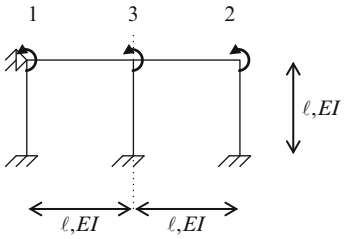

Fig. 7.41 A frame with three DOFs

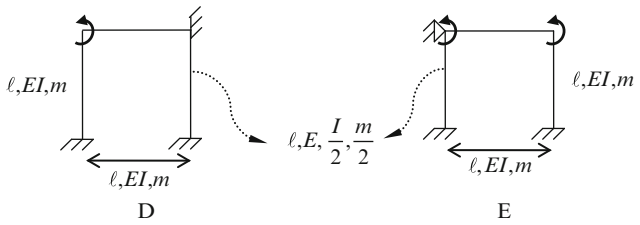

Fig. 7.42 The factors of the frame of Fig. 7.41

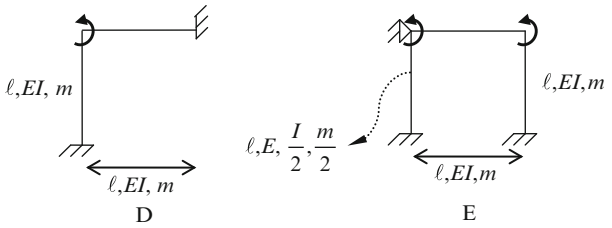

Fig. 7.43 Alternative illustration of the factors of the frame of Fig. 7.41

the determinant and eigenvalues of the free vibration are identical to those of the main structure as was desired.

Therefore, the factors E and D obtained from this algorithm have the same properties as those of the main structure, and the problem is solved by constructing the submatrices $\mathbf{K}_D, \mathbf{M}_D$ and $\mathbf{K}_E, \mathbf{M}_E$.

Example 7.10. Consider the frame shown in Fig. 7.41, which is constrained against sway. This frame has three DOFs. It is assumed that the frame has symmetric elastic properties with respect to the two planes of symmetry.

The factors D and E are obtained using the algorithm (b) step by step as shown in Fig. 7.42.

These factors can be considered as shown in Fig. 7.43.

The submatrices corresponding to these two factors are obtained, and their characteristic equations lead to the eigenfrequencies required as follows:

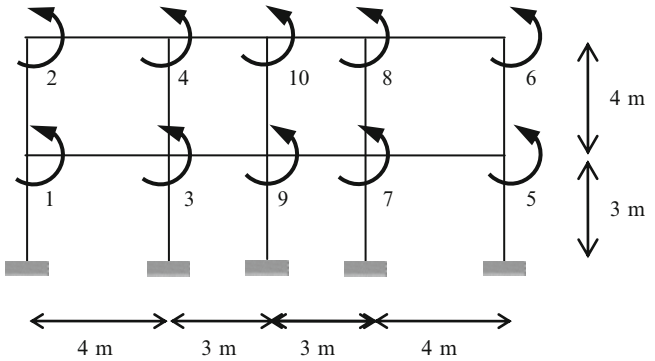

Fig. 7.44 A frame with four spans

$$
\begin{aligned}
&\mathbf{K}_{\mathrm{D}} = \left[\frac{4\mathrm{EI}}{\ell} + \frac{4\mathrm{EI}}{\ell}\right] = \left[\frac{8\mathrm{EI}}{\ell}\right] \quad \text{and } \mathbf{M}_{\mathrm{D}} = \left[\frac{4\mathrm{m}\ell^3}{420} + \frac{4\mathrm{m}\ell^3}{420}\right] = \left[\frac{8m\ell^3}{420}\right] \\
&\det\left[\mathbf{K}_{\mathrm{D}} - \omega^2\mathbf{M}_{\mathrm{D}}\right] = 0 \Rightarrow \omega_1^2 = \frac{420\mathrm{EI}}{\mathrm{m}\ell^4} \\
&\mathbf{K}_{\mathrm{E}} = \begin{bmatrix} \frac{4\mathrm{EI}}{\ell} + \frac{4\mathrm{EI}}{\ell} & \frac{2\mathrm{EI}}{\ell} \\ \frac{2\mathrm{EI}}{\ell} & \frac{4\mathrm{EI}}{\ell} + \frac{4\left(\frac{\mathrm{EI}}{2}\right)}{\ell} \end{bmatrix} = \begin{bmatrix} \frac{4\mathrm{EI}}{\ell} + \frac{4\mathrm{EI}}{\ell} & \frac{2\mathrm{EI}}{\ell} \\ \frac{2\mathrm{EI}}{\ell} & \frac{4\mathrm{EI}}{\ell} + \frac{4\left(\frac{\mathrm{EI}}{2}\right)}{\ell} \end{bmatrix} \\
&\mathbf{M}_{\mathrm{E}} = \begin{bmatrix} \frac{4\mathrm{m}\ell^3}{420} + \frac{4\mathrm{m}\ell^3}{420} & \frac{-3\mathrm{m}\ell^3}{420} \\ \frac{-3\mathrm{m}\ell^3}{420} & \frac{4\mathrm{m}\ell^3}{420} + \frac{4\left(\frac{\mathrm{EI}}{2}\right)\ell^3}{420} \end{bmatrix} \det\left[\mathrm{K}_{\mathrm{E}} - \omega^2\mathrm{M}_{\mathrm{E}}\right] = 0 \\
&\Rightarrow \omega_2^2 = \frac{525\mathrm{EI}}{\mathrm{m}\ell^4} \\
&\Rightarrow \omega_3^2 = \frac{378\mathrm{EI}}{\mathrm{m}\ell^4}.
\end{aligned}
\tag{7.88}
$$

Example 7.11. Consider the frame with an even number of spans as shown in Fig. 7.44, where the frame has 10 DOFs without side sway and 12 DOFs with side sway.

In the case of non-sway, the factors D and E are obtained as (Fig. 7.45)

In this case, the eigensolution of a 10×10 matrix is transformed into the eigensolution of two 4×4 and 6×6 matrices.

In the sway case, the factors D and E are obtained as shown in Fig. 7.46.

The factors of the main frame in the case of sway and non-sway are identical. Only the factor E has the translation DOF.

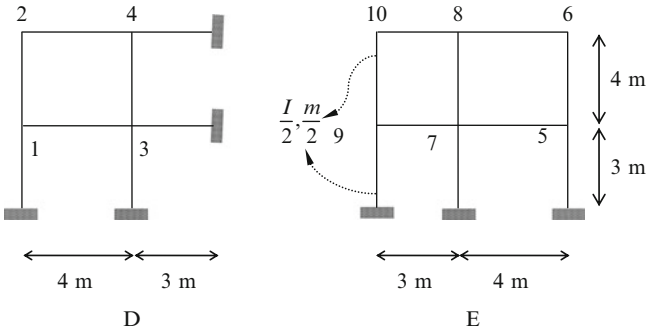

Fig. 7.45 Factors D and E for the non-sway frame

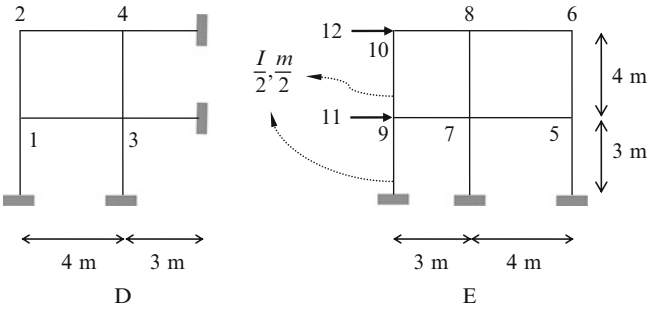

Fig. 7.46 Factors D and E for the sway frame

7.4.3 Discussion

Decomposition and healing process presented in this part reduce the dimensions of the matrices for dynamic analysis of the symmetric frames. Therefore, for large-scale problems the accuracy of calculation increases and the cost of computation decreases.

It can be observed that for the symmetric frames, one of the factors is common for sway and non-sway cases. Therefore, if a frame has n symmetric DOFs, then for both sway and non-sway cases, we will have common results. As an example, for a 10-storey frame with Form II symmetry, the natural frequencies can be obtained by three matrices of dimensions 45×45, 45×45 and 55×55 in place of two matrices of dimensions 100×100 and 90×90. This results in a considerable saving in computational time.

7.5 Eigenfrequencies of Symmetric Planar Trusses via Weighted Graph Symmetry and New Canonical Forms

In this part two methods are presented for calculating the eigenfrequencies of structures. The first approach is graph theoretical and uses graph symmetry. The graph models are decomposed into submodels and healing processes are employed such that the union of the eigenvalues of the healed submodels contain the eigenvalues of the entire model. The second method has an algebraic nature and uses special canonical forms.

7.5.1 Modified Symmetry Forms

In this section, two modified forms are introduced, and methods are presented for constructing a suitable weighted graph. These graphs are then decomposed, and healings are performed to maintain the eigen-properties of the entire graph.

It should be mentioned that the Form II is applicable to the graph matrices like Laplacian and adjacency matrices, or to the structural matrices when the structure has only one degree of freedom per node, while Form A is defined for trusses with two degrees of freedom per node. The same reasoning holds for the Form III and Form B symmetry introduced in the subsequent subsections.

7.5.1.1 Symmetry of Form A (Modified Form II Symmetry)

For trusses with axis of symmetry passing through some members, we have the Form A symmetry, as shown in Fig. 7.47a. The main reason for not being able to employ the previously developed forms of symmetry for calculating the eigenfrequencies of truss structures is due to the existence of oblique cross members. These members affect the entries of the stiffness and mass matrices and change the sign for some of the entries. Separation of the horizontal and vertical DOFs, as shown in Fig. 7.47b, results in stiffness matrices of the symmetric trusses for the case where the axis of symmetry does not pass through the nodes as follows:

First the nodes in the left-hand side (LHS) of the symmetry axis are numbered followed by the numbering of the nodes in the right-hand side (RHS). Now the horizontal DOFs (along x-axis) are first numbered, and then the vertical DOFs (in y-direction) are numbered for the LHS. A similar numbering is then performed for the DOFs of the RHS.

Pattern of the weighted block adjacency matrix **M** is as follows:

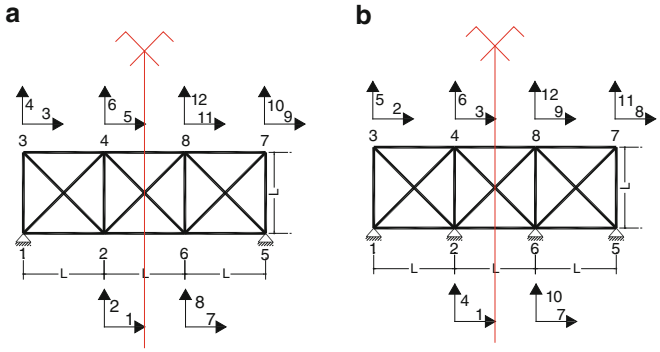

Fig. 7.47 Modified numbering of the DOFs (Form A). (**a**) Initial numbering. (**b**) Modified numbering

$$\mathbf{M} = \begin{array}{c} \begin{matrix} \text{LHS} & & \text{RHS} & \\ \text{H} & \text{V} & \text{H} & \text{V} \end{matrix} \\ \begin{bmatrix} \mathbf{A} & \mathbf{C} & \mathbf{D} & \mathbf{F} \\ \mathbf{C} & \mathbf{B} & \mathbf{F} & \mathbf{E} \\ \mathbf{D} & -\mathbf{F} & \mathbf{A} & -\mathbf{C} \\ -\mathbf{F} & \mathbf{E} & -\mathbf{C} & \mathbf{B} \end{bmatrix} \end{array} \begin{matrix} H \\ V \\ H \\ V \end{matrix} \begin{matrix} \\ \text{LHS} \\ \\ \text{RHS} \end{matrix} \tag{7.89}$$

Conditions for symmetry are as follows:
All the submatrices are symmetric, except **F** which is antisymmetric.

$$\mathbf{A}^{\mathrm{t}} = \mathbf{A}\,, \quad \mathbf{B}^{\mathrm{t}} = \mathbf{B}\,, \quad \mathbf{C}^{\mathrm{t}} = \mathbf{C}\,, \quad \mathbf{D}^{\mathrm{t}} = \mathbf{D} \;\text{ and }\; \mathbf{F}^{\mathrm{t}} = -\mathbf{F}\ . \tag{7.90}$$

Here $\mathbf{F}^{\mathrm{t}} = -\mathbf{F}$ corresponds to the interaction of the horizontal DOFs of the LHS nodes and the vertical DOFs of the RHS and vice versa.

Performing the following permutations, we transform the matrix **M** into the Schur's form:

$$\xrightarrow[\mathrm{C}_2 = \mathrm{C}_2 - \mathrm{C}_4]{\mathrm{C}_2 = \mathrm{C}_1 + \mathrm{C}_3} \quad \mathbf{M} = \begin{bmatrix} \mathbf{A}+\mathbf{D} & \mathbf{C}-\mathbf{F} & \mathbf{D} & \mathbf{F} \\ \mathbf{C}+\mathbf{F} & \mathbf{B}-\mathbf{E} & \mathbf{F} & \mathbf{E} \\ \mathbf{A}+\mathbf{D} & -\mathbf{F}+\mathbf{C} & \mathbf{A} & -\mathbf{C} \\ -\mathbf{F}-\mathbf{C} & \mathbf{E}-\mathbf{B} & -\mathbf{C} & \mathbf{B} \end{bmatrix}, \tag{7.91}$$

$$\xrightarrow[R_4 = R_4 + R_2]{R_3 = R_3 - R_1} \quad \mathbf{M} = \left[\begin{array}{cc|cc} \mathbf{A}+\mathbf{D} & \mathbf{C}-\mathbf{F} & \mathbf{D} & \mathbf{F} \\ \mathbf{C}+\mathbf{F} & \mathbf{B}-\mathbf{E} & \mathbf{F} & \mathbf{E} \\ \hline \mathbf{0} & \mathbf{0} & \mathbf{A}-\mathbf{D} & -\mathbf{C}-\mathbf{F} \\ \mathbf{0} & \mathbf{0} & \mathbf{F}-\mathbf{C} & \mathbf{B}+\mathbf{E} \end{array}\right]. \tag{7.92}$$

Thus,

$$\mathrm{Det}[\mathbf{M}] = \underbrace{\mathrm{Det}\begin{bmatrix}\mathbf{A}+\mathbf{D} & \mathbf{C}-\mathbf{F}\\ \mathbf{C}+\mathbf{F} & \mathbf{B}-\mathbf{E}\end{bmatrix}}_{\mathbf{S}} * \underbrace{\mathrm{Det}\begin{bmatrix}\mathbf{A}-\mathbf{D} & -\mathbf{C}-\mathbf{F}\\ -\mathbf{C}+\mathbf{F} & \mathbf{B}+\mathbf{E}\end{bmatrix}}_{\mathbf{T}}. \tag{7.93}$$

Therefore, the eigenvalues of $\mathbf{M}$ can be obtained as

$$\lambda(\mathbf{M}) = \lambda(\mathbf{S}) \cup \lambda(\mathbf{T}). \tag{7.94}$$

It should be noted that $\mathbf{S}$ and $\mathbf{T}$ are both symmetric, because $\mathbf{F}$ is antisymmetric and the remaining submatrices are symmetric. The above relationships provide the basis of the algebraic method for trusses with odd number of bays.

7.5.1.2 Symmetry of Form B (Modified Form III Symmetry)

For trusses with axis of symmetry passing through central nodes, we have the Form B symmetry, as shown in Fig. 7.48. First the nodes in the LHS of the symmetry axis are numbered followed by the numbering of the nodes in the RHS, and then the central nodes on the axis of symmetry are numbered. Now the horizontal DOFs (along x-axis) are first numbered, and then the vertical DOFs (in y-direction) are numbered for the LHS. A similar numbering is then performed for the DOFs of the RHS. Finally, the horizontal DOFs (in x-direction) followed by the vertical DOFs (in y-direction) for the central nodes on the axis of symmetry.

Pattern of the matrix $\mathbf{M}$ is as follows:

$$\mathbf{M} = \left[\begin{array}{cc|cc|cc} \mathbf{A} & \mathbf{C} & \mathbf{D} & \mathbf{F} & \mathbf{G} & \mathbf{I} \\ \mathbf{C} & \mathbf{B} & \mathbf{F} & \mathbf{E} & \mathbf{I} & \mathbf{H} \\ \hline \mathbf{D} & -\mathbf{F} & \mathbf{A} & -\mathbf{C} & \mathbf{G} & -\mathbf{I} \\ -\mathbf{F} & \mathbf{E} & -\mathbf{C} & \mathbf{B} & -\mathbf{I} & \mathbf{H} \\ \hline \mathbf{G}^{\mathrm{t}} & \mathbf{I}^{\mathrm{t}} & \mathbf{G}^{\mathrm{t}} & -\mathbf{I}^{\mathrm{t}} & \mathbf{J} & \mathbf{L} \\ \mathbf{I}^{\mathrm{t}} & \mathbf{H}^{\mathrm{t}} & -\mathbf{I}^{\mathrm{t}} & \mathbf{H}^{\mathrm{t}} & \mathbf{L} & \mathbf{K} \end{array}\right]. \tag{7.95}$$

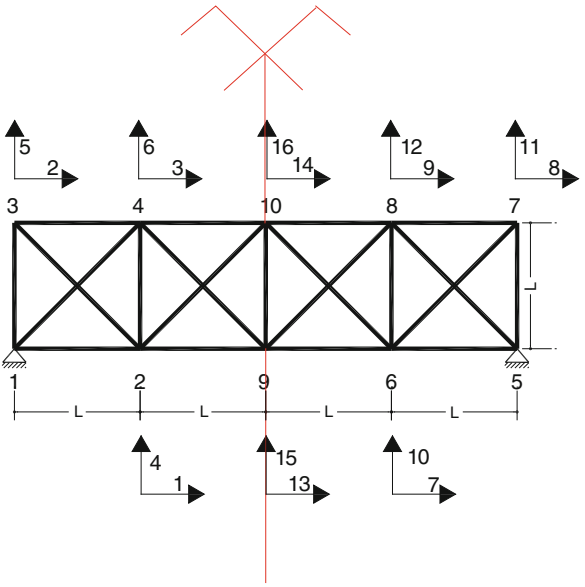

Fig. 7.48 A symmetric truss with the axis passing through central nodes

Nodes on the LHS of the axis | Nodes on the RHS of the axis | Nodes on the axis of symmetry

$$\xrightarrow{\text{Column permutations}} \left[\begin{array}{cc|cc|cc} \mathbf{A} & \mathbf{C} & \mathbf{G} & \mathbf{I} & \mathbf{D} & \mathbf{F} \\ \mathbf{B} & \mathbf{B} & \mathbf{H} & \mathbf{G} & \mathbf{F} & \mathbf{E} \\ \hline \mathbf{D} & -\mathbf{F} & \mathbf{G} & -\mathbf{I} & \mathbf{A} & -\mathbf{C} \\ -\mathbf{F} & \mathbf{E} & -\mathbf{I} & \mathbf{H} & -\mathbf{C} & \mathbf{B} \\ \hline \mathbf{G}^t & \mathbf{I}^t & \mathbf{J} & \mathbf{0} & \mathbf{G}^t & -\mathbf{J}^t \\ \mathbf{J}^t & \mathbf{H}^t & \mathbf{0} & \mathbf{K} & -\mathbf{J}^t & \mathbf{H}^t \end{array}\right], \tag{7.96}$$

Nodes on the LHS of the axis | Nodes on the RHS of the axis | Nodes on the axis of symmetry

$$\xrightarrow{\text{Exchange of rows}} \left[\begin{array}{cc|cc|cc} \mathbf{A} & \mathbf{C} & \mathbf{G} & \mathbf{I} & \mathbf{D} & \mathbf{F} \\ \mathbf{C} & \mathbf{B} & \mathbf{I} & \mathbf{H} & \mathbf{F} & \mathbf{E} \\ \hline \mathbf{G}^t & \mathbf{I}^t & \mathbf{J} & \mathbf{0} & \mathbf{G}^t & -\mathbf{I}^t \\ \mathbf{I}^t & \mathbf{H}^t & \mathbf{0} & \mathbf{K} & -\mathbf{I}^t & \mathbf{H}^t \\ \hline \mathbf{D} & -\mathbf{F} & \mathbf{G} & -\mathbf{I} & \mathbf{A} & -\mathbf{C} \\ -\mathbf{F} & \mathbf{E} & -\mathbf{I} & \mathbf{H} & -\mathbf{C} & \mathbf{B} \end{array}\right], \tag{7.97}$$

Nodes on the LHS of the axis | Nodes on the RHS of the axis | Nodes on the axis of symmetry

$$\xrightarrow[C_2 = C_2 - C_4]{C_2 = C_1 + C_3} \left[\begin{array}{cc|cc|cc} \mathbf{A+D} & \mathbf{C-F} & \mathbf{G} & \mathbf{I} & \mathbf{D} & \mathbf{F} \\ \mathbf{C+F} & \mathbf{B-E} & \mathbf{I} & \mathbf{H} & \mathbf{F} & \mathbf{E} \\ \hline \mathbf{2G^t} & \mathbf{2I^t} & \mathbf{J} & \mathbf{0} & \mathbf{G^t} & \mathbf{-I^t} \\ \mathbf{0} & \mathbf{0} & \mathbf{0} & \mathbf{K} & \mathbf{-I^t} & \mathbf{H^t} \\ \hline \mathbf{A+D} & \mathbf{-F+C} & \mathbf{G} & \mathbf{-I} & \mathbf{A} & \mathbf{-C} \\ \mathbf{-F-C} & \mathbf{E-B} & \mathbf{-I} & \mathbf{H} & \mathbf{-C} & \mathbf{B} \end{array}\right] \tag{7.98}$$

Now the following Schur's form is obtained as

$$\xrightarrow[R_6 = R_6 + R_2]{R_5 = R_5 - R_1} \left[\begin{array}{ccc|ccc} \mathbf{A+D} & \mathbf{C-F} & \mathbf{G} & \mathbf{I} & \mathbf{D} & \mathbf{F} \\ \mathbf{C+F} & \mathbf{B-E} & \mathbf{I} & \mathbf{H} & \mathbf{F} & \mathbf{E} \\ \mathbf{2G^t} & \mathbf{2I^t} & \mathbf{J} & \mathbf{0} & \mathbf{G^t} & \mathbf{-I^t} \\ \hline \mathbf{0} & \mathbf{0} & \mathbf{0} & \mathbf{K} & \mathbf{-I^t} & \mathbf{H^t} \\ \mathbf{0} & \mathbf{0} & \mathbf{0} & \mathbf{-2I} & \mathbf{A-D} & \mathbf{-C-F} \\ \mathbf{0} & \mathbf{0} & \mathbf{0} & \mathbf{2H} & \mathbf{-C+F} & \mathbf{B+E} \end{array}\right]. \tag{7.99}$$

Interchanging the 4–6 rows and columns, we obtain

$$\text{Det}\,[\mathbf{M}] = \text{Det}\,\underset{\mathbf{S}}{\left[\begin{array}{ccc} \mathbf{A+D} & \mathbf{C-F} & \mathbf{G} \\ \mathbf{C+F} & \mathbf{B-E} & \mathbf{I} \\ \mathbf{2G^t} & \mathbf{2I^t} & \mathbf{J} \end{array}\right]} * \underset{\mathbf{t}}{\left[\begin{array}{ccc} \mathbf{A-D} & \mathbf{-C-F} & \mathbf{-2I} \\ \mathbf{-C+F} & \mathbf{B+E} & \mathbf{2H} \\ \mathbf{-I^t} & \mathbf{H^t} & \mathbf{K} \end{array}\right]}. \tag{7.100}$$

Thus,

$$\lambda(\mathbf{M}) = \lambda(\mathbf{S}) \cup \lambda(\mathbf{T}). \tag{7.101}$$

Matrix **L** is always a null matrix due to the symmetry. We may move the nodes on the axis of symmetry in y-direction; these nodes should not be moved in x-direction.

The matrices **A**, **B**, **C**, **D** and **E** are symmetric and **F** is antisymmetric. These submatrices are $n \times n$, where n is the number of free nodes in each side of the axis of symmetry. **I**, **H** and **G** are $n \times m$ submatrices, where m is the number of node on the axis and **L**, **J** and **K** are $m \times m$ submatrices. **L** is replaced by the null matrix **0**.

The above relationships provide the basis of the algebraic method for trusses with an even number of bays.

7.5.1.3 Definitions: Stiffness and Mass Graphs

The stiffness graph of a truss structure with k degrees of freedom has k nodes, and the two nodes i and j are connected if the corresponding off-diagonal entry of the stiffness matrix is non-zero. The weight of each node as equal to the corresponding entry on the main diagonal, and the weight of each member connecting the nodes i and j is the same as the entry (i,j) of the stiffness matrix. The mass graph of a mass matrix is similarly constructed.

7.5.2 Numerical Results

In this section, three examples are presented and discussed in detail to illustrate the methods presented in the previous section.

Example 7.12. Consider the symmetric truss with an odd number of spans as shown in Fig. 7.49. For this truss, the axis of symmetry passes through four members.

The stiffness matrix will have the following form:

$$\mathbf{K} = \left[\begin{array}{cc|cc|cc|cc} \frac{2EA}{L}+\frac{EA}{2L'} & 0 & \frac{EA}{2L'} & 0 & -\frac{EA}{L} & -\frac{EA}{2L'} & 0 & -\frac{EA}{2L'} \\ 0 & \frac{EA}{L}+\frac{EA}{L'} & 0 & 0 & -\frac{EA}{2L'} & -\frac{EA}{L} & \frac{EA}{2L'} & 0 \\ \hline \frac{EA}{2L'} & 0 & \frac{EA}{L}+\frac{EA}{2L'} & -\frac{EA}{L} & 0 & -\frac{EA}{2L'} & 0 & -\frac{EA}{2L'} \\ 0 & 0 & -\frac{EA}{L} & \frac{EA}{L}+\frac{EA}{L'} & \frac{EA}{2L'} & 0 & -\frac{EA}{2L'} & 0 \\ \hline -\frac{EA}{L} & -\frac{EA}{2L'} & 0 & \frac{EA}{2L'} & \frac{2EA}{L}+\frac{EA}{2L'} & 0 & -\frac{EA}{2L'} & 0 \\ -\frac{EA}{2L'} & -\frac{EA}{L} & -\frac{EA}{2L'} & 0 & 0 & \frac{EA}{L}+\frac{EA}{L'} & 0 & 0 \\ \hline 0 & \frac{EA}{2L'} & 0 & -\frac{EA}{2L'} & -\frac{EA}{2L'} & 0 & \frac{EA}{L}+\frac{EA}{2L'} & -\frac{EA}{L} \\ -\frac{EA}{2L'} & 0 & -\frac{EA}{2L'} & 0 & 0 & 0 & -\frac{EA}{L} & \frac{EA}{L}+\frac{EA}{L'} \end{array}\right]. \tag{7.102}$$

The weighted graph corresponding to the above stiffness matrix can easily be constructed as shown in Fig. 7.50. Here, the weight of each node is identical to the corresponding entry on the main diagonal, and the weight of each member is the same as the (i,j)th entry of the matrix corresponding to that member.

The subgraphs are formed using the following algorithm:

After decomposing the graph into two subgraphs using the axis of symmetry, the following operations are performed:

(a) *The subgraph corresponding to S*:

1. If there is a direct member between the horizontal DOF of two symmetric nodes, then a directed ring should be added to the node of the LHS with a weight equal to the weight of the member.

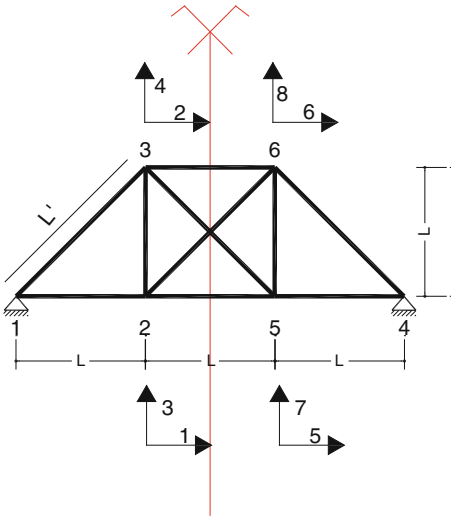

Fig. 7.49 A truss with an odd number of bays

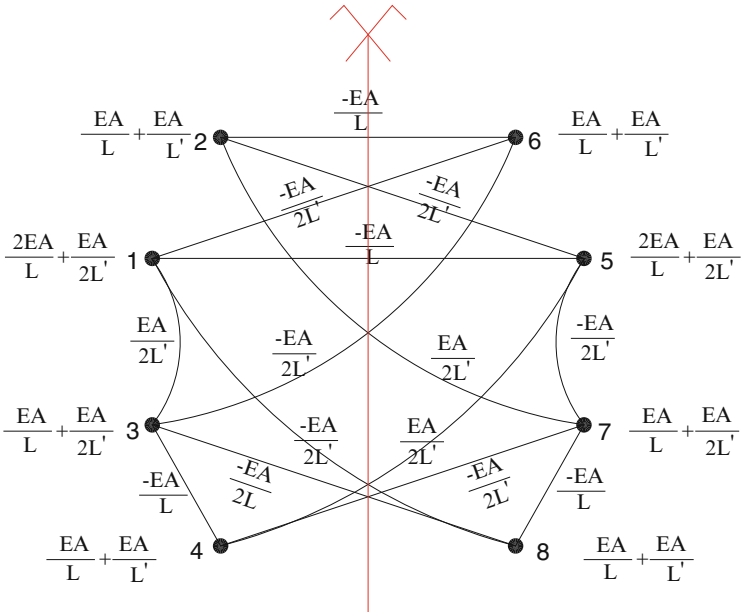

Fig. 7.50 Graph representation of the stiffness matrix

2. If there is a direct member between the vertical DOF of two symmetric nodes, then a directed ring should be added to the node of the RHS with a weight equal to the weight of the member having minus sign.

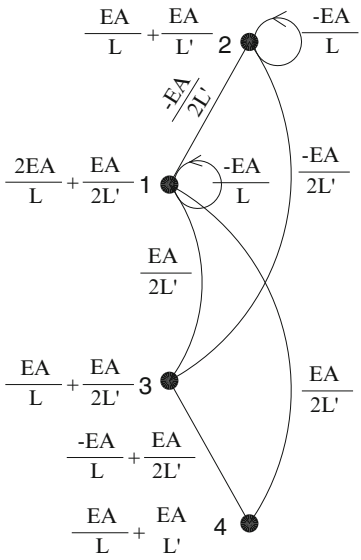

Fig. 7.51 Formation of the subgraph *S*

3. The oblique members cut by the axis of symmetry, which connect the horizontal (or vertical) DOFs, are in dual form, and the weight of one of them should be added to the weight of the member connecting the corresponding nodes. Addition should be replaced by subtraction for vertical DOFs.
4. The weight of the members connecting the horizontal and vertical DOFs is equal to the weight of the existing member between these two nodes minus the weight of the connecting member of the node corresponding to the horizontal DOF to the node corresponding to the vertical DOF, as shown in Fig. 7.51.

The stiffness matrix corresponding to the subgraph of Fig. 7.51 is formed as

$$S = \begin{bmatrix} \frac{EA}{L} + \frac{EA}{2L'} & \frac{-EA}{2L'} & \frac{EA}{2L'} & \frac{EA}{2L'} \\ \frac{-EA}{2L'} & \frac{EA}{L'} & \frac{-EA}{2L'} & 0 \\ \frac{EA}{2L'} & \frac{-EA}{2L'} & \frac{EA}{L} + \frac{EA}{2L'} & \frac{-EA}{L} + \frac{EA}{2L'} \\ \frac{EA}{2L'} & 0 & \frac{-EA}{L} + \frac{EA}{2L'} & \frac{EA}{L} + \frac{EA}{L'} \end{bmatrix} \tag{7.103}$$

(b) *The subgraph corresponding to T*:
After decomposing the graph into two subgraphs at the cut by the axis of symmetry, the following operations should be performed:

1. If there is a direct link between any node in the right-hand side and the LHS, then a loop is added to the subgraph in the RHS which has a weight equal to the weight of that node with reverse sign.

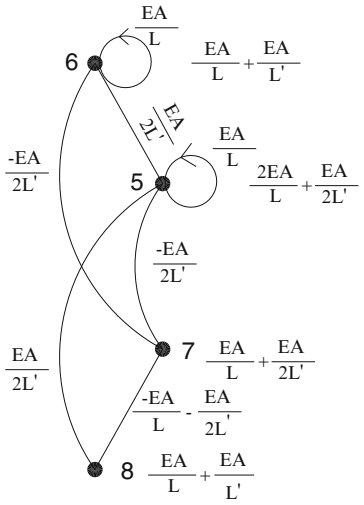

Fig. 7.52 Formation the subgraph T

2. If there is a direct link between the vertical DOFs of the LHS and the RHS, then a directed loop is added to the subgraph in the RHS which has a weight equal to the weight of that link member.
3. The oblique members connecting the horizontal DOF (or vertical), which are cut, are necessarily dual, and we should reduce the weight of one of them from the link between two corresponding nodes in one side of the symmetry axis (right-hand side). We make addition for the vertical DOFs.
4. The weight of the member connecting the horizontal and vertical DOFs is equal to the weight of the existing member between these two nodes (in the RHS of the axis) plus the weight of the member connecting the node corresponding to the horizontal DOF (in the same side of the axis) to the node corresponding to the vertical DOF in the other side of the symmetry axis.

The stiffness matrix corresponding to the subgraph of Fig. 7.52 is formed as

$$\mathbf{T} = \begin{bmatrix} \frac{3EA}{L} + \frac{EA}{2L'} & \frac{EA}{2L'} & \frac{-EA}{2L'} & \frac{EA}{2L'} \\ \frac{EA}{2L'} & \frac{2EA}{L} + \frac{EA}{L'} & \frac{-EA}{L'} & 0 \\ \frac{-EA}{2L'} & \frac{-EA}{2L'} & \frac{EA}{L} + \frac{EA}{2L'} & \frac{-EA}{L} - \frac{EA}{2L'} \\ \frac{EA}{2L'} & 0 & \frac{-EA}{L} - \frac{EA}{2L'} & \frac{EA}{L} + \frac{EA}{L'} \end{bmatrix}. \tag{7.104}$$

Similarly, the mass matrix is formed as

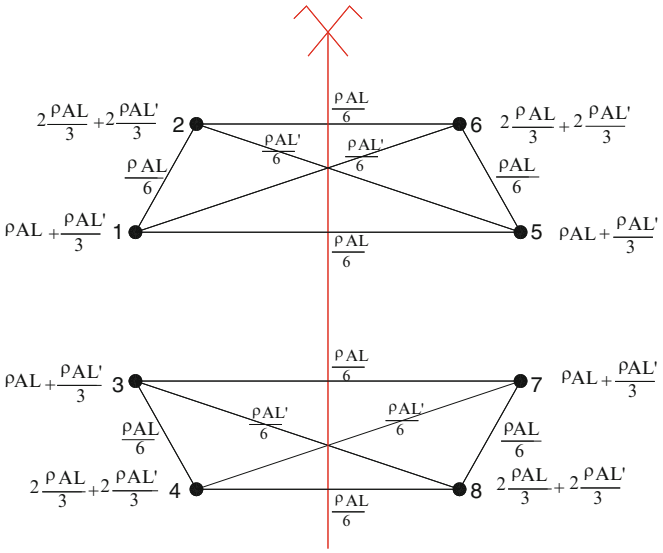

Fig. 7.53 Graph representation of the mass matrix

$$\mathbf{M} = \left[\begin{array}{cc|cc|cc|cc} \rho AL + \frac{\rho AL'}{3} & \frac{\rho AL}{6} & 0 & 0 & \frac{\rho AL}{6} & \frac{\rho AL'}{6} & 0 & 0 \\ \frac{\rho AL}{6} & \frac{2\rho AL}{3} + \frac{2\rho AL'}{3} & 0 & 0 & \frac{\rho AL'}{6} & \frac{\rho AL}{6} & 0 & 0 \\ \hline 0 & 0 & \rho AL + \frac{\rho AL'}{3} & \frac{\rho AL}{6} & 0 & 0 & \frac{\rho AL}{6} & \frac{\rho AL'}{6} \\ 0 & 0 & \frac{\rho AL}{6} & \frac{2\rho AL}{3} + \frac{2\rho AL'}{3} & 0 & 0 & \frac{\rho AL'}{6} & \frac{\rho AL}{6} \\ \hline \frac{\rho AL}{6} & \frac{\rho AL'}{6} & 0 & 0 & \rho AL + \frac{\rho AL'}{3} & \frac{\rho AL}{6} & 0 & 0 \\ \frac{\rho AL'}{6} & \frac{\rho AL}{6} & 0 & 0 & \frac{\rho AL}{6} & \frac{2\rho AL}{3} + \frac{2\rho AL'}{3} & 0 & 0 \\ \hline 0 & 0 & \frac{\rho AL}{6} & \frac{\rho AL'}{6} & 0 & 0 & \rho AL + \frac{\rho AL'}{3} & \frac{\rho AL}{6} \\ 0 & 0 & \frac{\rho AL'}{6} & \frac{\rho AL}{6} & 0 & 0 & \frac{\rho AL}{6} & \frac{2\rho AL}{3} + \frac{2\rho AL'}{3} \end{array}\right]. \tag{7.105}$$

Graph representation of the mass matrix is illustrated in Fig. 7.53. The subgraphs are formed utilising the previous algorithm as follows:

(a) *The subgraph corresponding to S*:
This subgraph is shown in Fig. 7.54. The mass matrix corresponding to the subgraph shown in Fig. 7.54 is constructed as

$$\mathbf{S} = \left[\begin{array}{cc|cc} \frac{7\rho AL}{6} + \frac{\rho AL'}{3} & \frac{\rho AL}{6} + \frac{\rho AL'}{6} & 0 & 0 \\ \frac{\rho AL}{6} + \frac{\rho AL'}{6} & \frac{5\rho AL}{6} + \frac{2\rho AL'}{3} & 0 & 0 \\ \hline 0 & 0 & \frac{5\rho AL}{6} + \frac{\rho AL'}{3} & \frac{\rho AL}{6} - \frac{\rho AL'}{6} \\ 0 & 0 & \frac{\rho AL}{6} - \frac{\rho AL'}{6} & \frac{\rho AL}{2} + \frac{2\rho AL'}{3} \end{array}\right]. \tag{7.106}$$

(b) *The subgraph corresponding to T*:
This subgraph is shown in Fig. 7.55. The mass matrix corresponding to this subgraph is as follows:

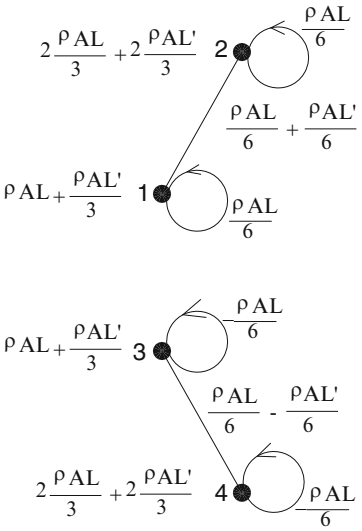

Fig. 7.54 Formation of the subgraph *S*

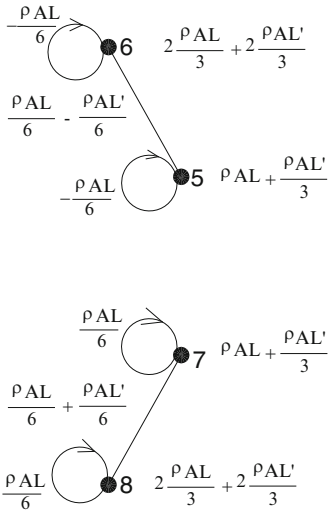

Fig. 7.55 Formation of the subgraph T

$$\mathrm{T} = \begin{bmatrix} \frac{5\rho AL}{6} + \frac{\rho AL'}{3} & \frac{\rho AL}{6} - \frac{\rho AL'}{6} & 0 & 0 \\ \frac{\rho AL}{6} - \frac{\rho AL'}{6} & \frac{\rho AL}{2} + \frac{2\rho AL'}{3} & 0 & 0 \\ 0 & 0 & \frac{7\rho AL}{6} + \frac{\rho AL'}{3} & \frac{\rho AL}{6} + \frac{\rho AL'}{6} \\ 0 & 0 & \frac{\rho AL}{6} + \frac{\rho AL'}{6} & \frac{5\rho AL}{6} + \frac{2\rho AL'}{3} \end{bmatrix}. \tag{7.107}$$

Considering, $E = 2.07 \times 10^7$ kN/m $L = 100$ cm, $I = 100$ cm^2 and $\rho = 78$ kN/m^3 and $A = 10$ cm^2 the frequencies of the structure are calculated as

$$\omega_S = [16.251, 20.608, 37.51, 40.229]$$
$$\omega_T = [8.294, 42.680, 45.403, 55.909]$$
$$\omega = \omega_S \cup \omega_T = [16.251, 20.608, 37.51, 40.229, 8.294, 42.680, 45.403, 55.909]. \tag{7.108}$$

Using the algebraic approach formulated in Sect. 3.1, identical eigenfrequencies are obtained. The eigenvectors are then calculated and the mode shapes are obtained, Fig. 7.56.

Example 7.13. Consider the symmetric truss with an even number of spans as shown in Fig. 7.57. For this truss, the axis of symmetry passes through two nodes.

The stiffness matrix of the structure shown in Fig. 7.58 has the Form B symmetry as follows:

$$\mathbf{K} = \begin{bmatrix}
\frac{2EA}{L}+\frac{EA}{2L'} & 0 & \frac{EA}{2L'} & 0 & 0 & 0 & 0 & 0 & -\frac{EA}{L} & -\frac{EA}{2L'} & 0 & -\frac{EA}{2L'} \\
0 & \frac{EA}{L}+\frac{EA}{L'} & 0 & 0 & 0 & 0 & 0 & 0 & -\frac{EA}{2L'} & -\frac{EA}{L} & \frac{EA}{2L'} & 0 \\
\frac{EA}{2L'} & 0 & \frac{EA}{L}+\frac{EA}{2L'} & -\frac{EA}{L} & 0 & 0 & 0 & 0 & 0 & -\frac{EA}{2L'} & 0 & -\frac{EA}{2L'} \\
0 & 0 & -\frac{EA}{L} & \frac{EA}{L}+\frac{EA}{L'} & 0 & 0 & 0 & 0 & \frac{EA}{2L'} & 0 & -\frac{EA}{2L'} & 0 \\
0 & 0 & 0 & 0 & \frac{2EA}{L}+\frac{EA}{2L'} & 0 & -\frac{EA}{2L'} & 0 & -\frac{EA}{L} & -\frac{EA}{2L'} & 0 & \frac{EA}{2L'} \\
0 & 0 & 0 & 0 & 0 & \frac{EA}{L}+\frac{EA}{L'} & 0 & 0 & -\frac{EA}{2L'} & -\frac{EA}{L} & -\frac{EA}{2L'} & 0 \\
0 & 0 & 0 & 0 & -\frac{EA}{2L'} & 0 & \frac{EA}{L}+\frac{EA}{2L'} & -\frac{EA}{L} & 0 & \frac{EA}{2L'} & 0 & -\frac{EA}{2L'} \\
0 & 0 & 0 & 0 & 0 & 0 & -\frac{EA}{L} & \frac{EA}{L}+\frac{EA}{L'} & -\frac{EA}{2L'} & 0 & -\frac{EA}{2L'} & 0 \\
-\frac{EA}{L} & -\frac{EA}{2L'} & 0 & \frac{EA}{2L'} & -\frac{EA}{L} & -\frac{EA}{2L'} & 0 & -\frac{EA}{2L'} & \frac{2EA}{L}+\frac{EA}{L'} & 0 & 0 & 0 \\
-\frac{EA}{2L'} & -\frac{EA}{L} & -\frac{EA}{2L'} & 0 & -\frac{EA}{2L'} & -\frac{EA}{L} & \frac{EA}{2L'} & 0 & 0 & \frac{2EA}{L}+\frac{EA}{L'} & 0 & 0 \\
0 & \frac{EA}{2L'} & 0 & -\frac{EA}{2L'} & 0 & -\frac{EA}{2L'} & 0 & -\frac{EA}{2L'} & 0 & 0 & \frac{EA}{L}+\frac{EA}{L'} & -\frac{EA}{L} \\
-\frac{EA}{2L'} & 0 & -\frac{EA}{2L'} & 0 & \frac{EA}{2L'} & 0 & -\frac{EA}{2L'} & 0 & 0 & 0 & -\frac{EA}{L} & \frac{EA}{L}+\frac{EA}{L'}
\end{bmatrix}. \tag{7.109}$$

Graph representation of the stiffness matrix is illustrated in Fig. 7.58.

7.5.2.1 Symmetry Property of the Graph Representation of the Stiffness Matrix

1. The graph is symmetric with respect to the axis passing through the nodes corresponding to the central DOFs.
2. The weight of the node i is equal to the (i,i)th entry of the stiffness (or mass) matrix, and it is symmetric with respect to the axis.

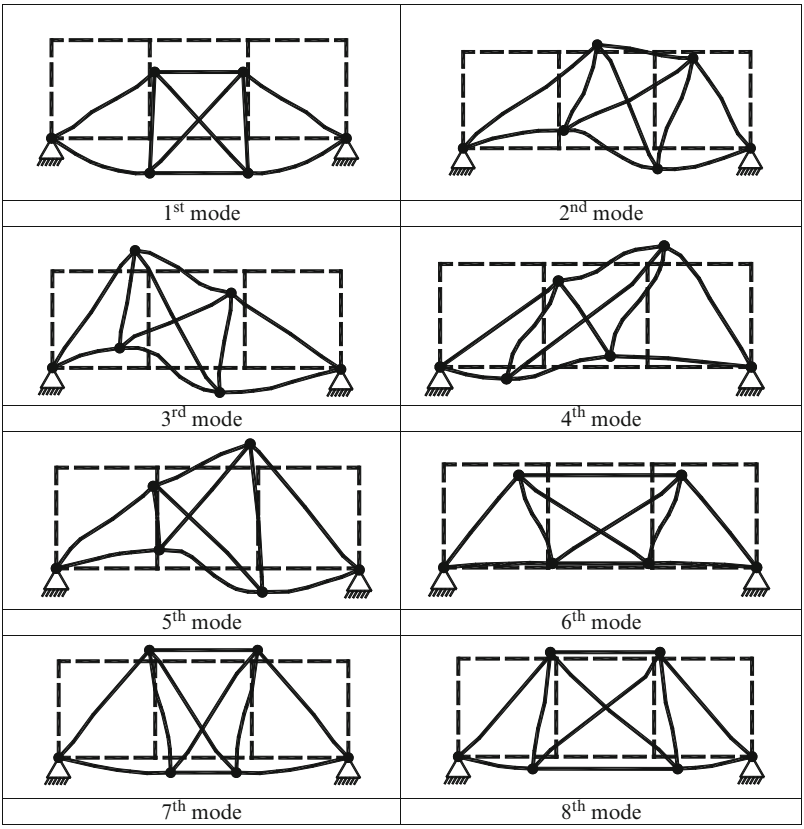

Fig. 7.56 The natural mode shapes of Example 7.12

3. The weight of the member connecting the nodes i and j is equal to the (i,j)th entry of the stiffness (or mass) matrix. The weight between the x DOFs (the upper part of the graph) and the weight of the member between y DOFs (lower part of the graph) are symmetric with respect to the axis of symmetry (the corresponding members are identical), and the weight of the members between x and y DOFs in two sides of the axis of symmetry is antisymmetric (equal members with reverse signs). Finally there should be no link member between x and y DOFs of the central nodes, that is, the submatrix **L** of the stiffness (or mass) matrices should be null matrix. This had been proven differently.

7.5.2.2 Formation of the Subgraphs

The subgraphs are constructed utilising the following algorithm:

We subdivide the graph into two subgraphs by removing the members cut by the axis of symmetry. The subgraph in the LHS corresponds to the matrix **S**, and the one

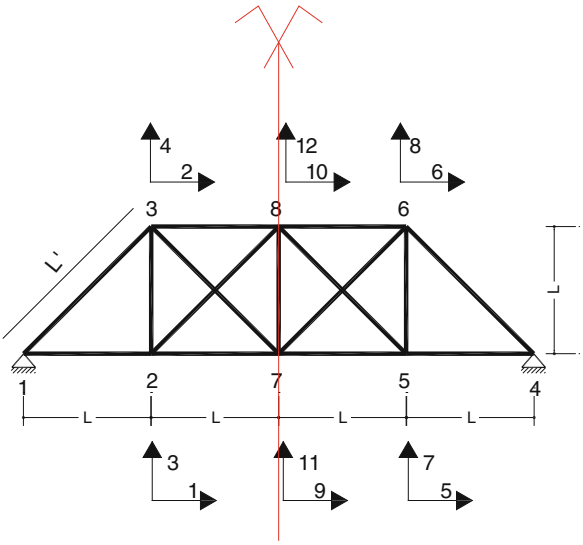

Fig. 7.57 A truss with an even number of bays

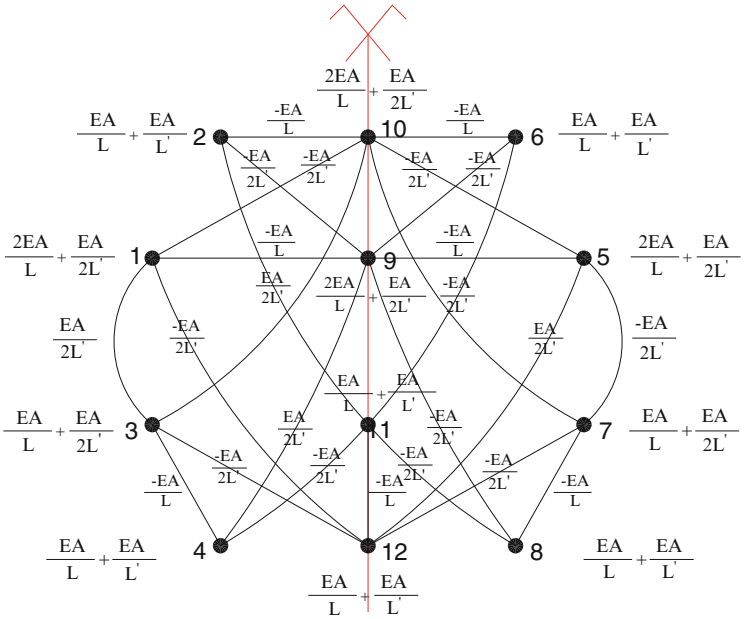

Fig. 7.58 Graph representation of the stiffness matrix

in the RHS corresponds to **T**. For the graphs on the axis of symmetry, the upper nodes on the axis corresponding to the horizontal DOFs are associated to S and the bottom nodes on the axis corresponding to the vertical DOFs are associated to T.

The weight of the nodes and all the members (which may exist between the nodes on the axis) are left unchanged.

(a) *The subgraph corresponding to S*:
If there exists a member between any node of the LHS (nodes 5, 6, 7 and 8) and the central nodes (the existing nodes in Figs. 7.57 and 7.58), then a directed member is added from the central node towards the node in the LHS with a weight equal to that of the existing member. The weight of the directed member from i to j is added to the entry S_{ij}.

The stiffness matrix corresponding to the subgraph shown in Fig. 7.59 is constructed as

$$\mathbf{K}_S = \begin{bmatrix} \frac{2EA}{L} + \frac{EA}{2L'} & 0 & \frac{EA}{2L'} & 0 & -\frac{EA}{s} & -\frac{EA}{2L'} \\ 0 & \frac{EA}{L} + \frac{EA}{L'} & 0 & 0 & -\frac{EA}{2L'} & -\frac{EA}{L} \\ \frac{EA}{2L'} & 0 & \frac{EA}{L} + \frac{EA}{2L'} & -\frac{EA}{L} & 0 & -\frac{EA}{2L'} \\ 0 & 0 & -\frac{EA}{L} & \frac{EA}{L} + \frac{EA}{L'} & \frac{EA}{2L'} & 0 \\ -\frac{2EA}{L} & -\frac{EA}{L'} & 0 & -\frac{EA}{L'} & \frac{2EA}{L} + \frac{EA}{L'} & 0 \\ -\frac{EA}{L'} & -\frac{2EA}{L} & -\frac{EA}{L'} & 0 & 0 & \frac{2EA}{L} + \frac{EA}{L'} \end{bmatrix}. \quad (7.110)$$

(b) *The subgraph corresponding to T*:
The weight of the nodes and the possible existing members are left unchanged. If there exists a member between the DOFs of the RHS (nodes 5, 6, 7 and 8) and the central nodes (the existing nodes in Figs. 7.59 and 7.60), then another directed member is added from the LHS node towards the central node with a weight equal to that of the existing member. For the added directed member, the weight of the member from i to j is added to the entry T_{ij}.

The stiffness matrix corresponding to the subgraph T, shown in Fig. 7.60, is constructed in the following:

$$\mathbf{K}_T = \begin{bmatrix} \frac{2EA}{L} + \frac{EA}{2L'} & 0 & -\frac{EA}{2L'} & 0 & 0 & \frac{EA}{L'} \\ 0 & \frac{EA}{L} + \frac{EA}{L'} & 0 & 0 & -\frac{EA}{L'} & 0 \\ -\frac{EA}{2L'} & 0 & \frac{EA}{L} + \frac{EA}{2L'} & -\frac{EA}{L} & 0 & -\frac{EA}{L'} \\ 0 & 0 & -\frac{EA}{L} & \frac{EA}{L} + \frac{EA}{L'} & -\frac{EA}{L'} & 0 \\ 0 & -\frac{EA}{2L'} & 0 & -\frac{EA}{2L'} & \frac{EA}{L} + \frac{EA}{L'} & -\frac{EA}{L} \\ \frac{EA}{2L'} & 0 & -\frac{EA}{2L'} & 0 & -\frac{EA}{L} & \frac{EA}{L} + \frac{EA}{L'} \end{bmatrix}. \quad (7.111)$$

For the mass matrix, a similar operation is performed.

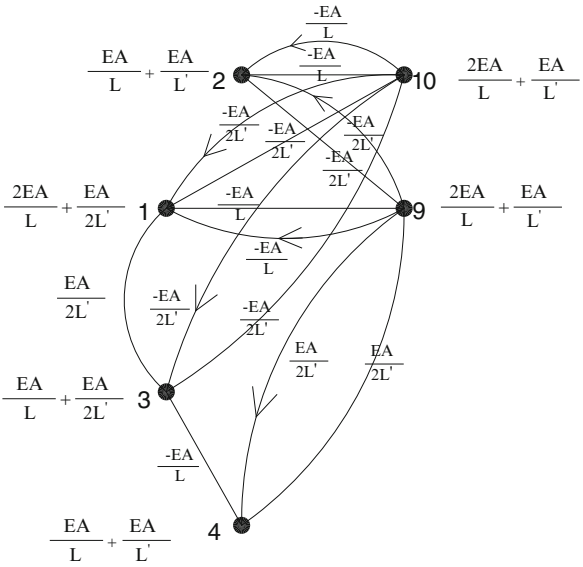

Fig. 7.59 Formation the subgraph *S*

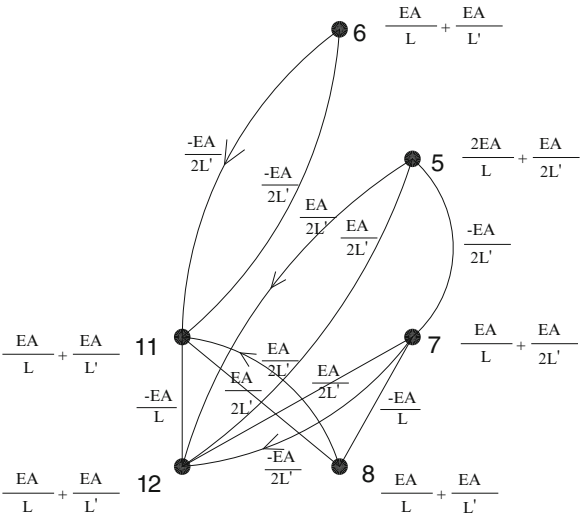

Fig. 7.60 Formation the subgraph *T*

$$\mathbf{M}=\begin{bmatrix}
\rho AL+\frac{\rho AL'}{3} & \frac{\rho AL}{6} & 0 & 0 & 0 & 0 & 0 & 0 & \frac{\rho AL}{6} & \frac{\rho AL'}{6} & 0 & 0\\
\frac{\rho AL}{6} & \frac{2\rho AL}{3}+\frac{2\rho AL'}{3} & 0 & 0 & 0 & 0 & 0 & 0 & \frac{\rho AL'}{6} & \frac{\rho AL}{6} & 0 & 0\\
0 & 0 & \rho AL+\frac{\rho AL'}{3} & \frac{\rho AL}{6} & 0 & 0 & 0 & 0 & 0 & 0 & \frac{\rho AL}{6} & \frac{\rho AL'}{6}\\
0 & 0 & \frac{\rho AL}{6} & \frac{2\rho AL}{3}+\frac{2\rho AL'}{3} & 0 & 0 & 0 & 0 & 0 & 0 & \frac{\rho AL'}{6} & \frac{\rho AL}{6}\\
0 & 0 & 0 & 0 & \rho AL+\frac{\rho AL'}{3} & \frac{\rho AL}{6} & 0 & 0 & \frac{\rho AL}{6} & \frac{\rho AL'}{6} & 0 & 0\\
0 & 0 & 0 & 0 & \frac{\rho AL}{6} & \frac{2\rho AL}{3}+\frac{2\rho AL'}{3} & 0 & 0 & \frac{\rho AL'}{6} & \frac{\rho AL}{6} & 0 & 0\\
0 & 0 & 0 & 0 & 0 & 0 & \rho AL+\frac{\rho AL'}{3} & \frac{\rho AL}{6} & 0 & 0 & \frac{\rho AL}{6} & \frac{\rho AL'}{6}\\
0 & 0 & 0 & 0 & 0 & 0 & \frac{\rho AL}{6} & \frac{2\rho AL}{3}+\frac{2\rho AL'}{3} & 0 & 0 & \frac{\rho AL'}{6} & \frac{\rho AL}{6}\\
\frac{\rho AL}{6} & \frac{\rho AL'}{6} & 0 & 0 & \frac{\rho AL}{6} & \frac{\rho AL'}{6} & 0 & 0 & \rho AL+\frac{2\rho AL'}{3} & \frac{\rho AL}{6} & 0 & 0\\
\frac{\rho AL'}{6} & \frac{\rho AL}{6} & 0 & 0 & \frac{\rho AL'}{6} & \frac{\rho AL}{6} & 0 & 0 & \frac{\rho AL}{6} & \rho AL+\frac{2\rho AL'}{3} & 0 & 0\\
0 & 0 & \frac{\rho AL}{6} & \frac{\rho AL'}{6} & 0 & 0 & \frac{\rho AL}{6} & \frac{\rho AL'}{6} & 0 & 0 & AL+\frac{2\rho AL'}{3} & \frac{\rho AL}{6}\\
0 & 0 & \frac{\rho AL'}{6} & \frac{\rho AL}{6} & 0 & 0 & \frac{\rho AL'}{6} & \frac{\rho AL}{6} & 0 & 0 & \frac{\rho AL}{6} & \rho AL+\frac{2\rho AL'}{3}
\end{bmatrix}. \tag{7.112}$$

The graph representation of the mass matrix with the Form B symmetry is illustrated in Fig. 7.61.

The subgraphs are constructed utilising the previous algorithm.

(a) *The subgraph corresponding to S:*
The mass matrix corresponding to the subgraph, shown in Fig. 7.62, is formed as

$$\mathbf{M}_S=\begin{bmatrix}
\rho AL+\frac{\rho AL'}{3} & \frac{\rho AL}{6} & 0 & 0 & \frac{\rho AL}{6} & \frac{\rho AL'}{6}\\
\frac{\rho AL}{6} & \frac{2\rho AL}{3}+\frac{2\rho AL'}{3} & 0 & 0 & \frac{\rho AL'}{6} & \frac{\rho AL}{6}\\
0 & 0 & \rho AL+\frac{\rho AL'}{3} & \frac{\rho AL}{6} & 0 & 0\\
0 & 0 & \frac{\rho AL}{6} & \frac{2\rho AL}{3}+\frac{2\rho AL'}{3} & 0 & 0\\
\frac{\rho AL}{3} & \frac{\rho AL'}{3} & 0 & 0 & \rho AL+\frac{2\rho AL'}{3} & \frac{\rho AL}{6}\\
\frac{\rho AL'}{3} & \frac{\rho AL}{3} & 0 & 0 & \frac{\rho AL}{6} & \rho AL+\frac{2\rho AL'}{3}
\end{bmatrix}. \tag{7.113}$$

(b) *The subgraph corresponding to T:*
The mass matrix corresponding to the subgraph, shown in Fig. 7.63, is as follows:

$$\mathbf{M}_T=\begin{bmatrix}
\rho AL+\frac{\rho AL'}{3} & \frac{\rho AL}{6} & 0 & 0 & 0 & 0\\
\frac{\rho AL}{6} & \frac{2\rho AL}{3}+\frac{2\rho AL'}{3} & 0 & 0 & 0 & 0\\
0 & 0 & \rho AL+\frac{\rho AL'}{3} & \frac{\rho AL}{6} & \frac{\rho AL}{3} & \frac{\rho AL'}{3}\\
0 & 0 & \frac{\rho AL}{6} & \frac{2\rho AL}{3}+\frac{2\rho AL'}{3} & \frac{\rho AL'}{3} & \frac{\rho AL}{3}\\
0 & 0 & \frac{\rho AL}{6} & \frac{\rho AL'}{6} & \rho AL+\frac{2\rho AL'}{3} & \frac{\rho AL}{6}\\
0 & 0 & \frac{\rho AL'}{6} & \frac{\rho AL}{6} & \frac{\rho AL}{6} & \rho AL+\frac{2\rho AL'}{3}
\end{bmatrix}. \tag{7.114}$$

Considering $E = 2.07 \times 10^7\,\mathrm{kN/m}$, $L = 100$ cm, $I = 100\,\mathrm{cm}^4$ and $\rho = 78\,\mathrm{kN/m}^3$ and, the frequencies of the structure are calculated as

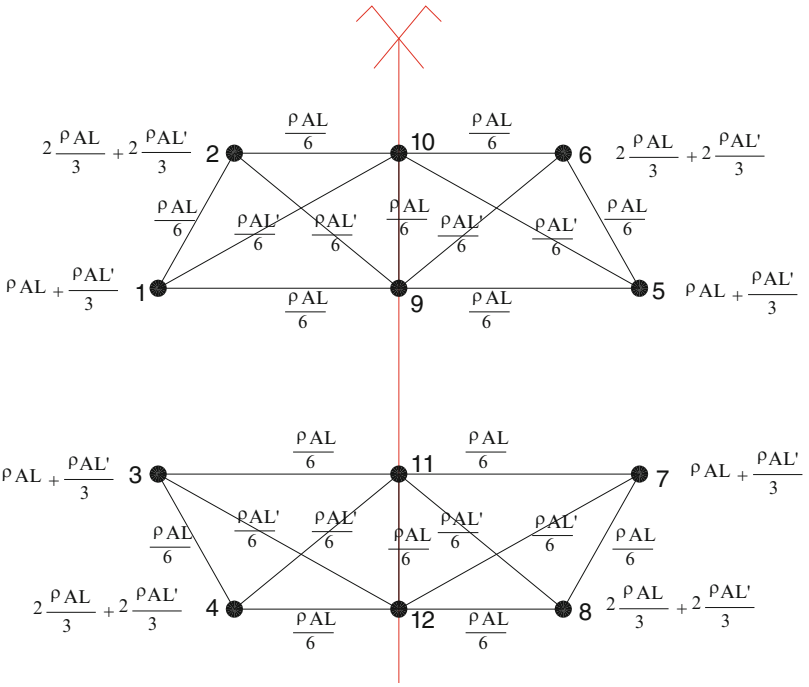

Fig. 7.61 Graph representation of the mass matrix

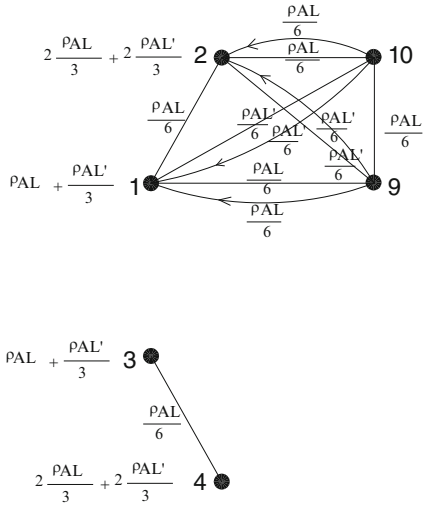

Fig. 7.62 Formation of the subgraph *S*

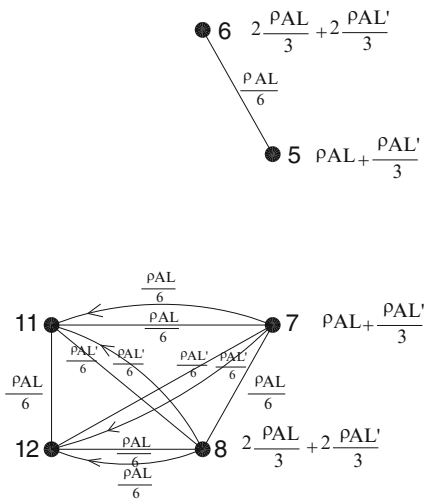

Fig. 7.63 Formation of the subgraph T

$$\omega_T = [48.908, 42.227, 37.548, 31.368, 26.525, 5.447],$$
$$\omega_S = [11.886, 14.184, 11.722, 42.890, 45.349, 59.192],$$
$$\omega = \omega_T \cup \omega_S = [48.908, 42.227, 37.548, 31.368, 26.525, 5.447, 11.886, 14.184, 11.722, 42.890, 45.349, 59.192]. \quad (7.115)$$

Using the algebraic approach formulated in Sect. 3.2, identical eigenfrequencies are obtained. The eigenvectors are then calculated and the mode shapes are obtained. The first four mode shapes are illustrated in Fig. 7.64.

Important Notes: In the main graph there is no member between the nodes in the two sides of the symmetry axis, since the submatrices **D**, **E** and **F** are null matrices. The reason is the existence of a member directly connecting two nodes in two sides of the symmetry axis. If there exist such members, then the submatrices **D**, **E** and **F** will not be null, and for finding the subgraphs S and T and only for such members, one should act as was described in the algorithm for the Form B symmetry. For other members with the present pattern with nodes in two sides of the axis connected to the central node, the above algorithm should be employed. This problem can be recognised by investigating the similarity between the Form A and Form B canonical symmetries. Part of the matrices **S** and **T** in Form A are exactly the same as submatrices **S** and **T** in Form B.

Example 7.14. Consider a planar 2D truss with the symmetry axis passing through central members (truss with odd number of spans), as shown in Fig. 7.65.

Considering L = 100 cm, I = 100 cm^4, E = 201 kN/mm^2 and $\rho = 78\,\text{kN/m}^3$, $A = 10\,\text{cm}^2$, the eigenfrequencies of the structure are calculated as:

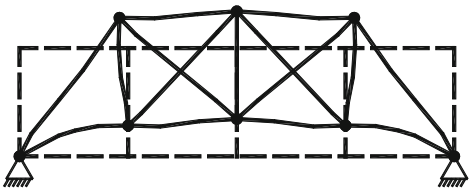

1st mode

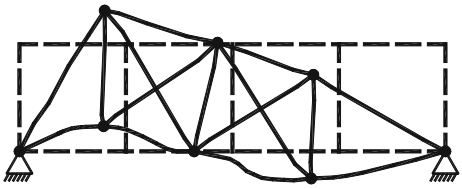

2nd mode

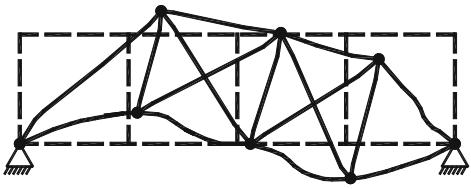

3rd mode

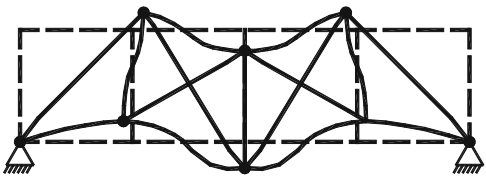

4th mode

Fig. 7.64 The first four natural mode shapes of Example 7.13

$$\omega_S = \begin{bmatrix} 26.83, 42.78, 92.36, 108.31, 150.23, 159.69, 169.32, 171.32, 180.91, \\ 201.74, 225.75, 230.13, 233.65, 293.60 \end{bmatrix},$$

$$\omega_T = \begin{bmatrix} 11.40, 58.91, 76.81, 122.52, 140.75, 174.27, 177.88, 183.17, 217.99, \\ 223.18, 233.94, 235.82, 259.0, 322.24 \end{bmatrix},$$

$$\omega = \omega_S \cup \omega_T = \begin{bmatrix} 26.83, 42.78, 92.36, 108.31, 150.23, 159.69, 169.32, 171.32, 180.91, \\ 201.74, 225.75, 230.13, 233.65, 293.60, 11.40, 58.91, 76.81, 122.52, \\ 140.75, 174.27, 177.88, 183.17, 217.99, 223.18, 233.94, 235.82, \\ 259.0, 322.24 \end{bmatrix} \tag{7.116}$$

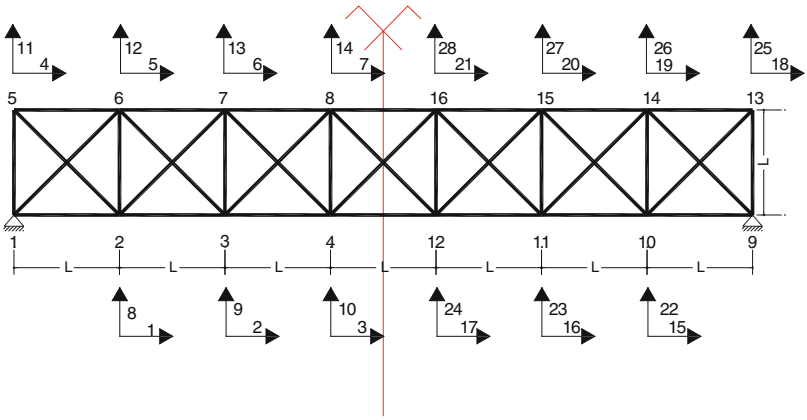

Fig. 7.65 A 7-bay symmetric truss

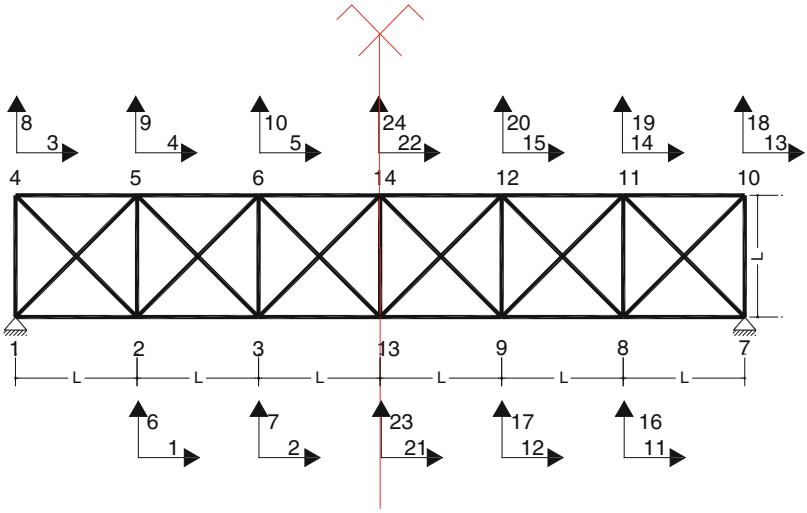

Fig. 7.66 A 6-bay truss

Using the algebraic approach formulated in Sect. 3.1, identical eigenfrequencies are obtained.

Example 7.15. Consider a planar 2D trusses that passes symmetry axes on middle nodes (truss with even number of spans) as shown in Fig. 7.66.

Considering L = 100 cm, I = 100 cm^4, E = 201 kN/mm^2 and $\rho = 78\,kN/m^3$, $A = 10\,cm^2$, the eigenfrequencies of the structure are calculated as:

$$\omega_K = \begin{bmatrix} 319.33, 247.61, 32.86, 50.60, 235.05, 226.08, 210.38, 111.94, 119.87, 162.88, \\ 175.33, 177.43 \end{bmatrix},$$

$$\omega_H = \begin{bmatrix} 15.17, 73.08, 86.37, 142.5, 157.8, 170.21, 182.37, 189.58, 225.17, 226.63 \\ 234.2, 284.92 \end{bmatrix},$$

$$\omega = \omega_K \cup \omega_H = \begin{bmatrix} 319.33, 247.61, 32.86, 50.60, 235.05, 226.08, 210.38, 111.94, \\ 119.87, 162.88, 175.33, 177.43, 15.17, 73.08, 86.37, 142.5, 157.8, \\ 170.21, 182.37, 189.58, 225.17, 226.63, 234.2, 284.92 \end{bmatrix} \tag{7.117}$$

Using the algebraic approach formulated in Sect. 3.2, identical eigenfrequencies are obtained.

Though in this part the examples are selected from small trusses, however, the method shows its potential more when applied to large-scale structures. For comparison of the required time for calculating the eigenvalues of matrices with and without decomposition, matrices of various dimensions are considered having sparsity between 30 % and 40 %, and MATLAB is employed for these calculations.

7.5.3 Discussion

In this part two new canonical forms are introduced and weighted graph are associated with these forms. Decomposition and healing processes are presented to perform on these graphs in order to reduce the dimensions of the problem for free vibration analysis of the symmetric trusses. Therefore, the accuracy of calculation increases, and the cost of the computation decreases. The previously developed methods were unable to deal with cross-link members of structures with more than one DOF per node, while the new forms defined here overcome this difficulty. Calculation of the eigenfrequencies can also be performed using the relationships presented in Sects. 3.1 and 3.2 for trusses with odd and even numbers of bays, respectively.

It should be mentioned that for automatic numbering of the degrees of freedom (or nodal numbering suitable for the canonical forms), additional algorithm is required.

The present method is also applicable to similar eigensolution problems such as stability analysis of symmetric trusses for calculating their critical loads. This approach can easily be generalised to free vibration analysis of space trusses.

7.6 General Canonical Forms for Analytical Solution of Problems in Structural Mechanics

In this part new forms are introduced for efficient eigensolution of special tri-diagonal and penta-diagonal matrices. Applications of these forms are illustrated using problems from mechanics of structures.

7.6.1 Definitions

The polynomial $p(\lambda) = \det(\mathbf{A} - \lambda\mathbf{I})$ is called the *characteristic polynomial* of $\mathbf{A}$. The roots of $p(\lambda) = 0$ are the *eigenvalues* of $\mathbf{A}$. Since the degree of the characteristic polynomial $p(\lambda)$ equals to N, the dimension of $\mathbf{A}$ has N roots, so $\mathbf{A}$ has N eigenvalues. A non-zero vector $\mathbf{x}$ satisfying $\mathbf{Ax} = \lambda\mathbf{x}$ is an *eigenvector* for the eigenvalue λ.

The easiest matrix for which the eigenvalues can be calculated is a diagonal matrix, whose eigenvalues are simply its diagonal entries. Equally easy is a triangular matrix, whose eigenvalues are also its diagonal entries. A matrix can have complex eigenvalues, since the roots of its characteristic polynomial may be real or complex. Therefore, there is not always a real triangular matrix with the same eigenvalues as a real general matrix, since a real triangular matrix can only have real eigenvalues. Thus, one must either use complex numbers or look beyond real triangular matrices for canonical forms for real matrices. For this purpose, it is sufficient to consider block triangular matrices, that is, matrices of the form

$$\mathbf{A} = \begin{bmatrix} \mathbf{A}_{11} & \mathbf{A}_{12} & . & . & . & \mathbf{A}_{1N} \\ & \mathbf{A}_{22} & . & . & . & \mathbf{A}_{2N} \\ & & . & . & . & . \\ & & & . & . & . \\ & & & & . & . \\ & & & & & \mathbf{A}_{NN} \end{bmatrix}, \tag{7.118}$$

where each $\mathbf{A}_{ii}$ is square and all entries below $\mathbf{A}_{ii}$ blocks are zero. It can easily be shown that the characteristic polynomial $\det(\mathbf{A} - \lambda\mathbf{I})$ of $\mathbf{A}$ is the product $\prod_{i=1}^{N} \det(\mathbf{A}_{ii} - \lambda\mathbf{I})$ of the characteristic polynomial of the $\mathbf{A}_{ii}$, and therefore, the set $\lambda(\mathbf{A})$ of eigenvalues of $\mathbf{A}$ is the union $\cup_{i=1}^{N} \lambda(\mathbf{A}_{ii})$ of the sets of eigenvalues of the diagonal blocks $\mathbf{A}_{ii}$.

7.6.2 *Decomposition of a Tri-diagonal Matrix*

Consider a block tri-diagonal matrix as:

$$\mathbf{F} = \begin{bmatrix} \mathbf{A} & \mathbf{B} & & & & & & & \\ \mathbf{B} & \mathbf{C} & \mathbf{B} & & & & & & \\ & \mathbf{B} & \mathbf{C} & \mathbf{B} & & & & & \\ & & \cdot & \cdot & \cdot & & & & \\ & & & \cdot & \cdot & \cdot & & & \\ & & & & \cdot & \cdot & \cdot & & \\ & & & & & \mathbf{B} & \mathbf{C} & \mathbf{B} & \\ & & & & & & \mathbf{B} & \mathbf{C} & \mathbf{B} \\ & & & & & & & \mathbf{B} & \mathbf{A} \end{bmatrix}, \tag{7.119}$$

where **A**, **B** and **C** are m × m matrix blocks. The matrix **F** contains n blocks in each row and n blocks in each column. A matrix **M** in the form of **F** will be denoted by $\mathbf{M}_{mn} = \mathbf{F}(\mathbf{A}_m, \mathbf{B}_m, \mathbf{C}_m)_{mn}$.

7.6.2.1 Canonical Form I

Now consider the following tri-diagonal matrix:

$$\begin{aligned} &\mathbf{M}_{\mathbf{mn}} = \mathbf{F}(\mathbf{A}_\mathbf{m},\ \mathbf{B}_\mathbf{m},\ \mathbf{A}_\mathbf{m})_{\mathbf{mn}}, \\ &\text{where}\ \ \mathbf{A}_\mathbf{m} = \mathbf{F}(a, b, a)_\mathbf{m}\ \ \textbf{and}\ \ \mathbf{B}_\mathbf{m} = \mathbf{F}(c, d, c)_\mathbf{m}. \end{aligned} \tag{7.120}$$

Consider $\mathbf{T}_k = \mathbf{F}(0,1,0)_k$ with eigenvalues λ_k, and denote the unit matrix by $\mathbf{I}_k$, where k is the dimension of the square matrices $\mathbf{T}_k$ and $\mathbf{I}_k$. The matrix $\mathbf{M}_{mn}$ can be decomposed as

$$\mathbf{M}_{mn} = \mathbf{I}_n \otimes \mathbf{A}_m + \mathbf{T}_n \otimes \mathbf{B}_m, \tag{7.121}$$

where ⊗ denotes the Kronecker product of two matrices as defined in Sect. 4.9. Substituting the following relationships in Eq. 7.121,

$$\mathbf{A}_m = (a\mathbf{I}_m + b\mathbf{T}_m) \ \ \text{and}\ \mathbf{B}_m = (c\mathbf{I}_m + d\mathbf{T}_m) \tag{7.122}$$

results in

$$\mathbf{M}_{mn} = a\mathbf{I}_n \otimes \mathbf{I}_m + b\mathbf{I}_n \otimes \mathbf{T}_m + c\mathbf{T}_n \otimes \mathbf{I}_m + d\mathbf{T}_n \otimes \mathbf{T}_m. \tag{7.123}$$

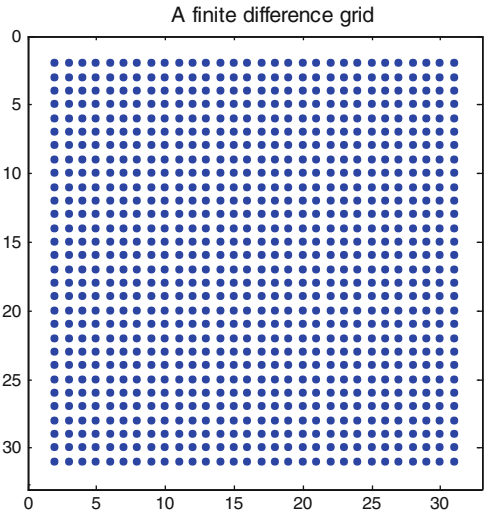

Fig. 7.67 A square domain and its grid points

It is readily verified that the eigenvalues of $\mathbf{T}_n \otimes \mathbf{T}_m$ are $\lambda_m\lambda_n$, and therefore,

$$\lambda = a + b\lambda_m + c\lambda_n + d\lambda_m\lambda_n. \tag{7.124}$$

7.6.2.2 Applications

For problems where the second derivatives are present, the application of finite difference method leads to matrices of canonical Form I. As an example, consider the solution of the Laplace equation using the finite difference method. The parameters of λ in Eq. 7.124 for this case are as follows:

$$a = 4,\ b = -1,\ c = -1,\ \text{and } d = 0, \tag{7.125}$$

leading to

$$\lambda = 4 - \lambda_m - \lambda_n. \tag{7.126}$$

Now consider the solution of the Laplace equation in a square domain, Fig. 7.50, with $N = 4$ ($m = n = 4$).

In general case, for a path P_n with n nodes, the adjacency and Laplacian matrices are in the form $P_n = F(a,b,a)$, and the corresponding eigenvalues can be obtained by (Fig. 7.67)

$$\lambda = a + 2b\cos\frac{k\pi}{n+1} \quad \text{for } k = 1,\ldots,n. \tag{7.127}$$

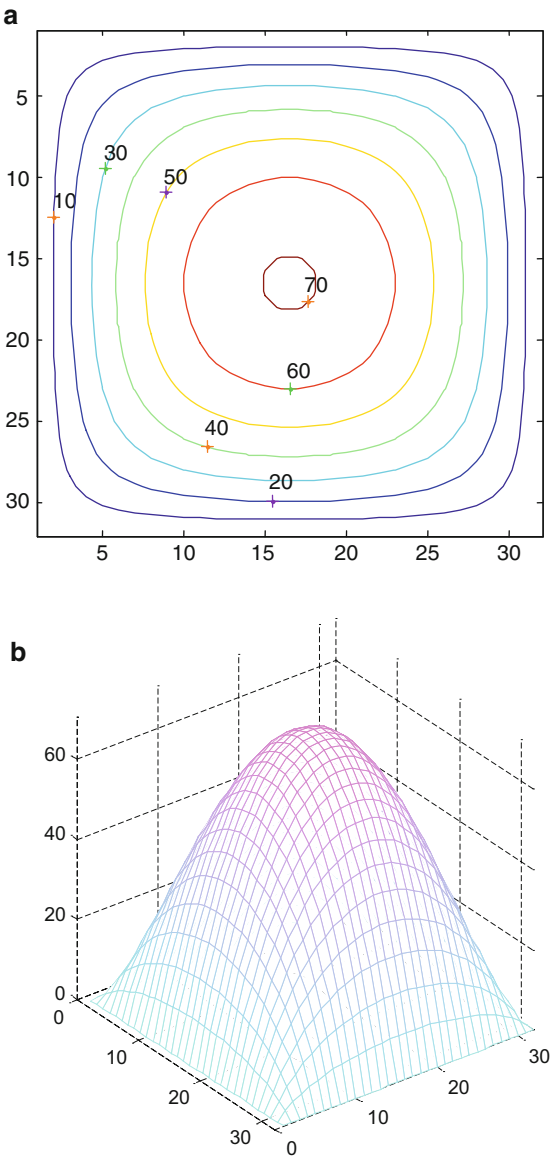

Fig. 7.68 Distributions of the first eigenvector in 2D and 3D spaces. (**a**) Components of the first eigenvector in 2D space. (**b**) Components of the first eigenvector in 3D space

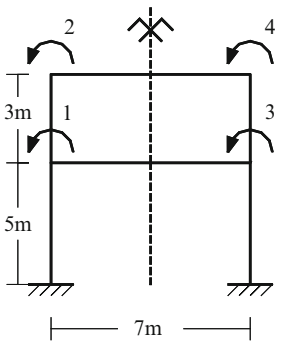

Fig. 7.69 A symmetric frame with sway

For $\mathbf{T}_m = \mathbf{F}(0,1,0)$ one obtains $\lambda_m = 2\cos\frac{k\pi}{n+1}$, and for maximum, $\lambda_4 = 2\cos\frac{\pi}{5} = 1.6180$, leading to $\lambda = 4 - 1.6180 - 1.6180 = 0.7639$ which is quite close to the exact value. Figures 7.68a and 7.69b show the distribution of the components of the corresponding first eigenvector, over the grid points, in two- and three-dimensional spaces, respectively.

7.6.3 *A New Form for Efficient Solution of Eigenproblem*

7.6.3.1 A General Block Diagonal Tri-diagonal Matrix

Consider a block tri-diagonal matrix as

$$\mathbf{M} = \left[\begin{array}{cc|cc|cc} x & 3 & 0 & 2 & 0 & 0 \\ 4 & x & x & 0 & 0 & 0 \\ \hline 0 & 2 & x & 3 & 0 & 2 \\ x & 0 & 4 & x & x & 0 \\ \hline 0 & 0 & 0 & 2 & x & 3 \\ 0 & 0 & x & 0 & 4 & x \end{array}\right] \tag{7.128}$$

with x as some diagonal and non-diagonal entries. We are interested to find x such that the determinant of $\mathbf{M}$ becomes zero. This matrix has the canonical Form I as introduced in the previous section, and it can be expressed as $\mathbf{P}_m = \mathbf{F}(\mathbf{A}_2,\mathbf{B}_2,\mathbf{A}_2)$. The corresponding eigenvalues can be obtained as

$$\lambda = \mathbf{A}_2 + 2\mathbf{B}_2\cos\frac{k\pi}{n+1};\ k = 1,\ldots,n. \tag{7.129}$$

Now one can substitute the corresponding submatrices for $\mathbf{A}_2$ and $\mathbf{B}_2$, leading to

$$\lambda = \begin{bmatrix} \mathrm{x} & 3 \\ 4 & \mathrm{x} \end{bmatrix} + 2\begin{bmatrix} 0 & 2 \\ \mathrm{x} & 0 \end{bmatrix} \cos\frac{\mathrm{k}\pi}{4};\ \mathrm{k} = 1, \ldots, 3. \tag{7.130}$$

For $\det(\mathbf{M}) = 0$, the determinant of $\lambda_{\mathbf{M}}$ for k = 1,2,3 should be set to zero, that is,

$$\begin{aligned} &\det\left(\begin{bmatrix} \mathrm{x} & 3 \\ 4 & \mathrm{x} \end{bmatrix} + 2\begin{bmatrix} 0 & 2 \\ \mathrm{x} & 0 \end{bmatrix} \cos\frac{\pi}{4}\right) = 0 \Rightarrow \mathrm{x} = 10.4695,\ \ \mathrm{x} = -2.2268, \\ &\det\left(\begin{bmatrix} \mathrm{x} & 3 \\ 4 & \mathrm{x} \end{bmatrix} + 2\begin{bmatrix} 0 & 2 \\ \mathrm{x} & 0 \end{bmatrix} \cos\frac{2\pi}{4}\right) = 0 \Rightarrow \mathrm{x} = 3.4641,\ \ \mathrm{x} = -3.4641, \\ &\det\left(\begin{bmatrix} \mathrm{x} & 3 \\ 4 & \mathrm{x} \end{bmatrix} + 2\begin{bmatrix} 0 & 2 \\ \mathrm{x} & 0 \end{bmatrix} \cos\frac{3\pi}{4}\right) = 0 \Rightarrow \mathrm{x} = 0.7159,\ \ \mathrm{x} = -0.9586. \end{aligned} \tag{7.131}$$

These are exactly the same eigenvalues obtained from $\det(\mathbf{M}) = 0$.
For the special case n = 2, we have

$$\mathbf{M} = \begin{bmatrix} \mathbf{A} & \mathbf{B} \\ \mathbf{B} & \mathbf{A} \end{bmatrix}, \tag{7.132}$$

resulting in

$$\begin{aligned} &\det\left(\mathbf{A} + 2\cos\frac{\pi}{3}\mathbf{B}\right) = 0 \\ &\det\left(\mathbf{A} - 2\cos\frac{\pi}{3}\mathbf{B}\right) = 0 \end{aligned} \Rightarrow \begin{array}{l} \det(\mathbf{A} + \mathbf{B}) = 0 \\ \det(\mathbf{A} - \mathbf{B}) = 0 \end{array}. \tag{7.133}$$

In general, one can write

$$\det(\mathbf{M}) = 0 \ \Rightarrow \det\left(\mathbf{A} + 2\cos\frac{\mathrm{k}\pi}{\mathrm{n}+1}\mathbf{B}\right) = 0 \ \text{ for } \mathrm{i} = 1, 2, \ldots, \mathrm{n}. \tag{7.134}$$

Example 7.16. Consider the symmetric frame as shown in Fig. 7.69. The numbering for DOFs is chosen that a Form II symmetry is provided for the structural matrices. For all the members, EI is taken as 'a' and the unit length mass is assumed to be 10 kg/m.

The stiffness and mass matrices are formed as

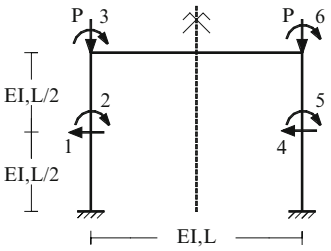

Fig. 7.70 A portal frame with six DOF

$$\mathbf{K} = \mathrm{a}\left[\begin{array}{cc|cc} \frac{284}{105} & \frac{2}{3} & \frac{2}{7} & 0 \\ \frac{2}{3} & \frac{40}{21} & 0 & \frac{2}{7} \\ \hline \frac{2}{7} & 0 & \frac{284}{105} & \frac{2}{3} \\ 0 & \frac{2}{7} & \frac{2}{3} & \frac{40}{21} \end{array}\right] \quad \text{and}$$

$$\mathbf{M} = \left[\begin{array}{cc|cc} \frac{990}{21} & \frac{-81}{42} & \frac{-1029}{42} & 0 \\ \frac{-81}{42} & \frac{740}{21} & 0 & \frac{-1029}{42} \\ \hline \frac{-1029}{42} & 0 & \frac{990}{21} & \frac{-81}{42} \\ 0 & \frac{-1029}{42} & \frac{-81}{42} & \frac{740}{21} \end{array}\right]. \tag{7.135}$$

The matrix $[\mathbf{K} - \omega^2\mathbf{M}]$ has a Form II pattern, Eq. 7.132, and using Eq. 7.133, we have

$$\begin{aligned} \det\begin{bmatrix} 2.41 - 71.6\mathrm{x} & 0.67 + 2\mathrm{x} \\ 0.67 + 2\mathrm{x} & 1.61 - 59.7\mathrm{x} \end{bmatrix} &= 0 \\ \det\begin{bmatrix} 2.99 - 22.6\mathrm{x} & 0.67 + 2\mathrm{x} \\ 0.67 + 2\mathrm{x} & 2.19 - 10.7\mathrm{x} \end{bmatrix} &= 0 \end{aligned} \tag{7.136}$$

where $\mathrm{x} = \frac{\omega^2}{\mathrm{a}}$, leading to the following natural frequencies:

$$\begin{aligned} \mathrm{x}_1 = 0.019 \Rightarrow \omega_1^2 = 0.019\mathrm{a} \quad \mathrm{x}_3 = 0.102 \Rightarrow \omega_3^2 = 0.102\mathrm{a}, \\ \mathrm{x}_2 = 0.042 \Rightarrow \omega_2^2 = 0.042\mathrm{a} \quad \mathrm{x}_4 = 0.252 \Rightarrow \omega_4^2 = 0.252\mathrm{a}. \end{aligned} \tag{7.137}$$

Example 7.17. Consider a one-span frame as shown in Fig. 7.70. The columns are subdivided into two elements. Therefore, the frame has six DOFs as illustrated in the figure. The stiffness matrix of the structure is assembled as follows:

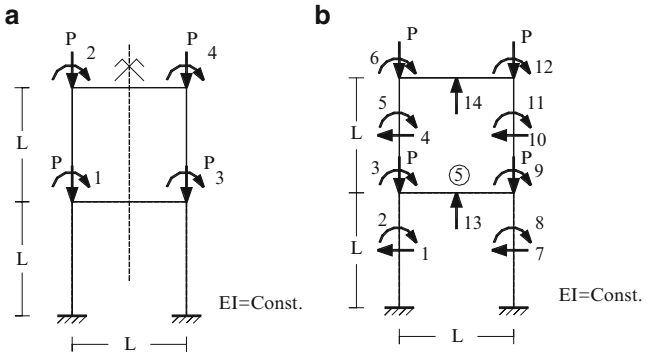

Fig. 7.71 A one-bay two-storey frame. (**a**) Four degrees of freedom. (**b**) Fourteen degrees of freedom

$$\mathbf{K} = \frac{EI}{L^3}\left[\begin{array}{ccc|ccc} 192 & 0 & -48 & 0 & 0 & 0 \\ 0 & 64 & 16 & 0 & 0 & 0 \\ -48 & 16 & 36 & 0 & 0 & 2 \\ \hline 0 & 0 & 0 & 192 & 0 & -48 \\ 0 & 0 & 0 & 0 & 64 & 16 \\ 0 & 0 & 2 & -48 & 16 & 36 \end{array}\right] - \frac{P}{L}\left[\begin{array}{ccc|ccc} \frac{24}{5} & 0 & \frac{-1}{5} & 0 & 0 & 0 \\ 0 & \frac{8}{15} & \frac{-1}{15} & 0 & 0 & 0 \\ \frac{-1}{5} & \frac{-1}{15} & \frac{4}{15} & 0 & 0 & 0 \\ \hline 0 & 0 & 0 & \frac{24}{5} & 0 & \frac{-1}{5} \\ 0 & 0 & 0 & 0 & \frac{8}{15} & \frac{-1}{15} \\ 0 & 0 & 0 & \frac{-1}{5} & \frac{-1}{15} & \frac{4}{15} \end{array}\right]. \tag{7.138}$$

This matrix has Form II and the smallest eigenvalue corresponds to $P_{cr} = \frac{22.2097EI}{L^2}$. This is an approximate value compared to the real value as $P_{cr} = \frac{25.2EI}{L^2}$. A better result can be obtained by subdividing the columns into three elements and the beam into two elements.

Example 7.18. Consider a one-bay two-storey frame as shown in Fig. 7.71a. This example is studied with two different discretisations. In the first model, each column is considered as one element as in Fig. 7.71a, and in the second model, each column is subdivided into two elements as illustrated in Fig. 7.4.

For the first model $P_{cr} = \frac{19.75EI}{L^2}$, which is a crude answer.

For the second model shown in Fig. 7.71b, the stiffness matrix is formed as

$$\mathbf{K} = \frac{EI}{L^3}\left[\begin{array}{cccccc|cccccc}
192 & 0 & -48 & 0 & 0 & 0 & 0 & 0 & 0 & 0 & 0 & 0 \\
0 & 64 & 16 & 0 & 0 & 0 & 0 & 0 & 0 & 0 & 0 & 0 \\
-48 & 16 & 36 & 0 & 0 & 0 & 0 & 0 & 2 & 0 & 0 & 0 \\
0 & 0 & 0 & 192 & 0 & -48 & 0 & 0 & 0 & 0 & 0 & 0 \\
0 & 0 & 0 & 0 & 64 & 16 & 0 & 0 & 0 & 0 & 0 & 0 \\
0 & 0 & 0 & -48 & 16 & 36 & 0 & 0 & 0 & 0 & 0 & 2 \\
\hline
0 & 0 & 0 & 0 & 0 & 0 & 192 & 0 & -48 & 0 & 0 & 0 \\
0 & 0 & 0 & 0 & 0 & 0 & 0 & 64 & 16 & 0 & 0 & 0 \\
0 & 0 & 2 & 0 & 0 & 0 & -48 & 12 & 36 & 0 & 0 & 0 \\
0 & 0 & 0 & 0 & 0 & 0 & 0 & 0 & 0 & 192 & 0 & -48 \\
0 & 0 & 0 & 0 & 0 & 0 & 0 & 0 & 0 & 0 & 64 & 16 \\
0 & 0 & 0 & 0 & 0 & 2 & 0 & 0 & 0 & -48 & 16 & 36
\end{array}\right]$$

$$-\frac{P}{L}\left[\begin{array}{cccccc|cccccc}
\frac{48}{5} & 0 & \frac{-2}{5} & 0 & 0 & 0 & 0 & 0 & 0 & 0 & 0 & 0 \\
0 & \frac{16}{15} & \frac{-2}{15} & 0 & 0 & 0 & 0 & 0 & 0 & 0 & 0 & 0 \\
\frac{-2}{5} & \frac{-2}{15} & \frac{8}{15} & 0 & 0 & 0 & 0 & 0 & 0 & 0 & 0 & 0 \\
0 & 0 & 0 & \frac{24}{5} & 0 & \frac{-1}{5} & 0 & 0 & 0 & 0 & 0 & 0 \\
0 & 0 & 0 & 0 & \frac{8}{5} & \frac{-1}{15} & 0 & 0 & 0 & 0 & 0 & 0 \\
0 & 0 & 0 & \frac{-1}{5} & \frac{-1}{15} & \frac{4}{15} & 0 & 0 & 0 & 0 & 0 & 0 \\
\hline
0 & 0 & 0 & 0 & 0 & 0 & \frac{48}{5} & 0 & \frac{-2}{5} & 0 & 0 & 0 \\
0 & 0 & 0 & 0 & 0 & 0 & 0 & \frac{16}{15} & \frac{-2}{15} & 0 & 0 & 0 \\
0 & 0 & 0 & 0 & 0 & 0 & \frac{-2}{5} & \frac{-2}{15} & \frac{8}{15} & 0 & 0 & 0 \\
0 & 0 & 0 & 0 & 0 & 0 & 0 & 0 & 0 & \frac{24}{5} & 0 & \frac{-1}{5} \\
0 & 0 & 0 & 0 & 0 & 0 & 0 & 0 & 0 & 0 & \frac{8}{15} & \frac{-1}{15} \\
0 & 0 & 0 & 0 & 0 & 0 & 0 & 0 & 0 & \frac{-1}{5} & \frac{-1}{15} & \frac{4}{15}
\end{array}\right] \tag{7.139}$$

leading to $P_{cr} = \frac{11.1049EI}{L^2}$. Subdividing the columns into three elements and the beams into two elements leads to $P_{cr} = \frac{12.7554EI}{L^2}$. The exact value for the critical load is $P_{cr(exact)} = \frac{12.60EI}{L^2}$.

7.6.4 Canonical Penta-diagonal Form

7.6.4.1 Formulation

The numerical solution of some problems results in five-diagonal matrices. An example of this form is depicted in the following:

$$\mathbf{M}_{mn} = \begin{bmatrix} \mathbf{A} & \mathbf{B} & \mathbf{I} & & & & & & & \\ \mathbf{B} & \mathbf{A}+\mathbf{I} & \mathbf{B} & \mathbf{I} & & & & & & \\ \mathbf{I} & \mathbf{B} & \mathbf{A}+\mathbf{I} & . & . & & & & & \\ & . & . & . & . & . & & & & \\ & & . & . & . & . & . & & & \\ & & & . & . & . & . & . & & \\ & & & & . & . & . & \mathbf{B} & \mathbf{I} & \\ & & & & & . & \mathbf{B} & \mathbf{A}+\mathbf{I} & \mathbf{B} & \\ & & & & & & \mathbf{I} & \mathbf{B} & \mathbf{A} \end{bmatrix}_{n\times n}. \tag{7.140}$$

Using the Kronecker product, this matrix can be decomposed as

$$\mathbf{M}_{mn} = \mathbf{I}_n \otimes \mathbf{A}_m + \mathbf{T}_n \otimes \mathbf{B}_m + \mathbf{S}_n \otimes \mathbf{I}_m \tag{7.141}$$

where

$$\mathbf{T}_n = \mathbf{F}(0,1,0) \text{ and } \mathbf{S}_n = \begin{bmatrix} 0 & 0 & 1 & & & \\ 0 & 1 & 0 & 1 & & \\ 1 & 0 & 1 & . & . & \\ & 1 & . & . & . & . \\ & & . & . & . & . \\ & & & . & . & . \end{bmatrix}. \tag{7.142}$$

It can easily be verified that

$$\mathbf{S}_n = \mathbf{T}_n^2 - \mathbf{I}_n. \tag{7.143}$$

Therefore,

$$\begin{aligned} \mathbf{M}_{mn} &= \mathbf{I}_n \otimes \mathbf{A}_m + \mathbf{T}_n \otimes \mathbf{B}_m + \left(\mathbf{T}_n^2 - \mathbf{I}_n\right) \otimes \mathbf{I}_m \\ &= \mathbf{I}_n \otimes (\mathbf{A}_m - \mathbf{I}_m) + \mathbf{T}_n \otimes \mathbf{B}_m + \mathbf{T}_n^2 \otimes \mathbf{I}_m. \end{aligned} \tag{7.144}$$

In the last two terms, $\mathbf{T}_n$ cannot be factorised, since we have a matrix product and not a Kronecker product. Therefore, the eigenvalues of the last two terms are calculated to search for a possible equivalent matrix with the same eigenvalues:

$$\lambda_{\mathbf{T}_n \otimes \mathbf{B}_m + \mathbf{T}_n^2 \otimes \mathbf{I}_m} = \mathbf{B}_m \lambda_{\mathbf{T}_n} + \mathbf{I}_m \lambda_{\mathbf{T}_n^2}. \tag{7.145}$$

On the other hand, we have

$$\lambda_{\mathbf{T}_n^2} = (\lambda_{\mathbf{T}_n})^2 \tag{7.146}$$

Hence,

$$\lambda_{\mathbf{T}_n \otimes \mathbf{B}_m + \mathbf{T}_n^2 \otimes \mathbf{I}_m} = \lambda_{\mathbf{T}_n}(\mathbf{B}_m + \lambda_{\mathbf{T}_n}\mathbf{I}_m) = \lambda_{\mathbf{T}_n}\left(\mathbf{B}_m + 2\mathbf{I}_m \cos\frac{k\pi}{n+1}\right). \tag{7.147}$$

This is the same as the eigenvalue of the following matrix:

$$\mathbf{T}_n \otimes \left(\mathbf{B}_m + 2\mathbf{I}_m \cos\frac{k\pi}{n+1}\right). \tag{7.148}$$

Substituting in Eq. 7.144 leads to

$$\begin{aligned}\mathbf{M}_{mn} &= \mathbf{I}_n \otimes (\mathbf{A}_m - \mathbf{I}_m) + \mathbf{T}_n \otimes \mathbf{B}_m + \left(\mathbf{T}_n^2 \otimes \mathbf{I}_m\right) \\ &= \mathbf{I}_n \otimes (\mathbf{A}_m - \mathbf{I}_m) + \mathbf{T}_n \otimes \left(\mathbf{B}_m + 2\mathbf{I}_m \cos\frac{k\pi}{n+1}\right).\end{aligned} \tag{7.149}$$

It can be seen that we have again a canonical Form I expressed as

$$\mathbf{F}\left(\mathbf{A}_m - \mathbf{I}_m, \mathbf{B}_m\left(2\mathbf{I}_m \cos\frac{k\pi}{n+1}\right), \mathbf{A}_m - \mathbf{I}_m\right) \tag{7.150}$$

and the eigenvalues of this form should be calculated. Therefore, a five-diagonal form is transformed to a tri-diagonal form, and

$$\begin{aligned}\lambda_{\mathbf{M}} &= (\mathbf{A}_m - \mathbf{I}_m) + 2\cos\frac{k\pi}{n+1}\left(\mathbf{B}_m + 2\mathbf{I}_m\left(\cos\frac{k\pi}{n+1}\right)\right) \\ &= \mathbf{A}_m + 2\mathbf{B}_m \cos\frac{k\pi}{n+1} + \mathbf{I}_m\left(4\cos^2\frac{k\pi}{n+1} - 1\right) \\ &= \mathbf{A}_m + 2\mathbf{B}_m \cos\frac{k\pi}{n+1} + \mathbf{I}_m\left(1 + 2\cos\frac{2k\pi}{n+1}\right).\end{aligned} \tag{7.151}$$

Example 7.19. Consider a simply supported square thin plate as shown in Fig. 7.72. The buckling load of this plate under uniform compressive loads $N_x = N_y = N$ is required. The governing differential equation of the plate is

$$\frac{\partial^4 w}{\partial x^4} + 2\frac{\partial^4 w}{\partial x^2 y^2} + \frac{\partial^4 w}{\partial y^4} + \frac{N}{D}\left(\frac{\partial^2 w}{\partial x^2} + \frac{\partial^2 w}{\partial y^2}\right) = 0, \tag{7.152}$$

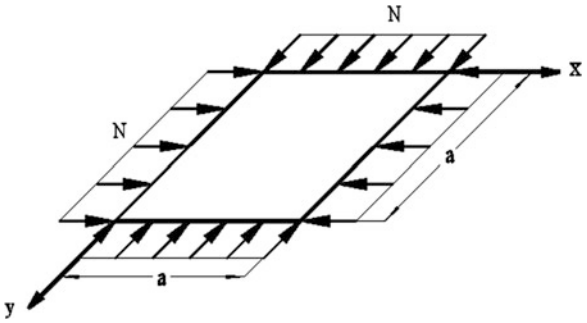

Fig. 7.72 A plate under biaxial compressive loading

or

$$\nabla^4 w + \frac{N}{D}\nabla^2 w = 0. \tag{7.153}$$

The exact solution of this problem is as follows:

$$N_{cr} = \frac{2\pi^2 D}{a^2} = \frac{19.7392D}{a^2}. \tag{7.154}$$

Using the finite difference method leads to a five-diagonal matrix with the pattern studied in the previous section. In a special case, when $n = 6$ (i.e. each edge is divided into six segments), the final form of $\mathbf{M}$ and the matrices $\mathbf{A}_m$ and $\mathbf{B}_m$ are as follows:

$$\mathbf{A}_5 = \mathbf{F}_5(18 - 4\alpha, \alpha - 8, 19 - 4\alpha), \mathbf{B}_5 = \mathbf{F}_5(\alpha - 8, 2, \alpha - 8), \text{ with}$$
$$\alpha = \frac{N\left(\frac{a}{6}\right)^2}{D} = \frac{Na^2}{36D}. \tag{7.155}$$

Therefore, $\det(\mathbf{M}) = 0$ leads to

$$\lambda_{\mathbf{M}} = \mathbf{A}_5 + 2\mathbf{B}_5 \cos\frac{k\pi}{6} + \mathbf{I}_5\left(1 + 2\cos\frac{2k\pi}{6}\right) = 0 \text{ for } k = 1, 2, \ldots, 5. \tag{7.156}$$

Thus, instead of the matrix $\mathbf{M}$ with different magnitudes of k, the smallest value for $k = 1$ should be calculated, the main aim being the calculation of the critical load. This reduces the dimension of the matrix from 25×25 to 5×5. The latter matrix can itself be reduced as

For $k = 1$,

$$\lambda_{\mathbf{M}} = \mathbf{F}(a, b, c)$$
$$= \mathbf{F}\left(8 - 4\alpha + 2\left(\cos\frac{\pi}{6}\right)(\alpha - 8) + 1 + 2\cos\frac{2\pi}{6}, \alpha - 8 + 4\cos\frac{\pi}{6},\right.$$
$$\left. 19 - 4\alpha + 2\left(\cos\frac{\pi}{6}\right)(\alpha - 8) + 1 + 2\cos\frac{2\pi}{6}\right). \tag{7.157}$$

Here c = a + 1, that is this matrix has a similar form to that of the five-diagonal matrix (7.22). Therefore, for calculating the eigenvalues, one can again employ the same relationship, leading to

$$\lambda_{\lambda_M} = 0 \Rightarrow \mathbf{A} + 2\mathbf{B}\cos\frac{k'\pi}{n+1} + \mathbf{I}\left(1 + 2\cos\frac{2k'\pi}{n+1}\right) = 0 \ . \tag{7.158}$$

For $k' = 1$, we have

$$\begin{aligned} &18 - 4\alpha + 2\left(\cos\frac{\pi}{6}\right)(\alpha - 8) + 1 + 2\cos\frac{2\pi}{6} + 2\cos\frac{\pi}{6}\left(\alpha - 8 + 4\cos\frac{\pi}{6}\right) \\ &+ \mathbf{I}\left(1 + 2\cos\frac{2\pi}{6}\right) = 0 \end{aligned} \tag{7.159}$$

with **I** being a 1 × 1 unit matrix. Therefore, the 5 × 5 matrix is further reduced to a 1 × 1 matrix, that is, one equation with one unknown. Thus,

$$\alpha = \frac{6 - 8\cos\frac{\pi}{6} + 2\cos\frac{2\pi}{6}}{1 - \cos\frac{\pi}{6}} = 0.5359 \Rightarrow \frac{N_{cr}a^2}{36D} = \alpha \Rightarrow N_{cr} = \frac{19.2923D}{a^2}. \tag{7.160}$$

7.6.4.2 Derivation of the Exact Solution

Having α in terms of the parameter n, the exact value of α can also be derived as follows:

$$\alpha_{ext} = \underset{n\to\infty}{\text{Limit}} \frac{6 - 8\cos\frac{\pi}{n} + 2\cos\frac{2\pi}{n}}{1 - \cos\frac{\pi}{n}}. \tag{7.161}$$

Using $\cos 2\theta = 2\cos^2\theta - 1$ leads to

$$\alpha_{ext} = \underset{n\to\infty}{\text{Limit}} \frac{4\left(1 - \cos\frac{\pi}{n}\right)^2}{1 - \cos\frac{\pi}{n}} = \underset{n\to\infty}{\text{Limit}}\ 4\left(1 - \cos\frac{\pi}{n}\right). \tag{7.162}$$

Employing the following trigonometric relation and approximating sin θ by θ, if $\theta \to 0$, then we have

$$1 - \cos\theta = 2\mathbf{sin}^2\frac{\theta}{2} \approx 2\left(\frac{\theta}{2}\right)^2 = \frac{\theta^2}{2}. \tag{7.163}$$

Therefore,

$$\alpha_{ext} = 4\frac{(\pi)^2}{2n^2} = \frac{2\pi^2}{n^2}. \tag{7.164}$$

Substituting for α, we have

$$\frac{N_{cr}\left(\frac{a}{n}\right)^2}{D} = \frac{2\pi^2}{n^2}, \tag{7.165}$$

leading to the exact value of the critical load

$$(N_{cr})_{ext} = \frac{2D\pi^2}{a^2} = \frac{19.7392D}{a^2}. \tag{7.166}$$

7.7 Numerical Examples for the Matrices as the Sum of Three Kronecker Products

Matrices that can be written as the sum of three Kronecker products are already introduced in Sects. 4.10 and 4.11. In this part, examples are included to show the efficiency of this decomposition approach.

In this section, five examples are presented from structural mechanics to illustrate the applicability and the efficiency of the present methods.

Example 7.20. Consider the truss shown in Fig. 7.73. The cross-sectional areas and the mass of the members are as follows:

Member	Cross-sectional area	Mass
1 and 2	A	m
3	1.5 A	3 m
4 and 5	1.5 A	2 m

The natural frequencies of the structure are required.

Using the finite element approach, the stiffness and mass matrices for a typical element are as follows:

$$[\mathbf{K}_i] = \frac{EA_i}{h_i}\begin{bmatrix} C^2 & CS & -C^2 & -CS \\ CS & S^2 & -CS & -S^2 \\ -C^2 & -CS & C^2 & CS \\ -CS & -S^2 & CS & S^2 \end{bmatrix}, \quad [\mathbf{M}_i] = \frac{m_i h_i}{6}\begin{bmatrix} 2 & 0 & 1 & 0 \\ 0 & 2 & 0 & 1 \\ 1 & 0 & 2 & 0 \\ 0 & 1 & 0 & 2 \end{bmatrix},$$

where $C = \cos\theta$ and $S = \sin\theta$.

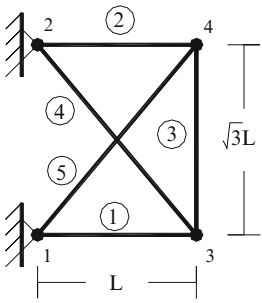

Fig. 7.73 A simple planar truss

After assembling the matrices of the elements for the entire structure and deleting the rows and columns corresponding to support nodes 1 and 2, we obtain

$$\mathbf{K} = \frac{\mathrm{EA}}{16\sqrt{3}\mathrm{L}} \begin{bmatrix} 32.9090 & -9 & 0 & 0 \\ -9 & 39.5885 & 0 & -24 \\ 0 & 0 & 32.9090 & 9 \\ 0 & -24 & 9 & 39.5885 \end{bmatrix},$$

$$\mathbf{M} = \frac{\mathrm{mL}}{16\sqrt{3}} \begin{bmatrix} 31.3960 & 0 & 8 & 0 \\ 0 & 31.3960 & 0 & 8 \\ 8 & 0 & 31.3960 & 0 \\ 0 & 8 & 0 & 31.3960 \end{bmatrix}. \det\left(\mathbf{K} - \mathbf{M}\omega^2\right) = 0.$$

It can be observed that **K** and **M** have no particular form as modelled; however, one can multiply a row and the corresponding column in (-1) such that the eigenvalues remain unchanged. If such operations are performed for the first row and column of **K** and the corresponding **M**, then we obtain a Form II matrix, and constructing **M** + **N** and **M** − **N**, the eigenvalues can be obtained as

$$\omega = \{0.5614,\ 0.8887,\ 1.2195,\ 1.6624\} \times \sqrt{\frac{\mathrm{EA}}{\mathrm{mL}^2}}.$$

Example 7.21. Using three finite elements we want to find the natural frequencies of the clamped beam shown in Fig. 7.74. The stiffness and mass matrices of a typical element are as follows:

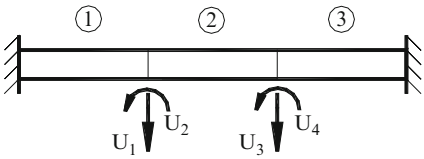

Fig. 7.74 A clamped beam with three elements

$$[\mathbf{K}_i] = \frac{EI_i}{L_i^3}\begin{bmatrix} 12 & 6L & -12 & 6L \\ 6L & 4L^2 & -6L & 2L^2 \\ -12 & -6L & 12 & -6L \\ 6L & 2L^2 & -6L & 4L^2 \end{bmatrix},$$

$$[\mathbf{M}_i] = \frac{\rho_i A_i L_i}{420}\begin{bmatrix} 156 & 22L & 54 & -13L \\ 22L & 4L^2 & 13L & -3L^2 \\ 54 & 13L & 156 & -22L \\ -13L & -3L^2 & -22L & 4L^2 \end{bmatrix}.$$

Assembling the matrices for the entire structure and applying the boundary conditions, the equation of vibration is as follows:

$$\frac{\rho AL}{420}\begin{bmatrix} 312 & 0 & 54 & -13L \\ 0 & 8L^2 & 13L & -3L^2 \\ 54 & 13L & 312 & 0 \\ -13L & -3L^2 & 0 & 8L^2 \end{bmatrix}\begin{bmatrix} \ddot{U}_1 \\ \ddot{U}_2 \\ \ddot{U}_3 \\ \ddot{U}_4 \end{bmatrix} + \frac{EI}{L^3}\begin{bmatrix} 24 & 0 & -12 & 6L \\ 0 & 8L^2 & -6L & 2L^2 \\ -12 & -6L & 24 & 0 \\ 6L & 2L^2 & 0 & 8L^2 \end{bmatrix}\begin{bmatrix} U_1 \\ U_2 \\ U_3 \\ U_4 \end{bmatrix} = \begin{bmatrix} 0 \\ 0 \\ 0 \\ 0 \end{bmatrix}$$

Here again one cannot see Form II matrices. However, multiplying the first row and column by (-1), such matrices can be constructed. Using their factors, similar to Example 7.20, the eigenvalues are obtained as

$$\omega = \{2.4961, 6.9893, 16.2561, 32.3059\} \times \sqrt{\frac{EI}{\rho AL^4}}.$$

Example 7.22. Consider a simply supported a $\times$ a square plate, as shown in Fig. 7.75. The load is applied in x-direction. Using the finite difference approach, the critical load of the plate is calculated.

Considering the governing differential equation as

$$\nabla^4 w + \frac{N_x}{D}\frac{\partial^2 w}{\partial x^2} = 0$$

and employing the finite difference method, the matrix **M** is obtained in the following form:

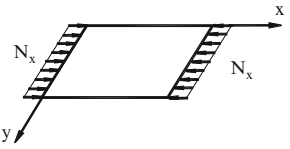

Fig. 7.75 A simply supported plate

$$\mathbf{M} = \mathbf{I} \otimes \mathbf{A} + \mathbf{T} \otimes \mathbf{B} + \mathbf{S} \otimes \mathbf{I} = \sum_{i=1}^{3} \mathbf{A}_i \otimes \mathbf{B}_i$$

where

$$\mathbf{B}_1 = \mathbf{F}(18 - 2x,\ x - 8, 19 - 2x, 1),\ \mathbf{B}_2 = \mathbf{F}(-8, 2, -8),$$
$$\mathbf{A}_2 = \mathbf{F}(0, 1, 0), \mathbf{A}_3 = \mathbf{F}(0, 0, 1, 1).$$

Since $\mathbf{A}_i\mathbf{A}_j = \mathbf{A}_j\mathbf{A}_i$ for each pair of i and j, then

$$\lambda_{\mathbf{M}} = \bigcup_{j=1}^{n} \left[\text{eig} \sum_{i=1}^{3} \lambda_j(\mathbf{A}_i)\mathbf{B}_i) \right]; \lambda_{\mathbf{A}_1} = 1,\ \lambda_{\mathbf{A}_2} = 2\cos\frac{k\pi}{n+1},$$
$$\lambda_{\mathbf{A}_3} = 1 + 2\cos\frac{2k\pi}{n+1}.$$

Once $\lambda_{\mathbf{M}}$ is calculated, it can be observed that it contains diagonal blocks and each block has the Form **F**. Thus, the diagonalisation is performed once again for each block, since $\mathbf{A}_i\mathbf{A}_j = \mathbf{A}_j\mathbf{A}_i$ still holds for these blocks.

For critical load (k = 1), we have

$$18 - 2x - 16\cos\frac{\pi}{m} + 1 + 2\cos\frac{2\pi}{m} + 2\cos\frac{\pi}{m}\left(x - 8 + 4\cos\frac{\pi}{m}\right)$$
$$+ 1\left(1 + 2\cos\frac{2\pi}{m}\right) = 0;\ m = n + 1$$
$$\Rightarrow x = \frac{4\left(3 - 4\cos\frac{\pi}{m} + \cos\frac{2\pi}{m}\right)}{\left(1 - \cos\frac{\pi}{m}\right)}.$$

In this relationship, $m \to \infty$ leads to an accurate value of the critical load as $x = \frac{4\pi^2}{m^2}$, where $1 - \cos\alpha \cong \frac{\alpha^2}{2}$ when $\alpha \to 0$. This result is in a good agreement with the exact value, which is

$$N_{cr} = \frac{xD}{\left(\frac{a}{m}\right)^2} = \frac{4\pi^2 D}{a^2}.$$

Example 7.23. In the previous example, suppose the supports with no loading are clamped, then the matrix **M** will still contain the decomposability property. In such a case,

$$\mathbf{A} = \mathbf{F}(20 - 2x, -8, 19 - 2x, 1), \quad \mathbf{B} = \mathbf{F}(x - 8, 2, x - 8).$$

Using Eq. 7.171, **M** appears in a block form and the block corresponding to $k = 1$ is

$$\mathbf{N} = \mathbf{F}\Big(20 - 2x + 2\cos\frac{\pi}{m}(x - 8) + 1 + 2\cos\frac{2\pi}{m}, \quad -8 + 4\cos\frac{\pi}{m},$$
$$19 - 2x + 2\cos\frac{\pi}{m}(x - 8) + 1 + 2\cos\frac{2\pi}{m}, 1\Big); \quad m = n + 1$$

$$\mathbf{A}_1 = \mathbf{F}(0, 1, 0, 0), \quad \mathbf{A}_2 = \mathbf{F}(0, 0, -1, 1).$$

Here, unlike the previous case, **N** does not satisfy $\mathbf{A}_i\mathbf{A}_j = \mathbf{A}_j\mathbf{A}_i$ and no further simplification is possible. Thus, one should form $\det(\mathbf{N}) = 0$ and solve it. Assuming $n = 8$, this solution leads to

$$x = 1.1073 \rightarrow N_{cr} = 7.1804\frac{\pi^2 D}{a^2}.$$

The exact value of the critical load is $N_{cr} = 7.69\dfrac{\pi^2 D}{a^2}$. Here, in place of the determinant of a 49×49 matrix, that of a 7×7 matrix is calculated. Choosing larger values for n, one can easily increase the accuracy of the finite difference approach. The present method reduces the size of a matrix to its square root. It should be added that for a rectangular plate when subdivided into equal lengths in x- and y-directions, similar forms will be formed.

Example 7.24. The natural bending and axial frequencies of the beam shown in Fig. 7.76 is required.

The differential equation governing the bending of this beam can be written as

$$\frac{d^4 w}{dx^4} - \beta^4 w = 0 \ \text{ where } \ \beta = \frac{\rho A\omega^2}{EI}.$$

Choosing $n + 1$ element for discretisation of the beam, the final matrix becomes an $n \times n$ matrix in the following form:

$$\mathbf{M} = \mathbf{F}(5, -4, 6, 1), = 5\mathbf{I} + (-4)\mathbf{T} + \mathbf{S}$$

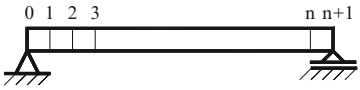

Fig. 7.76 A simple beam and its discretisation

where **T**, **S** and **I** commute two by two, and therefore, Eq. 7.171 can be employed leading to

$$\lambda_{\mathbf{M}} = 5 - 8\cos\alpha + (1 + 2\cos 2\alpha) = 6 - 8\cos\alpha + 2\cos 2\alpha = 4(1 - \cos\alpha)^2$$
$$= 16\sin^4\frac{\alpha}{2}$$
$$\alpha = \frac{k\pi}{m}; \quad m = n + 1.$$

On the other hand,

$$\omega_k = (\beta L)_k^2\sqrt{\frac{EI}{mL^4}} \quad (\beta L)_k^2 = (n+1)^2\sqrt{\lambda} = 4m^2\sin^2\frac{\alpha}{2}$$

leading to the exact answer as

$$n \to \infty \Rightarrow (\beta L)_k^2 = 4m^2\frac{k^2\pi^2}{4m^2} \Rightarrow (\beta L)_k = k\pi \Rightarrow \omega_k = (k\pi)^2\sqrt{\frac{EI}{mL^4}} \quad k = 1 : n.$$

For the axial vibration, the governing equation is as follows:

$$\frac{d^2U}{dx^2} + \alpha^2 U = 0$$

where

$$\alpha = \frac{\rho\omega^2}{E}.$$

In this case, the matrix corresponding to the finite difference will be a tri-diagonal matrix as $\mathbf{M} = \mathbf{F}(2,-1,2)$, and we have the following results:

$$\mathbf{M} = 2\mathbf{I} + (-1)\mathbf{T} \Rightarrow \lambda_{\mathbf{M}} = 2 + (-1)(2\cos\alpha) = 4\sin^2\frac{\alpha}{2},$$

$$\omega_k = \beta_k\sqrt{\frac{EA}{m}} \quad (\beta L)_k = (n+1)\sqrt{\lambda} = 2m\sin\frac{\alpha}{2},$$

$$n \to \infty \Rightarrow (\beta L)_k = 2m\frac{k\pi}{2m} = k\pi \Rightarrow \omega_k = \frac{k\pi}{L}\sqrt{\frac{EA}{m}}.$$

This is an exact answer. For a beam with clamped support, a similar approach leads to the exact result.

7.8 Symmetric Finite Element Formulation Using Canonical Forms: Truss and Frame Elements

In this part, canonical forms are used to decompose the symmetric line elements (truss and beam elements) into sub-elements of less the number of degrees of freedom (DOFs). Then the matrices associated with each sub-element are formed, and finally the matrices associated with each subsystem are combined to form the matrices of the prime element. Therefore, it becomes possible to find the pros and cons of this method and compare the efficiency and simplicity of the present approach to the existing methods.

7.8.1 Sign Convention

In this section, for computation of fundamental matrices for symmetric finite elements, the origin of the local coordinate system of the elements is taken at the centre of symmetry of the elements. Therefore, the symmetry axis or symmetry plane of each element will divide it into two parts: the positive half and the negative half.

If the symmetry axis passes through a node, that node will be numbered as node 1. Otherwise, node number 1 is usually chosen on the positive side of the element. Then, all of the nodes on the positive side are numbered sequentially. Having the nodes on the positive half of the element labelled, say from 1 (or 2) up to k, the rest of the nodes (nodes on the negative half of the element) must be numbered, considering the nodes of the positive side. This means that numbering of the negative side should be started with the node which is associated with the permutation of the first positive node, and is numbered as k + 1. Then, the reflection of the second positive node is labelled as k + 2, and this process is continued. The numbering process is terminated with the negative node which is permutation of the last positive node. Degrees of freedom (DOFs) of each node are numbered following the same rule.

Translation in positive direction and counterclockwise rotation for a positive node (node in the positive part of the element) define the positive translational and rotational DOFs for such nodes. Positive directions for negative nodes are selected such that the DOFs for a node and its reflection are the mirror of each other. For the node which is located at the centre of symmetry (if available), the positive directions can be selected arbitrarily. Figure 7.77 shows two one-dimensional (line) elements and numbering of the nodes and associated positive degrees of freedom, based on the convention described above.

For two- or three-dimensional elements, the general approach for numbering and defining the positive directions are the same. If an element has more than one

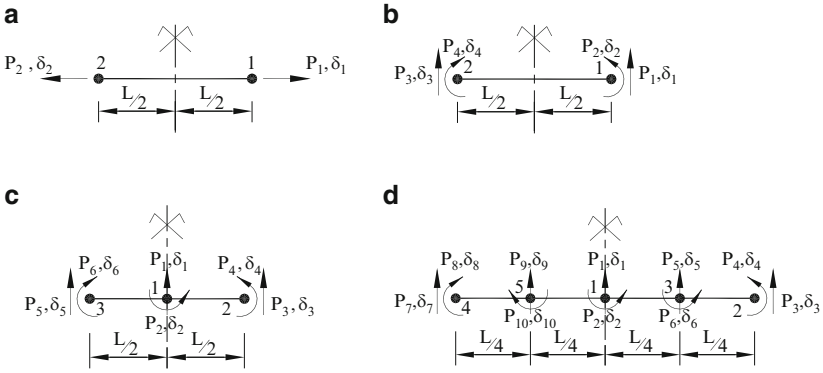

Fig. 7.77 Numbering of the nodes and the DOFs for symmetric line elements. (**a**) Two-node truss element. (**b**) Two-node beam element. (**c**) Three-node beam element. (**d**) Five-node beam element

plane of symmetry, in order to apply the strategy described above, first, one of the planes should be selected as the main plane, and then during the numbering process for positive points (and DOFs), other planes of symmetry are taken into account one by one. Figure 7.78 shows the numbering and positive DOFs for a plane element possessing two main planes of symmetry: 1–1 and 2–2, where plane 1–1 which is in bold, has been taken as the principal symmetry plane. The node in the positive–positive quarter has been selected as node 1, its image with respect to plane 2–2 is labelled as node 2 and then the negative nodes have been numbered with respect to the principal plane of symmetry (1–1). It should be noted that as soon as the positive DOFs for node 1 are fixed, the positive direction for the other DOFs will be determined by means of symmetry properties.

7.8.2 Truss Element

In this section, the properties of special symmetry form of the truss element shown in Fig. 7.77a are utilised in order to decompose the space of variables of this element into *subspaces of divisor and co-divisor*. This decreases the size of matrices and vectors which are involved in formulation of such element and therefore leads to a reduction in calculation time and computational effort.

Although such a reduction does not seem to be significant in small problem of a two-node truss element for which the matrices are 2 by 2, however, this simple example is selected in order to give an overview of the present method.

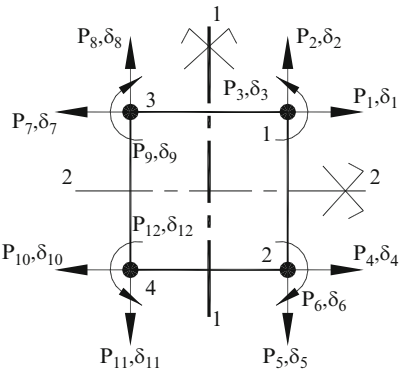

Fig. 7.78 Numbering of the nodes and DOFs for symmetric plane elements

The degrees of freedom of the truss element are collected in a vector **u**, which is called the *displacement vector* of the element:

$$\mathbf{u} = (\delta_1,\ \delta_2)^{\mathrm{t}}. \tag{7.167}$$

It is seen from the configuration of the element (Fig. 7.77a) that this element with the DOFs shown on it has the Form II symmetry. In such symmetric problems, where the only symmetry operation of the system is a symmetry plane, the symmetry analysis of the system will result in decomposition of the vector space of the problem into two independent subspaces, one of which is symmetric and the other is antisymmetric with respect to the plane of symmetry. It is also observed that the divisor C is always associated with the symmetric subspace and the co-divisor D is corresponded to the antisymmetric subspace. From now on, we denote these two subspaces as V_C and V_D, and we call them the divisor and the co-divisor subspaces, respectively.

Assuming that u varies linearly through the element, the linear displacement field within a truss element can be written in terms of the nodal displacements δ_1 and δ_2 as follows (it is noted that $u = \delta_1$ at node 1 and $u = \delta_2$ at node 2):

$$u = N_1.\ \delta_1 + N_2.\ \delta_2 \tag{7.168}$$

where $N_1 = \frac{1}{2} + \frac{x}{l}$ and $N_2 = \frac{1}{2} - \frac{x}{l}$ are the liner shape functions.

In general, the linear displacement field can be written as

$$u = a.x + b. \tag{7.169}$$

We can decompose such a field into two terms, namely, $(a.x)$ and (b). The first term $(a.x)$ shows the displacement field in which the translation of the positive nodes is in the positive direction and the translation of the associated negative nodes are in the negative direction with the same magnitude. Such a displacement field is symmetric with respect to the symmetry plane of the element. On the other hand,

the term (b) is a constant displacement in positive direction at all of the nodes of the element. This displacement field is antisymmetric with respect to the plane of symmetry.

Based on what was mentioned above, the overall displacement field u of the problem can be decomposed into two displacement fields, corresponding to the subspaces V_C and V_D; the first one is symmetric, which we denote it by u_C, and the second one is the field of the antisymmetric subspace V_D, which we denote it by u_D:

$$u_C = a.x \quad \text{and} \quad u_D = b. \tag{7.170}$$

If we denote the DOFs of the symmetric and antisymmetric subsystems (the basis vectors of subspaces V_C and V_D) by Δ_C and Δ_D, respectively, then by substituting the coordinate x = l/2 at node 1, we will have

$$\Delta_C = a.l/2 \;\Rightarrow\; a = \frac{2}{l}\Delta_C, \tag{7.171}$$

$$\Delta_D = b. \tag{7.172}$$

Thus, we can rewrite the equation of displacement fields of the subspaces (Eq. 7.170) as follows:

$$u_C = a.x = \left(\frac{2}{l}\Delta_C\right).x = \left(\frac{2}{l}x\right).\Delta_C \;\Rightarrow\; N_C = \frac{2}{l}x, \tag{7.173}$$

$$u_D = b = \Delta_D = (1).\Delta_D \;\Rightarrow\; N_D = 1, \tag{7.174}$$

where N_C and N_D are the shape functions of the divisor and co-divisor subspaces, respectively.

Now, having the shape function of the element decomposed into symmetric and antisymmetric sub-functions, we can readily find the matrices of the subsystems using potential energy approach.

- *Matrices of Each Subsystem:* The stiffness matrix of an element can be found using the strain energy of the element:

$$U_e = \frac{1}{2}\int_e \sigma^t \varepsilon A dx \tag{7.175}$$

in which $\sigma = E\varepsilon$ (Hooke's law), and ε is calculated from the strain–displacement relationship

$$\varepsilon = \frac{du}{dx}. \tag{7.176}$$

This relation can be written in terms of the element freedoms (δ_i) using the concept of the shape function

$$u = \sum N_i \delta_i \;\Rightarrow\; \varepsilon = \frac{d}{dx}\left(\sum N_i \delta_i\right) \tag{7.177}$$

which yields the matrix equation

$$\boldsymbol{\varepsilon} = \mathbf{B}.\boldsymbol{\delta} \tag{7.178}$$

where the matrix **B** is the *element strain–displacement matrix*.

Now the strain energy term of the element (Eq. 7.175) can be written as follows:

$$U_e = \frac{1}{2}\int_e (E\boldsymbol{\varepsilon})^t \boldsymbol{\varepsilon} A dx = \frac{1}{2}\int_e \boldsymbol{\delta}^t \mathbf{B}^t E \mathbf{B} \boldsymbol{\delta} A dx, \tag{7.179}$$

or

$$U_e = \frac{1}{2}\boldsymbol{\delta}^t \left(\int_e \mathbf{B}^t E \mathbf{B} A dx\right)\boldsymbol{\delta}. \tag{7.180}$$

Therefore, the stiffness matrix of the element will be obtained as

$$\mathbf{k}_e = \int_e \mathbf{B}^t E \mathbf{B} A dx. \tag{7.181}$$

Following the strategy described above, it is now possible to find the strain–displacement matrix **B** of each subspace, using its own shape function. Then the stiffness matrix of each subsystem can be calculated using Eq. 7.181, noting that integration should be carried out over only the positive half of the element.

For the divisor subspace V_C,

$$N_C = \frac{2}{l}x \;\Rightarrow\; u_C = N_C.\Delta_C = \frac{2}{l}x.\Delta_C,$$
$$\mathbf{B}_C = \frac{dN_C}{dx} = \left[\frac{2}{l}\right]. \tag{7.182}$$

Thus,

$$\mathbf{k}_C = EA\left[\int_0^{\frac{1}{2}} \left(\frac{2}{l}\right)\left(\frac{2}{l}\right) dx\right] = \left[\frac{2EA}{l}\right]. \tag{7.183}$$

Similarly, for the co-divisor subspace V_D,

$$N_D = 1 \Rightarrow \mathbf{B}_D = \frac{dN_D}{dx} = [0]. \tag{7.184}$$

Therefore,

$$\mathbf{k}_D = [0]. \tag{7.185}$$

Special attention should be paid to the physical interpretation of the stiffness matrices $\mathbf{k}_C$ and $\mathbf{k}_D$. The symmetric subsystem is associated with divisor subspace, with shape function $N_C = \frac{2}{l}x$ corresponding to a bar element in which the end nodes are moving away from the origin of the element with the same rate. The antisymmetric subsystem associated with the co-divisor subspace, on the other hand, is a bar element in which both of the end nodes are moving in the same direction and with the same rate; the stiffness in such a case will be vanished.

The consistent–mass matrix for an element can be found as

$$\mathbf{m} = \rho A \int_l \mathbf{N}^t.\mathbf{N}\, dx. \tag{7.186}$$

Thus, it is possible to find the mass matrices of the subsystems, using their own shape functions, in a similar manner to those of stiffness matrices:

$$\mathbf{m}_C = \rho A \int_0^{\frac{1}{2}} \left(\frac{2}{l}x\right)^2 dx = \left[\tfrac{1}{6}\rho AL\right], \tag{7.187}$$

$$\mathbf{m}_D = \rho A \int_0^{\frac{1}{2}} (1)^2 dx = \left[\tfrac{1}{2}\rho AL\right]. \tag{7.188}$$

- *Combination of the Subspaces and Finding the Matrices of the Element:* In order to extract the matrix of the symmetric element from its devisor and co-divisor matrices, the properties of the canonical Form II should be considered. One of the main advantages of the method based on linear algebra, compared to similar methods (such as group theory), is in this stage of the procedure.

As it was mentioned in Sect. 7.2.2, a symmetric matrix of canonical Form II has the following pattern:

$$\mathbf{M} = \left[\begin{array}{c|c} \mathbf{A} & \mathbf{B} \\ \hline \mathbf{B} & \mathbf{A} \end{array}\right].$$

For which, the divisor and co-divisor matrices are

$$\mathbf{C} = \mathbf{A} + \mathbf{B} \;\text{ and }\; \mathbf{D} = \mathbf{A} - \mathbf{B}.$$

Now, we have the divisor and co-divisor matrices for the symmetric truss element, and one can easily find the matrices of the main element, combining the condensed submatrices as follows:

$$\mathbf{A} = \tfrac{1}{2}(\mathbf{C} + \mathbf{D}) \;\text{ and }\; \mathbf{B} = \tfrac{1}{2}(\mathbf{C} - \mathbf{D}). \tag{7.189}$$

Thus, for the stiffness matrix, we will have

$$\mathbf{k}_A = \tfrac{1}{2}(\mathbf{k}_C + \mathbf{k}_D) = \frac{EA}{2l}[2+0] = \left[\frac{EA}{l}\right]. \tag{7.190}$$

$$\mathbf{k}_B = \tfrac{1}{2}(\mathbf{k}_C - \mathbf{k}_D) = \frac{EA}{2l}[2-0] = \left[\frac{EA}{l}\right], \tag{7.191}$$

which results in the stiffness matrix of the truss element as

$$\mathbf{k}_e = \frac{EA}{l}\left[\begin{array}{c|c} 1 & 1 \\ \hline 1 & 1 \end{array}\right]. \tag{7.192}$$

Similarly, for the consistent–mass matrix,

$$\mathbf{m}_A = \tfrac{1}{2}(\mathbf{m}_C + \mathbf{m}_D) = \frac{\rho AL}{2}\left[\frac{1}{6} + \frac{1}{2}\right] = \left[\frac{\rho AL}{3}\right], \tag{7.193}$$

$$\mathbf{m}_B = \tfrac{1}{2}(\mathbf{m}_C - \mathbf{m}_D) = \frac{\rho AL}{2}\left[\frac{1}{6} - \frac{1}{2}\right] = \left[-\frac{\rho AL}{6}\right], \tag{7.194}$$

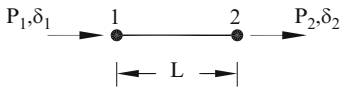

Fig. 7.79 Conventional node numbering and the positive DOFs for truss elements

$$\Rightarrow \mathbf{m}_e = \frac{\rho AL}{6}\left[\begin{array}{c|c} 2 & -1 \\ \hline -1 & 2 \end{array}\right]. \tag{7.195}$$

Finally, it should be noted that the above matrices are resulted using the sign convention described in Sect. 7.3. A more conventional node numbering and sign convention for truss elements is shown in Fig. 7.79. In order to convert the results to this convention, it is enough to reverse the sign of the first line and then the first column of the matrices. This action is physically justified as follows: An out-of-plane rotation on element of Fig. 7.77a will result in the same node numbering with the conventional element, Fig. 7.79. Then it is enough to change the positive direction for freedom δ_1 in order to make two elements completely identical. The final results are the well-known matrices of a two-dimensional truss element:

$$\mathbf{k}_e = \frac{EA}{l}\left[\begin{array}{c|c} 1 & -1 \\ \hline -1 & 1 \end{array}\right] \text{ and } \mathbf{m}_e = \frac{\rho \mathrm{AL}}{6}\left[\begin{array}{c|c} 2 & 1 \\ \hline 1 & 2 \end{array}\right]. \tag{7.196}$$

7.8.3 Beam Element

The concepts discussed for truss elements can be repeated here for the beam elements. The element of Fig. 7.77b clearly shows the canonical Form II symmetry. Again, the vector space of the problem can be decomposed into the symmetric divisor subspace and the antisymmetric co-divisor subspace.

The process starts with decomposition of the shape function of the displacement field. Whereas both the nodal displacements and nodal slopes are involved in a beam element, one should define Hermite shape functions, which satisfy nodal value and slope continuity requirements. Each of the shape functions is of cubic order represented by

$$N_i = a_i + b_i x + c_i x^2 + d_i x^3. \tag{7.197}$$

The displacement field of the element will be of cubic order, and the rotation of each point through the element will be calculated from the following quadratic equation:

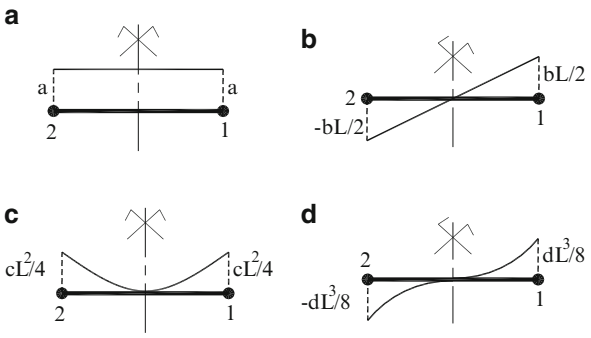

Fig. 7.80 Terms of v(x).
(**a**) v_1 = a: symmetric.
(**b**) v_2 = bx: antisymmetric.
(**c**) $v_3 = cx^2$: symmetric.
(**d**) $v_4 = dx^3$: antisymmetric

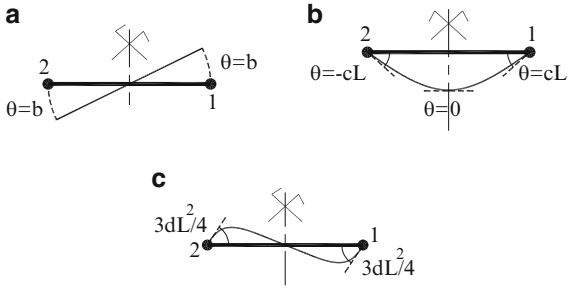

Fig. 7.81 Terms of $v'(x)$.
(**a**) $v'_1 = b$: antisymmetric.
(**b**) $v'_2 = 2cx$: symmetric.
(**c**) $v'_3 = 3dx^2$: antisymmetric

$$v(x) = a + bx + cx^2 + dx^3, \tag{7.198}$$

$$v'(x) = \frac{d}{dx}v(x) = b + 2cx + 3dx^2. \tag{7.199}$$

Each term of the displacement field equation and its first derivation (which shows the rotations) is studied individually in Figs. 7.80 and 7.81, respectively. Similar to what was mentioned for the truss element, we separate the symmetric and antisymmetric terms and allocate them to the divisor and co-divisor subspaces, respectively.

Based on Figs. 7.80 and 7.81, the displacement field of the element can be decomposed as follows:

For the divisor subspace,

$$\begin{aligned} v_C(x) &= a + cx^2, \\ v'_C(x) &= 2cx. \end{aligned} \tag{7.200}$$

For the co-divisor subspace,

$$v_D(x) = bx + dx^3,$$
$$v'_D(x) = b + 3dx^2. \tag{7.201}$$

At node 1 (x = l/2), we have

$$v_D = \Delta_{1D}, \quad v'_D = \Delta_{2D},$$
$$v_C = \Delta_{1C}, \quad v'_C = \Delta_{2C}. \tag{7.202}$$

The values of a, b, c and d can be found as follows:

$$\begin{Bmatrix} v_C \\ v'_C \end{Bmatrix} = \begin{bmatrix} 1 & x^2 \\ 0 & 2x \end{bmatrix} \begin{Bmatrix} a \\ c \end{Bmatrix} \Rightarrow \begin{Bmatrix} \Delta_{1C} \\ \Delta_{2C} \end{Bmatrix} = \begin{bmatrix} 1 & \frac{l^2}{4} \\ 0 & l \end{bmatrix} \begin{Bmatrix} a \\ c \end{Bmatrix} \Rightarrow \begin{cases} a = \Delta_{1C} - \frac{\Delta_{2C}}{4} \\ c = \frac{\Delta_{2C}}{l} \end{cases},$$

$$\begin{Bmatrix} v_D \\ v'_D \end{Bmatrix} = \begin{bmatrix} x & x^3 \\ 1 & 3x^2 \end{bmatrix} \begin{Bmatrix} b \\ d \end{Bmatrix} \Rightarrow \begin{Bmatrix} \Delta_{1D} \\ \Delta_{2D} \end{Bmatrix} = \begin{bmatrix} \frac{l}{2} & \frac{l^3}{8} \\ 1 & \frac{3l^2}{4} \end{bmatrix} \begin{Bmatrix} b \\ d \end{Bmatrix} \Rightarrow \begin{cases} b = \frac{3\Delta_{1D}}{l} - \frac{\Delta_{2D}}{2} \\ d = \frac{2\Delta_{2D}}{l^2} - \frac{4\Delta_{1D}}{l^3} \end{cases},$$

$$\Rightarrow \begin{Bmatrix} a \\ c \end{Bmatrix} = \begin{bmatrix} 1 & \frac{-l}{4} \\ 0 & \frac{1}{l} \end{bmatrix} \begin{Bmatrix} \Delta_{1C} \\ \Delta_{2C} \end{Bmatrix} \quad \text{and} \quad \begin{Bmatrix} b \\ d \end{Bmatrix} = \begin{bmatrix} \frac{3}{l} & \frac{-1}{2} \\ \frac{-4}{l^3} & \frac{2}{l^2} \end{bmatrix} \begin{Bmatrix} \Delta_{1D} \\ \Delta_{2D} \end{Bmatrix}. \tag{7.203}$$

Substituting these values in Eq. 7.202 results in

$$\begin{Bmatrix} v_C \\ v'_C \end{Bmatrix} = \begin{bmatrix} 1 & x^2 \\ 0 & 2x \end{bmatrix} \begin{bmatrix} 1 & \frac{-l}{4} \\ 0 & \frac{1}{l} \end{bmatrix} \begin{Bmatrix} \Delta_{1C} \\ \Delta_{2C} \end{Bmatrix} = \begin{bmatrix} 1 & \frac{x^2}{l} - \frac{l}{4} \\ 0 & \frac{2x}{l} \end{bmatrix} \begin{Bmatrix} \Delta_{1C} \\ \Delta_{2C} \end{Bmatrix}, \tag{7.204}$$

$$\begin{Bmatrix} v_D \\ v'_D \end{Bmatrix} = \begin{bmatrix} x & x^3 \\ 1 & 3x^2 \end{bmatrix} \begin{bmatrix} \frac{3}{l} & \frac{-1}{2} \\ \frac{-4}{l^3} & \frac{2}{l^2} \end{bmatrix} \begin{Bmatrix} \Delta_{1D} \\ \Delta_{2D} \end{Bmatrix}$$
$$= \begin{bmatrix} \frac{3x}{l} - 4\left(\frac{x}{l}\right)^3 & 2\frac{x^3}{l^2} - \frac{x}{2} \\ \frac{3}{l} - 12\frac{x^2}{l^3} & 3\left(\frac{x}{l}\right)^2 - \frac{1}{2} \end{bmatrix} \begin{Bmatrix} \Delta_{1D} \\ \Delta_{2D} \end{Bmatrix}. \tag{7.205}$$

Therefore, the shape function matrix of each subspace can be written as

$$\mathbf{N}_C = \left[1 \quad \frac{x^2}{l} - \frac{l}{4}\right] \text{ and } \mathbf{N}_D = \left[\frac{3x}{l} - 4\left(\frac{x}{l}\right)^3 \quad 2\frac{x^3}{l^2} - \frac{x}{2}\right]. \tag{7.206}$$

This is crucial for the continuation of the solution. Based on the potential energy approach, we can write the strain energy equation for a beam element as

$$U_e = \frac{1}{2}EI\left(\int_e \left(\frac{d^2v}{dx^2}\right)^2 dx\right) \tag{7.207}$$

in which

$$v = \mathbf{N}\delta \;\Rightarrow\; \frac{d^2v}{dx^2} = \left(\frac{d^2\mathbf{N}}{dx^2}\right)\delta$$

Thus, we have

$$U_e = \frac{1}{2}\delta^t\left(EI\int_e \left(\frac{d^2\mathbf{N}}{dx^2}\right)^t\left(\frac{d^2\mathbf{N}}{dx^2}\right)dx\right)\delta \tag{7.208}$$

which means that the stiffness matrix of the beam element can be calculated as

$$\mathbf{k}_e = EI\int_e \left(\frac{d^2\mathbf{N}}{dx^2}\right)^t\left(\frac{d^2\mathbf{N}}{dx^2}\right)dx. \tag{7.209}$$

Now it will be possible to find the stiffness matrix of each subsystem using the shape function matrix of its subspace, noting the fact that the integration should be carried out over only the positive half of the element:

For divisor subspace,

$$\frac{d^2\mathbf{N}_C}{dx^2} = \left[0 \quad \frac{2}{l}\right] \;\Rightarrow\; \left(\frac{d^2\mathbf{N}_C}{dx^2}\right)^t\left(\frac{d^2\mathbf{N}_C}{dx^2}\right) = \begin{bmatrix}0\\ \frac{2}{l}\end{bmatrix}\left[0 \quad \frac{2}{l}\right] = \begin{bmatrix}0 & 0\\ 0 & \frac{4}{l^2}\end{bmatrix}$$

$$\Rightarrow\; \mathbf{k}_C = EI\int_0^{\frac{l}{2}} \begin{bmatrix}0 & 0\\ 0 & \frac{4}{l^2}\end{bmatrix}dx = \frac{EI}{l^3}\begin{bmatrix}0 & 0\\ 0 & 2l^2\end{bmatrix}. \tag{7.210}$$

And for the co-divisor subspace,

$$\frac{d^2\mathbf{N}_D}{dx^2}=\begin{bmatrix}-\frac{24x}{l^3} & \frac{12x}{l^2}\end{bmatrix}\Rightarrow\left(\frac{d^2\mathbf{N}_D}{dx^2}\right)^t\left(\frac{d^2\mathbf{N}_D}{dx^2}\right)=\begin{bmatrix}-\frac{24x}{l^3}\\ \frac{12x}{l^2}\end{bmatrix}\begin{bmatrix}-\frac{24x}{l^3} & \frac{12x}{l^2}\end{bmatrix}$$

$$=12\times 12\begin{bmatrix}\frac{4x^2}{l^6} & -\frac{2x^2}{l^5}\\ -\frac{2x^2}{l^5} & \frac{x^2}{l^4}\end{bmatrix}$$

$$\Rightarrow\ \mathbf{k}_D=EI\int_0^{\frac{l}{2}}\begin{bmatrix}\frac{4x^2}{l^6} & -\frac{2x^2}{l^5}\\ -\frac{2x^2}{l^5} & \frac{x^2}{l^4}\end{bmatrix}dx=\frac{EI}{l^3}\begin{bmatrix}24 & -12l\\ -12l & 6l^2\end{bmatrix}. \tag{7.211}$$

It should be noted that both of the matrices $\mathbf{k}_C$ and $\mathbf{k}_D$ are symmetric. This is due to the fact that these are stiffness matrices of subsystems. Now it is easy to combine the matrices of the subsystems and find the factors of stiffness matrix of the element, based on what was mentioned for the truss element:

$$\mathbf{k}_A=\tfrac{1}{2}(\mathbf{k}_C+\mathbf{k}_D)=\frac{1}{2}\frac{EI}{l^3}\left(\begin{bmatrix}0 & 0\\ 0 & 2l^2\end{bmatrix}+\begin{bmatrix}24 & -12l\\ -12l & 6l^2\end{bmatrix}\right)$$

$$=\frac{EI}{l^3}\begin{bmatrix}12 & -6l\\ -6l & 4l^2\end{bmatrix}, \tag{7.212}$$

$$\mathbf{k}_B=\tfrac{1}{2}(\mathbf{k}_C-\mathbf{k}_D)=\frac{1}{2}\frac{EI}{l^3}\left(\begin{bmatrix}0 & 0\\ 0 & 2l^2\end{bmatrix}-\begin{bmatrix}24 & -12l\\ -12l & 6l^2\end{bmatrix}\right)$$

$$=\frac{EI}{l^3}\begin{bmatrix}-12 & 6l\\ 6l & -2l^2\end{bmatrix}. \tag{7.213}$$

Eventually, the stiffness matrix of the beam element will be as follows:

$$\mathbf{k}_e=\frac{EI}{l^3}\left[\begin{array}{cc|cc}12 & -6l & -12 & 6l\\ -6l & 4l^2 & 6l & -2l^2\\ \hline -12 & 6l & 12 & -6l\\ 6l & -2l^2 & -6l & 4l^2\end{array}\right]. \tag{7.214}$$

Other matrices of the element can be found exactly in the same manner as was described here, using the shape function matrices of the individual subspaces.

A beam element with classical system of nodal numbering and sign convention for DOFs is shown in Fig. 7.82. As it is seen, the element for which we derived the stiffness matrix (Fig. 7.77b) can coincide with this element by an out-of-plane rotation and changing the direction of DOF δ_2. Therefore, in order to adapt the

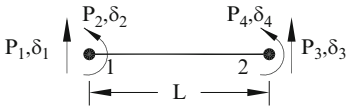

Fig. 7.82 Conventional node numbering and positive DOFs for beam elements

stiffness matrix of Eq. 7.214 to conventional form, it is enough to reverse the sign of the entries of the second line and the second column as follows:

$$\mathbf{k}_e = \frac{EI}{l^3}\left[\begin{array}{cc|cc} 12 & 6l & -12 & 6l \\ 6l & 4l^2 & -6l & 2l^2 \\ \hline -12 & -6l & 12 & -6l \\ 6l & 2l^2 & -6l & 4l^2 \end{array}\right]. \tag{7.215}$$

7.8.4 Discussion

In this part a new computational approach is presented for finding the matrices of elements in FEM, using the symmetry analysis of each element. Here, we first adapt the appearance of the element and its degrees of freedom with one of the canonical symmetry forms which are well known in linear algebra. This is done by the means of an appropriate numbering and sign convention. Then, we use the properties of the canonical forms in order to decompose the element into a number of sub-elements. This reduces the number of DOFs which are involved in forming the matrices of the element. In other words, we decompose the vector space of the first problem into a number of independent subspaces with smaller orders. Each of the resulted subspaces is physically associated with a symmetry type of the structure (this is the meaning of the symmetry analysis through which we decouple different symmetry modes of a symmetrical system). We use the concept of symmetry type of each subspace and the decomposition of the overall shape function of the element into a number of sub-functions, each of which corresponds to the symmetry type of one of the subspaces (e.g. symmetric and antisymmetric terms). When such a decomposition is valid and each sub-element has its own shape function, it will be very easy to form the matrices of each sub-element by means of one of the conventional methods – such as potential energy method – using its own shape function. Finally, we combine the matrices of different sub-elements, based on the properties of the canonical forms, and construct the matrix of the original element.

The method is originally inspired by group-theoretical methods which are presented in the literature, but the present approach involves less computational time and effort, and relatively less judgment is needed in this method, compared to the pure group-theoretical approach. Combination of matrices of sub-elements and forming the matrix of the main element is much easier and more direct in this

method, and in the case of elements with odd number of nodes, this approach seems to be more adaptable.

The present method can be more helpful in the case of complex elements having a number of nodes, where usually one of the canonical forms of symmetry exists; however, in this part, only the formulation for simple truss and beam elements is derived, since the focus of this part was on the general concepts. It should be noted that in the case of more complex elements, the same steps are involved. As an example, this idea can easily be applied to three-node and five-node line elements, where the symmetry of the element has the canonical Form III symmetry.

7.9 Eigensolution of Rotationally Repetitive Space Structures

In this part the eigensolution for calculating the buckling load and free vibration of systems are presented using a canonical form from linear algebra, known as circulant matrix. This form is block tri-diagonal matrices with additional corner blocks and occurs in matrices concerned with graph models associated with rotationally repetitive structures. In this method, the structure is decomposed into repeated substructures, and the solution for static analysis is obtained partially, and the problem of finding the eigenvalues and eigenvectors for buckling loads of the main structures is transformed into calculating those of their special repeating substructures.

7.9.1 Basic Formulation of the Used Stiffness Matrix

Basically, a rotationally repetitive structure is a structure constituting a cyclically symmetric configuration with angle of cyclic symmetry equal to θ as shown in symbolic manner in Fig. 7.83.

Let the configuration be divided by some imaginary lines or surfaces into $n = \frac{2\pi}{\theta}$ segments $S_1, S_2 \ldots S_n$. The segmental division must satisfy the following requirements:

A. An angle ψ_i belongs to each segment by which the direction of first DOFs of nodes allocated in that segment is defined, and this angle is an integer multiple of the angle θ. Obviously the nodes located in a segment will have a same angle ψ_i.
B. The imaginary segmental boundaries may not pass through any joint so that the segment to which a given joint belongs can be uniquely determined. The word 'joint' is used here to refer to a joint in the skeletal system but can be used as a nodal point in continuum, and this convention is followed throughout.

As the consequence of the above conditions, the segment can not contain any joint lying on the axis of symmetry.

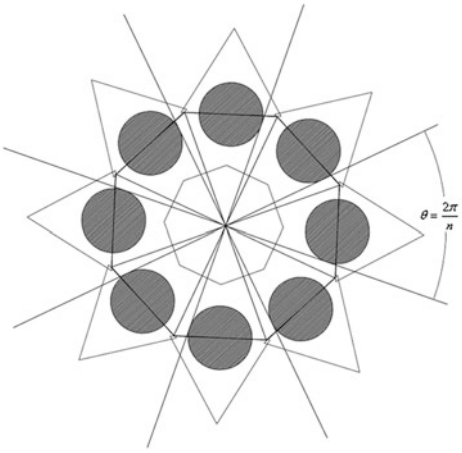

Fig. 7.83 Symbolic representation of a rotationally repetitive structure

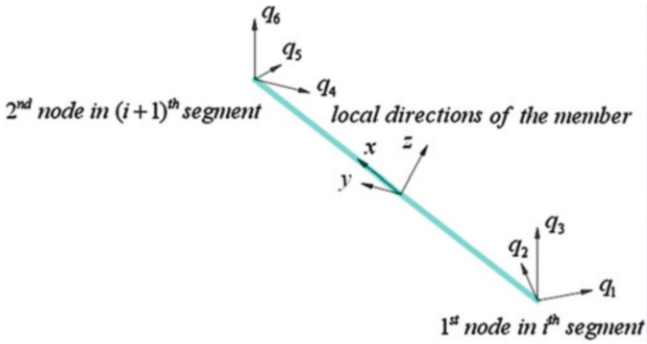

Fig. 7.84 A 3D beam element between two consecutive segments

The stiffness matrix of a typical element having nodes in different segments, that is, an element between two consecutive segments, is calculated as follows:

The stiffness matrix in the local (element) coordinate system is the common stiffness matrix for a 3D beam element (shown in Fig. 7.84); however, the transformation matrix from local coordinate system to the global coordinate system is as follows:

The stiffness matrix of each element is calculated in its local coordinate system and transformed into the global coordinate system (segmental directions) specified at its extreme nodes by the following transformation matrix:

$$\mathbf{T} = \begin{bmatrix} \mathbf{T}_{11} & & & \\ & \mathbf{T}_{11} & & \\ & & \mathbf{T}_{22} & \\ & & & \mathbf{T}_{22} \end{bmatrix},$$

$$\text{where } \mathbf{T}_{11} = \begin{bmatrix} T_{x1} & T_{x2} & T_{x3} \\ T_{y1} & T_{y2} & T_{y3} \\ T_{z1} & T_{z2} & T_{z3} \end{bmatrix} \text{ and } \mathbf{T}_{22} = \begin{bmatrix} T_{x4} & T_{x5} & T_{x6} \\ T_{y4} & T_{y5} & T_{y6} \\ T_{z4} & T_{z5} & T_{z6} \end{bmatrix}. \quad (7.216)$$

Here, T_{xi} is the cosine of the angle between x-axis (element direction from first point to second one) and direction of the ith degree of freedom in the global coordinate systems (segmental directions for DOFs), and the subscripts y and z are representatives for directions of principal axes in the cross section of the element. The overall stiffness matrix of the rotationally repetitive space structure is obtained by assembling the stiffness matrices of the elements which has a special canonical form introduced in Sect. 7.3.

Since each extreme node of a typical element shown in Fig. 7.1 has different segmental directions, these will have different ψ_i, and the transformation matrix between local coordinates and global coordinates will be as depicted in Eq. 7.206.

7.9.2 *A Canonical Form Associated with Rotationally Repetitive Structures*

In this section, a canonical form is presented for rotationally repetitive structures, and the efficient eigensolution via this form is followed. The methodology for nodal numbering is as follows:

The difference between the number of an arbitrarily selected node in an arbitrarily segment and the number of corresponding node in the adjacent segment is constant.

If the stiffness matrix of a rotationally repetitive structure is formed using the transformation of Eq. 7.214, then the following canonical form will be achieved.

$$\mathbf{M} = \begin{bmatrix} \mathbf{A} & \mathbf{B} & \mathbf{0} & \mathbf{0} & \dots & \mathbf{0} & \mathbf{0} & \mathbf{B}^t \\ \mathbf{B}^t & \mathbf{A} & \mathbf{B} & \mathbf{0} & \dots & \mathbf{0} & \mathbf{0} & \mathbf{0} \\ \mathbf{0} & \mathbf{B}^t & \mathbf{A} & \mathbf{B} & \dots & \mathbf{0} & \mathbf{0} & \mathbf{0} \\ \mathbf{0} & \mathbf{0} & \mathbf{B}^t & \ddots & \ddots & \mathbf{0} & \mathbf{0} & \mathbf{0} \\ \vdots & \vdots & \vdots & \ddots & \mathbf{A} & \mathbf{B} & \mathbf{0} & \mathbf{0} \\ \mathbf{0} & \mathbf{0} & \mathbf{0} & \mathbf{0} & \mathbf{B}^t & \mathbf{A} & \mathbf{B} & \mathbf{0} \\ \mathbf{0} & \mathbf{0} & \mathbf{0} & \mathbf{0} & \mathbf{0} & \mathbf{B}^t & \mathbf{A} & \mathbf{B} \\ \mathbf{B} & \mathbf{0} & \mathbf{0} & \mathbf{0} & \mathbf{0} & \mathbf{0} & \mathbf{B}^t & \mathbf{A} \end{bmatrix}. \quad (7.217)$$

From now on this canonical form will be referred to as block tri-diagonal matrix with corner blocks abbreviated as BTMCB.

7.9.3 Eigensolution for Finding Buckling Load of Structure with the BTMCB Form

Block diagonalisation of the BTMCB forms is discussed in Sect. 4.12, and here the eigensolution for finding the buckling load of rotationally repetitive structures, with no node on the axis of symmetry, and under vertical lumped loads located at the extreme nodes of the elements, is presented via the BTMCB form. The smallest eigenvalue shows the buckling load of the system, and the corresponding eigenvector is the buckling mode shape.

If the stiffness matrix of a rotationally repetitive structure is generated using the transformation matrix presented in Sect. 7.2, the BTMCB form will be achieved. In order to find the buckling load of the system, the geometric stiffness matrix of the structure should be generated.

If the segmental stiffness matrix for each segment of structure is separately generated, it can be observed that the segmental stiffness matrices are the same, and the displacements in different segmental coordinates are identical. From the latter fact, it can be realised that internal forces made in identical elements within any two arbitrarily selected segments due to displacements occurred in segmental coordinates are equal.

It is obvious that the values of entries in local geometric stiffness matrix for an element depend on forces made in its local degrees of freedom, and there are same displacements and consequently tantamount identical forces for similar elements in any two arbitrarily selected segments. As the transformation matrix should be the same for both of elastic stiffness and geometric stiffness matrices, a BTMCB form in geometric stiffness matrix similar to that of elastic stiffness matrix is expected.

After generating the global geometric stiffness matrix of structure as it was predicted, a similar BTMCB form will be obtained. Thus, the eigensolution for finding the eigenvalues of $|[\mathbf{K}^{e}] - P[\mathbf{K}^{g}]| = 0$ via this BTMCB form becomes possible. Here, $\mathbf{K}^{e}$ is the elastic stiffness matrix, and $\mathbf{K}^{g}$ is the geometric stiffness matrix of the structure. The process of calculation is as follows:

1.1 First the elastic stiffness matrices of elements are formed in their local coordinate system and then transformed into the global coordinates. These matrices are assembled to form the overall elastic stiffness matrix of the rotationally repetitive structure.
1.2 In this step, a static problem is solved, for the stiffness matrix calculated in the previous step and for the forces lumped in the nodes. This leads to the nodal displacements of the structure in the global coordinate system.
1.3 The results obtained in step 2 are used to calculated displacements in local coordinate system for each element.

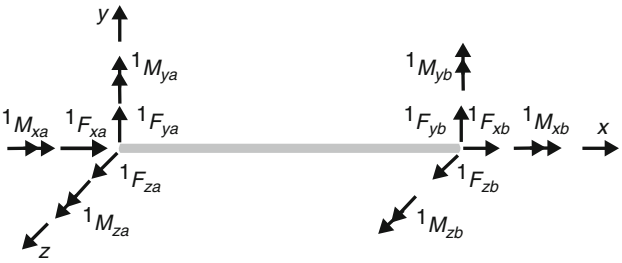

Fig. 7.85 The internal forces of a typical element in its local coordinate system

1.4 Using the displacements calculated in step 3 and local stiffness matrix of each element, the internal forces are computed in the local coordinate system of the element as defined in Fig. 7.85.

1.5 Utilising the internal forces calculated in step 4 in geometric stiffness matrix of a 3D beam element presented in Eq. 7.247, the local geometric stiffness matrix of elements is computed:

$$[\mathbf{K}^g] = \begin{bmatrix} a & c & & & & & -a & -c & & & \\ b & & d & g & -h & -a & -b & & l & -g & -h \\ & b & e & h & g & -c & & -b & m & h & -g \\ & & f & i & k & & -d & -e & -f & -i & -k \\ & & & j & & & -g & -h & -i & n & -o \\ & & & & j & & h & -g & -k & o & n \\ & & & & & & a & c & & & \\ & & & & & & b & & -l & g & h \\ & & & & & & & b & -m & -h & g \\ & sym & & & & & & & f & a & c \\ & & & & & & & & & j & \\ & & & & & & & & & & j \end{bmatrix} \tag{7.218}$$

where

$$a = \frac{^1M_{za}+^1M_{zb}}{L^2},\ b = \frac{6\,^1F_{xb}}{5L},\ c = -\frac{^1M_{ya}+^1M_{yb}}{L^2},\ d = \frac{^1M_{ya}}{L},\ e = \frac{^1M_{za}}{L}$$
$$f = \frac{^1F_{xb}J}{AL},\ g = \frac{^1M_{xb}}{L},\ h = -\frac{^1F_{xb}}{10},\ i = \frac{^1M_{za}+^1M_{zb}}{6},\ j = \frac{2\,^1F_{xb}L}{15},$$
$$k = -\frac{^1M_{ya}+^1M_{yb}}{6},\ l = \frac{^1M_{yb}}{L},\ m = \frac{^1M_{zb}}{L},\ n = -\frac{^1F_{xb}L}{30},\ o = -\frac{^1M_{xb}}{2}.$$

1.6 The process of assembling of the geometric stiffness matrices leads to the formation of the structural geometric stiffness matrix having the BTMCB form.

1.7 After calculating the geometric stiffness matrix of structure via the above six steps, the eigensolution with BTMCB form is performed as follows:

A. Extract the submatrices **A** and **B** from the geometric and elastic stiffness matrices using the mathematical process of Sect. 7.4 to construct an eigenproblem in the BTMCB form.
B. Generate the **H** matrix. This depends on the number of repetitive substructures; however, calculating its eigenvalues, λ_j, depends on the latter number being odd or even.
C. Generate the block matrices $\mathbf{BL}_{\mathrm{j}}$ from matrices **A** and **B** for both elastic and geometric stiffness matrices of the structure.
D. Define the block submatrices $\left(\mathbf{BL}_{\mathbf{K}^{\mathrm{g}-1}\mathbf{K}^{\mathrm{e}}}\right)_{\mathrm{j}}$ for each pair of blocks $\left(\mathbf{BL}_{\mathbf{K}^{\mathrm{g}}}\right)_{\mathrm{j}}$ and $\left(\mathbf{BL}_{\mathbf{K}^{\mathrm{e}}}\right)_{\mathrm{j}}$ via the following equation:

$$\left(\mathbf{BL}_{\mathbf{K}^{\mathrm{g}-1}\mathbf{K}^{\mathrm{e}}}\right)_{\mathrm{j}} = \left(\mathbf{BL}_{\mathbf{K}^{\mathrm{g}}}\right)_{\mathrm{j}}^{-1}\left(\mathbf{BL}_{\mathbf{K}^{\mathrm{e}}}\right)_{\mathrm{j}}. \tag{7.219}$$

E. Find the eigenvalues of the block matrices calculated in step D and gather all of the eigenvalues calculated by means of Eq. 7.249:

$$\mathrm{eig}\left(\mathbf{K}^{\mathrm{g}-1}\mathbf{K}^{\mathrm{e}}\right) = \bigcup_{\mathrm{j}=1}^{\mathrm{n}} \mathrm{eig}\left(\mathbf{BL}_{\mathbf{K}^{\mathrm{g}-1}\mathbf{K}^{\mathrm{e}}}\right)_{\mathrm{j}} = \bigcup_{\mathrm{j}=1}^{\mathrm{n}} \mathrm{eig}\left(\left(\mathbf{BL}_{\mathbf{K}^{\mathrm{g}}{}_{\mathrm{j}}}\right)^{-1}\left(\mathbf{BL}_{\mathbf{K}^{\mathrm{e}}{}_{\mathrm{j}}}\right)\right). \tag{7.220}$$

F. The eigenvector corresponding to each eigenvalue of block submatrix $\mathbf{BL}_{\mathbf{K}^{\mathrm{g}-1}\mathbf{K}^{\mathrm{e}}}$ is obtained by the following relationship:

$$\mathbf{BL}_{\mathrm{j}}\mathbf{Y}_{\mathrm{i}} = \mu_{\mathrm{i}}\mathbf{Y}_{\mathrm{i}}. \tag{7.221}$$

Each eigenvalue of the block matrix $\mathbf{BL}_{\mathrm{j}}$ obtained by Eq. 7.249 is an eigenvalue of $\mathrm{K}^{\mathrm{g}^{-1}}\mathrm{K}^{\mathrm{e}}$ matrix; however, the eigenvectors obtained by Eq. 7.250 need to be healed by a Kronecker product as

$$\boldsymbol{\phi}_{\mathrm{i}} = \mathbf{U}(\mathbf{e}_{\mathrm{j}} \otimes \mathbf{Y}_{\mathrm{i}}) = (\mathbf{X} \otimes \mathbf{I})(\mathbf{e}_{\mathrm{j}} \otimes \mathbf{Y}_{\mathrm{i}}) = \mathbf{X}\mathbf{e}_{\mathrm{j}} \otimes \mathbf{I}\mathbf{Y}_{\mathrm{i}} \quad \rightarrow \quad \boldsymbol{\phi}_{\mathrm{i}} = \mathbf{X}^{\mathrm{j}} \otimes \mathbf{Y}_{\mathrm{i}} \tag{7.222}$$

where $\mathbf{X}^{\mathrm{j}}$ is the eigenvector of corresponding to the j^{th} eigenvalue of the matrix **H**. The matrix **X** is calculated by Eq. 7.240. Finally, if an eigenvalue calculated by Eq. 7.249 is a simple one, the corresponding eigenvector will be real, but if the eigenvalue is a multiple root of the characteristic polynomial, the corresponding eigenvector will be complex. Adding two conjugate eigenvectors will result in the real eigenvectors for both of them.

7.9.4 *Eigensolution for Free Vibration of Structural Systems with the BTMCB Form*

Using the nodal numbering presented in Sect. 7.3, the elastic stiffness matrix of the structure shown in Fig. 7.1 is formed, as explained in Sect. 7.2. The corresponding lumped mass matrix is then generated by classic methods. The matrix corresponding to this dynamic set will be in the following BTMCB form:

$$[\mathbf{K}] - \omega^2[\mathbf{M}] = \begin{bmatrix} \mathbf{A} & \mathbf{B} & \mathbf{0} & \mathbf{0} & \dots & \mathbf{0} & \mathbf{0} & \mathbf{B}^t \\ \mathbf{B}^t & \mathbf{A} & \mathbf{B} & \mathbf{0} & \dots & \mathbf{0} & \mathbf{0} & \mathbf{0} \\ \mathbf{0} & \mathbf{B}^t & \mathbf{A} & \mathbf{B} & \dots & \mathbf{0} & \mathbf{0} & \mathbf{0} \\ \mathbf{0} & \mathbf{0} & \mathbf{B}^t & \ddots & \ddots & \mathbf{0} & \mathbf{0} & \mathbf{0} \\ \vdots & \vdots & \vdots & \ddots & \mathbf{A} & \mathbf{B} & \mathbf{0} & \mathbf{0} \\ \mathbf{0} & \mathbf{0} & \mathbf{0} & \mathbf{0} & \mathbf{B}^t & \mathbf{A} & \mathbf{B} & \mathbf{0} \\ \mathbf{0} & \mathbf{0} & \mathbf{0} & \mathbf{0} & \mathbf{0} & \mathbf{B}^t & \mathbf{A} & \mathbf{B} \\ \mathbf{B} & \mathbf{0} & \mathbf{0} & \mathbf{0} & \mathbf{0} & \mathbf{0} & \mathbf{B}^t & \mathbf{A} \end{bmatrix}. \tag{7.223}$$

Therefore, the natural frequencies and natural modes can be found by

$$\left|[\mathbf{K}] - \omega^2[\mathbf{M}]\right| = 0. \tag{7.224}$$

The eigenvalues and eigenvectors are denoted by ω_i and φ_i, respectively.

Applying the BTMCB form to Eq. 7.35 for calculating the eigenvalues and eigenvectors of the above set is similar to the process mentioned in Sect. 7.5. After generating the mass matrix of structure, the process of finding the natural frequencies and natural mode shapes can be performed as follows:

1.8 Extract the submatrices **A** and **B** from the mass and stiffness matrices using the mathematical process presented in Sect. 7.4.

1.9 Generate the **H** matrix, which depends on the number of repetitive substructures. Calculating the concerned eigenvalues, λ_j, depends on the latter number being odd or even.

1.10 Generate the block matrices $\mathbf{BL}_j$ from submatrices **A** and **B** for both elastic stiffness and mass matrices of structure.

1.11 Find m eigenvalues for each of n pairs of block matrices $(\mathbf{BL_M})_j$ and $(\mathbf{BL_{K^e}})_j$ calculated in the previous step by solving Eq. 7.254:

$$\left|\mathbf{BL}_{\mathbf{K^e}} - \omega^2\mathbf{BL}_{\mathbf{M}}\right|_j = 0 \;\Rightarrow\; \bigcup_{i=1}^{m} \omega_j{}^2. \tag{7.225}$$

1.12 Gather all of the eigenvalues calculated by Eq. 7.254 as in the following equation:

$$\zeta_i = {\omega_i}^2 = \bigcup_{j=1}^{n} \left(\bigcup_{i=1}^{m} {\omega_j}^2 \right). \tag{7.226}$$

1.13 The eigenvector corresponding to each eigenvalue of Eq. 7.255 is obtained as

$$\mathbf{B}\mathbf{L}_j\mathbf{V}_i = \zeta_i\mathbf{V}_i. \tag{7.227}$$

1.14 Each eigenvalue obtained by Eq. 7.37 is an eigenvalue of total system, but the eigenvectors obtained by Eq. 7.38 need to be healed by a Kronecker product as

$$\boldsymbol{\varphi}_i = \mathbf{U}\left(\mathbf{e}_j \otimes \mathbf{V}_i\right) = (\mathbf{X} \otimes \mathbf{I})\left(\mathbf{e}_j \otimes \mathbf{V}_i\right) = \mathbf{X}\mathbf{e}_j \otimes \mathbf{I}\mathbf{V}_i \rightarrow \boldsymbol{\varphi}_i = \mathbf{X}^j \otimes \mathbf{V}_i \tag{7.228}$$

where $\mathbf{X}^j$ is the eigenvector corresponding to the j^{th} eigenvalue of the **H** matrix, and the **X** matrix is calculated in the way shown in Eq. 7.240. Finally, if the eigenvalue calculated by Eq. 7.255 is a simple one, the corresponding eigenvector will be real; however, if the eigenvalue is a multiple root of characteristic polynomial, the corresponding eigenvector will be complex. Adding two conjugate eigenvectors will result in real eigenvectors for both of them.

7.9.5 Reducing Computational Efforts by Substructuring the System

In this section a substructuring method is used for finding the block submatrices **A** and **B** in mass and elastic stiffness matrices. As will be shown, less effort is needed to generate the corresponding submatrices in geometric stiffness matrix as a consequence of the aforementioned methodology.

The substructuring process may be performed as follows:

Step A. Generating the submatrices **A** and **B** in mass and elastic stiffness matrices: Using the segmental division introduced in Sect. 7.2, the nodes of the structure are divided into *n* subset of nodes. In order to find the required substructure, the nodes associated with three arbitrarily selected consecutive segments should be extracted from the set of all the nodes of the structure. After defining the nodes in substructure, the corresponding elements should be defined.

Thus, an adjacency submatrix between previously selected nodes should be specified by which the required submatrices can completely be generated. This adjacency matrix comprises all the elements existing in the intermediate segment as well as elements between the nodes in the intermediate segment

and the ones in two other segments. Calculating the mass and stiffness matrices for the aforementioned substructure leads to the formation of matrices in the following form:

$$[\mathbf{M}_{\text{substructure}}] = \begin{bmatrix} \mathbf{C} & \mathbf{B} & \mathbf{0} \\ \mathbf{B}^{\text{t}} & \mathbf{A} & \mathbf{B} \\ \mathbf{0} & \mathbf{B}^{\text{t}} & \mathbf{D} \end{bmatrix} \text{ and } [\mathbf{K}^{\text{elastic}}_{\text{substructure}}] = \begin{bmatrix} \mathbf{C} & \mathbf{B} & \mathbf{0} \\ \mathbf{B}^{\text{t}} & \mathbf{A} & \mathbf{B} \\ \mathbf{0} & \mathbf{B}^{\text{t}} & \mathbf{D} \end{bmatrix}. \quad (7.229)$$

Thus, we need bigger matrices to compute in order to extract the submatrices **A** and **B** from them.

Step B. Solution of the static problem:

As the structure has similar stiffness submatrices in different segments and the exterior loads applied to the structure are similar in different segments, the displacements will be identical as well. Since having the displacements in a segment is sufficient, therefore the solution of static problem merely for one segment will be adequate if the stiffness matrix of the substructure is calculated appropriately. The stiffness matrix of a segment is calculated by the following relationship:

$$\mathbf{K}^{\text{elastic}}_{\text{segment}} = \mathbf{A} + \mathbf{B} + \mathbf{B}^{\text{t}}. \quad (7.230)$$

The static problem which should be solved will be as follows:

$$[\mathbf{F}_{\text{segment}}] = \left[\mathbf{K}^{\text{elastic}}_{\text{segment}}\right][\mathbf{X}]. \quad (7.231)$$

Solving the above equation results in the displacements of an arbitrarily substructure in the global coordinate system.

Step C. Generating the submatrices Step **A** and Step **B** in the geometric stiffness matrix:

By calculating the transformation matrix of Sect. 7.2 for each element of the substructure defined in Step A and by pre-multiplying the aforementioned transformation matrix into displacements achieved in Step B for extreme nodes of the cited element, the displacements in local coordinate system will be calculated.

As the stiffness matrix of each element in its coordinate system is computable by elastic stiffness matrix for a 3D beam element and the displacement of the element in its coordinate system are calculated above by means of Eq. 7.260, the internal forces for each element can be calculated as

$$[\mathbf{F}_{\text{internal}}] = [\mathbf{K}_{\text{local}}][\mathbf{X}_{\text{local}}]. \quad (7.232)$$

Substituting the internal forces in Eq. 7.248 leads to the formation of the geometric stiffness matrix for each element, and the assembling process of

the matrices leads to the formation of a geometric stiffness matrix having the following form:

$$\left[\mathbf{K}^{\text{geometric}}_{\text{substructure}}\right] = \begin{bmatrix} \mathbf{C} & \mathbf{B} & \mathbf{0} \\ \mathbf{B}^{\mathrm{t}} & \mathbf{A} & \mathbf{B} \\ \mathbf{0} & \mathbf{B}^{\mathrm{t}} & \mathbf{D} \end{bmatrix}. \tag{7.233}$$

By the steps A to C of Sect. 7.7, the submatrices **A** and **B** of the mass, elastic and geometric stiffness matrices are calculated, and the process of eigensolution described in Sects. 7.5 and 7.6 for finding the buckling loads and natural frequencies of rotationally repetitive structure can be executed with the least efforts.

7.9.6 *Numerical Examples*

Examples for finding the first six buckling loads and the first six maximum periods for both solution methods for four dome structures are presented in this section. The results are compared to those obtained by considering the entire structure in the solution without using the symmetry property of the structures.

For all the structures, the density of the material is considered as 78.5 kN/m^3, and the modulus of elasticity is equal to 2e + 8 kN/m^2.

Example 7.25: Type 1 configuration Specifications of the first configuration are as follows:

Span = 145 m, height = 46.2 m, A = sweep angle = 65 (in degrees), number of cycles = 32 and number of members in a rib = 16.

Element cross-sectional properties consisting of pipes are as follows:

$$\text{Exterior diameter} = 0.3239\,\text{m},\ \text{thickness} = 0.01\,\text{m and cross-sectional area} = 0.00986\,\text{m}^2$$

The configuration of the dome presented and the selected substructure for computing the geometric and elastic stiffness matrices of the substructure are shown in Fig. 7.86. This substructure is selected such that its cyclic repetition covers the entire structure, and it has minimum number of elements with respect to this property.

The first six buckling loads and the first six maximum periods of the structure for both classic and present methods are presented in Table 7.1.

Example 7.26: Type 2 configuration Specifications of the second configuration are as follows:

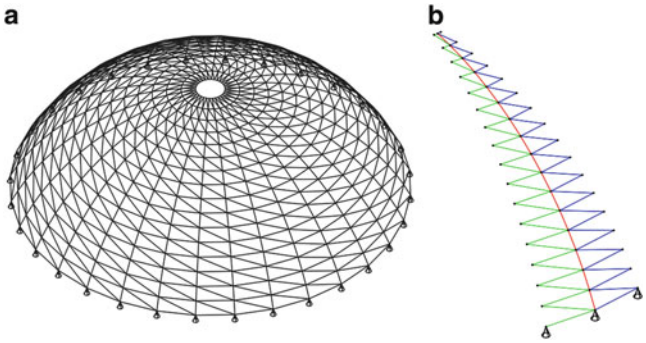

Fig. 7.86 A dome and the selected substructure (Example 7.25)

Table 7.1 Comparison of the results for Example 7.25

Method	First six buckling loads (kN)	Elapsed time (s)	First six periods (s)	Elapsed time (s)
Present method	67.111171586	1.56	0.054773	0.45
	67.363499398		0.054773	
	67.363499398		0.049093	
	68.140308485		0.049094	
	68.140308485		0.045122	
	69.504374950		0.039380	
Classic method	68.143713692	65.46	0.062228	88.46
	68.401052322		0.062228	
	68.401052322		0.050445	
	69.192595933		0.047125	
	69.192595933		0.047125	
	70.580117663		0.042186	
Time ratio $= \frac{\text{time for present method}}{\text{time for classic method}}$		0.024		0.0051

$$\text{Span} = 75\,\text{m},\ \text{height} = 23\ \text{m},\ \text{A} = \text{sweep angle} = 63.04\ (\text{in degrees}),$$
$$\text{number of cycles} = 16 \text{ and number of members in a rib} = 9.$$

Element cross-sectional properties consisting of pipes are as follows:

$$\text{Exterior diameter} = 0.273\,\text{m},\ \text{thickness} = 0.0063\,\text{m and cross-sectional area} = 0.00528\,\text{m}^2.$$

The configuration of the dome presented and the selected substructure for computing the geometric and elastic stiffness matrices of the substructure are shown in Fig. 7.5. This substructure is selected such that its cyclic repetition covers the entire structure, and it has minimum number of elements with respect to this property (Fig. 7.87).

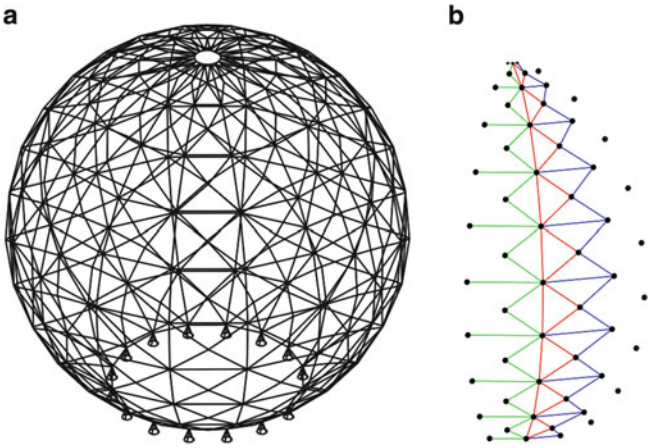

Fig. 7.87 A dome and the selected substructure (Example 7.26)

Table 7.2 Comparison of the results for Example 7.26

Method	First six buckling loads (kN)	Elapsed time (s)	First six periods (s)	Elapsed time (s)
Present method	42.626768260	2.71	1.076111	1.86
	42.950213071		1.076111	
	42.950213071		0.327777	
	44.038557461		0.230387	
	44.038557461		0.169891	
	46.324767177		0.169891	
Classic method	42.972754775	114	1.053611	138
	43.249623685		1.053611	
	43.370217133		0.322513	
	44.365376027		0.230462	
	44.517103987		0.163465	
	46.694711532		0.152487	
Time ratio $= \frac{\text{time for present method}}{\text{time for classic method}}$		0.024		0.014

The first six buckling loads and the first six maximum periods of the structure for both classic and the present methods are presented in Table 7.2.

Example 7.27: Type 3 configuration Specifications of the example, considered for first type of configurations are as follows:

Span = 69.28 m, height = 20 m, A = sweep angle = 60 (in degrees), number of cycles = 16 and number of members in a rib = 8.

Element cross-sectional properties (pipes) : Exterior diameter = 0.273 m, thickness = 0.016 m and cross-sectional area = 0.0129 m^2.

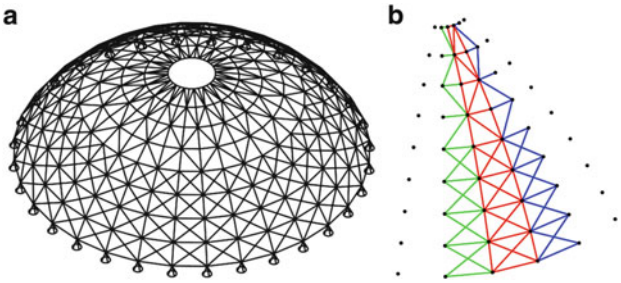

Fig. 7.88 A dome and the selected substructure (Example 7.27)

Table 7.3 Comparison of the results for Example 7.27

Method	First six buckling loads (kN)	Elapsed time (s)	First six periods (s)	Elapsed time (s)
Present method	64.849808347	2.43	0.182603	1.21
	65.051354899		0.182603	
	65.051354899		0.152094	
	65.592911269		0.152094	
	65.592911269		0.150714	
	66.519733355		0.150714	
Classic method	66.069444015	145	0.141674	186
	66.162547554		0.135081	
	66.416914783		0.135081	
	66.802945238		0.127772	
	67.024791100		0.127772	
	67.764475434		0.102673	
Time ratio $= \frac{\text{time for present method}}{\text{time for classic method}}$		0.017		0.007

The configuration of the dome presented and the selected substructure for computing the geometric and elastic stiffness matrices of the substructure are shown in Fig. 7.88. This substructure is selected such that its cyclic repetition covers the entire structure, and it has minimum number of elements with respect to this property (Fig. 7.88).

The first six buckling loads and the first six maximum periods of the structure for both classic and the present methods are presented in Table 7.3.

Example 7.28: Type 4 configuration Specifications of the example, considered for first type of configurations are as follows:

Span = 75 m, height = 12.97 m, diameter of gap inside = 45 m, A = sweep angle = 50 (in degrees), number of cycles = 24, number of members in a rib in upper layer = 4 and number of members in a rib in lower layer = 3.

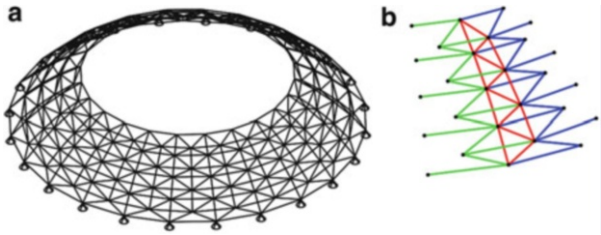

Fig. 7.89 A dome and the selected substructure (Example 7.28)

Table 7.4 Comparison of the results for Example 7.28

Method	First six buckling loads (kN)	Elapsed time (s)	First six periods (s)	Elapsed time (s)
Present method	53.150070147	0.89	0.169493	0.36
	53.776869149		0.169493	
	53.776869149		0.164238	
	55.744596127		0.164238	
	55.744596126		0.127169	
	59.338436596		0.127169	
Classic method	52.173264063	41.56	0.167541	55.56
	52.808894050		0.167541	
	52.808894051		0.163075	
	54.802130814		0.163075	
	54.802130814		0.125557	
	58.435492680		0.125557	
$Time\ ratio = \frac{time\ for\ present\ method}{time\ for\ classic\ method}$		0.022		0.007

Element cross-sectional properties (pipes) : Exterior diameter $= 0.1778\,\text{m}$, thickness $= 0.0063\,\text{m}$ and cross-sectional area $= 3.39\text{e} - 3\,\text{m}^2$.

The configuration of the dome presented and the selected substructure for computing the geometric and elastic stiffness matrices of the substructure are shown in Fig. 7.7. This substructure is selected such that its cyclic repetition covers the entire structure, and it has minimum number of elements with respect to this property (Fig. 7.89).

The first six buckling loads and the first six maximum periods of the structure for both classic and the present methods are presented in Table 7.4.

7.9.7 Concluding Remarks

Symmetry in rotationally repetitive structures results in the decomposition of the systems into smaller subsystems. The matrices corresponding to the detached

subsystems have diminutive dimension in comparison to the dimension of primary matrices. By the decomposition of the rotationally repetitive structures into subsystems, large eigenproblems transform into much more smaller eigenproblems. In fact, for a structure having n rotationally repeating segments, instead of finding the eigenvalues of an $nm \times nm$ matrix, one can n times calculate the eigenvalues of $m \times m$ matrix, where m is equal to the number of active degrees of freedom in a subsystem.

Besides, by applying the substructuring methodologies for eigensolution, there is no need to generate the entire mass, elastic stiffness and geometric stiffness matrices for the main structure. This leads to a drastical reduction in time and memory needed. Although the structures studied here are domes, the application of the presented method can easily be extended to other rotationally repetitive civil engineering structures such as cooling towers and chimneys or structures such as milling cutters, turbine bladed disks, gears and fan or pump impellers in mechanical engineering.

The saving in the required time and memory is divided into three parts:

1. Saving in time and memory due to calculating the mass, elastic and geometric stiffness matrices of subsystem; in fact, instead of generating the entire mass, elastic and geometric stiffness matrices of the structure, the associated matrices of the subsystem can be calculated, and the process of eigensolution can be pursued.
2. Saving in time and memory due to partial static analysis of the structure for buckling load problem.
3. Saving in time and memory due to calculating n times the eigenvalues and eigenvectors of a problem in dimensions of active DOFs in a subsystem instead of calculating the eigenvalues and eigenvector of a structure with an enormous number of DOFs.

References

1. Kaveh A, Sayarinejad MA (2004) Graph symmetry in dynamic systems. Comput Struct 82 (23–26):2229–2240
2. Kaveh A, Salimbahrami B (2007) Buckling load of symmetric frames using canonical forms. Comput Struct 85(11):1420–1430
3. Kaveh A, Salimbahrami B (2004) Eigensolutions of symmetric frames using graph factorization. Commun Numer Methods Eng 20:889–910
4. Kaveh A, Shahryari L (2010) Eigenfrequencies of symmetric planar trusses via weighted graph symmetry and new canonical forms. Eng Comput 27(3):409–439
5. Kaveh A, Rahami H (2005) New canonical forms for analytical solution of problems in structural mechanics. Commun Numer Methods Eng 21(9):499–513
6. Kaveh A, Rahami H (2007) Compound matrix block diagonalization for efficient solution of eigenproblems in structural mechanics. Acta Mech 188(3–4):155–166
7. Kaveh A, Nikbakht M (2007) Symmetric finite element formulation using linear algebra and canonical forms: truss and frame elements. Paper 130 from CCP: 86, ISBN 978-1-905088-17-1
8. Kaveh A, Nemati F (2010) Eigensolution of rotationally repetitive space structures using a canonical form. Int J Numer Methods Biomed Eng 26(12):1781–1796

Chapter 8
Graph Products Applied to the Analysis of Regular Structures

8.1 Introduction

In spite of considerable advances in computational capability of computers in recent years, efficient methods for more time-saving solutions of structures are of great interest. Large problems arise in many scientific and engineering problems. While the basic mathematical ideas are independent of the size of the matrices, the numerical determination of the displacement and internal forces becomes more complicated as the dimensions of matrices increase and their sparsity decreases. The use of prefabrication in industrialised building construction often results in structures with regular patterns of elements exhibiting symmetry of various types, and special methods are beneficial for efficient solution of such problems.

In the first part of this chapter, an efficient method is developed for the analysis of regular structures. A structure is called regular if its model can be formed by a graph product. Here, instead of direct solution of the equations corresponding to a regular structure or finding the inverse of the stiffness matrix directly, modal analysis is used, and eigenvectors are employed for calculating the displacements and then internal forces of the structures. For this purpose, first an efficient method is developed for calculating the eigenvectors of the product graphs, and then a method is presented for using these eigenvectors for evaluating the displacements of a structure [1].

In the second part, static analysis of structures with repeated patterns is presented. These structures are comprised of submodels each having different repeated pattern. As an example, considering a structure with two different repeated patterns, the nodal numbering is performed in such a manner that the resulting stiffness matrix of the structure contains two block-diagonal matrices. Thus, their inversion can easily be performed using regular matrices requiring smaller amount of computational time. In the second part, the modal analysis, free vibration and eigenfrequencies of such structures are studied. Here as well the stiffness and mass matrices are transformed into two block matrices forms and using dynamic

A. Kaveh, *Optimal Analysis of Structures by Concepts of Symmetry and Regularity*,
DOI 10.1007/978-3-7091-1565-7_8,

condensation and the matrix inversion which is involved in this condensation, the eigensolution is performed on matrices of lower dimensions [2].

The presented examples consist of 2D and 3D structures in which in some stories, the stiffnesses are changed due to the addition of some members taking the structures out of regularity. Apart from these, the power transition towers often having additional bracings in some levels are investigated. Other applications correspond to calculating the buckling loads and natural frequencies of regular plates driven to irregular forms by having different support conditions and some added parts.

In the third part, block circulant matrices and their properties are investigated. It is shown that a circulant matrix can be considered as the sum of Kronecker products in which the first components have the commutativity property with respect to multiplication. The important fact is that the method for block diagonalisation of these matrices is much simpler than the previously developed methods, and one does not need to find an additional matrix for orthogonalisation. As it will be shown not only the matrices corresponding to domes in the form of Cartesian product, strong Cartesian product and direct product are circulant, but for other structures such as diamatic domes, pyramid domes, flat double-layer grids and some family of transmission towers, these matrices are also block circulant [3].

8.2 Analysis of Repetitive Structures

8.2.1 Eigenvectors for Sum of the Kronecker Products

Let us assume $\mathbf{M}$ to be as the sum of some Kronecker products, as

$$\mathbf{M} = \sum_{i=1}^{k} (\mathbf{A}_i \otimes \mathbf{B}_i) \tag{8.1}$$

Now if the matrix $\mathbf{P}$ diagonalises all the $\mathbf{A}_i$s simultaneously, then it is previously shown that $\mathbf{U} = \mathbf{P} \otimes \mathbf{I}$ can also block diagonalise the matrix $\mathbf{M}$. The necessary and sufficient condition for $\mathbf{P}$ to exist is that all pairs of $\mathbf{A}_i$s commute, that is,

$$\mathbf{A}_i\mathbf{A}_j = \mathbf{A}_j\mathbf{A}_i. \tag{8.2}$$

Then,

$$\lambda_{\mathbf{M}} = \bigcup_{i=1}^{n} \mathrm{eig}(\mathbf{M}_i); \mathbf{M}_i = \sum_{j=1}^{k} \left(\lambda_i(\mathbf{A}_j)\mathbf{B}_j\right). \tag{8.3}$$

In this relation, the dimension of $\mathbf{A}_j$ is equal to n and that of $\mathbf{B}_j$ is equal to m.

We assume that the condition of Eq. 8.2 holds. Then both $\mathbf{A}_1$ and $\mathbf{A}_2$ can be diagonalised simultaneously with a vector like $\mathbf{u}$. Now considering $\mathbf{A}_1 = \mathbf{I}$, Eq. 8.3 becomes

$$\lambda_{\mathbf{M}} = \bigcup_{i=1}^{n} \text{eig}(\mathbf{M}_i); \mathbf{M}_i = \mathbf{B}_1 + \lambda_i(\mathbf{A}_2)\mathbf{B}_2. \tag{8.4}$$

Considering μ as the eigenvalue, and $\mathbf{v}$ as the eigenvector of $\mathbf{M}_i = \mathbf{B}_1 + \lambda_i(\mathbf{A}_2)\mathbf{B}_2$, we have

$$(\mathbf{B}_1 + \lambda\mathbf{B}_2)\mathbf{v} = \mu\mathbf{v}. \tag{8.5}$$

In the following, we will show that $\mathbf{u} \otimes \mathbf{v}$ will be an eigenvector of $\mathbf{M}$. Since

$$(\mathbf{A} \otimes \mathbf{B})(\mathbf{C} \otimes \mathbf{D}) = \mathbf{AC} \otimes \mathbf{BD}, \tag{8.6}$$

therefore,

$$(\mathbf{A}_1 \otimes \mathbf{B}_1 + \mathbf{A}_2 \otimes \mathbf{B}_2)(\mathbf{u} \otimes \mathbf{v}) = (\mathbf{A}_1\mathbf{u}) \otimes (\mathbf{B}_1\mathbf{v}) + (\mathbf{A}_2\mathbf{u}) \otimes (\mathbf{B}_2\mathbf{v}). \tag{8.7}$$

However, we have assumed $\mathbf{A}_1 = \mathbf{I}$; thus,

$$\mathbf{A}_1\mathbf{u} = \mathbf{u};\ \mathbf{A}_2\mathbf{u} = \lambda\mathbf{u}. \tag{8.8}$$

Considering Eqs. 8.5 and 8.8, the Eq. 8.7 becomes

$$\begin{aligned}(\mathbf{A}_1 \otimes \mathbf{B}_1 + \mathbf{A}_2 \otimes \mathbf{B}_2)(\mathbf{u} \otimes \mathbf{v}) &= \mathbf{u} \otimes (\mathbf{B}_1\mathbf{v}) + \lambda\mathbf{u} \otimes (\mathbf{B}_2\mathbf{v}) \\ &= \mathbf{u} \otimes (\mathbf{B}_1 + \lambda\mathbf{B}_2)\mathbf{v} = \mu(\mathbf{u} \otimes \mathbf{v}).\end{aligned} \tag{8.9}$$

This relationship shows that $\mathbf{u} \otimes \mathbf{v}$ is an eigenvector of $\mathbf{M}$.

Now if $\mathbf{A}_1 \neq \mathbf{I}$, then the proof will not change. This is because Eq. 8.1 will still hold, and using the QZ transformation, one can find two matrices $\mathbf{Q}$ and $\mathbf{Z}$ such that

$$\mathbf{QA}_1\mathbf{Z} = \mathbf{I};\ \mathbf{QA}_2\mathbf{Z} = \mathbf{D} \tag{8.10}$$

where $\mathbf{D}$ is a diagonal matrix and changes $\mathbf{A}_1$ into an $\mathbf{I}$ matrix.

Special Case: At this stage, it should be noted that if apart from $\mathbf{A}_1$ and $\mathbf{A}_2$, the two matrices $\mathbf{B}_1$ and $\mathbf{B}_2$ have the commutative property with respect to multiplication, then we will have

$$\text{eig}\left(\sum_{i=1}^{n} \mathbf{A}_i \otimes \mathbf{B}_i\right) = \sum_{i=1}^{n} \text{eig}(\mathbf{A}_i \otimes \mathbf{B}_i). \tag{8.11}$$

In this case, $\mathbf{v}$ should be such an eigenvector that diagonalises the two matrices $\mathbf{B}_1$ and $\mathbf{B}_2$ simultaneously. Now if μ is the corresponding eigenvalue, after using the QZ transformation and transforming $\mathbf{B}_2$ to $\mathbf{I}$, we will have

$$\mathbf{B}_2\mathbf{v} = \mathbf{v};\ \mathbf{B}_1\mathbf{v} = \mu\mathbf{v}. \tag{8.12}$$

In this way, Eq. 8.9 will be simplified as

$$(\mathbf{A}_1 \otimes \mathbf{B}_1 + \mathbf{A}_2 \otimes \mathbf{B}_2)(\mathbf{u} \otimes \mathbf{v}) = \mathbf{u} \otimes \mu\mathbf{v} + \lambda\mathbf{u} \otimes \mathbf{v} = (\mu + \lambda)(\mathbf{u} \otimes \mathbf{v}). \tag{8.13}$$

Hence, $\mathbf{u} \otimes \mathbf{v}$ is an eigenvector of $\mathbf{M}$, with the only difference is that here $\mathbf{v}$ is an eigenvector which simultaneously block diagonalises the matrices $\mathbf{B}_1$ and $\mathbf{B}_2$, while $\mathbf{v}$ had been previously considered as the eigenvector of $\mathbf{M}_i = \mathbf{B}_1 + \lambda_i(\mathbf{A}_2)\mathbf{B}_2$. It should be mentioned that this can be observed in the Laplacian matrix of a Cartesian product.

Having the eigenvalues, one can find the corresponding eigenvectors by an iterative approach. However, this is a numerical approach, while in here we will form the eigenvectors by an analytical approach and not a numerical one.

8.2.2 *Solution of Linear Equations via Eigenvalues and Eigenvectors*

In the following, the application of eigenvectors in the solution of a set of linear equations will be presented and later will be used in the analysis of a regular structure.

Suppose we want to solve the following set of equations:

$$\mathbf{M}\mathbf{x} = \mathbf{B}. \tag{8.14}$$

Exactly similar to the modal analysis, using a suitable transformation, we transform $\mathbf{x}$ to $\mathbf{y}$. This transformation can be written as

$$\{\mathbf{x}\}_n = \sum_{i=1}^{n} \{\boldsymbol{\varphi}\}_i \mathbf{y}_i \tag{8.15}$$

where $\{\boldsymbol{\varphi}\}_i$s are the eigenvectors of the matrix $\mathbf{M}$. Obviously these vectors are orthogonal. Thus, multiplying the two sides of Eq. 8.14 by $\{\boldsymbol{\varphi}\}_j^t$, we will have

$$\{\boldsymbol{\varphi}\}_j^t \mathbf{M} \{\boldsymbol{\varphi}\}_j \mathbf{y}_j = \lambda_j \mathbf{y}_j = \{\boldsymbol{\varphi}\}_j^t \mathbf{B}. \tag{8.16}$$

Considering $\mathbf{B}_j = \{\boldsymbol{\varphi}\}_j^t \mathbf{B}$, we will have

$$\mathbf{y}_j = \frac{\mathbf{B}_j}{\lambda_j} \Rightarrow \{\mathbf{x}\}_n = \sum_{i=1}^{n} \{\boldsymbol{\varphi}\}_i \mathbf{y}_i = \sum_{i=1}^{n} \{\boldsymbol{\varphi}\}_i \frac{\mathbf{B}_i}{\lambda_i} = \sum_{i=1}^{n} \frac{\{\boldsymbol{\varphi}\}_i \{\boldsymbol{\varphi}\}_i^t}{\lambda_i} \mathbf{B}. \tag{8.17}$$

Therefore, the unknowns of this matrix equation can be obtained without inverting the matrix. This is done by merely using the eigenvalues and eigenvectors, the calculation of both of which has been previously explained.

If $\mathbf{A}_i$ s and $\mathbf{B}_i$ s do not possess the commutativity property with respect to multiplication, then for the case $k = 2$, one can use QZ transformation for the solution. This transformation is introduced in Ref. [4]. Here, one does not need to calculate the stiffness matrix.

However, one can easily find $\mathbf{M}^{-1}$ having the eigenvalues and eigenvectors of $\mathbf{M}$. Having the matrix $\mathbf{V}$ of eigenvectors and the matrix $\mathbf{D}$ of eigenvalues in its diagonal, then $\mathbf{M} = \mathbf{V}\mathbf{D}\mathbf{V}^t$. Since the eigenvalues of $\mathbf{M}^{-1}$ are the inverse of those of $\mathbf{M}$ with identical eigenvectors, therefore,

$$\mathbf{M}^{-1} = \mathbf{V}\mathbf{D}^{-1}\mathbf{V}^t = \mathbf{V} \begin{bmatrix} \frac{1}{\lambda_1} & & & 0 \\ & \frac{1}{\lambda_2} & & \\ & & . & \\ & & . & \\ 0 & & & \frac{1}{\lambda_{m*n}} \end{bmatrix} \mathbf{V}^t. \tag{8.18}$$

In this relation, $\mathbf{D}^{-1}$ can easily be obtained by finding the inverse of the diagonal entries of $\mathbf{D}$. The eigenvector of such a matrix will be $\mathbf{u} \otimes \mathbf{v}$ in which $\mathbf{u}$ is a vector that diagonalises the two matrices $\mathbf{A}_1$ and $\mathbf{A}_2$ simultaneously, and $\mathbf{v}$ is the eigenvector of $\mathbf{M}_i = \sum_{j=1}^{k} \left(\lambda_i(\mathbf{A}_j)\mathbf{B}_j\right)$.

For a structure, if we want the stiffness matrix to be in the form of the sum of two Kronecker products, then for expressing the governing equation, the Cartesian coordinate system should be altered. This is obvious because a structure which is obtained by rotation of an element, due to rotational symmetry, the displacements under a symmetric loading will be in a radial direction, and therefore, these displacements will not be identical in x and y directions. Thus, for this case, a cylindrical coordinate will be more suitable. An example of such a case will be given in the following section.

8.2.3 Kronecker Product of a Path and a Cycle

Suppose we want to study a structure in the form of $P_m\ (X)_C\ C_n$. In general, one can show that the Laplacian matrix can be written as

$$\mathbf{M}_{mn} = \mathbf{G}_n(\mathbf{A}_m, \mathbf{B}_m, \mathbf{A}_m) = \mathbf{I}_n \otimes \mathbf{F}_m(1, -1, 2) + \mathbf{G}_n(2, -1, 2) \otimes \mathbf{I}_m \tag{8.19}$$

where

$$\mathbf{G}_n(\mathbf{A}_m, \mathbf{B}_m, \mathbf{C}_m) = \begin{bmatrix} \mathbf{A}_m & \mathbf{B}_m & & & & \mathbf{B}_m \\ \mathbf{B}_m & \mathbf{C}_m & . & & & \\ & . & . & . & & \\ & & . & . & . & \\ & & & . & \mathbf{C}_m & \mathbf{B}_m \\ \mathbf{B}_m & & & & \mathbf{B}_m & \mathbf{A}_m \end{bmatrix}_n \tag{8.20}$$

$$\text{and } \mathbf{F}_n(\mathbf{A}_m, \mathbf{B}_m, \mathbf{C}_m) = \begin{bmatrix} \mathbf{A}_m & \mathbf{B}_m & & & & \\ \mathbf{B}_m & \mathbf{C}_m & . & & & \\ & . & . & . & & \\ & & . & . & . & \\ & & & . & \mathbf{C}_m & \mathbf{B}_m \\ & & & & \mathbf{B}_m & \mathbf{A}_m \end{bmatrix}_n .$$

Therefore,

$$\text{eig}(\mathbf{M}_{mn}) = \bigcup_{i=1}^{n} \{\text{eig}[\mathbf{F}_m(1,-1,2) + \lambda_i(\mathbf{G}_n(2,-1,2))\mathbf{I}_m]\} \quad i = 1:n \tag{8.21}$$

where

$$\lambda_i(\mathbf{G}_n(2,-1,2)) = 2 - 2\cos\frac{2i\pi}{n} \quad : \quad i = 1:n. \tag{8.22}$$

It can be seen that here $\mathbf{F}_m(1,-1,2)$ is the Laplacian matrix of P_m and $\mathbf{G}_n(2,-1,2)$ is the Laplacian matrix of C_n. In this way we will have n matrices of dimension m.

Similarly for the direct product of P_m by C_n, we will have

$$\begin{aligned} \mathbf{M}_{mn} &= \mathbf{G}_n(\mathbf{A}_m, \mathbf{B}_m, \mathbf{C}_m) \\ &= \mathbf{I}_n \otimes 2\mathbf{F}_m(1,0,2) + \mathbf{G}_n(0,-1,0) \otimes \mathbf{F}_m(0,1,0). \end{aligned} \tag{8.23}$$

In this relation, we have $\lambda_i(\mathbf{G}_n(0,-1,0)) = -2\cos\frac{2i\pi}{n}$, and therefore,

$$\text{eig}(\mathbf{M}_{mn}) = \bigcup_{i=1}^{n} \left\{ \text{eig}\left[2\mathbf{F}_m(1,0,2) - 2\cos\frac{2i\pi}{n}\mathbf{F}_m(0,1,0) \right] \right\}. \tag{8.24}$$

For strong Cartesian product of P_m by C_n, this matrix will be as

$$\begin{aligned}\mathbf{M}_{mn} &= \mathbf{G}_n(\mathbf{A}_m, \mathbf{B}_m, \mathbf{C}_m) \\ &= \mathbf{I}_n \otimes 3\mathbf{F}_m(2,0,3) + \mathbf{G}_n(-1,-1,-1) \otimes \mathbf{F}_m(1,1,1).\end{aligned} \tag{8.25}$$

Here, we have $\lambda_i(\mathbf{G}_n(-1,-1,-1)) = -\left(1 + 2\cos\dfrac{2i\pi}{n}\right)$, and therefore,

$$\text{eig}(\mathbf{M}_{mn}) = \bigcup_{i=1}^{n} \left\{ \text{eig}\left[3\mathbf{F}_m(2,0,3) - \left(1 + 2\cos\frac{2i\pi}{n}\right)\mathbf{F}_m(1,1,1) \right] \right\}. \tag{8.26}$$

However, if we express the stiffness matrix of such a structure in a cylindrical coordinate system, since in the upper and lower part of the main diagonal block we obtain blocks which are the transpose of each other, therefore, the stiffness matrix can be expressed as the sum of three Kronecker products in the following form:

$$\mathbf{M} = \mathbf{A}_1 \otimes \mathbf{B}_1 + \mathbf{A}_2 \otimes \mathbf{B}_2 + \mathbf{A}_3 \otimes \mathbf{B}_3; \mathbf{A}_1 = \mathbf{I}; \mathbf{A}_3 = \mathbf{A}_2^t; \mathbf{B}_3 = \mathbf{B}_2^t \tag{8.27}$$

where

$$\mathbf{A}_3 = \mathbf{A}_2^t = \begin{bmatrix} 0 & 1 & & & & & 0 \\ & 0 & 1 & & & & \\ & & \cdot & \cdot & & & \\ & & & \cdot & \cdot & & \\ & & & & \cdot & 1 & \\ & & & & & 0 & 1 \\ 1 & & & & & & 0 \end{bmatrix}_n. \tag{8.28}$$

For calculating the eigenvalues of this matrix, after expanding the determinant, the solution of the corresponding characteristic equation will result in the nth roots of 1, containing n real and complex values, that is,

$$\det(\mathbf{A}_3 - \lambda\mathbf{I}) = 0 \Rightarrow \lambda^n = 1 \Rightarrow \lambda = \left\{ 1, e^{\frac{2\pi i}{n}}, e^{\frac{4\pi i}{n}}, \ldots, e^{\frac{2(n-1)\pi i}{n}} \right\}. \tag{8.29}$$

In what follows, we will show that all the above ideas can be applied to the analysis of repetitive structures.

8.2.4 An Illustrative Example

Suppose we want to study a structure in the form of the strong Cartesian product of P_2 by C_5. Three-dimensional and two-dimensional configurations of this structure are shown in Fig. 8.1. In these figures, the geometric properties and loading are specified. In fact, this structure is formed by two equilateral polygons with five

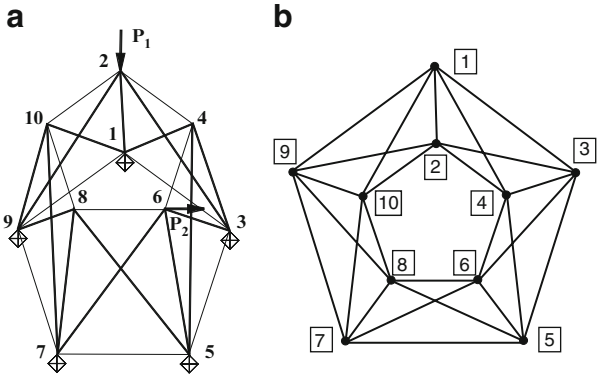

Fig. 8.1 Three- and two-dimensional views of a structure

edges, where the distance of the five external and internal nodes from their centres are 3 and 1.5, respectively. The external nodes 2, 4, 6, 8 and 10 are in the height of 1.5 m. All the cross-sectional areas are 5 cm^2 and the elastic modulus is taken as 200 kN/mm^2. The loads P_1 at node 2 is 30 kN and the load P_2 at node 6 is 20 kN. It can be seen that the loading is nonsymmetric.

If we form the stiffness matrix of this structure in the Cartesian coordinate, we will find out that it does not obey the pattern of the repetitive form (sum of Kronecker products). However, forming this matrix in the cylindrical coordinate system, the reduced stiffness matrix will have the following form:

$$\mathbf{M} = \mathbf{A}_1 \otimes \mathbf{B}_1 + \mathbf{A}_2 \otimes \mathbf{B}_2 + \mathbf{A}_3 \otimes \mathbf{B}_3; \mathbf{A}_1 = \mathbf{I}; \mathbf{A}_3 = \mathbf{A}_2^{\mathrm{t}}; \mathbf{B}_3 = \mathbf{B}_2^{\mathrm{t}}$$

where

$$\mathbf{B}_1 = 10^5 \begin{bmatrix} 0.6463 & 0 & -0.1867 \\ 0 & 1.2063 & 0 \\ -0.1867 & 0 & 0.3639 \end{bmatrix} \text{ and } \mathbf{B}_2 = 10^4 \begin{bmatrix} 1.9593 & 2.6967 & 0 \\ -2.6967 & -3.7117 & 0 \\ 0 & 0 & 0 \end{bmatrix}.$$

The matrices $\mathbf{A}_2$ and $\mathbf{A}_3$ are given in Eq. 8.28 and the corresponding eigenvalues are provided by Eq. 8.29. In this example, both matrices have the dimension equal to five.

$$\begin{aligned} \mathrm{eig}(\mathbf{A}_2) &= \left\{1, \mathrm{e}^{\frac{2\pi \mathrm{i}}{5}}, \mathrm{e}^{\frac{4\pi \mathrm{i}}{5}}, \mathrm{e}^{\frac{6\pi \mathrm{i}}{5}}, \mathrm{e}^{\frac{8\pi \mathrm{i}}{5}}\right\} \\ &= \{1, 0.3090 + 0.9511\mathrm{i}, -0.8090 + 0.5878\mathrm{i}, -0.8090 - 0.5878\mathrm{i}, \\ &\quad 0.3090 - 0.9511\mathrm{i}\}. \end{aligned}$$

The eigenvalues of the matrix $\mathbf{M}$ can be found using Eq. 8.15 as follows:

$$\mathrm{eig}(\mathbf{M}) = \bigcup_{\mathrm{i}=1}^{5} \left[\mathrm{eig}\left\{\mathbf{B}_1 + \lambda_{\mathrm{i}}(\mathbf{A}_2)\mathbf{B}_2 + \lambda_{\mathrm{i}}\left(\mathbf{A}_2^{\mathrm{t}}\right)\mathbf{B}_2^{\mathrm{t}}\right\}\right].$$

As an example, the biggest eigenvalue is calculated as $\lambda_{\max} = 1.0864\mathrm{e}5$.

The eigenvectors of this matrix are $\mathbf{u} \otimes \mathbf{v}$ where both $\mathbf{u}$ and $\mathbf{v}$ are introduced before. As an example the eigenvectors corresponding to the above-given eigenvalue are as

$$\{\boldsymbol{\varphi}\} = [1 \quad 1 \quad 1 \quad 1 \quad 1]^{t} \otimes [0.4330 \quad 0 \quad -0.1119]^{t}.$$

It should be noted that for a structure, the governing equation is $\mathbf{K}\Delta = \mathbf{P}$. In this equation, $\mathbf{K}$ is the reduced cylindrical stiffness matrix of the structure and $\mathbf{P}$ is the force vector which is expressed in the cylindrical coordinate system. Using Eq. 8.18, the displacements are found in the cylindrical coordinate system (ρ, θ, z) as

$$\Delta = \begin{matrix} \rho \\ \theta \\ z \end{matrix} \begin{bmatrix} 0.5330 & -0.2351 & 0.4221 & -0.2549 & -0.1770 \\ 0.0028 & 0.0924 & 0.2169 & 0.1621 & -0.1254 \\ 1.0978 & -0.1206 & 0.2166 & -0.1308 & -0.0908 \end{bmatrix}$$

and after transformation, the displacements are obtained in the Cartesian coordinate system (x, y, z) as

$$\Delta = \begin{matrix} x \\ y \\ z \end{matrix} \begin{bmatrix} -0.0028 & -0.2521 & 0.4236 & 0.2810 & 0.2071 \\ 0.5330 & 0.0152 & -0.2140 & 0.1110 & 0.0646 \\ 1.0978 & -0.1206 & 0.2166 & -0.1308 & -0.0908 \end{bmatrix}.$$

Here, the columns 1–5 contain the displacements of the nodes 2, 4, 6, 8 and 10 in the specified directions.

8.2.5 *Algorithm for the Analysis*

The analysis of a repetitive structure can be summarised as follows. It should be noted that the loading of the structure can be nonsymmetric.

Step 1. Form the stiffness matrix in the cylindrical coordinate system and express it in the form

$$\mathbf{M} = \sum_{i=1}^{m} \mathbf{A}_i \otimes \mathbf{B}_i.$$

Step 2. Determine the eigenvalues of the matrix $\mathbf{M}$ using the relationship

$$\text{eig}(\mathbf{M}) = \bigcup_{j=1}^{k} \left[\text{eig} \left\{ \sum_{i=1}^{m} \lambda_j(\mathbf{A}_i)\mathbf{B}_i \right\} \right],$$

where k is the dimension of the matrix $\mathbf{A}_i$.

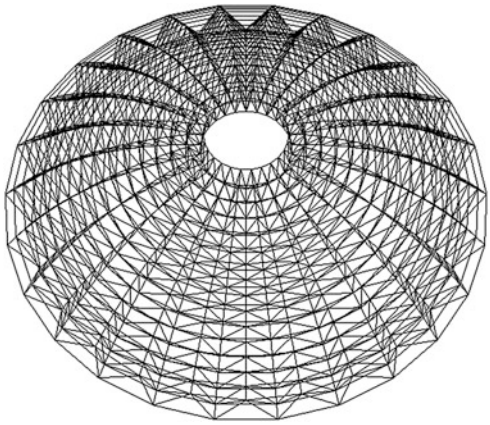

Fig. 8.2 A double-layer dome

Step 3. Determine the vector u which digonalises the matrices $\mathbf{A}_i$ simultaneously.
Step 4. Determine the vector v which is the eigenvector of the matrix

$$\mathbf{M}_i = \sum_{i=1}^{m} \{\lambda_j(\mathbf{A}_i)\mathbf{B}_i\}.$$

If the two matrices $\mathbf{B}_1$ and $\mathbf{B}_2$ also commute with respect to multiplication, then it is only sufficient to determine v such that it diagonalises these two matrices simultaneously.

Step 5. Determine the eigenvector of $\mathbf{M}$ which is the Kronecker product of the two vectors determined in Step 3 and Step 4, that is, $\boldsymbol{\varphi} = \mathbf{u} \otimes \mathbf{v}$.

Step 6. Determine the displacements in the cylindrical coordinate system using the following relationship and change the results into the Cartesian coordinate system:

$$\{\boldsymbol{\Delta}\}_n = \sum_{i=1}^{n} \frac{\{\boldsymbol{\varphi}\}_i \{\boldsymbol{\varphi}\}_i^t}{\lambda_i} \mathbf{P}.$$

8.2.6 Numerical Examples

In this section, three examples corresponding to different types of structures are studied using the present method.

Example 8.1. A double-layer dome is considered as shown in Fig. 8.2. The top layer is C_{26} $(X)_C$ P_{15} and the bottom layer is C_{26} $(X)_C$ P_{14}. Each node at the bottom layer is connected to four adjacent nodes in the top layer. The stiffness matrix of this structure has the following form:

$$\mathbf{K}_{mk}=\begin{bmatrix}
\mathbf{E}_m & \mathbf{H}_m & -\mathbf{I}_m & & & & & & \mathbf{0}\\
\mathbf{H}_m^t & \mathbf{E}_m+2\mathbf{I}_m & \mathbf{H}_m^t & -\mathbf{I}_m & & & & & \\
-\mathbf{I}_m & \mathbf{H}_m & \mathbf{E}_m+3\mathbf{I}_m & \mathbf{H}_m & . & & & & \\
 & -\mathbf{I}_m & \mathbf{H}_m^t & . & . & . & & & \\
 & & . & . & . & . & & & \\
 & & & . & . & . & . & & \\
 & & & & & & \mathbf{E}_m+3\mathbf{I}_m & \mathbf{H}_m & -\mathbf{I}_m\\
 & & & & & & \mathbf{H}_m^t & \mathbf{E}_m+2\mathbf{I}_m & \mathbf{H}_m^t\\
\mathbf{0} & & & & & & -\mathbf{I}_m & \mathbf{H}_m & \mathbf{E}_m
\end{bmatrix}_{k\times k}$$

This is a penta-diagonal block matrix and in the two diagonals adjacent to the main diagonal, $\mathbf{H}_m^t$ and $\mathbf{H}_m$ are alternately changed. Thus, the stiffness matrix can be expressed as

$$\mathbf{K}_{mk}=\mathbf{I}_k\otimes\mathbf{E}_m+\mathbf{C}_k\otimes\mathbf{H}_m+\mathbf{C}_k^t\otimes\mathbf{H}_m^t+\mathbf{D}_k\otimes\mathbf{I}_m=\sum_{i=1}^{4}\mathbf{A}_i\otimes\mathbf{B}_i$$

where

$$\mathbf{C}_k=\begin{bmatrix}
0 & 1 & & & & & & \\
0 & 0 & 0 & & & & & \\
 & 1 & 0 & 1 & & & & \\
 & & 0 & 0 & 0 & & & \\
 & & & 1 & . & . & & \\
 & & & & . & . & . & \\
 & & & & & . & . & \\
 & & & & & & . & .
\end{bmatrix}_k,\quad
\mathbf{D}_k=\begin{bmatrix}
0 & 0 & -1 & & & & & & \\
0 & 2 & 0 & . & & & & & \\
-1 & 0 & 3 & . & . & & & & \\
 & . & . & . & . & . & & & \\
 & & . & . & . & . & . & & \\
 & & & . & . & . & . & . & \\
 & & & & . & . & 3 & 0 & -1\\
 & & & & & . & 0 & 2 & 0\\
 & & & & & & -1 & 0 & 0
\end{bmatrix}_k$$

$$\mathbf{E}_m=\mathbf{G}_m(5,-1,5),\quad
\mathbf{H}_m=\begin{bmatrix}
-1 & 0 & & & & & & -1\\
-1 & -1 & 0 & & & & & \\
 & . & . & . & & & & \\
 & & . & . & . & & & \\
 & & & . & . & . & & \\
 & & & & . & . & . & \\
 & & & & & . & . & \\
 & & & & & & . & \\
 & & & & & & -1 & 0\\
0 & & & & & & -1 & -1
\end{bmatrix}_m.$$

Here, under an arbitrary loading, with the bottom nodes being fixed, instead of inverting a matrix of dimension $26\times 28\times 3=2{,}184$, we need to calculate the

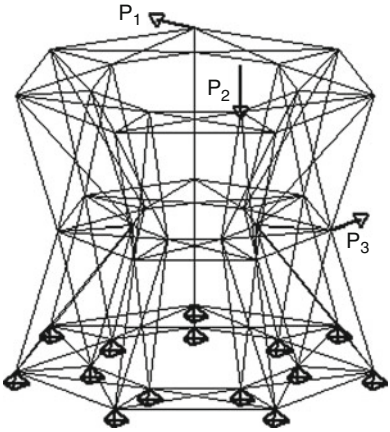

Fig. 8.3 A space structure with lexicographic model $G(X)_{LG}H$

eigenvalues (step 2) and the eigenvectors (step 4) of a matrix of dimension $28 \times 3 = 84$, where 3 is the DOFs of each node. Then, the vector u is calculated which diagonalises the matrices A_i (after $i = 26$) simultaneously (step 3) and after finding the Kronecker product of these two vectors (step 5), using the relationship of step 6, all the displacements can be calculated. For calculating the eigenvalues, we use the following approach.

Here, $\mathbf{K}$ is the sum of four Kronecker products. First we control $\mathbf{A}_i$s and $\mathbf{B}_i$s for commutative property. Here, B_is have this property. Since two matrices $\mathbf{M} = \sum_i (\mathbf{A}_i \otimes \mathbf{B}_i)$ and $\mathbf{N} = \sum_i (\mathbf{B}_i \otimes \mathbf{A}_i)$ are similar, we interchange $\mathbf{A}_i$s and $\mathbf{B}_i$s. Since the eigenvalue does not change, therefore, we can write

$$\mathrm{eig}(\mathbf{K}_{mk}) = \mathrm{eig} \sum_{i=1}^{4} (\mathbf{A}_i \otimes \mathbf{B}_i) = \mathrm{eig} \left(\sum_{i=1}^{4} \mathbf{B}_i \otimes \mathbf{A}_i \right)$$

Therefore,

$$\mathrm{eig}(\mathbf{K}_{mk}) = \bigcup_{j=1}^{m} \left[\mathrm{eig} \left\{ \sum_{i=1}^{4} \lambda_j(\mathbf{B}_i)\mathbf{A}_i \right\} \right]$$

Example 8.2. The model of a space structure is considered as the lexicographic product of $G(X)_{LG}H$ with $G = C_7(X)_C\ P_4$ and $H = P_2$, Fig. 8.3. All the nodes at the bottom layer are constrained against movement, and the loading is nonsymmetric as illustrated in the figure.

For this example, instead of inverting a matrix of dimension $2 \times 14 \times 3 = 84$, we need to calculate the eigenvalues (step 2) and the eigenvectors (step 4) of a matrix of dimension $4 \times 3 = 12$, where 3 is the DOFs of each node. Then, the vector $\mathbf{u}$ is calculated which diagonalises the matrices $\mathbf{A}_i$ (after $i = 7$)

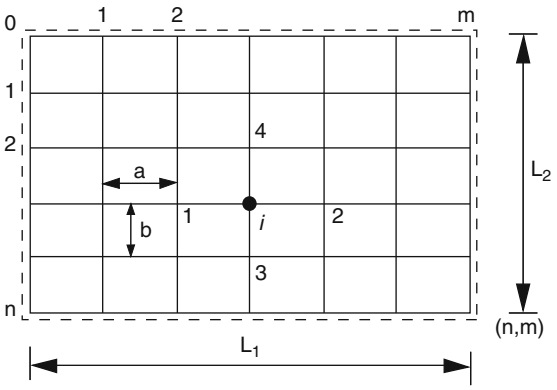

Fig. 8.4 A simply supported rectangular plate

simultaneously (step 3) and after finding the Kronecker product of these two vectors (step 5), using the relationship of step 6, all the displacements can be calculated.

Example 8.3. Consider a simply supported rectangular plate under a uniform load of intensity P_0, as shown in Fig. 8.4. We want to calculate the deflection and the moment at different points of this plate. This example is included to show the applicability of the present method for non-repetitive models.

Here, we use finite difference method, since the form of the corresponding coefficient matrix is such that it can be expressed as the sum of Kronecker products. The subdivision of the plate is shown in Fig. 8.4.

The theoretical solution of this problem can be obtained from the following governing equation:

$$\nabla^4 w = \frac{\partial^4 w}{\partial x^4} + 2\frac{\partial^4 w}{\partial x^2 \partial y^2} + \frac{\partial^4 w}{\partial y^4} = \frac{P}{D}.$$

The solution of this equation using the finite difference results in a penta-diagonal block matrix, the solution of which is already discussed in Example 8.1. The above equation can be transformed into the following two equations of lower order [5]:

$$\nabla^2 M = \frac{\partial^2 M}{\partial x^2} + \frac{\partial^2 M}{\partial y^2} = -P; \quad \nabla^2 w = \frac{\partial^2 w}{\partial x^2} + \frac{\partial^2 w}{\partial y^2} = -\frac{M}{D}.$$

Since we want to change the governing equation into its finite difference form, therefore, it is much simpler to use the above two equations which have lower order. From one equation, we should find one of the bending moments in terms of the external force, and in the next equation, this moment should be entered as the solution in order to calculate the deflection. The transformation of these equations into finite difference form is performed as follows:

$$(M_1 + M_2 + M_3 + M_4 - 4M_i) = -P_i a^2;$$
$$(w_1 + w_2 + w_3 + w_4 - 4w_i) = -M_i a^2.$$

Which is written for the *i*th node and as it can be seen from Fig. 8.4, the nodes 1–4 are the nodes adjacent to this node. The length of the subdivisions in both directions are considered to be identical and equal to a, that is, (b = a)**.**

The important point in using these two relationships is that the form of the coefficient matrices for both should be identical, and it is enough to be calculated once. Considering the external load as P_0 and subdividing the plate in two direction with m and n nodes, the Laplacian matrix ∇^2 will be obtained as

$$\nabla^2 = \mathbf{I}_n \otimes \mathbf{F}_m(-4, 1, -4) + \mathbf{F}_n(0, 1, 0) \otimes \mathbf{I}_m = \mathbf{A}_1 \otimes \mathbf{B}_1 + \mathbf{A}_2 \otimes \mathbf{B}_2 = \mathbf{C}.$$

An important point in the above matrix is that both $\mathbf{A}_1$ and $\mathbf{A}_2$, and $\mathbf{B}_1$ and $\mathbf{B}_2$ have the commutative property with respect to multiplication, and therefore, the eigenvalues and eigenvectors can be calculated much simpler.

The two equations of this problem can be expressed as follows:

$$\nabla^2 \mathbf{M} = -P \Rightarrow [\mathbf{I}_n \otimes \mathbf{F}_m(-4, 1, -4) + \mathbf{F}_n(0, 1, 0) \otimes \mathbf{I}_m]\{\mathbf{M}\} = -\{P_0\} \Rightarrow [\mathbf{C}]\{\mathbf{M}\} = -\{P_0\}a^2$$

$$\nabla^2 \mathbf{w} = -\frac{M}{D} \Rightarrow [\mathbf{I}_n \otimes \mathbf{F}_m(\mathbf{-4}, \mathbf{1}, \mathbf{-4}) + \mathbf{F}_n(\mathbf{0}, \mathbf{1}, \mathbf{0}) \otimes \mathbf{I}_m]\{\mathbf{w}\} = -\left\{\frac{M}{D}\right\} \Rightarrow [\mathbf{C}]\{\mathbf{w}\} = -\left\{\frac{M}{D}\right\}a^2.$$

The solution of the first equation, using Eq. 8.18, will be as follows:

$$\{\mathbf{M}\} = -P_0 a^2 \sum_i \frac{\{\boldsymbol{\varphi}\}_i \{\boldsymbol{\varphi}\}_i^t}{\lambda_i}.$$

Therefore, only the calculation of λ_i and $\{\boldsymbol{\varphi}\}_i$ is needed. In this case, one can use Eq. 8.11 for calculating the eigenvalues and eigenvectors; the matrix **C** can be diagonalised. Thus, we will have

$$\begin{aligned} \mathrm{eig}(\mathbf{C}) &= \mathrm{eig}\{\mathbf{I}_n \otimes \mathbf{F}_m(-4, 1, -4) + \mathbf{F}_n(0, 1, 0) \otimes \mathbf{I}_m\} \\ &= \mathrm{eig}(\mathbf{I}_n \otimes \mathbf{F}_m(-4, 1, -4)) + \mathrm{eig}(\mathbf{F}_n(0, 1, 0) \otimes \mathbf{I}_m) \end{aligned}$$

On the other hand, we know that the eigenvalues of a matrix in the form of $\mathbf{F}_n$ are as follows:

$$\text{eig}(\mathbf{F}_n(a,b,a)) = a + 2b\cos\left(\frac{i\pi}{n+1}\right); \quad i = 1:n.$$

The eigenvectors are as follows:

$$\{\boldsymbol{\varphi}\}_j^k = \sin\left(\frac{kj\pi}{n+1}\right); \quad \{\boldsymbol{\varphi}\}_1^k = \sin\left(\frac{k\pi}{n+1}\right); \quad j = 1:n.$$

Since we have $\text{eig}(\mathbf{C}\otimes\mathbf{D}) = \text{eig}(\mathbf{C})\text{eig}(\mathbf{D})$, therefore,

$$\begin{aligned}\lambda = \text{eig}(\mathbf{C}) &= \text{eig}(\mathbf{F}_m(-4,1,-4)) + \text{eig}(\mathbf{F}_n(0,1,0)) \\ &= -4 + 2\cos\frac{i\pi}{n+1} + 2\cos\frac{j\pi}{m+1} \qquad i = 1:n; j = 1:m.\end{aligned}$$

Since in this case both $\mathbf{A}_1$ and $\mathbf{A}_2$, and $\mathbf{B}_1$ and $\mathbf{B}_2$ have the commutative property with respect to multiplication, therefore, $\mathbf{u}$ and $\mathbf{v}$ are the eigenvectors which diagonalise these pair of matrices simultaneously. The Kronecker product of these eigenvectors is the eigenvector of $\mathbf{C}$, and we have

$$\{\boldsymbol{\varphi}\} = \sin\left(\frac{kj\pi}{n+1}\right)\otimes\sin\left(\frac{k'j'\pi}{m+1}\right); \quad j = 1:n; j' = 1:m.$$

Therefore, the eigenvalues and eigenvectors can be calculated with two simple relationships, and one does not need to perform lengthy matrix operations. This is because the matrix has become diagonal and not block diagonal.

After this simple calculation, we use a similar approach for the second equation. Having the solution of the first equation (moments in each node), the deflections can be obtained by the following equation:

$$\{\mathbf{w}\} = -\frac{1}{D}a^2\sum_i \frac{\{\boldsymbol{\varphi}\}_i\{\boldsymbol{\varphi}\}_i^t}{\lambda_i}\{\mathbf{M}\}.$$

In order to clarify the problem, we consider a numerical example. Suppose we have a square plate with edge length of L and the number of subdivisions is six in each direction. Then, the number of nodes will be five in each direction and using the above relationships, the eigenvalues will be as

$$\lambda = \text{eig}(\mathbf{C}) = -4 + 2\cos\frac{i\pi}{6} + 2\cos\frac{j\pi}{6} \qquad i = 1:5; j = 1:5$$

$$\lambda = \{-7.4641, -6.7321, \ldots, -1.2679, -0.5359\}$$

The corresponding eigenvectors can easily be obtained. As an example, the first eigenvector is obtained as

$$\{\boldsymbol{\varphi}\}_1 = \sin\left(\frac{j\pi}{6}\right) \otimes \sin\left(\frac{'j'\pi}{6}\right); \quad j = 1:5; j' = 1:5$$

$$\{\boldsymbol{\varphi}\}_1 = \left\{0.5, \frac{\sqrt{3}}{2}, 1, \frac{\sqrt{3}}{2}, 0.5\right\} \otimes \left\{0.5, \frac{\sqrt{3}}{2}, 1, \frac{\sqrt{3}}{2}, 0.5\right\}$$
$$= \left\{0.25, \frac{\sqrt{3}}{4}, \ldots, \frac{\sqrt{3}}{4}, 0.25\right\}$$

Therefore,

$$\{\mathbf{M}\} = -P_0\left(\frac{L}{6}\right)^2 \sum_i \frac{\{\boldsymbol{\varphi}\}_i \{\boldsymbol{\varphi}\}_i^t}{\lambda_i}; \quad a = \frac{L}{6}$$

$$\{\mathbf{M}\} = \{0.0264, 0.390, 0.427, 0.390, \ldots, 0.0264\} P_0 L^2.$$

Now, all these values are put in the right-hand side of the deflection equation in the form of a vector. As it was mentioned, for the solution of the second equation, the eigenvalues and eigenvectors are similar to those of the previous case. Thus,

$$\{\mathbf{w}\} = -\frac{1}{D} a^2 \sum_i \frac{\{\boldsymbol{\varphi}\}_i \{\boldsymbol{\varphi}\}_i^t}{\lambda_i} \{\mathbf{M}\} = \{0.0011, 0.0019, 0.0021, \ldots, 0.0011\} \frac{P_0 L^4}{D}.$$

As an example, the deflection at the central node will be $\frac{0.00405 P_0 L^4}{D}$. This deflection can be calculated by analytical methods as $\frac{0.00406 P_0 L^4}{D}$. Considering $n = 5$, we will have a small error in the fifth digit. It should be mentioned that this error belongs to the finite difference formulation and not the method being used. Even if the number of subdivisions is increased, a similar performance will be observed. It can be seen that using the present method requires no inversion or direct solution of equations, and only the eigenvalues and eigenvectors of generators should be calculated. This calculation appeared in the form of simple relationships because of the simplicity of the forms of the generators.

The remaining operation can easily be performed. As an example, for $\upsilon = 0.3$, the bending moments at the centre of the plate will be

$$M_x = M_y = (1 + \upsilon)\frac{M_m}{2} = 0.046875 P_0 L^2$$

It should be noted that for a nonsymmetric loading, the solution process does not change and the eigenvalues and eigenvectors will be the same and only the solution vector will be different.

The method presented in this chapter simplifies the analysis of the regular structures to a great extend. This method avoids the direct solution of equations

corresponding to the stiffness matrix, and analysis of large-scale structures requires the formation of much smaller matrices. Thus, using this method, much bigger structures can be solved with a higher speed.

The application of this method is not confined to regular structures. It can be used in the solution of the problems where the corresponding solution matrix can be written in the form of the sum of some Kronecker products. In Example 8.3, a finite difference solution of a plate has been included in this chapter to illustrate this point of view.

When the structures contain cut-outs or some modifications are performed on their regular models, the problem can still be dealt with incorporating the results of the recent developments [6, 7].

8.3 Static and Modal Analyses of Structures with Different Repeated Patterns

Now suppose a number of nodes or members are added to a model. One of the iterative methods for such a problem is condensation in which some DOFs are eliminated and some others are maintained. As a well-known approach of this kind, one can refer to the Guyan's method. This method is a static condensation approach in which the DOFs of the inertia terms are ignored. After that, for reducing the error in the static condensation, in the solution of dynamic problems, other amendments are performed by the researcher. One such an amendment is that of Paz, which can be considered as the generalisation of the static condensation. Other methods are also introduced, where the inverse of the stiffness matrix is obtained using the Taylor's series expansion. Recent approach can be found in Refs. [8–10]. Pellegrino and Calladine [11, 12] have avoided the inversion of the stiffness matrix using the SVD of the equilibrium matrix of the structure.

In the present section, some concepts of the force method are utilised; however, unlike the standard force method where the selected primary structure is determinate, here it is indeterminate and constitutes the regular part of the structure, and the internal forces of the additional members which make the structure irregular are selected as redundants. Here, the primary structure can be analysed using concepts of graph theory and/or group theory.

In this section, the main aim is to perform static and modal analysis of those structures which have different repeated patterns. These types of structures have regularity and irregularities in their model. Using a suitable nodal numbering, we transform the stiffness and mass matrices into two block-diagonal forms, the inverse of the stiffness matrix of the corresponding regular part becomes available, and the static, dynamic, free vibration and natural frequencies of the structure can be obtained.

First a brief introduction is provided to the previously developed methods on eigensolution of regular structures. This section is organised in three parts consisting of eigenvalues, eigenvectors and solution of a set of linear equations.

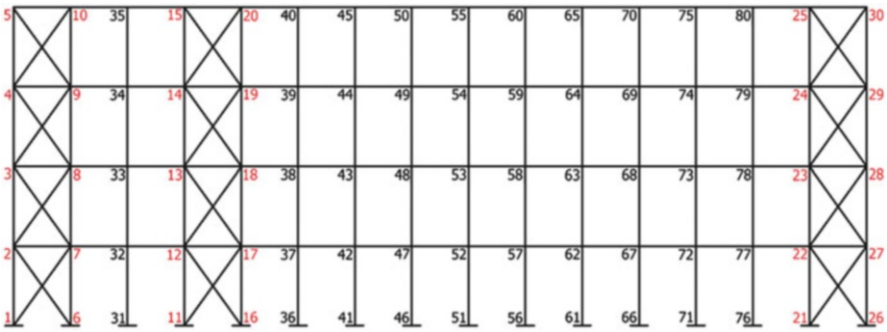

Fig. 8.5 A plane frame with repeated submodels and its nodal ordering

8.3.1 Static Analysis of Structures with Repeated Patterns

In this section, the present method is described with the help of an example. Suppose we want to perform a static analysis of the structure shown in Fig. 8.5, using the stiffness method. It can be seen that in this structure, two different types of repetitions are involved. One part has a regular form which fulfils the conditions of Eq. 8.2 and for which the eigenvalues, eigenvectors and the inverse of the stiffness matrix can easily be obtained. For this purpose, as it can be seen in the figure, first the irregular nodes (nodes 1–30) are numbered (identified in red colour), followed by numbering the internal nodes (nodes 31–80) which belong to the regular submodel. After assembling the stiffness matrix and forming the reduced stiffness matrix $\mathbf{K}$, we have

$$\mathbf{K} = \begin{bmatrix} \mathbf{K}_{\mathrm{mm}} & \mathbf{K}_{\mathrm{ms}} \\ \mathbf{K}_{\mathrm{ms}} & \mathbf{K}_{\mathrm{ss}} \end{bmatrix} \tag{8.30}$$

where the subscript m corresponds to the nodes numbered from 1 to 30 and the subscript s belongs to the nodes numbered from 31 to 80. The matrix $\mathbf{K}$ in this example have dimension 192.

Showing the inverse of the matrix $\mathbf{K}$ by $\mathbf{D}$, we have [13]

$$\begin{aligned} \mathbf{K}^{-1} = \mathbf{D} &= \begin{bmatrix} \mathbf{D}_{\mathrm{mm}} & \mathbf{D}_{\mathrm{ms}} \\ \mathbf{D}_{\mathrm{ms}}^{\mathrm{t}} & \mathbf{D}_{\mathrm{ss}} \end{bmatrix} \\ \boldsymbol{\Gamma} &= \mathbf{K}_{\mathrm{mm}} - \mathbf{K}_{\mathrm{ms}}\mathbf{K}_{\mathrm{ss}}^{-1}\mathbf{K}_{\mathrm{ms}}^{\mathrm{t}} \\ \mathbf{D}_{\mathrm{mm}} &= \boldsymbol{\Gamma}^{-1} \\ \mathbf{D}_{\mathrm{ms}} &= -\boldsymbol{\Gamma}^{-1}\mathbf{K}_{\mathrm{ms}}\mathbf{K}_{\mathrm{ss}}^{-1} \\ \mathbf{D}_{\mathrm{ss}} &= \mathbf{K}_{\mathrm{ss}}^{-1} - \mathbf{K}_{\mathrm{ss}}^{-1}\mathbf{K}_{\mathrm{ms}}^{\mathrm{t}}\mathbf{D}_{\mathrm{ms}}^{\mathrm{t}} \end{aligned} \tag{8.31}$$

The above process indicates that for finding the inverse of a matrix of dimension 192, using this method, the inverse of two matrices $\mathbf{K}_{ss}$ and Γ of dimensions 120 and 72 should be found. But the matrix $\mathbf{K}_{ss}$ is a block matrix of the following form:

$$\mathbf{K}_{ss} = \begin{bmatrix} \mathbf{A} & \mathbf{0} & \mathbf{0} & & . & . & \mathbf{0} \\ \mathbf{0} & \mathbf{A} & \mathbf{B} & \mathbf{0} & & & \\ \mathbf{0} & \mathbf{B}^t & \mathbf{A} & . & . & & \\ . & \mathbf{0} & . & . & . & \mathbf{0} & \\ . & & . & . & . & \mathbf{B} & \mathbf{0} \\ & & & \mathbf{0} & \mathbf{B}^t & \mathbf{A} & \mathbf{B} \\ \mathbf{0} & & & & \mathbf{0} & \mathbf{B}^t & \mathbf{A} \end{bmatrix}. \tag{8.32}$$

The $\mathbf{K}_{ss}$ matrix is a block matrix of dimension 10 with each block having dimension 12. Separating the matrix $\mathbf{A}$ as an independent block, one can show that the matrix $\mathbf{K}_{ss}$ has the following form:

$$\mathbf{K}_{ss} = \begin{bmatrix} \mathbf{A} & \mathbf{0} \\ \mathbf{0} & \mathbf{R}_9(\mathbf{A}, \mathbf{B}, \mathbf{B}^t) \end{bmatrix} \tag{8.33}$$

where the form $\mathbf{R}$ is defined as

$$\mathbf{R}_n(\mathbf{A}, \mathbf{B}, \mathbf{B}^t) = \begin{bmatrix} \mathbf{A} & \mathbf{B} & \mathbf{0} & \mathbf{0} & . & . & \mathbf{0} \\ \mathbf{B}^t & \mathbf{A} & \mathbf{B} & \mathbf{0} & & & \\ \mathbf{0} & \mathbf{B}^t & \mathbf{A} & . & . & & \\ . & \mathbf{0} & . & . & . & \mathbf{0} & \\ . & & . & . & . & \mathbf{B} & \mathbf{0} \\ & & & \mathbf{0} & \mathbf{B}^t & \mathbf{A} & \mathbf{B} \\ \mathbf{0} & & & & \mathbf{0} & \mathbf{B}^t & \mathbf{A} \end{bmatrix}. \tag{8.34}$$

This form is exactly identical to the matrix arising from the finite element analysis of repeated structures. Considering the block-diagonal nature of the matrix $\mathbf{K}_{ss}$, its inverse can be found as follows:

$$\mathbf{K}_{ss}^{-1} = \begin{bmatrix} \mathbf{A}^{-1} & \mathbf{0} \\ \mathbf{0} & \mathbf{R}_9^{-1}(\mathbf{A}, \mathbf{B}, \mathbf{B}^t) \end{bmatrix}. \tag{8.35}$$

Therefore, we need to find the inverse of $\mathbf{R}$.

For calculating the eigenvalues and eigenvectors of a block circulant matrices, there are very simple relationships [14]. If the matrix $\mathbf{R}$ contains two blocks of $\mathbf{B}$ and $\mathbf{B}^t$ at its corners, we will obtain such a matrix. Therefore, we express $\mathbf{R}$ in the following form:

$$\mathbf{R}=\mathbf{K}'+\mathbf{K}''\Rightarrow \begin{bmatrix} \mathbf{A} & \mathbf{B} & \mathbf{0} & \mathbf{0} & . & . & \mathbf{0} \\ \mathbf{B}^{\mathrm{t}} & \mathbf{A} & \mathbf{B} & \mathbf{0} & & & \\ \mathbf{0} & \mathbf{B}^{\mathrm{t}} & \mathbf{A} & \mathbf{B} & & & \\ \mathbf{0} & \mathbf{0} & \mathbf{B}^{\mathrm{t}} & \mathbf{A} & & & \\ . & & & & . & & \\ . & & & & & . & \mathbf{B} \\ \mathbf{0} & & & & & \mathbf{B}^{\mathrm{t}} & \mathbf{A} \end{bmatrix}_{9\times 9} =$$

$$\begin{bmatrix} \mathbf{A} & \mathbf{B} & \mathbf{0} & \mathbf{0} & . & . & \mathbf{B}^{\mathrm{t}} \\ \mathbf{B}^{\mathrm{t}} & \mathbf{A} & \mathbf{B} & \mathbf{0} & & & \\ \mathbf{0} & \mathbf{B}^{\mathrm{t}} & \mathbf{A} & \mathbf{B} & & & \\ \mathbf{0} & \mathbf{0} & \mathbf{B}^{\mathrm{t}} & \mathbf{A} & & & \\ . & & & & . & & \\ . & & & & & . & \mathbf{B} \\ \mathbf{B} & & & & & \mathbf{B}^{\mathrm{t}} & \mathbf{A} \end{bmatrix}_{9\times 9} + \begin{bmatrix} \mathbf{0} & \mathbf{0} & \mathbf{0} & \mathbf{0} & . & . & -\mathbf{B}^{\mathrm{t}} \\ \mathbf{0} & \mathbf{0} & \mathbf{0} & \mathbf{0} & & & \\ \mathbf{0} & \mathbf{0} & \mathbf{0} & \mathbf{0} & & & \\ \mathbf{0} & \mathbf{0} & \mathbf{0} & \mathbf{0} & & & \\ . & & & & . & & \\ . & & & & & . & \mathbf{0} \\ -\mathbf{B} & & & & & \mathbf{0} & \mathbf{0} \end{bmatrix}_{9\times 9} . \tag{8.36}$$

Showing the inverse of the matrix $\mathbf{K}'$ by $\mathbf{E}$, we will have

$$\mathbf{R}^{-1}=[\mathbf{K}'+\mathbf{K}'']^{-1}=\left\{\mathbf{K}'\left\{\mathbf{I}+\mathbf{K}''^{-1}\mathbf{K}''\right\}\right\}^{-1}=[\mathbf{I}+\mathbf{E}\mathbf{K}'']^{-1}\mathbf{E}. \tag{8.37}$$

Interchanging the position of the rows and columns corresponding to block 9 with those of block 2 from matrices $\mathbf{K}''$ and $\mathbf{E}$, the corresponding matrices will change to a form with two blocks as

$$\overline{\mathbf{K}}''=\begin{bmatrix} \mathbf{0} & -\mathbf{B}^{\mathrm{t}} & \mathbf{0} & \mathbf{0} & & & & & \\ -\mathbf{B} & \mathbf{0} & \mathbf{0} & & & & & & \\ & . & . & . & & & & & \\ & & . & . & . & & & & \\ & & & . & . & . & & & \\ & & & & . & . & . & & \\ & & & & & . & . & . & \\ & & & & & & . & \mathbf{0} & \mathbf{0} \\ \mathbf{0} & & & & & & & \mathbf{0} & \mathbf{0} \end{bmatrix}_{9\times 9} = \begin{bmatrix} \mathbf{K}_1 & \mathbf{0} \\ \mathbf{0} & \mathbf{0} \end{bmatrix}$$

$$\mathbf{K}_1=-\mathbf{R}_2(\mathbf{0},\mathbf{B}^{\mathrm{t}},\mathbf{B}) \tag{8.38}$$

where $\overline{\mathbf{K}}''$ is the same as $\mathbf{K}''$ after interchanging the last row with the second row and the last column with the second column.

Now, considering the method presented in [3] and Eq. 8.23, we obtain the following:

$$[\mathbf{I}+\mathbf{E}\mathbf{K}'']^{-1}\mathbf{E} = \left(\begin{bmatrix}\mathbf{I} & \mathbf{0}\\ \mathbf{0} & \mathbf{I}\end{bmatrix} + \begin{bmatrix}\mathbf{E}_{11} & \mathbf{E}_{12}\\ \mathbf{E}_{21} & \mathbf{E}_{22}\end{bmatrix}\begin{bmatrix}\mathbf{K}_1 & \mathbf{0}\\ \mathbf{0} & \mathbf{0}\end{bmatrix}\right)^{-1}\mathbf{E}$$
$$= \begin{bmatrix}\mathbf{I}+\mathbf{E}_{11}\mathbf{K}_1 & \mathbf{0}\\ \mathbf{E}_{21}\mathbf{K}_1 & \mathbf{I}\end{bmatrix}^{-1}\mathbf{E} = \begin{bmatrix}(\mathbf{I}+\mathbf{E}_{11}\mathbf{K}_1)^{-1} & \mathbf{0}\\ -\mathbf{E}_{21}\mathbf{K}_1(\mathbf{I}+\mathbf{E}_{11}\mathbf{K}_1)^{-1} & \mathbf{I}\end{bmatrix}\mathbf{E} \quad (8.39)$$

The inverse of $\mathbf{K}'$ can be obtained using its eigenvalues, since

$$\mathbf{K}' = \mathbf{I}\otimes\mathbf{A} + \mathbf{H}\otimes\mathbf{B} + \mathbf{H}^{t}\otimes\mathbf{B}^{t} = \sum_{i=1}^{3}\mathbf{A}_i\otimes\mathbf{B}_i \quad (8.40)$$

where $\mathbf{H}$ is a circulant matrix of the following form:

$$\mathbf{H} = \begin{bmatrix}0 & 1 & 0 & 0 & . & . & 0\\ 0 & 0 & 1 & 0 & & & \\ 0 & 0 & 0 & 1 & & & \\ 0 & 0 & 0 & 0 & & & \\ . & & & & . & & \\ . & & & & & . & 1\\ 1 & & & & & 0 & 0\end{bmatrix}_{9\times 9}. \quad (8.41)$$

$\mathbf{H}$ is an orthogonal matrix, and the two matrices $\mathbf{H}$ and $\mathbf{H}^{t}$ commute with respect to multiplication, that is,

$$\mathbf{H}\mathbf{H}^{t} = \mathbf{H}^{t}\mathbf{H} = \mathbf{I}. \quad (8.42)$$

Therefore, considering Eqs. 8.3 and 8.26, the eigenvalues of $\mathbf{K}'$ will be obtained as follows:

$$\mathrm{eig}(\mathbf{K}') = \bigcup_{i=1}^{n}\mathrm{eig}(\mathbf{K}'_i);\quad \mathbf{K}'_i = \lambda_i(\mathbf{A}_1)\mathbf{B}_1 + \lambda_i(\mathbf{A}_2)\mathbf{B}_2 + \lambda_i(\mathbf{A}_3)\mathbf{B}_3. \quad (8.43)$$

After calculating the eigenvalues and using Eqs. 8.19 and 8.23, the inverse of $\mathbf{K}'$ is obtained. As it can be seen, in this method, instead of finding the inverse of $\mathbf{R}$ of dimension 108, we need the inverse of two regular matrices $\mathbf{K}'$ and $\mathbf{I}+\mathbf{E}_{11}\mathbf{K}_1$ (Eq. 8.39). The relationships corresponding to finding the inverse of the matrix $\mathbf{R}$ can also be obtained simpler as

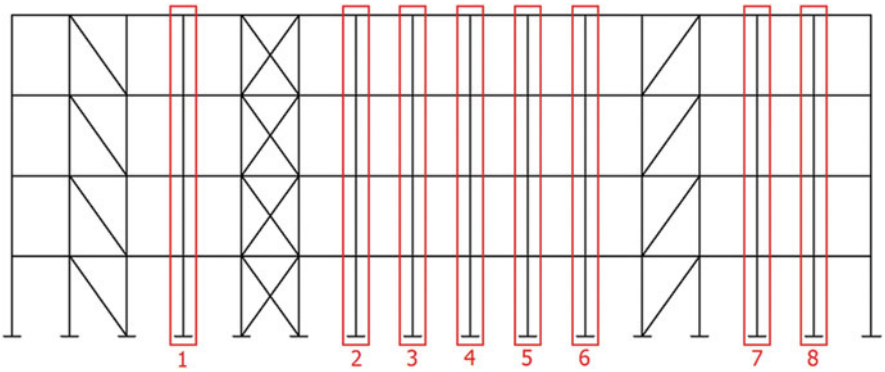

Fig. 8.6 A structural model with a repeated submodels

$$\mathbf{R}(\mathbf{A},\mathbf{B},\mathbf{B}^{\mathrm{t}}) \Rightarrow \begin{bmatrix} \mathbf{A} & \mathbf{B} & \mathbf{0} & \mathbf{0} & . & . & \mathbf{0} \\ \mathbf{B}^{\mathrm{t}} & \mathbf{A} & \mathbf{B} & \mathbf{0} & & & \\ \mathbf{0} & \mathbf{B}^{\mathrm{t}} & \mathbf{A} & \mathbf{B} & & & \\ \mathbf{0} & \mathbf{0} & \mathbf{B}^{\mathrm{t}} & \mathbf{A} & & & \\ . & & & & . & & \\ . & & & & & . & \mathbf{B} \\ \mathbf{0} & & & & & \mathbf{B}^{\mathrm{t}} & \mathbf{A} \end{bmatrix} = \begin{bmatrix} \mathbf{B}^{\mathrm{t}} & \mathbf{0} \\ \mathbf{0} & \mathbf{0} \\ \mathbf{0} & \mathbf{0} \\ \mathbf{0} & \mathbf{0} \\ & \\ . & . \\ \mathbf{0} & \mathbf{B} \end{bmatrix}$$

$$\begin{bmatrix} \mathbf{0} & \mathbf{0} & \mathbf{0} & \mathbf{0} & . & . & \mathbf{I} \\ \mathbf{I} & \mathbf{0} & \mathbf{0} & \mathbf{0} & . & . & \mathbf{0} \end{bmatrix} = \mathbf{K}' - \mathbf{UV}$$

$$\Rightarrow \mathbf{R}^{-1}(\mathbf{A},\mathbf{B},\mathbf{B}^{\mathrm{t}}) = (\mathbf{K}' - \mathbf{UV})^{-1}$$

$$= \mathbf{K}'^{-1} + \mathbf{K}'^{-1}\mathbf{U}\left(\mathbf{I} - \mathbf{V}\mathbf{K}'^{-1}\mathbf{U}\right)^{-1}\mathbf{V}\mathbf{K}'^{-1}. \tag{8.44}$$

As it can be seen from the above relationship, in this type of formulation, in order to find **R,** we should invert two matrices. One is the inverse of $\mathbf{I} - \mathbf{V}\mathbf{K}'^{-1}\mathbf{U}$ which is the same as $\mathbf{I} + \mathbf{E}_{11}\mathbf{K}_1$, and in this example, it is a matrix with two blocks each being of dimension 12. The other one is $\mathbf{K}'$ which is the sum of three Kronecker products and its eigenvalues, and thus, its inverse can easily be found. Finally, the inversion of a matrix of dimension 192 is changed to calculating eigenvalues of 10 matrices of dimension 12, one inverse of a matrix of dimension 24 and one inverse of a matrix of dimension 72.

In summary, here, matrices with repeated patterns do not satisfy Eq. 8.2, and by employing some matrix operations, their inversion is altered to the inversion of decomposable block matrices. In this way, a simple relationship is found for the inversion of structural matrices of finite element models with repeated patterns using an analytical method. Finally, it should briefly be mentioned that the method of nodal ordering is performed in the present approach. In general, the connectivity of the regular part of the structural model follows a fixed pattern. As an example, in Fig. 8.6, the nodes which are

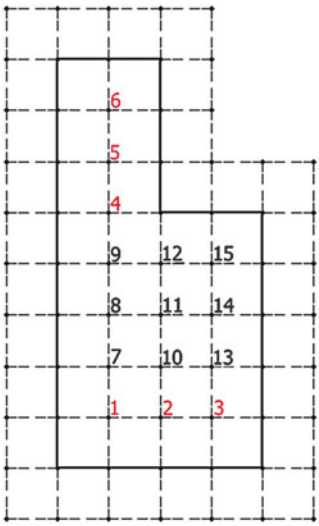

Fig. 8.7 A plate with nodal numbering for finite difference method

encircled in rectangles (identified in red) have a repeated pattern which is different with the remaining part. In the present method, these patterns are identified and the corresponding nodes are numbered, followed by numbering the nodes of the remaining part of the model. The important point is that these repeated parts can situate in different positions in the model. As it can be seen from Fig. 8.6, the structure is braced in different forms; however, there exists eight fixed repeated submodels.

8.4 Free Vibration Analysis of Irregular Structure Comprising of Regular Parts

Now, suppose we want to perform the modal analysis of the structure shown in Fig. 8.7 and find its natural eigenfrequencies. Here, we use dynamic condensation for calculating the eigenfrequencies. Similar to static analysis, first we perform a suitable nodal ordering to form the reduced stiffness matrix in the form of Eq. 8.16 and $\mathbf{K}_{ss}$ in the form of Eq. 8.18. In a similar way, the mass matrix is obtained in the following form:

$$\mathbf{M} = \begin{bmatrix} \mathbf{M}_{mm} & \mathbf{M}_{ms} \\ \mathbf{M}_{ms}^{t} & \mathbf{M}_{ss} \end{bmatrix} \tag{8.45}$$

where the subscript m corresponds to the nodes 1–30 and the subscript *s* corresponds to nodes 31–80. The aim is to solve the following eigenvalue problem:

$$(\mathbf{K} - \lambda_i \mathbf{M})\Phi_i = \mathbf{0}; \quad i = 1 : n \tag{8.46}$$

where n = 192. One can express the above equation as

$$\left(\begin{bmatrix} \mathbf{K}_{mm} & \mathbf{K}_{ms} \\ \mathbf{K}_{ms}^{t} & \mathbf{K}_{ss} \end{bmatrix} - \lambda \begin{bmatrix} \mathbf{M}_{mm} & \mathbf{M}_{ms} \\ \mathbf{M}_{ms}^{t} & \mathbf{M}_{ss} \end{bmatrix}\right)\begin{pmatrix} \Phi_m \\ \Phi_s \end{pmatrix} = \begin{pmatrix} \mathbf{0} \\ \mathbf{0} \end{pmatrix}. \tag{8.47}$$

Using the improved dynamic condensation of [15], instead of solving the above problem, the problem of corresponding eigenvalues is defined as the following, and iteration is performed on it.

$$\left(\mathbf{K}^0 - \lambda_r^0 \mathbf{M}^0\right)\Phi_r^{\mathbf{0}} = \mathbf{0}; \quad r = 1 : m \tag{8.48}$$

where m = 72, and $\mathbf{K}^0$ and $\mathbf{M}^0$ are as follows:

$$\mathbf{K}^0 = \mathbf{K}_{mm} - \mathbf{K}_{ms}\mathbf{K}_{ss}^{-1}\mathbf{K}_{ms}^{t} \tag{8.49}$$

$$\mathbf{M}^0 = \mathbf{M}_{mm} - \mathbf{M}_{ms}\mathbf{K}_{ss}^{-1}\mathbf{K}_{ma}^{t} - \mathbf{K}_{ms}\mathbf{K}_{ss}^{-1}\mathbf{K}_{ms}^{t} + \mathbf{K}_{ms}\mathbf{K}_{ss}^{-1}\mathbf{M}_{ss}\mathbf{K}_{ss}^{-1}\mathbf{K}_{ms}^{t}. \tag{8.50}$$

According to the existing relationships for iteration in dynamic condensation, λ^0 and Φ^0 obtained from Eq. 8.34 are modified until the eigenvectors are obtained with the required accuracy.

As it can be seen, using this method, instead of solving an eigenvalue problem of dimension 192, in this example, it is sufficient to find the inverse of $\mathbf{K}_{ss}$ of dimension 120 and solve an eigenvalue problem common to $\mathbf{K}^0$ and $\mathbf{M}^0$ which is of dimension 72.

The closed-form solution of the inverse of $\mathbf{K}_{ss}$ can be obtained using Eqs. 8.27, 8.28, and 8.29 utilising the eigenvalues of 10 matrices of dimension 12 and the inverse of a matrix of dimension 24. The eigenvalue problem of dimension 72 is solved by an iterative dynamic condensation. It should be mentioned that the advantage of using dynamic condensation is that it does not need additional inversion and merely requires some matrix multiplication.

8.4.1 Illustrative Examples

Example 8.4. In this example, the aim is to calculate the buckling load and eigenfrequencies of a simple-fixed beam. Here, the central finite difference method is utilised. The equation of buckling and vibration of this beam are as follows:

$$\frac{d^4w}{dx^4} + \frac{N}{EI}\frac{d^2w}{dx^2} = 0; \quad \lambda = \frac{N}{EI}h^2$$

$$\frac{d^4w}{dx^4} - \beta^4 w = 0; \quad \beta = \frac{\rho\omega^2}{EI}; \quad \lambda = (\beta h)^4.$$

It is obvious that the two end nodes of the beam are different because of having different boundary conditions while the intermediate nodes are similar. Selecting $n = 10$ for the calculation, first the two end nodes ($m = 2$) and then the intermediate nodes ($s = 8$) should be numbered.

Using the finite difference equations, the final equations to be solved are as follows:

$$(\mathbf{A} - \lambda_i \mathbf{B})\Phi_i = 0 \Rightarrow \left(\begin{bmatrix} \mathbf{A}_{mm} & \mathbf{A}_{ms} \\ \mathbf{A}_{ms}^t & \mathbf{A}_{ss} \end{bmatrix} - \lambda \begin{bmatrix} \mathbf{B}_{mm} & \mathbf{B}_{ms} \\ \mathbf{B}_{ms}^t & \mathbf{B}_{ss} \end{bmatrix} \right) \begin{pmatrix} \Phi_m \\ \Phi_s \end{pmatrix} = \begin{pmatrix} \mathbf{0} \\ \mathbf{0} \end{pmatrix}$$

where

$$\mathbf{A}_{mm} = \begin{bmatrix} 7 & 0 \\ 0 & 5 \end{bmatrix}; \quad \mathbf{A}_{ss} = \mathbf{F}_8(6, -4, 6, 1); \quad \mathbf{A}_{ms} = \begin{bmatrix} -4 & 1 & 0 & 0 & 0 & 0 & 0 & 0 \\ 0 & 0 & 0 & 0 & 0 & 0 & 1 & -4 \end{bmatrix}.$$

Also the matrix $\mathbf{B}$ for buckling will be as follows:

$$\mathbf{B}_{mm} = 2\mathbf{I}_2; \quad \mathbf{B}_{ss} = \mathbf{F}_8(2, -1, 2); \quad \mathbf{B}_{ms} = \begin{bmatrix} -1 & 0 & 0 & 0 & 0 & 0 & 0 & 0 \\ 0 & 0 & 0 & 0 & 0 & 0 & 0 & -1 \end{bmatrix},$$

and for the problem of vibration, we have $\mathbf{B} = \mathbf{I}_{10}$.

The matrix $\mathbf{A}_{ss}$ has dimension 8 and it is penta-diagonal. Thus, it can be written as

$$\mathbf{A}_{ss} = \mathbf{F}_8(6, -4, 6, 1) = \sum_{i=1}^{3} (\mathbf{A}_i \otimes \mathbf{B}_i).$$

Since $t_1 = \frac{a_i - c_i}{d_i}$ and $t_2 = \frac{a_i - c_i + d_i}{b_i}$ for three matrices $\mathbf{A}_i$ are identical, therefore, $\mathbf{A}_i\mathbf{A}_j = \mathbf{A}_j\mathbf{A}_i$. Thus, $\mathbf{A}_{ss}$ is decomposed into eight numerical blocks. Therefore, in this example, one needs only to solve an eigenvalue problem of dimension $m = 2$.

Example 8.5. In this example, the aim is to calculate the buckling load of a plate with some additional part. Here, first the internal nodes are numbered for which the eigenvalues can be calculated. We have the subgraph S with $s = 9$ nodes and the remaining nodes for the subgraph M with $m = 6$ nodes. It should be mentioned that the number of nodes is purposely chosen low for a better illustration of the approach. The nodal numbering is illustrated in Fig. 8.7.

The governing differential equation of the problem for the case when the loading is in x-direction will be as follows:

$$\nabla^4 w + \frac{N_x}{D} \frac{\partial^2 w}{\partial x^2} = 0.$$

Using the finite difference method, a similar set of equations to that of the previous example should be solved with the only difference that we have

$$\mathbf{A}_{ss} = \begin{bmatrix} \mathbf{E} & \mathbf{F} & \mathbf{I} \\ \mathbf{F} & \mathbf{E}+\mathbf{I} & \mathbf{F} \\ \mathbf{I} & \mathbf{F} & \mathbf{E} \end{bmatrix}; \ \mathbf{E} = \begin{bmatrix} 19 & -8 & 1 \\ -8 & 19 & -8 \\ 1 & -8 & 19 \end{bmatrix}; \ \mathbf{F} = \begin{bmatrix} -8 & 2 & 0 \\ 2 & -8 & 2 \\ 0 & 2 & -8 \end{bmatrix}.$$

In general, $\mathbf{A}_{ss}$ is a penta-diagonal block matrix, and since the nodes are chosen from the regular part of the model satisfying the condition $\mathbf{A}_i\mathbf{A}_j = \mathbf{A}_j\mathbf{A}_i$, thus, the eigenvalues and its inverse can easily be found using the relationships (8.16). Also we have

$$\mathbf{B}_{ss} = \begin{bmatrix} \mathbf{2I} & \mathbf{-I} & \mathbf{0} \\ \mathbf{-I} & \mathbf{2I} & \mathbf{-I} \\ \mathbf{0} & \mathbf{-I} & \mathbf{2I} \end{bmatrix}.$$

Therefore, here, finding the eigenvalues of a matrix of dimension $n = 15$ is changed to the calculation of the eigenvalues of three matrices of dimension 3 and one matrix of dimension 6. The smallest eigenvalue is obtained as $\lambda = 1.7673$ in four iterations, while the exact value is $\lambda = 1.7597$.

Example 8.6. In this example, the aim is to find the buckling load of a square plate with side length a. The supports at two edges are simple and the other two sides fixed. The load is applied in x-direction. The plate is divided into eight segments in each side. Obviously the entries of the corresponding matrix will be different for internal nodes and external nodes. Thus, here, $s = 25$ and the remaining nodes belong to the subgraph M with $m = 24$ nodes. The nodal numbering is illustrated in Fig. 8.8.

Here, the matrix $\mathbf{A}_{ss}$ will be as

$$\mathbf{A}_{ss} = \mathbf{F}_5(\mathbf{E}, \mathbf{F}, \mathbf{E}, \mathbf{I}); \ \mathbf{E} = \mathbf{F}_5(20, -8, 20, 1); \ \mathbf{F} = \mathbf{F}_5(-8, 2, -8).$$

Also we have

$$\mathbf{B}_{ss} = \mathbf{I}_5 \otimes \mathbf{F}_5(2, -1, 2).$$

The rest of the calculation is similar to that of the previous example.

Example 8.7. This example is taken from Ref. [16]. A mass–spring system is considered as shown in Fig. 8.9. Here, the numbering is altered and first the two end nodes are numbered $(m = 2)$ followed by the numbering of the remaining intermediate nodes $(s = 28)$.

With this numbering, the matrices **K** and **M** will have the following forms:

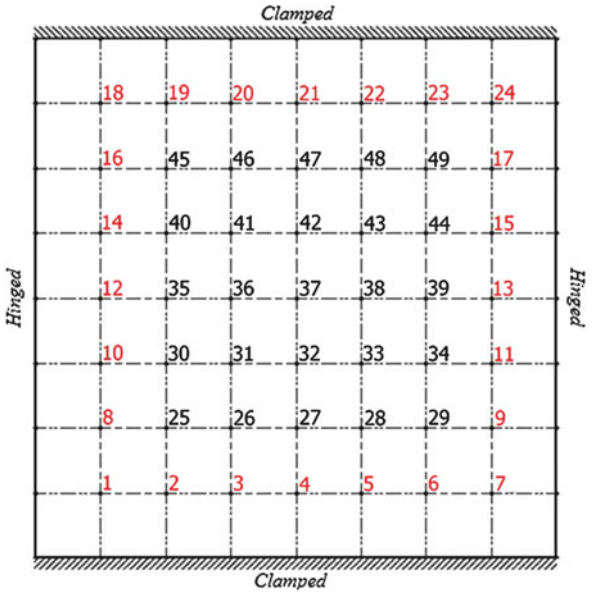

Fig. 8.8 A plate with different boundary conditions and its nodal numbering

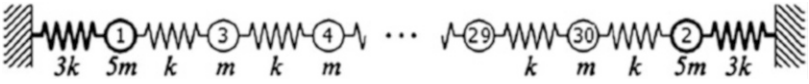

Fig. 8.9 A system of mass–spring and its numbering

$$\mathbf{K} = \begin{bmatrix} \mathbf{K}_{mm} & \mathbf{K}_{ms} \\ \mathbf{K}_{ms}^{t} & \mathbf{K}_{ss} \end{bmatrix}; \quad \mathbf{M} = \begin{bmatrix} \mathbf{M}_{mm} & \mathbf{M}_{ms} \\ \mathbf{M}_{ms}^{t} & \mathbf{M}_{ss} \end{bmatrix}$$

where

$$\mathbf{K}_{mm} = 4k\mathbf{I}_2; \quad \mathbf{K}_{ss} = k\mathbf{F}_{28}(2,-1,2); \quad \mathbf{K}_{ms} = k\begin{bmatrix} -1 & 0 & . & . & 0 & 0 \\ 0 & 0 & . & . & 0 & -1 \end{bmatrix}_{2\times 28}$$

$$\mathbf{M}_{mm} = 5m\mathbf{I}_2; \quad \mathbf{M}_{ss} = m\mathbf{I}_{28}; \quad \mathbf{M}_{ms} = m\mathbf{Z}_{2\times 28}$$

where $\mathbf{Z}$ is a matrix with all zero entries. The eigenvalues of $\mathbf{K}_{ss}$ are given in the form of a simple relationship in [17].

$$\text{eig}(\mathbf{K}_{ss}) = \text{eig}(\mathbf{F}_s(2,-1,2)) = 2 - 2\cos\frac{k\pi}{s+1}; \quad k = 1:s.$$

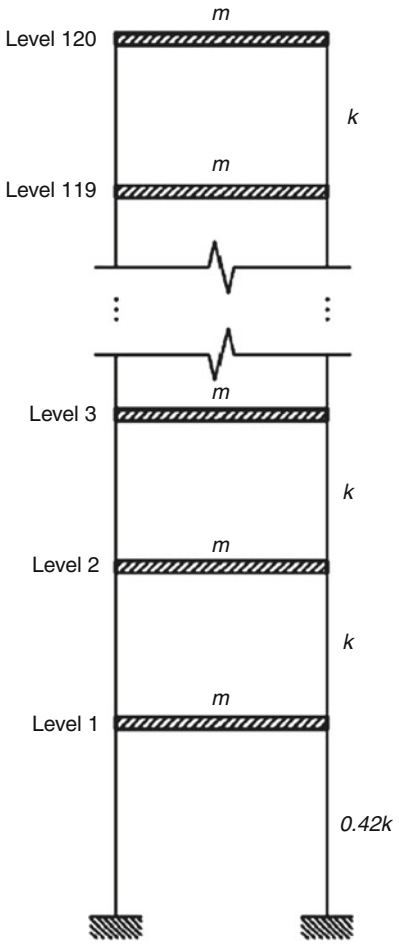

Fig. 8.10 A one-bay 120-storey shear frame

Therefore, one needs to solve an eigenvalue problem of dimension $\mathrm{m} = 2$ compared to the need for solution of an eigenvalue problem of dimension 12 in Ref. [16].

The smallest eigenvalue obtained from an exact method is $\lambda = 0.0112\mathrm{k/m}$, and using the present method after only four iterations, $\lambda = 0.0106\mathrm{k/m}$ is achieved.

Example 8.8. In this example, we want to find the eigenfrequencies of a 120-storey shear frame shown in Fig. 8.10. Here, the stiffness of the first storey is different with the remaining stories.

This example is taken from Ref. [16]. Here, first the nodes of the first and the last stories are numbered $(\mathrm{m} = 2)$ followed by those of the other stories $(\mathrm{s} = 118)$. The **K** and **M** matrices will have the following forms:

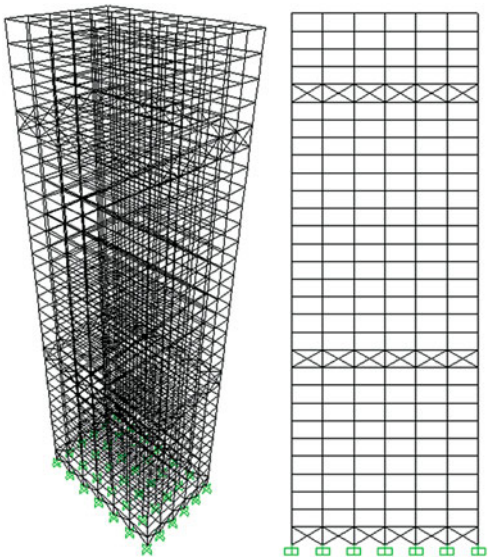

Fig. 8.11 The 3D model of a 30-storey frame and its elevation

$$\mathbf{K}_{\text{mm}} = \text{k}\begin{bmatrix} 1.42 & 0 \\ 0 & 1 \end{bmatrix};\quad \mathbf{K}_{\text{ss}} = \text{k}\mathbf{F}_{118}(2,-1,2);$$

$$\mathbf{K}_{\text{ms}} = \text{k}\begin{bmatrix} -1 & 0 & . & . & 0 & 0 \\ 0 & 0 & . & . & 0 & -1 \end{bmatrix}_{2\times 118}$$

$$\mathbf{M}_{\text{mm}} = \text{m}\mathbf{I}_2;\quad \mathbf{M}_{\text{ss}} = \text{m}\mathbf{I}_{118};\quad \mathbf{M}_{\text{ms}} = \text{m}\mathbf{Z}_{2\times 118}$$

The calculations will be identical to the previous example. Thus, only an eigenvalue problem of dimension $\text{m} = 2$ should be solved, compared to the method in [16] which requires the solution of a problem of dimension 16.

The smallest eigenvalue obtained from an exact method is $\omega = 01^{-2}\sqrt{1.6610\,\frac{\text{k}}{\text{m}}}$, and using the present method after only six iterations, the exact value is achieved.

Example 8.9. Figure 8.11 shows a 30-storey frame and in each storey it contains 42 columns and 78 beams. The supports of the structure are fixed in both directions. The physical and mechanical properties of the 3D frame for bending and truss elements are as follows:

$$\text{E} = 2.1\text{e}11\text{N/m}^2,\ \rho = 78500\text{N/m}^3, \text{I}_\text{x} = 6.572\text{e} - 5\text{m}^4, \text{I}_\text{y} = 3.301\text{e} - 6\text{m}^4,$$
$$\text{A} = 4.265\text{e} - 3\text{m}^2.$$

This means that the cross sections and physical properties of beams and bracings in all the stories are identical, 22 truss elements are added to the outer faces of the structure in stories 1, 11 and 26 to increase the stiffness of the structure. These elements take the structure out for regularity and make it an irregular one. Here,

applying the present method, the problem can efficiently be analysed. The suitable nodal numbering decomposes the stiffness and mass matrices into two parts, and these parts can separately be analysed.

For the free vibration analysis of this 3D frame, suitable nodal numbering is performed by ordering the nodes of the stories 1, 10, 11, 25, 26 and 30 first, followed by ordering the remaining nodes starting from lower stories and carrying on to the upper ones.

In this structure, each storey contains 42 free nodes and each node has six DOFs. Therefore, the reduced stiffness matrix is of dimension 7560×7560. As it is mentioned in dynamic condensation, the stiffness and mass matrices will be decomposed into two blocks of dimension m and s. The subscript m in this example corresponds to the nodes 1–42, 379–462, 1008–1092 and 1218–1260, and subscript belongs to the remaining nodes. It should be mentioned that the numbering starts from the first storey since the nodes of the structure at ground level are all fixed and are deleted from the overall stiffness matrix.

In this method, instead of solving a direct eigenvalue problem of dimension 7560×7560, we need to find the inverse of a matrix of dimension 6048×6048 corresponding to $\mathbf{K}_{ss}$ and solve an eigenvalue problem of a dimension 1512×1512. However, as it will be observed, the inverse of $\mathbf{K}_{ss}$ can be found simpler using its eigenvalues. The pattern of $\mathbf{K}_{ss}$ matrix for this example is as follows:

$$\mathbf{K}_{ss} = \begin{bmatrix} \mathbf{R}_8(\mathbf{A}, \mathbf{B}, \mathbf{B}^t) & \mathbf{0} & \mathbf{0} \\ \mathbf{0} & \mathbf{R}_{13}(\mathbf{A}', \mathbf{B}', \mathbf{B}'^t) & \mathbf{0} \\ \mathbf{0} & \mathbf{0} & \mathbf{R}_3(\mathbf{A}, \mathbf{B}, \mathbf{B}^t) \end{bmatrix}$$

where the matrices $\mathbf{A}$ and $\mathbf{B}$ have dimension 252×252. It is obvious that the inverse of the matrix $\mathbf{K}_{ss}$ can be expressed in the following form:

$$\mathbf{K}_{ss} = \begin{bmatrix} \mathbf{R}_8^{-1}(\mathbf{A}, \mathbf{B}, \mathbf{B}^t) & \mathbf{0} & \mathbf{0} \\ \mathbf{0} & \mathbf{R}_{13}^{-1}(\mathbf{A}', \mathbf{B}', \mathbf{B}'^t) & \mathbf{0} \\ \mathbf{0} & \mathbf{0} & \mathbf{R}_3^{-1}(\mathbf{A}, \mathbf{B}, \mathbf{B}^t) \end{bmatrix}$$

and for finding the inverse of the matrix $\mathbf{R}$, Eq. 8.30 will be utilised.

For the tower of this example, instead of solving a direct eigenvalue problem of dimension 7560×7560, we need to find the eigenvalues for 13 matrices of dimension 252, inverse of 3 matrices of dimension 504 and an eigenvalue problem of a common matrix of dimension 1512×1512.

After analysis of the structure with aforementioned properties, the angular frequency of this example is obtained as $\omega = 1.417\text{rad/s}$ and the period is obtained as $T = 4.435\text{s}$.

Example 8.10. Consider the tower shown in Fig. 8.12. This tower consists of bar elements, wherein the stories 1, 7, 13, 14, 20 have additional bracings and in the remaining stories, it has only one element. The supports of the structure in both

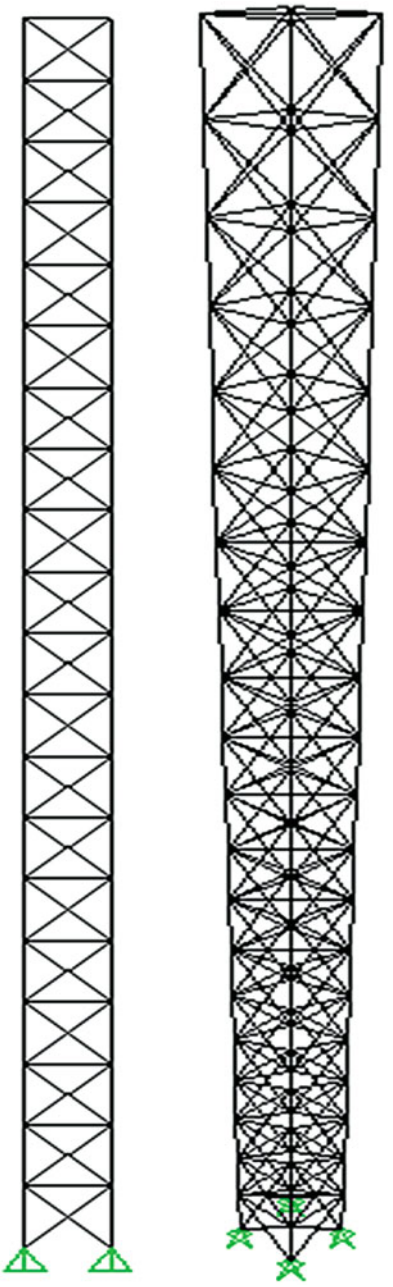

Fig. 8.12 The 3D model and elevation of a tower

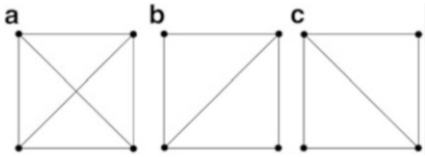

Fig. 8.13 (**a**) Plan of the stories 1, 7, 13, 14 and 20; (**b**) plan of the stories 2–7 and 15–19; (**c**) plan of the stories 8–12

directions are pin-jointed. The physical and mechanical properties of the 3D truss structure are as follows:

$$\mathrm{E} = 2.1\mathrm{e}11\mathrm{N/m}^2,\ \rho = 78500\mathrm{N/m}^3,\ \mathrm{A} = 4.265\mathrm{e} - 3\mathrm{m}^2.$$

This means the cross section and physical properties of the truss elements are identical in all the stories. In the stories 1, 7, 13, 14 and 20, two bar elements are added in order to increase the stiffness of the structure. These elements change the regular structure to an irregular one. Using the method of this chapter, employing a suitable nodal numbering, the stiffness and mass matrices are decomposed into two parts and each can separately be analysed.

For free vibration analysis of this 3D truss, first the nodes in the ceilings of the stories 1, 7, 13, 14 and 20 are numbered and then the remaining stories are numbered starting from the bottom storey moving to the top stories (Figs. 8.12 and 8.13).

This structure has four free nodes in each storey and each node has three translational DOFs. The structure has 20 stories, and therefore, its reduced stiffness matrix is of dimension 240×240. The stiffness and mass matrices are subdivided into two blocks of dimensions m and s. In this example, the subscript m corresponds to the nodes 1–4, 24–28, 48–56 and 76–80, and the subscript s corresponds to the remaining nodes.

For this example, instead of solving a direct eigenvalue problem of dimension 240×240, we need the inverse of a matrix of dimension 180×180 corresponding $\mathbf{K}_{\mathrm{ss}}$ and solve an eigenvalue problem of dimension 60×60. The matrix $\mathbf{K}_{\mathrm{ss}}$ in this example has the following form:

$$\mathbf{K}_{\mathrm{ss}} = \begin{bmatrix} \mathbf{R}_5(\mathbf{A}, \mathbf{B}, \mathbf{B}^{\mathrm{t}}) & \mathbf{0} & \mathbf{0} \\ \mathbf{0} & \mathbf{R}_5\left(\mathbf{A}', \mathbf{B}', \mathbf{B}'^{\mathrm{t}}\right) & \mathbf{0} \\ \mathbf{0} & \mathbf{0} & \mathbf{R}_5(\mathbf{A}, \mathbf{B}, \mathbf{B}^{\mathrm{t}}) \end{bmatrix}$$

where each matrix $\mathbf{A}$ and $\mathbf{B}$ have dimension 12×12. The inverse of this matrix is as follows:

$$\mathbf{K}_{\mathrm{ss}} = \begin{bmatrix} \mathbf{R}_5^{-1}(\mathbf{A}, \mathbf{B}, \mathbf{B}^{\mathrm{t}}) & \mathbf{0} & \mathbf{0} \\ \mathbf{0} & \mathbf{R}_5^{-1}\left(\mathbf{A}', \mathbf{B}', \mathbf{B}'^{\mathrm{t}}\right) & \mathbf{0} \\ \mathbf{0} & \mathbf{0} & \mathbf{R}_5^{-1}(\mathbf{A}, \mathbf{B}, \mathbf{B}^{\mathrm{t}}) \end{bmatrix}.$$

In order to find the inverse of $\mathbf{R}$, the Eq. 8.30 is utilised.

For this example, instead of solving a direct eigenvalue problem of dimension 240×240, we need to find the eigenvalues for 10 matrices of dimension 12, inverse of 2 matrices of dimension 24 and an eigenvalue problem of a common matrix of dimension 60×60.

After analysis of the structure with aforementioned properties, the angular frequency of this example is obtained as $\omega = 2.2116\text{rad/s}$ and the period is obtained as $T = 2.969\text{s}$. Obviously by increasing the number of stories of the structure, the power of the present method will become more apparent.

8.4.2 Discussion

In this chapter, structures are studied which have some kind of repeated patterns; however, they cannot be considered as regular structures. Even we can have models that can be regular, but the theorems previously proven for product graphs are not applicable, one example of which is the strong Kronecker products.

In this chapter, wherever we have the problem of inverting a matrix, a closed-form solution is utilised. For calculating the eigenvalues, a dynamic condensation method is employed. Though this method has an iterative nature, however, the corresponding operations are addition and multiplication. For analysis, we need to find the inverse of the matrix corresponding to the regular structure only once for which a closed-form solution is employed.

For the case when the aim is the static analysis, for inversion a closed-form solution is used. Choosing part of the model for which decomposition is applicable, one can utilise the dynamic condensation. This is because this method requires only the inversion of the matrix for the part that can easily be performed. Though this method is considered as an iterative approach, however, the inversion is performed only once, and the iterative part consists of only simple matrix additions and multiplications. This inversion corresponds to the regular part of the structure for which closed-form solution is available.

When we face an irregular structure which contains some regular parts, first we number the nodes corresponding to irregular part and show the blocks of the stiffness and mass matrices of this part with subscript m. According to the dynamic condensation, one should solve an eigenvalue problem of size equal to the dimension of this matrix. We should also find the inverse of a matrix of dimension equal to the nodes contained in the regular part of the structure. In solving the inverse of the matrices, we will have matrices of the form $\mathbf{R}_{\text{n}}(\mathbf{A}, \mathbf{B}, \mathbf{B}^{\text{t}})$, and if these matrices have n blocks and each block is of dimension l, then for the inversion, we should perform n time eigenvalue problem of dimension l and once the inverse of $\mathbf{I} + \mathbf{E}_{11}\mathbf{K}_1$ or $\mathbf{I} - \mathbf{V}\mathbf{K}'^{-1}\mathbf{U}$ with dimension $2l$ will be needed.

In order to compare the present method with the direct approach, the computation time and the number of different operations are provided in Table 8.1 for the last two examples. The considerable difference of the computational time shows the superiority of the present approach.

Table 8.1 Comparison of the computational time for the direct and present methods for Examples 8.9 and 8.10

	Direct method		Present method			
	Common eigenvalue	CPU time (s)	Inverse	Eigenvalue	Common eigenvalue	CPU time (s)
Example 8.9	1 matrix of 7560 × 7560	1,008.59146	3 matrices of 504 × 504	13 matrices of 252 × 252	1 matrix of 1512 × 1512	2.73376
Example 8.10	1 matrix of 240 × 240	0.8750	2 matrices of 24 × 24	10 matrices of 12 × 12	One matrix of 60 × 60	0.015

8.5 Block Circulant Matrices and Applications in Free Vibration Analysis of Cyclically Repetitive Structures

In this part, block circulant matrices and their properties are investigated. Circulant matrix can be considered as the sum of Kronecker products in which the first components have the commutativity property with respect to multiplication. The important fact is that the method for block diagonalisation of these matrices is much simpler than the previously developed methods, and one does not need to find an orthogonaliser matrix. As it will be shown that only the matrices corresponding to domes in the form of Cartesian product, strong Cartesian product and direct product are circulant, but for other structures such as diamatic domes, pyramid domes, flat double-layer grids and some family of transmission towers, these matrices are also block circulant.

8.5.1 Some Basic Definitions and Concepts of Block Circulant Matrices

In general, a block circulant matrix can be written as

$$\mathbf{C} = \begin{bmatrix} \mathbf{A}_1 & \mathbf{A}_2 & . & . & \mathbf{A}_{n-1} & \mathbf{A}_n \\ \mathbf{A}_n & \mathbf{A}_1 & . & . & \mathbf{A}_{n-2} & \mathbf{A}_{n-1} \\ . & . & . & . & . & . \\ . & . & . & . & . & . \\ \mathbf{A}_3 & \mathbf{A}_4 & . & . & \mathbf{A}_1 & \mathbf{A}_2 \\ \mathbf{A}_2 & \mathbf{A}_3 & . & . & \mathbf{A}_n & \mathbf{A}_1 \end{bmatrix}. \tag{8.51}$$

The entries of a block circulant matrix can also be numbers. Then, the matrix is known as a *circulant matrix*. The following circulant matrix is a good example of such a matrix:

$$\mathbf{P}_4 = \begin{bmatrix} 0 & 0 & 0 & 1 & 0 & 0 & 0 & 0 \\ 0 & 0 & 0 & 0 & 1 & 0 & 0 & 0 \\ 0 & 0 & 0 & 0 & 0 & 1 & 0 & 0 \\ 0 & 0 & 0 & 0 & 0 & 0 & 1 & 0 \\ 0 & 0 & 0 & 0 & 0 & 0 & 0 & 1 \\ 1 & 0 & 0 & 0 & 0 & 0 & 0 & 0 \\ 0 & 1 & 0 & 0 & 0 & 0 & 0 & 0 \\ 0 & 0 & 1 & 0 & 0 & 0 & 0 & 0 \end{bmatrix}. \tag{8.52}$$

4

This matrix also fulfils the definition of a permutation matrix, since each row and column contains only one entry as 1 and the remaining entries are zeros. The index 4 shows that the non-zero entry starts at column 4 and in each subsequent row moves one column ahead. With this definition, obviously we will have $\mathbf{P}_1 = \mathbf{I}$, where $\mathbf{I}$ is a unit matrix. Now, one can easily show that for two n-dimensional circulant matrices $\mathbf{A}$ and $\mathbf{B}$, we have $\mathbf{AB} = \mathbf{BA}$. This is because if the entries of $\mathbf{A}$ and $\mathbf{B}$ are a and b, respectively, then the ijth entry of $\mathbf{AB}$ and $\mathbf{BA}$ will be

$$(\mathbf{AB})_{ij} = \sum_{k=1}^{n} a_{n+1-i+k} b_{j-k+1}; \quad (\mathbf{BA})_{ij} = \sum_{k=1}^{n} b_{n+1-i+k} a_{j-k+1}. \tag{8.53}$$

Since for a circulant matrix $\mathbf{C}$ we have $c_{n+k} = c_k$, therefore, the equality of the two expressions in Eq. 8.2 becomes obvious.

We want to define $\mathbf{C}$ in terms of the permeation matrices of type $\mathbf{P}_i$. Therefore, some properties of these matrices are provided in the subsequent section.

8.5.2 Some Properties of Permutation Matrices

In this section, some of the properties of the permutation matrices are discussed.

1. Since the permutation matrices are special cases of circulant matrices, therefore, we have

$$\mathbf{P}_i \mathbf{P}_j = \mathbf{P}_j \mathbf{P}_i \tag{8.54}$$

2. Calculation of different powers of $\mathbf{P}_i$:
   It can easily be shown that different powers of a permutation matrix are permutation matrices, that is,

$$\mathbf{P}_i^m = \mathbf{P}_j, \tag{8.55}$$

and in the special case if $\mathbf{P}_i$ has dimension n, then

$$\mathbf{P}_i^n = \mathbf{P}_1 = \mathbf{I}; \quad \text{inv}(\mathbf{P}_i) = \mathbf{P}_i^t = \mathbf{P}_i^{n-1}. \tag{8.56}$$

3. The eigenvalues of the matrix $\mathbf{P}_i$:
   First we calculate the eigenvalues of

$$\mathbf{P}_2 = \begin{bmatrix} 0 & 1 & & & & & \\ & 0 & 1 & & & & \\ & & . & . & & & \\ & & & . & 1 & & \\ & & & & 0 & 1 & \\ & & & & & 0 & \\ 1 & & & & & & \end{bmatrix}. \tag{8.57}$$

The characteristic equation of this matrix is formed as follows:

$$\begin{aligned} \text{Poly}(\mathbf{P}_2) &= \det(\mathbf{P}_2 - \lambda\mathbf{I}) = \lambda^n - 1 = 0 \Rightarrow \lambda = \sqrt[n]{1} = \left(e^{\frac{2\pi i}{n}}\right)^k = \omega^k; \\ i &= \sqrt{-1}; k = 0 : n-1. \end{aligned} \tag{8.58}$$

It is obvious that for calculating the eigenvalues of $\mathbf{P}_i$, the same equation should be written. Therefore, the eigenvalues of $\mathbf{P}_i$ will be obtained from the same relationship, with $i \neq 1$. In this way, $\mathbf{P}_i$ and $\mathbf{P}_j$ are similar, that is, these have identical eigenvalues.

4. The eigenvectors of $\mathbf{P}_i$:
   If we assume

$$\mathbf{v} = \left\{1, \omega, \omega^2, \ldots, \omega^{(n-1)}\right\}^t \tag{8.59}$$

where $\omega = e^{\frac{2\pi i}{n}}$ is defined according to Eq. 8.58, then

$$\mathbf{P}_2\mathbf{v} = \left\{\omega, \omega^2, \ldots, \omega^{(n-1)}, 1\right\}^t = \omega\mathbf{v}. \tag{8.60}$$

This means that v is an eigenvector of $\mathbf{P}_2$. With a simple calculation similar to the above case, it can be observed that $\mathbf{v}_k$, which is the generalised form of $\mathbf{v}$, is also an eigenvector of $\mathbf{P}_2$, where

$$\mathbf{v}_k = \left\{1, \omega^k, \omega^{2k}, \ldots, \omega^{(n-1)k}\right\}^t. \tag{8.61}$$

The eigenvectors corresponding to $\mathbf{P}_i$ can similarly be obtained.

5. The block diagonaliser matrix of $\mathbf{P}_i$:
   Using Eq. 8.61 and considering $\omega = e^{2\pi i/n}$, it can be seen that the inner product of two vectors $\mathbf{v}_i$ and $\mathbf{v}_j$ is as follows:

$$\left(\mathbf{v}_i, \mathbf{v}_j\right) = \sum_{k=0}^{n-1} \omega^{(i-j)k} = \begin{cases} 0 & i \neq j \\ n & i = j \end{cases}. \tag{8.62}$$

This means that the following vector will be a base vector.

$$\mathbf{e} = \frac{1}{\sqrt{n}}\{\mathbf{v}_0, \mathbf{v}_1, \ldots, \mathbf{v}_{n-1}\}. \tag{8.63}$$

Therefore, the unity matrix $\mathbf{E}$ defined in the following form diagonalises the matrix $\mathbf{P}_i$:

$$\mathbf{E} = \frac{1}{\sqrt{n}} \begin{bmatrix} 1 & 1 & 1 & . & 1 \\ 1 & \omega & \omega^2 & . & \omega^{n-1} \\ 1 & \omega^2 & \omega^4 & . & \omega^{2(n-1)} \\ . & . & . & . & . \\ 1 & \omega^{n-1} & \omega^{2(n-1)} & . & \omega^{(n-1)(n-1)} \end{bmatrix}. \tag{8.64}$$

In this way, we will have

$$\mathbf{DP}_i = \mathbf{E}^* \mathbf{P}_i \mathbf{E} = \begin{bmatrix} 1 & & & & 0 \\ & \omega & & & \\ & & \omega^2 & & \\ & & & . & \\ & & & & . \\ 0 & & & & \omega^{n-1} \end{bmatrix}. \tag{8.65}$$

This is a diagonal matrix, and the symbol * is used for the conjugate transposition.

8.5.3 Some Properties of Block Circulant Matrices

Considering the above definition, the block circulant matrix $\mathbf{C}$ of Eq. 8.60 can be expressed as

$$\mathbf{C} = \mathbf{P}_1 \otimes \mathbf{A}_1 + \mathbf{P}_2 \otimes \mathbf{A}_2 + \ldots + \mathbf{P}_n \otimes \mathbf{A}_n = \sum_{i=1}^{n} (\mathbf{P}_i \otimes \mathbf{A}_i). \tag{8.66}$$

Similar to the characteristic equation of rotation matrix with numerical entries, we define the matrix function $\mathbf{H}(x)$ in the following form:

$$\begin{cases} \mathbf{H} : \mathbf{C} \rightarrow \mathbf{C}^2 \\ \mathbf{H}(x) = \sum_{i=1}^{n} \left(\mathbf{x}^{i-1} \otimes \mathbf{A}_i \right) \end{cases}. \tag{8.67}$$

Here, in general, $\mathbf{C}$ contains a set of complex numbers. Obviously, if x is a number, then one can omit the symbol $\otimes$. In any case, the output of this function is a matrix.

With this definition and with the help of Eq. 8.55, we will have

$$\mathbf{C} = \mathbf{H}(\mathbf{P}_2). \tag{8.68}$$

Since the eigenvalues of the matrix $\mathbf{P}_i$ are obtained as ω^k, one can see that the eigenvalues of $\mathbf{C}$ will be the union of the eigenvalues of the matrices $\mathbf{H}(\omega^k)$.

Using Eq. 8.64, we define the matrix $\mathbf{F}$ as

$$\mathbf{F} = \mathbf{E} \otimes \mathbf{I} \tag{8.69}$$

Now, we show that $\mathbf{F}^*\mathbf{CF}$ is block diagonal.

$$(\mathbf{A} \otimes \mathbf{B})(\mathbf{C} \otimes \mathbf{D}) = \mathbf{AC} \otimes \mathbf{BD}; \quad (\mathbf{A} \otimes \mathbf{B})^t = \mathbf{A}^t \otimes \mathbf{B}^t. \tag{8.70}$$

Therefore,

$$\mathbf{F}^*\mathbf{CF} = (\mathbf{E}^t \otimes \mathbf{I}^t)\left\{\sum_{i=1}^{n} (\mathbf{P}_i \otimes \mathbf{A}_i)\right\}(\mathbf{E} \otimes \mathbf{I}) = \sum_{i=1}^{n} (\mathbf{E}^*\mathbf{P}_i \otimes \mathbf{A}_i)(\mathbf{E} \otimes \mathbf{I})$$
$$= \sum_{i=1}^{n} (\mathbf{E}^*\mathbf{P}_i\mathbf{E} \otimes \mathbf{A}_i). \tag{8.71}$$

As it was mentioned before, the unitary matrix $\mathbf{E}$ diagonalises $\mathbf{P}_i$, and therefore,

$$\mathbf{F}^*\mathbf{CF} = \sum_{i=1}^{n} (\mathbf{DP}_i \otimes \mathbf{A}_i) \tag{8.72}$$

This shows that the matrix is a block-diagonal one. The important point is that using Eq. 8.65 and the definition of $\mathbf{H}(x)$ in Eq. 8.67, we will have

$$\mathbf{F}^*\mathbf{CF} = \sum_{i=1}^{n} (\mathbf{DP}_i \otimes \mathbf{A}_i) = \begin{bmatrix} \mathbf{H}(1) & & & & \mathbf{0} \\ & \mathbf{H}(\omega) & & & \\ & & \mathbf{H}(\omega^2) & & \\ & & & \ddots & \\ \mathbf{0} & & & & \mathbf{H}(\omega^{n-1}) \end{bmatrix}. \tag{8.73}$$

Therefore, we should obtain the union of the eigenvalues of the diagonal block matrices. An important result of this equation is that

$$\det(\mathbf{C}) = \prod_{i=0}^{n-1} \det\{\mathbf{H}(\omega^i)\}. \tag{8.74}$$

For calculating the eigenvectors of $\mathbf{C}$, we assume $\mathbf{u}$ to be the eigenvectors corresponding to each submatrix of $\mathbf{H}(\omega^i)$. In that case, using Eq. 8.59, we form the vector $\mathbf{v}$.

Now, we show that $\mathbf{v} \otimes \mathbf{u}$ is an eigenvector of $\mathbf{C}$. Using Eq. 8.70, we have

$$\left\{\sum_{i=1}^{n}(\mathbf{P}_i \otimes \mathbf{A}_i)\right\}(\mathbf{v} \otimes \mathbf{u}) = \sum_{i=1}^{n}(\mathbf{P}_i\mathbf{v} \otimes \mathbf{A}_i\mathbf{u}) = \sum_{i=1}^{n}\left(\omega^{i-1}\mathbf{v} \otimes \mathbf{A}_i\mathbf{u}\right)$$
$$= \left\{\sum_{i=1}^{n}\left(\omega^{i-1} \otimes \mathbf{A}_i\right)\right\}(\mathbf{v} \otimes \mathbf{u}). \tag{8.75}$$

Considering Eq. 8.67, we have

$$\mathbf{H}\left(\omega^i\right) = \sum_{i=1}^{n}\left(\omega^{i-1} \otimes \mathbf{A}_i\right). \tag{8.76}$$

Therefore,

$$\left\{\sum_{i=1}^{n}(\mathbf{P}_i \otimes \mathbf{A}_i)\right\}(\mathbf{v} \otimes \mathbf{u}) = \mathbf{H}\left(\omega^i\right)(\mathbf{v} \otimes \mathbf{u}). \tag{8.77}$$

This shows that $\mathbf{H}\left(\omega^i\right)$ are eigenvalues of $\mathbf{C}$, and also $\mathbf{v} \otimes \mathbf{u}$ are the corresponding eigenvectors.

For clarification, we present a simple example. Suppose we want to calculate the eigenvalues and eigenvectors of the following block circulant matrix:

$$\mathbf{C} = \begin{bmatrix} \mathbf{M} & \mathbf{0} & \mathbf{N} & \mathbf{R} & \mathbf{0} \\ \mathbf{0} & \mathbf{M} & \mathbf{0} & \mathbf{N} & \mathbf{R} \\ \mathbf{R} & \mathbf{0} & \mathbf{M} & \mathbf{0} & \mathbf{N} \\ \mathbf{N} & \mathbf{R} & \mathbf{0} & \mathbf{M} & \mathbf{0} \\ \mathbf{0} & \mathbf{N} & \mathbf{R} & \mathbf{0} & \mathbf{M} \end{bmatrix}.$$

Then, $\mathbf{H}(\mathrm{x})$ will be in the following form:

$$\mathbf{H}(\mathrm{x}) = \mathbf{x}^0 \otimes \mathbf{M} + \mathbf{x}^2 \otimes \mathbf{N} + \mathbf{x}^3 \otimes \mathbf{R}.$$

We have also

$$\omega^k = \left(e^{\frac{2\pi i}{n}}\right)^k = \{1,\ \ 0.3090 \pm 0.9511^*i, -0.8090 \pm 0.5878^*i\};\ k = 0:4.$$

Therefore, five eigenvalues are obtained. Now, we should substitute each one in $\mathbf{H}(\mathrm{x})$ and then calculate the eigenvalues of each submatrices. As an example, for $\mathrm{x} = 0.3090 + 0.9511^*i$, we will have

$$\mathbf{K} = \mathbf{H}(0.3090 + 0.9511^*i)$$
$$= \mathbf{M} + (0.3090 + 0.9511^*i)^2\mathbf{N} + (0.3090 + 0.9511^*i)^3\mathbf{R}.$$

It can be observed that the process is very simple. It should be mentioned that using the previously developed method, we had to calculate $\mathbf{C} = \sum_{i=1}^{n} (\mathbf{P}_i \otimes \mathbf{A}_i)$ and considering the pair-wise commutativity property of $\mathbf{P}_i$ with respect to multiplication, we had to form an orthogonal matrix which simultaneously diagonalises all the $\mathbf{P}_i$s. This was a lengthy process which is avoided in the present method.

For calculating the eigenvectors, we should form $\mathbf{u}$ and $\mathbf{v}$. Using Eq. 8.59, we will have

$$\mathbf{v} = \{1,\ 0.3090 + 0.9511^{*}\mathrm{i}, -0.8090 + 0.5878^{*}\mathrm{i}, -0.8090 - 0.5878^{*}\mathrm{i},\ 0.3090 - 0.9511^{*}\mathrm{i}\}^{\mathrm{t}}.$$

Also we should calculate $\mathbf{u}$ for each submatrix $\mathbf{H}(\omega^{\mathrm{i}})$. As an example, for the submatrix $\mathbf{K}$ which we discussed in the above, one can obtain k eigenvectors, with k being the dimension of the matrix $\mathbf{M}$. Finally $\mathbf{v} \otimes \mathbf{u}$ eigenvectors of $\mathbf{C}$ will be constructed.

8.5.4 *The Complete Study of a Simple Example*

In this section, the above steps are applied to the eigensolution of a simple structure. One of the well-known domes is called diamatic dome, as shown in Fig. 8.14a. Unlike many other domes in this structure, the number of nodes in each horizontal ring is not constant, and in each ring, some number of nodes is added. Therefore, one cannot easily formulate the corresponding problem as the sum of Kronecker products. A similar problem arises in pyramids, shown in Fig. 8.14b. As an example of these two domes, the view and plan of a diamatic and a pyramid domes are shown in Fig. 8.14a, b, respectively. Both domes have 7 faces, 882 edges and 316 nodes.

In order to be able to provide the details of the problem, a smaller structure is considered, as shown in Fig. 8.15. In this dome, we have 4 faces, 60 edges and 25 nodes, with nodes being numbered as illustrated in Fig. 8.15b. First we consider the model as a graph, and then we find the eigenvalues of its Laplacian matrix. In Example 8.11 of the next section, the natural eigenfrequencies of the same pyramid, as a space structure, will be calculated.

The pattern of the Laplacian matrix of this graph will be as follows:

$$\mathbf{L}_{mn+k} = \begin{bmatrix} \mathbf{A}_m & \mathbf{B}_m & \mathbf{0} & \mathbf{B}_m^{t} & \mathbf{P}_{mk} \\ \mathbf{B}_m^{t} & \mathbf{A}_m & \mathbf{B}_m & \mathbf{0} & \mathbf{P}_{mk} \\ \mathbf{0} & \mathbf{B}_m^{t} & \mathbf{A}_m & \mathbf{B}_m & \mathbf{P}_{mk} \\ \mathbf{B}_m & \mathbf{0} & \mathbf{B}_m^{t} & \mathbf{A}_m & \mathbf{P}_{mk} \\ \mathbf{P}_{mk}^{t} & \mathbf{P}_{mk}^{t} & \mathbf{P}_{mk}^{t} & \mathbf{P}_{mk}^{t} & \mathbf{R}_k \end{bmatrix}$$

where $m = 6$, $n = 4$ and $k = 1$. Using the method of Ref. [18], we can perform the following transformation:

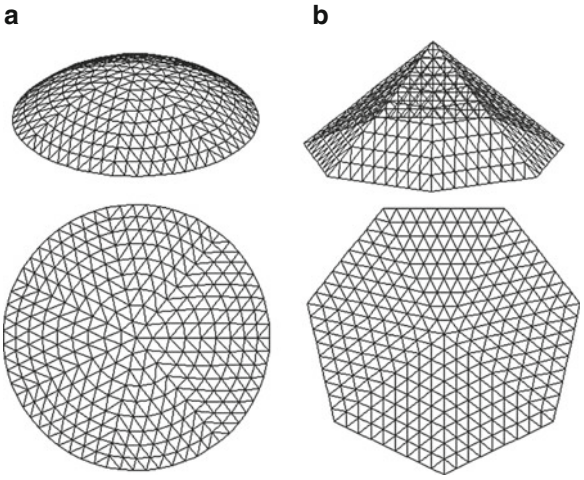

Fig. 8.14 View and plane of two dome structures. (**a**) A diamatic dome (**b**) A pyramid dome

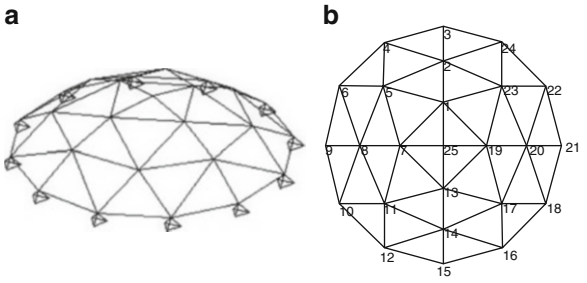

Fig. 8.15 A diamatic dome and the corresponding nodal numbering. (**a**) A three-dimensional view of a dome (**b**) Nodal numbering

$$
\mathbf{L}_{4(m+k)} = \left[\begin{array}{cc|cc|cc|cc}
\mathbf{A} & \mathbf{P} & \mathbf{B} & \mathbf{P} & \mathbf{0} & \mathbf{P} & \mathbf{B^t} & \mathbf{P} \\
16\frac{\mathbf{P^t}}{4} & \frac{\mathbf{R}}{4} & \frac{\mathbf{P^t}}{4} & \frac{\mathbf{R}}{4} & \frac{\mathbf{P^t}}{4} & \frac{\mathbf{R}}{4} & \frac{\mathbf{P^t}}{4} & \frac{\mathbf{R}}{4} \\
\hline
\mathbf{B^t} & \mathbf{P} & \mathbf{A} & \mathbf{P} & \mathbf{B} & \mathbf{P} & \mathbf{0} & \mathbf{P} \\
\frac{\mathbf{P^t}}{4} & \frac{\mathbf{R}}{4} & \frac{\mathbf{P^t}}{4} & \frac{\mathbf{R}}{4} & \frac{\mathbf{P^t}}{4} & \frac{\mathbf{R}}{4} & \frac{\mathbf{P^t}}{4} & \frac{\mathbf{R}}{4} \\
\hline
\mathbf{0} & \mathbf{P} & \mathbf{B^t} & \mathbf{P} & \mathbf{A} & \mathbf{P} & \mathbf{B} & \mathbf{P} \\
\frac{\mathbf{P^t}}{4} & \frac{\mathbf{R}}{4} & \frac{\mathbf{P^t}}{4} & \frac{\mathbf{R}}{4} & \frac{\mathbf{P^t}}{4} & \frac{\mathbf{R}}{4} & \frac{\mathbf{P^t}}{4} & \frac{\mathbf{R}}{4} \\
\hline
\mathbf{B} & \mathbf{P} & \mathbf{0} & \mathbf{P} & \mathbf{B^t} & \mathbf{P} & \mathbf{A} & \mathbf{P} \\
\frac{\mathbf{P^t}}{4} & \frac{\mathbf{R}}{4} & \frac{\mathbf{P^t}}{4} & \frac{\mathbf{R}}{4} & \frac{\mathbf{P^t}}{4} & \frac{\mathbf{R}}{4} & \frac{\mathbf{P^t}}{4} & \frac{\mathbf{R}}{4}
\end{array}\right]
$$

$$
= \begin{bmatrix}
\mathbf{M} & \mathbf{N} & \mathbf{W} & \mathbf{S} \\
\mathbf{S} & \mathbf{M} & \mathbf{N} & \mathbf{W} \\
\mathbf{W} & \mathbf{S} & \mathbf{M} & \mathbf{N} \\
\mathbf{N} & \mathbf{W} & \mathbf{S} & \mathbf{M}
\end{bmatrix}.
$$

It can be seen that this matrix is also a circulant matrix, and we can therefore easily calculate its eigenvalues. Here, the $\mathbf{H}(\mathrm{x})$ matrix can be written as

$$\mathbf{H}(\mathrm{x}) = \mathbf{x}^0 \otimes \mathbf{M} + \mathbf{x}^1 \otimes \mathbf{N} + \mathbf{x}^2 \otimes \mathbf{W} + \mathbf{x}^3 \otimes \mathbf{S}.$$

Also we have

$$\omega^{\mathrm{k}} = \left(\mathrm{e}^{\frac{2\pi \mathrm{i}}{4}}\right)^{\mathrm{k}} = \{\pm 1, \pm \mathrm{i}\}; \quad \mathrm{k} = 0:3.$$

Thus, as an example, for $\mathrm{x} = -\mathrm{i}$, we will have

$$\mathbf{H}(-\mathrm{i}) = \mathbf{M} - \mathrm{i}\mathbf{N} - \mathbf{W} + \mathrm{i}^*\mathbf{S}$$
$$= \begin{bmatrix} 6 & -1 & 0 & 0 & -1-\mathrm{i} & 0 & 0 \\ -1 & 6 & -1 & -1 & -1-\mathrm{i} & -\mathrm{i} & 0 \\ 0 & -1 & 3 & -1 & 0 & -\mathrm{i} & 0 \\ 0 & -1 & -1 & 4 & -1 & -1 & 0 \\ -1+\mathrm{i} & -1+\mathrm{i} & 0 & -1 & 6 & -1 & 0 \\ 0 & \mathrm{i} & \mathrm{i} & -1 & -1 & 4 & 0 \\ 0 & 0 & 0 & 0 & 0 & 0 & 0 \end{bmatrix}.$$

The eigenvalues of this matrix are as follows:

$$\mathrm{eig}(\mathbf{H}(-\mathrm{i})) = \{0, 0.7790, 3.2321, 4.3397, 5.4909, 7.3844, 7.7739\}.$$

In a similar manner for other x's, we obtain the submatrices and their eigenvalues. It should be noted that as it is explained in [18], here we will have three additional zeros among the answers which should be deleted from the final set of eigenvalues.

Here as well if we want to use the previously developed methods, the corresponding matrix will be expressed as the sum of four Kronecker products, and we should find an orthogonal matrix which simultaneously diagonalises the first components of the four parts of this sum. While in here, we could obtain four submatrices for four values of x. It should be noted that all the dome structures consisting of Cartesian, strong Cartesian and direct products investigated previously in [19] will have circulant matrices.

8.6 Complementary Examples

Example 8.11. In this example, a structure is considered as shown in Fig. 8.16. We want to calculate the frequencies and the natural modes of this structure under its

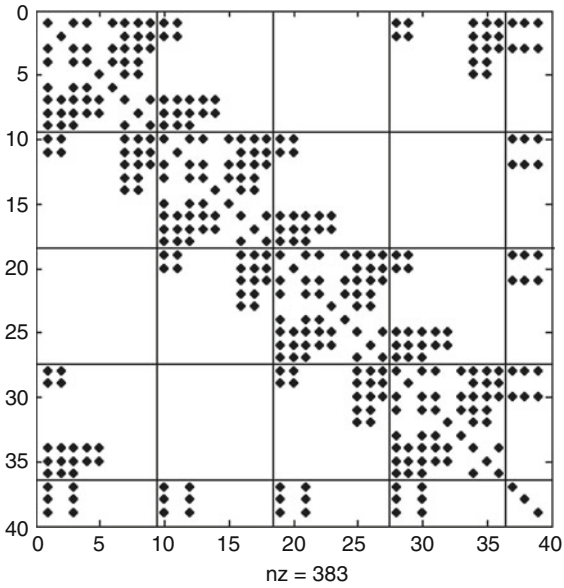

Fig. 8.16 The patterns of the stiffness and mass matrices of Example 8.11

self-weight. The area for all the cross sections are considered as 5 cm^2, the elastic modulus is taken as 200 kN/mm^2 (MPa). For all the elements, $\rho = 78.5\ kN/m^3$.

Similar to Ref. [19], first the stiffness and mass matrices are constructed in a cylindrical coordinate system. Here, the stiffness and mass matrices will have a similar pattern to that of the Laplacian matrix of the previous example, with the only difference that the dimensions will be threefold bigger. These matrices have the following patterns:

$$\mathbf{K} = \begin{bmatrix} \mathbf{A}_m & \mathbf{B}_m & \mathbf{0} & \mathbf{B}_m^t & \mathbf{P}_{mk} \\ \mathbf{B}_m^t & \mathbf{A}_m & \mathbf{B}_m & \mathbf{0} & \mathbf{P}_{mk} \\ \mathbf{0} & \mathbf{B}_m^t & \mathbf{A}_m & \mathbf{B}_m & \mathbf{P}_{mk} \\ \mathbf{B}_m & \mathbf{0} & \mathbf{B}_m^t & \mathbf{A}_m & \mathbf{P}_{mk} \\ \mathbf{P}_{mk}^t & \mathbf{P}_{mk}^t & \mathbf{P}_{mk}^t & \mathbf{P}_{mk}^t & \mathbf{R}_k \end{bmatrix}; \quad \mathbf{M} = \begin{bmatrix} \mathbf{A}_m & \mathbf{B}_m & \mathbf{0} & \mathbf{B}_m^t & \mathbf{P}_{mk} \\ \mathbf{B}_m^t & \mathbf{A}_m & \mathbf{B}_m & \mathbf{0} & \mathbf{P}_{mk} \\ \mathbf{0} & \mathbf{B}_m^t & \mathbf{A}_m & \mathbf{B}_m & \mathbf{P}_{mk} \\ \mathbf{B}_m & \mathbf{0} & \mathbf{B}_m^t & \mathbf{A}_m & \mathbf{P}_{mk} \\ \mathbf{P}_{mk}^t & \mathbf{P}_{mk}^t & \mathbf{P}_{mk}^t & \mathbf{P}_{mk}^t & \mathbf{R}_k \end{bmatrix}$$

where $m = 18$, $n = 4$ and $k = 3$. It can be observed that here the last block column has three numerical columns in place of a single one. Therefore, in performing the algorithm for decomposing this block column to other blocks, we consider three additional zero columns next to each block matrix. In this case, the stiffness and mass matrices will have the following form after deleting the rows and columns corresponding to the support nodes.

It can be seen that the mass matrix is not diagonal, and one cannot calculate the eigenvalue for the free vibration merely by considering the stiffness matrix. Thus, the $\mathbf{K} - \mathbf{M}\omega^2$ matrix is constructed as

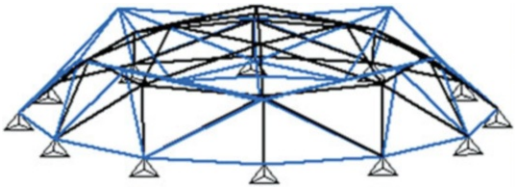

Fig. 8.17 The sixth natural mode of the structure in Example 8.11

$$\mathbf{K}-\mathbf{M}\omega^2=\begin{bmatrix}\mathbf{M}_K-\mathbf{M}_M\omega^2 & \mathbf{N}_K-\mathbf{N}_M\omega^2 & \mathbf{W}_K-\mathbf{W}_M\omega^2 & \mathbf{S}_K-\mathbf{S}_M\omega^2\\ \mathbf{S}_K-\mathbf{S}_M\omega^2 & \mathbf{M}_K-\mathbf{M}_M\omega^2 & \mathbf{N}_K-\mathbf{N}_M\omega^2 & \mathbf{W}_K-\mathbf{W}_M\omega^2\\ \mathbf{W}_K-\mathbf{W}_M\omega^2 & \mathbf{S}_K-\mathbf{S}_M\omega^2 & \mathbf{M}_K-\mathbf{M}_M\omega^2 & \mathbf{N}_K-\mathbf{N}_M\omega^2\\ \mathbf{N}_K-\mathbf{N}_M\omega^2 & \mathbf{W}_K-\mathbf{W}_M\omega^2 & \mathbf{S}_K-\mathbf{S}_M\omega^2 & \mathbf{M}_K-\mathbf{M}_M\omega^2\end{bmatrix}.$$

This is also a circulant matrix. Therefore, $\mathbf{H}(x)$ can be written as

$$\begin{aligned}\mathbf{H}(x)=&\mathbf{x}^0\otimes\left(\mathbf{M}_K-\mathbf{M}_M\omega^2\right)+\mathbf{x}^1\otimes\left(\mathbf{N}_K-\mathbf{N}_M\omega^2\right)+\mathbf{x}^2\otimes\left(\mathbf{W}_K-\mathbf{W}_M\omega^2\right)\\&+\mathbf{x}^3\otimes\left(\mathbf{S}_K-\mathbf{S}_M\omega^2\right).\end{aligned}$$

We also have

$$\omega^k=\left(e^{\frac{2\pi i}{4}}\right)^k=\{\pm1,\pm i\};\quad k=0:3.$$

For all values of x, the submatrices $\mathbf{H}(x)$ are obtained in terms of ω, and equating them to zero, the corresponding eigenvalues are calculated. The largest period of this structure is obtained as $T_1=0.0826$. For the construction of the eigenvectors, as we mentioned before, $\mathbf{u}$ and $\mathbf{v}$ should be calculated. Then using Eq. 8.59, we obtain

$$\omega=e^{\frac{2\pi i}{4}}=i\Rightarrow\mathbf{v}=\left\{1,\omega,\omega^2,\ldots,\omega^{(n-1)}\right\}^t=\{1,i,-1,i\}^t.$$

For all values of $\mathbf{u}$, the submatrices $\mathbf{H}\left(\omega^i\right)$ are calculated, and finally the vibrating modes $\mathbf{v}\otimes\mathbf{u}$ are obtained. As an example, for the 6th period ($T_6=0.0456$), the 6th natural mode is shown in Fig. 8.17.

Example 8.12. A flat double-layer grid is considered as shown in Fig. 8.18. The support nodes are illustrated in darker points. As it can be seen, we have also an additional support at the middle of the structure. Similar to the previous example, all the cross sections are considered as 5 cm^2, the elastic modulus is taken as 200 kN/mm^2 (MPa). For all the elements, $\rho=78.5\ kN/m^3$. One can consider this structure as eight triangular-shaped substructures (segments) with eight common boundaries (interfaces).

A nodal numbering similar to that of Fig. 8.15b is performed in here. The numbering starts with the interface of two segments followed by numbering the internal node of this segment except the middle node. The other interface of this

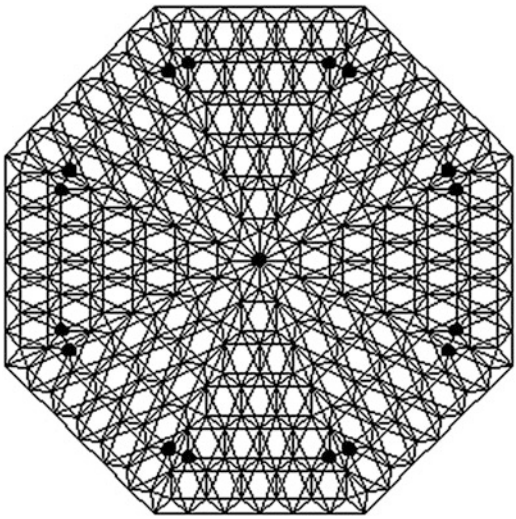

Fig. 8.18 A flat double-layer grid

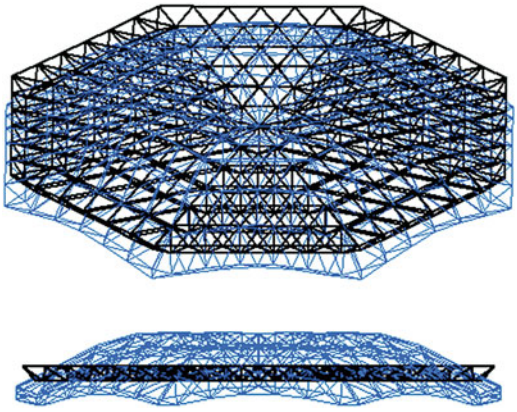

Fig. 8.19 The third vibrating mode of a flat double-layer grid

segment is numbered followed by the internal nodes of the second segment. This process is cyclically repeated until all the nodes except the middle node are numbered. The middle node is numbered last. Here as well the stiffness and mass matrices are formed in a cylindrical coordinate system. These matrices are also circulant and eight blocks submatrices are obtained. In this example, the first period is calculated as $T_1 = 0.0113$ and the third period is obtained as $T_3 = 0.0102$. As an example, the vibrating mode corresponding to the 3rd period is illustrated in Fig. 8.19.

Example 8.13. In this example, a transmission tower, shown in Fig. 8.20, is investigated. The height of this tower is 58 m, and its plan is a square of length 6 m at the bottom which is reduced to 2 m at the top. The height is divided into 29 panels of 2 m. Here as well we obtain the stiffness and mass matrices in a cylindrical coordinate system, and then we form $\mathbf{K} - \mathbf{M}\omega^2$ as

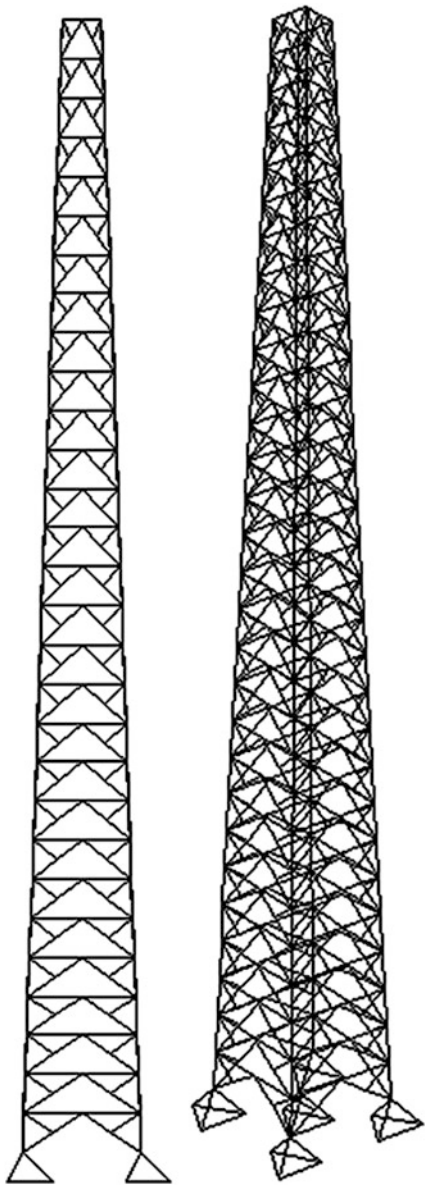

Fig. 8.20 A transmission tower and one of its views

$$\mathbf{K}-\mathbf{M}\omega^2=\begin{bmatrix}\mathbf{A}_\mathrm{K}-\mathbf{A}_\mathrm{M}\omega^2 & \mathbf{B}_\mathrm{K}-\mathbf{B}_\mathrm{M}\omega^2 & \mathbf{0} & \mathbf{C}_\mathrm{K}-\mathbf{C}_\mathbf{M}\omega^\mathbf{2}\\ \mathbf{C}_\mathrm{K}-\mathbf{C}_\mathrm{M}\omega^2 & \mathbf{A}_\mathrm{K}-\mathbf{A}_\mathrm{M}\omega^2 & \mathbf{B}_\mathrm{K}-\mathbf{B}_\mathrm{M}\omega^2 & \mathbf{0}\\ \mathbf{0} & \mathbf{C}_\mathrm{K}-\mathbf{C}_\mathrm{M}\omega^2 & \mathbf{A}_\mathrm{K}-\mathbf{A}_\mathrm{M}\omega^2 & \mathbf{B}_\mathrm{K}-\mathbf{B}_\mathrm{M}\omega^2\\ \mathbf{B}_\mathrm{K}-\mathbf{B}_\mathrm{M}\omega^2 & \mathbf{0} & \mathbf{C}_\mathrm{K}-\mathbf{C}_\mathrm{M}\omega^2 & \mathbf{A}_\mathrm{K}-\mathbf{A}_\mathrm{M}\omega^2\end{bmatrix}$$

which is a circulant matrix. Thus, $\mathbf{H}(\mathrm{x})$ will be in the following form:

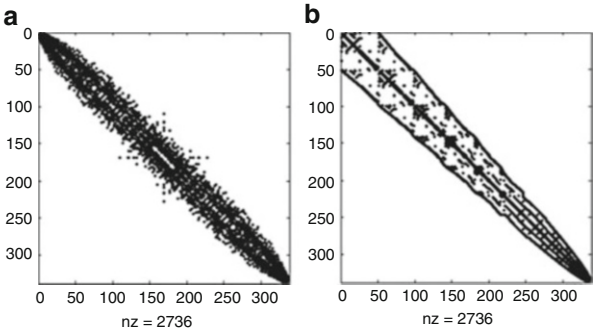

Fig. 8.21 Forms of the Laplacian matrices after reordering the nodes of the graph model. (**a**) Ordered by Fiedler vector (**b**) Ordered by the reverse Cuthill–McKee

$$\mathbf{H}(\mathrm{x}) = \mathbf{x}^0 \otimes \left(\mathbf{A}_\mathrm{K} - \mathbf{A}_\mathrm{M}\omega^2\right) + \mathbf{x}^1 \otimes \left(\mathbf{B}_\mathrm{K} - \mathbf{B}_\mathrm{M}\omega^2\right) + \mathbf{x}^3 \otimes \left(\mathbf{C}_\mathrm{K} - \mathbf{C}_\mathrm{M}\omega^2\right).$$

Also we have

$$\omega^\mathrm{k} = \left(\mathrm{e}^{\frac{2\pi \mathrm{i}}{4}}\right)^\mathrm{k} = \{\pm 1, \pm \mathrm{i}\}; \quad \mathrm{k} = 0:3.$$

For all values of x, the submatrices $\mathbf{H}(\mathrm{x})$ are obtained in terms of ω, and equating them to zero, the corresponding eigenvalues are calculated. It should be noted that if we want to model them as trusses, then for analysis, all the nodes together with their incident members which are situated on a plane should be connected to the ground by an artificial member; otherwise, we will have local instability and the determinant of the reduced stiffness matrix will also be zero.

Example 8.14. The main aim of this example is to use the eigenvectors for optimal nodal numbering of structures. Consider the graph model of the Example 8.12. After the formation of its Laplacian matrix and calculating the second eigenvalue, the corresponding eigenvector, known as the Fiedler vector, is constructed and its entries are ordered for reducing the profile of the stiffness matrix. Here, the Laplacian matrix is a circulant matrix and one can easily calculate the eigenvalues and eigenvectors using the present method. For this example, the second eigenvalue is obtained as $\lambda_2 = 0.1070$. The result of ordering is compared to that of the reverse Cuthill–McKee method. The profile and bandwidth by the Fiedler vector are $\mathrm{B} = 60$; $\mathrm{P} = 7755$ and those of the reverse Cuthill–McKee are $\mathrm{B} = 52$; $\mathrm{P} = 10332$. The patterns of both cases are illustrated in Fig. 8.21.

In this chapter, the block circulant matrices are introduced, and their properties are employed in an efficient free vibration analysis of cyclically repetitive structures. These properties are applied to dome structures, cyclic double-layer grids and transmission towers. The method is also applied to nodal numbering of structures for profile reduction of stiffness matrices. The presented approach is highly efficient and results in a considerable reduction of the dimension of eigenproblems. This method can also be employed in the forced vibration using the approach developed in [20].

References

1. Kaveh A, Rahami H (2010) An efficient analysis of repetitive structures generated by graph products. Int J Numer Methods Eng 84(1):108–126
2. Kaveh A, Rahami H, Mehanpour H (2012) Static and modal analyses of structures with different repeated patterns. Adv Eng Software 51:1–9
3. Kaveh A, Rahami H (2011) Block circulant matrices and applications in free vibration analysis of cyclically repetitive structures. Acta Mech 217(1–2):51–62
4. Kaveh A, Rahami H (2008) Topology and graph products; eigenproblems in optimal structural analysis. Commun Numer Methods Eng 24:929–945
5. Szilard R (2004) Theories and applications of plate analysis: classical, numerical and engineering methods. Wiley, New York
6. Kaveh A, Alinejad B (2010) Graph products with specified domains for configuration processing and formation of the adjacency matrices. Eng Comput 27(2):205–224
7. Kaveh A, Rahami H (2010) Eigenvalues of the adjacency and Laplacian matrices for modified regular structural models. Int J Numer Methods Biomed Eng 26(12):1836–1855
8. Choi D, Kim H, Cho M (2008) Iterative method for dynamic condensation combined with substructuring scheme. J Sound Vib 317:199–218
9. Guedri M, Bouhaddi N, Majed R (2006) Reduction of the stochastic finite element models using a robust dynamic condensation method. J Sound Vib 297:123–145
10. Lin R, Xia Y (2003) A new eigensolution of structures via dynamic condensation. J Sound Vib 266:93–106
11. Pellegrino S, Calladine CR (1986) Matrix analysis of statically and kinematically indeterminate frameworks. Int J Solids Struct 22:409–428
12. Pellegrino S (1993) Structural computations with the singular-value decomposition of the equilibrium matrix. Int J Solids Struct 30:3025–3035
13. Kardestuncer H (1974) Elementary matrix analysis of structures. McGraw-Hill Inc, New York
14. Kaveh A, Rahami H, Mirghaderi SR, Ardalan Asl M (2013) Analysis of near-regular structures using the force method. Eng Comput 30(1):21–48
15. Rongming L, Yong X (2003) A new eigensolution of structures via dynamic condensation. J Sound Vib 266:93–106
16. Kaveh A, Fazli H (2011) Approximate eigensolution of locally modified regular structures using a substructuring technique. Comput Struct 89:529–537
17. Kaveh A, Rahami H (2006) Block diagonalization of adjacency and Laplacian matrices for graph product; applications in structural mechanics. Int J Numer Methods Eng 68:33–63
18. Kaveh A, Rahami H (2008) Factorization for efficient solution of eigenproblems of adjacency and Laplacian matrices for graph products. Int J Numer Methods Eng 75:58–82
19. Kaveh A, Rahami H (2004) An efficient method for decomposition of regular structures using graph products. Int J Numer Methods Eng 61:1797–1808
20. Rahami H, Kaveh A (2008) Forced vibration of symmetric structures. Commun Numer Methods Eng 241:393–406

Chapter 9
Graph Products Applied to the Locally Modified Regular Structures Using Direct Methods

9.1 Introduction

In the first part of this chapter, a method is presented for eigensolution of a non-regular model. First, the nodes of the non-regular part of such model are ordered followed by ordering the nodes of the regular part. With this ordering, the graph matrices will be separated into two blocks. The eigensolution of the non-regular part can be performed by an iterative method, and those of the regular part can easily be calculated using decomposition approaches studied in the previous chapters. Some numerical examples are included to illustrate the efficiency of the new method [1].

In the second part, structures transformable to regular forms are studied. Here, two cases are investigated. In the first case, the effect of different boundary conditions on these structures is explored, and in the second case, the effect of adding or removing members and nodes is studied. In some structures, the graph model is regular and different boundary conditions change the corresponding block matrices into non-regular ones. In some other structures, the addition or removal of nodes and/or members changes the structure into a regular one. Here, an efficient method is presented for dealing with the above-mentioned irregularities [2].

9.2 Analysis of Non-regular Graphs Using the Results of Regular Models via an Iterative Method

In this part, an efficient method is presented for the analysis of non-regular graphs and structures which contain regular submodels. Efficient decomposition methods are presented for some classes of regular models in the previous parts. For non-regular structures, iterative methods are often used.

In the present method, for a non-regular model, first the nodes of the non-regular part are ordered followed by numbering the nodes of the regular part. With this

A. Kaveh, *Optimal Analysis of Structures by Concepts of Symmetry and Regularity*,
DOI 10.1007/978-3-7091-1565-7_9,

ordering, the graph and structural matrices are separated into two blocks. The eigensolution of the regular part is easily calculated using the decomposition approaches and that of non-regular part is performed by an iterative method. Some numerical examples are included to illustrate the efficiency of the new method [1].

9.2.1 Main Method

In this method, with transforming the matrices of graphs and structures into block form and employing dynamic condensation, the eigenvalues are calculated. For simplicity, a graph for which the eigenvalues can be calculated using the above-mentioned method (or any other method) is denoted by S. The dimension of the matrices of this graph is denoted by s which corresponds to the DOFs which is supposed to be omitted. We also assume that the primary matrices have dimension equal to n.

In general, we aim at solving the following eigenvalue problem:

$$(\mathbf{A} - \lambda_i \mathbf{B})\Phi_i = 0 \quad ; \quad i = 1 : n \tag{9.1}$$

This matrix can be decomposed into two parts having dimensions of m and s, where $n = m + s$. It is obvious s corresponds to the part for which the inverse can be found using the previously developed methods.

$$\left(\begin{bmatrix} \mathbf{A}_{mm} & \mathbf{A}_{ms} \\ \mathbf{A}_{ms}^t & \mathbf{A}_{ss} \end{bmatrix} - \lambda \begin{bmatrix} \mathbf{B}_{mm} & \mathbf{B}_{ms} \\ \mathbf{B}_{ms}^t & \mathbf{B}_{ss} \end{bmatrix} \right) \begin{pmatrix} \Phi_m \\ \Phi_s \end{pmatrix} = \begin{pmatrix} \mathbf{0} \\ \mathbf{0} \end{pmatrix} \tag{9.2}$$

According to [3], the calculation can be summarised as follows:

First, we obtain $\mathbf{A}^0$ and $\mathbf{B}^0$ using the following relationships:

$$\mathbf{A}^0 = \mathbf{A}_{mm} - \mathbf{A}_{ms}\mathbf{A}_{ss}^{-1}\mathbf{A}_{ms}^t \tag{9.3}$$

$$\mathbf{B}^0 = \mathbf{B}_{mm} - \mathbf{B}_{ms}\mathbf{A}_{ss}^{-1}\mathbf{A}_{ms}^t - \mathbf{A}_{ms}\mathbf{A}_{ss}^{-1}\mathbf{B}_{ms}^t + \mathbf{A}_{ms}\mathbf{A}_{ss}^{-1}\mathbf{B}_{ss}\mathbf{A}_{ss}^{-1}\mathbf{A}_{ms}^t. \tag{9.4}$$

Therefore, up to here, we need an inversion of a matrix of dimension s.

Now, the magnitudes of λ^0 and Φ^0 are found from the following eigensolution:

$$(\mathbf{A}^0 - \lambda_r^0 \mathbf{B}^0)\Phi_r^{\mathbf{0}} = \mathbf{0}; \quad r = 1 : m \tag{9.5}$$

It is obvious that the dimension of the calculation is m which is equal to the number of additional nodes contained in the corresponding structural graph with respect to the graph S.

Now for calculating the rth eigenvalue, we will have

$$\lambda_r^{(0)} = \lambda_r^0 \text{ and } \Phi_r^{(0)} = \Phi_r^0; \quad r = 1 : m \tag{9.6}$$

$$\mathbf{t}_d^{(0)} = \mathbf{A}_{ss}^{-1}(\mathbf{B}_{ms}^t + \mathbf{B}_{ss}\mathbf{t}_G) \text{ and } \mathbf{t}_G = -\mathbf{A}_{ss}^{-1}\mathbf{A}_{ms}^t \tag{9.7}$$

These values are the preliminary values, and the iteration should be performed until convergence is achieved. These operations for the k th iteration are as follows:

$$\begin{aligned}
\mathbf{t}_d^{(k)} &= \mathbf{A}_{ss}^{-1}(\mathbf{B}_{ms}^t + \mathbf{B}_{ss}\mathbf{t}_G) + \lambda_r^{(k-1)}\mathbf{A}_{ss}^{-1}\mathbf{B}_{ss}\mathbf{t}_d^{(k-1)} \\
\Delta\mathbf{B}^{(k)} &= \lambda_r^{(k-1)}(\mathbf{B}_{ms} + \mathbf{t}_G^t\mathbf{B}_{ss})\mathbf{t}_d^{(k)} \\
\mathbf{B}^{(k)} &= \mathbf{B}^0 + \Delta\mathbf{B}^{(k)} \\
\overline{\lambda}_r^{(k)} &= \lambda_r^0 \frac{\left(\Phi_r^0\right)^t \mathbf{B}^{(0)} \Phi_r^{(k-1)}}{\left(\Phi_r^0\right)^t \mathbf{B}^{(k)} \Phi_r^{(k-1)}} \\
\Phi_r^{(k)} &= \overline{\lambda}_r^{(k)} \sum_{i=1}^{m} \frac{\Phi_r^0 \left(\Phi_i^0\right)^t}{\lambda_i^0 - \overline{\lambda}_r^{(k)}} \Delta\mathbf{B}^{(k)} \Phi_r^{(k-1)} \\
\lambda_r^{(k)} &= \lambda_r^0 \frac{\left(\Phi_r^0\right)^t \mathbf{B}^0 \Phi_r^{(k)}}{\left(\Phi_r^0\right)^t \mathbf{B}^{(k)} \Phi_r^{(k)}}.
\end{aligned} \tag{9.8}$$

This iteration for the r th eigenvalue will be continued until the following condition is fulfilled:

$$\left|\lambda_r^{(k)} - \lambda_r^{(k-1)}\right| / \lambda_r^{(k)} \leq \varepsilon. \tag{9.9}$$

As it can be seen from Eqs. 9.3 ,9.4, and 9.5, all the calculations consist of only the inversion of a matrix $\mathbf{A}_{ss}$ and finding the eigenvalues of two matrices of dimension m only once and substituting in Eq. 9.8, and no additional matrix operations are needed.

It should be noted that in structural problems, the smallest eigenvalues and, in the graph Laplacian matrices, the second eigenvalues are of importance.

It can be recognised that in the present method, ordering plays an important role. According to the above explanations, first a subgraph S of the graph is selected. This part is selected such that the inverse of the corresponding matrix can be calculated. The remaining part of the model is denoted as M. For nodal ordering, first the nodes of M and then the nodes of S are numbered.

Here, applications of this method in graph and structural problems are described. One of these applications is the calculation of the eigenvalues of the Laplacian matrices of direct and strong Cartesian graph products. For these products, the Laplacian matrices can be expressed as the sum of two Kronecker products. We define the following penta-diagonal block matrix:

$$\mathbf{F}_n(\mathbf{A},\mathbf{B},\mathbf{C},\mathbf{D}) = \begin{bmatrix} \mathbf{A} & \mathbf{B} & \mathbf{D} & & & & & & \\ \mathbf{B} & \mathbf{C} & \mathbf{B} & \mathbf{D} & & & & & \\ \mathbf{D} & \mathbf{B} & \mathbf{C} & \mathbf{B} & & & & & \\ & \mathbf{D} & . & . & . & & & & \\ & & & . & . & . & & & \\ & & & & . & . & . & \mathbf{D} & \\ & & & & & \mathbf{B} & \mathbf{C} & \mathbf{B} & \mathbf{D} \\ & & & & & \mathbf{D} & \mathbf{B} & \mathbf{C} & \mathbf{B} \\ & & & & & & \mathbf{D} & \mathbf{B} & \mathbf{A} \end{bmatrix}_{n\times n}. \tag{9.10}$$

In this matrix, the blocks **A**, **B**, **C** and **D** are m × m submatrices. It should be mentioned that when this matrix is used with three arguments, then we will have $\mathbf{D} = \mathbf{0}$.

In this way, for the direct product, we will have

$$\mathbf{M}_{ef} = \mathbf{F}_f(0,1,0) \otimes \mathbf{F}_e(0,-1,0) + \mathbf{F}_f(1,0,2) \otimes \mathbf{F}_e(1,0,2), \tag{9.11}$$

and for strong Cartesian product, we have

$$\mathbf{M}_{ef} = \mathbf{F}_f(1,1,1) \otimes \mathbf{F}_e(-1,-1,-1) + \mathbf{F}_f(2,0,3) \otimes \mathbf{F}_e(2,0,3) \tag{9.12}$$

Here, both terms are in the form $\mathbf{A}_1 \otimes \mathbf{B}_1 + \mathbf{A}_2 \otimes \mathbf{B}_2$. However, in both terms, $\mathbf{A}_1\mathbf{A}_2 \neq \mathbf{A}_2\mathbf{A}_1$. Thus, one cannot block diagonalise using the given form.

In Sect. 6.7, members were added to the four edges of the graph to perform the calculations. This changes $\mathbf{A}_2$ and $\mathbf{B}_2$ in the direct product to $2\mathbf{I}$, and in strong Cartesian product, it changes to $3\mathbf{I}$ to provide the decomposability condition. However, it is shown that one does not need to alter $\mathbf{B}_2$ and changes on $\mathbf{A}_2$ is sufficient for block diagonalisation.

Since the addition of members to all four edges of the graph is unnecessary and two opposite edges are sufficient (e.g. upper and lower edges), thus $\mathbf{M}_{ef}$ can be written as

$$\mathbf{M}_{ef} = \mathbf{I}_f \otimes (\mathbf{A}+\mathbf{B})_e + \mathbf{F}_f(1,-1,2) \otimes (-\mathbf{B})_e \tag{9.13}$$

Since in this case $\mathbf{I}_f\mathbf{T}_f = \mathbf{T}_f\mathbf{I}_f$; therefore, $\mathbf{M}_{ef}$ can be diagonalised and we have

$$\mathrm{eig}(\mathbf{M}_{ef}) = \bigcup_{i=1}^{f} \{\mathrm{eig}[\mathbf{A}_e - (1+2\cos\frac{i\pi}{f})\mathbf{B}_e]\} \tag{9.14}$$

Due to the change on the primary graph, the magnitude of λ_2 will have some approximation. In order to improve this approximation, one can use Rayleigh's method. In this method, there is no need to add member to the edges of the model. Details of this approach will be illustrated in Example 9.1. Using a suitable numbering scheme and decomposing the Laplacian matrix of the graphs which are not similar to the product graphs, one can calculate the eigenvalues, as shown in Example 9.2. In this

example, utilising the Fiedler's vector obtained from the second eigenvalue of the Laplacian matrix of the model, suitable nodal ordering is obtained.

Another application of the present method is finding the eigenvalues of two graphs connected to each other, as illustrated in Example 9.3. In this example, using the Fiedler's vector, the graph can be bisected.

Another example of this application is the study of the graphs which become a standard product graph after the addition of some members, Example 9.4.

In relation with structures, the buckling load and vibration frequencies of beams and plates are investigated. The considered beam contains different supports such that the corresponding matrix does not match with previously developed canonical forms, and hence, the existing relationships cannot be directly used, Example 9.5. The plates are selected such that they have either an additional part with respect to regular model (Example 9.6), or it has different boundary conditions (Example 9.7). Apart from these, the vibration frequency of a mass–spring system is studied (Example 9.8), and a shear structure having masses at some nodes having different stiffnesses (Example 9.9) is investigated. As it will be seen, a variety of problems can be solved using the present method. This application can also be extended to some problems in other fields of engineering.

9.2.2 Numerical Examples

Example 9.1. In this example, the aim is to find the eigenvalues of the Laplacian matrix of a graph in the form of strong Cartesian product. The strong Cartesian product $P_4\ (X)_{SC}\ P_5$ is shown in Fig. 9.1. The main problem is that the upper and lower nodes are not identical to the intermediate nodes and if only the intermediate nodes are considered, then one can find the eigenvalues followed by the inverse of the corresponding matrix. Therefore, for nodal ordering, first the upper and lower nodes are labelled followed by the numbering of the intermediate nodes.
Considering the above nodal ordering, the Laplacian matrix is decomposed into two blocks as follows:

$$\mathbf{L} = \begin{bmatrix} \mathbf{L}_{mm} & \mathbf{L}_{ms} \\ \mathbf{L}_{ms}^{t} & \mathbf{L}_{ss} \end{bmatrix}$$

Here, $m = 8$ and $s = 12$. Therefore, instead of calculating the eigenvalues of a matrix of dimension 20, only a matrix of dimension 12 is inversed together with an eigensolution of dimension 8. The $\mathbf{L}_{ss}$ matrix is in the following form:

$$\mathbf{L}_{ss} = \begin{bmatrix} \mathbf{A} & \mathbf{B} & \mathbf{0} \\ \mathbf{B} & \mathbf{A} & \mathbf{B} \\ \mathbf{0} & \mathbf{B} & \mathbf{A} \end{bmatrix} = \mathbf{F}_3(\mathbf{A},\mathbf{B},\mathbf{A}) = \mathbf{I}_3 \otimes \mathbf{F}_4(5,-1,8) + \mathbf{F}_3(0,1,0) \otimes \mathbf{F}_4(-1,-1,-1)$$

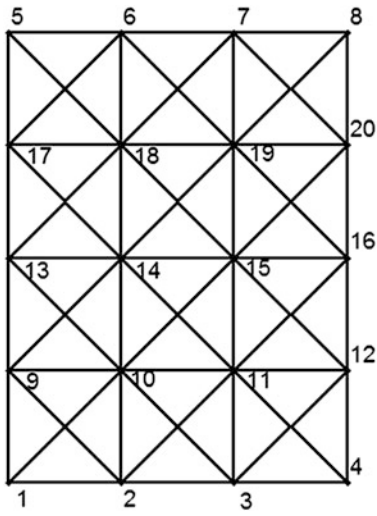

Fig. 9.1 The strong Cartesian product P_5 $(X)_{SC}$ P_4 and its nodal numbering

The important point is that for inverting $\mathbf{L}_{ss}$, there is no need for direct calculations since in this matrix $\mathbf{A}_1\mathbf{A}_2 = \mathbf{A}_2\mathbf{A}_1$, and eigenvalues can easily be obtained by $\lambda_{\mathbf{M}} = \bigcup_{i=1}^{n} \text{eig}(\mathbf{M}_i)$; $\mathbf{M}_i = \sum_{j=1}^{k} (\lambda_i(\mathbf{A}_j)\mathbf{B}_j)$, and the inversion is performed employing Eq. 9.1. Thus, we have

$$\lambda_{\mathbf{L}} = \bigcup_{i=1}^{3} [\lambda_i(\mathbf{I}_3)\mathbf{F}_4(5,-1,8) + \lambda_i(\mathbf{F}_3(0,1,0)\mathbf{F}_4(-1,-1,-1)]$$

In this way, instead of solving an eigenvalue problem of dimension 20, the eigenvalues of three matrices of dimension 4 and one of dimension 8 should be calculated.

Example 9.2. In Fig. 9.2a, a graph is shown which is similar to strong Cartesian product, and the only difference is that the crossing points are considered as nodes belonging the subgraph S. The remaining nodes are contained in the subgraph M. Using the aforementioned numbering, the matrix $\mathbf{L}_{ss}$ will be equal to $4\mathbf{I}_6$, where $\mathbf{I}$ is a unit matrix. Therefore, $\mathbf{L}_{ss}^{-1} = \frac{1}{4}\mathbf{I}_6$, and it is sufficient to calculate the eigenvalues of a matrix of dimension $m = 12$. It should be mentioned that for calculating the eigenvalues of this matrix similar to the previous example, one can decompose the graph into two subgraphs with $m = 6$ and $s = 6$. For this example, the second eigenvalue of the Laplacian matrix is obtained as $\lambda_2 = 0.7226$**.**
As an application, the eigenvector of this eigenvalue, known as the Fiedler vector, is obtained for Fig. 9.2a, and the nodal ordering is performed for reducing the profile of the stiffness matrix. The Fiedler vector is as

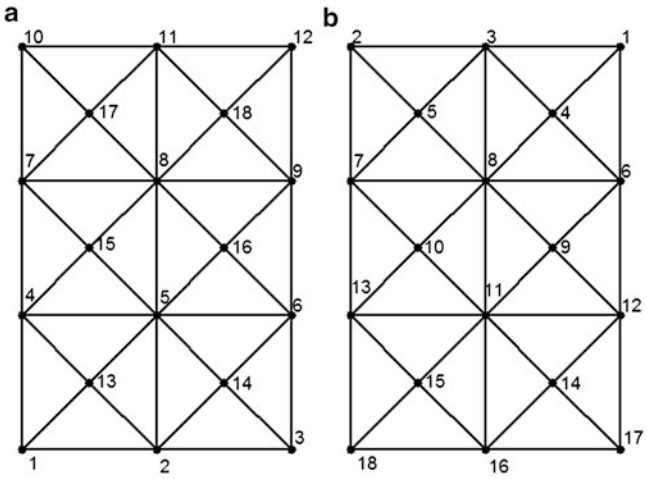

Fig. 9.2 (**a**) The graph introduced in Example 8.12, (**b**) nodal ordering using Fiedler's vector

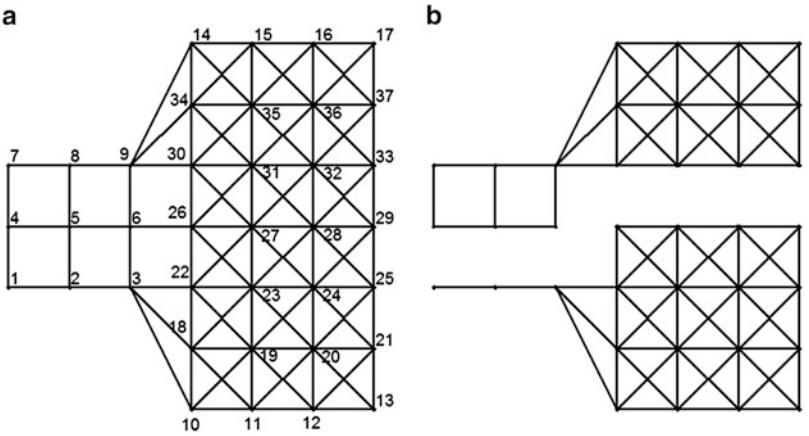

Fig. 9.3 (**a**) Two graphs connected to each other and the nodal numbering, (**b**) partitioning of the graph

$$\begin{aligned}\mathbf{v}_2 = \{&0.3156, 0.3074, 0.3156, 0.1375, 0.1365, 0.1375, -0.1375, -0.1365,\\ &-0.1375, -0.1356, -0.3074,\\ &-0.3156, 0.2737, 0.2737, 0, 0, -0.2737, -0.2737\}\end{aligned}$$

Ordering the nodes according to this vector, the new nodal numbers are obtained as illustrated in Fig. 9.2b.

Example 9.3. In this example, we want to calculate the eigenvalues of graph obtained by connecting two subgraphs. An example of such a graph is illustrated

in Fig. 9.3a. One subgraph is the product graph $P_7\ (X)_{SC}\ P_4$, and the other one is the product graph $P_3\ (X)_C\ P_3$. In nodal numbering, one should pay special attention to the block which should be inverted, and its eigenvalues should be calculable. Similar to the previous example, the intermediate part of the strong Cartesian product is considered and numbered, and the remaining nodes are numbered next. Therefore, for this graph, we have

$$\mathbf{L} = \begin{bmatrix} \mathbf{L}_{mm} & \mathbf{L}_{ms} \\ \mathbf{L}_{ms}^{t} & \mathbf{L}_{ss} \end{bmatrix}$$

Here, we have $m = 17$ and $s = 20$. With this numbering and inverting a matrix of dimension 20, we will face an eigenvalue problem of dimension 17. In the matrix $\mathbf{L}_{ss}$, we have the following form:

$$\mathbf{L}_{ss} = \mathbf{F}_5(\mathbf{A}, \mathbf{B}, \mathbf{A}) = \mathbf{I}_5 \otimes \begin{bmatrix} 6 & -1 & 0 & 0 \\ -1 & 8 & -1 & 0 \\ 0 & -1 & 8 & -1 \\ 0 & 0 & -1 & 5 \end{bmatrix} + \mathbf{F}_5(0,1,0) \otimes \mathbf{F}_4(-1,-1,-1)$$

In this way, instead of inverting a matrix of dimension 20, one should find the eigensolution of five matrices of dimension 4 to be employed in

$$\mathbf{M}^{-1} = \mathbf{V}\mathbf{D}^{-1}\mathbf{V}^{t} = \mathbf{V} \begin{bmatrix} 1/\lambda_1 & & & 0 \\ & 1/\lambda_2 & & \\ & & . & \\ & & & . \\ 0 & & & 1/\lambda_{m^*n} \end{bmatrix} \mathbf{V}^{t}$$

In this problem, the relationships (8.58) are used twice, and $\lambda_2 = 0.3078$ is obtained, while the exact answer is $\lambda_2 = 0.3101$. As an application, this eigenvalue is used to find the Fiedler's vector. Ordering the entries of this vector, the model can be bisected such that the two obtained subgraphs have identical number of members and the number of members connecting the two subgraphs is minimum. Figure 9.3b shows these two subgraphs. This approach is extensively employed in parallel computing.

Example 9.4. We want to study a graph obtained by addition of two members to the product graph $P_5\ (X)_{SC}\ C_4$. The Laplacian matrix of this graph will have the following form, and its eigenvalues can be calculated as follows:

$$\mathbf{L}_{mn} = \mathbf{F}_n(\mathbf{A}_m, \mathbf{B}_m, \mathbf{C}_m)$$

$$\mathbf{A}_m = \mathbf{G}_m(5,-1,5),\ \mathbf{B}_m = \mathbf{G}_m(-1,-1,-1) \text{ and } \mathbf{C}_m = \mathbf{G}_m(8,-1,8)$$

Since

$$\mathbf{A}_m = 6\mathbf{I}_m + \mathbf{B}_m, \quad \mathbf{C}_m = 9\mathbf{I}_m + \mathbf{B}_m,$$

therefore,

$$\mathbf{L}_{mn} = \mathbf{F}(6\mathbf{I}_m + \mathbf{B}_m, \mathbf{B}_m, 9\mathbf{I}_m + \mathbf{B}_m) = 3\mathbf{F}_n(2,0,3) \otimes \mathbf{I}_m + \mathbf{F}_n(1,1,1) \otimes \mathbf{B}_m$$

We know that

$$\text{eig}(\mathbf{B}_m) = -(1 + 2\cos\frac{2k\pi}{m}) \quad k = 1 : m$$

using

$$\text{eig}(\sum (\mathbf{A}_i \otimes \mathbf{B}_i)) = \text{eig}(\sum (\mathbf{B}_i \otimes \mathbf{A}_i))$$

We have

$$\text{eig } (\mathbf{L}_{mn}) = \text{eig}\{\mathbf{I}_m \otimes 3\mathbf{F}_n(2,0,3) + \mathbf{B}_m \otimes \mathbf{F}_n(1,1,1)\}$$

since both $\mathbf{I}_m$ and $\mathbf{B}_m$ commute in the multiplication; thus, we have

$$\text{eig } (\mathbf{L}_{mn}) = \bigcup_{k=1}^{m} [\text{eig}\{3\mathbf{F}_n(2,0,3) - (1 + 2\cos\frac{2k\pi}{m})\mathbf{F}_n(1,1,1)\}]$$

As it can be observed from Fig. 9.4, we have $m = 12$ and $s = 8$. Here, the matrix $\mathbf{L}_{ss}$ has the following form:

$$\mathbf{L}_{ss} = \mathbf{G}_4(\mathbf{A}, \mathbf{B}, \mathbf{A}); \quad \mathbf{A} = \begin{bmatrix} 8 & -1 \\ -1 & 8 \end{bmatrix}; \quad \mathbf{B} = -\mathbf{I}_4$$

where

$$\mathbf{G}_n(\mathbf{A}_m, \mathbf{B}_m, \mathbf{C}_m) = \begin{bmatrix} \mathbf{A}_m & \mathbf{B}_m & & & & & & & \mathbf{B}_m \\ \mathbf{B}_m & \mathbf{C}_m & \mathbf{B}_m & & & & & & \\ & \mathbf{B}_m & \mathbf{C}_m & \mathbf{B}_m & & & & & \\ & & \cdot & \cdot & \cdot & & & & \\ & & & \cdot & \cdot & \cdot & & & \\ & & & & \cdot & \cdot & \cdot & & \\ & & & & & \mathbf{B}_m & \mathbf{C}_m & \mathbf{B}_m & \\ & & & & & & \mathbf{B}_m & \mathbf{C}_m & \mathbf{B}_m \\ \mathbf{B}_m & & & & & & & \mathbf{B}_m & \mathbf{A}_m \end{bmatrix}_n.$$

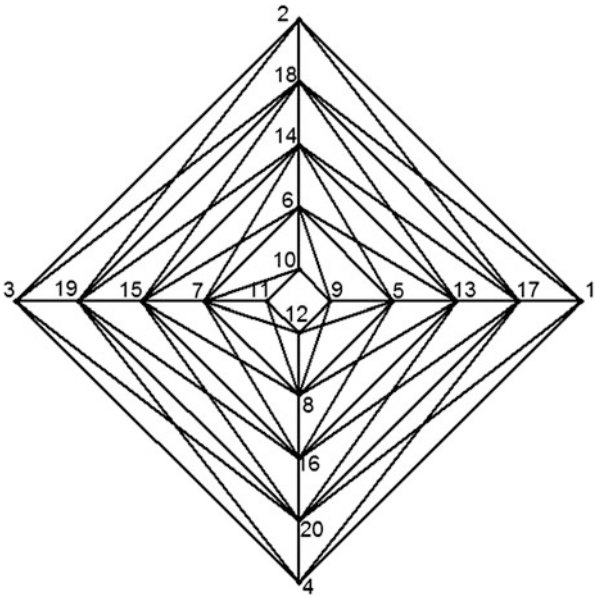

Fig. 9.4 The product graph $P_5\ (X)_{SC}\ C_4$ with two deleted members

For this matrix, $\mathbf{A}_1\mathbf{A}_2 = \mathbf{A}_2\mathbf{A}_1$**,** and therefore, the calculation of the eigenvalues and the inverse of the matrix become feasible. In this example, repeating the relationships (9.8), one obtains $\lambda_2 = 1.1001$**,** while the exact answer is $\lambda_2 = 1.1027$.

Example 9.5. In this example, we want to calculate the buckling load and the natural frequency of a fixed-simple ended bending beam. The calculation is performed using the finite difference approach. The buckling and vibration equation of this beam can be expressed as

$$\frac{d^4w}{dx^4} + \frac{N}{EI}\frac{d^2w}{dx^2} = 0;\ \ \lambda = \frac{N}{EI}h^2$$

$$\frac{d^4w}{dx^4} - \beta^4 w = 0;\ \ \beta = \frac{\rho\omega^2}{EI};\ \ \lambda = (\beta h)^4$$

It is obvious that the nodes of the two sides are different because of having different boundary conditions; however, the internal nodes have identical conditions. Choosing $n = 10$ for the calculation, first we should number the two sides ($m = 2$) followed by the internal nodes ($s = 8$).

Using the finite difference method, the following equations should be solved:

$$(\mathbf{A} - \lambda_i\mathbf{B})\Phi_i = 0 \Rightarrow \left(\begin{bmatrix} \mathbf{A}_{mm} & \mathbf{A}_{ms} \\ \mathbf{A}_{ms}^t & \mathbf{A}_{ss} \end{bmatrix} - \lambda\begin{bmatrix} \mathbf{B}_{mm} & \mathbf{B}_{ms} \\ \mathbf{B}_{ms}^t & \mathbf{B}_{ss} \end{bmatrix}\right)\begin{pmatrix} \Phi_m \\ \Phi_s \end{pmatrix} = \begin{pmatrix} \mathbf{0} \\ \mathbf{0} \end{pmatrix}$$

where

$$\mathbf{A}_{mm} = \begin{bmatrix} 7 & 0 \\ 0 & 5 \end{bmatrix};\ \mathbf{A}_{ss} = \mathbf{F}_8(6,-4,6,1);\ \mathbf{A}_{ms} = \begin{bmatrix} -4 & 1 & 0 & 0 & 0 & 0 & 0 & 0 \\ 0 & 0 & 0 & 0 & 0 & 0 & 1 & -4 \end{bmatrix}$$

The matrix **B** for buckling will have the following form:

$$\mathbf{B}_{mm} = 2\mathbf{I}_2;\ \mathbf{B}_{ss} = \mathbf{F}_8(2,-1,2);\ \mathbf{B}_{ms} = \begin{bmatrix} -1 & 0 & 0 & 0 & 0 & 0 & 0 & 0 \\ 0 & 0 & 0 & 0 & 0 & 0 & 0 & -1 \end{bmatrix}$$

And for vibration problem, we will have $\mathbf{B} = \mathbf{I}_{10}$.

The matrix $\mathbf{A}_{ss}$ has dimension equal to 8, and it is a penta-diagonal matrix. Therefore, we can express it as

$$\mathbf{A}_{ss} = \mathbf{F}_8(6,-4,6,1) = \sum_{i=1}^{3} (\mathbf{A}_i \otimes \mathbf{B}_i)$$

Since the values of $t_1 = \dfrac{a_i - c_i}{d_i}$ and $t_2 = \dfrac{a_i - c_i + d_i}{b_i}$ are identical for all three matrices $\mathbf{A}_i$, therefore $\mathbf{A}_i\mathbf{A}_j = \mathbf{A}_j\mathbf{A}_i$. Thus, $\mathbf{A}_{ss}$ can be decomposed into eight numerical blocks [3]. Hence, in this example, only an eigenvalue problem of dimension $m = 2$ should be solved.

Example 9.6. In this example, the aim is to calculate the buckling load of a plate with some additional part. Here, first the internal nodes are numbered for which the eigenvalues can be calculated. We have the subgraph S with $s = 9$ nodes and the remaining nodes for the subgraph **M** with $m = 6$ nodes. It should be mentioned that the number of nodes is purposely chosen low for a better illustration of the approach. The nodal numbering is illustrated in Fig. 9.5.

The governing differential equation of the problem for the case when the loading is in x-direction will be as follows:

$$\nabla^4 w + \frac{N_x}{D}\frac{\partial^2 w}{\partial x^2} = 0$$

Using the finite difference method, a similar set of equations to that of the previous example should be solved with the only difference that we have:

$$\mathbf{A}_{ss} = \begin{bmatrix} \mathbf{E} & \mathbf{F} & \mathbf{I} \\ \mathbf{F} & \mathbf{E}+\mathbf{I} & \mathbf{F} \\ \mathbf{I} & \mathbf{F} & \mathbf{E} \end{bmatrix};\ \mathbf{E} = \begin{bmatrix} 19 & -8 & 1 \\ -8 & 19 & -8 \\ 1 & -8 & 19 \end{bmatrix};\ \mathbf{F} = \begin{bmatrix} -8 & 2 & 0 \\ 2 & -8 & 2 \\ 0 & 2 & -8 \end{bmatrix}$$

In general, $\mathbf{A}_{ss}$ is a penta-diagonal block matrix, and since the nodes are chosen from the regular part of the model satisfying the condition $\mathbf{A}_i\mathbf{A}_j = \mathbf{A}_j\mathbf{A}_i$, thus, the

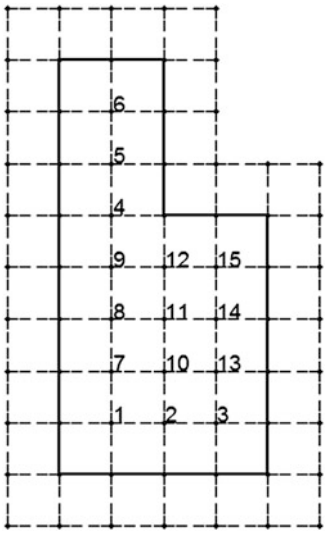

Fig. 9.5 A plate with nodal numbering for finite difference method

eigenvalues and its inverse can easily be found using the relationships (8.58). Also we have

$$\mathbf{B}_{ss} = \begin{bmatrix} 2\mathbf{I} & -\mathbf{I} & \mathbf{0} \\ -\mathbf{I} & 2\mathbf{I} & -\mathbf{I} \\ \mathbf{0} & -\mathbf{I} & 2\mathbf{I} \end{bmatrix}$$

Therefore, here, finding the eigenvalues of a matrix of dimension $n = 15$ is changed to the calculation of the eigenvalues of three matrices of dimension 3 and one matrix of dimension 6. The smallest eigenvalue is obtained as $\lambda = 1.7673$ in four iterations, while the exact value is $\lambda = 1.7597$.

Example 9.7. In this example, the aim is to find the buckling load of a square plate with side length a. The supports at two edges are simple and the other two sides fixed. The load is applied in x-direction. The plate is divided into eight segments in each side. Obviously, the entries of the corresponding matrix will be different for internal nodes and external nodes. Thus, here, $s = 25$, and the remaining nodes belong to the subgraph M with $m = 24$ nodes. The nodal numbering is illustrated in Fig. 9.6.

Here, the matrix $\mathbf{A}_{ss}$ will be as

$$\mathbf{A}_{ss} = F_5(\mathbf{E}, \mathbf{F}, \mathbf{E}, \mathbf{I});\ \mathbf{E} = \mathbf{F}_5(20, -8, 20, 1);\ \mathbf{F} = \mathbf{F}_5(-8, 2, -8)$$

Also we have

$$\mathbf{B}_{ss} = \mathbf{I}_5 \otimes \mathbf{F}_5(2, -1, 2)$$

The rest of the calculation is similar to that of the previous example.

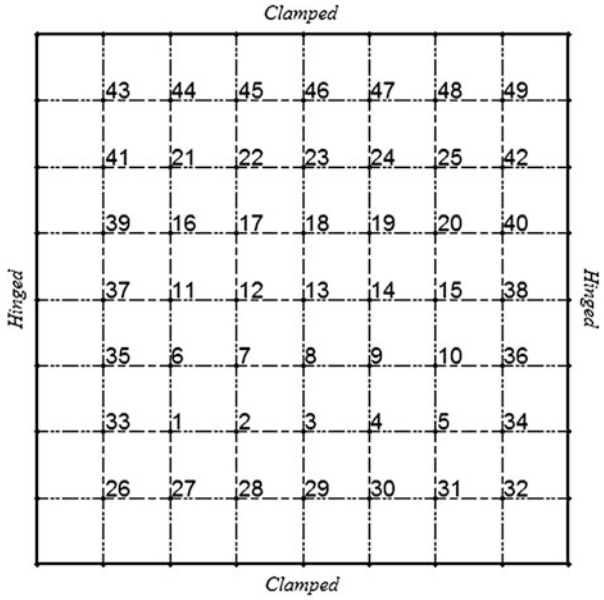

Fig. 9.6 A plate with different boundary conditions and its nodal numbering

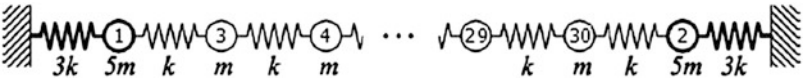

Fig. 9.7 A system of mass–spring and its numbering

Example 9.8. This example is taken from Ref. [4]. A mass–spring system is considered as shown in Fig. 9.7. Here, the numbering is altered, and first the two end nodes are numbered ($m = 2$) followed by the numbering of the remaining intermediate nodes ($s = 28$).

With this numbering, the matrices $\mathbf{K}$ and $\mathbf{M}$ will have the following forms:

$$\mathbf{K} = \begin{bmatrix} \mathbf{K}_{mm} & \mathbf{K}_{ms} \\ \mathbf{K}_{ms}^{t} & \mathbf{K}_{ss} \end{bmatrix}; \quad \mathbf{M} = \begin{bmatrix} \mathbf{M}_{mm} & \mathbf{M}_{ms} \\ \mathbf{M}_{ms}^{t} & \mathbf{M}_{ss} \end{bmatrix}$$

where

$$\mathbf{K}_{mm} = 4k\mathbf{I}_2; \quad \mathbf{K}_{ss} = k\mathbf{F}_{28}(2, -1, 2); \quad \mathbf{K}_{ms} = k\begin{bmatrix} -1 & 0 & . & . & 0 & 0 \\ 0 & 0 & . & . & 0 & -1 \end{bmatrix}_{2\times 28}$$

$$\mathbf{M}_{mm} = 5m\mathbf{I}_2; \quad \mathbf{M}_{ss} = m\mathbf{I}_{28}; \quad \mathbf{M}_{ms} = m\mathbf{Z}_{2\times 28}$$

where $\mathbf{Z}$ is a matrix with all zero entries. The eigenvalues of $\mathbf{K}_{ss}$ are given in the form of a simple relationship in [5].

$$\text{eig}(\mathbf{K}_{ss}) = \text{eig}(\mathbf{F}_s(2,-1,2)) = 2 - 2\cos\frac{k\pi}{s+1} \quad ; \quad k = 1:s$$

Therefore, one needs to solve an eigenvalue problem of dimension $m = 2$ compared to the need for solution of an eigenvalue problem of dimension 12 in Ref. [4].

The smallest eigenvalue obtained from an exact method is $\lambda = 0.0112\frac{k}{m}$, and using the present method after only four iterations, $\lambda = 0.0106\frac{k}{m}$ is achieved.

Example 9.9. This example is taken from Ref. [4]. Here, first the nodes of the first and the last stories are numbered ($m = 2$) followed by those of the other stories ($s = 118$). The $\mathbf{K}$ and $\mathbf{M}$ matrices will have the following forms:

$$\mathbf{K}_{mm} = k\begin{bmatrix} 1.42 & 0 \\ 0 & 1 \end{bmatrix}; \quad \mathbf{K}_{ss} = k\mathbf{F}_{118}(2,-1,2);$$

$$\mathbf{K}_{ms} = k\begin{bmatrix} -1 & 0 & . & . & 0 & 0 \\ 0 & 0 & . & . & 0 & -1 \end{bmatrix}_{2\times 118}$$

$$\mathbf{M}_{mm} = m\mathbf{I}_2; \quad \mathbf{M}_{ss} = m\mathbf{I}_{118}; \quad \mathbf{M}_{ms} = m\mathbf{Z}_{2\times 118}$$

The calculations will be identical to the previous example. Thus, only an eigenvalue problem of dimension $m = 2$ should be solved, compared to the method in [4] which requires the solution of a problem of dimension 16.

The smallest eigenvalue obtained from an exact method is $\omega = 10^{-2}\sqrt{1.6610\frac{k}{m}}$, and using the present method after only six iterations, the exact value is achieved.

9.2.3 *Discussion*

In this chapter, the analysis of those graphs and non-regular structures is studied from which a regular model can be extracted, and inversion is performed using the previously developed methods.

The method developed in this chapter is an iterative approach, and its important feature is that it performs the inversion and eigensolution on matrices' smaller dimension than the matrix of the original model only once. This means that in the iterations of this method, we have only numerical calculations and not matrix calculation. It is seen that after decomposition, the dimensions of the matrices are reduced. The examples contain both graph and structural ones. In the graph examples,

we have studied the problems which have models obtained from product graphs with addition of some members. This means non-regular graph products are obtained by adding some members. Connecting two graphs is also investigated. In relation with structures, the buckling load and vibration frequencies of the beam and plates are studied. Examples are selected from those having either additional parts compared to a regular model, or different boundary conditions are involved in the structure.

9.3 Application of Kronecker Product to the Analysis of Modified Regular Structures

The problem of inverting matrices associated with modified regular structures can be treated more efficiently using an approach that takes into account the solutions of well-formed matrices of the main regular structures. Here, a well-formed matrix is defined as a matrix with a canonical form for which the inversion is carried out using much simpler formulations. Using such an approach, one may consider various types of modifications. For example, different boundary conditions can be treated using this method. Also in the analysis of some structures such as plates with irregular boundaries using the FD method, the present approach can efficiently be used, employing the solution of the plate with regular configuration.

In what follows, first the method for calculating the inverse of block matrices is discussed and then a method is presented for finding the inverse of those matrices which are transformable to regular ones. Finally, the application of this method is illustrated through some examples [2].

9.3.1 Inversion of Block Matrices

First, we should note that in matrix algebra, the inverse of a block matrix can be obtained in terms of the inverse of its blocks by a special formulation. However, such an operation requires the inversion of the blocks involved. Here, we will observe that considering the eigenvalues and eigenvectors of block matrices, such calculation can be simplified.

Suppose the form of the matrix to be investigated be as follows:

$$\mathbf{M}_{\mathrm{mn}} = \mathbf{A}_1 \otimes \mathbf{B}_1 + \mathbf{A}_2 \otimes \mathbf{B}_2 \tag{9.15}$$

where n is the dimension of the matrices $\mathbf{A}_1$ and $\mathbf{A}_2$, and m is the dimension of the matrices $\mathbf{B}_1$ and $\mathbf{B}_2$. We consider two cases. In the first case, $\mathbf{A}_1\mathbf{A}_2 = \mathbf{A}_2\mathbf{A}_1$, then using the eigenvalues, the inverse of $\mathbf{M}$ can easily be obtained. In the second case, $\mathbf{A}_1\mathbf{A}_2 \neq \mathbf{A}_2\mathbf{A}_1$, and we should use QZ factorisation.

In the first case, the two matrices $\mathbf{A}_1$ and $\mathbf{A}_2$ commute with respect to multiplication, and one can find the eigenvalues using the following relationship:

$$\lambda_{\mathbf{M}} = \bigcup_{i=1}^{n} \mathrm{eig}(\mathbf{M}_i); \quad \mathbf{M}_i = \lambda_i(\mathbf{A}_1)\mathbf{B}_1 + \lambda_i(\mathbf{A}_2)\mathbf{B}_2 \tag{9.16}$$

It is obvious that if $\mathbf{V}$, the matrix containing the eigenvectors and $\mathbf{D}$, is a diagonal matrix containing the eigenvalues of a symmetric matrix $\mathbf{M}$, then we have $\mathbf{M} = \mathbf{V}\mathbf{D}\mathbf{V}^t$. Since the eigenvalues of $\mathbf{M}^{-1}$ are the inverse of those of $\mathbf{M}$, and the eigenvectors are identical, therefore,

$$\mathbf{M}^{-1} = \mathbf{V}\mathbf{D}^{-1}\mathbf{V}^t = \mathbf{V}\begin{bmatrix} 1/\lambda_1 & & & 0 \\ & 1/\lambda_2 & & \\ & & . & \\ & & & . \\ 0 & & & 1/\lambda_{m^*n} \end{bmatrix}\mathbf{V}^t \tag{9.17}$$

where $\mathbf{D}^{-1}$ can easily be obtained by inverting the diagonal entries of $\mathbf{D}$. The eigenvector of such a matrix will be in the form of $\mathbf{u} \otimes \mathbf{v}$ in which $\mathbf{u}$ is a vector that diagonalises both matrices $\mathbf{A}_1$ and $\mathbf{A}_2$ simultaneously and $\mathbf{v}$ which is an eigenvector of $\mathbf{M}_i = \lambda_i(\mathbf{A}_1)\mathbf{B}_1 + \lambda_i(\mathbf{A}_2)\mathbf{B}_2$ as discussed in the previous chapters.

In the second case, if $\mathbf{A}_1$ and $\mathbf{A}_2$ do not commute with respect to multiplication, then QZ decomposition should be used. This decomposition is introduced previously, and here only the inverting process is reintroduced.

In this case, consider $\mathbf{y} = \mathbf{M}\mathbf{x}$, where $\mathbf{M}$ has the form of Eq. 9.15. Natural approach will lead to $\mathbf{x} = \mathbf{M}^{-1}\mathbf{y}$. Here, one can use QZ decomposition. However, instead of inversion, we consider appropriate transformations to make $\mathbf{M}$ a diagonal matrix and inversion can then be achieved by inverting the diagonal entries. For this purpose, decomposition should be performed such that instead of $\mathbf{T}$, we end up with a diagonal $\mathbf{D}$. We use QZ decomposition as

$$\begin{cases} \mathbf{T}_A = \mathbf{Q}\mathbf{A}\mathbf{Z} \\ \mathbf{T}_B = \mathbf{Q}\mathbf{B}\mathbf{Z} \end{cases} \qquad \alpha = \mathrm{diag}(\mathbf{T}_A)\ ,\ \beta = \mathrm{diag}(\mathbf{T}_B) \tag{9.18}$$

α and β are the entries on the main diagonal of $\mathbf{T}_A$ and $\mathbf{T}_B$, respectively.

Substitute $\mathbf{U} = \mathbf{K}^{-1}$ with the following:

$$\mathbf{K}(:,i) = \begin{cases} \mathbf{A}\mathbf{V}(:,i) & |\alpha_i| \geq |\beta_i| \\ \mathbf{B}\mathbf{V}(:,i) & \text{elsewhere} \end{cases} \qquad (\mathbf{V} = \mathbf{Z}^t) \tag{9.19}$$

Then unlike the previous case, we have $\mathbf{V} = \mathbf{Z}^t$, but $\mathbf{U} \neq \mathbf{Q}^t$, and $\mathbf{U}\mathbf{A}\mathbf{V}$ is a diagonal matrix:

$$\mathbf{y} = (\mathbf{A}_1 \otimes \mathbf{B}_1 + \mathbf{A}_2 \otimes \mathbf{B}_2)\mathbf{x} \tag{9.20}$$

Considering

$$\mathbf{U_A A_1 V_A} = \mathbf{D_1} \ , \ \mathbf{U_A A_2 V_A} = \mathbf{D_2} \ , \ \mathbf{U_B B_1 V_B} = \mathbf{D_3} \ , \ \mathbf{U_B B_2 V_B} = \mathbf{D_4}, \quad (9.21)$$

we have

$$(\mathbf{U_A} \otimes \mathbf{U_B})\mathbf{y} = (\mathbf{U_A} \otimes \mathbf{U_B})(\mathbf{A_1} \otimes \mathbf{B_1} + \mathbf{A_2} \otimes \mathbf{B_2})\mathbf{x} \quad (9.22)$$

Substituting

$$\mathbf{x} = (\mathbf{V_A} \otimes \mathbf{V_B})\bar{\mathbf{x}}, \quad \bar{\mathbf{y}} = (\mathbf{U_A} \otimes \mathbf{U_B})\mathbf{y}, \quad (9.23)$$

we have

$$\bar{\mathbf{y}} = (\mathbf{D_1} \otimes \mathbf{D_3} + \mathbf{D_2} \otimes \mathbf{D_4})\bar{\mathbf{x}} \quad (9.24)$$

Having $\mathbf{y}, \bar{\mathbf{y}}$ can be calculated, and since the matrix in prentices is diagonal, $\bar{\mathbf{x}}$ and then $\mathbf{x}$ can be calculated. It should be noted that in using these transformations, the calculations are performed on $\mathbf{A}_1, \mathbf{A}_2, \mathbf{B}_1$ and $\mathbf{B}_2$ having dimensions similar to that of the repetitive blocks. Thus, the amount of calculations is reduced considerably.

9.3.2 Proposed Method

Most of the research results presented in the past were concentrated on structural forms having support conditions for which the structural matrices could be expressed as the sum of some Kronecker products. In such cases, using the corresponding theorems, one can simplify the calculations using the block matrices. In general, a structure can have supports leading to non-regular forms which make these calculations impossible. The structure can also have a geometry which can be transformed into regular models by adding some members and nodes. The main aim of this chapter is to study such cases, and as an example, the calculations will be performed on the matrices corresponding to FD solutions.

9.3.2.1 The Effect of Different Boundary Conditions

In order to clarify the problem, suppose that we want to calculate the maximum deflection of the plate shown in Fig. 9.8. This plate is uniformly loaded, and it is simply supported in three edges and clamed in the other edge.

The governing equation for this problem is as follows [6]:

$$\nabla^4 \mathrm{w} = \frac{\partial^4 \mathrm{w}}{\partial \mathrm{x}^4} + 2\frac{\partial^4 \mathrm{w}}{\partial \mathrm{x}^2 \partial \mathrm{y}^2} + \frac{\partial^4 \mathrm{w}}{\partial \mathrm{y}^4} = \frac{\mathrm{p}}{\mathrm{D}} \Rightarrow \mathrm{D} = \frac{\mathrm{Et}^3}{12(1-\upsilon^2)} \quad (9.25)$$

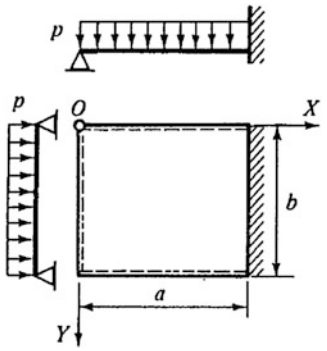

Fig. 9.8 A plate with simple supports in three edges and clapped in one edge under a uniform loading

If the length of the subdivisions in both directions are taken as h, for a typical joint (i,j), we will have

$$\begin{aligned}&20w(i,j)-8[w(i,j-1)+w(i+1,j)+w(i,j+1)+w(i-1,j)]\\&+2[w(i-1,j-1)+w(i+1,j-1)+w(i+1,j+1)+w(i-1,j+1)]\\&+[w(i,j-2)+w(i+2,j)+w(i,j+2)+w(i-2,j)]=\frac{ph^4}{D}\end{aligned}\tag{9.26}$$

It should be noted that the nodal numbering is performed such that the nodes corresponding to the claimed supports and the corresponding nodes in the other side of the plate are first numbered, followed by the numbering of the remaining nodes. As an example, if we consider the numbers of subdivisions in the X and Y directions as 7 and 6, respectively, the nodal numbering should be performed as illustrated in Fig. 9.9. In this way, writing the FD equations and imposing the boundary conditions, we will obtain the following matrix:

$$\begin{aligned}&[\mathbf{C}]\{\mathbf{w}\}=-\{\mathbf{p}\}\frac{h^4}{D}\\&\Rightarrow\begin{bmatrix}\mathbf{C}_{11}&\mathbf{C}_{12}\\\mathbf{C}_{21}&\mathbf{C}_{22}\end{bmatrix}\begin{Bmatrix}\mathbf{w}_1\\\mathbf{w}_2\end{Bmatrix}=-\frac{h^4}{D}\begin{Bmatrix}\mathbf{p_1}\\\mathbf{p_2}\end{Bmatrix};\quad \mathbf{C}_{21}=\mathbf{C}_{12}^{t}\end{aligned}\tag{9.27}$$

where the decomposed submatrices are as follows:

$$\mathbf{C}_{11}=\mathbf{F}_5(\mathbf{A}_2,\mathbf{B}_2,\mathbf{A}_2+\mathbf{I}_2,\mathbf{I}_2);\ \mathbf{A}_2=\begin{bmatrix}20&0\\0&18\end{bmatrix}\ ;\ \mathbf{B}_2=-8\times\mathbf{I}_2$$

$$\begin{aligned}&\mathbf{C}_{22}=\mathbf{F}_5(\mathbf{A}_4,\mathbf{B}_4,\mathbf{A}_4+\mathbf{I}_4,\mathbf{I}_4);\ \ \mathbf{A}_4=\mathbf{F}_4(19,-8,19,1);\\&\mathbf{B}_4=\mathbf{F}_4(-8,2,-8)\end{aligned}$$

$$\mathbf{C}_{12}=\mathbf{F}_5(\mathbf{A}_{4\times2},\mathbf{B}_{4\times2},\mathbf{A}_{4\times2})\ \ ;\ \ \mathbf{A}_{4\times2}=\begin{bmatrix}-8&1&0&0\\0&0&1&-8\end{bmatrix};\ \mathbf{B}_{4\times2}=\begin{bmatrix}2&0&0&0\\0&0&0&2\end{bmatrix}$$

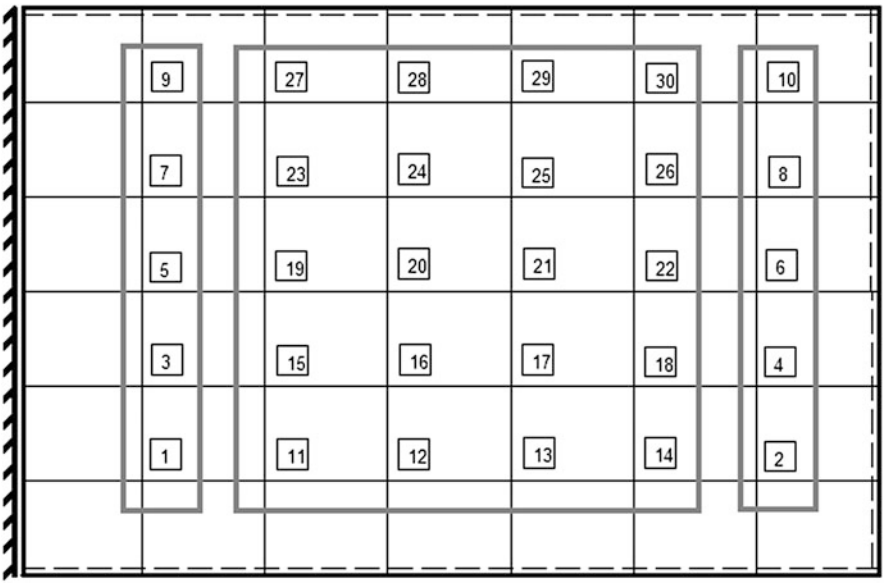

Fig. 9.9 Nodal numbering of the plate for the FD method

where $\mathbf{I}$ is a unit matrix and

$$\mathbf{F}_{\mathrm{m}}(\mathbf{A},\mathbf{B},\mathbf{C},\mathbf{D}) = \begin{bmatrix} \mathbf{A} & \mathbf{B} & \mathbf{D} & & & \mathbf{0} \\ \mathbf{B} & \mathbf{C} & \mathbf{B} & . & & \\ \mathbf{D} & \mathbf{B} & . & . & . & \\ & . & . & . & \mathbf{B} & \mathbf{D} \\ & & . & \mathbf{B} & \mathbf{C} & \mathbf{B} \\ \mathbf{0} & & & \mathbf{D} & \mathbf{B} & \mathbf{A} \end{bmatrix}_{\mathrm{m}} \tag{9.29}$$

If the fourth argument of $\mathbf{F}$ is not present, then the above matrix becomes a block tri-diagonal matrix.

Considering the different boundary conditions and using the above-mentioned nodal numbering, one can observe repetitive block forms in all the submatrices (even in the submatrix $\mathbf{C}_{21} = \mathbf{C}_{12}^{\mathrm{t}}$ which is a rectangular matrix).

Therefore, solving Eq. 9.17 in block form, we will have

$$\begin{cases} \{\mathbf{w}_2\} = -\dfrac{\mathrm{h}^4}{\mathrm{D}}\mathbf{C}_{22}^{-1}[\{\mathbf{p}_2\} + \mathbf{C}_{21}\{\mathbf{w}_1\}] \\ \{\mathbf{w}_1\} = -\dfrac{\mathrm{h}^4}{\mathrm{D}}[\mathbf{C}_{11} - \mathbf{C}_{12}\mathbf{C}_{22}^{-1}\mathbf{C}_{21}]^{-1}[\{\mathbf{p}_1\} - \mathbf{C}_{12}\mathbf{C}_{22}^{-1}\{\mathbf{p}_2\}] \end{cases} \tag{9.30}$$

It can be seen that in these relationships, we do not need to find the inverse of $\mathbf{C}_{11} - \mathbf{C}_{12}\mathbf{C}_{22}^{-1}\mathbf{C}_{21}$ and $\mathbf{C}_{22}$. The important point is that, as we will see, the inverse of

$\mathbf{C}_{11}$ and $\mathbf{C}_{22}$ can easily be found, and we need only to invert $\mathbf{C}_{11} - \mathbf{C}_{12}\mathbf{C}_{22}^{-1}\mathbf{C}_{21}$ which is a matrix with identical dimension to that of $\mathbf{C}_{11}$. Since in most of the numerical methods like FD, the number of subdivisions is generally high, therefore, the dimension of the matrix $\mathbf{C}_{11}$ is less than that of $\mathbf{C}_{22}$, and from the second row, the matrix $\mathbf{w}_2$ should be calculated; otherwise, we should first calculate $\mathbf{w}_1$.

Now, we consider the inversion of $\mathbf{C}_{11}$ and $\mathbf{C}_{22}$ matrices. These matrices are block five-diagonal matrices. As an example, the inverse of $\mathbf{C}_{22}$ can be expressed as

$$\begin{aligned}\mathbf{C}_{22} &= \mathbf{F}(\mathbf{A}, \mathbf{B}, \mathbf{A} + \mathbf{I}, \mathbf{I}) = \mathbf{I} \otimes \mathbf{A} + \mathbf{F}(0, 1, 0) \otimes \mathbf{B} + \mathbf{F}(0, 0, 1, 1) * \mathbf{I} \\ &= \sum_{i=1}^{3} \mathbf{A}_i \otimes \mathbf{B}_i \end{aligned} \tag{9.31}$$

Since we have three Kronecker products, therefore, one cannot use QZ transformation of inversion. However, since $\mathbf{A}_i\mathbf{A}_j = \mathbf{A}_j\mathbf{A}_i$, therefore, we first use Eq. 9.16 and obtain

$$\lambda_{\mathbf{C}_{22}} = \bigcup_{i=1}^{5} \text{eig}(\mathbf{M}_i); \mathbf{M}_i = \mathbf{A} + \lambda_i(\mathbf{F}(0, 1, 0))\mathbf{B} + \lambda_i(\mathbf{F}(0, 0, 1, 1))\mathbf{I} \tag{9.32}$$

The vector u which diagonalises the three matrices $\mathbf{I_5}$, $\mathbf{F}(0, 1, 0)$ and $\mathbf{F}(0, 0, 1, 1)$ simultaneously will then be calculated followed by the vector $\mathbf{v}$, that is, the eigenvector of $\mathbf{M}_i = \mathbf{A} + \lambda_i(\mathbf{F}(0, 1, 0))\mathbf{B} + \lambda_i(\mathbf{F}(0, 0, 1, 1))\mathrm{I}$. The columns of the matrix $\mathbf{V}$ are equal to $\mathbf{u} \otimes \mathbf{v}$. In this way, using Eq. 9.17, the $\mathbf{C}_{22}^{-1}$ will be obtained.

In relation with $\mathbf{C}_{22}$**,** it is important to note that this matrix is exactly the same as the matrix we had for the plate with four edges being simply supported. In fact the role of different support conditions is reflected in $\mathbf{C}_{11}$ and $\mathbf{C}_{21} = \mathbf{C}_{12}^{t}$.

For inverting the submatrix $\mathbf{C}_{11}$, a similar calculations can be carried out. If we only want to calculate the moments, we have to adopt a similar process. In this case, we will have block tri-diagonal matrix which can be expressed as the sum of two Kronecker products and the process of calculation will not be different.

9.3.2.2 Structures Transformable to Regular Forms

In the following, we study the analysis of plates. In general, one needs to calculate the moments and deflection of the plates where its geometry can be changed into regular figures by adding or deleting some parts. Then using the FD method and after writing the corresponding equations for the regular plate, the results of the main plate are obtained.

As an example, we want to calculate the moments and deflection of the plate in Fig. 9.10a. This plate is pinned at its boundary nodes. For solution, FD method is employed. As it can be seen for simplicity and because of the irregularity of the

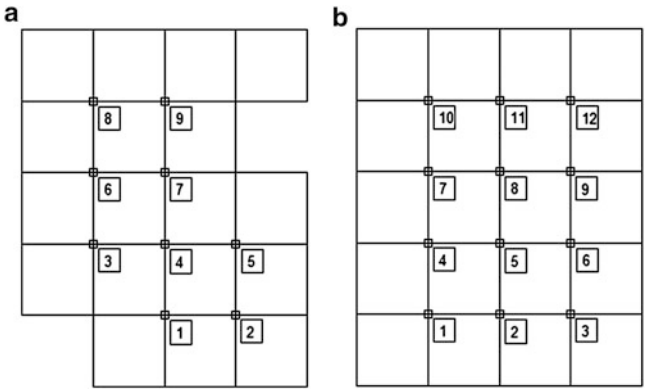

Fig. 9.10 Completion of (**a**) as (**b**) for having a regular block matrix

plate, nine nodes are selected. Obviously for more irregularity, the distance between the nodes should be reduced by increasing the number of subdivisions.

First, we transform the plate into a complete plate as shown in Fig. 9.10b, and with new numbering, the inverse of the matrix of the FD equations of this plate can be calculated.

The governing relationships for this problem are as follows:

$$[\mathbf{C}_{(b)}]\{\mathbf{M}\} = -\{\mathbf{P}\}a^2 \Rightarrow \{\mathbf{M}\} = -[\mathbf{H}]\{\mathbf{P}\}a^2 \Rightarrow [\mathbf{H}] = [\mathbf{C}_{(b)}]^{-1} \tag{9.33}$$

By partitioning this matrix, we have

$$\begin{Bmatrix} \mathbf{M}_1 \\ \mathbf{M}_2 \end{Bmatrix} = -\begin{bmatrix} \mathbf{H}_{11} & \mathbf{H}_{12} \\ \mathbf{H}_{21} & \mathbf{H}_{22} \end{bmatrix} \begin{Bmatrix} \mathbf{P}_1 a^2 \\ \mathbf{P}_2 a^2 \end{Bmatrix} \tag{9.34}$$

which can be expressed as

$$\begin{Bmatrix} \mathbf{M}'_1 \\ \mathbf{0} \end{Bmatrix} = -\begin{bmatrix} \mathbf{H}_{11} & \mathbf{H}_{12} \\ \mathbf{H}_{21} & \mathbf{H}_{22} \end{bmatrix} \begin{Bmatrix} \mathbf{P}_1 a^2 \\ \mathbf{P}'_2 a^2 \end{Bmatrix} \tag{9.35}$$

Here, $\mathbf{H}_{22}$ corresponds to the added nodes (three nodes), and $\mathbf{H}_{11}$ corresponds to the remaining nodes. Thus,

$$\mathbf{M}'_1 = -[\mathbf{H}_{11}\mathbf{P}_1 + \mathbf{H}_{12}\mathbf{P}'_2]a^2; \quad \mathbf{P}'_2 = -\mathbf{H}_{22}^{-1}\mathbf{H}_{21}\mathbf{P}_1 \tag{9.36}$$

Combining these two equations leads to

$$\mathbf{M}'_1 = -[\mathbf{H}_{11} - \mathbf{H}_{12}\mathbf{H}_{22}^{-1}\mathbf{H}_{21}]\mathbf{P}_1 a^2 \Rightarrow \mathbf{C}_{(a)}^{-1} = \mathbf{H}_{11} - \mathbf{H}_{12}\mathbf{H}_{22}^{-1}\mathbf{H}_{21} \tag{9.37}$$

Ultimately, the deflection of the plate is obtained as

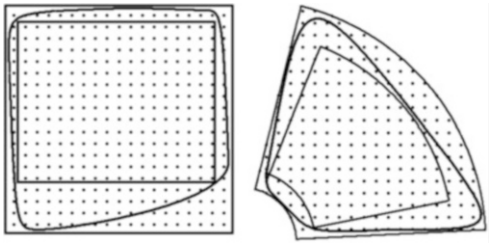

Fig. 9.11 Transformation of two non-regular plates to regular rectangular- and sector of a circle-shaped plates

$$[\mathbf{C}_{(a)}]\{\mathbf{W}'\} = -\frac{\mathbf{M}_1'}{D}a^2 \Rightarrow \{\mathbf{W}'\} = -[\mathbf{H}_{11} - \mathbf{H}_{12}\mathbf{H}_{22}^{-1}\mathbf{H}_{21}]\frac{\mathbf{M}_1'}{D}a^2 \tag{9.38}$$

where $D = Et^3/12(1 - v^2)$.

In Example 9.10, it can be seen that the selected grid for discretisation of the plate for FD analysis has certain extra parts than a standard graph product.

The point is that in some plates, it is easier to consider it in the form of a sector of a circle in place of considering it as a rectangular model. Example 9.11 investigates a plate using this approach.

In any case, we should know that a rectangular or a sector of a circle can be inscribed in a circle or can be circumscribed in it, in both cases of which the calculations lead to the inversion of a matrix with dimension equal to the number of nodes added or deleted. As an example, in Fig. 9.11 for both irregular plates, in analysis by FD method, both cases of the plates inscribed in a circle or circumscribe it are illustrated.

9.3.3 Numerical Examples

Example 9.10. In this problem, a plate discretised as shown in Fig. 9.12 for FD analysis contains parts more than that of a standard product graph. In the previous section, we studied a plate smaller than its circumferential bigger plate, while in here, we create a regular product graph which is inside the plate. Partitioning the stiffness matrix of this plate into two parts and having the inverse of the created product graph, the solution of the problem becomes feasible.

Here, the equations are written for Fig. 9.12a, and ultimately, the results are obtained for Fig. 9.12b. The governing relationship here is as follows:

$$[\mathbf{C}_{(a)}]\{\mathbf{M}\} = -\{\mathbf{P}\}a^2 \Rightarrow \begin{bmatrix} \mathbf{C}_{11} & \mathbf{C}_{12} \\ \mathbf{C}_{21} & \mathbf{C}_{22} \end{bmatrix} \begin{Bmatrix} \mathbf{M}_1 \\ \mathbf{M}_2 \end{Bmatrix} = -\begin{Bmatrix} \mathbf{P}_1 a^2 \\ \mathbf{P}_2 a^2 \end{Bmatrix}$$

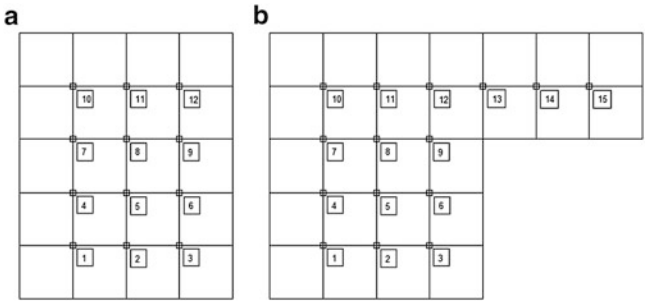

Fig. 9.12 Reduction of (**b**) to obtain (**a**) for having a regular block matrix

Therefore,

$$\begin{cases} \{\mathbf{M}_1\} = \mathbf{C}_{11}^{-1}[\{\mathbf{P}_1\}a^2 - \mathbf{C}_{12}\{\mathbf{M}_2\}] \\ \{\mathbf{M}_2\} = [\mathbf{C}_{22} - \mathbf{C}_{21}\mathbf{C}_{11}^{-1}\mathbf{C}_{12}]^{-1}[\{\mathbf{P}_2\} - \mathbf{C}_{21}\mathbf{C}_{11}^{-1}\{\mathbf{P}_1\}]a^2 \end{cases}$$

Substituting $\mathbf{M}_2$ in $\mathbf{M}_1$, and due to the ease of inverting $\mathbf{C}_{11}$, it is enough to find the inverse of a matrix having dimension equal to that of $\mathbf{C}_{22}$, that is, we calculate $[\mathbf{C}_{22} - \mathbf{C}_{21}\mathbf{C}_{11}^{-1}\mathbf{C}_{12}]^{-1}$.
Now, we calculate the deflection as follows:

$$\begin{bmatrix} \mathbf{C}_{11} & \mathbf{C}_{12} \\ \mathbf{C}_{21} & \mathbf{C}_{22} \end{bmatrix} \begin{Bmatrix} \mathbf{W}_1 \\ \mathbf{W}_2 \end{Bmatrix} = -\frac{1}{\mathrm{D}} \begin{Bmatrix} \mathbf{M}_1 \\ \mathbf{M}_2 \end{Bmatrix}$$

Thus,

$$\begin{cases} \{\mathbf{W}_1\} = \mathbf{C}_{11}^{-1}\left[-\dfrac{\mathbf{M_1}}{\mathrm{D}} - \mathbf{C}_{12}\{\mathbf{W}_2\}\right] \\ \{\mathbf{W}_2\} = [\mathbf{C}_{22} - \mathbf{C}_{21}\mathbf{C}_{11}^{-1}\mathbf{C}_{12}]^{-1}\left[\mathbf{C}_{21}\mathbf{C}_{11}^{-1}\dfrac{\mathbf{M_1}}{\mathrm{D}} - \dfrac{\mathbf{M_2}}{\mathrm{D}}\right] \end{cases}$$

In this way, the inverse of the same matrix $[\mathbf{C}_{22} - \mathbf{C}_{21}\mathbf{C}_{11}^{-1}\mathbf{C}_{12}]$ which resulted the bending moments is obtained for calculating the deflections.

Example 9.11. Here, we study a plate which is convertible to the sector of a circle. As it can be seen from Fig. 9.13a, this plate can be converted into the quarter of a circle by adding some parts, and writing the finite difference equations in the polar coordinate system as developed in [7], it has become complete as shown in Fig. 9.13b. It should be noted that all the supports are pinned around the edges.
The finite difference matrix for the plate with hole in Fig. 9.13a is a 5-by-5 non-rectangular one. Adding three nodes, the plate changes into a quarter of a circle

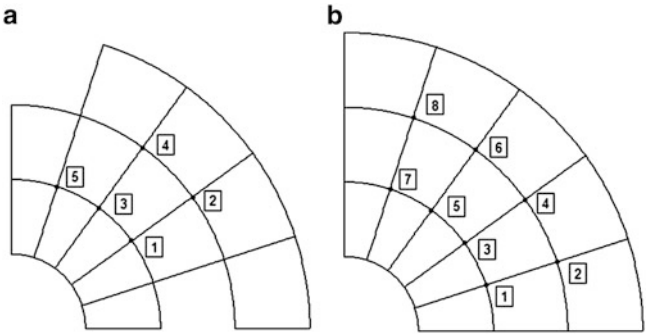

Fig. 9.13 Completion of (**a**) to obtain (**b**) for having regular block matrix in polar coordinate system

having eight nodes, and the corresponding FD matrix takes the form F which can easily be inverted using Eq. 9.17:

$$\mathbf{C}_{(b)} = \mathbf{F}_4(\mathbf{A}_2, \mathbf{B}_2, \mathbf{A}_2) = \mathbf{I}_4 \otimes \mathbf{A}_2 + \mathbf{F}_4(0,1,0) \otimes \mathbf{B}_2$$

$$\mathbf{A}_2 = \begin{bmatrix} 2(1+\frac{25}{\pi^2}) & \frac{5}{4} \\ \frac{5}{6} & 2(1+\frac{100}{9\pi^2}) \end{bmatrix} \Rightarrow \mathbf{B}_2 = \begin{bmatrix} \frac{25}{\pi^2} & 0 \\ 0 & \frac{100}{9\pi^2} \end{bmatrix}$$

In this way, using the relationships of Example 9.10, one needs to invert only a matrix of dimension 3 corresponding to the added nodes.

9.3.4 Concluding Remarks

The method presented in this chapter extends the applications of the previous methods developed for the analysis of regular structures based on the stiffness method and some concepts from graph products. In some of the examples previously investigated, adding or removing some nodes and/or members changes the models into non-regular ones, or similarly, the use of different support conditions may alter the repetitive nature of the corresponding block matrices. In such cases, first the matrices are partitioned in such a way that the effect of the support conditions and the remaining part of the structure are separated, and the analysis is performed using the regularity property. Thus, the support conditions do not need to be regular, and different supports can be present in the structure. For the most recent work on this topic the read may refer to Kaveh et al. [8].

References

1. Rahami H, Kaveh A, Mehanpour H (2012) Optimal analysis of non-regular graphs using the results of regular models via an iterative method. Int J Optim Civil Eng 2:153–171
2. Kaveh A, Rahami H, Mehanpour H (2013) Application of Kronecker product to the analysis of modified regular structures. Iranian J Sci Technol (in press)
3. Kaveh A, Rahami H (2006) Block diagonalization of adjacency and Laplacian matrices for graph product; applications in structural mechanics. Int J Numer Meth Eng 68:33–63
4. Kaveh A, Fazli H (2011) Approximate eigensolution of locally modified regular structures using a substructuring technique. Comput Struct 89:529–537
5. Kaveh A, Rahami H (2010) An efficient analysis of repetitive structures generated by graph products. Int J Numer Meth Eng 84:108–126
6. Szilard R (2004) Theories and applications of plate analysis: classical, numerical and engineering methods. Wiley, New York
7. Ugural AC (1981) Stresses in plates and shells. McGraw-Hill, New York
8. Kaveh A, Rahami H, Mirghaderi SR, Ardalan Asl M (2013) Analysis of near-regular structures using the force method. Eng Comput 30(1):21–48

Chapter 10
Graph Products Applied to the Regular and Locally Modified Regular Structures Using Iterative Methods

10.1 Introduction

In this chapter, graph products are employed to study various kinds of regular structural patterns. The emphasis is on the eigensolution of the finite element models associated with such structures. However, the methods developed here can also be used for static and dynamic analysis as well. In Sect. 10.2, various symmetric and regular structural patterns and their corresponding canonical matrix forms are investigated. It is demonstrated that using the idea of matrix decomposition, one can simplify the eigenproblem associated with the regular model under consideration. In Sect. 10.3, we extend our investigation to structural models with a dominant regular pattern, which need to be slightly perturbed or modified in order to be considered as purely regular. There are plenty of such examples in structural mechanics applications; we can refer to the local refinement of a regularly meshed finite element model, small cut-outs extracted from a structural model and non-regular constraints imposed on a regular model as a few examples. The idea of matrix decomposition is further extended in order to develop numerical methods to deal with such cases. The concept of modification seems also to be attractive in dealing with nonconforming matrix forms, such as those associated with translational regular patterns. Using this concept in conjunction with substructuring techniques, an approximate method is presented in Sect. 10.4 for efficient solution of the corresponding eigenproblem.

10.2 Eigensolution of Symmetric and Regular Structures Using Canonical Forms

A fundamental approach towards exploiting symmetry and regularity in structural mechanics problems is through the decomposition of the structural matrices. In this regard, theory of groups and their representations has been extensively used as a

A. Kaveh, *Optimal Analysis of Structures by Concepts of Symmetry and Regularity*,
DOI 10.1007/978-3-7091-1565-7_10,

standard tool. Group theory is known as the mathematical language of symmetry [1]. However, the concepts of group theory may appear to be complicated for an unfamiliar user, and this may be a non-appealing feature from the viewpoint of an engineer compared to a mathematician. An engineer considers the symmetry as a simplifying property of a structure and also expects the method for exploiting this property to be simple enough. Matrix canonical forms are developed as an alternative to represent the underlying mathematical operations more conveniently. Canonical forms were originated from eigenproblems associated with symmetric graphs and then were extended to graph products. Using the method of canonical forms, one considers directly the patterns of the stiffness and mass matrices, instead of using projection operators in group theoretic methods, to construct invariant subspaces. A local symmetry-adapted coordinate system is employed in which the matrices assume the desired forms. Then, the invariant subspaces are constructed using the properties of the established matrix patterns. This method has several advantages. Firstly, it is simple and easy to understand. Secondly, the full matrices need not be constructed at all, and it is adequate to determine a small portion of the matrix, that is, its repeating blocks. Thirdly, the final decomposed matrices (block-diagonal forms) can be presented in a closed-form solution.

The generalised eigenproblem associated with a regular structure may be expressed as follows:

$$\mathbf{K\Phi} = \omega^2\, \mathbf{M\Phi} \tag{10.1}$$

where $\mathbf{K}$ and $\mathbf{M}$ of order N are the stiffness and mass matrices, ω is the natural frequency and $\mathbf{\Phi}$ is the matrix of eigenvectors. Matrices associated with regular structure may be represented in special block forms known as canonical forms. Different kinds of canonical forms can be decomposed by transforming the matrices into block-diagonal forms using a suitable orthogonal matrix $\mathbf{T}$. The transformed stiffness and mass matrices are

$$\mathbf{K}^{(\mathrm{BD})} = \mathbf{T}^{\mathrm{t}}\mathbf{KT} \text{ and } \mathbf{M}^{(\mathrm{BD})} = \mathbf{T}^{\mathrm{t}}\mathbf{MT} \tag{10.2}$$

where $\mathbf{K}^{(\mathrm{BD})}$ and $\mathbf{M}^{(\mathrm{BD})}$ each have the same block-diagonal form. Using the transformation (10.2), the eigenproblem of the regular model is reduced to several smaller decoupled eigenproblems, which produces dramatic simplification and saving in the computations.

In this section, the most common matrix canonical forms are reviewed, and those symmetric and regular structural configurations that can be explained through such forms are investigated. The invariant subspaces are formulated, and the closed-form solution for the block-diagonalised matrix is provided for each case. Here, only the stiffness matrix is considered, since the pattern of the mass matrix is the same.

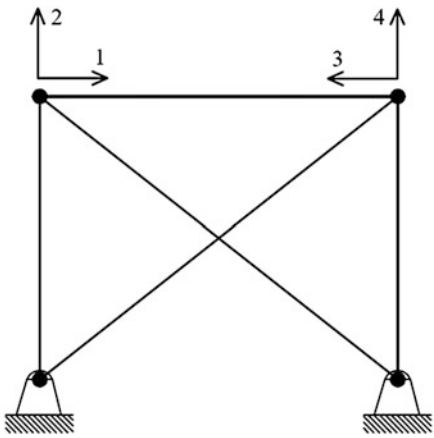

Fig. 10.1 Bilateral symmetry

10.2.1 Canonical Form II

This is the simplest matrix form that can be associated with structural models having a bilateral symmetry. Consider the pin-jointed truss shown in Fig. 10.1 as a simple example. Using a symmetry-adapted local coordinate system as depicted in this figure, the stiffness matrix can be written in the following form:

$$\mathbf{K} = \left[\begin{array}{c|c} \mathbf{A} & \mathbf{B} \\ \hline \mathbf{B} & \mathbf{A} \end{array}\right] \tag{10.3}$$

where $\mathbf{A}$ and $\mathbf{B}$ are $m \times m$ matrices.

Let $\mathbf{q}$ denote the matrix of eigenvectors for the adjacency matrix of a two-node path graph

$$\mathbf{q} = \frac{1}{\sqrt{2}} \begin{bmatrix} 1 & 1 \\ -1 & 1 \end{bmatrix}. \tag{10.4}$$

Then, we define the block-orthonormal matrix $\mathbf{Q}$ as follows:

$$\mathbf{Q} = \mathbf{q} \otimes \mathbf{I}_{\mathrm{m}} = \frac{1}{\sqrt{2}} \begin{bmatrix} \mathbf{I}_{\mathrm{m}} & \mathbf{I}_{\mathrm{m}} \\ -\mathbf{I}_{\mathrm{m}} & \mathbf{I}_{\mathrm{m}} \end{bmatrix}, \tag{10.5}$$

where $\mathbf{I}_{\mathrm{m}}$ denotes the identity matrix of order m. Using matrix $\mathbf{Q}$ as defined in Eq. 10.5, one can transform $\mathbf{K}$ into block-diagonal form

$$\tilde{\mathbf{K}} = \mathbf{Q}^{\mathrm{t}}\mathbf{K}\mathbf{Q} = \left[\begin{array}{c|c} \mathbf{A} - \mathbf{B} & \mathbf{0} \\ \hline \mathbf{0} & \mathbf{A} + \mathbf{B} \end{array}\right]. \tag{10.6}$$

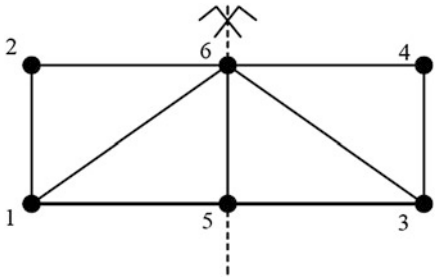

Fig. 10.2 Bilateral symmetry with a kernel

10.2.2 Canonical Form III

The basic Form III is written as follows:

$$\mathbf{L} = \begin{bmatrix} \mathbf{A} & \mathbf{B} & \mathbf{P} \\ \mathbf{B} & \mathbf{A} & \mathbf{P} \\ \mathbf{P}^t & \mathbf{P}^t & \mathbf{C} \end{bmatrix}, \tag{10.7}$$

where we assume that $\mathbf{A}$ and $\mathbf{B}$ are $m \times m$ matrices and $\mathbf{C}$ is a $k \times k$ matrix.

This form can be associated with graph models having bilateral symmetry, in which some nodes lie on the axis (plane) of symmetry. For example, consider the graph shown in Fig. 10.2. The Laplacian matrix of this graph is given by

$$\mathbf{L} = \left[\begin{array}{cc|cc|cc} 3 & -1 & 0 & 0 & -1 & -1 \\ -1 & 2 & 0 & 0 & 0 & -1 \\ \hline 0 & 0 & 3 & -1 & -1 & -1 \\ 0 & 0 & -1 & 2 & 0 & -1 \\ \hline -1 & 0 & -1 & 0 & 3 & -1 \\ -1 & -1 & -1 & -1 & -1 & 5 \end{array}\right].$$

One can easily verify that $\mathbf{Q}$ in block form Eq. 10.8 is the right choice for an orthonormal basis

$$\mathbf{Q} = \left[\begin{array}{c|c} \mathbf{q} \otimes \mathbf{I}_m & \mathbf{0} \\ \hline \mathbf{0} & \mathbf{I}_k \end{array}\right], \tag{10.8}$$

where $\mathbf{q}$ is defined in Eq. 10.4. Now performing the transformation on Form III (matrix $\mathbf{L}$ in Eq. 10.7), we arrive at

$$\tilde{\mathbf{L}} = \mathbf{Q}^t\mathbf{L}\mathbf{Q} = \left[\begin{array}{c|cc} \mathbf{A}-\mathbf{B} & \mathbf{0} & \mathbf{0} \\ \hline \mathbf{0} & \mathbf{A}+\mathbf{B} & \sqrt{2}\mathbf{P} \\ \mathbf{0} & \sqrt{2}\mathbf{P}^t & \mathbf{C} \end{array}\right]. \tag{10.9}$$

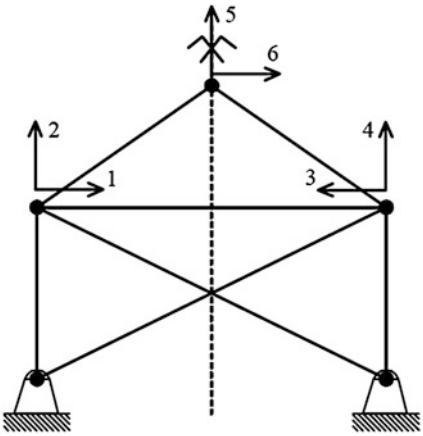

Fig. 10.3 Bilateral symmetric structure with a kernel

Form III can be extended to structural models with bilateral symmetry in which some nodal points are located on the plane of symmetry. We use the term 'kernel' for the points falling on the symmetry plane. As a simple example, consider the pin-jointed truss in Fig. 10.3. Let us partition the set of DOFs corresponding to kernel points into 'stationary' and 'reversing' DOFs according to the behaviour of a DOF with respect to the reflection across the symmetry plane. For example, in Fig. 10.3, DOF numbers 5 and 6 are the set of 'stationary' and 'reversing' DOFs, respectively.

Partitioning the set of DOFs in this way, the stiffness matrix takes the following form:

$$\mathbf{K} = \left[\begin{array}{cc|cc} \mathbf{A} & \mathbf{B} & \mathbf{P} & \mathbf{S} \\ \mathbf{B} & \mathbf{A} & \mathbf{P} & -\mathbf{S} \\ \hline \mathbf{P}^{\mathrm{t}} & \mathbf{P}^{\mathrm{t}} & \mathbf{C}_{\mathrm{s}} & \mathbf{0} \\ \mathbf{S}^{\mathrm{t}} & -\mathbf{S}^{\mathrm{t}} & \mathbf{0} & \mathbf{C}_{\mathrm{r}} \end{array}\right]. \tag{10.10}$$

The orthonormal basis for the two invariant subspaces of $\mathbf{K}$ is constructed as follows:

$$\mathbf{Q} = \left[\begin{array}{cc|cc} \mathbf{q}_1 \otimes \mathbf{I}_{\mathrm{m}} & \mathbf{0} & \mathbf{q}_2 \otimes \mathbf{I}_{\mathrm{m}} & \mathbf{0} \\ \mathbf{0} & \begin{bmatrix} \mathbf{0}_{\mathrm{s}} \\ \mathbf{I}_{\mathrm{r}} \end{bmatrix} & \mathbf{0} & \begin{bmatrix} \mathbf{I}_{\mathrm{s}} \\ \mathbf{0}_{\mathrm{r}} \end{bmatrix} \end{array}\right], \tag{10.11}$$

where $\mathbf{q}_1$ and $\mathbf{q}_2$ are the columns of $\mathbf{q}$ as defined in Eq. 10.4. Using the above basis, matrix $\mathbf{K}$ in Eq. 10.10 is decomposed as follows:

$$\tilde{\mathbf{K}} = \mathbf{Q}^{\mathrm{t}}\mathbf{K}\mathbf{Q} = \left[\begin{array}{cc|cc} \mathbf{A}-\mathbf{B} & -\sqrt{2}\mathbf{S} & \mathbf{0} & \mathbf{0} \\ -\sqrt{2}\mathbf{S}^{\mathrm{t}} & \mathbf{C}_{\mathrm{r}} & \mathbf{0} & \mathbf{0} \\ \hline \mathbf{0} & \mathbf{0} & \mathbf{A}+\mathbf{B} & \sqrt{2}\mathbf{P} \\ \mathbf{0} & \mathbf{0} & \sqrt{2}\mathbf{P}^{\mathrm{t}} & \mathbf{C}_{\mathrm{s}} \end{array}\right]. \tag{10.12}$$

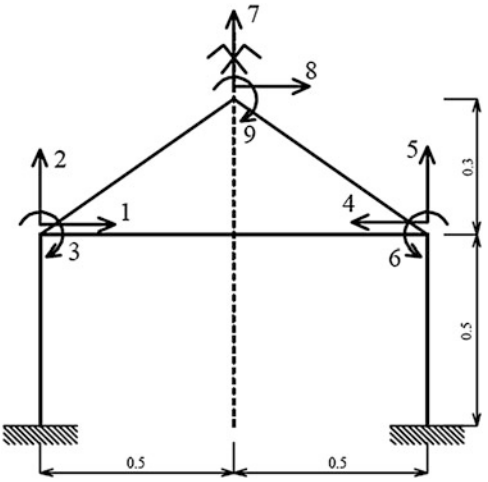

Fig. 10.4 A bilateral symmetric frame with kernel

As a numerical example, consider the frame structure shown in Fig. 10.4. The frame is composed of beam elements with elastic modulus E and moment of inertia I. Numbering the DOFs as demonstrated in this figure, the stiffness matrix takes the form Eq. 10.10, with the following submatrices:

$$\mathbf{A} = \mathrm{EI}\begin{bmatrix} 2.734 & 0.44 & 0.057 \\ 0.44 & 3.348 & 0.32 \\ 0.057 & 0.32 & 4.622 \end{bmatrix}, \quad \mathbf{C}_\mathrm{s} = \mathrm{EI}[1.95]\,\mathbf{B} = \mathrm{EI}\begin{bmatrix} 1 & 0 & 0 \\ 0 & -0.372 & -0.186 \\ 0 & -0.186 & 0.907 \end{bmatrix},$$

$$\mathbf{C}_\mathrm{r} = \mathrm{EI}\begin{bmatrix} 1.95 & 0.268 \\ 0.268 & 2.962 \end{bmatrix}, \qquad \mathbf{S} = \mathrm{EI}\begin{bmatrix} -0.975 & -0.134 \\ -0.439 & 0.134 \\ 0.134 & -1.347 \end{bmatrix} \mathbf{P} = \mathrm{EI}\begin{bmatrix} -0.439 \\ -0.975 \\ -0.134 \end{bmatrix},$$

and the decomposed matrix $\tilde{\mathbf{K}}$ in Eq. 10.12 is formed as

$$\tilde{\mathbf{K}} = \mathrm{EI}\left[\begin{array}{ccccc|cccc} 1.734 & 0.439 & 0.057 & 1.378 & 0.189 & & & & \\ & 3.720 & 0.506 & 0.621 & -0.189 & & & & \\ & & 3.715 & -0.189 & 1.905 & & \mathbf{0} & & \\ & \mathrm{sym} & & 1.950 & 0.267 & & & & \\ & & & & 2.962 & & & & \\ \hline & & & & & 3.738 & 0.439 & 0.057 & -0.621 \\ & & \mathbf{0} & & & & 2.975 & 0.134 & -0.378 \\ & & & & & & & 5.529 & -0.1892 \\ & & & & & \mathrm{sym} & & & 1.950 \end{array}\right]$$

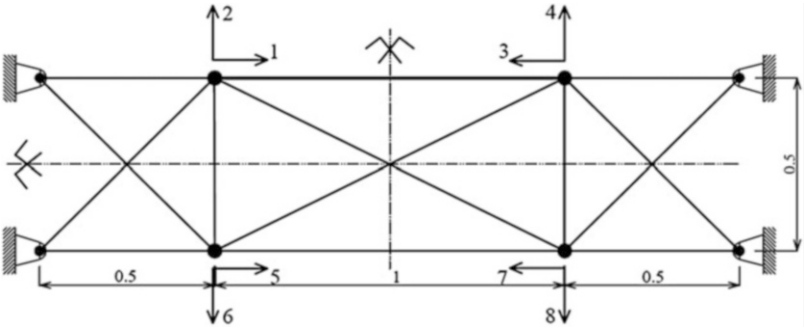

Fig. 10.5 A structure with two bilateral symmetries

10.2.3 Nested Form II

This form is a generalisation of Form II, where the blocks inside Form II have a Form II themselves. This form can be associated with structures having two perpendicular planes of symmetry. The general pattern of nested Form II can be represented as

$$\mathbf{K} = \left[\begin{array}{c|c|c|c} \mathbf{A} & \mathbf{B}_1 & \mathbf{B}_2 & \mathbf{B}_3 \\ \hline \mathbf{B}_1 & \mathbf{A} & \mathbf{B}_3 & \mathbf{B}_2 \\ \hline \mathbf{B}_2 & \mathbf{B}_3 & \mathbf{A} & \mathbf{B}_1 \\ \hline \mathbf{B}_3 & \mathbf{B}_2 & \mathbf{B}_1 & \mathbf{A} \end{array}\right], \tag{10.13}$$

where each block of the matrix is $m \times m$.

As an example, consider the pin-jointed truss shown in Fig. 10.5. The elastic modulus and cross-sectional area for each member are E and a, respectively. With a proper selection and numbering of local coordinates as depicted in this figure, the stiffness matrix takes the form Eq. 10.13 with the following submatrices:

$$\mathbf{A} = \mathrm{Ea}\begin{bmatrix} 4.422 & 0.349 \\ 0.349 & 2.886 \end{bmatrix}, \qquad \mathbf{B}_1 = \mathrm{Ea}\begin{bmatrix} 1 & 0 \\ 0 & 0 \end{bmatrix}, \qquad \mathbf{B}_2 = \mathrm{Ea}\begin{bmatrix} 0 & 0 \\ 0 & 2 \end{bmatrix},$$
$$\mathbf{B}_3 = \mathrm{Ea}\begin{bmatrix} 0.716 & -0.358 \\ -0.358 & 0.179 \end{bmatrix}.$$

Matrix $\mathbf{Q}$ is constructed as follows:

$$\mathbf{Q} = \mathbf{Q}_1\mathbf{Q}_2, \tag{10.14}$$

where

$$\mathbf{Q}_1 = \mathbf{q} \otimes \mathbf{I}_{2\mathrm{m}}, \text{ and } \mathbf{Q}_2 = \left[\begin{array}{c|c} \mathbf{q} \otimes \mathbf{I}_{\mathrm{m}} & \mathbf{0} \\ \hline \mathbf{0} & \mathbf{q} \otimes \mathbf{I}_{\mathrm{m}} \end{array}\right], \tag{10.15}$$

where $\mathbf{q}$ is the matrix defined in Eq. 10.4.

Using the basis of Eq. 10.14, one can decompose the stiffness matrix into the following form:

$$\tilde{\mathbf{K}} = \mathbf{Q}^{\mathrm{t}}\mathbf{K}\mathbf{Q} = \begin{bmatrix} \mathbf{A}-\mathbf{B}_1-\mathbf{B}_2+\mathbf{B}_3 & \mathbf{0} & \mathbf{0} & \mathbf{0} \\ \mathbf{0} & \mathbf{A}+\mathbf{B}_1-\mathbf{B}_2+\mathbf{B}_3 & \mathbf{0} & \mathbf{0} \\ \mathbf{0} & \mathbf{0} & \mathbf{A}-\mathbf{B}_1+\mathbf{B}_2+\mathbf{B}_3 & \mathbf{0} \\ \mathbf{0} & \mathbf{0} & \mathbf{0} & \mathbf{A}+\mathbf{B}_1+\mathbf{B}_2+\mathbf{B}_3 \end{bmatrix}. \tag{10.16}$$

The numerical values for the example considered are as follows:

$$\tilde{\mathbf{K}} = \begin{bmatrix} 4.138 & -0.0084 & & & & & & \\ -0.0084 & 1.065 & & & & & & \\ & & 4.707 & 0.707 & & & \mathbf{0} & \\ & & 0.707 & 0.707 & & & & \\ & & & & 2.707 & 0.707 & & \\ & & & & 0.707 & 4.707 & & \\ & & \mathbf{0} & & & & 6.138 & -0.0084 \\ & & & & & & -0.0084 & 5.065 \end{bmatrix}$$

10.2.4 Nested Form III

This form may be composed of a Form II nested by Form III blocks, or otherwise, it may consist of a Form III nested by Form II blocks, and in a general setting, it may be composed of a Form III nested by Form III blocks. This form is associated with structures having two perpendicular planes of symmetry in which one or both of the planes pass through some of the structural nodes. As an example, consider the frame structure shown in Fig. 10.6. Each element of the frame has a unit length, a moment of inertia equal to I and the elastic modulus E. Numbering the nodal DOFs as depicted in this figure, the stiffness matrix takes the following form:

$$\mathbf{K} = \left[\begin{array}{cccc|cccc} \mathbf{A} & \mathbf{B}_1 & \mathbf{P} & \mathbf{S} & \mathbf{B}_2 & & & \\ \mathbf{B}_1 & \mathbf{A} & \mathbf{P} & -\mathbf{S} & & \mathbf{B}_2 & & \\ \mathbf{P}^{\mathrm{t}} & \mathbf{P}^{\mathrm{t}} & \mathbf{C}_{\mathrm{s}} & \mathbf{0} & & & \mathbf{B}_{\mathrm{s}} & \\ \mathbf{S}^{\mathrm{t}} & -\mathbf{S}^{\mathrm{t}} & \mathbf{0} & \mathbf{C}_{\mathrm{r}} & & & & \mathbf{B}_{\mathrm{r}} \\ \hline \mathbf{B}_2 & & & & \mathbf{A} & \mathbf{B}_1 & \mathbf{P} & \mathbf{S} \\ & \mathbf{B}_2 & & & \mathbf{B}_1 & \mathbf{A} & \mathbf{P} & -\mathbf{S} \\ & & \mathbf{B}_{\mathrm{s}} & & \mathbf{P}^{\mathrm{t}} & \mathbf{P}^{\mathrm{t}} & \mathbf{C}_{\mathrm{s}} & \mathbf{0} \\ & & & \mathbf{B}_{\mathrm{r}} & \mathbf{S}^{\mathrm{t}} & -\mathbf{S}^{\mathrm{t}} & \mathbf{0} & \mathbf{C}_{\mathrm{r}} \end{array}\right]. \tag{10.17}$$

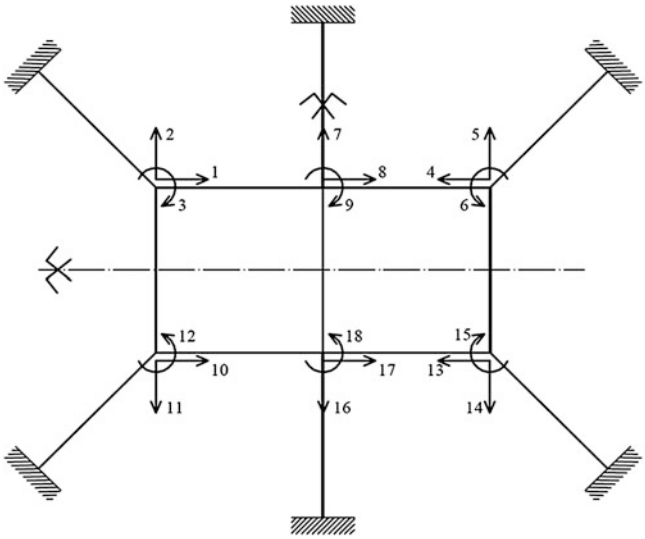

Fig. 10.6 Bilateral symmetric frame structure with kernel nodes

This is a Form II nested by Form III blocks. The numerical values of the submatrices for this example are as follows:

$$\mathbf{B}_1 = \mathbf{0}_3,\ \mathbf{B}_2 = \mathrm{EI}\begin{bmatrix} -0.372 & 0 & -0.186 \\ 0 & 1 & 0 \\ -0.186 & 0 & 0.907 \end{bmatrix},\ \mathbf{A} = \mathrm{EI}\begin{bmatrix} 2.059 & -0.313 & 0.054 \\ -0.313 & 2.059 & 0.054 \\ 0.054 & 0.054 & 3.279 \end{bmatrix},$$

$$\mathbf{P} = \mathrm{EI}\begin{bmatrix} 0 \\ -0.372 \\ -0.186 \end{bmatrix},\ \mathbf{S} = \mathrm{EI}\begin{bmatrix} -1 & 0 \\ 0 & 0.186 \\ 0 & -0.907 \end{bmatrix}\ \mathbf{C}_\mathrm{s} = \mathrm{EI}[2.745],\ \mathbf{C}_\mathrm{r} = \mathrm{EI}\begin{bmatrix} 2.745 & 0 \\ 0 & 4.373 \end{bmatrix},$$

Construction of matrix $\mathbf{Q}$ is straightforward using the successive transformations as follows:

$$\begin{aligned} &\mathbf{Q} = \mathbf{Q}_1\mathbf{Q}_2, \\ &\mathbf{Q}_1 = \mathbf{q} \otimes \mathbf{I}_{2\mathrm{m}+\mathrm{k}},\ \text{and}\ \mathbf{Q}_2 = \left[\begin{array}{c|c} \mathbf{Q}^{(\mathrm{III})} & \mathbf{0} \\ \hline \mathbf{0} & \mathbf{Q}^{(\mathrm{III})} \end{array}\right], \end{aligned} \tag{10.18}$$

where

$$\mathbf{Q}^{(\mathrm{III})} = \left[\begin{array}{cc|cc} \mathbf{q}_1 \otimes \mathbf{I}_\mathrm{m} & \mathbf{0} & \mathbf{q}_2 \otimes \mathbf{I}_\mathrm{m} & \mathbf{0} \\ \mathbf{0} & \begin{bmatrix} \mathbf{0}_\mathrm{s} \\ \mathbf{I}_\mathrm{r} \end{bmatrix} & \mathbf{0} & \begin{bmatrix} \mathbf{I}_\mathrm{s} \\ \mathbf{0}_\mathrm{r} \end{bmatrix} \end{array}\right] \tag{10.19}$$

Using the basis of Eq. 10.18, the decomposed stiffness matrix is obtained as

$$\tilde{\mathbf{K}} = \begin{bmatrix} \mathbf{A}-\mathbf{B_1}-\mathbf{B_2} & -\sqrt{2}\mathbf{S} & & & & & & & \\ -\sqrt{2}\mathbf{S^t} & \mathbf{C_r}-\mathbf{B_r} & & & & & & & \\ & & \mathbf{A}+\mathbf{B_1}-\mathbf{B_2} & \sqrt{2}\mathbf{P} & & \mathbf{0} & & & \\ & & \sqrt{2}\mathbf{P^t} & \mathbf{C_r}-\mathbf{B_r} & & & & & \\ & & & & \mathbf{A}-\mathbf{B_1}+\mathbf{B_2} & -\sqrt{2}\mathbf{S} & & & \\ & & & & -\sqrt{2}\mathbf{S^t} & \mathbf{C_r}+\mathbf{B_r} & & & \\ & & & & & & \mathbf{A}+\mathbf{B_1}+\mathbf{B_2} & \sqrt{2}\mathbf{P} & \\ & & & & & & \sqrt{2}\mathbf{P^t} & \mathbf{C_s}+\mathbf{B_s} & \end{bmatrix} \tag{10.20}$$

10.2.5 Generalised Form II

Canonical Form II can be generalised into the following pattern:

$$\mathbf{L} = \begin{bmatrix} \mathbf{A} & \mathbf{B} & & & \\ \mathbf{B} & \mathbf{A} & \mathbf{B} & & \\ & \ddots & \ddots & \ddots & \\ & & \mathbf{B} & \mathbf{A} & \mathbf{B} \\ & & & \mathbf{B} & \mathbf{A} \end{bmatrix}_{mn\times mn}, \tag{10.21}$$

where each block is of order m and there are n blocks on the diagonal of the matrix.

Let λ_j (j=1, . . ., n) and $\mathbf{V} = [\mathbf{v}_1, \mathbf{v}_2, \ldots, \mathbf{v}_n]$ be the eigenvalues and the associated normalised eigenvectors of a path graph P_n, respectively. Then,

$$\mathbf{Q} = \mathbf{V} \otimes \mathbf{I}_m, \tag{10.22}$$

is the desired block-orthonormal matrix to decompose generalised Form II. The decomposed matrix is obtained as follows:

$$\tilde{\mathbf{L}} = \mathbf{Q}^t\mathbf{L}\mathbf{Q} = \begin{pmatrix} \mathbf{A}+\lambda_1\mathbf{B} & & & & \\ & \mathbf{A}+\lambda_2\mathbf{B} & & \mathbf{0} & \\ & & \ddots & & \\ & \mathbf{0} & & \mathbf{A}+\lambda_{n-1}\mathbf{B} & \\ & & & & \mathbf{A}+\lambda_n\mathbf{B} \end{pmatrix}. \tag{10.23}$$

Generalised Form II may appear in certain structural models exhibiting translational regularity. Translational regular structure (TRS) is defined as a regular model where at least one of its generators is a path. This type of regularity is more frequently encountered in engineering structures such as frames, trusses, shells and other types of structural and mechanical models. Unfortunately, very limited number of translational regular structures can be categorised as those possessing

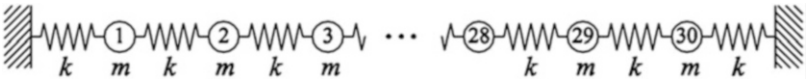

Fig. 10.7 A translational regular mass–spring system

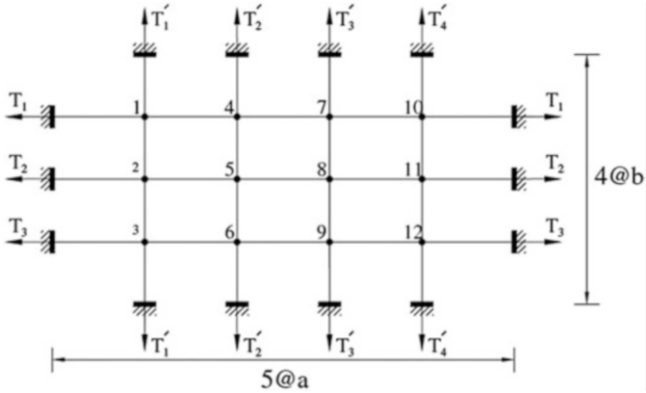

Fig. 10.8 A translational regular cable net

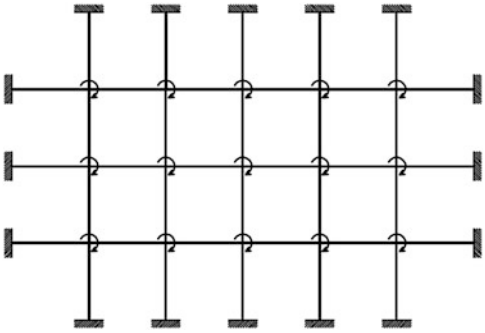

Fig. 10.9 A translational regular frame

generalised Form II matrix pattern. Examples are limited to systems with 1 degree of freedom per node such as the spring–mass systems (Fig. 10.7 also known as linear periodic systems), prestressed nets (Fig. 10.8) and frames with just rotational degrees of freedom (Fig. 10.9).

The problem is that for a general TRS such as the two-dimensional truss shown in Fig. 10.10, the block matrix **B** cannot be made symmetric, and hence, the stiffness matrix will look like

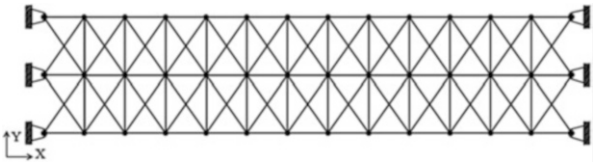

Fig. 10.10 A translational regular 2D truss

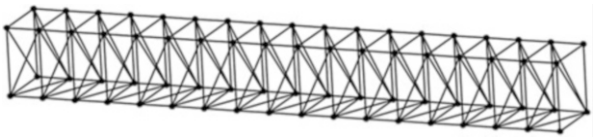

Fig. 10.11 A translational regular 3D truss

$$\mathbf{K}^{(\mathrm{TR})} = \begin{bmatrix} \mathbf{A} & \mathbf{B} & & & \\ \mathbf{B}^{\mathrm{t}} & \mathbf{A} & \mathbf{B} & & \\ & \ddots & \ddots & \ddots & \\ & & \mathbf{B}^{\mathrm{t}} & \mathbf{A} & \mathbf{B} \\ & & & \mathbf{B}^{\mathrm{t}} & \mathbf{A} \end{bmatrix}_{\mathrm{mn}\times\mathrm{mn}} . \tag{10.24}$$

A more prevalent form of a TRS is the state of relaxed boundary conditions at two extremes, as for a 3D truss shown in Fig. 10.11. In this case, the corner blocks of (10.24) are altered such that the form

$$\mathbf{K}^{(\mathrm{TR})} = \begin{bmatrix} \mathbf{C} & \mathbf{B} & & & \\ \mathbf{B}^{\mathrm{t}} & \mathbf{A} & \mathbf{B} & & \\ & \ddots & \ddots & \ddots & \\ & & \mathbf{B}^{\mathrm{t}} & \mathbf{A} & \mathbf{B} \\ & & & \mathbf{B}^{\mathrm{t}} & \mathbf{D} \end{bmatrix}_{\mathrm{mn}\times\mathrm{mn}} . \tag{10.25}$$

becomes even more sophisticated to be handled through the decomposition. The general idea is that such forms may not be explicitly decomposed into n decoupled diagonal blocks; however, efficient methods may be devised in order to relate these forms or the corresponding mechanical systems to more convenient forms or systems. The author and his coworkers have an ongoing research on this area and have employed different techniques to exploit the potential of matrix canonical forms in the analysis of nonconforming cases similar to this one [2–4]. In Sect. 10.4, a method is presented for efficient handling of regular structures exhibiting matrix patterns similar to Eq. 10.25. The method is based on a physical interpretation of the problem, in which the regular structure is represented as a rotationally regular fabrication using the substructuring technique. Such a method provides a sound basis for efficient utilisation of decomposable matrix forms in the analysis of nonconforming matrix patterns.

10.2.6 Block Circulant Form

The common block circulant form is

$$\begin{bmatrix} \mathbf{A} & \mathbf{B} & & & \mathbf{B}^t \\ \mathbf{B}^t & \mathbf{A} & \mathbf{B} & & \\ & \ddots & \ddots & \ddots & \\ & & \mathbf{B}^t & \mathbf{A} & \mathbf{B} \\ \mathbf{B} & & & \mathbf{B}^t & \mathbf{A} \end{bmatrix}_{mn \times mn}, \tag{10.26}$$

where each block is $m \times m$ and there are n blocks on the diagonal.

This form is associated with 'rotationally regular' structures or structures having C_n symmetry. This form can be decomposed using a complex transformation matrix given by

$$\mathbf{Q} = \mathbf{V} \otimes \mathbf{I}_m, \tag{10.27}$$

where $\mathbf{V}$ is the matrix of complex eigenvectors of an n-circuit, whose columns are obtained from

$$\mathbf{v}_k = \begin{pmatrix} \xi^1 \\ \xi^2 \\ \vdots \\ \xi^n \end{pmatrix}, \tag{10.28}$$

where $\xi = e^{(2\pi k/n)}$ is the nth root of unity.

When submatrix $\mathbf{B}$ is symmetric, a 'reciprocal block circulant' (RBC) form is obtained:

$$\begin{bmatrix} \mathbf{A} & \mathbf{B} & & & \mathbf{B} \\ \mathbf{B} & \mathbf{A} & \mathbf{B} & & \\ & \ddots & \ddots & \ddots & \\ & & \mathbf{B} & \mathbf{A} & \mathbf{B} \\ \mathbf{B} & & & \mathbf{B} & \mathbf{A} \end{bmatrix}_{mn \times mn}. \tag{10.29}$$

This form is more attractive due to the fact that it can be decomposed using a real transformation. One can incorporate the real eigenvectors of a C_n into $\mathbf{V}$ in Eq. 10.27 to construct the transformation matrix $\mathbf{Q}$ for the corresponding RBC form. This form is associated with rotationally regular graph models that possess additional reflection symmetry between two successive subgraphs or equivalently the graph models with C_{nv} symmetry group.

For structural models that possess this type of symmetry, the situation is different, since the submatrix $\mathbf{B}$ cannot be made symmetric. However, as will be

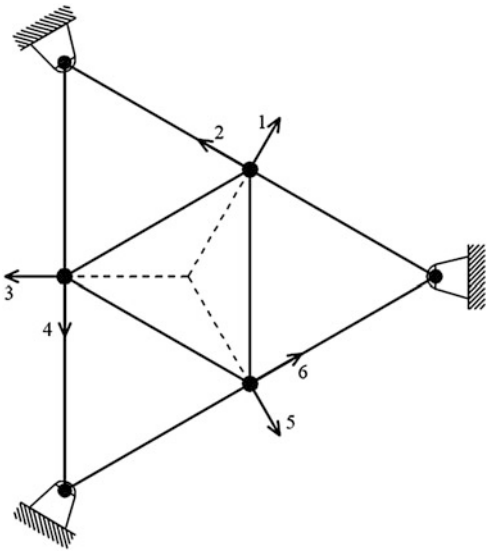

Fig. 10.12 Pin-jointed truss with C_{3v} symmetry

illustrated by numerous examples, with proper alignment and partitioning of local nodal coordinates, the same real invariant subspaces can be employed in the construction of the transformation matrix **Q**.

To illustrate the method for constructing invariant subspaces, let us consider the simple example of a pin-jointed truss depicted in Fig. 10.12. Each bar element has a unit length. The elastic modulus and cross-sectional area for each member are E and a, respectively.

A symmetry-adapted local coordinate system is selected such that the stiffness matrix takes the form

$$\mathbf{K} = \mathrm{Ea} \begin{bmatrix} \mathbf{A} & \mathbf{B} & \mathbf{B}^{\mathrm{t}} \\ \mathbf{B}^{\mathrm{t}} & \mathbf{A} & \mathbf{B} \\ \mathbf{B} & \mathbf{B}^{\mathrm{t}} & \mathbf{A} \end{bmatrix}. \tag{10.30}$$

Partitioning the coordinate variables of each node into radial and tangent directions, or more specifically into nodal coordinates which are symmetric between the two consecutive nodes and those which are antisymmetric or reversing, the blocks of the matrix can further be partitioned as follows:

$$\mathbf{A} = \begin{bmatrix} \mathbf{A}_{\mathrm{s}} & \\ & \mathbf{A}_{\mathrm{r}} \end{bmatrix}, \ \mathbf{B} = \begin{bmatrix} \mathbf{B}_1 & \mathbf{B}_3 \\ -\mathbf{B}_3^{\mathrm{t}} & \mathbf{B}_2 \end{bmatrix}, \ \text{and } \mathbf{B}^{\mathrm{t}} = \begin{bmatrix} \mathbf{B}_1 & -\mathbf{B}_3 \\ \mathbf{B}_3^{\mathrm{t}} & \mathbf{B}_2 \end{bmatrix}. \tag{10.31}$$

The numerical values of the above submatrices for the example considered are presented below:

$$\mathbf{A} = \begin{bmatrix} 1.5 & 0 \\ 0 & 2.5 \end{bmatrix}, \ \mathbf{B} = \begin{bmatrix} 0.75 & 0.433 \\ -0.433 & -0.25 \end{bmatrix}.$$

The eigenvalues of the C_3 are $\{-1, -1, 2\}$. Let $[\mathbf{v}_1, \mathbf{v}_2, \mathbf{v}_3]$ denote three eigenvectors associated with these eigenvalues, respectively. We construct invariant subspaces associated with repeated eigenvalue -1 as follows:

$$\mathbf{Q}_1 = \left[\mathbf{v}_1 \otimes \begin{bmatrix} 1 \\ 0 \end{bmatrix} \middle| \ \mathbf{v}_2 \otimes \begin{bmatrix} 0 \\ 1 \end{bmatrix} \right],$$

and

$$\mathbf{Q}_2 = \left[\mathbf{v}_2 \otimes \begin{bmatrix} 1 \\ 0 \end{bmatrix} \middle| \ \mathbf{v}_1 \otimes \begin{bmatrix} 0 \\ 1 \end{bmatrix} \right].$$

For the simple eigenvalue 2, the invariant subspace is constructed as

$$\mathbf{Q}_3 = [\mathbf{v}_3 \otimes \mathbf{I}_2],$$

and the matrix consisting of the complete set of invariant subspaces is

$$\mathbf{Q} = [\mathbf{Q}_1 | \mathbf{Q}_2 | \mathbf{Q}_3].$$

The above formulation is generalised to an RBC form of order mn, where each block is partitioned according to Eq. 10.31; hence, $\mathrm{m} = \mathrm{m_s} + \mathrm{m_r}$. Let λ_k be a repeated eigenvalue of C_n. Let $\mathbf{v}_\mathrm{k}$ and $\mathbf{v}_{\mathrm{k}+1}$ denote the eigenvectors associated with this eigenvalue. The invariant subspaces associated with repeated eigenvalue λ_k are constructed as follows:

$$\mathbf{Q}_\mathrm{k} = \left[\mathbf{v}_\mathrm{k} \otimes \begin{bmatrix} \mathbf{I}_\mathrm{m} \\ 0 \end{bmatrix} \middle| \mathbf{v}_{k+1} \otimes \begin{bmatrix} 0 \\ \mathbf{I}_{\mathrm{m_r}} \end{bmatrix} \right], \tag{10.32}$$

and

$$\mathbf{Q}_{k+1} = \left[\mathbf{v}_{k+1} \otimes \begin{bmatrix} \mathbf{I}_{m_s} \\ 0 \end{bmatrix} \middle| \mathbf{v}_k \otimes \begin{bmatrix} 0 \\ \mathbf{I}_{m_r} \end{bmatrix} \right]. \tag{10.33}$$

For the simple eigenvalue λ_k and the associated eigenvector $\mathbf{v}_\mathrm{k}$, the invariant subspace is constructed as

$$\mathbf{Q}_\mathrm{k} = [\mathbf{V}_\mathrm{k} \otimes \mathbf{I}_\mathrm{m}], \tag{10.34}$$

and the matrix of all invariant subspaces is constructed as

$$\mathbf{Q} = [\mathbf{Q}_1|\cdots|\mathbf{Q}_n]. \tag{10.35}$$

Now, using the transformation matrix of Eq. 10.35 one can obtain the decomposed form of the matrix as

$$\tilde{\mathbf{K}} = \mathbf{Q}^t\mathbf{K}\mathbf{Q} = \mathrm{Ea}\begin{bmatrix} \tilde{\mathbf{K}}_1 & & \\ & \ddots & \\ & & \tilde{\mathbf{K}}_n \end{bmatrix}. \tag{10.36}$$

Each diagonal block in $\tilde{\mathbf{K}}$ can be obtained directly from the following formulations, without the need to perform the complete transformation (10.36).

$$\tilde{\mathbf{K}}_k = \begin{bmatrix} \mathbf{A}_s + \lambda_k\mathbf{B}_1 & \pm\gamma_k\mathbf{B}_3 \\ \pm\gamma_k\mathbf{B}_3^t & \mathbf{A}r + \lambda_k\mathbf{B}_2 \end{bmatrix}; k = 1, \ldots, n. \tag{10.37}$$

In this relation, $\gamma_k = \sqrt{4 - \lambda_k^2}$.

Referring back to the example considered in Fig. 10.12, Eq. 10.37 yields the following decomposition:

$$\tilde{\mathbf{K}}_1 = \begin{bmatrix} \mathbf{A}_s - \mathbf{B}_1 & \sqrt{3}\mathbf{B}_3 \\ \sqrt{3}\mathbf{B}_3^t & \mathbf{A}_r - \mathbf{B}_2 \end{bmatrix}; \tilde{\mathbf{K}}_2 = \begin{bmatrix} \mathbf{A}_s - \mathbf{B}_1 & -\sqrt{3}\mathbf{B}_3 \\ -\sqrt{3}\mathbf{B}_3^t & \mathbf{A}_r - \mathbf{B}_2 \end{bmatrix} \text{ and}$$

$$\tilde{\mathbf{K}}_3 = \begin{bmatrix} \mathbf{A}_s + 2\mathbf{B}_1 & \mathbf{0} \\ \mathbf{0} & \mathbf{A}_r + 2\mathbf{B}_2 \end{bmatrix}$$

For another example, consider the frame structure with C_{6v} symmetry as shown in Fig. 10.13. Each element of the frame has a unit length, a moment of inertia equal to I and the elastic modulus *E*. The numerical value of the cross-sectional area is taken as $a = 20 \times \mathrm{I}$. Using the local symmetry-adapted coordinates as depicted in this figure, the stiffness matrix takes the following form:

$$\mathbf{K} = \mathrm{EI}\begin{bmatrix} \mathbf{A} & \mathbf{B} & & & & \mathbf{B}^t \\ \mathbf{B}^t & \mathbf{A} & \mathbf{B} & & & \\ & \mathbf{B}^t & \mathbf{A} & \mathbf{B} & & \\ & & \mathbf{B}^t & \mathbf{A} & \mathbf{B} & \\ & & & \mathbf{B}^t & \mathbf{A} & \mathbf{B} \\ \mathbf{B} & & & & \mathbf{B}^t & \mathbf{A} \end{bmatrix}$$

Each block of the stiffness matrix above is partitioned with regard to 'stationary' and 'reversing' coordinates as follows:

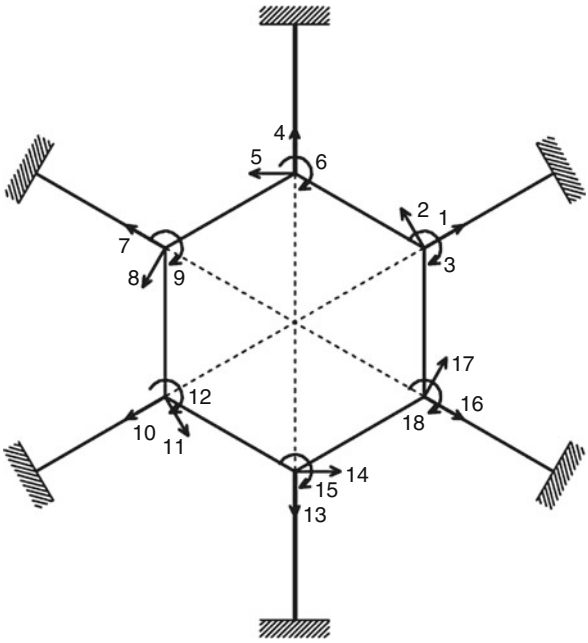

Fig. 10.13 A frame with C_{6v} symmetry

$$\mathbf{A} = \begin{bmatrix} \mathbf{A}_s & \\ & \mathbf{A}_r \end{bmatrix} = \left[\begin{array}{c|cc} 30.559 & 0 & 0 \\ \hline 0 & 30.559 & 0 \\ 0 & 0 & 3.280 \end{array}\right],$$

and

$$\mathbf{B} = \begin{bmatrix} \mathbf{B}_1 & \mathbf{B}_3 \\ -\mathbf{B}_3^t & \mathbf{B}_2 \end{bmatrix} = \left[\begin{array}{c|cc} 4.720 & 8.821 & -0.161 \\ \hline -8.821 & -14.907 & -0.093 \\ 0.161 & -0.093 & -0.907 \end{array}\right].$$

The eigenvalues of the C_6 are $\{-2, -1, -1, 1, 1, 2\}$. The invariant subspaces associated with repeated eigenvalues are constructed as follows:

$$\mathbf{Q}_k = \left[\begin{array}{ccc|ccc} & \mathbf{v}_k & \otimes \begin{bmatrix} 1 \\ 0 \\ 0 \end{bmatrix} & & \mathbf{v}_{k+1} & \otimes \begin{bmatrix} 0 & 0 \\ 1 & 0 \\ 0 & 1 \end{bmatrix} \end{array}\right],$$

$$\mathbf{Q}_{k+1} = \left[\begin{array}{ccc|ccc} & \mathbf{v}_{k+1} & \otimes \begin{bmatrix} 1 \\ 0 \\ 0 \end{bmatrix} & & \mathbf{v}_k & \otimes \begin{bmatrix} 0 & 0 \\ 1 & 0 \\ 0 & 1 \end{bmatrix} \end{array}\right]$$

where $\mathbf{v}_k$ and $\mathbf{v}_{k+1}$ are the eigenvectors of C_6 associated with a repeated eigenvalue.

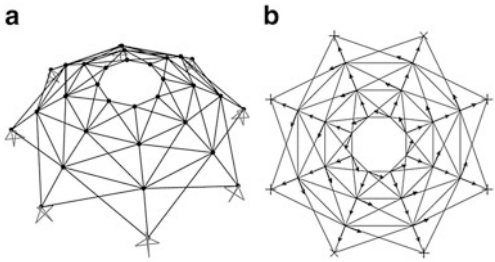

Fig. 10.14 A single-layer space truss of P_3 by C_8 strong Cartesian product

For the simple eigenvalues, the invariant subspace is constructed as

$$\mathbf{Q}_k = [\mathbf{v}_k \otimes \mathbf{I}_3]$$

where $\mathbf{v}_k$ is the eigenvector of C_6 associated with a simple eigenvalue.

And the complete set of invariant subspaces is

$$\mathbf{Q} = [\mathbf{Q}_1|\cdots|\mathbf{Q}_6].$$

The diagonal blocks of $\tilde{\mathbf{K}}$ are obtained using Eq. 10.37 for k = 1,..., 6. The results are as follows:

$$\tilde{\mathbf{K}}_1 = \begin{bmatrix} \mathbf{A}_s - 2\mathbf{B}_1 & \mathbf{0} \\ \mathbf{0} & \mathbf{A}_r - 2\mathbf{B}_2 \end{bmatrix}, \tilde{\mathbf{K}}_2 = \begin{bmatrix} \mathbf{A}_s - \mathbf{B}_1 & \sqrt{3}\mathbf{B}_3 \\ \sqrt{3}\mathbf{B}_3^t & \mathbf{A}_r - \mathbf{B}_2 \end{bmatrix}$$

$$\tilde{\mathbf{K}}_3 = \begin{bmatrix} \mathbf{A}_s - \mathbf{B}_1 & -\sqrt{3}\mathbf{B}_3 \\ -\sqrt{3}\mathbf{B}_3^t & \mathbf{A}_r - \mathbf{B}_2 \end{bmatrix}, \tilde{\mathbf{K}}_4 = \begin{bmatrix} \mathbf{A}_s + \mathbf{B}_1 & \sqrt{3}\mathbf{B}_3 \\ \sqrt{3}\mathbf{B}_3^t & \mathbf{A}_r + \mathbf{B}_2 \end{bmatrix}, \tilde{\mathbf{K}}_5 = \begin{bmatrix} \mathbf{A}_s + \mathbf{B}_1 & -\sqrt{3}\mathbf{B}_3 \\ \mathbf{0} & \mathbf{A}_r + \mathbf{B}_2 \end{bmatrix}$$

$$\tilde{\mathbf{K}}_6 = \begin{bmatrix} \mathbf{A}_s + 2\mathbf{B}_1 & 0 \\ 0 & \mathbf{A}_r + 2\mathbf{B}_2 \end{bmatrix}$$

As the final example for RBC form, consider the pin-jointed one-layer dome with C_{8v} symmetry as shown in Fig. 10.14a. Each node of the structure has three translational degrees of freedom. The local symmetry-adapted coordinates are shown in Fig. 10.14b. Radial and vertical degrees of freedom are the 'stationary' DOFs, while the tangent DOFs are regarded as 'reversing'. The stiffness matrix takes the following form:

$$\mathbf{K} = \begin{bmatrix} \mathbf{A} & \mathbf{B} & & \mathbf{B}^t \\ \mathbf{B}^t & \mathbf{A} & \ddots & \\ & \ddots & \ddots & \mathbf{B} \\ \mathbf{B} & & \mathbf{B}^t & \mathbf{A} \end{bmatrix}_{72\times 72},$$

where each block is 9×9 and there are eight blocks on the diagonal. Each block of the stiffness matrix is given in the partitioned form as

$$\mathbf{A} = \begin{bmatrix} \mathbf{A}_s & \\ & \mathbf{A}_r \end{bmatrix}, \quad \mathbf{B} = \begin{bmatrix} \mathbf{B}_1 & \mathbf{B}_3 \\ -\mathbf{B}_3^t & \mathbf{B}_2 \end{bmatrix}, \quad \text{and } \mathbf{B}^t = \begin{bmatrix} \mathbf{B}_1 & \mathbf{B}_3 \\ \mathbf{B}_3^t & \mathbf{B}_2 \end{bmatrix},$$

where $\mathbf{A}_s$ is 6×6 associated with radial and vertical degrees of freedom (DOFs) and $\mathbf{A}_r$ is 3×3 associated with tangential DOFs.

The eigenvalues of the C_8 are $\{-2, -\sqrt{2}, -\sqrt{2},\ 0.0,\ 0.0, -\sqrt{2}, -\sqrt{2},\ 2\}$. The invariant subspaces are computed using the Eqs. 10.32, 10.33, 10.34, and 10.35, and the diagonal blocks of $\tilde{\mathbf{K}}$ are obtained from the closed-form solution (10.37), for k = 1,. . ., 8. The results are

$$\tilde{\mathbf{K}}_1 = \begin{bmatrix} \mathbf{A}_s - 2\mathbf{B}_1 & 0 \\ 0 & \mathbf{A}_r - 2\mathbf{B}_2 \end{bmatrix}, \quad \tilde{\mathbf{K}}_2 = \begin{bmatrix} \mathbf{A}_s - \sqrt{2}\mathbf{B}_1 & -\sqrt{2}\mathbf{B}_3 \\ -\sqrt{2}\mathbf{B}_3^t & \mathbf{A}_r - \sqrt{2}\mathbf{B}_2 \end{bmatrix}$$

$$\tilde{\mathbf{K}}_3 = \begin{bmatrix} \mathbf{A}_s - \mathbf{B}_1 & \sqrt{2}\mathbf{B}_3 \\ -2\mathbf{B}_3^t & \mathbf{A}_r - \sqrt{2}\mathbf{B}_2 \end{bmatrix}, \quad \tilde{\mathbf{K}}_4 = \begin{bmatrix} \mathbf{A}_s & 2\mathbf{B}_3 \\ 2\mathbf{B}_3^t & \mathbf{A}_r \end{bmatrix},$$

$$\tilde{\mathbf{K}}_5 = \begin{bmatrix} \mathbf{A}_s & -2\mathbf{B}_3 \\ -2\mathbf{B}_3^t & \mathbf{A}_r \end{bmatrix}, \quad \tilde{\mathbf{K}}_6 = \begin{bmatrix} \mathbf{A}_s + \sqrt{2}\mathbf{B}_1 & -\sqrt{2}\mathbf{B}_3 \\ -\sqrt{2}\mathbf{B}_3^t & \mathbf{A}_r + \sqrt{2}\mathbf{B}_2 \end{bmatrix}$$

$$\tilde{\mathbf{K}}_7 = \begin{bmatrix} \mathbf{A}_s + \sqrt{2}\mathbf{B}_1 & \sqrt{2}\mathbf{B}_3 \\ \sqrt{2}\mathbf{B}_3^t & \mathbf{A}_r + \sqrt{2}\mathbf{B}_2 \end{bmatrix}, \quad \tilde{\mathbf{K}}_8 = \begin{bmatrix} \mathbf{A}_s + 2\mathbf{B}_1 & \mathbf{0} \\ \mathbf{0} & \mathbf{A}_r + 2\mathbf{B}_2 \end{bmatrix}$$

These results can be verified with those of a direct transformation of $\mathbf{K}$ as follows:

$$\tilde{\mathbf{K}} = \mathbf{Q}^t\mathbf{K}\mathbf{Q} = \begin{bmatrix} \tilde{\mathbf{K}}_1 & & \\ & \ddots & \\ & & \tilde{\mathbf{K}}_8 \end{bmatrix}.$$

10.2.7 Augmented Block Circulant (ABC) Form

This form is obtained from a block circulant form augmented by a kernel block. The kernel block is linked to all other blocks through the same bridging block. The form looks like

$$\mathbf{L}_{mn+k} = \begin{pmatrix} \mathbf{A} & \mathbf{B} & \ddots & & \mathbf{B} & \mathbf{P} \\ \mathbf{B} & \mathbf{A} & \mathbf{B} & \mathbf{0} & & \mathbf{P} \\ \ddots & \mathbf{B} & \ddots & \ddots & \ddots & \vdots \\ & \mathbf{0} & \ddots & \mathbf{A} & \mathbf{B} & \mathbf{P} \\ \mathbf{B} & & \ddots & \mathbf{B} & \mathbf{A} & \mathbf{P} \\ \mathbf{P}^t & \mathbf{P}^t & \cdots & \mathbf{P}^t & \mathbf{P}^t & \mathbf{C} \end{pmatrix}, \tag{10.38}$$

where $\mathbf{C}$ is the kernel block of order k, $\mathbf{P}$ the bridging block, and $\mathbf{0}$ is zero matrix of order m.

This form is associated with rotationally regular product graphs with a kernel component, or from the viewpoint of symmetry, those graph models with C_{nv} symmetry where the axis of rotation passes through some nodes of the graph. The form is easily decomposed using the following procedure:

Let $\lambda_j (j = 1, \ldots, n)$ be the eigenvalues of the C_n sorted in an ascending order. Let $\mathbf{V} = [\mathbf{v}_1, \mathbf{v}_2, \ldots, \mathbf{v}_n]$ be the orthogonal matrix of the normalised eigenvectors associated with the eigenvalues λ_j. Clearly $\lambda_n = 2$, and

$$\mathbf{v}_n = \frac{1}{\sqrt{n}}[1, 1, \ldots, 1]_n^t. \tag{10.39}$$

Now, define the block-orthonormal matrix $\mathbf{Q}$ as

$$\mathbf{Q} = \left[\begin{array}{c|c} \mathbf{V} \otimes \mathbf{I}_m & \mathbf{0} \\ \hline \mathbf{0} & \mathbf{I}_k \end{array}\right]. \tag{10.40}$$

Choosing matrix $\mathbf{Q}$ in this way, it is easily verified that matrix $\mathbf{L}$ of Eq. 10.38 can be transformed into

$$\tilde{\mathbf{L}} = \mathbf{Q}^t \mathbf{L} \mathbf{Q} = \begin{bmatrix} \tilde{\mathbf{L}}_1 & & & \\ & \tilde{\mathbf{L}}_2 & & \\ & & \ddots & \\ & & & \tilde{\mathbf{L}}_n \end{bmatrix}, \tag{10.41}$$

where

$$\tilde{\mathbf{L}}_j = \mathbf{A} + \lambda_j \mathbf{B}; \quad (j = 1, \ldots, n-1), \tag{10.42}$$

and

$$\tilde{\mathbf{L}}_n = \begin{pmatrix} \mathbf{A} + 2\mathbf{B} & \sqrt{n}\mathbf{P} \\ \sqrt{n}\mathbf{P}^t & \mathbf{C} \end{pmatrix}. \tag{10.43}$$

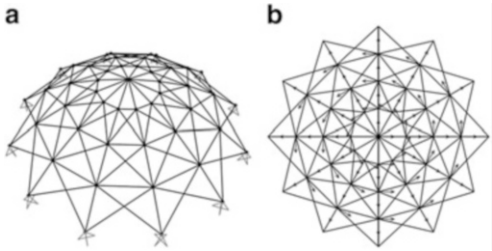

Fig. 10.15 A single-layer space truss of P_3 by C_{12} strong Cartesian product having a kernel node

Rotationally regular structures with a kernel component fall in the category of ABC forms; however, the form may be slightly different from Eq. 10.38. A kernel is one or more structural nodes which are located on the axis of rotation symmetry. As an example, consider a single-layer pin-jointed dome depicted in Fig. 10.15a. Its model consists of a strong Cartesian product of P_3 by C_{12}. The kernel is composed of a single node at the apex. The local symmetry-adapted coordinates are shown in Fig. 10.15b. Local coordinates for the kernel are aligned arbitrarily.

Let us partition the set of kernel DOFs into 'stationary' and 'rotating' DOFs according to the behaviour of a DOF with respect to the rotation around the axis of rotation symmetry. For example, the vertical component of displacement is the 'stationary' DOF, and the two horizontal components comprise the 'rotating' set. With such a partitioning, the ABC form of stiffness matrix for rotationally regular structures with a kernel looks like

$$\mathbf{K}^{(\mathrm{ABC})} = \begin{pmatrix} \mathbf{A} & \mathbf{B} & & & \mathbf{B}^{\mathrm{t}} & \mathbf{P} & \mathbf{S} \\ \mathbf{B}^{\mathrm{t}} & \mathbf{A} & \mathbf{B} & \mathbf{Z} & & \mathbf{P} & \mathbf{S}\mathbf{T}_{\theta} \\ & \mathbf{B}^{\mathrm{t}} & \ddots & \ddots & & \mathbf{P} & \mathbf{S}\mathbf{T}_{\theta} \\ & \mathbf{Z} & \ddots & \mathbf{A} & \mathbf{B} & \vdots & \vdots \\ & & & \mathbf{B}^{\mathrm{t}} & \mathbf{A} & \mathbf{P} & \mathbf{S}\mathbf{T}_{(\mathrm{n}-1)\theta} \\ \mathbf{P}^{\mathrm{t}} & \mathbf{P}^{\mathrm{t}} & \mathbf{P}^{\mathrm{t}} & \cdots & \mathbf{P}^{\mathrm{t}} & \mathbf{C}_{\mathrm{s}} & \mathbf{0} \\ \mathbf{S}^{\mathrm{t}} & \mathbf{T}_{\theta}^{\mathrm{t}}\mathbf{S}^{\mathrm{t}} & \mathbf{T}_{\theta}^{\mathrm{t}}\mathbf{S}^{\mathrm{t}} & \cdots & \mathbf{T}_{(\mathrm{n}-1)\theta}^{\mathrm{t}}\mathbf{S}^{\mathrm{t}} & \mathbf{0} & \mathbf{C}_{\mathrm{r}} \end{pmatrix}. \tag{10.44}$$

where **A** and **B** can be partitioned according to Eq. 10.31. The bridging matrices **P** and **S** can be partitioned accordingly into

$$\mathbf{P} = \begin{bmatrix} \mathbf{P}_{\mathrm{s}} \\ \hline \mathbf{P}_{\mathrm{r}} \end{bmatrix} \text{ and } \mathbf{S} = \begin{bmatrix} \mathbf{S}_{\mathrm{s}} \\ \hline \mathbf{S}_{\mathrm{r}} \end{bmatrix}. \tag{10.45}$$

The kernel matrix **C** is partitioned into diagonal blocks $\mathbf{C}_{\mathrm{s}}$ and $\mathbf{C}_{\mathrm{r}}$ of order c_s and c_r, respectively ($k = c_s + c_r$). $\mathbf{T}_{\mathrm{j}\theta}$ is the rotation matrix of radius $\mathrm{j}\theta$ ($\mathrm{j} = 1 : \mathrm{n} - 1$), where $\theta = \frac{2\pi}{\mathrm{n}}$.

Now, we construct the invariant subspaces as follows: As before, let $\lambda_{\mathrm{j}} (\mathrm{j} = 1, \ldots, \mathrm{n})$ be the eigenvalues of the C_{n} sorted in an ascending order, and let $\mathbf{V} = [\mathbf{v}_1, \mathbf{v}_2, \ldots, \mathbf{v}_{\mathrm{n}}]$ be the matrix of the corresponding normalised eigenvectors.

The invariant subspaces $[\mathbf{Q}_1,\ \mathbf{Q}_2, \ldots,\ \mathbf{Q}_n]$ are computed using the relations (10.32, 10.33, 10.34, and 10.35) for single and repeating eigenvalues. Then, the set is augmented as follows to get the required $\mathbf{Q}$ matrix:

$$\mathbf{Q} = \left[\begin{array}{c|c|c|c|c|c|c} \multicolumn{4}{c|}{\left[\mathbf{Q}_1 \mid \mathbf{Q}_2 \mid \cdots \mid \mathbf{Q}_{n-1}\right]} & \mathbf{0} & \mathbf{Q}_n & \mathbf{0} \\ \multicolumn{4}{c|}{\mathbf{0}} & \left[\begin{array}{c}\mathbf{0}\\ \mathbf{I}_{cr}\end{array}\right] & \mathbf{0} & \left[\begin{array}{c}\mathbf{I}_{cs}\\ \mathbf{0}\end{array}\right] \end{array}\right]. \tag{10.46}$$

The decomposed form of the stiffness matrix is then obtained as

$$\tilde{\mathbf{K}} = \mathbf{Q}^t \mathbf{K}^{(ABC)} \mathbf{Q} = \begin{bmatrix} \tilde{\mathbf{K}}_1 & & \\ & \ddots & \\ & & \tilde{\mathbf{K}}_{n-1} \end{bmatrix}, \tag{10.47}$$

where the diagonal blocks $\tilde{\mathbf{K}}_j$ are obtained directly from the relations

$$\tilde{\mathbf{K}}_j = \begin{bmatrix} \mathbf{A}_s + \lambda_j \mathbf{B}_1 & \pm\gamma_j \mathbf{B}_3 \\ \pm\gamma_j \mathbf{B}_3^T & \mathbf{A}_r + \lambda_j \mathbf{B}_2 \end{bmatrix} \ (j = 1, \ldots,\ n-3), \tag{10.48}$$

and

$$\tilde{\mathbf{K}}_{n-2} = \begin{bmatrix} \mathbf{A}_s + \lambda_{n-2}\mathbf{B}_1 & \gamma_{n-2}\mathbf{B}_3 & & & \eta\mathbf{S}_s \\ \gamma_{n-2}\mathbf{B}_3^t & \mathbf{A}_r + \lambda_{n-2}\mathbf{B}_2 & & & \eta\mathbf{S}_r\mathbf{E} \\ & & \mathbf{A}_s + \lambda_{n-2}\mathbf{B}_1 & -\gamma_{n-2}\mathbf{B}_3 & \eta\mathbf{S}_s\mathbf{E} \\ & & -\gamma_{n-2}\mathbf{B}_3^t & \mathbf{A}_r + \lambda_{n-2}\mathbf{B}_2 & \eta\mathbf{S}_r \\ \eta\mathbf{S}_s^t & \eta\mathbf{E}_s^t\mathbf{S}_r^t & \eta\mathbf{E}^t\mathbf{S}_r^t & \eta\mathbf{S}_r^t & \mathbf{C}_r \end{bmatrix}, \tag{10.49}$$

where $\lambda_{n-2} = \lambda_{n-1} = 2\cos\left(\frac{2\pi}{n}\right)$ is the second largest eigenvalue of C_n, $\gamma_j = \sqrt{4 - \lambda_j^2}$, $\eta = \sqrt{\frac{n}{2}}$, and $\mathbf{E}$ is a block-diagonal matrix of order c_r with 2×2 diagonal blocks:

$$\bar{\mathbf{E}} = \begin{bmatrix} 0 & 1 \\ -1 & 0 \end{bmatrix}. \tag{10.50}$$

The last diagonal block of $\tilde{\mathbf{K}}$ is obtained from

$$\tilde{\mathbf{K}}_{n-1} = \begin{bmatrix} \mathbf{A}_s + 2\mathbf{B}_1 & \mathbf{0} & \sqrt{n}\mathbf{P}_s \\ \mathbf{0} & \mathbf{A}_r + 2\mathbf{B}_2 & \sqrt{n}\mathbf{P}_r \\ \sqrt{n}\mathbf{P}_s^t & \sqrt{n}\mathbf{P}_r^t & \mathbf{C}_s \end{bmatrix}. \tag{10.51}$$

For example, let us formulate the decomposed stiffness matrix for the single-layer dome of Fig. 10.15a. The eigenvalues of the C_{12} are

$\{-2, -\sqrt{3}, -\sqrt{3}, -1, -1, 0, 0, 1, 1, \sqrt{3}, \sqrt{3}, 2\}$, and using (10.48, 10.49, and 10.51), we obtain

$$\tilde{\mathbf{K}}_1 = \begin{bmatrix} \mathbf{A}_s - 2\mathbf{B}_1 & \\ & \mathbf{A}_r - 2\mathbf{B}_2 \end{bmatrix},$$

$$\tilde{\mathbf{K}}_2,\ \tilde{\mathbf{K}}_3 = \begin{bmatrix} \mathbf{A}_s - \sqrt{3}\mathbf{B}_1 & \pm\mathbf{B}_3 \\ \pm\mathbf{B}_3^t & \mathbf{A}_r - \sqrt{3}\mathbf{B}_2 \end{bmatrix},$$

$$\tilde{\mathbf{K}}_4,\ \tilde{\mathbf{K}}_5 = \begin{bmatrix} \mathbf{A}_s - \mathbf{B}_1 & \pm\sqrt{3}\mathbf{B}_3 \\ \pm\sqrt{3}\mathbf{B}_3^t & \mathbf{A}_r - \mathbf{B}_2 \end{bmatrix},$$

$$\tilde{\mathbf{K}}_6,\ \tilde{\mathbf{K}}_7 = \begin{bmatrix} \mathbf{A}_s & \pm 2\mathbf{B}_3 \\ \pm 2\mathbf{B}_3^t & \mathbf{A}_r \end{bmatrix},$$

$$\tilde{\mathbf{K}}_8,\ \tilde{\mathbf{K}}_9 = \begin{bmatrix} \mathbf{A}_s + \mathbf{B}_1 & \pm\sqrt{3}\mathbf{B}_3 \\ \pm\sqrt{3}\mathbf{B}_3^t & \mathbf{A}_r + \mathbf{B}_2 \end{bmatrix},$$

$$\tilde{\mathbf{K}}_{10} = \begin{bmatrix} \mathbf{A}_s + \sqrt{3}\mathbf{B}_1 & \mathbf{B}_3 & & & \sqrt{6}\mathbf{S}_s \\ \mathbf{B}_3^t & \mathbf{A}_r + \sqrt{3}\mathbf{B}_2 & & & \sqrt{6}\mathbf{S}_r\mathbf{E} \\ & & \mathbf{A}_s + \sqrt{3}\mathbf{B}_1 & -\mathbf{B}_3 & \sqrt{6}\mathbf{S}_s\mathbf{E} \\ & & -\mathbf{B}_3^t & \mathbf{A}_r + \sqrt{3}\mathbf{B}_2 & \sqrt{6}\mathbf{S}_r \\ \sqrt{6}\mathbf{S}_s^t & \sqrt{6}\mathbf{E}^t\mathbf{S}_s^t & \sqrt{6}\mathbf{E}^t\mathbf{S}_s^t & \sqrt{6}\mathbf{S}_s^t & \mathbf{C}_r \end{bmatrix}$$

$$\tilde{\mathbf{K}}_{11} = \begin{bmatrix} \mathbf{A}_s + 2\mathbf{B}_1 & & \sqrt{12}\mathbf{P}_s \\ & \mathbf{A}_r + 2\mathbf{B}_2 & \sqrt{12}\mathbf{P}_r \\ \sqrt{12}\mathbf{P}_s^t & \sqrt{12}\mathbf{P}_r^t & \mathbf{C}_s \end{bmatrix}$$

10.3 Eigensolution of Locally Modified Regular Structures Using Iterative Methods

In this section, we present two numerical methods for the efficient eigensolution of the modified regular structural models. We refer to the unmodified purely regular structure as the *base model*. The fundamental assumption of this section is that the matrices associated with the base models possess canonical forms which could be decomposed using one of the formulations given in Sect. 10.2. This is a great computational advantage that could be exploited efficiently in developing numerical algorithms for the eigensolution of the modified regular models.

The generalised eigenvalue problem for free vibration of a modified regular structure without damping may be expressed as follows:

$$(\mathbf{K} + \mathbf{E}\Delta\ \mathbf{k}\ \mathbf{E}^t)\mathbf{u} = \lambda(\mathbf{M} + \mathbf{E}\Delta\ \mathbf{m}\ \mathbf{E}^t)\mathbf{u}, \tag{10.52}$$

where $\mathbf{K}$ and $\mathbf{M}$ of order N are the stiffness and mass matrices of the base model, $\mathbf{\Delta k}$ and $\mathbf{\Delta m}$ of order m are the modification parts and λ is the natural frequency squared. $\mathbf{E}$ is a Boolean matrix of association between the set of m modified DOFs and N base DOFs.

In Sect. 10.3.1, an algorithm is presented based on single vector iterations by employing the complete set of modal information from the base model. The eigenproblem is transformed from the Cartesian coordinates into generalised coordinates, and the transformed problem is solved for a few frequencies and mode shapes using the shifted inverse iteration method.

In Sect. 10.3.2, we present a numerical method for the approximate eigensolution of the modified regular structures based on a free interface substructuring technique. The proposed method has the advantage that it does not rely on the complete eigensolution of the base model and instead uses a few eigenvalues and eigenvectors together with higher-order approximations from the base model. This information is used to reduce the governing eigenproblem while preserving the sparsity of the matrices.

10.3.1 Eigensolution of Locally Modified Regular Structures Using Shifted Inverse Iteration Method

Let $\mathbf{\Phi}$ denote the orthonormal matrix of eigenvectors corresponding to the base model. The following relations hold:

$$\mathbf{\Phi}^{\mathrm{t}}\mathbf{K}\mathbf{\Phi} = \mathbf{\Lambda}, \tag{10.53}$$

and

$$\mathbf{\Phi}^{\mathrm{t}}\mathbf{M}\ \mathbf{\Phi} = \mathbf{I}, \tag{10.54}$$

where $\mathbf{I}$ is the identity matrix and $\mathbf{\Lambda}$ denotes the diagonal matrix of the squared frequencies.

Let us transform the displacement vector $\mathbf{u}$ to generalised coordinates as

$$\mathbf{u} = \mathbf{\Phi q}, \tag{10.55}$$

Then, the eigenproblem of the modified regular structure (Eq. 10.52) is transformed to

$$(\mathbf{\Lambda} + \psi\Delta\mathbf{k}\ \psi^{\mathrm{t}})\mathbf{q} = \lambda(\mathbf{I} + \psi\Delta\ \mathbf{m}\ \psi^{\mathrm{t}})\mathbf{q}, \tag{10.56}$$

where $\boldsymbol{\psi} = \mathbf{\Phi}^{\mathrm{t}}\mathbf{E}$.

Suppose that we are interested in those eigenvalues λ close to a specified value λ_0. We shift the origin to λ_0 in Eq. 10.56 as follows:

$$[\mathbf{\Lambda} + \psi\Delta\mathbf{k}\ \psi^t - \lambda_0(\mathbf{I} + \psi\Delta\ \mathbf{m}\ \psi^t)]\ \mathbf{q} = (\lambda - \lambda_0)(\mathbf{I} + \psi\Delta\ \mathbf{m}\ \psi^t)\mathbf{q}. \tag{10.57}$$

Rearranging Eq. 10.57 yields

$$[\mathbf{\Lambda_s} + \psi(\Delta\mathbf{k} - \lambda_0\Delta\ \mathbf{m})\ \psi^t]\ \mathbf{q} = (\lambda - \lambda_0)(\mathbf{I} + \psi\Delta\ \mathbf{m}\ \psi^t)\mathbf{q}, \tag{10.58}$$

where $\mathbf{\Lambda_s} = \mathbf{\Lambda} - \lambda_0\ \mathbf{I}$..

Let us write

$$\bar{\mathbf{\Lambda}}_\mathbf{s} = [\mathbf{\Lambda_s} + \psi(\Delta\mathbf{k} - \lambda_0\Delta\ \mathbf{m})\psi^t]\ . \tag{10.59}$$

Multiplying Eq. 10.58 by the inverse of $\bar{\mathbf{\Lambda}}_s$ and setting $\theta = \frac{1}{(\lambda - \lambda_0)}$, we obtain

$$\theta\ \mathbf{q} = \bar{\mathbf{\Lambda}}_\mathbf{s}^{-1}(\mathbf{I} + \psi\ \Delta\mathbf{m}\ \psi^t)\mathbf{q}\ . \tag{10.60}$$

The inversion $\bar{\mathbf{\Lambda}}_\mathbf{s}^{-1}$ is calculated using the well-known *Sherman–Morrison–Woodbury* formula

$$\bar{\mathbf{\Lambda}}_\mathbf{s}^{-1} = \left(\mathbf{\Lambda_s}^{-1} - \mathbf{\Lambda_s}^{-1}\psi\mathbf{C_s}^{-1}\ \psi^t\mathbf{\Lambda_s}^{-1}\right), \tag{10.61}$$

where

$$\mathbf{C_s} = \left((\Delta\mathbf{k}\text{-}\lambda_0\Delta\mathbf{m})^{-1} + \psi^t\mathbf{\Lambda_s}^{-1}\psi\right). \tag{10.62}$$

If the inversion $(\Delta\mathbf{k} - \lambda_0\,\Delta\mathbf{m})^{-1}$ does not exist (and it is often the case), then Eqs. 10.61 and 10.62 should be revised as follows:

$$\bar{\mathbf{\Lambda}}_\mathbf{s}^{-1} = \left(\mathbf{\Lambda_s}^{-1} - \mathbf{\Lambda_s}^{-1}\psi\mathbf{C_s}^{-1}(\Delta\mathbf{k}\text{-}\lambda_0\Delta\mathbf{m})\ \psi^t\mathbf{\Lambda_s}^{-1}\right), \tag{10.63}$$

where

$$\mathbf{C_s} = \left(\mathbf{I_m} + (\Delta\mathbf{k} - \lambda_0\Delta\mathbf{m})\psi^t\mathbf{\Lambda_s}^{-1}\psi\right). \tag{10.64}$$

Equation 10.60 is in the form of a standard eigenvalue problem that can be solved for a few largest eigenvalues θ and the corresponding eigenvectors using the power method. These eigenvalues correspond to the values of λ closest to λ_0. The only tough term in Eqs. 10.61 or 10.63 is the inversion $\mathbf{C_s}^{-1}$. This term changes every time we apply a different shift λ_0 to the origin. However, the number of modified DOFs is of much smaller order *m*. In our implementation, this inversion is more

efficiently conducted by LU decomposition with partial pivoting instead of full matrix inversion.

In the following, the necessary matrix vector operations for one step of vector iterations are demonstrated through a subroutine. Let q_k and q_{k+1} be the successive vectors in the kth iteration step. Let $\mathbf{\Lambda}$ denote the vector of diagonal entries of $\mathbf{\Lambda_s}$, and let the operator ./(point divide) denote the array division between two vectors. If a matrix is point divided by a vector, its columns will array-wise be divided by that vector.

Subroutine 1.

$$\mathbf{U} = \Psi./\Lambda$$
$$\eta_1 = q_k + \Psi\Delta\mathbf{m}\Psi^t q_k$$
$$\eta_2 = \eta_1./\Lambda$$
$$\eta_3 = \Psi^t\eta_2$$
$$\eta_3 = (\Delta\mathbf{k} - \lambda_0\ \Delta\mathbf{m})\eta_3$$
$$\text{Solve for } \eta_4 \text{ from } (\mathbf{I}_m + (\Delta\mathbf{k} - \lambda_0\ \Delta\mathbf{m})\Psi^t\mathbf{U})\eta_4 = \eta_3$$
$$q_{k+1} = \eta_2 - \mathbf{U}\eta_4$$
$$q_{k+1} = \frac{q_{k+1}}{\left\|q_{k+1}\right\|_2 + q_{k+1}^t\Psi\Delta\mathbf{m}\Psi^t q_{k+1}}$$

10.3.1.1 Initialisation, Shift and Deflation

Any non-zero vector q_0 perpendicular to the subspace spanned by the previously calculated eigenvectors can be used as the initial or starting vector. The starting vector is normalised using the following normalisation operation:

$$q_0 = \frac{q_0}{\|q_0\|_2 + q_0^t\Psi\Delta\mathbf{m}\Psi^t q_0.} \tag{10.65}$$

The eigenvalue estimated from normalised vector $\mathbf{q}$ is calculated as

$$\lambda = \mathbf{q}^t(\mathbf{\Lambda} + \psi\ \Delta\mathbf{k}\ \psi^t)\mathbf{q}. \tag{10.66}$$

The convergence of the algorithm depends to a great extent on the choice of appropriate shifts. Equation 10.67 demonstrates the rate of convergence towards the eigenvalue λ_1 which is closest to the selected shift λ_0 (see, e.g. [5]). Also in this equation, λ_2 is the second closest eigenvalue to λ_0. Although introducing a new shift λ_0 requires some matrices to be modified, the extra matrix calculations are compensated for by a remarkable reduction in the number of iterations:

$$\left\|\lambda^{k} - \lambda_1\right\| = O\left(\frac{\lambda_1 - \lambda_0}{\lambda_2 - \lambda_0}\right)^{k}. \tag{10.67}$$

In the experiments of this chapter, we use a multiple of the eigenvalue obtained in the previous step, as the shift value for the current step. The coefficient is taken as 0.98. For the first shift, a small number close to zero ($\varepsilon = 1e-4$) is assumed.

Another feature incorporated into the algorithm is that the speed of convergence is monitored and once it drops below a certain level, then the shift value is changed to the current estimate of the eigenvalue, and the calculations continue after the new shift is applied. This happens when there exist two eigenvalues very close to each other and the shift used is not close enough to one of them, such that the ratio in the right-hand side of Eq. 10.67 is very close to unity. As mentioned before, application of a new shift involves extra matrix computations, but these are compensated by the improved rate of convergence towards the eigenpair sought.

For computing the eigenpairs one by one, it is necessary to prevent the algorithm from converging to previously obtained quantities or technically deflate for the previous information. Deflation is carried out by restricting the current vector to the complementary subspace of the already computed eigenvectors. Let $\mathbf{Q}$ denote the set of j computed orthonormal eigenvectors. The projection operator that orthogonolises (j + 1)th eigenvector against the computed eigenvectors is defined by

$$\mathbf{P} = \mathbf{I} - \mathbf{Q}\mathbf{Q}^{t}(\mathbf{I} + \psi\ \Delta\mathbf{m}\ \psi^{t}) \tag{10.68}$$

The projected vector is normalised using Eq. 10.65 and then used in the iteration process. During the iterations, it is necessary to frequently orthogonalise the current vector against the existing vectors in order to prevent convergence to an unwanted eigenvector. If we define the dominant eigenvector as an already computed eigenvector with the closest eigenvalue to the current shift, then the frequency of re-orthogonalisation can be determined by examining the component of the current vector which is in the direction of the dominant eigenvector. If this component exceeds the specified limit, then the orthogonalisation is carried out.

10.3.1.2 The Algorithm

In the following, necessary steps towards the calculation of a few frequencies and eigenmodes of a modified regular structure are presented in an algorithm to facilitate a quick review of the proposed method:

(1) Obtain the eigensolution of the base model employing a block-diagonalisation technique (i.e. $\mathbf{\Phi}$ and $\mathbf{\Lambda}$ from Eq. 10.53).
(2) Set ($\lambda_0 = \varepsilon = 1e-4$), $k = 0$, $\mathbf{q}_k = \mathbf{e}_1$ and $tol = 10^{-12}$.
(3) Repeat for the number of requested eigenpairs:

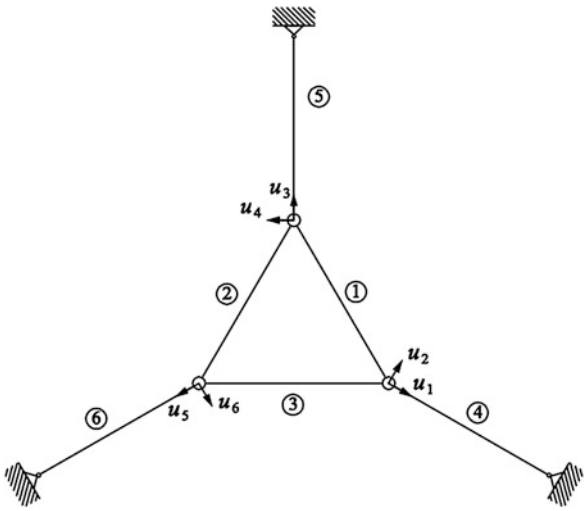

Fig. 10.16 A pin-jointed planar truss

1. Repeat until convergence:
   1.1 Update **q** through subroutine 1.
   1.2 If **Q** is not empty, then replace **q** with its projection into $\mathbf{Q}^{\perp}$ using the operator **P** in Eq. 10.68.
   1.3 If the rate of convergence is not improved more than 5 % between two successive iterations, then change the shift λ_0 to the current estimate of the eigenvalue (Eq. 10.66). Update matrices using the new shift.
   1.4 Check for convergence.
2. Calculate λ from Eq. 10.66; add **q** to **Q** and λ to the set of requested eigenvalues.
3. Set $k = 0$; initialise $\mathbf{q}_k$ with a vector perpendicular to **Q**.
4. Select a new shift λ_0 and update the matrices.

(4) Calculate the requested mode shapes from Eq. 10.55.

10.3.1.3 Numerical Experiments

Example 10.1. Consider the planar, pin-jointed truss depicted in Fig. 10.16. The structure is composed of six identical elastic bars, each having the stiffness EA, length L and a uniform mass *m* per unit length. The model possesses symmetry properties and serves as our *base* structure. The structure has six DOFs, and hence, the mass and stiffness matrices are each 6×6. The nodal degrees of freedom are expressed in a local symmetry-adapted coordinate system as depicted for each node in Fig. 10.16. With this convention, the stiffness matrix takes the form

$$\mathbf{K} = \begin{bmatrix} \mathbf{K}_1 & \mathbf{K}_2 & \mathbf{K}_2^t \\ \mathbf{K}_2^t & \mathbf{K}_1 & \mathbf{K}_2 \\ \mathbf{K}_2 & \mathbf{K}_2^t & \mathbf{K}_1 \end{bmatrix}$$

with the following submatrices:

$$\mathbf{K}_1 = \left(\frac{EA}{4L}\right) \begin{bmatrix} 10 & 0 \\ 0 & 2 \end{bmatrix},$$

and

$$\mathbf{K}_2 = \left(\frac{EA}{4L}\right) \begin{bmatrix} 3 & \sqrt{3} \\ -\sqrt{3} & -1 \end{bmatrix}.$$

The consistent mass matrix has the form

$$\mathbf{M} = \begin{bmatrix} \mathbf{M}_1 & \mathbf{M}_2 & \mathbf{M}_2^t \\ \mathbf{M}_2^t & \mathbf{M}_1 & \mathbf{M}_2 \\ \mathbf{M}_2 & \mathbf{M}_2^t & \mathbf{M}_1 \end{bmatrix},$$

with the following components:

$$\mathbf{M}_1 = \left(\frac{mL}{12}\right) \begin{bmatrix} 12 & 0 \\ 0 & 12 \end{bmatrix},$$

and

$$\mathbf{M}_2 = \left(\frac{mL}{12}\right) \begin{bmatrix} -1 & -\sqrt{3} \\ \sqrt{3} & -1 \end{bmatrix}.$$

Let us define the Kronecker product:

$$\mathbf{H} = \begin{bmatrix} \frac{\sqrt{3}}{3} & \frac{-\sqrt{3}}{6-0.5i} & \frac{-\sqrt{3}}{6+0.5i} \\ \frac{\sqrt{3}}{3} & \frac{\sqrt{3}}{3} & \frac{\sqrt{3}}{3} \\ \frac{\sqrt{3}}{3} & \frac{-\sqrt{3}}{6+0.5i} & \frac{-\sqrt{3}}{6-0.5i} \end{bmatrix} \otimes \mathbf{I}_2,$$

where $\mathbf{I}_2$ is the identity matrix of order two, and $i = \sqrt{-1}$.

Using the above unitary matrix $\mathbf{H}$, the stiffness and mass matrices are transformed into block-diagonal matrices:

$$\mathbf{H}^{*}\mathbf{K}\mathbf{H} = \mathbf{Diag}(\overline{\mathbf{K}}_{\mathrm{i}})_{\mathrm{i}=1:3}$$
$$= \begin{bmatrix} \mathbf{K}_1 + \mathbf{K}_2^{(+)} & & \\ & \mathbf{K}_1 - 0.5\mathbf{K}_2^{(+)} + \mathrm{i}\sqrt{3}/2\mathbf{K}_2^{(-)} & \\ & & \mathbf{K}_1 - 0.5\mathbf{K}_2^{(+)} - \mathrm{i}\sqrt{3}/2\mathbf{K}_2^{(-)} \end{bmatrix}$$

and

$$\mathbf{H}^{*}\mathbf{K}\mathbf{H} = \mathbf{Diag}(\overline{\mathbf{M}}_{\mathrm{i}})_{\mathrm{i}=1:3}$$
$$= \begin{bmatrix} \mathbf{M}_1 + \mathbf{M}_2^{(+)} & & \\ & \mathbf{M}_1 - 0.5\mathbf{M}_2^{(+)} + \mathrm{i}\sqrt{3}/2\mathbf{M}_2^{(-)} & \\ & & \mathbf{M}_1 - 0.5\mathbf{M}_2^{(+)} - \mathrm{i}\sqrt{3}/2\mathbf{M}_2^{(-)} \end{bmatrix}$$

where (.)* denotes the conjugate transpose, and we have

$$\mathbf{K}_2^{(+)} = \mathbf{K}_2 + \mathbf{K}_2^{\mathrm{t}}, \text{ and } \mathbf{K}_2^{(-)} = \mathbf{K}_2 - \mathbf{K}_2^{\mathrm{t}},$$

and

$$\mathbf{M}_2^{(+)} = \mathbf{M}_2 + \mathbf{M}_2^{\mathrm{t}}, \text{ and } \mathbf{M}_2^{(-)} = \mathbf{M}_2 - \mathbf{M}_2^{\mathrm{t}}.$$

Each decomposed system $\bar{\mathbf{K}}_{\mathrm{i}}, \bar{\mathbf{M}}_{\mathrm{i}}(\mathrm{i} = 1:3)$ is solved to obtain $\overline{\mathbf{V}}_{\mathrm{i}}, \overline{\mathbf{\Lambda}}_{\mathrm{i}}(\mathrm{i} = 1:3)$ such that

$$\overline{\mathbf{V}}_{\mathrm{i}}^{*}\overline{\mathbf{K}}_{\mathrm{i}}\overline{\mathbf{V}}_{\mathrm{i}} = \overline{\mathbf{\Lambda}}_{\mathrm{i}}, \text{ and } \mathbf{V}_{\mathrm{i}}^{*}\mathbf{M}_{\mathrm{i}}\mathbf{V}_{\mathrm{i}} = \mathbf{I}; (\mathrm{i} = 1:3).$$

Putting them together, we have

$$\mathbf{V}^{*}\mathbf{H}^{*}\mathbf{K}\mathbf{H}\mathbf{V} = \mathbf{\Lambda}; \text{ and } \mathbf{V}^{*}\mathbf{H}^{*}\mathbf{M}\mathbf{H}\mathbf{V} = \mathbf{I},$$

where

$$\mathbf{V} = \mathbf{Diag}(\bar{\mathbf{V}}_{\mathrm{i}})_{\mathrm{i}=1:3}; \mathbf{\Lambda} = \mathbf{Diag}\left(\bar{\mathbf{\Lambda}}_{\mathrm{i}}\right)_{\mathrm{i}=1:3}.$$

Hence, the orthonormal matrix $\mathbf{\Phi}$ in Eq. 10.53 is obtained as

$$\mathbf{\Phi} = \mathbf{H}\mathbf{V}.$$

$\mathbf{\Phi}$ is the requested matrix of modal vectors for the base structure, and $\mathbf{\Lambda}$ is the diagonal matrix of the natural frequencies squared. Our calculations lead to

$$\mathbf{\Lambda} = \left(3\mathrm{EA}/\mathrm{mL}^2\right)\mathbf{Diag}(0, 0.0898, 0.898, 0.8352, 0.8352, 1.6).$$

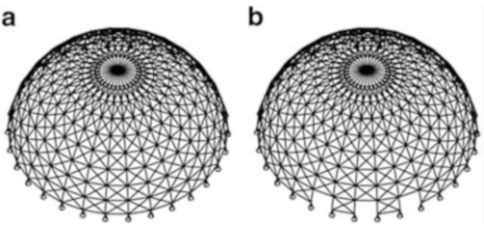

Fig. 10.17 A double-layer dome (**a**), the modified structure (**b**)

and

$$\mathbf{\Phi} = \begin{bmatrix} 0 & 0.101 & -0.002 & 0.105 & 0.181 & 0.182 \\ -0.182 & 0.003 & 0.180 & -0.127 & 0.073 & 0 \\ 0 & -0.049 & 0.088 & 0.105 & -0.181 & 0.182 \\ -0.182 & -0.158 & -0.088 & 0.127 & 0.073 & 0 \\ 0 & -0.052 & -0.087 & -0.209 & 0 & 0.182 \\ -0.182 & 0.155 & -0.093 & 0 & -0.147 & 0 \end{bmatrix}.$$

Now, suppose that we are going to modify the base structure by changing the cross-sectional area of member 4 to $2A$ and consequently its distributed mass to $2m$. The necessary modification matrices are

$$\Delta\mathbf{k} = \left(\frac{\mathrm{EA}}{4\mathrm{L}}\right)\begin{bmatrix} 4 & 0 \\ 0 & 0 \end{bmatrix}; \text{ and } \Delta\mathbf{m} = \left(\frac{\mathrm{mL}}{12}\right)\begin{bmatrix} 12 & 0 \\ 0 & 12 \end{bmatrix},$$

and the associate matrix $\mathbf{E}$ is

$$\mathbf{E}^{\mathrm{t}} = \begin{bmatrix} 1 & 0 & 0 & 0 & 0 & 0 \\ 0 & 1 & 0 & 0 & 0 & 0 \end{bmatrix}.$$

Hence, matrix Ψ in Eq. 10.56 reads

$$\Psi^{\mathrm{t}} = \mathbf{E}^{\mathrm{t}}\mathbf{\Phi} = \begin{bmatrix} 0 & 0.101 & -0.002 & 0.105 & 0.181 & 0.182 \\ -0.182 & 0.003 & 0.180 & -0.127 & 0.073 & 0 \end{bmatrix},$$

and we have necessary information to go through the iterations and obtain the modified frequencies

$$\omega^2 = \left(\frac{3\mathrm{EA}}{\mathrm{mL}^2}\right)\{0,0.0699,0.1121,0.6542,0.7325,1.3971\}$$

Example 10.2. Figure 10.17a depicts a single-layer dome composed of pin-jointed bar elements. The model is a strong Cartesian product $C_{30} \otimes P_9$ augmented by a node at the apex. Each node of the structure has three translational DOFs. The

Table 10.1 Some natural frequencies and periods of the *base* structure

Mode no.	Frequency (rad/s)	Period (sec)
1	55.212314958242	0.113800432239
2	57.412197701472	0.109439902298
3	57.412197701563	0.109439902298
4	64.249800343827	0.097793071318
5	64.249800343980	0.097793071318
6	75.862375410463	0.082823471756
7	75.862375410605	0.082823471756
8	91.832588278479	0.068419995831
9	91.832588278676	0.068419995831
10	110.911771332569	0.056650301692
11	110.911771332718	0.056650301692
12	131.101366502565	0.047926161830

bottom nodes of the dome are all constrained in three directions. This leads to a total of 720 DOFs for the entire structure. The diameter of the dome is 32 m, and its height is 13.6 m. The bar elements have a uniform cross-sectional area of $a = 6.41\ \text{cm}^2$, and the Young's modulus is considered to be $E = 2.1 \times 10^{11}\ \text{N/m}^2$. For simplicity, a concentrated mass of 80 kg in each node is assumed.

The free vibration analysis of the base structure depicted in Fig. 10.17a is performed using a procedure for decomposition of stiffness and mass matrices. The prerequisite to this is to transform the stiffness and mass matrices from the global coordinates to a local symmetry-adapted coordinate system as discussed in the previous example. With such a transformation, the stiffness and mass matrices would take the augmented block circulant form as illustrated in Sect. 10.2.7. All the frequencies and mode shapes of the base structure are calculated using the formulations presented in the aforementioned section. Table 10.1 shows a few lower frequencies and the corresponding periods obtained from the decomposition method.

Now, suppose that we are interested in the effects of eliminating some diagonal elements on the vibration behaviour of the base structure. As an example, consider the modified structure obtained by eliminating six diagonal bars as depicted in Fig. 10.17b. A total number of six nodes are affected by this modification, and hence, the modification matrices $\boldsymbol{\Delta}\mathbf{k}$ and $\boldsymbol{\Delta}\mathbf{m}$ in Eq. 10.52 are 18 by 18 each. The first 12 eigenfrequencies and mode shapes of the modified structure are obtained using the proposed method and the direct inverse iteration method. The results obtained from the two methods are in good agreement with each other. Table 10.2 summarises the frequencies and corresponding periods of the modified structure. The total time required by the proposed method to complete the iterations together with the solution of the base structure was 0.285 s. The direct inverse iterations required 7.68 s to complete the solution for 12 eigenpairs, indicating that the proposed method performed 27 times faster in the case of this example.

Table 10.2 The 12 lowest natural frequencies and the periods of the *modified* structure

Mode no.	Frequency (rad/s)	Period (sec)
1	43.059838267156	0.145917531510
2	45.126505414274	0.139234918581
3	45.994210412664	0.136608178525
4	52.618417941081	0.119410380491
5	52.958200044459	0.118644238322
6	62.757775486842	0.100118037302
7	63.028029548635	0.099688747247
8	76.447643302369	0.082189391795
9	77.938683888095	0.080617031155
10	94.133449645646	0.066747636795
11	95.074919920548	0.066086674724
12	116.686047209274	0.053846929067

10.3.2 Approximate Eigensolution of Locally Modified Regular Structures Using a Substructuring Technique

With a closer look at problem (10.52), its connection with two other extensively investigated eigenproblems in structural mechanics is realised. The first one is structural dynamic reanalysis problem, which deals with efficient use of natural frequencies and modes obtained from a previous analysis to derive the response of the new modified structure, without extensive additional computations. Approximate methods for eigenvalue reanalysis based on Taylor's series expansion have been proposed [6, 7]. However, these methods are not suitable for significant modifications. Rank-one modification of the eigenproblem has been the subject of research for quite some time [8, 9]. However, these methods rely on the complete eigensolution of the original system, which is prohibitively expensive for large-scale systems. Carey et al. [10] proposed a block Lanczos method to calculate a few lowest eigenvalues based on the information obtained in the solution of a few eigenvalues for the original system. They employed a clever idea of using starting Lanczos vectors which span the column space of the matrix $\mathbf{E}$ in Eq. 10.52. The modification problem that we are going to address in this chapter however differs from the reanalysis problem due to the block-diagonalisable structure of $\mathbf{K}$ and $\mathbf{M}$, as mentioned before. This is an occasion that offers great opportunities in eigensolution and linear solution of the corresponding equations and will be efficiently employed in the proposed method of this chapter. Nevertheless, the method developed here is directly applicable to reanalysis problems as well.

Another problem of structural mechanics related to the subject matter is the dynamic substructuring [11]. There are basically two methods available in literature for the eigenvalue problem of substructuring. Kron's method is one of them, where the problem reduces to solving a non-linear eigenvalue problem involving the Kron's matrix [12, 13]. Sehmi [14] applied the Lanczos algorithm to Kron's method and showed that operation count decreases dramatically compared to the classic solutions of Kron's scalar equation. However, a remarkable drawback of Kron's

substructuring is the need to calculate all eigenpairs of each substructure primarily. This is very time consuming, since only the first a few eigensolutions are generally of interest for most applications. Weng et al. [15] improved the Kron's substructuring method using modal truncation approximation. They incorporated the first-order and the second-order residual flexibility approximations of the higher modes. The other well-known method of dynamic substructuring is the component mode synthesis (CMS), where a non-linear eigenvalue problem is avoided by restricting the solution to a certain subspace [16, 17]. CMS methods are classified as free interface, fixed interface and hybrid methods. MacNeal introduced the residual flexibility to include the static effects of higher normal modes [18]. Rozenblum applied an associated isostatic subset method to calculate the residual modes for positive semi-definite stiffness matrices [19]. Rixen proposed a dual Craig–Bampton formulation of the CMS method [20].

Most of the structural applications require just a few lower eigenfrequencies and their corresponding modal vectors. This information can be obtained much more easily and quickly for the base model due to block-diagonalisable structure of its matrices. Hence, it is natural to express the dynamic behaviour of a modified model in terms of eigenmodes of its base model. Higher eigenmodes can be estimated by static modes deduced from residual flexibility of the base model. Again, the decomposable structure of the matrices associated with the base model is of central importance in constructing such approximations. In this section, we provide a substructure-assembled formulation of problem (10.52) and describe how a truncated modal basis together with static modes deduced from residual flexibility of the base model can be used to reduce the governing eigenproblem into a much smaller problem while maintaining the sparsity.

10.3.2.1 Free Interface Substructure Formulation for the Modified Regular Structure

Let us assume that, with respect to eigenvalue problem (10.52), the perturbations $\boldsymbol{\Delta k}$ and $\boldsymbol{\Delta m}$ correspond to a substructure interacting with the *base model* of $\mathbf{K}$ and $\mathbf{M}$. This substructure is not required to be a meaningful substructure as illustrated in Example 4. Partitioning the model into these two components and using internal forces $\mathbf{f}$ on the interface DOFs between the two substructures, the linear dynamic behaviour of each part is governed by the local eigenequations

$$\mathbf{Ku} - \lambda\mathbf{Mu} + \mathbf{Ef} = \mathbf{0}, \tag{10.69}$$

and

$$\boldsymbol{\Delta k}\mathbf{v} - \lambda\boldsymbol{\Delta m}\mathbf{v} - \mathbf{f} = \mathbf{0}. \tag{10.70}$$

The compatibility between the two substructures is enforced by

$$\mathbf{E}^{\mathrm{t}}\mathbf{u} - \mathbf{v} = \mathbf{0}. \tag{10.71}$$

Putting them together, Eqs. 10.69, 10.70, and 10.71 can be written in block form

$$\begin{bmatrix} \mathbf{K} & \mathbf{0} & \mathbf{E} \\ \mathbf{0} & \Delta\mathbf{k} & -\mathbf{I} \\ \mathbf{E}^{\mathrm{t}} & -\mathbf{I} & \mathbf{0} \end{bmatrix} \begin{bmatrix} \mathbf{u} \\ \mathbf{v} \\ \mathbf{f} \end{bmatrix} - \lambda \begin{bmatrix} \mathbf{M} & & \\ & \Delta\mathbf{m} & \\ & & \mathbf{0} \end{bmatrix} \begin{bmatrix} \mathbf{u} \\ \mathbf{v} \\ \mathbf{f} \end{bmatrix} = \mathbf{0}. \tag{10.72}$$

Vector $\mathbf{f}$ is also known as Lagrange multipliers. The assembled system (10.72) is of order $N + 2\,m$ and has for general solution N eigenvalues λ.

10.3.2.2 Modal Truncation

Let $\mathbf{\Phi}$ be the matrix of M-orthonormal eigenvectors and $\mathbf{\Lambda}$ the diagonal matrix of eigenvalues associated with the eigenproblem of the base model. Hence, the following relations hold:

$$\mathbf{\Phi}^{\mathrm{t}}\mathbf{K}\mathbf{\Phi} = \mathbf{\Lambda} \text{ and } \mathbf{\Phi}^{\mathrm{t}}\mathbf{M}\mathbf{\Phi} = \mathbf{I}. \tag{10.73}$$

Let us define a cut-off eigenvalue λ_{c} and suppose that we are interested in those eigenvalues λ of Eq. 10.52 that

$$\lambda << \lambda_{\mathrm{c}}. \tag{10.74}$$

Now, partition $\mathbf{\Lambda}$ into lower and higher eigenvalues based on the cut-off value λ_{c} as

$$\mathbf{\Lambda} = \begin{bmatrix} \mathbf{\Lambda}_{\mathrm{l}} & \\ & \mathbf{\Lambda}_{\mathrm{h}} \end{bmatrix}. \tag{10.75}$$

Let the corresponding partitioning of $\mathbf{\Phi}$ be

$$\mathbf{\Phi} = [\,\mathbf{\Phi}_{\mathrm{l}} \;\; \mathbf{\Phi}_{\mathrm{h}}\,]. \tag{10.76}$$

Using modal coordinates $\mathbf{q}$ defined by

$$\mathbf{u} = \mathbf{\Phi}_{\mathrm{l}}\mathbf{q}_{\mathrm{l}} + \mathbf{\Phi}_{\mathrm{h}}\mathbf{q}_{\mathrm{h}}. \tag{10.77}$$

and premultiplying the problem (10.69) by $\mathbf{\Phi}_{\mathrm{h}}^{\mathrm{t}}$, it can be deduced that

$$\mathbf{\Lambda}_{\mathrm{h}}\mathbf{q}_{\mathrm{h}} - \lambda\mathbf{q}_{\mathrm{h}} + \mathbf{\Phi}_{\mathrm{h}}^{\mathrm{t}}\mathbf{E}\mathbf{f} = \mathbf{0}. \tag{10.78}$$

Premultiplying Eq. 10.78 by $\boldsymbol{\Lambda}_{\mathrm{h}}{}^{-1}$ and putting $\lambda\,\boldsymbol{\Lambda}_{\mathrm{h}}{}^{-1} \approx 0$ due to the assumption (10.74), we arrive at

$$\mathbf{q}_{\mathrm{h}} = -\boldsymbol{\Lambda}_{\mathrm{h}}^{-1}\boldsymbol{\Phi}_{\mathrm{h}}^{\mathrm{t}}\mathbf{E}\mathbf{f}. \tag{10.79}$$

Substituting Eq. 10.79 into Eq. 10.77, we obtain the following approximation for vector $\mathbf{u}$:

$$\mathbf{u} \approx \boldsymbol{\Phi}_{\mathrm{l}}\mathbf{q}_{\mathrm{l}} - \mathbf{G}_{\mathrm{res}}\mathbf{E}\mathbf{f}, \tag{10.80}$$

where

$$\mathbf{G}_{\mathrm{res}} = \boldsymbol{\Phi}_{\mathrm{h}}\boldsymbol{\Lambda}_{\mathrm{h}}{}^{-1}\boldsymbol{\Phi}_{\mathrm{h}}{}^{\mathrm{t}} \tag{10.81}$$

is the residual flexibility of the base model.

In summary, we construct the following approximation of the coordinate vectors and Lagrange multipliers for the reduction of the eigenproblem (10.72):

$$\begin{bmatrix}\mathbf{u}\\ \mathbf{v}\\ \mathbf{f}\end{bmatrix} \approx \mathbf{T}\begin{bmatrix}\mathbf{q}_{\mathrm{l}}\\ \mathbf{v}\\ \mathbf{f}\end{bmatrix} \approx \begin{bmatrix}\boldsymbol{\Phi}_{\mathrm{l}} & \mathbf{0} & -\mathbf{G}_{\mathrm{res}}\mathbf{E}\\ \mathbf{0} & \mathbf{I} & \mathbf{0}\\ \mathbf{0} & \mathbf{0} & \mathbf{I}\end{bmatrix}\begin{bmatrix}\mathbf{q}_{\mathrm{l}}\\ \mathbf{v}\\ \mathbf{f}\end{bmatrix}, \tag{10.82}$$

10.3.2.3 The Reduced Eigenproblem

Using the approximation (10.82), we will reduce the assembled system (10.72). First, notice the following properties of the residual flexibility matrix

$$\begin{aligned}&\mathbf{G}_{\mathrm{res}}^{\mathrm{t}} = \mathbf{G}_{\mathrm{res}},\ \ \mathbf{G}_{\mathrm{res}}\mathbf{K}\mathbf{G}_{\mathrm{res}} = \mathbf{G}_{\mathrm{res}}\\ &\boldsymbol{\Phi}_{\mathrm{l}}^{\mathrm{t}}\mathbf{K}\mathbf{G}_{\mathrm{res}} = \mathbf{0},\ \ \boldsymbol{\Phi}_{\mathrm{l}}^{\mathrm{t}}\mathbf{M}\mathbf{G}_{\mathrm{res}} = \mathbf{0}.\end{aligned} \tag{10.83}$$

The reduced eigenproblem of the modified regular structure is then obtained by using the transformation (10.82) as follows:

$$\tilde{\mathbf{K}}\begin{bmatrix}\mathbf{q}_{\mathrm{l}}\\ \mathbf{v}\\ \mathbf{f}\end{bmatrix} - \lambda\tilde{\mathbf{M}}\begin{bmatrix}\mathbf{q}_{\mathrm{l}}\\ \mathbf{v}\\ \mathbf{f}\end{bmatrix} = 0, \tag{10.84}$$

with the reduced matrices

$$\tilde{\mathbf{K}} = \begin{bmatrix} \boldsymbol{\Lambda}_1 & \mathbf{0} & \boldsymbol{\Phi}_1^{\mathrm{t}}\mathbf{E} \\ \mathbf{0} & \Delta\mathbf{k} & -\mathbf{I} \\ \mathbf{E}^{\mathrm{t}}\boldsymbol{\Phi}_1 & -\mathbf{I} & \mathbf{F}_{\mathrm{res}} \end{bmatrix} \text{ and } \tilde{\mathbf{M}} = \begin{bmatrix} \mathbf{I} & & \mathbf{0} \\ & \Delta\mathbf{m} & \\ \mathbf{0} & & \mathbf{M}_{\mathrm{res}} \end{bmatrix}, \tag{10.85}$$

where

$$\mathbf{F}_{\mathrm{res}} = -\mathbf{E}^{\mathrm{t}}\mathbf{G}_{\mathrm{res}}\mathbf{E}, \quad \mathbf{M}_{\mathrm{res}} = \mathbf{E}^{\mathrm{t}}\mathbf{G}_{\mathrm{res}}\mathbf{M}\mathbf{G}_{\mathrm{res}}\mathbf{E}. \tag{10.86}$$

$\boldsymbol{\Lambda}_1$ and $\boldsymbol{\Phi}_1$ correspond to the calculated eigenvalues and eigenmodes of the base structure also called the *master* modes. They include zero eigenvalue and the corresponding rigid-body modes of the base model if available. However, the calculations differ in constructing the residual flexibility matrix, with or without the rigid-body modes.

10.3.2.4 Evaluation of the Residual Flexibility Matrix

In general case, stiffness matrix $\mathbf{K}$ of the base model may be positive semi-definite. First, we discuss the evaluation of $\mathbf{G}_{\mathrm{res}}$ when $\mathbf{K}$ is positive definite.

Positive-Definite Stiffness Matrix

In this case, $\mathbf{K}$ is nonsingular, and using the following result:

$$\mathbf{K}^{-1} = \boldsymbol{\Phi}\boldsymbol{\Lambda}^{-1}\boldsymbol{\Phi}^{\mathrm{t}} = \boldsymbol{\Phi}_1\boldsymbol{\Lambda}_1^{-1}\boldsymbol{\Phi}_1^{\mathrm{t}} + \boldsymbol{\Phi}_{\mathrm{h}}\boldsymbol{\Lambda}_{\mathrm{h}}^{-1}\boldsymbol{\Phi}_{\mathrm{h}}^{\mathrm{t}}. \tag{10.87}$$

we conclude that

$$\mathbf{G}_{\mathrm{res}} = \mathbf{K}^{-1} - \boldsymbol{\Phi}_1\boldsymbol{\Lambda}_1^{-1}\boldsymbol{\Phi}_1^{\mathrm{t}}. \tag{10.88}$$

The inversion $\mathbf{K}^{-1}$ is constructed using the block-diagonal transform of $\mathbf{K}$ (Eq. 10.2) as

$$\mathbf{K}^{-1} = \mathbf{T}\left[\mathbf{K}^{(\mathrm{BD})}\right]^{-1}\mathbf{T}^{\mathrm{t}}. \tag{10.89}$$

Positive Semi-Definite Stiffness Matrix

In this case, there are rigid-body modes present in the calculated modal matrix $\boldsymbol{\Phi}_1$, and they should be suppressed first to obtain the elastic part of the response, from which the residual flexibility is then calculated.

Let us partition the M-orthonormal modal matrix $\boldsymbol{\Phi}$ as follows:

$$\mathbf{\Phi} = [\mathbf{\Phi}_{\mathrm{l}}, \mathbf{\Phi}_{\mathrm{h}}] = [\mathbf{\Phi}_{\mathrm{r}}, \mathbf{\Phi}_{\mathrm{a}}, \mathbf{\Phi}_{\mathrm{h}}] = [\mathbf{\Phi}_{\mathrm{r}}, \mathbf{\Phi}_{\mathrm{e}}], \tag{10.90}$$

where $\mathbf{\Phi}_{\mathrm{r}}$ is the matrix of the rigid-body modes, $\mathbf{\Phi}_{\mathrm{a}}$ the matrix of calculated eigenvectors of non-zero eigenvalues and $\mathbf{\Phi}_{\mathrm{e}} = [\mathbf{\Phi}_{\mathrm{a}}, \mathbf{\Phi}_{\mathrm{h}}]$ the elastic eigenvectors.

The response of the following system:

$$\mathbf{K}\mathbf{x} = \mathbf{F}_0 \tag{10.91}$$

is composed of the rigid-body response $\mathbf{x}_{\mathrm{r}}$ and an elastic response $\mathbf{x}_{\mathrm{e}}$. The elastic response can be expressed in terms of eigenvalues and eigenmodes as

$$\mathbf{x}_{\mathrm{e}} = \left[\mathbf{\Phi}_{\mathrm{e}}\mathbf{\Lambda}_{\mathrm{e}}^{-1}\mathbf{\Phi}_{\mathrm{e}}^{\mathrm{t}}\right]\mathbf{F}_0 = \left[\mathbf{\Phi}_{\mathrm{a}}\mathbf{\Lambda}_{\mathrm{a}}^{-1}\mathbf{\Phi}_{\mathrm{a}}^{\mathrm{t}} + \mathbf{\Phi}_{\mathrm{h}}\mathbf{\Lambda}_{\mathrm{h}}^{-1}\mathbf{\Phi}_{\mathrm{h}}^{\mathrm{t}}\right]\mathbf{F}_0 = \mathbf{G}_{\mathrm{e}}\mathbf{F}_0. \tag{10.92}$$

Hence, the residual flexibility matrix $\mathbf{G}_{\mathrm{res}}$ can be obtained, provided that we have already calculated the elastic flexibility matrix $\mathbf{G}_{\mathrm{e}}$. The relation is

$$\mathbf{G}_{\mathrm{res}} = \mathbf{G}_{\mathrm{e}} - \mathbf{\Phi}_{\mathrm{a}}\mathbf{\Lambda}_{\mathrm{a}}^{-1}\mathbf{\Phi}_{\mathrm{a}}^{\mathrm{t}}. \tag{10.93}$$

The elastic flexibility matrix $\mathbf{G}_{\mathrm{e}}$ is calculated using an inertia relief procedure to remove the rigid-body modes. Let $\mathbf{R}$ be the orthogonal projector onto the complement space of $\mathbf{\Phi}_{\mathrm{r}}$, defined by

$$\mathbf{R} = (\mathbf{I} - \mathbf{\Phi}_{\mathrm{r}}\mathbf{\Phi}_{\mathrm{r}}^{\mathrm{t}}\mathbf{M}). \tag{10.94}$$

It can be shown [18, 19] that

$$\mathbf{G}_{\mathrm{e}} = \mathbf{R}\overline{\mathbf{G}}_{\mathrm{e}}\mathbf{R}^{\mathrm{t}}, \tag{10.95}$$

where $\bar{\mathbf{G}}_{\mathrm{e}}$ is the elastic flexibility matrix relative to a set of imposed constraints. $\bar{\mathbf{G}}_{\mathrm{e}}$ may be obtained by taking the stiffness matrix $\mathbf{K}$ which is singular, deleting rows and columns corresponding to constrained DOFs, inverting the resulting matrix and expanding back to the original size by adding zeros. If we use the block-diagonal transform $\mathbf{K}^{(\mathrm{BD})}$ of (10.2) instead of $\mathbf{K}$ for inversion, then we will have

$$\mathbf{G}_{\mathrm{e}} = \mathbf{R}\mathbf{T}\overline{\mathbf{G}}_{\mathrm{e}}^{(\mathrm{BD})}\mathbf{T}^{\mathrm{t}}\mathbf{R}^{\mathrm{t}}, \tag{10.96}$$

where $\overline{\mathbf{G}}_{\mathrm{e}}^{(\mathrm{BD})}$ is obtained from $\mathbf{K}^{(\mathrm{BD})}$ in an analogous way to that of $\overline{\mathbf{G}}_{\mathrm{e}}$. It should be noted that in the actual implementations, the inverse matrices are not computed explicitly, and the calculations are performed much more efficiently using LU decomposition with partial pivoting.

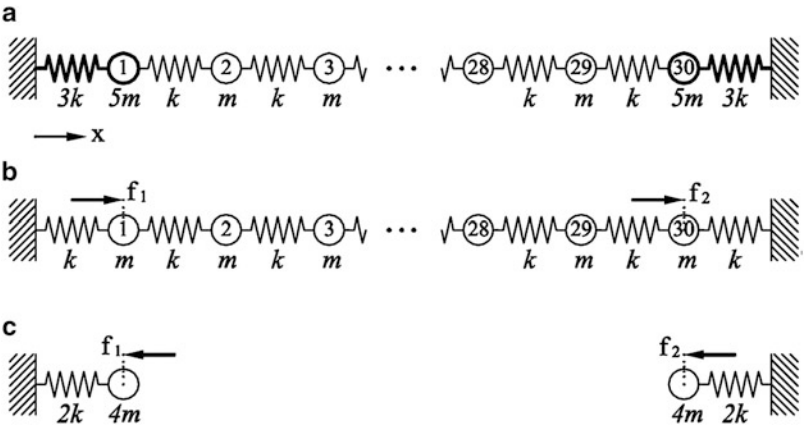

Fig. 10.18 (**a**) Mass–spring system, (**b**) the base system, (**c**) modification part

10.3.2.5 Numerical Experiments

Example 10.3. Consider the mass–spring system depicted in Fig. 10.18a. The system is composed of 30 point masses connected together with identical springs of stiffness k. Two end points are connected to the ground with springs of stiffness $3k$. Each point has a single degree of freedom in the x-direction with a concentrated mass m, except for the two end points with mass $5m$.
The system is decomposed into a regular model in Fig. 10.18b which serves as our base model and a small modification part as shown in Fig. 10.18c. The interface forces $\mathbf{f}$ acting between the two subsystems are also depicted in these figures.
The mass matrix of the base system is a diagonal matrix with entries equal to m. The stiffness has the form

$$\mathbf{K} = \mathrm{k}\begin{bmatrix} 2 & -1 & 0 & \dots & 0 \\ -1 & 2 & -1 & & \\ 0 & . & . & . & 0 \\ & & -1 & 2 & -1 \\ 0 & \dots & 0 & -1 & 2 \end{bmatrix}$$

This is a matrix of Toeplitz type, and its eigenvalues and eigenvectors can be given by

$$\lambda_{\mathrm{j}} = \mathrm{k}\left(2 - 2\cos\left(\frac{\mathrm{j}\pi}{31}\right)\right) \text{ and } \boldsymbol{\varphi}_{\mathrm{j}} = \begin{bmatrix} \sin\left(\frac{1\mathrm{j}\pi}{31}\right) \\ \sin\left(\frac{2\mathrm{j}\pi}{31}\right) \\ \sin\left(\frac{3\mathrm{j}\pi}{31}\right) \\ \vdots \\ \sin\left(\frac{30\mathrm{j}\pi}{31}\right) \end{bmatrix}, \quad (\text{for } \mathrm{j} = 1, 2, \dots, 30)$$

Table 10.3 Comparison of the results for Example 10.3

	$\lambda/\left(\frac{k}{m}\right)$		
Index	Present method	Direct method	Relative error (%)
1	0.011196179375082	0.011196152245938	0.000242308
2	0.04456671315552	0.044565589843171	0.002520582
3	0.09943251737941	0.099414548792035	0.018074404
4	0.174489925521154	0.1744322737405	0.033051097
5	0.267571530235334	0.267309789748227	0.097916536
6	0.373992592569361	0.373760051611776	0.062216643

Table 10.4 Comparison of the natural periods and mode shapes – Example 10.4

	T(sec)			
Index	Present method	Direct method	Relative error (%)	Mode shape error
1	2.437620492749	2.437629071982	0.00035195	6.9E-07
2	0.812544240652	0.812569812820	0.00314707	6.9E-07
3	0.487529859089	0.487574215574	0.00909738	1.8E-06
4	0.348241329684	0.348302251895	0.01749119	5.6E-06
5	0.270853657868	0.270938450909	0.03129605	1.4E-05
6	0.221614561259	0.221715019183	0.04530948	6.9E-07

Stiffness, mass and association matrices corresponding to modification subsystem are as follows:

$$\mathbf{\Delta k} = k\begin{bmatrix} 2 & 0 \\ 0 & 2 \end{bmatrix},\ \mathbf{\Delta m} = m\begin{bmatrix} 4 & 0 \\ 0 & 4 \end{bmatrix},\ \text{and } \mathbf{E}^t = \begin{bmatrix} 1 & 0 & \dots & 0 & 0 \\ 0 & 0 & \dots & 0 & 1 \end{bmatrix}_{2\times 30}$$

Utilising only eight eigenvalues and eigenmodes from the base system, that is,

$$\mathbf{\Lambda}_1 = \begin{bmatrix} \lambda_1 & & & \\ & \cdot & & \\ & & \cdot & \\ & & & \cdot \\ & & & \lambda_8 \end{bmatrix} \text{ and } \mathbf{\Phi}_1 = [\varphi_1 \quad \dots \quad \varphi_8],$$

we calculate the residual modes, $\mathbf{G}_{res}\mathbf{E}$, using an LU decomposition of $\mathbf{K}$. Next, we use this information to construct the reduced eigenproblem (10.84). In our case, matrices $\tilde{\mathbf{K}}$ and $\tilde{\mathbf{M}}$ are 12 by 12 each. The reduced problem in turn is solved using a sparse eigensolver of MATLAB software to obtain the first six eigenvalues as shown in Table 10.3. The system eigenvalues are also obtained using a direct method that solves the eigenproblem (10.52) of the modified system without reducing the problem size. The results are compared in Table 10.3 to see how much accuracy can be obtained in estimating the lower eigenvalues of the original system using the proposed method.

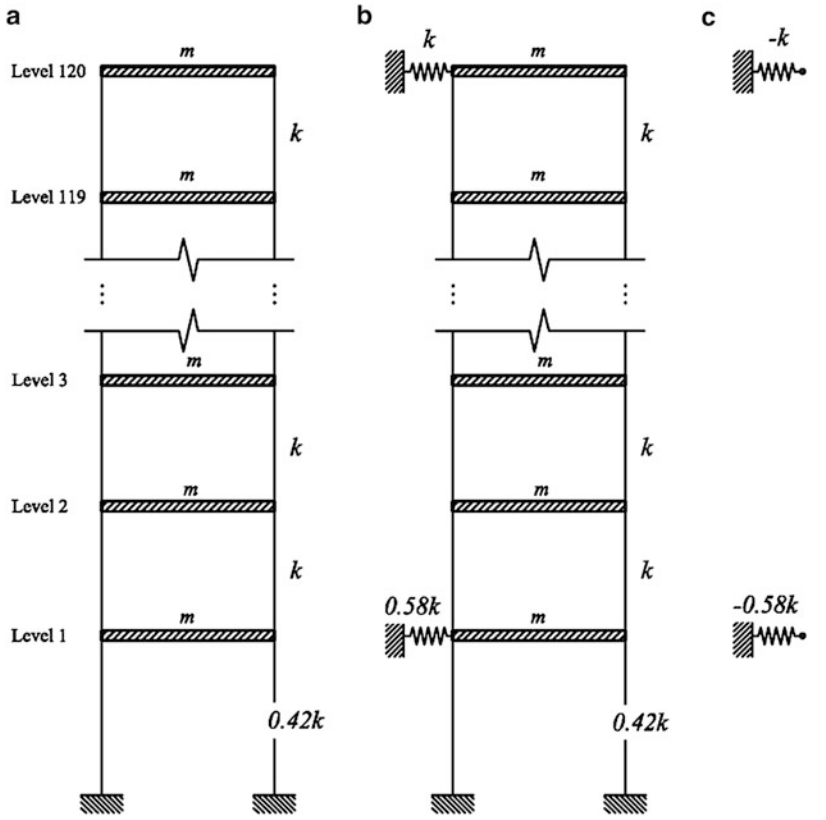

Fig. 10.19 A shear building (**a**), the base structure (**b**), the modification part (**c**)

It can be seen from the Table 10.3 that lower eigenvalues are estimated more accurately, and the relative error increases with the index of eigenvalues. Note that the relative error of an estimated eigenvalue is proportional to the ratio of that eigenvalue to the cut-off value. The cut-off value is the lower eigenvalue in the set $\mathbf{\Lambda}_h$. In this example, the cut-off value is the 9th eigenvalue of the base system ($\lambda_9 = 0.775788034904674$), because we used only eight of them as master eigenvalues. Hence, the eigenvalues that are well below this value are approximated more accurately. With reference to Table 10.3, it is realised that the maximum relative error is less than 0.1% which is a sufficient accuracy for usual engineering applications.

Example 10.4. This example demonstrates that the modification part need not be a meaningful substructure. Consider a 120-storey shear building depicted in Fig. 10.19a. Each floor has a total mass m concentrated at the floor level. The 2^{nd}-last stories are identical, each of lateral stiffness k. The first storey has a lateral stiffness $0.42k$.

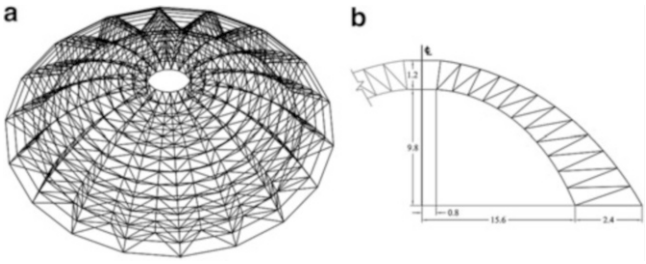

Fig. 10.20 A double-layer dome

In Fig. 10.19b, necessary springs are attached to the building at the first and the last floor levels in order to create a base structure with a regular stiffness matrix of order 120 × 120. The mass matrix is a diagonal matrix with diagonal elements m. Figure 10.19c shows the modification part. It is observed that springs with negative stiffness are introduced. Although a negative stiffness spring is not a meaningful substructure, it does not affect the algorithm because the formulations are developed based on the algebraic equilibrium equations partitioned using the Lagrange multipliers and no further assumptions are made regarding the modification matrices.

Table 10.4 presents the first six natural periods of the structure obtained using the present method and a direct method, assuming m = 5 t, and k = 200 × 10^3 kN/m.

Only 16 modes of the base structure are employed in the calculations using the proposed method. The corresponding cut-off value is (T_{17} = 0.071757536). The lower modes obtained here have periods well over the cut-off value, and hence, the relative errors in Table 10.4 are very small. Also presented in this table are the mode shape errors. The mode shape error is a measure of the angle between two vectors. It is calculated using the following relations:

$$\cos^2\theta = \frac{|\tilde{\mathbf{u}}^t\mathbf{u}|^2}{(\tilde{\mathbf{u}}^t\tilde{\mathbf{u}})(\mathbf{u}^t\mathbf{u})}, \tag{10.97}$$

and

$$\text{Mode shape error} = 1 - \cos^2\theta. \tag{10.98}$$

In these relations, $\mathbf{u}$ and $\tilde{\mathbf{u}}$ are the mode shapes calculated using the direct method and the proposed method, respectively, and θ is the angle between the two modes.

With reference to Table 10.4, one can deduce that the obtained mode shapes are very satisfactory.

Example 10.5. Consider a double-layer dome as shown in Fig. 10.20a. The top layer is the Cartesian product $C_n(X)_C P_m$, and the bottom layer is the Cartesian product $C_n(X)_C P_{m-1}$. Each node of the bottom layer is connected to four adjacent

Table 10.5 Some natural frequencies and periods of the *base* structure

Index	Frequency (rad/s)	Period (sec)
1	23.431111403210	0.268155667013
2	23.431111403210	0.268155667013
3	55.640554754627	0.112924562576
4	55.640554754627	0.112924562576
5	75.374657678647	0.083359387634
6	75.374657678647	0.083359387634
7	88.464767135800	0.071024719904
8	93.539922378078	0.067171162296
9	93.539922378078	0.067171162296
10	97.325211855081	0.064558660469
11	97.325211855081	0.064558660469
12	104.411745166515	0.060176997302
13	104.411745166515	0.060176997302
14	127.183813251247	0.049402397574
15	133.506590117543	0.047062735268
16	133.506590117543	0.047062735268

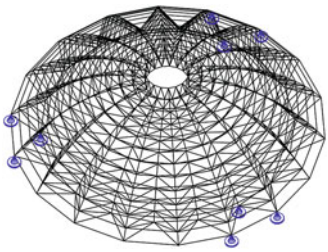

Fig. 10.21 The dome with supports

nodes in the top layer. Here n = 18, and m = 13. Figure 10.20b shows a cross section of the dome in elevation and some dimensions in metric units. The top and bottom arcs are divided into equal length segments by cross members. The structure is built of pin-jointed bar elements having cross-sectional area $a = 6.41$ cm^2, and elastic modulus is $E = 2.1 \times 10^{11}$ N/m^2. For simplicity, a concentrated mass of 80 kg in each node is assumed. Each node of the structures has three translational DOFs.

The eigenproblem associated with free vibration of the base model is transformed from global Cartesian coordinates into a local symmetry-adapted coordinate system in which stiffness and mass matrices become block diagonalisable and are easily solved to obtain the first 60 eigenfrequencies and eigenmodes constituting the master modes of the base structure. Table 10.5 presents the results for the first 16 non-zero natural frequencies (the six zero frequencies associated with rigid-body modes are discarded) and the corresponding natural periods. Calculations are performed at double-precision arithmetic and on a computer with Intel® Core ™2 Duo CPU 2.33 GHz and 2 GB of RAM, which was running Microsoft Windows XP Professional Service Pack 3.

Now consider the addition of some supports to the base structure as shown in Fig. 10.21. We use the penalty method to impose the constraints. In the penalty

Table 10.6 Comparison of the result for the *supported* structure

	Present method		Direct method			
	Total run time: 0.085		Total run time: 14.45			
Index	Frequency (rad/s)	Period (sec)	Frequency (rad/s)	Period (sec)	Relative error (%)	Mode shape error
1	37.642300	0.166918	37.641876	0.166920	0.001124	2.9E-08
2	37.642304	0.166918	37.641877	0.166920	0.001134	2.9E-08
3	44.171008	0.142247	44.169672	0.142251	0.003023	1.1E-07
4	55.887582	0.112425	55.883364	0.112434	0.007546	3.5E-07
5	55.888028	0.112425	55.883364	0.112434	0.008344	3.5E-07
6	66.621251	0.094312	66.608203	0.094331	0.019585	6.5E-07
7	74.902147	0.083885	74.893256	0.083895	0.011870	1.2E-06
8	74.902249	0.083885	74.893256	0.083895	0.012006	1.2E-06
9	88.104846	0.071315	88.101864	0.071317	0.003385	1.6E-06
10	94.670128	0.066369	94.635720	0.066393	0.036345	2.0E-06
11	94.673700	0.066367	94.635720	0.066393	0.040117	2.0E-06
12	103.415690	0.060757	103.384328	0.060775	0.030326	3.6E-06
13	108.461801	0.057930	108.403330	0.057961	0.053910	3.9E-06
14	108.466249	0.057928	108.403330	0.057961	0.058009	3.9E-06
15	114.514228	0.054868	114.484645	0.054882	0.025833	1.1E-05
16	126.344589	0.049731	126.213492	0.049782	0.103761	1.2E-05

method, matrix $\mathbf{K}$ is updated to $\mathbf{K} + \mathbf{E}\boldsymbol{\Delta}\mathbf{k}\mathbf{E}^{t}$, with $\boldsymbol{\Delta}\mathbf{k}$ being a diagonal matrix of penalty numbers. The penalty numbers are taken as 10^6 times the largest diagonal coefficient in the structure stiffness matrix. The results of the analysis using the proposed method with 60 master modes and also a direct sparse eigensolver of the MATLAB software are presented in Table 10.6 for the first 16 natural frequencies and the corresponding natural periods. Note that the supported structure has no rigid-body modes due to sufficient restraining of the structure.

Comparing the results in Tables 10.5 and 10.6, it can be verified that the fundamental period of the supported structure is decreased compared to that of the base structure, due to contribution of the supports to total structural stiffness. With reference to Table 10.6, one can observe that relative errors range from a negligible to 0.1 % for the last estimated natural period, indicating that the accuracy of the obtained results is satisfactory. The mode shapes are verified by the angles between them using Eq. 10.98. For simple eigenvalues, Eq. 10.97 is used to measure the angle between the corresponding mode shapes. For multiple eigenvalues, it is possible for the algorithm to calculate a different basis for the associated eigenspace. Hence, the subspaces spanned by the set of orthonormal eigenvectors associated with the multiple eigenvalue should be tested against each other. For this purpose, the angle between two equi-dimensional subspaces with orthonormal bases $\tilde{\mathbf{U}}$ and $\mathbf{U}$ is calculated from the following equation [21]:

$$\cos^2\theta = \det^2(\mathbf{M}). \tag{10.99}$$

where

$$\mathbf{M} = \tilde{\mathbf{U}}^t\mathbf{U}. \tag{10.100}$$

In these relations, $\cos^2\theta \approx 1$ is an indication of similarity between the two eigenspaces. Referring to Table 10.6, it can be deduced that the mode shapes are obtained with reasonable approximations.

Comparing the run times for the two methods, it is obvious that in the case of this example (1,350 DOFs), the proposed method presents a 169-fold reduction in the workload.

In order to further investigate the efficiency of the proposed method in the analysis of large-scale structural models, more test cases are considered here for comparison. The base models are similar to Fig. 10.20a in general configurations but are different in the number of DOFs and dimensions. The support conditions are similar to those configured in Fig. 10.21.

Table 10.7 summarises all the cases considered here for calculation of the first 16 frequencies and mode shapes. Also presented in this table are the results for the two extreme natural periods of the obtained sequence calculated using the proposed method and the direct method. The proposed method was implemented using 60 master modes from the base models. Again, relative errors indicate that the estimated natural periods are within the acceptable tolerance. Figure 10.22 demonstrates CPU times required to accomplish the calculations, using the proposed method and the direct method. Referring to this figure, it can be argued that it is in average 63 times faster to use the proposed method to estimate a few frequencies and mode shapes of locally modified regular structures, if the results are considered acceptable within a 0.1 % tolerance.

10.4 Substructure Representation for Efficient Eigensolution of Regular Structures

An extensively investigated canonical form, for which decomposition methods both for graph and structural models are readily available now, is the block circulant form as discussed in Sect. 10.2.6. This form may be associated with *rotational regular* (RR) models. Structural and mechanical models having this type of regularity are also called rotational periodic or cyclic repeated structures. Different types of domes, space structures, cooling towers, pipes, blades and many others fall in this category. The general pattern of the matrices associated with a *rotational regular structure* (RRS) can be represented by (10.26). Yet, for another type of widespread regularity pattern observed in structural models, that is, the *translational regularity*, there has not been reported any general method of decomposition

Table 10.7 Test cases considered

N number of DOFs	T_1(sec)			T_{16}(sec)		
	Present method	Direct method	Relative error (%)	Present method	Direct method	Relative error (%)
405	0.089649413	0.08965344	0.004492	0.034740328	0.034746611	0.018084
900	0.148331364	0.148334766	0.002293	0.045631364	0.045714109	0.181004
1,350	0.166918203	0.166920087	0.001129	0.049730545	0.0497822	0.103761
1,998	0.218556893	0.218558488	0.000730	0.06150333	0.061557176	0.087474
2,646	0.322415076	0.322416958	0.000584	0.07302754	0.073081879	0.074353
3,834	0.419528925	0.419530885	0.000467	0.092386593	0.092445018	0.063200
3,960	0.431754283	0.431755896	0.000374	0.094488851	0.094539638	0.053720
5,112	0.543525801	0.543527426	0.000299	0.113638535	0.113690448	0.045662

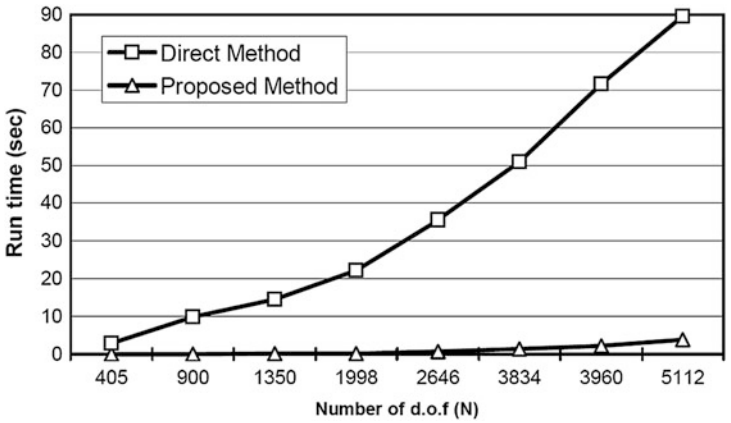

Fig. 10.22 Run time comparison for calculation of the first 16 eigenpairs

in the literature. *Translational regular structures* (TRS), also well known as linear periodic, are more frequently encountered in engineering structures such as frames, trusses, shells and other types of structural and mechanical models. Decomposition of the matrices associated with such models is entangled due to non-commuting pattern and the occurrence of inconsistent corner blocks at the corresponding canonical forms. This problem was discussed in Sect. 10.2.5 under the title "Generalised Form II". The general pattern of the matrices associated with a TRS can be given by Eq. 10.25.

It would be promising to try to relate the behaviour of a translational regular system to that of a rotational regular one, in order to take the computational advantages offered by the decomposable structure of the latter. For this purpose, the TRS can be represented as RRS using the established substructuring techniques. One such representation has been proposed by Garvey and Penny [22]. In this reference, a TRS is represented as an RRS by identifying the first and the last bay with each other and hence reducing the size of the model by the size of one bay.

Two classes of substructuring, that is, Kron's method [12] and Hurty method [16], have been employed for the solution of the resulting problem.

The representation provided by Garvey and Penny has two major shortcomings, so that it becomes inappropriate for the regular models considered in this chapter. First, the two ends of a TRS are identified (connected together) at nodal points, and in order for the representation to be correct, no overlapping of elements or nodal masses should be created in the identification process. The regular models studied here may not lead to an RRS, if represented in this way. Second, the substructure representation method proposed by Garvey and Penny does not reduce the resulting matrices, and hence, it is not obvious how much saving can be achieved in computational effort by using this method. Most of the structural applications require just a few lower eigenfrequencies and their corresponding modal vectors. Hence, it is essential for a substructuring technique to be able to reduce the size of the problem using suitable approximations, so that the required frequencies and mode shapes can be computed more efficiently and with acceptable accuracy.

In this section, a different substructure representation for TRS is proposed using a dual formulation. The dual formulation of general substructuring problem is due to Rixen [20]. Instead of using displacement constraints to identify the two ends of a TRS, the Lagrange multipliers or equivalently the interface forces are used to represent a TRS as a modification of its RR counterpart. The Lagrange multipliers are introduced as balancing forces to eliminate the effects of the imposed modifications. Using a dual description for substructure representation of TRS has the advantage that the response of the corresponding RRS including its natural modes and static response could be directly incorporated into a reduction basis. This basis is then used to reduce the dual system. The reduction is a key step in substructuring process and determines the efficiency of the proposed method.

10.4.1 Substructure Representation of TRS

The generalised eigenvalue problem for free vibration of a translational regular structure may be expressed as follows:

$$\mathbf{K}_{\mathrm{TR}}\mathbf{u} - \lambda\mathbf{M}_{\mathrm{TR}}\mathbf{u} = \mathbf{0}, \tag{10.101}$$

where $\mathbf{u}$ is the mode shape vector, λ the natural frequency squared and $\mathbf{K}_{\mathrm{TR}}$ and $\mathbf{M}_{\mathrm{TR}}$ of order *mn* are the stiffness and mass matrices, each having a block pattern similar to (10.25). This matrix pattern is associated with a TRS consisting of n sequential blocks each having m DOFs. As an example, consider a 2D truss shown in Fig 10.23a. In this example, $\mathrm{m} = 4$ and $\mathrm{n} = 5$. Now, to construct an RR representation, let us introduce artificial members as depicted in dashed lines in Fig. 10.23b to connect the nodes of the first and the last blocks. This manipulation is tantamount to modification of stiffness and mass matrices as follows:

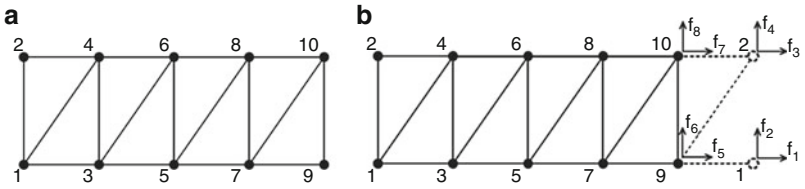

Fig. 10.23 (**a**) A TR structural model, (**b**) the RR representation

$$\mathbf{K}_{RR} = \mathbf{K}_{TR} + \mathbf{E}\Delta\ \mathbf{k}\ \mathbf{E}^t;\ \mathbf{M}_{RR} = \mathbf{M}_{TR} + \mathbf{E}\Delta\ \mathbf{m}\ \mathbf{E}^t. \tag{10.102}$$

The artificial modifications are performed in such a way that the resulting $\mathbf{K}_{RR}$ and $\mathbf{M}_{RR}$ matrices represent an RRS, having block patterns similar to (10.26). $\boldsymbol{\Delta}\mathbf{k}$ and $\boldsymbol{\Delta}\mathbf{m}$ are of order $2m$. $\mathbf{E}$ of order mn by $2m$ is a Boolean matrix of association between the set of $2m$ modified DOFs and mn base DOFs

$$\mathbf{E}^t = \begin{bmatrix} \mathbf{I}_m & \mathbf{0} & \mathbf{0} & \dots & \mathbf{0} \\ \mathbf{0} & \dots & \mathbf{0} & \mathbf{0} & \mathbf{I}_m \end{bmatrix}_{2m\times mn}. \tag{10.103}$$

Dynamic Equation (10.101) can still be satisfied with the modified matrices (10.102), introducing the vector of Lagrange multipliers $\mathbf{f}$ as follows:

$$\mathbf{K}_{RR}\mathbf{u} - \lambda\mathbf{M}_{RR}\mathbf{u} - \mathbf{E}\mathbf{f} = \mathbf{0}. \tag{10.104}$$

$\mathbf{f}$ is a $2m$ by 1 vector of the Lagrange multipliers or equivalently interface forces introduced at the modified nodes to balance the effects of the imposed modifications. Note that the eigenpairs (λ, $\mathbf{u}$) are the response parameters of the free vibrating TRS, and the fabricated RRS is forced by vector $\mathbf{f}$ to exhibit such a response. Hence, vector $\mathbf{f}$ is determined solely by the artificial modification imposed on the TRS. This can be demonstrated by the equation

$$\boldsymbol{\Delta}\mathbf{k}\mathbf{v} - \lambda\boldsymbol{\Delta}\mathbf{m}\mathbf{v} + \mathbf{f} = \mathbf{0}. \tag{10.105}$$

Compatibility is satisfied by

$$\begin{bmatrix} \mathbf{E}^t & -\mathbf{I}_{2n} \end{bmatrix} \begin{bmatrix} \mathbf{u} \\ \mathbf{v} \end{bmatrix} = \mathbf{0}. \tag{10.106}$$

Putting the set of Eqs. 10.104, 10.105, and 10.106 altogether, the system equation can be assembled in the following block form:

$$\begin{bmatrix} \mathbf{K}_{RR} & \mathbf{0} & \mathbf{E} \\ \mathbf{0} & -\boldsymbol{\Delta}\mathbf{k} & -\mathbf{I} \\ \mathbf{E}^t & -\mathbf{I} & \mathbf{0} \end{bmatrix} \begin{bmatrix} \mathbf{u} \\ \mathbf{v} \\ \mathbf{f} \end{bmatrix} - \lambda \begin{bmatrix} \mathbf{M}_{RR} & & \mathbf{0} \\ & -\boldsymbol{\Delta}\mathbf{m} & \\ \mathbf{0} & & \mathbf{0} \end{bmatrix} \begin{bmatrix} \mathbf{u} \\ \mathbf{v} \\ \mathbf{f} \end{bmatrix} = \mathbf{0}. \tag{10.107}$$

The order of the assembled system (10.107) is $mn + 4m$ and has for general solution mn eigenvalues λ, discarding $4m$ infinite eigenvalues introduced due to redundancy of the system equations. The order of the system should be reduced using appropriate approximations, to facilitate efficient calculation of a few requested lower eigenpairs.

10.4.2 Modal Truncation

As mentioned before, matrices associated with an RRS can be decomposed by transforming them into block-diagonal forms. Decomposition procedure involves the construction of an orthogonal matrix $\mathbf{T}$, such that

$$\mathbf{K}^{(\mathrm{BD})} = \mathbf{T}^{\mathrm{t}}\mathbf{K}_{\mathrm{RR}}\mathbf{T} \text{ and } \mathbf{M}^{(\mathrm{BD})} = \mathbf{T}^{\mathrm{t}}\mathbf{M}_{\mathrm{RR}}\mathbf{T}, \tag{10.108}$$

each have the same block-diagonal form.

Using such a transformation, the analysis of an RRS can be reduced to several smaller decoupled subproblems. The response of the system is then obtained much more easily and quickly by solving the reduced subsystems.

The procedure for reducing the eigenproblem (10.107) associated with a TRS is much the same as the one employed in the previous section for the modified regular structures. Let $\mathbf{\Phi}$ denote the matrix of $\mathbf{M}_{\mathrm{RR}}$-orthonormal eigenvectors and $\mathbf{\Lambda}$ be the diagonal matrix of eigenvalues of the RRS. Hence, the following relations hold:

$$\mathbf{\Phi}^{\mathrm{t}}\mathbf{K}_{\mathrm{RR}}\mathbf{\Phi} = \mathbf{\Lambda} \text{ and } \mathbf{\Phi}^{\mathrm{t}}\mathbf{M}_{\mathrm{RR}}\mathbf{\Phi} = \mathbf{I}. \tag{10.109}$$

Let us define a cut-off eigenvalue λ_{c} and suppose that we are interested in those eigenvalues λ of Eq. 10.101 or the equivalent assemblage (10.107), such that

$$\lambda << \lambda_{\mathrm{c}}. \tag{10.110}$$

Now, partition $\mathbf{\Lambda}$ into the lower and higher eigenvalues based on the cut-off value λ_{c} as

$$\mathbf{\Lambda} = \begin{bmatrix} \mathbf{\Lambda}_{\mathrm{l}} & \\ & \mathbf{\Lambda}_{\mathrm{h}} \end{bmatrix}, \tag{10.111}$$

where $\mathbf{\Lambda}_{\mathrm{l}}$ is the set of eigenvalues less than λ_{c} and $\mathbf{\Lambda}_{\mathrm{h}}$ is the set of eigenvalues greater than or equal to λ_{c}. Let the corresponding partitioning of $\mathbf{\Phi}$ be

$$\mathbf{\Phi} = [\,\mathbf{\Phi}_{\mathrm{l}} \quad \mathbf{\Phi}_{\mathrm{h}}\,]. \tag{10.112}$$

Using modal coordinates $\mathbf{q}$ defined by

$$\mathbf{u} = \mathbf{\Phi}_{\mathrm{l}}\mathbf{q}_{\mathrm{l}} + \mathbf{\Phi}_{\mathrm{h}}\mathbf{q}_{\mathrm{h}}, \tag{10.113}$$

and premultiplying Eq. 10.104 by $\mathbf{\Phi}_{\mathrm{h}}^{\mathrm{t}}$, it follows:

$$\mathbf{\Lambda}_{\mathrm{h}}\mathbf{q}_{\mathrm{h}} - \lambda\mathbf{q}_{\mathrm{h}} + \mathbf{\Phi}_{\mathrm{h}}^{\mathrm{t}}\mathbf{E}\mathbf{f} = \mathbf{0}. \tag{10.114}$$

Premultiplying Eq. 10.114 by $\mathbf{\Lambda}_{\mathrm{h}}^{-1}$ and putting $\lambda\mathbf{\Lambda}_{\mathrm{h}}^{-1} \approx \mathbf{0}$ due to the assumption (10.110), we arrive at

$$\mathbf{q}_{\mathrm{h}} \cong -{\mathbf{\Lambda}_{\mathrm{h}}}^{-1}\,\mathbf{\Phi}_{\mathrm{h}}^{\mathrm{t}}\,\mathbf{E}\,\mathbf{f}. \tag{10.115}$$

Substituting into Eq. 10.113 from Eq. 10.115, we obtain the following approximation for vector **u:**

$$\mathbf{u} \cong \mathbf{\Phi}_{\mathrm{l}}\mathbf{q}_{\mathrm{l}} - \mathbf{G}_{\mathrm{res}}\mathbf{E}\mathbf{f}, \tag{10.116}$$

where

$$\mathbf{G}_{\mathrm{res}} = \mathbf{\Phi}_{\mathrm{h}}\mathbf{\Lambda}_{\mathrm{h}}^{-1}\mathbf{\Phi}_{\mathrm{h}}^{\mathrm{t}} \tag{10.117}$$

is the residual flexibility of the RR model.

In summary, we construct the following approximation of the coordinate vectors and the Lagrange multipliers for the reduction of eigenproblem (10.107):

$$\begin{bmatrix}\mathbf{u}\\ \mathbf{v}\\ \mathbf{f}\end{bmatrix} \cong \mathbf{T}_{\mathrm{dual}}\begin{bmatrix}\mathbf{q_l}\\ \mathbf{v}\\ \mathbf{f}\end{bmatrix} = \begin{bmatrix}\mathbf{\Phi}_{\mathrm{l}} & \mathbf{0} & -\mathbf{G}_{\mathrm{res}}\mathbf{E}\\ \mathbf{0} & \mathbf{I} & \mathbf{0}\\ \mathbf{0} & \mathbf{0} & \mathbf{I}\end{bmatrix}\begin{bmatrix}\mathbf{q_l}\\ \mathbf{v}\\ \mathbf{f}\end{bmatrix}. \tag{10.118}$$

10.4.3 Reduced Eigenproblem

Using the approximation (10.118), we will reduce the assembled system (10.107). First, notice the following properties of the residual flexibility matrix:

$$\begin{aligned}&\mathbf{G}_{\mathrm{res}}^{\mathrm{t}} = \mathbf{G}_{\mathrm{res}}, \quad \mathbf{G}_{\mathrm{res}}\mathbf{K}_{\mathrm{RR}}\mathbf{G}_{\mathrm{res}} = \mathbf{G}_{\mathrm{res}},\\ &\mathbf{\Phi}_{\mathrm{l}}^{\mathrm{t}}\mathbf{K}_{\mathrm{RR}}\mathbf{G}_{\mathrm{res}} = \mathbf{0}, \quad \mathbf{\Phi}_{\mathrm{l}}^{\mathrm{t}}\mathbf{M}_{\mathrm{RR}}\mathbf{G}_{\mathrm{res}} = \mathbf{0}.\end{aligned} \tag{10.119}$$

The reduced eigenproblem of the modified regular structure is then obtained by using transformation (10.118) as

$$\tilde{\mathbf{K}}\begin{bmatrix}\mathbf{q}_l\\ \mathbf{v}\\ \mathbf{f}\end{bmatrix} - \lambda\tilde{\mathbf{M}}\begin{bmatrix}\mathbf{q}_l\\ \mathbf{v}\\ \mathbf{f}\end{bmatrix} = \mathbf{0}, \tag{10.120}$$

with the reduced matrices

$$\tilde{\mathbf{K}} = \begin{bmatrix}\boldsymbol{\Lambda}_l & \mathbf{0} & \boldsymbol{\Phi}_l^t\mathbf{E}\\ \mathbf{0} & -\Delta\mathbf{k} & -\mathbf{I}\\ \mathbf{E}^t\boldsymbol{\Phi}_l & -\mathbf{I} & \mathbf{F}_{\text{res}}\end{bmatrix} \text{ and } \mathbf{M} = \begin{bmatrix}\mathbf{I} & & \mathbf{0}\\ & -\Delta\mathbf{m} & \\ \mathbf{0} & & \mathbf{M}_{\text{res}}\end{bmatrix}, \tag{10.121}$$

where

$$\mathbf{F}_{\text{res}} = -\mathbf{E}^t\mathbf{G}_{\text{res}}\mathbf{E}, \quad \mathbf{M}_{\text{res}} = \mathbf{E}^t\mathbf{G}_{\text{res}}\mathbf{M}_{\text{RR}}\mathbf{G}_{\text{res}}\mathbf{E}. \tag{10.122}$$

$\boldsymbol{\Lambda}_l$ and $\boldsymbol{\Phi}_l$ correspond to the calculated eigenvalues and eigenmodes of the RRS. $\boldsymbol{\Phi}_l$ is also called the *master* modes. These include rigid-body modes of the RRS if they are present. Hence, $\boldsymbol{\Lambda}_l$ may contain zero eigenvalues corresponding to rigid-body modes. The calculations differ in constructing the residual flexibility matrix, with or without the presence of rigid-body modes.

10.4.4 Evaluation of the Residual Flexibility Matrix

In general case, stiffness matrix $\mathbf{K}_{\text{RR}}$ of the rotational regular model may be positive semi-definite. The residual flexibility $\mathbf{G}_{\text{res}}$ may be evaluated for positive-definite and positive semi-definite $\mathbf{K}_{\text{RR}}$ using a procedure similar to that outlined in Sect. 10.3.2.4.

10.4.5 Numerical Experiments

Example 10.6. Consider the regular graph model shown in Fig. 10.24a. The Laplacian matrix of this graph has the following block form:

$$\mathbf{L}_{\text{TR}} = \begin{bmatrix}\mathbf{C} & \mathbf{B} & & & & \\ \mathbf{B}^t & \mathbf{A} & \mathbf{B} & & & \\ & \ddots & \ddots & \ddots & & \\ & & \mathbf{B}^t & \mathbf{A} & \mathbf{B} & \\ & & & \mathbf{B}^t & \mathbf{D} & \end{bmatrix}_{20\times 20}.$$

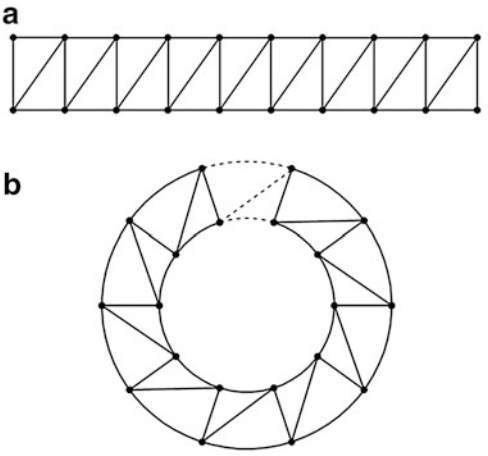

Fig. 10.24 (**a**) A TR graph model, (**b**) the RR representation

It consists of 10 diagonal 2-by-2 blocks with the following submatrices:

$$\mathbf{A} = \begin{bmatrix} 4 & -1 \\ -1 & 4 \end{bmatrix}, \ \mathbf{B} = \begin{bmatrix} -1 & 0 \\ -1 & -1 \end{bmatrix}, \ \mathbf{C} = \begin{bmatrix} 2 & -1 \\ -1 & 3 \end{bmatrix}, \ \mathbf{D} = \begin{bmatrix} 3 & -1 \\ -1 & 2 \end{bmatrix}.$$

The aim is to estimate the first non-zero eigenvalue of the Laplacian matrix using the proposed method and compare the accuracy of the result with a direct method of solution. In Fig. 10.24b, a rotationally regular representation of the graph model is constructed by adding some artificial elements depicted in dashed lines. The corresponding modification to Laplacian $\mathbf{L}_{\mathrm{TR}}$ is defined by

$$\mathbf{L}_{\mathrm{RR}} = \mathbf{L}_{\mathrm{TR}} + \mathbf{E}\Delta\mathbf{L}\mathbf{E}^{\mathrm{t}},$$

with the following submatrix:

$$\Delta\mathbf{L} = \begin{bmatrix} \mathbf{A} - \mathbf{C} & \mathbf{B}^{\mathrm{t}} \\ \mathbf{B} & \mathbf{A} - \mathbf{D} \end{bmatrix}.$$

The first step of solution by the proposed method is to obtain necessary information from the rotational regular model, taking the advantage of its block-diagonalised Laplacian matrix. This information includes a few eigenvalues and eigenvectors together with a linear solution to get $\mathbf{G}_{\mathrm{res}}\mathbf{E}$ using the procedure discussed in Sect. 10.4.4. In Table 10.8, some of the eigenvalues obtained from the RR model are presented.

The next step is to solve the reduced eigenproblem (10.120) with the following matrices:

Table 10.8 Some eigenvalues of the RR model – Example 10.6

Index	Eingenvalue
1	0.000000
2	0.479853
3	0.479853
4	1.763932
5	1.763932
6	3.442463
7	3.442463

Table 10.9 Comparison of the results for Example 10.6

	λ_2		
Number of master modes	Present method	Direct method	Relative error (%)
3	0.123795	0.122312	1.212135
5	0.122830	0.122312	0.422924
7	0.122612	0.122312	0.245107

$$\tilde{\mathbf{K}} = \begin{bmatrix} \mathbf{\Lambda}_l & \mathbf{0} & \mathbf{\Phi}_l^t\mathbf{E} \\ \mathbf{0} & -\Delta\mathbf{L} & -\mathbf{I} \\ \mathbf{E}^t\mathbf{\Phi}_l & -\mathbf{I} & -\mathbf{E}\mathbf{G}_{res}\mathbf{E} \end{bmatrix} \text{ and } \tilde{\mathbf{M}} = \begin{bmatrix} \mathbf{I} & & \mathbf{0} \\ & \mathbf{0} & \\ \mathbf{0} & & \mathbf{E}^t\mathbf{G}_{res}\mathbf{G}_{res}\mathbf{E} \end{bmatrix},$$

in order to estimate the requested eigenvalues for the TR model. This problem is solved using different number of eigenpairs $\mathbf{\Lambda}_l$ and $\mathbf{\Phi}_l$ from the RR model, and the first non-zero eigenvalue (λ_2) is obtained as shown in Table 10.9. It is observed that the accuracy of the result is improved by increasing the number of contributing master modes.

Note that the relative error of an estimated eigenvalue is proportional to the ratio of that eigenvalue to the cut-off value [22]. The cut-off value is the lower eigenvalue in the set $\mathbf{\Lambda}_h$. In this example, λ_2 is estimated with about 0.25 % error, using seven master modes. The cut-off value for this case is the 7th eigenvalue of the RR model (3.442463, from Table 10.8). Hence, the relative error is proportional to $0.122312/3.442463 = 0.0355$. The accuracy may be considered as satisfactory; however, better approximations can be obtained for large-scale problems as demonstrated in the following examples.

Example 10.7. A translational regular model of a two-dimensional truss is considered for free vibration analysis, as shown in Fig. 10.25. The structure is composed of pin-jointed steel bar elements having cross-sectional area $a = 16.01$ cm^2. The elastic modulus is $E = 2.1 \times 10^{11}$ N/m^2. Horizontal elements are 1 m in length, and vertical elements have a length of 1.2 m. The structure is clamped at the two ends. For simplicity, the mass of the structure is assumed to be concentrated at the nodal points, with a magnitude of 800 kg at each node. Each node of the structure has two translational DOFs, and hence, the total degree of freedom for the structure is 72.

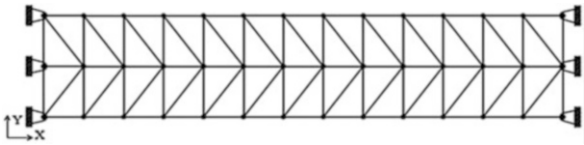

Fig. 10.25 A TR truss model

The stiffness matrix can be written in the following canonical form:

$$\mathbf{K}_{\mathrm{TR}} = \begin{bmatrix} \mathbf{A} & \mathbf{B} & & & & \\ \mathbf{B}^{\mathrm{t}} & \mathbf{A} & \mathbf{B} & & & \\ & \ddots & \ddots & \ddots & & \\ & & \mathbf{B}^{\mathrm{t}} & \mathbf{A} & \mathbf{B} & \\ & & & \mathbf{B}^{\mathrm{t}} & \mathbf{A} & \end{bmatrix}_{72\times 72}$$

The blocks of the matrix are 6 by 6 each, and there are a total of 12 blocks on the diagonal. The necessary modification to the stiffness matrix in order to represent an RR model is given by

$$\Delta\mathbf{k} = \begin{bmatrix} \mathbf{0} & \mathbf{B}^{\mathrm{t}} \\ \mathbf{B} & \mathbf{0} \end{bmatrix}_{12\times 12}.$$

The mass matrix is diagonal and does not require any modification. The resulting stiffness matrix associated with RR representation, has the following pattern:

$$\mathbf{K}_{\mathrm{RR}} = \begin{bmatrix} \mathbf{A} & \mathbf{B} & & & & \mathbf{B}^{\mathrm{t}} \\ \mathbf{B}^{\mathrm{t}} & \mathbf{A} & \mathbf{B} & & & \\ & \ddots & \ddots & \ddots & & \\ & & \mathbf{B}^{\mathrm{t}} & \mathbf{A} & \mathbf{B} & \\ \mathbf{B} & & & \mathbf{B}^{\mathrm{t}} & \mathbf{A} & \end{bmatrix}_{72\times 72}.$$

The eigenproblem associated with free vibration of the RR model is easily solved using matrix decomposition to obtain different numbers of required eigenvectors as the master modes of RR structure. The associated isostatic modes are also obtained using the procedure discussed in Sect. 10.4.4. Then, this information is utilised to form the reduced matrices in Eq. 10.121 using different number of master modes. The reduced problem in Eq. 10.120 is solved in each case to obtain four natural periods and mode shapes of the initial TR structure. The natural mode shapes are shown in Fig. 10.26.

The results of the analysis by the proposed method employing 7, 12 and 16 master modes are compared with a direct sparse eigensolver of the MATLAB software in Table 10.10. It is demonstrated in Fig. 10.27 that very satisfactory results can be obtained using adequate number of master modes. According to this

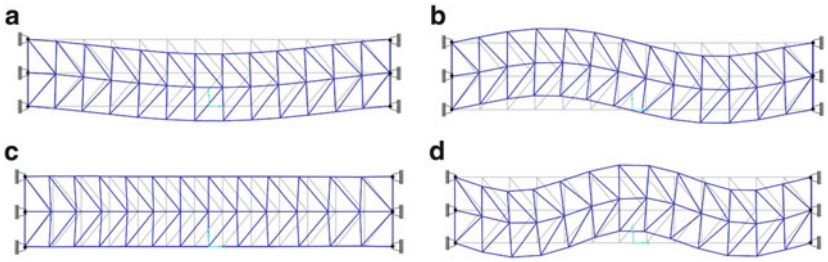

Fig. 10.26 Natural modes of the TRS, (**a**) first, (**b**) second, (**c**) third and (**d**) fourth mode

Table 10.10 Comparison of the natural periods and mode shapes – Example 10.7

		Mode number			
		1	2	3	4
Direct method	T(sec)	0.123632941	0.059508732	0.040227673	0.037383425
Present method with seven master modes	T(sec)	0.123632008	0.059499666	0.039706865	0.037339264
	Relative error (%)	0.000754	0.015235	1.294650	0.118130
	Mode shape error	3.9E-06	1.1E-05	1.8E-05	1.2E-05
Present method with 12 master modes	T(sec)	0.123632645	0.059501690	0.040219806	0.037376774
	Relative error (%)	0.000239	0.011835	0.019555	0.017791
	Mode shape error	1.2E-06	1.6E-06	3.6E-06	2.0E-06
Present method with 16 master modes	T(sec)	0.123632874	0.059507609	0.040219806	0.037382283
	Relative error (%)	0.000054	0.001887	0.019555	0.003053
	Mode shape error	2.9E-08	1.1E-07	6.5E-07	3.5E-07

graph, using 12 and 16 master modes, all the four natural periods are estimated with a relative error well below 0.1 %, which is a sufficient accuracy for usual engineering applications.

The mode shape errors are also reported in Table 10.10. It is concluded that the obtained mode shapes are very satisfactory.

Example 10.8. Consider a square prismatic truss structure, shown in Fig. 10.28a. Horizontal and vertical members are 1 m and 0.5 m long, respectively. Members are made of steel with a mass density of $\rho = 8.7 \times 10^3$ kg/m^3 and the modulus of elasticity $E = 2.0 \times 10^{11}$ Pa. Each member has a cross-sectional area: $A = 9.14$ cm^2. Total height of structure is 10.5 m. Each node of the structure

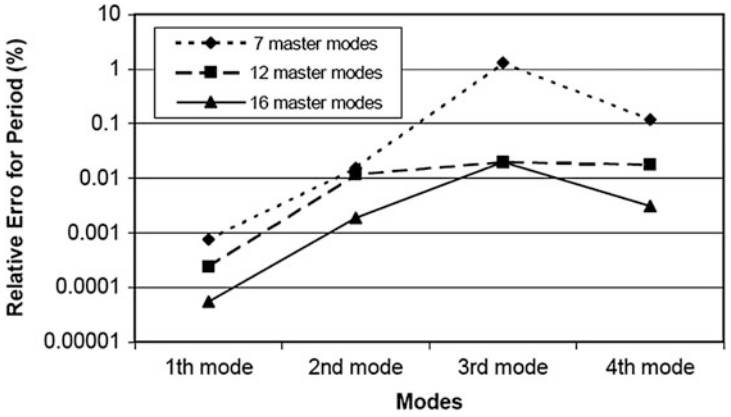

Fig. 10.27 Relative errors of estimated natural periods

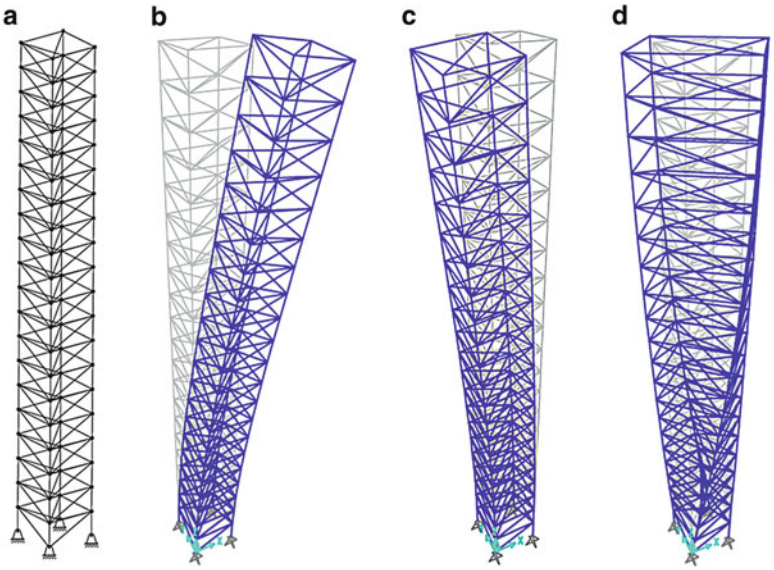

Fig. 10.28 (**a**) A translationally regular truss, (**b**) first, (**c**) second and (**d**) third natural modes of vibration

has three translational DOFs, and the total number of DOFs for the structure amounts to 252. The structure vibrates under its own mass. Three natural periods and mode shapes of the structure are sought. A lumped mass approach is taken for evaluation of the mass matrix. Stiffness and mass matrices have the following canonical forms:

$$\mathbf{K}_{TR} = \begin{bmatrix} \mathbf{A} & \mathbf{B} & & & \\ \mathbf{B}^t & \mathbf{A} & \mathbf{B} & & \\ & \ddots & \ddots & \ddots & \\ & & \mathbf{B}^t & \mathbf{A} & \mathbf{B} \\ & & & \mathbf{B}^t & \mathbf{C} \end{bmatrix}_{252\times252}, \quad \mathbf{M}_{TR} = \begin{bmatrix} \mathbf{m} & & & & \\ & \mathbf{m} & & & \\ & \ddots & \ddots & \ddots & \\ & & & \mathbf{m} & \\ & & & & \bar{\mathbf{m}} \end{bmatrix}_{252\times252}$$

The block submatrices are 12 by 12 each, and 21 such blocks are present on the diagonals of each stiffness and mass matrix.

Necessary modifications to stiffness and mass matrices are imposed by using the following submatrices:

$$\Delta\mathbf{k} = \begin{bmatrix} \mathbf{0} & \mathbf{B}^t \\ \mathbf{B} & \mathbf{A}-\mathbf{C} \end{bmatrix}_{24\times24}, \quad \Delta\mathbf{m} = \begin{bmatrix} \mathbf{0} & \mathbf{0} \\ \mathbf{0} & \mathbf{m}-\bar{\mathbf{m}} \end{bmatrix}_{24\times24},$$

in order to turn the TRS into an RRS which has associated stiffness and mass matrices with the following patterns:

$$\mathbf{K}_{RR} = \begin{bmatrix} \mathbf{A} & \mathbf{B} & & & \mathbf{B}^t \\ \mathbf{B}^t & \mathbf{A} & \mathbf{B} & & \\ & \ddots & \ddots & \ddots & \\ & & \mathbf{B}^t & \mathbf{A} & \mathbf{B} \\ \mathbf{B} & & & \mathbf{B}^t & \mathbf{A} \end{bmatrix}_{252\times252}, \quad \mathbf{M}_{RR} = \begin{bmatrix} \mathbf{m} & & & & \\ & \mathbf{m} & & & \\ & \ddots & \ddots & \ddots & \\ & & & \mathbf{m} & \\ & & & & \mathbf{m} \end{bmatrix}_{252\times252}$$

Table 10.11 summarises the results for the three natural periods obtained from the direct method and the proposed method with 7, 12 and 16 master modes form the RRS. The accuracy of the mode shapes is also examined using Eq. 10.98. These mode shapes are depicted in Fig. 10.28b–d. Calculations are performed at double-precision arithmetic and on a computer with Intel® Core ™2 Duo CPU 2.33 GHz and 2 GB of RAM, which was running Microsoft Windows XP Professional Service Pack 3.

With reference to Table 10.11, it is observed that satisfactory approximations are obtained for both natural periods and mode shapes of the TRS using the proposed method. One can conclude that using 16 master modes (about five times the required number of natural modes), the periods are estimated with less than 0.01 % error, indicating that the accuracy of the obtained results is very satisfactory.

The CPU times required to accomplish the calculations using the proposed method and the direct method using a sparse eigensolver of MATLAB software are also presented in this table. The time spent by the present method is slightly increased with the incorporation of more master modes. However, the time savings are remarkable compared with the direct method. It can be argued that the present method in the worst case performs nearly 40 times faster than the direct method to estimate a few natural periods and mode shapes of the regular structure, with an acceptable approximation.

Table 10.11 Comparison of the natural periods and mode shapes – Example 10.8

	Mode number		
	1	2	3
Direct method			
T(sec)	0.213472734	0.196085485	0.062959495
CPU time (sec)	4.168		
Present method with seven master modes			
T(sec)	0.213387095	0.19602602	0.06292555
Relative error (%)	0.040117	0.030326	0.053910
Mode shape error	4.7E-06	1.0E-05	5.8E-05
CPU time (sec)	0.0671		
Present method with 12 master modes			
T(sec)	0.213447395	0.196061943	0.06294718
Relative error (%)	0.011870	0.012006	0.019555
Mode shape error	1.3E-06	7.2E-06	2.4E-05
CPU time (sec)	0.0825		
Present method with 16 master modes			
T(sec)	0.213470313	0.196079557	0.06295474
Relative error (%)	0.001134	0.003023	0.007546
Mode shape error	6.9E-07	1.8E-06	5.6E-06
CPU time (sec)	0.105		

References

1. Armstrong MA (1988) Groups and symmetry. Springer, Berlin
2. Kaveh A, Fazli H (2010) Eigensolution of augmented graph products using shifted inverse iteration method. Int J Numer Methods Eng 83:558–574
3. Kaveh A, Fazli H (2010) Eigensolution of locally modified regular structures using shifted inverse iteration method. In: Topping BHV, Adam JM, Pallarés FJ, Bru R, Romero ML (eds) Proceedings of the 10th international conference on computational structural technology, Valencia
4. Kaveh A, Fazli H (2011) Approximate eigensolution of locally modified regular structures using a substructuring technique. Comput Struct 89:529–537
5. Parlett BN (1988) The symmetric eigenvalue problem. Prentice-Hall Inc, Englewood Cliffs
6. Bendiksen OO (1987) Mode localization phenomena in large space structures. AIAA J 25:1241–1248
7. Wang BP, Pilkey WD (1986) Eigenvalue reanalysis of locally modified structures using a generalized Rayleigh's method. AIAA J 24:983–990
8. Golub GH (1973) Some modified matrix eigenvalue problems. SIAM Rev 15:318–334
9. Arbenz P, Golub GH (1988) On the spectral decomposition of Hermitian matrices modified by low rank perturbations with applications. SIAM J Matrix Anal Appl 9:40–58
10. Carey MM, Golub GH, Law KH (1994) A Lanczos-based method for structural dynamic reanalysis problems. Int J Numer Methods Eng 7:2857–2883
11. Lui SH (2000) Domain decomposition methods for eigenvalue problems. J Comput Appl Math 117:17–34
12. Kron G (1957–1959) Diakoptics piecewise solution of large-scale systems. A series of chapters in the Electrical Journal, London
13. Lui SH (1998) Kron's method for symmetric eigenvalue problems. J Comput Appl Math 98:35–48

14. Sehmi NS (1986) Lanczos algorithm applied to Kron's method. Int J Numer Methods Eng 23:1857–1872
15. Weng S, Xia Y, Xu YL, Zhou XQ, Zhu HP (2009) Improved substructuring method for eigensolutions of large-scale structures. J Sound Vib 3:718–736
16. Hurty WC (1965) Dynamic analysis of structural systems using component modes. AIAA J 3:678–685
17. Craig RJ, Bampton M (1968) Coupling of substructures for dynamic analyses. AIAA J 6:1313–1319
18. MacNeal RH (1971) A hybrid method of component mode synthesis. Comput Struct 1:581–601
19. Rozenblum G (1985) Modal synthesis: generalization of MacNeal's method; theoretical basis. Comput Meth Appl Mech Eng 48:139–154
20. Rixen DJ (2004) A dual Craig-Bampton method for dynamic substructuring. J Comput Appl Math 168:383–391
21. Gunawan H, Neswan O, Budhi WS (2005) A formula for angles between subspaces of inner product spaces. Contrib Algebra Geom 46:311–320
22. Garvey SD, Penny JE (1994) Representing periodic structures efficiently as substructures. J Sound Vib 178:79–94

Chapter 11
Group Theory and Applications in Structural Mechanics

11.1 Introduction

Group theory is known as the mathematical language of the symmetry, and the representation theory is the powerful means of group theory in analysis of physical problems. Methods are available for studying symmetry in science and engineering using the theory of groups, Stiefel and Fässler [1] and Boardman et al. [2]. Methods for symmetry analysis of physical systems are developed in crystallogy and quantum mechanics for decomposing the problems of complicated symmetric systems. Although in structural mechanics, such techniques have not been introduced as much as in other fields of science, the method has been successfully utilised in different cases. Zingoni [3, 4] has studied the application of group theory in bifurcation problems, dynamic problems and in finite element method. Application of the group theory in the force method of structural analysis can be found in the joint work of Zingoni et al. [5]. Healy and Treacy [6] have developed innovative methods by combination of symmetry properties of structures with repeated substructures and the group theoretic method. Kaveh and Nikbakht have implemented methods based on group theory for decomposition of the problems of topological graphs [7], vibration analysis of simple dynamic systems [8] and the stability analysis of symmetric frames with simple forms of symmetry [9, 10].

This chapter consists of the following two parts:

In the first part basic concepts of symmetry, regularity, symmetry groups and representation theory are provided.

In the second part, the properties of structures having symmetry forms are studied. Physical interpretation for the mathematical subproblems resulted in the process of decomposition is found. This enables one to examine the new physical systems in order to find a potential for further decomposition. For this purpose, first a swift review of the methods developed in previous works is presented and then the extension of such techniques for more complicated problems is studied. The problems with subsystems having new symmetric properties are considered, and a method for finding such new symmetry properties in these systems is presented.

A. Kaveh, *Optimal Analysis of Structures by Concepts of Symmetry and Regularity*,
DOI 10.1007/978-3-7091-1565-7_11, © Springer-Verlag Wien 2013

In the third part, a methodology is developed for efficient calculation of buckling loads for frame structures having high-order symmetry properties in order to reduce the size of their associated eigenvalue problems. This is achieved by decomposing the second-order stiffness matrix of a symmetric model into submatrices using representation of its symmetry group, via a step-by-step approach. The physical interpretation of the resulted submatrices is shown as substructures (factors), and the possibility of further decomposition is then investigated for each of the constructed submodels. Due to the similarity transformation, the constructed submatrices contain the eigenvalues of the main structural matrix. The buckling load of the entire structure is obtained by calculating the buckling loads of its factors. The methods of the present chapter provide a mathematical foundation and a logical means to deal with symmetry, in place of looking for various boundary conditions to be imposed for symmetric structures, as in the traditional methods. Examples are provided to illustrate the simplicity and efficiency of the present method [10].

11.2 Basic Concepts of Symmetry Groups and Representation Theory

11.2.1 Definition of a Group

A group is a set G together with a multiplication on G which satisfies three axioms:

1. The multiplication is associative, that is to say $(xy)z = x(yz)$ for any three (not necessarily distinct) elements from G.
2. There is an element e in G, called an identity element, such that $xe = x = ex$ for every x in G.
3. Each element x of G has an (so-called) inverse x^{-1} which belongs to the set G and satisfies $x^{-1}x = e = xx^{-1}$.

The *order* of G is the number of its elements; element 'e' in the above definition is called *identity* element, and x^{-1} is said to be the *inverse* of element x. If $xy = yx$ for any two elements x and y of the group G, then G is called an *abelian group*.

A *subgroup* of a group G is a subset of G, which itself forms a group under the multiplication of G.

11.2.2 Classes of a Group

If x and g are two elements of a group G, then $g^{-1}xg$ will definitely be a member of G. Let us call this element as y. Thus, $y = g^{-1}xg$.

This relation is expressed in the words by saying that y is a *similarity transformation* of x by g. It is also said that x and y are *conjugate*. Conjugate elements have a number of important properties: every element is conjugate with itself; if x is conjugate with y, then y is conjugate with x; if x is conjugate with y and z, then y and z will be conjugate with each other. A complete set of elements that are conjugate with each other is called a *class* of the group.

11.2.3 Symmetry and Symmetry Operations

The symmetry of a body is described by introducing the set of all those transformations which preserve the distance between all pairs of points of the body and maps the body into coincidence with itself; either the result of the transformation is equivalent or it is identical with the primary arrangement. Each of these transformations is called a *symmetry operation* of the body, which can be in one of the following forms:

1. Proper rotation about an axis of symmetry (C_n), in which the angle of rotation is $\theta = \frac{2\pi}{n}$. If there is more than one axis of symmetry for the object, the axis associated with the largest value of n – or the smallest value of θ – is called *principal axis*.
2. Reflection in planes of symmetry (σ_l), in which l connotes to the type of symmetry plane:
   - If the plane is perpendicular to the principal axis, it is called *horizontal plane* (σ_h).
   - If the plane encompasses the principal axis, it is called *vertical plane* (σ_v).
   - If the plane consists of principal axis and passes through the bisector of the angle between two C_2 axes perpendicular to the principal axis, it is called *dihedral plane* (σ_d).
3. Rotation reflection or improper rotation, which is denoted by S_n, represents a rotation through an angle $\frac{2\pi}{n}$ about an improper axis, followed by a reflection in the plane perpendicular to the axis of rotation. It is pointed out that this operation is significant when each of the rotation and reflection are not individually among the symmetry operations of the object.
4. Inversion through the centre of symmetry which is a special case of S_n with $n = 2$, is denoted by (i).
5. Identical symmetry (e), which maps an arbitrary object into itself, is one of the symmetry operations of any given object, either symmetric or asymmetric.

A number of symmetric skeletal structures and their symmetry operators are depicted in Fig. 11.1. The interpretation of principal axis is simply shown in the grid of Fig. 11.1a, where there are two C_2 axes and one C_4 axis. Based on the above definitions, the latter will be the principal axis of the structure. The symmetry centre

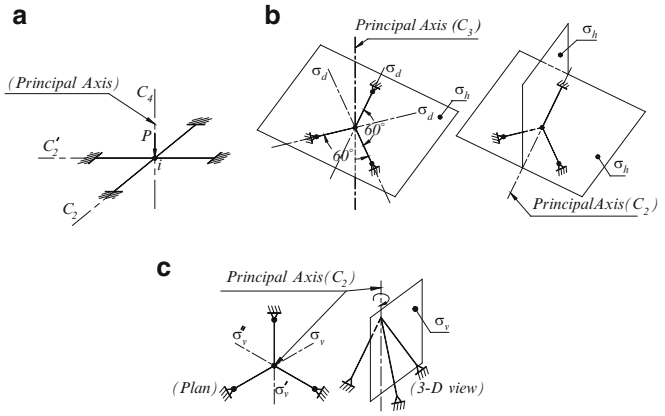

Fig. 11.1 Symmetric skeletal structures and their symmetry operators. (**a**) A grid. (**b**) Planar frames. (**c**) A 3-D frame

of this grid is joint 'i'. The concept of different kinds of symmetry planes can be recognised from the planar frames of Fig. 11.1b and the three-dimensional frame of Fig. 11.1c.

11.2.4 Symmetry Group

Symmetry operations of an object under the combination of transformation operations comprise a group, which is called a *symmetry group*. Symmetry groups are classified based on symmetry operations which make a group up. Figure 11.2 shows some symmetric structures and their symmetry groups. The symmetry group of a finite body is sometimes referred to as the *point group*. There are several methods for categorising the point groups. In Fig. 11.2, the point groups are named based on *Schoenflies method* – which is more conventional than the other approaches. The procedure of this method can be widely found in literature [11, 12]. This method will be utilised in this chapter.

11.2.5 Representation Theory

If a group T of linear operators $\widehat{T}_{gi}$ in a space R^n is *homomorphic* to finite group G with elements $g_1, g_2, \ldots, g_m$ (i.e. to each g_i, there correspond a number of operators

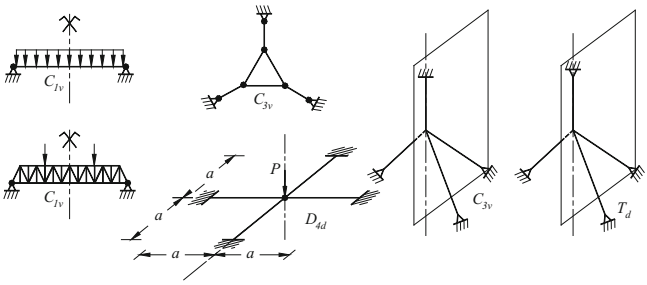

Fig. 11.2 Symmetry groups associated with some symmetrical structures

$(\widehat{T}_{gi})$ but to each operator $\widehat{T}_{gi}$, there corresponds only one definite element g_i, and moreover, this correspondence is preserved under group multiplication), then the group T is said to form a *representation* of G. The effect of any operator $\widehat{T}_{gi}$ on each of the unit vectors **e** of the space R^n can be shown as follows:

$$\hat{T}_{gi}.e = \sum_{r=1}^{n} D_{rk}(g_i) \; . \; e_r \tag{11.1}$$

It is clear that to each element g_i of the group G, a matrix $\mathbf{D}(g_i)$ can be assigned. The unit element of the group is associated with the unit matrix **I**, and the inverse elements are associated with inverse matrices. It can be easily shown that

$$\mathbf{D}(g_i) \; .\mathbf{D}(g_j) = \mathbf{D}(g_i g_j) \tag{11.2}$$

Therefore, it is possible to say that the matrices $\mathbf{D}(g_i)$ form a representation of order n of the group G. The trace of the matrix $\mathbf{D}(g_i)$ is known as the *character* of g_i, denoted by $\chi(g_i)$. The space R^n is the representation space, and the basis of this space is the basis of the representation. It is clear that the set of matrices **D** is a function of the selected basis of the representation. Suppose the vector **e** be the basis of space R^n. If the basis is transformed by a linear transformation:

$$\mathbf{e}' = \mathbf{Q}.\mathbf{e} \tag{11.3a}$$

in which **Q** is the $n \times n$ transformation matrix, then the representation matrices will undergo a similarity transformation as follows:

$$\mathbf{D}' = \mathbf{Q}^{-1}.\mathbf{D}.\mathbf{Q} \tag{11.3b}$$

Suppose that a representation **D** of the group G is given in a space R^n. If in the space R^n there is a subspace $R^k (k < n)$ which is invariant under all the transformations **D** (i.e. for any $\mathbf{x} \in R^k$, we have $\mathbf{D}.\mathbf{x} \in R^k$), the representation is

called a *reducible representation* (*redrep*). On the other hand, if we cannot define an invariant subspace R_k in space R^n, the representation will be named an *irreducible representation* (*irrep*).

Let us take the first k unit vectors in the space R^n as the unit vectors of the subspace R^k. The representation matrix will then have the following form:

$$\mathbf{D} = \left[\begin{array}{cccc|ccc} \mathbf{D}_{11} & \mathbf{D}_{12} & \dots & \mathbf{D}_{1,k} & \mathbf{D}_{1,k+1} & \dots & \mathbf{D}_{1,n} \\ \mathbf{D}_{21} & \mathbf{D}_{22} & \dots & \mathbf{D}_{2,k} & \mathbf{D}_{2,k+1} & \dots & \mathbf{D}_{2,n} \\ \vdots & \vdots & \dots & \vdots & \vdots & & \vdots \\ \mathbf{D}_{k,1} & \mathbf{D}_{k,2} & \dots & \mathbf{D}_{k,k} & \mathbf{D}_{k,k+1} & \dots & \mathbf{D}_{k,n} \\ \hline \mathbf{0} & \mathbf{0} & \dots & \mathbf{0} & \mathbf{D}_{k+1,k+1} & \dots & \mathbf{D}_{k+1,n} \\ \vdots & \vdots & \dots & \vdots & \vdots & \dots & \vdots \\ \mathbf{0} & \mathbf{0} & \dots & \mathbf{0} & \mathbf{D}_{n,k+1} & \dots & \mathbf{D}_{n,n} \end{array}\right]$$

It can be shown that if a redrep **D** is unitary, then the orthogonal component of the subspace R^k, denoted by R^{n-k}, is also invariant under the transformations **D** [13]. Now, if the unit vectors of the subspace R^k are taken as the first k unit vectors and the remaining n−k unit vectors are taken as the unit vectors of the subspace R^{n-k}, the representation matrix will have the following block-diagonal form:

$$\mathbf{D} = \left[\begin{array}{cccc|ccc} \mathbf{D}_{11} & \mathbf{D}_{12} & \dots & \mathbf{D}_{1,k} & \mathbf{0} & \dots & \mathbf{0} \\ \mathbf{D}_{21} & \mathbf{D}_{22} & \dots & \mathbf{D}_{2,k} & \mathbf{0} & \dots & \mathbf{0} \\ \vdots & \vdots & \dots & \vdots & \vdots & & \vdots \\ \mathbf{D}_{k,1} & \mathbf{D}_{k,2} & \dots & \mathbf{D}_{k,k} & \mathbf{0} & \dots & \mathbf{0} \\ \hline \mathbf{0} & \mathbf{0} & \dots & \mathbf{0} & \mathbf{D}_{k+1,k+1} & \dots & \mathbf{D}_{k+1,n} \\ \vdots & \vdots & \dots & \vdots & \vdots & \dots & \vdots \\ \mathbf{0} & \mathbf{0} & \dots & \mathbf{0} & \mathbf{D}_{n,k+1} & \dots & \mathbf{D}_{n,n} \end{array}\right]$$

If the space R can be resolved into invariant subspaces, in each of which an irrep is realised, then the representation **D** is fully reducible. With a suitable choice of unit vectors of the space, the matrix of this representation will have the following block-diagonal form, where α is the total number of classes of group G:

$$\mathbf{D} = \left[\begin{array}{c|c|c|c|c} \mathbf{D}^{(1)} & \mathbf{0} & \cdots & \mathbf{0} & \mathbf{0} \\ \hline \mathbf{0} & \mathbf{D}^{(2)} & \cdots & \mathbf{0} & \mathbf{0} \\ \hline \vdots & \vdots & \ddots & \vdots & \vdots \\ \hline \mathbf{0} & \mathbf{0} & \ldots & \mathbf{D}^{(\alpha-1)} & \mathbf{0} \\ \hline \mathbf{0} & \mathbf{0} & \cdots & \mathbf{0} & \mathbf{D}^{(\alpha)} \end{array}\right] \tag{11.4}$$

Any representation of a finite group is always equivalent to a unitary representation, and based on the foregoing discussion, it will always be either irreducible or fully reducible. For the second case, we can reduce all the matrices of the representation to block-factored matrices with the same pattern of diagonal blocks by going over the new system of unit vectors for the space.

Any symmetry group has α irreps, the details of which are presented in a table called *character table*. Comprehensive lists of character tables for common symmetry groups are available [12, 13, 14, 15]. It is conventional to show irreps with $\gamma^{(\mu)}$ and redreps with $\Gamma^{(\mu)}$.

The reduction process of a reducible representation into irreps would correspondingly divide the vector space R^n into a number of *group-invariant subspaces* $V^{(\mu)}$, such that none of these subspaces can be divided into further group-invariant subspaces of smaller dimension. In representation theory for symmetry groups, *idempotents* are defined as the projection operators which nullify all vectors of a given vector space other than those which belong to a particular subspace associated with a specific symmetry type. Thus, these operators can be used to transform the normal variables of a problem (spanning the vector space R^n) into orthogonal sets, each spanning a subspace $V^{(\mu)}$ of the vector space R^n. The idempotent operator $P^{(\mu)}$, which is defined associated to the subspace $V^{(\mu)}$ and its range is $V^{(\mu)}$, can be found via the Eq. 11.2 in which m_μ denotes the dimension of $\gamma^{(\mu)}$, Ref. [6]:

$$P^{(\mu)} \equiv \left(\frac{m_\mu}{m}\right) \sum_{i=1}^{m} \left[\chi\left(\gamma_i{}^{(\mu)}\right)\mathbf{\Gamma}_i\right] \tag{11.5}$$

The dimension of $V^{(\mu)}$ is given as

$$n_\mu \equiv \left(\frac{m_\mu}{m}\right) \sum_{i=1}^{m} \left[\chi\left(\gamma_i{}^{(\mu)}\right)\chi(\mathbf{\Gamma}_i)\right] \tag{11.6}$$

If $\gamma^{(\mu)}$ is absolutely irreducible and $m_\mu > 1$, then $V^{(\mu)}$ can be further decomposed into mutually orthogonal subspaces

$$V^{(\mu)} = \sum_{i=1}^{m_\mu} \oplus V^{(\mu i)} \tag{11.7}$$

It can be shown that the set of basis vectors for each subspace $V^{(\mu i)}\left(i = 1, 2 \ldots n_\mu\right)$ are physically indistinguishable from each other, which means that a solution for any required physical properties based on subspace $V^{(\mu 1)}$ must be identical to that based on any subspaces $V^{(\mu i)}$. Thus, only one of subspaces $V^{(\mu i)}$ actually needs to be considered, whereas such $V^{(\mu)}$ subspaces (in which $m_\mu > 1$) are always associated with the same set of eigenvalues (which in the conventional sense, constitute multiple roots of the problem). Decomposition of subspace $V^{(\mu)}$ into subspaces $V^{(\mu i)}\left(i = 1, 2, \ldots, n_\mu\right)$, and derivation of the associated basis vectors for a given problem, may be achieved directly by splitting idempotent $P^{(\mu)}$ into components $P^{(\mu i)}\left(i = 1, 2, \ldots, n_\mu\right)$ defined as below [6]:

$$P^{(\mu i)} \equiv \left(\frac{m_\mu}{m}\right) \sum_{j=1}^{m} \left[\gamma_j^{(\mu)}\right]_{i1} \mathbf{\Gamma}_j \tag{11.8}$$

in which $\left[\gamma_j^{(\mu)}\right]_{i1}$ denotes the i1-th entry of the matrix $\gamma_j^{(\mu)}$.

For more information on the representations and other properties of symmetry groups, one should refer to Refs. [11, 12, 13, 14, 15].

11.3 Stability Analysis of Hyper Symmetric Skeletal Structures Using Group Theory

11.3.1 A Review of the Present Method Through a Simple Example

In order to illustrate the method for decomposition of the buckling analysis of a symmetric system, with the aid of group theory, a simple example is studied in this section. In this section, formulas and equations which are widely used throughout the chapter are presented.

A symmetric, non-sway planar rigid frame is considered, as shown in Fig. 11.3.

The step-by-step method, which leads to the decomposition of such a problem using group theory, is described in the following. This method is described thoroughly in Ref. [7].

Step 1. *Recognition of point group of the structure*. The symmetry of a body is described by introducing the set of all those transformations which preserve the

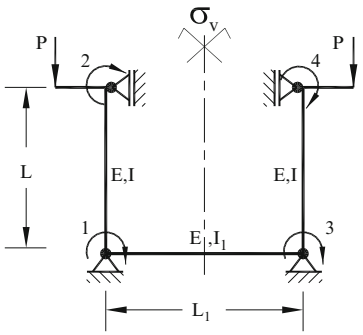

Fig. 11.3 Symmetric, non-sway planar frame with four DOFs

distance between all pairs of points of the body and map the body into coincidence with itself. The result of the transformation is either equivalent or it is identical to the primary arrangement. Each of these transformations is called a *symmetry operation* of the body. A *symmetry operator* such as an axis or a plane of symmetry induces additional properties to the system corresponding to which a symmetry operation is defined. Symmetry operators and their associated symmetry operations are identified with the same notations. As an example, associated with a symmetry axis C_4 (symmetry operator), two different operations can be defined: C_4 (rotation about the axis, with the angle of rotation $\theta = \frac{2\pi}{4}$) and $C_4{}^{-1}$ (rotation about the same axis, with the angle of rotation $\theta = \frac{2\pi}{4}$). For finite objects (bodies of finite extension), symmetry operations can be classified as follows: proper rotation about an axis (C_n); reflection in the planes of symmetry (σ_l); rotation, reflection or improper rotation (S_n is a C_n rotation followed by a reflection in a plane normal vector of which is the axis of rotation); inversion through the centre of symmetry (i), and identical symmetry (e) which maps any arbitrary object into itself and is one of the symmetry operations of any given object, either symmetric or asymmetric.

If there is more than one axis of symmetry for the object, the axis associated with the largest value of n – or the smallest value of θ – is called the *principal axis*. It should be noted that if a plane is perpendicular to the principal axis, it is called *horizontal plane* (σ_h); if the plane encompasses the principal axis, it is called *vertical plane* (σ_v); and if the plane consists of principal axis and passes through the bisector of the angle between two C_2 axes, perpendicular to the principal axis, it is called *dihedral plane* (σ_d). More detailed illustrations of symmetry operators and symmetry operations can be found in Refs. [7, 12].

The set of all symmetry operations of a finite body under the combination of transformation operations comprise an abstract group, which is called *symmetry group* or *point group*. Symmetry groups are classified based on symmetry operations which make up a group. The *Schöenflies method* is utilised in this chapter for naming the symmetry groups. This method has been described thoroughly in Refs. [11, 12].

The first step in solving a problem is finding the main symmetry operators and then the point group of the symmetric system. For the present problem, it is possible

Table 11.1 Character table of the group C_{1v}

C_{1v}	e	σ_v
$\gamma^{(1)}$	1	1
$\gamma^{(2)}$	1	−1

to distinguish only one vertical plane of symmetry – which has been shown as σ_v in Fig. 11.3. Based on the *Schöenflies method*, such a symmetry group is known as C_{1v}, which consists of two elements: $\{e, \sigma_v\}$. Once the point group of a structure is recognised, it is possible to find the properties of the group – such as its symmetry classes and irreducible representations – which are collected in a table which is called the *characteristic table*. As an example, Table 11.1 shows the characteristic table of the group C_{1v}.

Step 2. *Selecting a basis for n-dimensional vector space of the problem*. Such a basis can be any set of algebraic functions or vectors which span the vector space R^n of the problem. In stability analysis of a structure, the dimension of the problem is equal to the number of DOFs of the system. Therefore, in this chapter, the displacement vector of the structure is used as the basis of n-dimensional space of problems associated with a structure having n DOFs. It should be noted that in the formulation of structural matrices in this chapter, the degrees of freedom corresponding to the shear and axial deformations are neglected for the beam elements. The former assumption is due to the existence of rigid diaphragm in frame structures which constraints the horizontal translations of different nodes of a plan relative to each other. The latter assumption, on the other hand, has the meaning of neglecting shear stiffness compared to the flexural stiffness of the beam, which is a common assumption in most of the analyses. It should be noted that the method presented here is general and is independent of these simplifying assumptions.

If we show the generalised displacement (either translational or rotational) at each DOF (i) of the structure as u_i, the displacement vector of the problem will be as follows:

$$\mathbf{u} = (u_1,\ u_2,\ u_3,\ u_4)^t.$$

Step 3. *Forming the redreps (reducible representation) table of the point group on space R^n*. As it was mentioned before, each symmetry operation of a symmetry group can be introduced as a transformation, with respect to an arbitrary basis in the vector space R^n. The matrix representing such a transformation, then will be called a *reducible representation (redrep)* and is shown with $\mathbf{\Gamma}_i$ for the i-th symmetry operation of the group. For discrete systems, it is possible to construct the $\mathbf{\Gamma}_i$ (the reducible representation) implicitly as follows:

If $\mathbf{u}$ is an arbitrary displacement field, then each $\mathbf{\Gamma}_i$ is defined so that its action on the vector field $(\mathbf{\Gamma}_i\mathbf{u})$ 'mimics' one of the symmetry operations in group G [6]. Thus, in this chapter, $\mathbf{\Gamma}_i\mathbf{u}$ will be directly obtained by affecting each symmetry operation of group G to the basis of R^n (selected in step 2), and $\chi(\mathbf{\Gamma}_i)$ (trace of the matrix $\mathbf{\Gamma}_i$)

Table 11.2 Representation of C_{1v} on R^4

Element	Γ_i	$\Gamma_i.\mathbf{u}$	$\chi(\Gamma_i)$
e	Γ_1	$(u_1, u_2, u_3, u_4)^t$	4
σ_v	Γ_2	$(-u_3, -u_4, -u_1, -u_2)^t$	0

will be the number of DOFs which remain unchanged under this transformation. For the current example, Table 11.2 shows the redreps of the point group C_{1v}.

Step 4. *Finding the dimension of each subspace* $V^{(\mu)}$. Having the character table and the redreps of the symmetry group, it is now possible to find the dimension of each subspace (i.e. the scale of each decomposed subproblem which should be solved) using Eq. 11.7.

$$n_1 = \frac{1}{2}[(1 \times 4) + (1 \times 0)] = 2 \text{ and } n_2 = \frac{1}{2}[(1 \times 4) + (-1 \times 0)] = 2$$

It means that a problem with four DOFs will be substituted with two problems, each of which is of dimension 2.

Step 5. *Recognition of subspaces corresponded to multiple roots.* If the dimension of an absolutely irreducible representation (m_μ) is greater than '1', it can be further decomposed into mutually orthogonal subspaces. In this step, such subspaces are specified. The dimension of an irrep (irreducible representation) can be found from the character table of the group. Information on the representation theory of the groups and definitions of irrep, redrep and the character table can be found in the Sect 11.2. The character of element 'e' – the identical symmetry– in each representation is always equal to the dimension of that representation. Thus, from Table 11.1, it can be seen that both of the irreps of the group C_{1v} are of dimension 1 and step 5 does not include this group.

Step 6. *Finding idempotents associated with each subspace*. Idempotents are defined as operators associated with different group-invariant subspaces. Each subspace is the range of its associated idempotent when operating on the space of the main problem. The idempotent of subspaces with $m_\mu = 1$ is calculated using Eq. 11.5, and the idempotents corresponding to the subspaces recognised in step 5 can be calculated from

$$P^{(1)} = \frac{1}{2}[(1 \times \Gamma_1) + (1 \times \Gamma_2)] = \frac{\Gamma_1 + \Gamma_2}{2} \text{ and } P^{(2)} = \frac{1}{2}[(1 \times \Gamma_1) + (-1 \times \Gamma_2)] = \frac{\Gamma_1 - \Gamma_2}{2}$$

It should be noted that the idempotent operators of a group are among the properties of that group, and once the idempotents are found for a specific symmetry group, they can be used for similar problems having the same symmetry group.

Step 7. *Decomposition of basis of vector space* R^n *and finding the basis of each subspace*. This can be achieved by the means of affecting idempotent operators to

the basis of R^n. Subspace $V^{(\mu)}$ is the range of the idempotent $P^{(\mu)}$. Thus, each $P^{(\mu)}\mathbf{u}$ results in a combination of vectors which totally span the subspace $V^{(\mu)}$. Though there is no unique choice for the vectors spanning each subspace, different sets of bases result in the same eigenvalues for the subspace. In this chapter, spanning vectors of the subspace $V^{(\mu)}$ are derived from the result of $P^{(\mu)}\mathbf{u}$ and are then normalised in order to become unit vectors. These unit basis vectors are denoted by $\boldsymbol{\psi}_i^{(\mu)}\left(i = 1, 2 \ldots n_\mu\right)$ and are known as the symmetry modes of the system.

Subspace $V^{(1)}$ = Range $P^{(1)}$; $P^{(1)}.\mathbf{u} = \frac{\Gamma_1+\Gamma_2}{2}.\mathbf{u}$.

With the aid of Table 11.2, this equation yields $\frac{\Gamma_1+\Gamma_2}{2}.\mathbf{u} = (\alpha,\ \beta, -\alpha, -\beta)^t$.

where $\alpha = \frac{u_1-u_3}{2}$, $\beta = \frac{u_2-u_4}{2}$.

Hence, the unit vectors spanning $V^{(1)}$ are as follows:

$$\boldsymbol{\psi}_1^{(1)} = \frac{1}{\sqrt{2}}(1,0,-1,0)^t \text{ and } \boldsymbol{\psi}_2^{(1)} = \frac{1}{\sqrt{2}}(0,1,0,-1)^t.$$

Similarly, subspace $V^{(2)}$ = Range $P^{(2)}$; $P^{(2)}.\mathbf{u} = \frac{\Gamma_1-\Gamma_2}{2}.\mathbf{u}$ yields the symmetry modes as

$$\boldsymbol{\psi}_1^{(2)} = \frac{1}{\sqrt{2}}(1,0,1,0)^t \text{ and } \boldsymbol{\psi}_2^{(2)} = \frac{1}{\sqrt{2}}(0,1,0,1)^t.$$

It is possible to illustrate different symmetry modes $\left(\boldsymbol{\psi}_i^{(\mu)}\right)$ of the structure corresponding to different group-invariant subspaces. Each representation gives rise to a specific symmetry class and generally, the subspaces $V^{(\mu)}$ partition distinct classes of subsymmetry of the original structure [6]. This is apparent from Fig. 11.4.

Up to this stage, the general space of the problem has been decomposed into the subspaces which are called group-invariant subspaces. Now, it is the time to study the special case of buckling analysis of the structure.

$$\left(\mathbf{K}_O - P.\mathbf{K}_G\right) . \boldsymbol{\varphi} = \mathbf{0}. \tag{11.9}$$

Consider the well-known generalised eigenvalue problem associated with the buckling equation of a structural system. Here, $\mathbf{K}_O$ is the n × n first-order (linear or elastic) stiffness matrix which shows the bending effects, $\mathbf{K}_G$ is the n × n geometric (initial stress) stiffness matrix which results from the presence of axial load in a member, P is an eigenvalue which shows a buckling load of the system and φ is the corresponding buckling mode shape. If the structural system related to Eq. 11.9 is involved in a symmetry group (say G), then group representation theory can be used to construct an n × n orthogonal matrix **T** such that similarity transformations of $\mathbf{K}_O$ and $\mathbf{K}_G$ matrices by **T** result in *block factorisation* of those matrices in a similar pattern, that is,

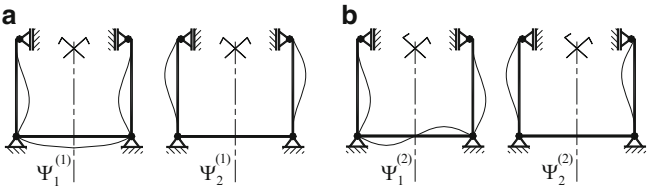

Fig. 11.4 Symmetry modes of the planar frame. (**a**) Subspace $V^{(1)}$: symmetric. (**b**) Subspace $V^{(2)}$: antisymmetric

$$\tilde{\mathbf{K}}_{\mathrm{O}} \equiv \mathbf{T}^{\mathrm{t}}.\ \mathbf{K}_{\mathrm{O}}.\ \mathbf{T} \quad \text{and} \quad \tilde{\mathbf{K}}_{\mathrm{G}} \equiv \mathbf{T}^{\mathrm{t}}.\ \mathbf{K}_{\mathrm{G}}.\ \mathbf{T} \tag{11.10}$$

in which both $\tilde{\mathbf{K}}_{\mathrm{O}}$ and $\tilde{\mathbf{K}}_{\mathrm{G}}$ have the same *block-diagonal* form. Of course, this reduces (11.10) to a number of smaller *uncoupled* eigenvalue problems. Therefore, we should now form the orthogonal matrix **T**.

Step 8. *Assembling of matrix* ***T*** *and block diagonalisation of the matrices* $\boldsymbol{K}_O$ *and* $\boldsymbol{K}_G$. Orthogonal matrix **T** in Eq. 11.10 has the normal basis vectors of subspaces (symmetry modes) as its columns, that is,

$$\mathbf{T} = \left[\mathbf{T}^{(1)}\ \mathbf{T}^{(2)}\ \ \ldots\ \mathbf{T}^{(\alpha)}\right] \tag{11.11}$$

in which

$$\mathbf{T}^{(\mu)} = \left[\boldsymbol{\Psi}_1^{(\mu)}\quad \boldsymbol{\Psi}_2^{(\mu)}\quad \ldots\quad \boldsymbol{\Psi}_{n_\mu}^{(\mu)}\right] \tag{11.12}$$

This is the matrix corresponding to similarity transformation under which the block factorisation of the matrices $\mathbf{K}_{\mathrm{O}}$ and $\mathbf{K}_{\mathrm{G}}$ is performed. Thus,

$$\mathbf{T} = \frac{1}{\sqrt{2}}\begin{bmatrix} 1 & 0 & 1 & 0 \\ 0 & 1 & 0 & 1 \\ -1 & 0 & 1 & 0 \\ 0 & -1 & 0 & 1 \end{bmatrix}.$$

The stiffness matrix of the structure can be written as

$$\mathbf{K} = \frac{\mathrm{EI}}{\mathrm{L}^3}\left[\begin{array}{cc|cc} 4+4\alpha & 2 & 2\alpha & 0 \\ 2 & 4 & 0 & 0 \\ \hline 2\alpha & 0 & 4+4\alpha & 2 \\ 0 & 0 & 2 & 4 \end{array}\right] - \frac{\mathrm{P}}{\mathrm{L}}\left[\begin{array}{cc|cc} \frac{2}{15} & -\frac{1}{30} & 0 & 0 \\ -\frac{1}{30} & \frac{2}{15} & 0 & 0 \\ \hline 0 & 0 & \frac{2}{15} & -\frac{1}{30} \\ 0 & 0 & -\frac{1}{30} & \frac{2}{15} \end{array}\right]$$

where $\alpha = \frac{\mathrm{I_1 L}^3}{\mathrm{I L_1}^3}$.

Therefore, the similarity transformation of stiffness matrix under the transformation matrix **T** can now be performed:

$$\mathbf{T}^t.\,\mathbf{K}\,.\,\mathbf{T} = \frac{EI}{L^3}\left[\begin{array}{cc|cc} 4+2\alpha & 2 & 0 & 0 \\ 2 & 4 & 0 & 0 \\ \hline 0 & 0 & 4+6\alpha & 2 \\ 0 & 0 & 2 & 4 \end{array}\right] - \frac{P}{L}\left[\begin{array}{cc|cc} \frac{2}{15} & -\frac{1}{30} & 0 & 0 \\ -\frac{1}{30} & \frac{2}{15} & 0 & 0 \\ \hline 0 & 0 & \frac{2}{15} & -\frac{1}{30} \\ 0 & 0 & -\frac{1}{30} & \frac{2}{15} \end{array}\right].$$

This shows that the problem has been decomposed into two subproblems, each of which is associated with one of the diagonal blocks.

Step 9. *Solving characteristic value problem in each subspace and finding buckling loads*. Now it is possible to solve Eq. 11.9 and find the eigenvalues in each of the subspaces $V^{(1)}$ and $V^{(2)}$ separately, for which the Eq. 11.9 changes into

$$\left(\mathbf{K}_O^{(\mu)} - P.\mathbf{K}_O^{(\mu)}\right).\,\boldsymbol{\varphi}^{(\mu)} = \mathbf{0}. \tag{11.13}$$

It should be noted that the eigenvalues (buckling loads) obtained from the individual subspaces $V^{(1)}$ and $V^{(2)}$ are the actual eigenvalues of the original problem, because a similarity transformation on a matrix preserves its eigenvalues.

For example, if we suppose that $\alpha = 1$ in our problem, the buckling loads will be found as follows:

$$\text{Subspace } V^{(1)};\ \det\begin{bmatrix} 6-\frac{2}{15}\lambda & 6+\frac{1}{30}\lambda \\ 2+\frac{1}{30}\lambda & 4-\frac{2}{15}\lambda \end{bmatrix} 0 \ \Rightarrow\ \lambda_1{}^{(1)} = 71.1293,\ \lambda_2{}^{(1)} = 16.8707$$

$$\text{Subspace } V^{(2)};\ \det\begin{bmatrix} 6-\frac{2}{15}\lambda & 6+\frac{1}{30}\lambda \\ 2+\frac{1}{30}\lambda & 4-\frac{2}{15}\lambda \end{bmatrix} = 0 \ \Rightarrow\ \lambda_1{}^{(2)} = 97.9473,\ \lambda_2{}^{(2)} = 22.0527$$

where $\lambda = \frac{PL^2}{EI}$. Thus, the critical load of the frame will be $P_{cr} = 16.8707\frac{EI}{L^2}$. The actual value of critical load of this structure is $P_{cr} = 12.8881\frac{EI}{L^2}$. It is possible to improve the result by dividing the members of the structure into more elements. If this happens, the number of DOFs and the scale of the problem will consequently increase. As an example, if we divide each column into two elements as shown in Fig. 11.5, the structure will have eight generalised DOFs and the stiffness matrix will be an 8×8 matrix, which leads to a critical load as $P_{cr} = 14.3547\frac{EI}{L^2}$. A similar step-by-step approach in this case results in the orthogonal matrix $\mathbf{T}$ as follows:

$$\mathbf{T} = \begin{bmatrix} \mathbf{I}_{4\times4} & \mathbf{I}_{4\times4} \\ -\mathbf{I}_{4\times4} & \mathbf{I}_{4\times4} \end{bmatrix} \quad \text{in which } \mathbf{I}_{4\times4} = \begin{bmatrix} 1 & & & \\ & 1 & & \\ & & 1 & \\ & & & 1 \end{bmatrix}.$$

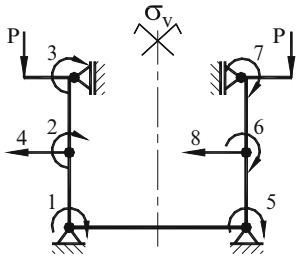

Fig. 11.5 Modelling each column with two elements

This matrix can decompose the 8×8 stiffness matrix into two submatrices of dimension 4. Finding the eigenvalues of the latter is much easier than calculating the eigenvalues of the original matrices of dimension 8.

The efficiency of the above method becomes more apparent for large-scale problems with finer discretised elements. Another case, where the application of the group theoretical method becomes beneficial and leads to considerable reduction, is the case of structures with more complicated forms of symmetry. This is the main focus of the present chapter and will be studied thoroughly in the following sections.

11.3.2 More Complicated Forms of Symmetry

The previous section was a short review on what has been presented before in Ref. [9]. As mentioned in the previous section, although the method is systematic and exact, its efficiency can be more obvious in problems including matrices of large dimensions or problems with complex symmetrical properties. Such problems can be categorised as follows:

- Problems of super structures with numerous degrees of freedom such as large-scale space structures.
- Problems with fine mesh discretisations.
- Problems of structures having a number of symmetry properties, referred to as *hyper symmetric structures* in this chapter. It should be noted that the term 'hyper symmetry' is adopted here for symmetric problems of finite groups with high orders (i.e. structures with geometries having numbers of symmetry operations), and it should not be taken identical to hyper symmetry used in theoretical physics. We are still dealing with ordinary finite groups, but they are of higher orders compared to symmetry groups associated with simple symmetric problems such as the one studied in the previous section.

The methodology of solving the first category of problems is exactly the same as what was mentioned in Sect. 11.2. Exactly the same steps should be taken, and similar results will be concluded. Problems of the second category have been studied to some extent in Ref. [9], and for fine mesh discretisations, the general

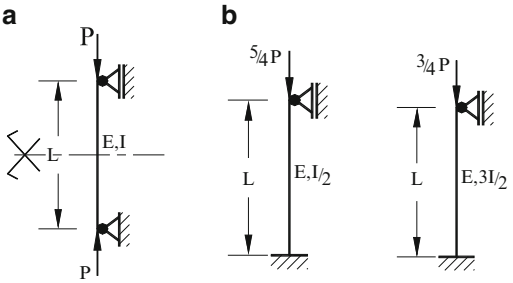

Fig. 11.6 A column element and its factors. (**a**) Column element. (**b**) Factors C and D

method is applicable. On the other hand, the last category consisting of problems with hyper symmetry should be under special attention, and in this chapter, we study such problems in two separate parts. In Ref. [9], four cases have been reported in each of which, one plane of symmetry bisects one or more beams or passes through one or more points of beams. In order to enter to the subject of hyper symmetry, it is necessary to complete these cases by considering the situation in which a plane of symmetry bisects a column element.

11.4 Finding the Factors of a Symmetric Column Element

A symmetric column with two rotational DOFs, under axial force P, having bending stiffness E I and length L is shown in Fig. 11.6a. The symmetry axis is perpendicular to the axis of the column. For such a symmetry, the shear DOFs are not active.

The stiffness matrix of such a column is as follows:

$$\mathbf{K} = \frac{\mathrm{EI}}{\mathrm{L}^3}\begin{bmatrix} 4 & 2 \\ 2 & 4 \end{bmatrix} - \frac{\mathrm{P}}{\mathrm{L}}\begin{bmatrix} \frac{2}{15} & \frac{1}{30} \\ \frac{1}{30} & \frac{2}{15} \end{bmatrix}.$$

If the method described in Sect. 11.2 is utilised, this matrix will be block-factorised as below:

$$\mathbf{K} = \frac{\mathrm{EI}}{\mathrm{L}^3}\left[\begin{array}{c|c} 6 & 0 \\ \hline 0 & 2 \end{array}\right] - \frac{\mathrm{P}}{\mathrm{L}}\left[\begin{array}{c|c} \frac{1}{10} & 0 \\ \hline 0 & \frac{1}{6} \end{array}\right].$$

Therefore, the factors of such a problem will be two substructures, denoted by C and D, with the following stiffness matrices:

$$\text{Factor C}: \quad \mathbf{K}_{\mathrm{O}} = \frac{\mathrm{EI}}{\mathrm{L}^3}[6] \quad \text{and} \quad \mathbf{K}_{\mathrm{G}} = \frac{1}{\mathrm{L}}\left[\frac{1}{10}\right]$$

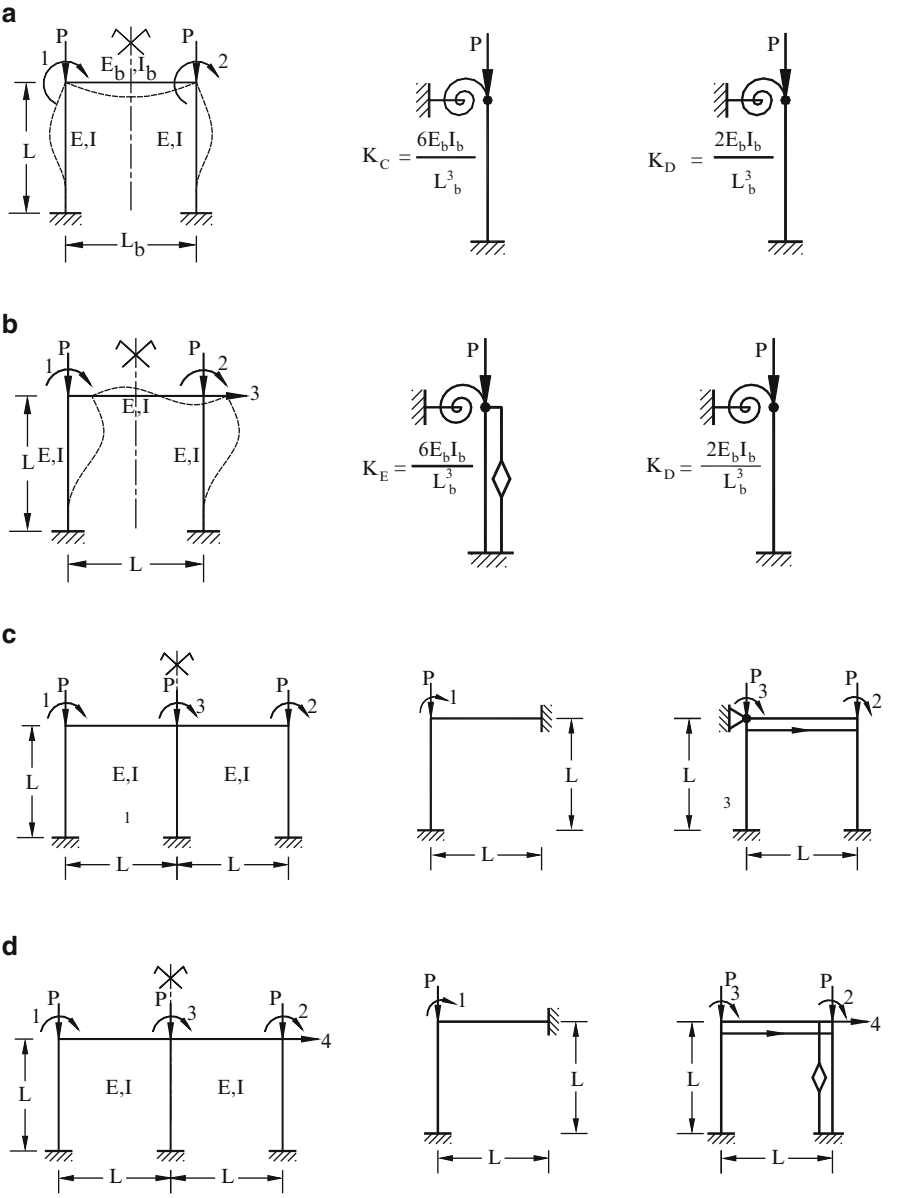

Fig. 11.7 Different cases of symmetric, planar frames and their factors. (**a**) Non-sway frame with odd number of spans. (**b**) Sway frame with odd number of spans. (**c**) Non-sway frame with even number of spans. (**d**) Sway frame with even number of spans

$$\text{Factor D}: \quad \mathbf{K}_O = \frac{EI}{L^3}[2] \quad \text{and} \quad \mathbf{K}_G = \frac{1}{L}\left[\frac{1}{6}\right]$$

Such sets of linear and geometric stiffness matrices are associated with two substructures C and D, as shown in Fig. 11.6b. Thus, from now on, we can substitute each column which has a plane of symmetry, with two columns C and D, each of which has one DOF.

We can now summarise the result of decomposition of different cases having symmetry, based on previous works [9] and the later result. In Fig. 11.7, the results previously obtained have been presented. In this figure, a virtual column element and a directed beam element are introduced (Fig. 11.7b, c, respectively). The stiffness matrices of such virtual elements which are used to form the mechanical representation of the factors are as follows:

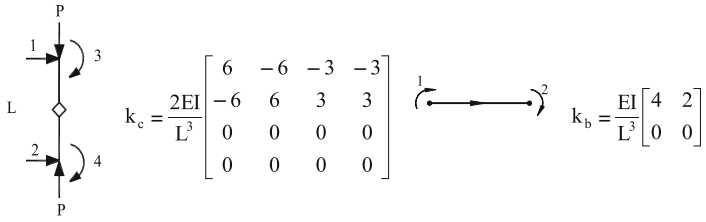

For more information on the cases shown in Fig. 11.7, see Ref. [9].

11.4.1 Hyper Symmetry

The problems of hyper symmetry – as introduced in the previous section – will be studied in this part as two different categories.

11.5 Symmetric Frames Having Numerous Symmetry Operators

When a structure has several symmetry operators, its symmetry group will have a higher order (order of a finite group is defined as the total number of its components). Such groups have more symmetry classes and consequently, more irreducible representations. Point groups such as C_2, C_{2v}, C_{3v}, C_{4v} and C_{6v}, which are conventional among the symmetric planar structures, are the examples of such symmetry groups. As mentioned, in such problems, there are more symmetry classes which means that more symmetry modes are distinguishable for the structure and more group-invariant subspaces will be produced during the process of

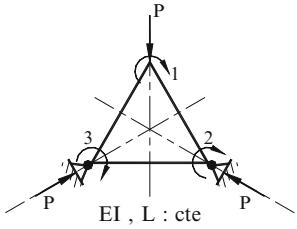

Fig. 11.8 Symmetric frame of group C_{3v}

decomposing the vector space of the problem. Also in such point groups, usually there are irreducible representations of dimensions greater than one. As it is mentioned in step 5, in such cases, there is the possibility of further decomposition of group-invariant subspace, which can be considerably beneficial in reducing the number of operations.

Example 11.1. As the first example of this category of problems, the triangular, planar frame shown in Fig. 11.8 is considered.

Step 1. As it is shown in Fig. 11.8, this structure has three vertical planes of symmetry, namely σ_v, σ'_v, and σ''_v as its symmetry operators. This set of symmetry operators introduces the symmetry group C_{3v}. The complete set of symmetry operations associated with this point group is as follows:

$$\{e,\ C_3,\ {C_3}^{-1},\ \sigma_v,\ \sigma'_v,\ \sigma''_v\}.$$

Table 11.3 shows the characteristic table of this group. The first column of this table shows the names of the irreducible representations presented in different rows, in the nomenclature proposed by Mulliken, and rather common in the modern literature. Such symbols are called *Mulliken symbols* and are in the general forms of A_i, B_i, E_i, T_i (or F_i), A'_i, A'', etc. For more details on this system of classification, one can refer to [12].

Step 2. Having three rotational DOFs, the displacement vector of this structure will be

$$\mathbf{u} = (u_1,\ u_2,\ u_3)^t$$

Step 3. Applying each of the symmetry operations of the group on the basis vector **u**, the reducible representation of the group C_{3v}, on space R^3 are resulted as presented in Table 11.4.

Step 4. By the aid of Tables 11.3 and 11.4, the dimensions of subspaces are found as

$$n_1 = \frac{3 + (-1) + (-1) + (-1)}{6} = 0,\ n_2 = \frac{3 + (-1) \times [(-1) + (-1) + (-1)]}{6} = 1,$$
$$n_3 = \frac{2}{6}(2 \times 3) = 2 \times 1.$$

Table 11.3 Character table of group C_{3v}

C_{3V}	e	$2C_3$	$3\,\sigma_v$
A_1	1	1	1
A_2	1	1	−1
E	2	−1	0

Table 11.4 Representation of C_{3v} on R^3

Element	Γ_i	$\Gamma_i.\mathbf{u}$	$\chi(\Gamma_i)$
E	Γ_1	u	3
C3	Γ_2	$(u_3, u_1, u_2)^t$	0
C_3^{-1}	Γ_3	$(u_2, u_3, u_1)^t$	0
σ_v	Γ_4	$(-u_1, -u_3, -u_2)^t$	−1
σ'_v	Γ_5	$(-u_2, -u_1, -u_3)^t$	−1
σ''_v	Γ_6	$(-u_3, -u_2, -u_1)^t$	−1

Step 5. As it is seen in Table 11.3, the third irrep of the group C_{3v} is of dimension 2. Thus, the third group-invariant subspace $V^{(3)}$ can further be decomposed into two identical subspaces $V^{(31)}$ and $V^{(32)}$, and calculation of eigenvalue for one of them is sufficient.

Step 6. Eq. 11.5 is used to find the idempotent operator associated with subspace $V^{(2)}$:

$$P^{(2)} = \frac{(\Gamma_1 + \Gamma_2 + \Gamma_3 - \Gamma_4 - \Gamma_5 - \Gamma_6)}{6}$$

Idempotent of the subspace $V^{(31)}$ is found via Eq. 11.8 as follows:

$$P^{(31)} = \frac{(2\Gamma_1 - \Gamma_2 - \Gamma_3 - \Gamma_4 - \Gamma_5 + 2\Gamma_6)}{6}.$$

It should be noted that for calculating the idempotent $P^{(31)}$, the two-dimensional irrep E is considered as shown in Table 11.5.

Step 7. When each of the idempotent operations found in the previous step is applied to the basis **u**, the following results are obtained:

$$P^{(2)}.\mathbf{u} = (\alpha, \alpha, \alpha)^t \text{ and } P^{(31)}.\mathbf{u} = (\beta, 0, -\beta)^t.$$

From which, the basis vectors of subspaces are extracted as

$$\boldsymbol{\psi}_1^{(2)} = \frac{1}{\sqrt{3}}(1,1,1)^t \text{ and } \boldsymbol{\psi}_1^{(31)} = \frac{1}{\sqrt{2}}(1,0,-1)^t.$$

Such basis vectors (symmetry modes of the structure) are depicted in Fig. 11.9. For this purpose, counterclockwise rotation is assumed to be positive.

Table 11.5 The third irreducible representation of C_{3v}

Element	E	C_3	C_3^{-1}	σ_v	σ'_v	σ''_v
E	$\begin{bmatrix} 1 & 0 \\ 0 & 1 \end{bmatrix}$	$\begin{bmatrix} -\frac{1}{2} & -\frac{\sqrt{3}}{2} \\ \frac{\sqrt{3}}{2} & -\frac{1}{2} \end{bmatrix}$	$\begin{bmatrix} -\frac{1}{2} & \frac{\sqrt{3}}{2} \\ \frac{\sqrt{3}}{2} & \frac{1}{2} \end{bmatrix}$	$\begin{bmatrix} -\frac{1}{2} & \frac{\sqrt{3}}{2} \\ \frac{\sqrt{3}}{2} & \frac{1}{2} \end{bmatrix}$	$\begin{bmatrix} -\frac{1}{2} & -\frac{\sqrt{3}}{2} \\ \frac{\sqrt{3}}{2} & \frac{1}{2} \end{bmatrix}$	$\begin{bmatrix} 1 & 0 \\ 0 & -1 \end{bmatrix}$

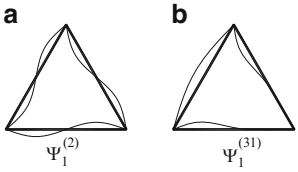

Fig. 11.9 Symmetry modes of the structure. (**a**) Subspace $V^{(1)}$. (**b**) Subspace $V^{(2)}$

Step 8. The orthogonal matrix **T** is formed as follows:

$$\mathbf{T} = \begin{bmatrix} \frac{1}{\sqrt{3}} & \frac{1}{\sqrt{2}} \\ \frac{1}{\sqrt{3}} & 0 \\ \frac{1}{\sqrt{3}} & -\frac{1}{\sqrt{2}} \end{bmatrix}.$$

Similarity transformation of stiffness matrix of the structure under matrix **T** ultimately leads to decomposition of the problem, and the stiffness matrices of subspaces are then resulted in the form of diagonal blocks as follows:

$$\mathbf{K} = \frac{EI}{L^3}\begin{bmatrix} 8 & 2 & 2 \\ 2 & 8 & 2 \\ 2 & 2 & 8 \end{bmatrix} - \frac{P}{L}\begin{bmatrix} 0.154 & -0.019 & -0.019 \\ -0.019 & 0.154 & -0.019 \\ -0.019 & -0.019 & 0.154 \end{bmatrix}$$

leading to

$$\mathbf{T}^t.\ \mathbf{K}\ .\ \mathbf{T} = \frac{EI}{L^3}\left[\begin{array}{c|c} 12 & 0 \\ \hline 0 & 6 \end{array}\right] - \frac{P}{L}\left[\begin{array}{c|c} 0.1155 & 0 \\ \hline 0 & 0.1732 \end{array}\right]$$

As it is seen, a 3×3 stiffness matrix is decomposed into two one-dimensional submatrices. The submatrix of subspace $V^{(31)}$ is a double-repeating root, and the buckling load which is calculated associated to this submatrix should be repeated twice in order to complete the set of all the three buckling loads of the system.

Step 9. The buckling load of the symmetrical frame is associated with its smallest eigenvalue. Therefore, from subspace $V^{(31)}$, it is concluded that $P_{cr} = 34.642\ \frac{EI}{L^2}$.

Discussion: In the Example 11.1, there was a group-invariant subspace with repeating roots. As it was mentioned before, this case occurs when the subspace is associated with an irrep of dimension two or more, and such subspaces can further

be decomposed. Here, we want to show that subspaces $V^{(31)}$ and $V^{(32)}$ are physically identical to each other.

Idempotent operation $P^{(32)}$ can be calculated from Eq. 11.3a, using Table 11.5 as

$$P^{(32)} = \frac{\sqrt{3}}{6}(-\Gamma_2 + \Gamma_3 + \Gamma_4 - \Gamma_5).$$

By applying this operator on basis vector $\mathbf{u}$, we find out that

$$P^{(32)}.\mathbf{U} = (\gamma, 0, -\gamma)^t$$

in which

$$\gamma = \frac{\sqrt{3}}{6}(-u_1 + 2u_2 - u_3).$$

It is seen that the basis vector of subspace $V^{(32)}$ is the same as $V^{(31)}$. Thus, they are associated with the same symmetry modes.

Example 11.2. The previous example was a frame with only three DOFs and during the decomposition process, one of its subspaces was unused (subspace $V^{(1)}$). This means that one can suppose some additional symmetry modes could be supposed for a larger problem of group C_{3v}, which are missed here due to the small dimension of the problem.

In the second example, a frame of higher dimension is studied. Figure 11.10 shows a planar, symmetric, non-sway frame with 14 DOFs. Both elastic and geometry stiffness matrices are 14×14.

Step 1. The structure has a C_2 axis as its principal axis and two vertical planes of symmetry. The symmetry group of such a symmetrical shape is C_{2v}. This group has four irreps of dimension 1. The character table of group C_{2v} is presented in Table 11.6.

Step 2. By collecting all of the rotational DOFs of the structure in the displacement vector, we have

$$\mathbf{u} = (u_1,\ u_2,\ u_3,\ u_4, \ldots,\ u_{12},\ u_{13},\ u_{14})^t.$$

Step 3. The representation table of the structure on R^{14} is presented in Table 11.7.

Step 4. From Table 11.7, it is found that $n_1 = n_3 = 3$ and $n_2 = n_4 = 4$, which means that the problem with 14 DOFs will be decomposed into two subproblems of dimension 3 and 2 subproblems of dimension 4.

Step 5. As it is seen in its characteristic table, group C_{2v} does not have any irreps of dimension two or more. Thus, all of the group-invariant subspaces are non-decomposable.

Step 6. The idempotent operators of group C_{2v} are found as follows:

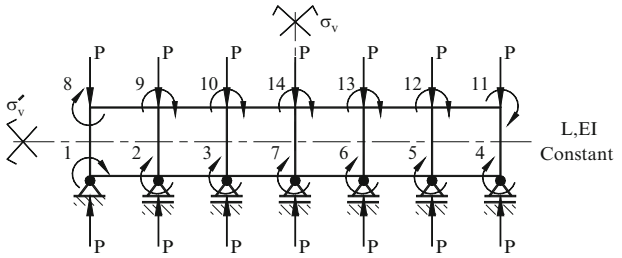

Fig. 11.10 Symmetric frame of group C_{2v}

Table 11.6 Character table of group C_{2v}

C_{2v}	E	C_2	σ_v	σ'_v
A_1	1	1	1	1
A_2	1	1	−1	−1
B_1	1	−1	1	−1
B_2	1	−1	−1	1

Table 11.7 Representation of C_{2v} on R^{14}

Element	Γ_i	$\Gamma_i.\mathbf{u}$	$\chi(\Gamma_i)$
e	Γ_1	$(u_1,\ u_2,\ u_3,\ u_4, \ldots,\ u_{12},\ u_{13},\ u_{14})^t$	14
C_2	Γ_2	$(u_{11},\ u_{12},\ u_{13},\ u_8, u_9, \ldots,\ u_2,\ u_3,\ u_7)^t$	0
σ_v	Γ_3	$(-u_4, -u_5, -u_6, -u_1, -u_2, \ldots, -u_9, -u_{10}, -u_{14})^t$	−2
σ'_v	Γ_4	$(-u_8, -u_9, -u_{10}, -u_{11}, -u_{12}, \ldots, -u_4, -u_5, -u_6, -u_7)^t$	0

$$P(1) = \frac{\Gamma_1 + \Gamma_2 + \Gamma_3 + \Gamma_4}{4},\ P(2) = \frac{\Gamma_1 + \Gamma_2 - \Gamma_3 - \Gamma_4}{4},$$
$$P(3) = \frac{\Gamma_1 - \Gamma_2 + \Gamma_3 - \Gamma_4}{4},\ P(4) = \frac{\Gamma_1 - \Gamma_2 - \Gamma_3 + \Gamma_4}{4}.$$

Steps 7 and 8. When the idempotents found in step 6 are applied on the displacement vector of the structure and the results are separated and normalised, the symmetry modes of the system are found as the columns of the matrix **T**. In this matrix, each partition shows the set of basis vectors of one subspace.

$$\mathbf{T}=\left[\begin{array}{ccc|cccc|ccc|cccc}
1 & 0 & 0 & 1 & 0 & 0 & 0 & 1 & 0 & 0 & 1 & 0 & 0 & 0 \\
0 & 1 & 0 & 0 & 1 & 0 & 0 & 0 & 1 & 0 & 0 & 1 & 0 & 0 \\
0 & 0 & 1 & 0 & 0 & 1 & 0 & 0 & 0 & 1 & 0 & 0 & 1 & 0 \\
-1 & 0 & 0 & 1 & 0 & 0 & 0 & -1 & 0 & 0 & 1 & 0 & 0 & 0 \\
0 & -1 & 0 & 0 & 1 & 0 & 0 & 0 & -1 & 0 & 0 & 1 & 0 & 0 \\
0 & 0 & -1 & 0 & 0 & 1 & 0 & 0 & 0 & -1 & 0 & 0 & 1 & 0 \\
0 & 0 & 0 & 0 & 0 & 0 & \sqrt{2} & 0 & 0 & 0 & 0 & 0 & 0 & \sqrt{2} \\
-1 & 0 & 0 & 1 & 0 & 0 & 0 & 1 & 0 & 0 & -1 & 0 & 0 & 0 \\
0 & -1 & 0 & 0 & 1 & 0 & 0 & 0 & 1 & 0 & 0 & -1 & 0 & 0 \\
0 & 0 & -1 & 0 & 0 & 1 & 0 & 0 & 0 & 1 & 0 & 0 & -1 & 0 \\
1 & 0 & 0 & 1 & 0 & 0 & 0 & -1 & 0 & 0 & -1 & 0 & 0 & 0 \\
0 & 1 & 0 & 0 & 1 & 0 & 0 & 0 & -1 & 0 & 0 & -1 & 0 & 0 \\
0 & 0 & 1 & 0 & 0 & 1 & 0 & 0 & 0 & -1 & 0 & 0 & -1 & 0 \\
0 & 0 & 0 & 0 & 0 & 0 & \sqrt{2} & 0 & 0 & 0 & 0 & 0 & 0 & -\sqrt{2}
\end{array}\right].$$

Step 9. The final result of decomposition of the stiffness matrix of the system is found from similarity transformation of this matrix under matrix **T**. This, results in a block-factored matrix with four diagonal blocks as follows:

$$\mathbf{T}^{t}.\mathbf{K}.\mathbf{T}=\frac{EI}{L^3}\left[\begin{array}{ccc|ccc|ccc|ccc}
24 & 8 & 0 & & & & & & & & & \\
8 & 40 & 8 & & & & & & & & & \\
0 & 8 & 40 & & & & & & & & & \\
\hline
 & & & 40 & 8 & 0 & 0 & & & & & \\
 & & & 8 & 56 & 8 & 0 & & & & & \\
 & & & 0 & 8 & 56 & 8\sqrt{2} & & & & & \\
 & & & 0 & 0 & 8\sqrt{2} & 56 & & & & & \\
\hline
 & & & & & & & 40 & 8 & 0 & & \\
 & & & & & & & 8 & 56 & 8 & & \\
 & & & & & & & 0 & 8 & 56 & & \\
\hline
 & & & & & & & & & & 24 & 8 & 0 & 0 \\
 & & & & & & & & & & 8 & 40 & 8 & 0 \\
 & & & & & & & & & & 0 & 8 & 40 & 8\sqrt{2} \\
 & & & & & & & & & & 0 & 0 & 8\sqrt{2} & 40
\end{array}\right]$$

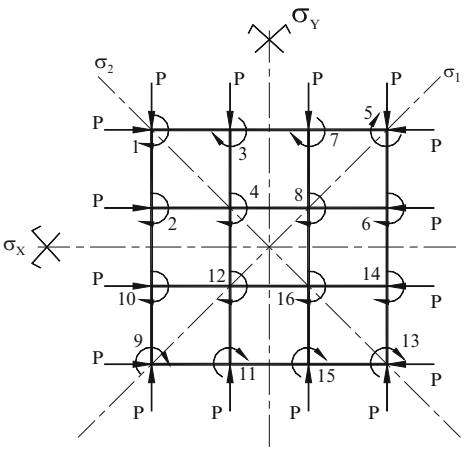

Fig. 11.11 Symmetric frame of group C_{4v}

$$-\frac{P}{L}\left[\begin{array}{cccc|cccc|cc|ccc}
0.66 & 0 & 0 & & & & & & & & & & \\
0 & 0.66 & 0 & & & & & & & & & & \\
0 & 0 & 0.66 & & & & & & & & & & \\
\hline
 & & & 0.399 & 0 & 0 & 0 & & & & & & \\
 & & & 0 & 0.399 & 0 & 0 & & & & & & \\
 & & & 0 & 0 & 0.399 & 0 & & & & & & \\
 & & & 0 & 0 & 0 & 0.399 & & & & & & \\
\hline
 & & & & & & & 0.399 & 0 & 0 & & & \\
 & & & & & & & 0 & 0.399 & 0 & & & \\
 & & & & & & & 0 & 0 & 0.399 & & & \\
\hline
 & & & & & & & & & & 0.66 & 0 & 0 & 0 \\
 & & & & & & & & & & 0 & 0.66 & 0 & 0 \\
 & & & & & & & & & & 0 & 0 & 0.66 & 0 \\
 & & & & & & & & & & 0 & 0 & 0 & 0.66
\end{array}\right]$$

Step 10. Subspace $V^{(4)}$ includes the smallest eigenvalue, and therefore, the critical load of the structure is calculated as follows:

$$\mathbf{K}^{(4)} = \frac{EI}{L^3}\begin{bmatrix} 24 & 8 & 0 & 0 \\ 8 & 40 & 8 & 0 \\ 0 & 8 & 40 & 8\sqrt{2} \\ 0 & 0 & 8\sqrt{2} & 40 \end{bmatrix} - \frac{P}{L}\begin{bmatrix} 0.66 & 0 & 0 & 0 \\ 0 & 0.66 & 0 & 0 \\ 0 & 0 & 0.66 & 0 \\ 0 & 0 & 0 & 0.66 \end{bmatrix}$$

$$\mathrm{Det}(\mathbf{K}) = 0 \Rightarrow P_{cr} = 29.8018\frac{EI}{L^2}$$

Table 11.8 Character table of group C_{4v}

C_{4V}	e	$2C_4$	C_2	$2\sigma_v$	$2\sigma_d$
A_1	1	1	1	1	1
A_2	1	1	1	−1	−1
B_1	1	−1	1	1	−1
B_2	1	−1	1	−1	1
E	2	0	−2	0	0

Table 11.9 Final results of Example 11.3

Subspace	Linear stiffness matrix ($\mathbf{K}_O$)	Geometric stiffness matrix ($\mathbf{K}_G$)	Eigenvalues $\left(\times \frac{L^2}{EI}\right)$
$V^{(1)}$	$\frac{EI}{L^3}[10]$	$\frac{1}{L}\left[\frac{13}{30}\right]$	{23, 0771}
$V^{(2)}$	$\frac{EI}{L^3}\begin{bmatrix} 8 & 2\sqrt{2} & 0 \\ 2\sqrt{2} & 14 & 2\sqrt{2} \\ 0 & 2\sqrt{2} & 20 \end{bmatrix}$	$\frac{1}{L}\begin{bmatrix} \frac{4}{15} & -\frac{\sqrt{2}}{30} & 0 \\ -\frac{\sqrt{2}}{30} & \frac{11}{30} & -\frac{\sqrt{2}}{30} \\ 0 & -\frac{\sqrt{2}}{30} & \frac{14}{30} \end{bmatrix}$	{20, 38.183, 60.002}
$V^{(3)}$	$\frac{EI}{L^3}\begin{bmatrix} 8 & 2\sqrt{2} & 0 \\ 2\sqrt{2} & 10 & 2\sqrt{2} \\ 0 & 2\sqrt{2} & 12 \end{bmatrix}$	$\frac{1}{L}\begin{bmatrix} \frac{4}{15} & -\frac{\sqrt{2}}{30} & 0 \\ -\frac{\sqrt{2}}{30} & \frac{13}{30} & -\frac{\sqrt{2}}{30} \\ 0 & -\frac{\sqrt{2}}{30} & \frac{6}{10} \end{bmatrix}$	{11.00, 23.077, 42.858}
$V^{(4)}$	$\frac{EI}{L^3}[14]$	$\frac{1}{L}\left[\frac{11}{30}\right]$	{38.182}
$V^{(51)}$ or $V^{(52)}$	$\frac{EI}{L^3}\begin{bmatrix} 8 & 2 & 2 & 0 \\ 2 & 10 & 0 & 2 \\ 2 & 0 & 14 & 2 \\ 0 & 2 & 2 & 16 \end{bmatrix}$	$\frac{1}{L}\begin{bmatrix} \frac{4}{15} & -\frac{1}{30} & -\frac{1}{30} & 0 \\ -\frac{1}{30} & \frac{13}{30} & 0 & -\frac{1}{30} \\ -\frac{1}{30} & 0 & \frac{11}{30} & -\frac{1}{30} \\ 0 & -\frac{1}{30} & -\frac{1}{30} & \frac{16}{30} \end{bmatrix}$	{15.287, 30, 30, 51.863}

It is seen that solving a problem of dimension 14 is replaced with small problems of dimensions 3 and 4.

Example 11.3. This example shows the efficiency of the method, when a rather large-scale problem is involved in a group of higher order. Figure 11.11 shows a symmetrical frame with 16 rotational DOFs and symmetrical loading. Having a C_2 axis as the principal axis, two vertical planes σ_x and σ_y, and two dihedral planes σ_1 and σ_2, the symmetry group of the structure is C_{4v}. This group has eight elements consisting of $\{e,\ C_4,\ {C_4}^{-1},\ C_2,\ \sigma_x,\ \sigma_y,\ \sigma_1,\ \sigma_2\}$. These elements are categorised in five symmetry classes. The symmetry classes and the irreps are shown in characteristic table of the group (Table 11.8).

It is seen that the fifth irrep of the group is of dimension 2. Therefore, in this problem, again there is a subspace with two sets of identical answers (doubly repeated roots). If the step-by-step method is used for the decomposition of this problem, the real space R^{16} of the problem will be decomposed into five subspaces: two subspaces of dimension 1 ($V^{(1)}$ and $V^{(4)}$), two subspaces of dimension 3 ($V^{(2)}$ and $V^{(3)}$) and a subspace of dimension 8 ($V^{(5)}$). The latter is associated with doubly repeated roots and can be further decomposed into four-dimensional subspaces $V^{(51)}$ and $V^{(52)}$, one of which is enough to be solved.

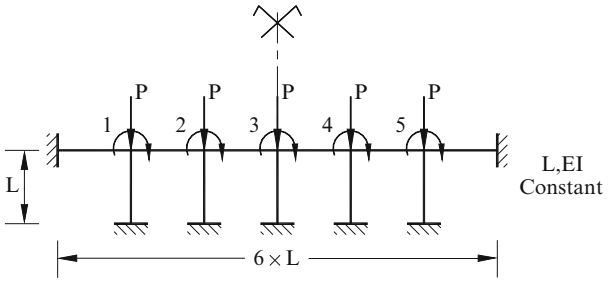

Fig. 11.12 Symmetric, planar, non-sway frame of group C_{1v}

Final results of decomposition of this problem with group theoretical method are presented in Table 11.9. The critical load of the structure is in subspace $V^{(3)}$ and is equal to $P_{cr} = 12.0002\frac{EI}{L^2}$. The results of this example show the strong ability of the method in reducing the dimension of a large problem with rather advanced symmetric properties. Here, problems of dimensions 1, 3 and 4 are solved instead of a 16 dimensional problem.

11.5.1 Frames with Symmetrical Factors

The general solution of the examples presented up to now is based on finding the symmetry group of the symmetric structure and using the representation theory in order to find a similarity transformation which can block diagonalise the mechanical matrices of the system. This is more or less the basis of most of the methods which use group theory in structural mechanics. The output of most of these methods is a number of submatrices of lower dimensions. Now in this section, we want to work on these submatrices in order to present a physical interpretation for them. Then, we examine such physical models associated with the submatrices in order to find if further decomposition is feasible. It should be noted at this stage that frequently some additional symmetry properties are present after factorisation of a symmetric configuration, but a review on literature of group theoretic methods in structural mechanics shows that almost none of them take these new properties into account. This is due to the fact that the new symmetries can hardly be recognised from the matrices which arise in group theoretic methods. A physical interpretation on the output matrices is necessary in order to find their new symmetry operations. Here, such an interpretation will be presented.

In Sect. 11.3, the factors resulting from decomposition of different cases of symmetric frames were introduced and illustrated in Fig. 11.7. Such factors are the mechanical models of decomposed submatrices mentioned above. Thus, it is possible now to study either the mathematical or the mechanical model of a symmetrical system and its factors. In the following, some examples are studied to clarify the procedure.

Table 11.10 Representation of C_{1v} on R^5

Element	Γ_i	$\Gamma_i.\mathbf{u}$	$\chi(\Gamma_i)$
e	Γ_1	$(u_1, u_2, u_3, u_4, u_5)^t$	5
σ_v	Γ_2	$-(u_5, u_4, u_3, u_2, u_1)^t$	−1

Example 11.4. As a very simple example, the non-sway, planar frame of Fig. 11.12 is studied. This structure has five rotational DOFs and one vertical plane of symmetry. The general stiffness matrix of this structure is formed as

$$\mathbf{K} = \frac{EI}{L^3}\begin{bmatrix} 12 & 2 & 0 & 0 & 0 \\ 2 & 12 & 2 & 0 & 0 \\ 0 & 2 & 12 & 2 & 0 \\ 0 & 0 & 2 & 12 & 2 \\ 0 & 0 & 0 & 2 & 12 \end{bmatrix} - \frac{P}{L}$$
$$\times \begin{bmatrix} 0.1333 & 0 & 0 & 0 & 0 \\ 0 & 0.1333 & 0 & 0 & 0 \\ 0 & 0 & 0.1333 & 0 & 0 \\ 0 & 0 & 0 & 0.1333 & 0 \\ 0 & 0 & 0 & 0 & 0.1333 \end{bmatrix}.$$

The solution of the problem by means of the group theoretic method consists of the following steps:

Step 1. The symmetry group of the structure is C_{1v}, which we had before in the illustrative example of Sect. 11.2.

Step 2. We choose the displacement vector $\mathbf{u} = (u_1,\ u_2,\ u_3,\ u_4,\ u_5)^t$ as the basis of vector space R^5.

Step 3. Representation of group C_{1v} with respect to the basis $\mathbf{u}$ is shown in Table 11.10.

Step 4. The dimensions of subspaces are calculated as follows:

$$n_1 = \frac{1}{2}[(1 \times 5) + (1 \times (-1))] = 2 \quad \text{and} \quad n_2 = \frac{1}{2}[(1 \times 5) + (-1 \times (-1))] = 3.$$

This means that this five-dimensional problem can be reduced to a two-dimensional and a three-dimensional problem.

Step 5. Both of the irreps of group C_{1v} are one-dimensional.

Step 6. The idempotents of group C_{1v} are calculated as before.

Step 7. Application of the idempotents on the basis vector $\mathbf{u}$ is as follows:

$$P(1).\mathbf{u} = \frac{\Gamma_1 + \Gamma_2}{2}.\mathbf{u} = (\alpha_1,\ \beta_1, 0, -\beta_1, -\alpha_1)^t \quad \text{and} \quad P(1).\mathbf{u} = \frac{\Gamma_1 - \Gamma_2}{2}.\mathbf{u}$$
$$= (\alpha_2,\ \beta_2,\ \gamma_2,\ \beta_2, \alpha_2)^t.$$

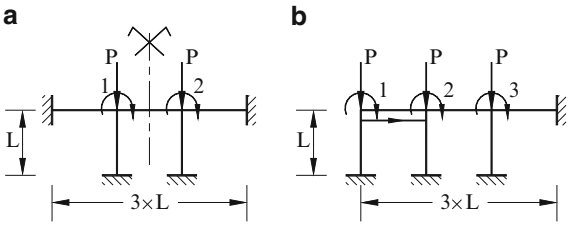

Fig. 11.13 Mechanical model of factors of Example 11.4. (**a**) Subspace $V^{(1)}$. (**b**) Subspace $V^{(2)}$

Step 8. The symmetry modes, which result for this problem, are collected in matrix **T**:

$$\mathbf{T} = \frac{1}{\sqrt{2}} \left[\begin{array}{cc|ccc} 1 & 0 & 1 & 0 & 0 \\ 0 & 1 & 0 & 1 & 0 \\ 0 & 0 & 0 & 0 & \sqrt{2} \\ 0 & -1 & 0 & 1 & 0 \\ -1 & 0 & 1 & 0 & 0 \end{array}\right].$$

Step 9. Finally, the block diagonalisation is resulted as

$$\mathbf{T}^{t}.\mathbf{K}.\mathbf{T} = \frac{EI}{L^3} \left[\begin{array}{cc|ccc} 12 & 2 & & & \\ 2 & 12 & & & \\ \hline & & 12 & 2 & 0 \\ & & 2 & 12 & 2\sqrt{2} \\ & & 0 & 2\sqrt{2} & 12 \end{array}\right] - \frac{P}{L}$$

$$\times \left[\begin{array}{cc|ccc} 0.1333 & 0 & & & \\ 0 & 0.1333 & & & \\ \hline & & 0.1333 & 0 & 0 \\ & & 0 & 0.1333 & 0 \\ & & 0 & 0 & 0.1333 \end{array}\right].$$

Now the eigenvalues in each subspace can be found and the solution will be terminated. On the other hand, by the aid of Fig. 11.7, we can illustrate the physical model of each set of arisen diagonal blocks, as shown in Fig. 11.13. As can be seen from this figure, the subproblem of subspace $V^{(1)}$ has a new symmetry operator, a vertical plane which determines the symmetry group C_{1v} for this subsystem. Thus, it is possible to perform the step-by-step method for the subsystem $V^{(2)}$ and perform further decomposition.

By numbering the DOFs of factor $V^{(1)}$ as shown in Fig. 11.13a, the results of the further decomposition are as follows:

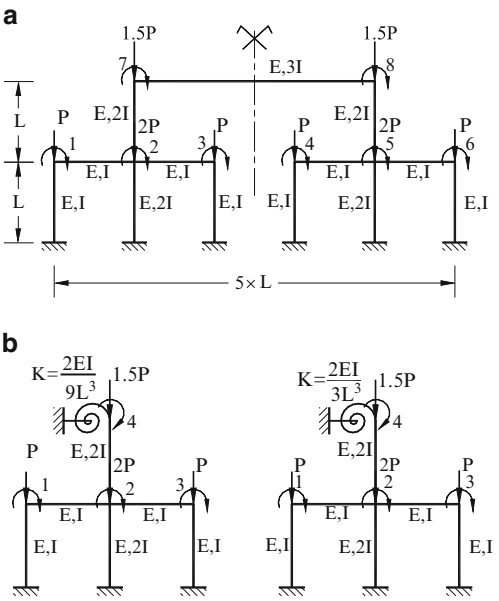

Fig. 11.14 A symmetric structure and its symmetrical factors. (**a**) Symmetric structure. (**b**) Factors of the structure

Table 11.11 The results of Example 11.5

Subspace $V^{(1)}$

$$\mathbf{K} = \frac{EI}{L^3}\begin{bmatrix} 8 & 2 & 0 & 0 \\ 2 & 24 & 2 & 4 \\ 0 & 2 & 8 & 0 \\ 0 & 4 & 0 & 8.222 \end{bmatrix} - \frac{P}{L}\begin{bmatrix} 0.1333 & 0 & 0 & 0 \\ 0 & 0.4667 & 0 & -0.05 \\ 0 & 0 & 0.1333 & 0 \\ 0 & -0.05 & 0 & 0.2 \end{bmatrix}$$

Subspace $V^{(1-1)}$

$$\mathbf{K} = \frac{EI}{L^3}[16] - \frac{P}{L}[0.2667]$$

Subspace $V^{(1-2)}$

$$\mathbf{K} = \frac{EI}{L^3}\begin{bmatrix} 16 & 5.66 & 0 \\ 5.66 & 48 & 8 \\ 0 & 8 & 16.44 \end{bmatrix} - \frac{P}{L}\begin{bmatrix} 0.267 & 0 & 0 \\ 0 & 0.93 & -0.1 \\ 0 & -0.1 & 0.4 \end{bmatrix}$$

Subspace $V^{(2)}$

$$\mathbf{K} = \frac{EI}{L^3}\begin{bmatrix} 8 & 2 & 0 & 0 \\ 2 & 24 & 2 & 4 \\ 0 & 2 & 8 & 0 \\ 0 & 4 & 0 & 8.667 \end{bmatrix} - \frac{P}{L}\begin{bmatrix} 0.1333 & 0 & 0 & 0 \\ 0 & 0.4667 & 0 & -0.05 \\ 0 & 0 & 0.1333 & 0 \\ 0 & -0.05 & 0 & 0.2 \end{bmatrix}$$

Subspace $V^{(2-1)}$

$$\mathbf{K} = \frac{EI}{L^3}[16] - \frac{P}{L}[0.2667]$$

Subspace $V^{(2-2)}$

$$\mathbf{K} = \frac{EI}{L^3}\begin{bmatrix} 16 & 5.66 & 0 \\ 5.66 & 48 & 8 \\ 0 & 8 & 17.33 \end{bmatrix} - \frac{P}{L}\begin{bmatrix} 0.267 & 0 & 0 \\ 0 & 0.93 & -0.1 \\ 0 & -0.1 & 0.4 \end{bmatrix}$$

$$\mathbf{T}^{(1)} = \frac{1}{\sqrt{2}}\begin{bmatrix} 1 & 1 \\ -1 & 1 \end{bmatrix} \Rightarrow \mathbf{T}^{(1)^{t}}.\mathbf{K}^{(1)}.\mathbf{T}^{(1)}$$

$$= \frac{EI}{L^3}\left[\begin{array}{c|c} 10 & 0 \\ \hline 0 & 14 \end{array}\right] - \frac{P}{L}\left[\begin{array}{c|c} 0.1333 & 0 \\ \hline 0 & 0.1333 \end{array}\right]$$

Example 11.5. As another simple example, the structure shown in Fig. 11.14a is considered. The group theoretical method decomposes the eight-dimensional matrices of this structure into two factors, each of which is of dimension 4. These factors are shown in Fig. 11.14b. As it can be seen, both of the factors are again structures with symmetry group C_{1v}. Therefore, they can be decomposed in turn. The mathematical results of such decompositions are summarised in Table 11.11. It is concluded from this table that the one-dimensional subproblems resulted from decomposition of both of the subspaces $V^{(1)}$ and $V^{(2)}$ are identical and only one of them is enough to be solved.

It should be noted that there is a basic difference between two categories of the problems of hyper symmetry (the structures studied in Sect. 4.1 and the problems studied in Sect. 4.2). The first category consists of the systems which have a number of symmetry operators and exhibits all of their symmetrical properties in the original structure. In this case, group theory is able to recognise all of the symmetry modes of the structure immediately and can perform the decomposition of different modes simultaneously. But the second category includes the structures with some hidden symmetrical properties that group theory cannot recognise directly. In such problems, it is necessary to have a physical interpretation of the outputs to find the extra symmetrical properties of the structure. Therefore, it is recommended to perform both procedures in all of the problems simultaneously – especially the problems of complicated symmetry forms – in order to profit from all the symmetrical potentials of the system.

11.5.2 Discussions

The decomposition method for symmetric problems of canonical forms presented in the previous chapters is extended to the problems with symmetry groups having higher orders. The factorisation of the symmetric structures has the following advantages:

1. The DOFs of the problem are reduced.
2. The computational time and effort are decreased.

References

1. Stiefel E, Fässler A (1979) Gruppentheoretische Methoden und ihre Anwendung. Teubner Studienbücher, Mathematik, Stuttgart
2. Boardman AD, O'Conner DE, Young PA (1973) Symmetry and its applications in science. McGraw-Hill, London
3. Zingoni A (1996) An efficient computational scheme for the vibration analysis of high-tension cable nets. J Sound Vib 189:55–79
4. Zingoni A (1996) Truss and beam finite elements revisited: a derivation based on displacement-field decomposition. Int J Space Struct 11:371–380
5. Zingoni A, Pavlovic MN, Zlokovic GM (1995) A symmetry-adapted flexibility approach for multi-storey space frames: general outline and symmetry-adapted redundants. Struct Eng Rev 7:107–119
6. Healey TJ, Treacy JA (1991) Exact block diagonalization of large eigenvalue problems for structures with symmetry. Int J Numer Methods Eng 31:265–285
7. Kaveh A, Nikbakht M (2007) Block diagonalization of Laplacian matrices of symmetric graphs via group theory. Int J Numer Methods Eng 69:908–947
8. Kaveh A, Nikbakht M (2006) Decomposition of symmetric mass–spring vibrating systems using groups, graphs, and linear algebra. Commun Numer Methods Eng 23:639–664
9. Kaveh A, Nikbakht M (2006) Buckling load of symmetric plane frames using canonical forms and group theory. Acta Mech 185:89–128
10. Kaveh A, Nikbakht M (2008) Stability analysis of hyper symmetric skeletal structures using group theory. Acta Mech 200:177–197
11. Hammermesh M (1962) Group theory and its application to physical problems. Dover Publication, New York
12. Albert Cotton F (1990) Chemical applications of group theory. Wiley, New York
13. Petrashen MI, Trifonov ED (1969) Group theory in quantum mechanics. Iliffe Books Ltd, London
14. Armstrong MA (1988) Groups and symmetry. Springer, New York
15. Miller W Jr (1972) Symmetry groups and their applications. Academic, New York

Chapter 12
Graph–Group Method for the Analysis of Symmetric-Regular Structures

12.1 Introduction

In this chapter, a combined graph–group method is presented for eigensolution of special graphs. The study of symmetric graphs with regularity is the main objective of this study. Many structural models are regular and usually have symmetric configurations. Here, the proposed method operates symmetry analysis of the entire structure utilising the symmetry properties of its simple generators. The model of a structure is considered as a product graph, and the Laplacian matrix, as one of the most important matrices associated with a graph, is studied. Characteristic problem of this matrix is investigated using symmetry analysis via group theory enriched by graph theory. The decomposition of Laplacian matrix of such graphs is performed in a step-by-step manner, based on the presented method. This method focuses on simple paths which generate large networks and finds the eigenvalues of the network using the analysis of the simple generators. Group theory is utilised as the main tool, improved by some concepts of graph products. As an application of the method, a benchmark problem of group theory from structural mechanics is studied. Vibration of cable nets is analysed and the frequencies of the networks are calculated using a hybrid graph–group method [1].

12.2 Symmetry Groups of Graph Products

Symmetry groups and representation theory were presented in the previous chapter.

Based on the definition, two groups G and G' are *isomorphic* if there is a bijection φ from G to G' which satisfies

$$\varphi(xy) = \varphi(x)\varphi(y) \text{ for all } x, y \in G. \tag{12.1}$$

A. Kaveh, *Optimal Analysis of Structures by Concepts of Symmetry and Regularity*,
DOI 10.1007/978-3-7091-1565-7_12, © Springer-Verlag Wien 2013

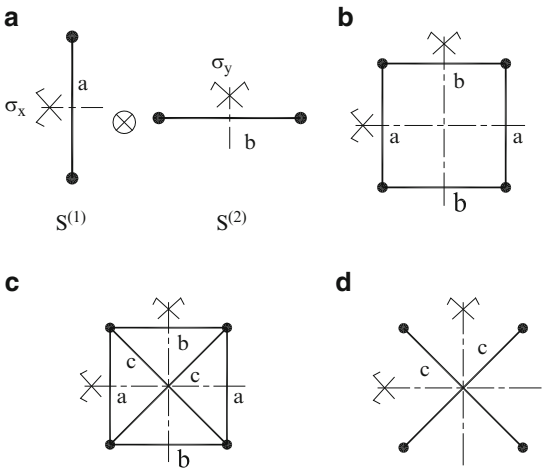

Fig. 12.1 Two weighted P_2 graphs and their products. (**a**) Two simple P_2 graphs. (**b**) The Cartesian product. (**c**) The strong Cartesian product. (**d**) The direct product

The function φ is called an *isomorphism* between G and G'. When groups G and G' are said to be isomorphic, there will be a one-by-one correspondence between their elements and these elements combine in the same manner. That is, if $x \rightarrow x'$, and $y \rightarrow y'$, then $xy \rightarrow x'y'$, in which $x, y \in G$, and $x', y' \in G'$.

Symmetry of the graphs which can be expressed as product of two paths is studied in this section, via group theory. This is illustrated through simple examples. Weighted graphs are selected here in order to show the symmetric (or asymmetric) properties of the generators and resulted graph. It should also be noted that application of graph theory in structural analysis mostly includes the use of the weighted graphs as the structural models [2]. The weights are assigned just to the elements for brevity.

Example 12.1. Two simple paths $S^{(1)}$ and $S^{(2)}$, each of which consists of two nodes and one element are shown in Fig. 12.1a. Such paths are called P_2. Different products of these generators, introduced in Sect. 12.2, are shown in Fig. 12.1b–d. Attention to different products of these generators and also other generators shows that the symmetry types of all three products for two given generators are the same. Therefore, we focus on Cartesian product of the graphs. Obviously, the discussion can easily be applied to the two other forms of the graph products.

Let us study the symmetry group of the generators first. Each of the P_2 paths of Fig. 12.1a has only a vertical plane of symmetry as the symmetry operator, which defines a symmetry operation σ_v. Such a symmetry group is called C_{1v}, the elements of which are $\{e, \sigma_v\}$. One can write the symmetry groups of these graphs as follows:

$$S^{(1)}: \; C_{1V} = \{e, \; \sigma_x\}, \quad S^{(2)}: \; C'_{1V} = \{e, \; \sigma_y\}. \tag{12.2}$$

Cartesian product of these two subgraphs (Fig. 12.1b) has two vertical planes of symmetry (σ_x and σ_y), plus an axis of symmetry which is perpendicular to the plane of the graph and is the intersection of the vertical planes of symmetry. A C_2 operation is defined associated to this axis, which is the rotation with an angle of $\theta = \pi$. The symmetry group of such a configuration is called C_{2V}, including the symmetry operations: {e, C_2, σ_v, σ'_v}. Here, the operators σ_v and σ'_v are σ_x and σ_y, respectively. This means that the Cartesian product of two graphs with symmetry group C_{1v} results in a symmetric graph of symmetry group C_{2V}.

$$S: \; C_{2V} = \{e, C_2, \; \sigma_x, \; \sigma_y\}. \tag{12.3}$$

Now, if we construct the direct product of symmetry groups C_{1v} and C'_{1v} in Eq. 12.2, based on the rule described in Sect. 11.5, we will have

$$C_{1v} \times C'_{1v} = \{e, \sigma_x\} \otimes \{e, \sigma_y\} = \{(e, e), (\sigma_x, e), (e, \sigma_y), (\sigma_x, \sigma_y)\}. \tag{12.4}$$

Although this set does not seem similar to a symmetry group in the sense that we know, an isomorphism can be discovered between this and a well-known symmetry group. The following theorem is implemented in this regard.

Theorem. *If H and K are subgroups of G for which HK = G (i.e. every element of G can be expressed as a product of xy, for some x ∈ H and y ∈ K), if they have only the identity element in common, and if every element of H commutes with every element of K, then G is isomorphic to H × K* [3].

For the present example, a comparison between Eqs. 12.2 and 12.3 shows that both symmetry groups C_{1v} and C'_{1v} are the subgroups of symmetry group C_{2v}. It can also be shown that all of the elements of C_{2v} are expressible as the product of elements of C_{1v} and C'_{1v}. This is shown in Table 12.1.

The equivalence of $\sigma_x \cdot \sigma_y$ and C_2 (the last row of Table 12.1) is illustrated in Fig. 12.2.

On the other hand, C_{1v} and C'_{1v} merely have the identity element in common:

$$C_{1v} \cap C'_{1v} = \{e\}.$$

Finally, it is seen that the elements of C_{1v} and C'_{1v} are commutative to each other. Thus, C_{1v} and C'_{1v} have all of the conditions mentioned in the theorem, and based on this theorem, it is possible to say that $C_{1v} \times C'_{1v}$ *is isomorphic to* C_{2v}.

It is possible to show the one-by-one correspondence between the elements of $C_{1v} \times C'_{1v}$ and those of C_{2v} as follows:

$$(e, e) \overset{\cong}{\longleftrightarrow} e, \quad (\sigma_x, e) \overset{\cong}{\longleftrightarrow} \sigma_x, \quad (e, \sigma_y) \overset{\cong}{\longleftrightarrow} \sigma_y, \quad (\sigma_x, \sigma_y) \overset{\cong}{\longleftrightarrow} C_2.$$

The above discussion shows that when two symmetric paths $S^{(1)}$ and $S^{(2)}$ with symmetry groups $G^{(1)}$ and $G^{(2)}$ are composed together by the Cartesian product, they

Table 12.1 Element of C_{2v}

C_{2v}		C_{1v}		C'_{1v}
e	=	e	.	e
σ_x	=	σ_x	.	e
σ_y	=	e	.	σ_y
C_2	=	σ_x	.	σ_y

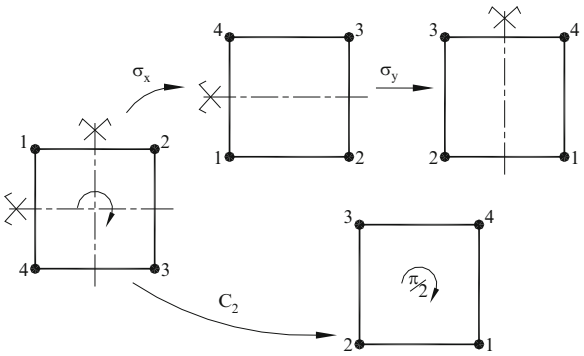

Fig. 12.2 Illustration of $\sigma_x \cdot \sigma_y$ being identical to C_2

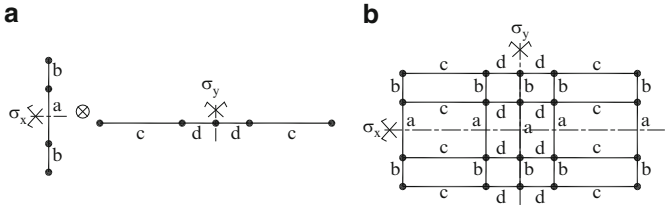

Fig. 12.3 Cartesian product of symmetric paths P_3 and P_4. (**a**) P_3 and P_4 paths with symmetry group C_{1v}. (**b**) Cartesian product of symmetric P_3 and P_4, with symmetry group $C_{2v} \cong C_{1v} \times C'_{1v}$

generate a symmetric graph S having symmetry group G, where $G \cong G^{(1)} \times G^{(2)}$. Here, ' $\cong$ ' is the symbol of isomorphism. In the product of two symmetric paths, $G^{(1)}$ and $G^{(2)}$ are usually the point group C_{1v}, and their Cartesian product will result in a symmetric graph of group C_{2v}. Figure 12.3 shows another example of this case.

Example 12.2. The Cartesian product of a symmetric weighted path and an asymmetric weighted path is studied in this example. Two paths are shown in Fig. 12.4: a symmetric path P_4 with symmetry group C_{1v} and an asymmetric path P_3. As mentioned before, the identical symmetry is one of the symmetry operations of all bodies, either symmetric or asymmetric. Thus, even the asymmetric graph $S^{(2)}$ has one symmetry operation $\{e\}$ and belongs to the symmetry group which is called C_1.

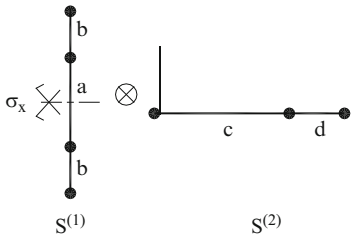

Fig. 12.4 Generators $S^{(1)}$ and $S^{(2)}$ (symmetric path P_4 and asymmetric path P_2)

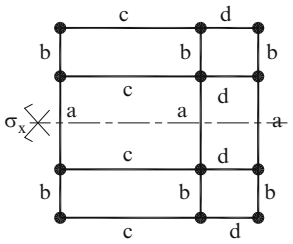

Fig. 12.5 Graph S: Cartesian product of generators $S^{(1)}$ and $S^{(2)}$

If these graphs are composed by the Cartesian product, they generate a new graph (say graph S). Let us predict the symmetry group of this graph from the symmetry groups of its generators. The direct product of the groups of generators will be as follows:

$$S^{(1)}; C_{1v} = \{e,\ \sigma_x\} \text{ and } S^{(2)};\ C_1 = \{e\}.$$

Therefore,

$$S = S^{(1)} \times S^{(2)}; \quad C_{1v} \times C_1 = \{e, \sigma_x\} \otimes \{e\} = \{(e,e), (\sigma_x, e)\}$$

where

$$(e,e) \overset{\cong}{\longleftrightarrow} e, \quad (\sigma_x, e) \overset{\cong}{\longleftrightarrow} \sigma_x.$$

This shows isomorphism with the set $\{e, \sigma_x\}$, which is the set of symmetry elements of group C_{1v}. Therefore, the product of graphs $S^{(1)}$ and $S^{(2)}$ will just have a vertical plane of symmetry (σ_x) and belongs to the symmetry group C_{1v}. Figure 12.5 approves accuracy of this prediction.

12.3 Symmetry Analysis of Product Graphs

Examples presented in the previous section show that in regular graphs which can be expressed as the product of two paths, symmetry properties of both of the repeating and binding generators define the symmetry of the product. It was shown that the symmetry group of the product graph is isomorphic to direct product of the symmetry groups of the generators.

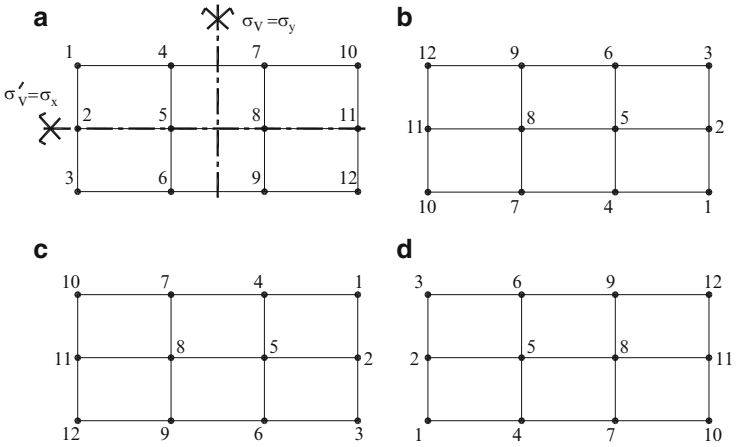

Fig. 12.6 Graph $G_1 = P_3\,(\mathrm{X})_{\mathrm{C}}\,P_4$ and its transformations under operators of the symmetry group C_{2v}. (**a**) Graph $P_3\,(\mathrm{X})_{\mathrm{C}}\,P_4$ and symmetry operation e. (**b**) Symmetry operation C_2. (**c**) I symmetry operation σ_y. (**d**) I symmetry operation σ_x

Now, we are going to show that the transformation matrix which decomposes any matrix associated to a symmetric-regular graph can be built using the generators of the graph. In order to highlight the improvement arisen by the method of the present section, a short review on conventional group theoretic method for decomposition of such graphs is presented first. This method has been developed before by Kaveh and Nikbakht [4] for decomposition of Laplacian matrix of a symmetric graph, and one can refer to this reference for further illustrations.

The method is described here briefly via the simple example of graph G_1, which is the Cartesian product of two paths P_3 and P_4, and was shown in Fig. 12.6. Symmetry operators of this graph are illustrated in Fig. 12.6a, with its symmetry operations in Fig. 12.6b–d.

Laplacian matrix of graph G_1 can be written as

$$\mathbf{L} = \begin{bmatrix}
2 & -1 & 0 & -1 & & & & & & & & \\
-1 & 3 & -1 & 0 & -1 & & & & & & & \\
0 & -1 & 2 & 0 & 0 & -1 & & & & \mathbf{0} & & \\
-1 & 0 & 0 & 3 & -1 & 0 & -1 & & & & & \\
 & -1 & 0 & -1 & 4 & -1 & 0 & -1 & & & & \\
 & & -1 & 0 & -1 & 3 & 0 & 0 & -1 & & & \\
 & & & -1 & 0 & 0 & 3 & -1 & 0 & -1 & & \\
 & & & & -1 & 0 & -1 & 4 & -1 & 0 & -1 & \\
 & & & & & -1 & 0 & -1 & 3 & 0 & 0 & -1 \\
 & & \mathbf{0} & & & & -1 & 0 & 0 & 2 & -1 & 0 \\
 & & & & & & & -1 & 0 & -1 & 3 & -1 \\
 & & & & & & & & -1 & 0 & -1 & 2
\end{bmatrix}. \tag{12.5}$$

Table 12.2 Reducible representation of C_{2v} on R^{12}

Element	Γ_i	$\Gamma_i\{\mathbf{u}\}$	$\chi(\Gamma_i)$
E	Γ_1	$\{u_1, u_2, u_3, u_4, u_5, u_6, u_7, u_8, u_9, u_{10}, u_{11}, u_{12}\}^t$	12
C_2	Γ_2	$\{u_{12}, u_{11}, u_{10}, u_9, u_8, u_7, u_6, u_5, u_4, u_3, u_2, u_1\}^t$	0
$\sigma_v(\sigma_y)$	Γ_3	$\{u_{10}, u_{11}, u_{12}, u_7, u_8, u_9, u_4, u_5, u_6, u_1, u_2, u_3\}^t$	0
$\sigma'_v(\sigma_x)$	Γ_4	$\{u_3, u_2, u_1, u_6, u_5, u_4, u_9, u_8, u_7, u_{12}, u_{11}, u_{10}\}^t$	4

Symmetry group of graph G_1 is C_{2v}. Figure 12.6 shows this graph under the effect of each of the four symmetry operations of this group. σ_y and σ_x, as the vertical planes of symmetry, are generally shown by σ_v and σ'_v in notation of the representation theory.

Graph G_1 includes 12 nodes, and its Laplacian is a 12×12 matrix, having 12 eigenvalues. This matrix can be decomposed into mutually independent submatrices of lower orders. In other words, we correlate all the nodes of the graph into a limited number of nodes, in each symmetry mode. Let us consider vector $\mathbf{u}$ as a basis vector, collecting all the nodes of the graph as its entries. This is the basis on which the Laplacian matrix of Eq. 12.5 was written.

$$\mathbf{u} = \{u_1, u_2, u_3, \ldots, u_{11}, u_{12}\}^{\mathrm{t}}.$$

Effect of each symmetry operation on this basis can be written using Fig. 12.6. When nodes are rearranged under each of the symmetry operations as shown in Fig. 12.6b, the vector $\mathbf{u}$ will be converted to a new vector (let us denote this by $\mathbf{u}'$). In this sense, symmetry operations can be considered as transformation operations, which transform $\mathbf{u}$ into $\mathbf{u}'$s.

Following this procedure for all of the symmetry operations of the symmetry group on the basis of vector $\mathbf{u}$, a set of transformation operations will arise, known as the *representation* of that group. In this example, using vector $\mathbf{u}$ (a 12-dimensional vector) results in a set of operations each of which is a 12-dimensional matrix. This set is called a *reducible representation (redrep)* of the group, conventionally shown by Γ. Complete set of representations $\Gamma.\mathbf{u}$'s are shown in Table 12.2. Such a representation can be reduced in dimension. It can be shown from representation theory that changing selected basis vector may arise in sets of matrices of lower dimensions. Each of these new sets will be another representation of the symmetry group, which is reduced in size. This process can be continued, and the dimension of resulted representations can be reduced more and more. As soon as there is no new basis, which can result in new representation of a lower dimension, the representation will be called an *irreducible representation (irrep)* of that symmetry group, shown by letter γ. It is possible to classify irreps of a symmetry group by means of characters. This is known as the *character table* of the group. Classes of the group form the columns of this table, while the rows are associated with different irreps. In this sense, each entry of the table shows the character of a class of the group in an irreducible representation. Comprehensive lists of such tables are widely available in different references [3, 5]. Table 12.3 is the character table of group C_{2v}.

Table 12.3 Character table of group C_{2v}

C_{2v}	e	C_2	σ_v	σ'_v
$\gamma^{(1)}$	1	1	1	1
$\gamma^{(2)}$	1	1	−1	−1
$\gamma^{(3)}$	1	−1	1	−1
$\gamma^{(4)}$	1	−1	−1	1

In the last column of Table 12.2, the characters of different representations can be found. These are calculated from those nodes that have been transformed into a coefficient of themselves under the symmetry operation. The character is the algebraic summation of these coefficients. In order to give an example, $\chi(\sigma_y)$ is calculated below:

$$\Gamma_4.\mathbf{u} = \left\{ u_3, \underset{\uparrow}{u_2}, u_1, u_6, \underset{\uparrow}{u_5}, u_4, u_9, \underset{\uparrow}{u_8}, u_7, u_{12}, \underset{\uparrow}{u_{11}}, u_{10} \right\}^t$$
$$\chi(\Gamma_4) = (+1+1+1+1) = 4.$$

Equation 12.12 provides the dimension of decomposed subgraphs. In this equation, m is the order of the point group, and $\gamma_i^{(\mu)}$s (i = *1,2,. . .,m*) are $m_\mu \times m_\mu$ matrices of redrep of the group. n_μ denotes the dimension of $V^{(\mu)}$ (the subspace associated with the μth subsystem), and $\chi(\mathbf{M})$ is the character (trace) for any given square matrix $\mathbf{M}$.

$$n_\mu = \frac{m_\mu}{m} \sum_1^m \left[\chi\left(\gamma_i^{(\mu)}\right) \chi(\Gamma_i) \right]. \tag{12.6}$$

Based on the above equation, and using Tables 12.2 and 12.3, one can easily find n_1=n_4=4 and n_2=n_3=2. This indicates that the symmetric graph G_1 can be decomposed into four independent subgraphs, and consequently, 12 × 12 Laplacian matrix of Eq. 12.5 is transformed into a block-diagonal matrix with two diagonal factors of dimension 4, and two diagonal factors of dimension 2. Each block is associated with one symmetry mode of the graph. A possible way to find these modes is using *idempotent* operators from the following equation [6]:

$$p^{(\mu)} = \frac{m_\mu}{m} \sum_1^m \left[\chi\left(\gamma_i^{(\mu)}\right) . \Gamma_i \right] \tag{12.7}$$

where $p^{(\mu)}$ is the idempotent associated with the subspace of the μ in the subgraph; $V^{(\mu)}$:

$$p^{(1)} = \frac{1}{4} \times [\Gamma_1 + \Gamma_2 + \Gamma_3 + \Gamma_4],\ p^{(2)} = \frac{1}{4} \times [\Gamma_1 + \Gamma_2 - \Gamma_3 - \Gamma_4],$$

$$p^{(3)} = \frac{1}{4} \times [\Gamma_1 - \Gamma_2 + \Gamma_3 - \Gamma_4],\ p^{(4)} = \frac{1}{4} \times [\Gamma_1 - \Gamma_2 - \Gamma_3 + \Gamma_4].$$

One can easily find the basis of each subspace $V^{(\mu)}$ as the range of idempotent $P^{(\mu)}$. It is enough to multiply the idempotent by the basis of the original vector space V and recognise independent sets that form the result. For example, for subspace $V^{(1)}$, we have

$$p^{(1)}.\mathbf{u} = \frac{\Gamma_1 + \Gamma_2 + \Gamma_3 + \Gamma_4}{4}.\mathbf{u} = \{\alpha, \beta, \alpha, \gamma, \theta, \gamma, \gamma, \theta, \gamma, \alpha, \beta, \alpha\}^t$$

in which

$$\alpha = \frac{u_1 + u_3 + u_{10} + u_{12}}{4},\ \beta = \frac{u_2 + u_{11}}{2},\ \gamma = \frac{u_4 + u_6 + u_7 + u_9}{4},\ \theta = \frac{u_5 + u_8}{2}.$$

From the above result, independent unit basis vectors of subspace $V^{(1)}$ can easily be extracted as follows:

$$\boldsymbol{\psi}_1{}^{(1)} = \frac{1}{2}\{1, 0, 1, 0, 0, 0, 0, 0, 0, 1, 0, 1\}^t,$$
$$\boldsymbol{\psi}_2{}^{(1)} = \frac{1}{\sqrt{2}}\{0, 1, 0, 0, 0, 0, 0, 0, 0, 0, 1, 0\}^t,$$

$$\boldsymbol{\psi}_3{}^{(1)} = \frac{1}{2}\{0, 0, 0, 1, 0, 1, 1, 0, 1, 0, 0, 0\}^t,$$
$$\boldsymbol{\psi}_4{}^{(1)} = \frac{1}{\sqrt{2}}\{0, 0, 0, 0, 1, 0, 0, 1, 0, 0, 0, 0\}^t.$$

Any set of the $\boldsymbol{\psi}_i{}^{(\mu)}$s, known as the *symmetry modes*, for a constant μ is associated to one symmetry type of the graph. This is shown in Fig. 12.7. In this figure, nodes, which contribute to a symmetry mode with positive sign, are shown in black points, and those which participate in the symmetry mode with negative sign are shown by the white points. It is found from this figure that the first subspace corresponds to a symmetric graph with respect to both σ_x and σ_y planes. In the second subspace, graph is antisymmetric with respect to both σ_x and σ_y, while in each of the third and fourth subspaces, the graph is symmetric with respect to one of the planes and antisymmetric with respect to the other one.

As it was shown before [4], the set of all symmetry modes with the same symmetry type (i.e. the symmetry modes of one subspace) can form the transformation matrix which can block diagonalise matrices of the graph. In other words, if we collect all of the $\boldsymbol{\psi}_i{}^{(\mu)}$s for a given μ, in an $n_\mu \times n_\mu$ matrix $\mathbf{T}^{(\mu)}$, then we will have

$$\mathbf{L}^{(\mu)} = \mathbf{T}^{(\mu)t}.\mathbf{L}.\mathbf{T}^{(\mu)}, \tag{12.8}$$

in which $\mathbf{L}^{(\mu)}$ is the given μth diagonal block of the block-factored Laplacian matrix $\mathbf{L}$. Therefore, Laplacian matrix $\mathbf{L}$ is decomposed into h submatrices, each of which

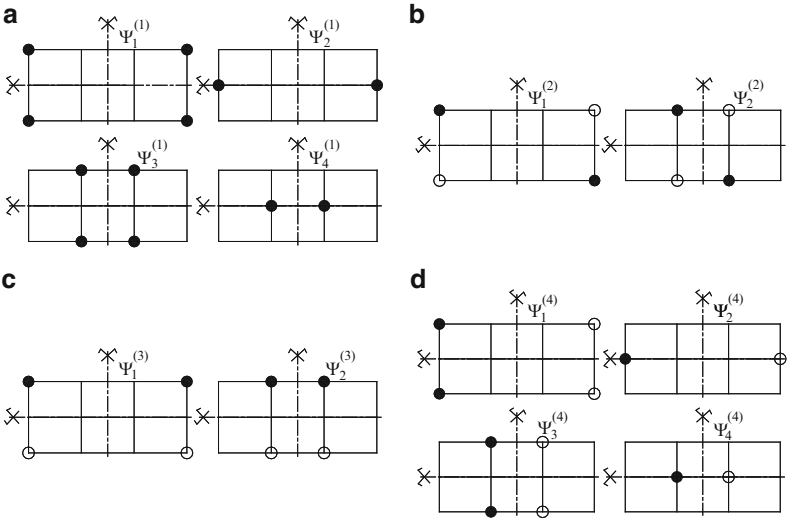

Fig. 12.7 Symmetry modes of Graph $G_1 = P_3\,(\mathrm{X})_\mathrm{C}\,P_4$. (**a**) Subspace $V^{(1)}$. (**b**) Subspace $V^{(2)}$. (**c**) I subspace $V^{(3)}$. (**d**) I subspace $V^{(4)}$

is associated with one of the subspaces. H is the number of classes of the symmetry group.

Instead of the above operations, it is possible to collect $\mathbf{T}^{(1)}$ to $\mathbf{T}^{(h)}$ together in an $n \times n$ matrix $\mathbf{T}$ and perform the procedures for all of the subspaces in one step as follows:

$$\bar{\mathbf{L}} = \mathbf{T}^t.\mathbf{L}.\mathbf{T} \tag{12.9}$$

in which $\bar{\mathbf{L}}$ is the block-diagonal Laplacian matrix of the graph.

$$\mathbf{T} = \frac{1}{2}\left[\begin{array}{cccc|cc|cc|cccc}
1 & 0 & 0 & 0 & 1 & 0 & 1 & 0 & 1 & 0 & 0 & 0 \\
0 & \sqrt{2} & 0 & 0 & 0 & 0 & 0 & 0 & 0 & \sqrt{2} & 0 & 0 \\
1 & 0 & 0 & 0 & -1 & 0 & -1 & 0 & 1 & 0 & 0 & 0 \\
0 & 0 & 1 & 0 & 0 & 1 & 0 & 1 & 0 & 0 & 1 & 0 \\
0 & 0 & 0 & \sqrt{2} & 0 & 0 & 0 & 0 & 0 & 0 & 0 & \sqrt{2} \\
0 & 0 & 1 & 0 & 0 & -1 & 0 & -1 & 0 & 0 & 1 & 0 \\
0 & 0 & 1 & 0 & 0 & -1 & 0 & 1 & 0 & 0 & -1 & 0 \\
0 & 0 & 0 & \sqrt{2} & 0 & 0 & 0 & 0 & 0 & 0 & 0 & -\sqrt{2} \\
0 & 0 & 1 & 0 & 0 & 1 & 0 & -1 & 0 & 0 & -1 & 0 \\
1 & 0 & 0 & 0 & -1 & 0 & 1 & 0 & -1 & 0 & 0 & 0 \\
0 & \sqrt{2} & 0 & 0 & 0 & 0 & 0 & 0 & 0 & -\sqrt{2} & 0 & 0 \\
1 & 0 & 0 & 0 & 1 & 0 & -1 & 0 & -1 & 0 & 0 & 0
\end{array}\right]. \tag{12.10}$$

It is proven in linear algebra that similarity transformation does not change the eigenvalues of a matrix. Therefore, it is possible to calculate the eigenvalues of two 2×2 and two 4×4 matrices instead of a 12×12 matrix.

$$\mathbf{L}^{(1)} = \begin{bmatrix} 1 & -\sqrt{2} & -1 & 0 \\ & 3 & 0 & -1 \\ & & 2 & -\sqrt{2} \\ Sym. & & & 3 \end{bmatrix}, \mathbf{L}^{(2)} = \begin{bmatrix} 2 & -1 \\ Sym. & 4 \end{bmatrix},$$

$$\mathbf{L}^{(3)} = \begin{bmatrix} 2 & -1 \\ Sym. & 2 \end{bmatrix}, \mathbf{L}^{(4)} = \begin{bmatrix} 2 & -\sqrt{2} & -1 & 0 \\ & 3 & 0 & -1 \\ & & 4 & -\sqrt{2} \\ Sym. & & & 5 \end{bmatrix}.$$

- *Graph–Group Method:* Procedure described above is the general group theoretic method for decomposition of symmetric graphs. However, when graph is regular (in the sense described before), graph product can enhance the method and reduce the volume of calculations. As it was seen, symmetry modes of regular graphs are combinations of symmetry modes of the generators. A method will be presented in this section based on finding symmetric and asymmetric modes of the factors and then combining these modes based on the character table of the product group. Steps of this method are described for this example in the following.

Step 1*: Finding symmetry group of the product graph:* When a graph is recognised as the product of two paths P_m and P_n, its symmetry group can be predicted as the direct product of the symmetry groups of the factors. This is proven in the previous section. Therefore, for this example, symmetry group of graph G_1 will be C_{2v}, which is the direct product of groups C_{1v}.

Step 2*: Finding symmetric and antisymmetric modes of the factors:* it can be possible to find symmetric and antisymmetric modes for a given path, with respect to its plane of symmetry (if available). These modes for each of the generators P_3 and P_4 of graph G_1 are shown in Fig. 12.8, based on the convention described for Fig. 12.7. These modes can be presented in matrix format as follows:

$$\mathbf{T}_{P3,Sym} = \begin{bmatrix} 1 & 0 \\ 0 & 1 \\ 1 & 0 \end{bmatrix}, \mathbf{T}_{P3,Anti-Sym} = \begin{bmatrix} 1 \\ 0 \\ -1 \end{bmatrix}, \mathbf{T}_{P4,Sym} = \begin{bmatrix} 1 & 0 \\ 0 & 1 \\ 0 & 1 \\ 1 & 0 \end{bmatrix} \text{ and}$$

$$\mathbf{T}_{P4,Anti-Sym} = \begin{bmatrix} 1 & 0 \\ 0 & 1 \\ 0 & -1 \\ -1 & 0 \end{bmatrix}.$$

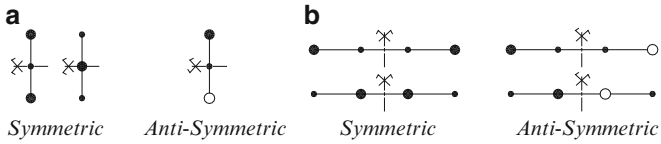

Fig. 12.8 Symmetric and antisymmetric modes of paths P_3 and P_4. (**a**) Repeating factor P_3. (**b**) Binding factor P_4

The entries of these matrices show independent nodes of associated path that are necessary for spanning the entire path in each of the symmetric and antisymmetric modes. These matrices will be called as the *mode matrices*.

Step 3: *Combining the mode matrices:* In order to reach to the symmetry modes of the product graph, different modes of the factors should be combined based on a specific order. For each subspace, character table of symmetry group of the product graph (found in step 1) governs this order.

For graph G_1, the character table of group C_{2v}, has been given previously in Table 12.3. For each subspace, mode matrices of the two factors contribute in either symmetric or antisymmetric form, based on the character of its symmetry operation in the irrep associated to that subspace. For example, in graph G_1, repeating factor (P_3) is associated with symmetry operation $\sigma_x(\sigma'_v)$. Characters of this operation in irreducible representations of group C_{2v} are as follows: +1, −1, −1 and +1. This means that subspaces $V^{(1)}$ and $V^{(4)}$ are symmetric, and subspaces $V^{(2)}$ and $V^{(3)}$ are antisymmetric with respect to the symmetry operation σ_x. Therefore, mode matrix of the repeating factor should contribute in its symmetric form in the first and the last subspace, and in its antisymmetric form, in the second and the third subspaces.

Combination of mode matrices of the factors should be based on the same rules of combination of their symmetry groups. Kronecker product (introduced in Sect. 12.3) is used for this purpose. Binding factor is the factor which controls the pattern of repeating, and therefore, its associated matrices should dictate the pattern of product matrix. Therefore, the mode matrix of the binding factor comes first in the Kronecker product. This can be described as follows:

$$\mathbf{T}^{(\mu)} = \mathbf{T}_{binding} \otimes \mathbf{T}_{repeating} \tag{12.11}$$

In order to more highlight the procedure, calculations for different subspaces are presented below:

$$\mathbf{T}^{(1)} = \mathbf{T}_{P4,Sym} \otimes \mathbf{T}_{P3,Sym} = \begin{bmatrix} 1 & 0 \\ 0 & 1 \\ 0 & 1 \\ 1 & 0 \end{bmatrix} \otimes \begin{bmatrix} 1 & 0 \\ 0 & 1 \\ 1 & 0 \end{bmatrix} = \begin{bmatrix} \begin{bmatrix} 1 & 0 \\ 0 & 1 \\ 1 & 0 \end{bmatrix} & & \\ & \begin{bmatrix} 1 & 0 \\ 0 & 1 \\ 1 & 0 \end{bmatrix} & \\ & \begin{bmatrix} 1 & 0 \\ 0 & 1 \\ 1 & 0 \end{bmatrix} & \\ & & \begin{bmatrix} 1 & 0 \\ 0 & 1 \\ 1 & 0 \end{bmatrix} \end{bmatrix} = \begin{bmatrix} 1 & 0 & 0 & 0 \\ 0 & 1 & 0 & 0 \\ 1 & 0 & 0 & 0 \\ 0 & 0 & 1 & 0 \\ 0 & 0 & 0 & 1 \\ 0 & 0 & 1 & 0 \\ 0 & 0 & 1 & 0 \\ 0 & 0 & 0 & 1 \\ 0 & 0 & 1 & 0 \\ 1 & 0 & 0 & 0 \\ 0 & 1 & 0 & 0 \\ 1 & 0 & 0 & 0 \end{bmatrix}$$

$$\mathbf{T}^{(2)} = \mathbf{T}_{P4,Anti-Sym} \otimes \mathbf{T}_{P3,Anti-Sym} = \begin{bmatrix} 1 & 0 \\ 0 & 1 \\ 0 & -1 \\ -1 & 0 \end{bmatrix} \otimes \begin{bmatrix} 1 \\ 0 \\ -1 \end{bmatrix}$$

$$= \begin{bmatrix} \begin{bmatrix} 1 \\ 0 \\ -1 \end{bmatrix} & & \\ & \begin{bmatrix} 1 \\ 0 \\ -1 \end{bmatrix} & \\ & -1 \times \begin{bmatrix} 1 \\ 0 \\ -1 \end{bmatrix} & \\ -1 \times \begin{bmatrix} 1 \\ 0 \\ -1 \end{bmatrix} & & \end{bmatrix} = \begin{bmatrix} 1 & 0 \\ 0 & 0 \\ -1 & 0 \\ 0 & 1 \\ 0 & 0 \\ 0 & -1 \\ 0 & -1 \\ 0 & 0 \\ 0 & 1 \\ -1 & 0 \\ 0 & 0 \\ 1 & 0 \end{bmatrix}$$

$$\mathbf{T}^{(3)} = \mathbf{T}_{P4,Sym} \otimes \mathbf{T}_{P3,Anti-Sym} = \begin{bmatrix} 1 & 0 \\ 0 & 1 \\ 0 & 1 \\ 1 & 0 \end{bmatrix} \otimes \begin{bmatrix} 1 \\ 0 \\ -1 \end{bmatrix} = \begin{bmatrix} \begin{bmatrix} 1 \\ 0 \\ -1 \end{bmatrix} & \\ & \begin{bmatrix} 1 \\ 0 \\ -1 \end{bmatrix} \\ & \begin{bmatrix} 1 \\ 0 \\ -1 \end{bmatrix} \\ \begin{bmatrix} 1 \\ 0 \\ -1 \end{bmatrix} & \end{bmatrix}$$

$$= \begin{bmatrix} 1 & 0 \\ 0 & 0 \\ -1 & 0 \\ 0 & 1 \\ 0 & 0 \\ 0 & -1 \\ 0 & 1 \\ 0 & 0 \\ 0 & -1 \\ 1 & 0 \\ 0 & 0 \\ -1 & 0 \end{bmatrix}$$

$$\mathbf{T}^{(4)} = \mathbf{T}_{P4,Anti-Sym} \otimes \mathbf{T}_{P3,Sym} = \begin{bmatrix} 1 & 0 \\ 0 & 1 \\ 0 & -1 \\ -1 & 0 \end{bmatrix} \otimes \begin{bmatrix} 1 & 0 \\ 0 & 1 \\ 1 & 0 \end{bmatrix}$$

$$= \begin{bmatrix} \begin{bmatrix} 1 & 0 \\ 0 & 1 \\ 1 & 0 \end{bmatrix} & \\ & \begin{bmatrix} 1 & 0 \\ 0 & 1 \\ 1 & 0 \end{bmatrix} \\ & -1 \times \begin{bmatrix} 1 & 0 \\ 0 & 1 \\ 1 & 0 \end{bmatrix} \\ -1 \times \begin{bmatrix} 1 & 0 \\ 0 & 1 \\ 1 & 0 \end{bmatrix} & \end{bmatrix} = \begin{bmatrix} 1 & 0 & 0 & 0 \\ 0 & 1 & 0 & 0 \\ 1 & 0 & 0 & 0 \\ 0 & 0 & 1 & 0 \\ 0 & 0 & 0 & 1 \\ 0 & 0 & 1 & 0 \\ 0 & 0 & -1 & 0 \\ 0 & 0 & 0 & -1 \\ 0 & 0 & -1 & 0 \\ -1 & 0 & 0 & 0 \\ 0 & -1 & 0 & 0 \\ -1 & 0 & 0 & 0 \end{bmatrix}.$$

Now it is enough to normalise the columns of $\mathbf{T}^{(\mu)}$s. The results are as follows. Comparison of Eq. 12.18 and the blocks of matrix $\mathbf{T}$ (Eq. 12.10) verifies the accuracy of the method.

$$\mathbf{T}^{(1)} = \frac{1}{2}\begin{bmatrix} 1 & 0 & 1 & 0 & 0 & 0 & 0 & 0 & 0 & 1 & 0 & 1 \\ 0 & \sqrt{2} & 0 & 0 & 0 & 0 & 0 & 0 & 0 & 0 & \sqrt{2} & 0 \\ 0 & 0 & 0 & 1 & 0 & 1 & 1 & 0 & 1 & 0 & 0 & 0 \\ 0 & 0 & 0 & 0 & \sqrt{2} & 0 & 0 & \sqrt{2} & 0 & 0 & 0 & 0 \end{bmatrix}^t \tag{12.12a}$$

$$\mathbf{T}^{(2)} = \frac{1}{2}\begin{bmatrix} 1 & 0 & -1 & 0 & 0 & 0 & 0 & 0 & 0 & -1 & 0 & 1 \\ 0 & 0 & 0 & 1 & 0 & -1 & -1 & 0 & 1 & 0 & 0 & 0 \end{bmatrix}^t \tag{12.12b}$$

$$\mathbf{T}^{(3)} = \frac{1}{2}\begin{bmatrix} 1 & 0 & -1 & 0 & 0 & 0 & 0 & 0 & 0 & 1 & 0 & -1 \\ 0 & 0 & 0 & 1 & 0 & -1 & 1 & 0 & -1 & 0 & 0 & 0 \end{bmatrix}^t \tag{12.12c}$$

$$\mathbf{T}^{(4)} = \frac{1}{2}\begin{bmatrix} 1 & 0 & 1 & 0 & 0 & 0 & 0 & 0 & 0 & -1 & 0 & -1 \\ 0 & \sqrt{2} & 0 & 0 & 0 & 0 & 0 & 0 & 0 & 0 & -\sqrt{2} & 0 \\ 0 & 0 & 0 & 1 & 0 & 1 & -1 & 0 & -1 & 0 & 0 & 0 \\ 0 & 0 & 0 & 0 & \sqrt{2} & 0 & 0 & -\sqrt{2} & 0 & 0 & 0 & 0 \end{bmatrix}^t . \tag{12.12d}$$

Step 4: *Decomposition of the matrices:* Matrices associated to the product graph can now be decomposed based on Eq. 12.8, using transformation matrices $\mathbf{T}^{(\mu)}$.

Strong Cartesian product of the factors P_3 and P_4 is shown in Fig. 12.9. This is another example of a symmetric-regular structure. It is seen that symmetry properties of this graph are exactly the same as those of graph G_1. These two graphs belong to the same symmetry group, and the same matrices $\mathbf{T}^{(\mu)}$ can be used to decompose the matrices of these two graphs. Laplacian matrix of graph G_2 is

$$\mathbf{L} = \begin{bmatrix} 3 & -1 & 0 & -1 & -1 & & & & & & & \\ -1 & 5 & -1 & -1 & -1 & -1 & & & & & & \\ 0 & -1 & 3 & 0 & -1 & -1 & 0 & & & \mathbf{0} & & \\ -1 & -1 & 0 & 5 & -1 & 0 & -1 & -1 & & & & \\ -1 & -1 & -1 & -1 & 8 & -1 & -1 & -1 & -1 & & & \\ & -1 & -1 & 0 & -1 & 5 & 0 & -1 & -1 & 0 & & \\ & & 0 & -1 & -1 & 0 & 5 & -1 & 0 & -1 & -1 & \\ & & & -1 & -1 & -1 & -1 & 8 & -1 & -1 & -1 & -1 \\ & & & & -1 & -1 & 0 & -1 & 5 & 0 & -1 & -1 \\ & & \mathbf{0} & & & 0 & -1 & -1 & 0 & 3 & -1 & 0 \\ & & & & & & -1 & -1 & -1 & -1 & 5 & -1 \\ & & & & & & & -1 & -1 & 0 & -1 & 3 \end{bmatrix} .$$

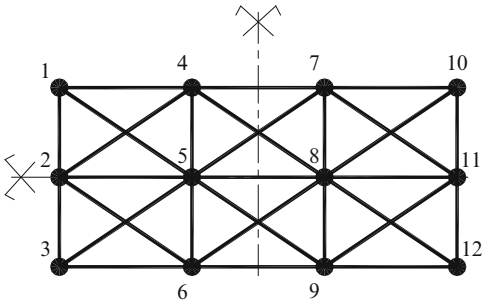

Fig. 12.9 Graph $G_2 = P_3\,(\mathrm{X})_{\mathrm{SC}}\,P_4$

This matrix can be decomposed into four submatrices, using Eq. 12.9, and transformation matrices $\mathbf{T}^{(1)}$ to $\mathbf{T}^{(4)}$ in Eq. 12.18:

$$\mathbf{L}^{(1)} = \begin{bmatrix} 3 & -\sqrt{2} & -1 & -\sqrt{2} \\ & 5 & -\sqrt{2} & -1 \\ & Sym & 4 & -2\sqrt{2} \\ & & & 7 \end{bmatrix}, \mathbf{L}^{(2)} = \begin{bmatrix} 3 & -1 \\ -1 & 6 \end{bmatrix}, \mathbf{L}^{(3)} = \begin{bmatrix} 3 & -1 \\ -1 & 4 \end{bmatrix} \text{ and}$$

$$\mathbf{L}^{(4)} = \begin{bmatrix} 3 & -\sqrt{2} & -1 & -\sqrt{2} \\ & 5 & -\sqrt{2} & -1 \\ & Sym & 6 & 0 \\ & & & 9 \end{bmatrix}.$$

Direct product of two paths P_3 and P_4 is another graph of symmetry group C_{2v}, Fig. 12.10a. Having 12 nodes, matrices $\mathbf{T}^{(\mu)}$ of Eq. 12.18 can be again used to decompose the 12×12 Laplacian matrix of the graph into diagonal blocks of dimensions two and four, similar to what was shown for graphs G_1 and G_2.

It should be noted that graph G_3 is composed of two independent graphs, which are shown in Fig. 12.10b. Since these graphs are identical to each other, one can just solve one of them and then repeat each of the eigenvalues twice to form the complete set of eigenvalues of the system. Therefore, half of the nodes are enough to be studied. This reduces the dimension of the problem to 6×6. Each of the new graphs has only one vertical plane of symmetry, and symmetry group of them is C_{1v}. Although this is a group of order two, with just two classes, the reduction of a 12×12 matrix to 6×6 is beneficial enough to considerably lower the computational time and effort.

Note: It is noted here that decomposition of Laplacian matrix of direct product and strong Cartesian product of two paths is not possible in graph theory by this time, without adding extra elements to the graph [7, 8]. Thus, for these cases, using a symmetry analysis in the way described seems inevitable.

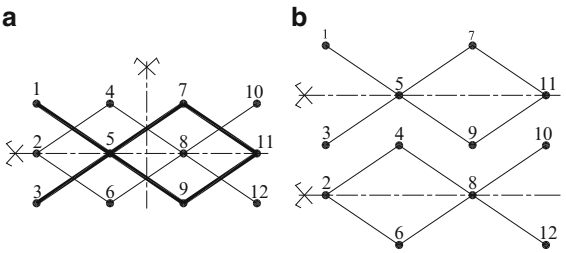

Fig. 12.10 Graph G_3, direct product of P_3 and P_4. (**a**) $G_3 = P_3\,(\mathrm{X})_{\mathrm{D}}\,P_4$. (**b**) G_3 as two disjoint graphs

12.4 Application in Analysis of Prestressed Cable Nets

In this section, vibration of prestressed cable nets is studied as a direct mechanical application of the proposed method. Analysis of cable networks which carry loads perpendicular to their plane has been interesting in structural mechanics, and especially for group theorists in this field. Such problems can be considered among benchmark problems of application of group theory in structural mechanics [9–11]. Here, we are going to use the method developed in the previous section for finding frequencies of such networks. For this purpose, first, a graph which is called *Net Graph* is mapped to the network, and then the natural frequencies are found as the eigenvalues of the Laplacian matrix of this graph. This leads to a considerable reduction in calculation efforts, and the dimension of matrices involved in the process of symmetry analysis.

- *Net graph for vibration of a cable network:* Fig. 12.11 shows one module of a cable network, which is formed from crossing of two perpendicular cables and comprises five nodes. Magnitude of pre tension forces in horizontal and vertical cables are assumed equal to T_x and T_y respectively. The net is supposed to support vertical loads at its nodes. Vertical load applied on node (i,j) is shown as $P_{i,j}$. A deformed position of the five-node module during free vibration of the net is shown in Fig. 12.11. Equilibrium of applied loads on this module in vertical direction results in

$$\begin{aligned}
&\sum F_z = 0;\\
&T_x(\sin\alpha_{i-1} - \sin\alpha_{i+1}) + T_y\left(\sin\alpha_{j-1} - siv\alpha_{j+1}\right) - P_{i,j} = 0\\
&\frac{T_x}{a}\left(2w_{i,j} - w_{i-1,j} - w_{i+1,j}\right) + \frac{T_y}{b}\left(2w_{i,j} - w_{i,j-1} - w_{i,j+1}\right) = P_{i,j}.
\end{aligned} \tag{12.13}$$

If we violate the equilibrium of the node (i,j) by imposing a negligible displacement $u_{i,j}$, vibration equation of the node can be found, using the following assumptions and simplifications:

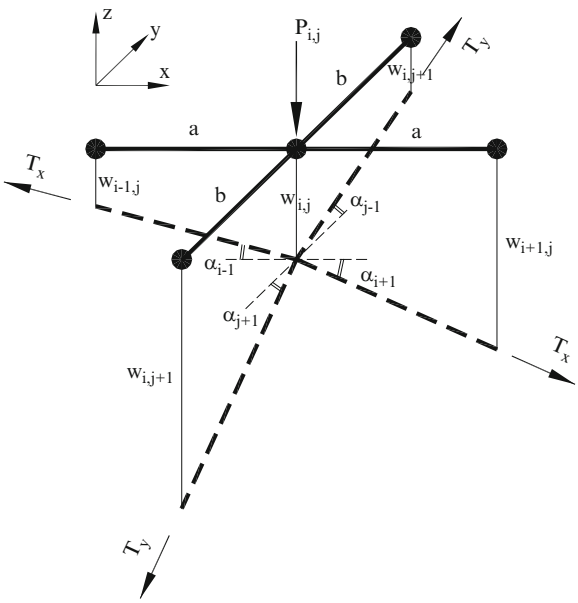

Fig. 12.11 One module of the cable net, comprising five nodes and four cable segments

1. Magnitudes of a and b stay constant during the vibration.
2. Cable segments stay straight between any two adjacent nodes and no local curve happens.
3. Prestressing forces in the cables are constant during the vibration of the net.

Based on these assumptions, dynamic equilibrium can be written for each node as follows:

$$\frac{T_x}{a}\left[2\left(w_{i,j}+u_{i,j}\right)-\left(w_{i-1,j}+u_{i-1,j}\right)-\left(w_{i+1,j}+u_{i+1,j}\right)\right]$$
$$+\frac{T_y}{b}\left[2\left(w_{i,j}+u_{i,j}\right)-\left(w_{i,j-1}+u_{i,j-1}\right)-\left(w_{i,j+1}+u_{i,j+1}\right)\right]-P_{i,j}+m_{i,j}.\ddot{u}_{i,j}=0.$$

Finally, this leads to the vibration equation of the node, as Eq. 12.14.

$$\frac{T_x}{a}\left(2u_{i,j}-u_{i-1,j}-u_{i+1,j}\right)+\frac{T_y}{b}\left(2u_{i,j}-u_{i,j-1}-u_{i,j+1}\right)+m_{i,j}.\ddot{u}_{i,j}=0. \qquad (12.14)$$

For a module with four extra nodes and totally eight cable segments, shown in Fig. 12.12, Eq. 12.13 can be modified by adding the following term to it:

$$\frac{T'}{c}\left(4u_{i,j}-u_{i-1,j-1}-u_{i+1,j-1}-u_{i-1,j+1}-u_{i+1,j+1}\right). \qquad (12.15)$$

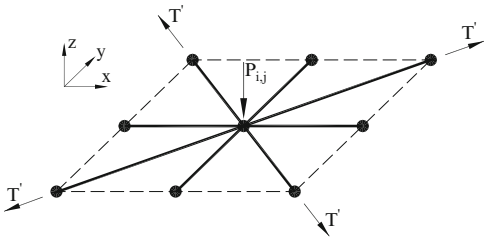

Fig. 12.12 A module of the cable net, composed of nine nodes and eight cable segments

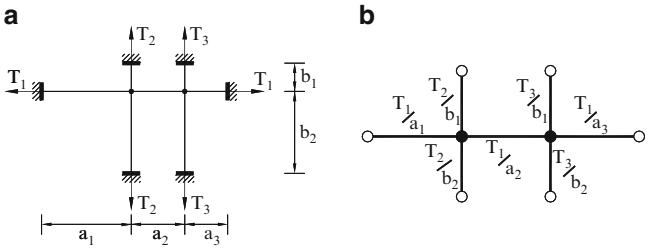

Fig. 12.13 A simple cable net and its associated net graph. (**a**) A net comprising of three cables. (**b**) Associated net graph

Here, a graph model is introduced for each cable net, by the means of which, it is possible to map the stiffness matrix of the system to the Laplacian matrix of the graph. Such transformation from the mechanical problem of vibrating prestressed cable nets to a mathematical problem in graph theory helps us to utilise the graph–group technique and develop it to the vibration analysis of such nets.

In the proposed graph model, each node of the cable net is shown as a vertex and each cable segment between two nodes is modelled as a weighted edge of the net graph. Figure 12.13 shows the net graph for a simple cable net consisting of three cables with prestressing forces T_1 to T_3. As illustrated in this figure, weight of an element associated to a cable segment of length l_i, with prestressing force T_i, equals to T_i/l_i. Each restrained node (support) is modelled as a null node in the net graph.

Laplacian matrix of the net graph is exactly the same as the stiffness matrix of the cable net. It should be noted here that although it is easily possible to introduce another graph associated to the mass matrix of the cable net, such a definition does not seem necessary. It is due to the fact that the mass matrices of such systems are always diagonal matrices – see Eq. 12.14 – and can easily be handled during decomposition process.

Example 12.3. Figure 12.14a shows a rectangular cable net with 15 nodes. Prestressing forces in all of the tendons are equal to T. Net graph of this network is presented in Fig. 12.14b, and factors of the net graph are shown in Fig. 12.14b. Laplacian matrix of graph NG_1 is the stiffness matrix of net N_1. This matrix is as

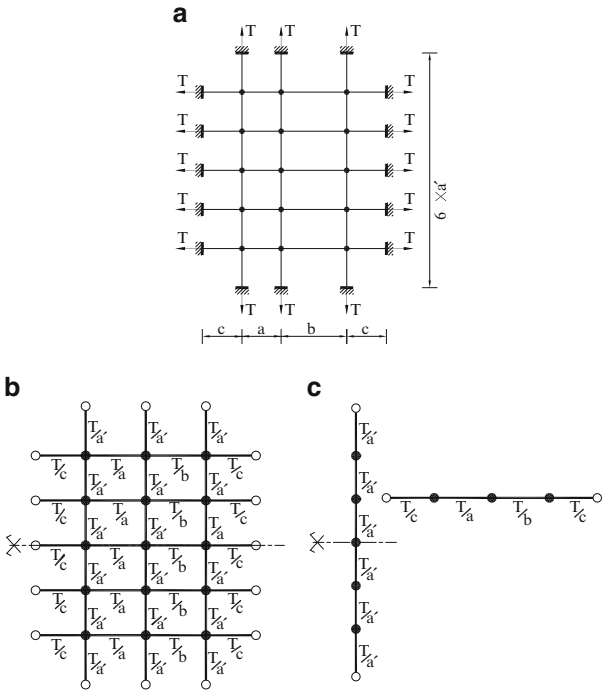

Fig. 12.14 A cable net with associated net graph and its factors. (**a**) Prestressed network N_1. (**b**) Net graph NG_1. (**c**) Factors of the net graph

Table 12.4 Character table of group C_{1v}

C_{2v}	e	σ_V
$\gamma^{(1)}$	1	1
$\gamma^{(2)}$	1	−1

shown in Eq. 12.16. Frequencies of the cable net are calculated as the eigenvalues of this matrix through the step-by-step method described in Sect. 12.5.

Step 1: Symmetry group of the repeating factor is C_{1v}, while the binding factor does not have any symmetry operation except the identical symmetry (e), which defines symmetry group C_1. Symmetry group of net graph NG_1 is the direct product of these two symmetry groups:

$$C_1 \otimes C_{1v} \cong C_{1v}.$$

Character table of this symmetry group is shown in Table 12.4.

$$\mathbf{L}=T\times\begin{bmatrix}
\alpha & -\frac{1}{a'} & 0 & 0 & 0 & -\frac{1}{a} & & & & & & & & & \\
 & \alpha & -\frac{1}{a'} & 0 & 0 & 0 & -\frac{1}{a} & & & & & & & & \\
 & & \alpha & -\frac{1}{a'} & 0 & 0 & 0 & -\frac{1}{a} & & & & & & & \\
 & & & \alpha & -\frac{1}{a'} & 0 & 0 & 0 & -\frac{1}{a} & & & & & & \\
 & & & & \alpha & 0 & 0 & 0 & 0 & -\frac{1}{a} & & & & & \\
 & & & & & \beta & -\frac{1}{a'} & 0 & 0 & 0 & -\frac{1}{b} & & & & \\
 & & & & & & \beta & -\frac{1}{a'} & 0 & 0 & 0 & -\frac{1}{b} & & & \\
 & & & & & & & \beta & -\frac{1}{a'} & 0 & 0 & 0 & -\frac{1}{b} & & \\
 & & & & & & & & \beta & -\frac{1}{a'} & 0 & 0 & 0 & -\frac{1}{b} & \\
 & & & & & & & & & \beta & 0 & 0 & 0 & 0 & -\frac{1}{b} \\
 & & & & \mathbf{SYM}. & & & & & & \gamma & -\frac{1}{a'} & 0 & 0 & 0 \\
 & & & & & & & & & & & \gamma & -\frac{1}{a'} & 0 & 0 \\
 & & & & & & & & & & & & \gamma & -\frac{1}{a'} & 0 \\
 & & & & & & & & & & & & & \gamma & -\frac{1}{a'} \\
 & & & & & & & & & & & & & & \gamma
\end{bmatrix} \tag{12.16}$$

in which

$$\begin{aligned}
\alpha &= \frac{1}{a}+\frac{1}{c}+\frac{2}{a'} \\
\beta &= \frac{1}{a}+\frac{1}{b}+\frac{2}{a'} \\
\gamma &= \frac{1}{b}+\frac{1}{c}+\frac{2}{a'}
\end{aligned}.$$

Step 2: Symmetric and antisymmetric deflections of repeating factor P_5 are shown in Fig. 12.14a, b. Binding factor P_3 in this example does not have any symmetry operation except the identical symmetry. Therefore, in any deflection shape of this factor, each node has its independent value. Mode matrix of a path P_n with such conditions will be $\mathbf{I_n}$, in which one non-zero entry is associated to each node of the path independently. Therefore, we will have

$$\mathbf{T}_{P5,Sym}=\begin{bmatrix}1 & & \\ & 1 & \\ & & 1 \\ & 1 & \\ 1 & & \end{bmatrix},\ \mathbf{T}_{P5,Anti-Sym}=\begin{bmatrix}1 & & \\ & & 1 \\ & & 0 \\ & & -1 \\ -1 & & \end{bmatrix},\ \mathbf{T}_{P3,ASym}=\begin{bmatrix}1 & & \\ & 1 & \\ & & 1\end{bmatrix}.$$

Step 3: Symmetry modes of the factors can now easily be combined based on Table 12.4

$$\mathbf{T}^{(1)} = \mathbf{T}_{P5,Sym} \otimes \mathbf{T}_{P3,ASym} = \begin{bmatrix} 1 & & \\ & 1 & \\ & & 1 \\ & 1 & \\ 1 & & \end{bmatrix} \otimes \begin{bmatrix} 1 & & \\ & 1 & \\ & & 1 \end{bmatrix} = \frac{1}{2} \begin{bmatrix} \mathbf{I}_{3\times3} & & \\ & \mathbf{I}_{3\times3} & \\ & & 2\mathbf{I}_{3\times3} \\ & \mathbf{I}_{3\times3} & \\ \mathbf{I}_{3\times3} & & \end{bmatrix}$$

$$\mathbf{T}^{(2)} = \mathbf{T}_{P5,AntiSym} \otimes \mathbf{T}_{P3,ASym} = \begin{bmatrix} 1 & & \\ & 1 & \\ & 0 & \\ & -1 & \\ -1 & & \end{bmatrix} \otimes \begin{bmatrix} 1 & & \\ & 1 & \\ & & 1 \end{bmatrix} = \frac{1}{2} \begin{bmatrix} \mathbf{I}_{3\times3} & & \\ & \mathbf{I}_{3\times3} & \\ & \mathbf{0}_{3\times3} & \\ & -\mathbf{I}_{3\times3} & \\ -\mathbf{I}_{3\times3} & & \end{bmatrix}.$$

Step 4: Stiffness matrix of the system is decomposed based on Eq. 12.9, using transformation matrices $\mathbf{T}^{(1)}$ and $\mathbf{T}^{(2)}$:

$$\mathbf{K}^{(1)} = \mathbf{L}^{(1)} = \mathbf{T}^{(1)^t} \times \mathbf{L} \times \mathbf{T}^{(1)}$$

$$= \frac{T}{4} \times \begin{bmatrix} \varepsilon & -\frac{2}{a'} & 0 & 0 & 0 & -\frac{1}{a'}-\frac{1}{a} & 0 & -\frac{2}{b} & 0 \\ & \varepsilon & -\frac{2}{a'} & 0 & 0 & 0 & -\frac{2}{a} & 0 & -\frac{2}{b} \\ & & \varepsilon & -\frac{1}{a'}-\frac{1}{b} & 0 & 0 & 0 & -\frac{2}{a} & 0 \\ & & & \xi & -\frac{1}{a'}-\frac{1}{a} & 0 & 0 & 0 & -\frac{2}{a'}-\frac{2}{a} \\ & & & & \varepsilon & -\frac{1}{a'}-\frac{1}{b} & 0 & 0 & 0 \\ & & & & & \eta & -\frac{2}{a'}-\frac{2}{b} & 0 & 0 \\ & & \mathbf{SYM.} & & & & \varsigma & -\frac{4}{a'} & 0 \\ & & & & & & & \varsigma & -\frac{4}{a'} \\ & & & & & & & & \varsigma \end{bmatrix}$$

$$\mathbf{K}^{(2)} = \mathbf{L}^{(2)} = \mathbf{T}^{(2)^t} \times \mathbf{L} \times \mathbf{T}^{(2)} = T \times \begin{bmatrix} \varepsilon & -\frac{2}{a'} & 0 & 0 & 0 & -\frac{1}{a'}-\frac{1}{a} \\ & \varepsilon & -\frac{2}{a'} & 0 & 0 & 0 \\ & & \varepsilon & -\frac{1}{a'}-\frac{1}{b} & 0 & 0 \\ & & & \xi & -\frac{1}{a'}+\frac{1}{a} & 0 \\ & & \mathbf{SYM.} & & \varepsilon & -\frac{1}{a'}+\frac{1}{b} \\ & & & & & \eta \end{bmatrix}$$

in which

$$\varepsilon = \frac{4}{a'} + \frac{1}{a} + \frac{1}{b} + \frac{2}{c}$$
$$\eta = \frac{4}{a'} + \frac{1}{a} + \frac{2}{b} + \frac{1}{c}$$
$$\xi = \frac{4}{a'} + \frac{2}{a} + \frac{1}{b} + \frac{1}{c}$$
$$\varsigma = \frac{8}{a'} + \frac{4}{a} + \frac{4}{b}.$$

Matrices $\mathbf{L}^{(1)}$ and $\mathbf{L}^{(2)}$ are similar to matrix $\mathbf{L}$. Therefore, the eigenvalues of stiffness matrix of the net will be the union of eigenvalues of matrices $\mathbf{L}^{(1)}$ and $\mathbf{L}^{(2)}$.

Natural frequencies of the net, which are the generalised eigenvalues of stiffness and mass matrices, can easily be calculated by just having the eigenvalues of the stiffness matrix. This is due to the fact that the mass matrix is diagonal:

$$\det(\mathbf{K} - \omega^2.\mathbf{M}) = \det(\mathbf{K} - m\omega^2.\mathbf{I}) = \det(\mathbf{K} - \lambda.\mathbf{I})$$

$$\lambda = m\omega^2 \Rightarrow \omega = \sqrt{\frac{\lambda}{m}} \tag{12.17}$$

in which λ is the eigenvalue of the stiffness matrix (or the Laplacian matrix of the net graph) and ω is the corresponding frequency of the cable net.

Example 12.4. Prestressed network N_2 shown in Fig. 12.15a is analysed as the second example. This problem has been formerly studied by Zingoni [10, 11] and solved through the conventional group theoretic method. Now we are going to use combined graph–group method. Stiffness matrix of the network is calculated as the Laplacian matrix of the net graph NG_2 which is illustrated in Fig. 12.15b:

$$\mathbf{K} = \mathbf{L} = \begin{bmatrix}
2(\frac{I}{a}+\frac{I'}{b}) & -\frac{I'}{b} & 0 & -\frac{I}{a} & & & & & & & & & \\
-\frac{I'}{b} & 2(\frac{I}{a}+\frac{I'}{b}) & -\frac{I'}{b} & 0 & -\frac{I}{a} & & & & & & & & \\
0 & -\frac{I'}{b} & 2(\frac{I}{a}+\frac{I'}{b}) & 0 & 0 & -\frac{I}{a} & & & & & & & \\
-\frac{I}{a} & 0 & 0 & 2(\frac{I}{a}+\frac{I'}{b}) & -\frac{I'}{b} & 0 & -\frac{I}{a} & & & & & & \\
 & -\frac{I}{a} & 0 & -\frac{I'}{b} & 2(\frac{I}{a}+\frac{I'}{b}) & -\frac{I'}{b} & 0 & -\frac{I}{a} & & & & & \\
 & & -\frac{I}{a} & 0 & -\frac{I'}{b} & 2(\frac{I}{a}+\frac{I'}{b}) & 0 & 0 & -\frac{I}{a} & & & & \\
 & & & -\frac{I}{a} & 0 & 0 & 2(\frac{I}{a}+\frac{I'}{b}) & -\frac{I'}{b} & 0 & -\frac{I}{a} & & & \\
 & & & & -\frac{I}{a} & 0 & -\frac{I'}{b} & 2(\frac{I}{a}+\frac{I'}{b}) & -\frac{I'}{b} & 0 & -\frac{I}{a} & & \\
 & & & & & -\frac{I}{a} & 0 & -\frac{I'}{b} & 2(\frac{I}{a}+\frac{I'}{b}) & 0 & 0 & -\frac{I}{a} & \\
 & & & & & & -\frac{I}{a} & 0 & 0 & 2(\frac{I}{a}+\frac{I'}{b}) & -\frac{I'}{b} & 0 & \\
 & & & & & & & -\frac{I}{a} & 0 & -\frac{I'}{b} & 2(\frac{I}{a}+\frac{I'}{b}) & -\frac{I'}{b} & \\
 & & & & & & & & -\frac{I}{a} & 0 & -\frac{I'}{b} & 2(\frac{I}{a}+\frac{I'}{b}) &
\end{bmatrix}.$$

Net graph NG_2 is the direct product of two paths P_3 and P_4. Such a product was studied formerly as graph G_1 in Chap. 5, and its transformation matrices $\mathbf{T}^{(1)}$ to $\mathbf{T}^{(4)}$ were presented in Eq. 12.12. These matrices can be used to decompose stiffness

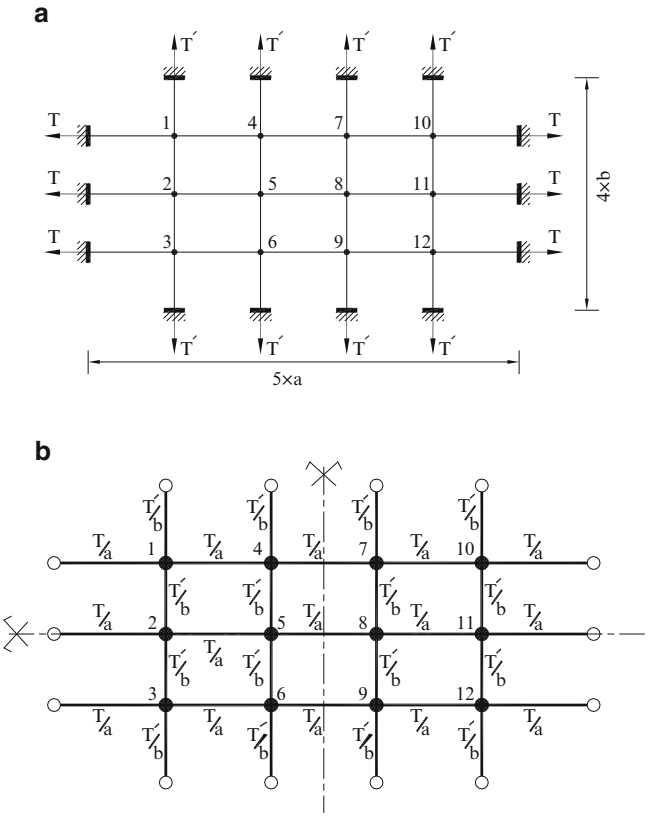

Fig. 12.15 Rectangular cable net N_2 and its associated net graph. (**a**) Rectangular network N_2. (**b**) Net graph NG_2, associated to net N_2

matrix of network N_2. If the magnitudes of the tension in horizontal and vertical cables are the same ($T' = T$), the results will be as follows:

$$\mathbf{K}^{(1)} = \frac{T}{ab}\begin{bmatrix} 2(a+b) & -\sqrt{2}a & -b & 0 \\ & 2(a+b) & 0 & -b \\ & & 2(a+b) & -\sqrt{2}a \\ Sym. & & & 2(a+b) \end{bmatrix}$$

$$\mathbf{K}^{(2)} = \frac{T}{ab}\begin{bmatrix} 2(a+b) & -b \\ Sym. & 2a+3b \end{bmatrix}, \mathbf{K}^{(3)} = \frac{T}{ab}\begin{bmatrix} 2(a+b) & -b \\ Sym. & 2a+b \end{bmatrix}$$

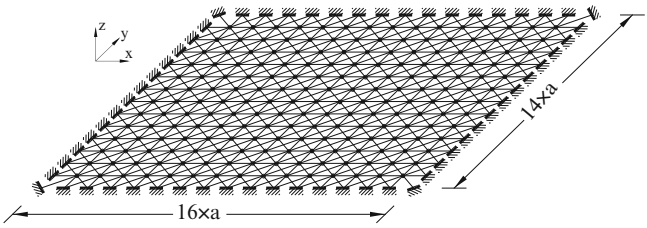

Fig. 12.16 Prestressed cable network N_3

$$\mathbf{K}^{(4)} = \frac{T}{ab}\begin{bmatrix} 2(a+b) & -\sqrt{2}a & -b & 0 \\ & 2(a+b) & 0 & -b \\ & & 2a+3b & -\sqrt{2}a \\ & Sym. & & 2a+3b \end{bmatrix}.$$

In presented examples, it was shown that instead of solving the characteristic equation for matrices of higher dimensions, some factors of lower dimensions are studied, resulting in a considerable saving in time and memory storage. In the first example, instead of analysing a 15×15 matrix, matrices of dimensions 9 and 6 are studied. This is the achievement of group theory. However, combination of group and graph product causes dealing with simple paths during the symmetry analysis. In other words, instead of working with a 15×15 matrix, 5×2 and 5×3 matrices are involved in a simple way in the group theoretic analysis. In the second example, working with 3×2, 3×1 and 4×2 matrices leads to decomposition of a 3×2 matrix to matrices of dimensions 4 and 2. Improvement which arises in symmetry analysis of structures by group theory, using the proposed method can be more highlighted in problems of larger scales. One example of such problems is presented as the last.

Example 12.5. Prestressed network $N3$ shown in Fig. 12.16 is composed of 13 horizontal and 15 vertical cables tied to each other by means of the crossed cables.

This network contains 195 nodes, which make the scale of stiffness and mass matrices of the system 195×195. Due to the symmetry of the system, group theory can be used to decompose it into independent subsystems of lower dimensions. However, existence of 195 nodes makes the symmetry analysis complicated as well.

Net graph of this network is the strong Cartesian product of two paths P_{13} and P_{15}. Therefore, the presented combined method can successfully be used to develop the symmetry analysis of the system. Symmetric and antisymmetric modes of the factors can easily be recognised and combined to form the symmetry transformation matrix of the whole system. In this example, instead of working with 195×195 matrices of the structure, $13 \times 6, 13 \times 7, 15 \times 7$ and 15×8 matrices associated with factors are involved in the process of analysis, which is a considerable achievement.

12.5 Discussion

A new method is presented in this chapter for symmetry analysis of regular structures. This is a combined method which uses the concept of graph products to improve the conventional group theoretic method for decomposition of symmetric graphs. The method is completely described for topological graphs, and then its mechanical application is presented. In this method, instead of studying the entire structure, its simple factors are studied, and transformation matrix which decomposes the structure is found as a combination of matrices of the factors. It is proved that symmetry group of such structures is always isomorphic to the direct product of symmetry groups of its generators. Therefore, after finding symmetric and antisymmetric modes of the factors, these are combined by direct (Kronecker) product, based on the character table of the product group (which is associated to the symmetry group of the original structure).

References

1. Kaveh A, Nikbakht M, Rahami H (2010) Improved group theoretic method using graphs products, for the analysis of symmetric-regular structures. Acta Mech 210(3–4):265–289
2. Kaveh A, Nikbakht M (2010) Improved group-theoretical method for eigenvalue problems of special symmetric structures, using graph theory. Adv Eng Soft 41:22–31
3. Armstrong MA (1988) Groups and symmetry. Springer, Berlin
4. Kaveh A, Nikbakht M (2007) Block diagonalization of Laplacian matrices of symmetric graphs via group theory. Int J Numer Methods Eng 69(5):908–947
5. Albert CF (1990) Chemical applications of group theory, Wiley, New York
6. Healey TJ, Treacy JA (1991) Exact block diagonalization of large eigenvalue problems for structures with symmetry. Int J Numer Methods Eng 31:265–285
7. Kaveh A, Rahami H (2008) Factorization for efficient solution of eigenproblems of adjacency and Laplacian matrices for graph products. Int J Numer Methods Eng 75(1):58–82
8. Pothen A, Simon H, Liou KP (1990) Partitioning sparse matrices with eigenvectors of graphs. SIAM J Matrix Anal Appl 11:430–452
9. Zloković GM (1989) Group theory and G-vector spaces in engineering structures, vibration, stability and statics. Ellis Horwood Limited, Chichester
10. Zingoni A (1996) An efficient computational scheme for the vibration analysis of high-tension cable nets. J Sound Vib 189:55–79
11. Zingoni A (2002) Group-theoretical applications in solid and structural mechanics: a review. Chapter 12. In: Topping BHV, Bittnar Z (eds) Computational structures technology. Saxe-Coburg, Edinburgh

Index

A. Kaveh, *Optimal Analysis of Structures by Concepts of Symmetry and Regularity*,
DOI 10.1007/978-3-7091-1565-7, © Springer-Verlag Wien 2013